

Topics in Current Chemistry 332

Gerhard Erker  
Douglas W. Stephan  
*Editors*

# Frustrated Lewis Pairs I

Uncovering and Understanding

 Springer

**332**

## **Topics in Current Chemistry**

*Editorial Board:*

K.N. Houk, Los Angeles, CA, USA

C.A. Hunter, Sheffield, UK

M.J. Krische, Austin, TX, USA

J.-M. Lehn, Strasbourg, France

S.V. Ley, Cambridge, UK

M. Olivucci, Siena, Italy

J. Thiem, Hamburg, Germany

M. Venturi, Bologna, Italy

C.-H. Wong, Taipei, Taiwan

H.N.C. Wong, Shatin, Hong Kong

For further volumes:

<http://www.springer.com/series/128>

## **Aims and Scope**

The series *Topics in Current Chemistry* presents critical reviews of the present and future trends in modern chemical research. The scope of coverage includes all areas of chemical science including the interfaces with related disciplines such as biology, medicine and materials science.

The goal of each thematic volume is to give the non-specialist reader, whether at the university or in industry, a comprehensive overview of an area where new insights are emerging that are of interest to larger scientific audience.

Thus each review within the volume critically surveys one aspect of that topic and places it within the context of the volume as a whole. The most significant developments of the last 5 to 10 years should be presented. A description of the laboratory procedures involved is often useful to the reader. The coverage should not be exhaustive in data, but should rather be conceptual, concentrating on the methodological thinking that will allow the non-specialist reader to understand the information presented.

Discussion of possible future research directions in the area is welcome.

Review articles for the individual volumes are invited by the volume editors.

**Readership: research chemists at universities or in industry, graduate students.**

Gerhard Erker · Douglas W. Stephan  
Editors

# Frustrated Lewis Pairs I

Uncovering and Understanding

With contributions by

K. Chernichenko · H. Eckert · G. Erker · T.M. Gilbert · S. Grimme ·  
F. Huang · G. Kehr · M. Leskelä · H. Li · G. Lu · I. Pápai · T. Repo ·  
B. Rieger · T.A. Rokob · B. Schirmer · F. Schulz · S. Schwendemann ·  
D.W. Stephan · V. Sumerin · Z.-X. Wang · T. Wiegand · L. Zhao

 Springer

*Editors*

Gerhard Erker  
Universität Münster  
Organisch-Chemisches Institut  
Münster  
Germany

Douglas W. Stephan  
University of Toronto  
Department of Chemistry  
Toronto  
Canada

ISSN 0340-1022

ISBN 978-3-642-36696-3

DOI 10.1007/978-3-642-36697-0

Springer Heidelberg New York Dordrecht London

ISSN 1436-5049 (electronic)

ISBN 978-3-642-36697-0 (eBook)

Library of Congress Control Number: 2013934529

© Springer-Verlag Berlin Heidelberg 2013

This work is subject to copyright. All rights are reserved by the Publisher, whether the whole or part of the material is concerned, specifically the rights of translation, reprinting, reuse of illustrations, recitation, broadcasting, reproduction on microfilms or in any other physical way, and transmission or information storage and retrieval, electronic adaptation, computer software, or by similar or dissimilar methodology now known or hereafter developed. Exempted from this legal reservation are brief excerpts in connection with reviews or scholarly analysis or material supplied specifically for the purpose of being entered and executed on a computer system, for exclusive use by the purchaser of the work. Duplication of this publication or parts thereof is permitted only under the provisions of the Copyright Law of the Publisher's location, in its current version, and permission for use must always be obtained from Springer. Permissions for use may be obtained through RightsLink at the Copyright Clearance Center. Violations are liable to prosecution under the respective Copyright Law.

The use of general descriptive names, registered names, trademarks, service marks, etc. in this publication does not imply, even in the absence of a specific statement, that such names are exempt from the relevant protective laws and regulations and therefore free for general use.

While the advice and information in this book are believed to be true and accurate at the date of publication, neither the authors nor the editors nor the publisher can accept any legal responsibility for any errors or omissions that may be made. The publisher makes no warranty, express or implied, with respect to the material contained herein.

Printed on acid-free paper

Springer is part of Springer Science+Business Media ([www.springer.com](http://www.springer.com))

# Preface

Up until recently, our understanding of the chemistry resulting from the combination of Lewis acids and bases had not evolved much since Lewis' time. In large part, the formation of Lewis acid–base adducts drew little interest as these systems were with a few notable exceptions perceived as thermodynamic sinks. However in 2006, we learned that certain combinations of Lewis acids and Lewis bases could coexist in solution and provide the possibility of new, synergistic reactions in which both reagents participate in the activation of  $H_2$ . This “archetypical” reaction was first demonstrated with Lewis pairs in which adduct formation was sterically frustrated. Subsequently we learned that such “frustrated Lewis pairs” (FLPs) could also be derived from weak electronic attractions between the acid and base, and that this notion was not limited to group 13/15 combinations.

The discovery of this seemingly simple concept led to the unprecedented application of FLPs in metal-free catalytic hydrogenations. Although the early developments were summarized in our 2010 review in *Angewandte Chemie*, the area has grown rapidly since then. Indeed, a number of creative and insightful contributions have broadened the range of FLP systems and led to dramatic developments including the activation of a variety of small molecules such as alkenes, alkynes,  $CO_2$ ,  $N_2O$ , and  $NO$ , among others. Theoretical studies have provided insight and understanding of this evolving area and exciting applications of FLPs in synthetic chemistry and catalysis continue to emerge.

These two volumes are a compilation of the state-of-the-art research concerning “FLPs” as of mid-2012. Over 20 researchers from around the globe have contributed chapters, detailing their inventive and astute contributions to this new and exciting area of the chemistry. These works cover a broad range of studies including synthetic chemistry, theoretical treatments, spectroscopic examinations, and catalytic applications. This breadth demonstrates the broad impact this work has had but furthermore speaks to the enormous potential for the future.

It has been our great pleasure to have acted as editors for these volumes. It is our hope that this collection will not only highlight the amazing growth of this area in only a few years, but will moreover influence others to take up the task of exploring or exploiting FLPs in their own chemistry.

Toronto, ON, Canada  
Münster, Germany

Douglas W. Stephan  
Gerhard Erker



# Contents

<b>Discovery of Frustrated Lewis Pairs: Intermolecular FLPs for Activation of Small Molecules</b> .....	1
Douglas W. Stephan	
<b>Intramolecular Frustrated Lewis Pairs: Formation and Chemical Features</b> .....	45
Gerald Kehr, Sina Schwendemann, and Gerhard Erker	
<b>Frustrated Lewis Pair Mediated Hydrogenations</b> .....	85
Douglas W. Stephan and Gerhard Erker	
<b>Amine-Borane Mediated Metal-Free Hydrogen Activation and Catalytic Hydrogenation</b> .....	111
Victor Sumerin, Konstantin Chernichenko, Felix Schulz, Markku Leskelä, Bernhard Rieger, and Timo Repo	
<b>Hydrogen Activation by Frustrated Lewis Pairs: Insights from Computational Studies</b> .....	157
Tibor András Rokob and Imre Pápai	
<b>Quantum Chemistry of FLPs and Their Activation of Small Molecules: Methodological Aspects</b> .....	213
Birgitta Schirmer and Stefan Grimme	
<b>Computational Design of Metal-Free Molecules for Activation of Small Molecules, Hydrogenation, and Hydroamination</b> .....	231
Zhi-Xiang Wang, Lili Zhao, Gang Lu, Haixia Li, and Fang Huang	



<b>Computational Studies of Lewis Acidity and Basicity in Frustrated Lewis Pairs</b> .....	267
Thomas M. Gilbert	
<b>Solid-State NMR as a Spectroscopic Tool for Characterizing Phosphane–Borane Frustrated Lewis Pairs</b> .....	291
Thomas Wiegand, Hellmut Eckert, and Stefan Grimme	
<b>Index</b> .....	347

# Discovery of Frustrated Lewis Pairs: Intermolecular FLPs for Activation of Small Molecules

Douglas W. Stephan

**Abstract** The discovery of *frustrated Lewis pairs* is described, as well as the ability of these intermolecular systems to react with a range of small molecules.

**Keywords** Alkynes · B–H bond activation · C–F bond activation · CO<sub>2</sub> activation · Frustrated Lewis pairs · Heterolytic activation of disulfide · Heterolytic cleavage of dihydrogen · N<sub>2</sub>O activation · Olefins · Ring-openings

## Contents

1	Introduction .....	2
1.1	Discovering Metal-Free Hydrogen Activation .....	5
1.2	Frustrated Lewis Pairs .....	8
1.3	Scope of Chapter .....	9
2	Heterolytic H <sub>2</sub> Activation by Intermolecular FLPs .....	9
2.1	Phosphine/Borane FLPs .....	10
2.2	Carbene/Borane FLPs .....	12
2.3	Nitrogen Bases/Boranes FLPs .....	12
2.4	Mechanistic Considerations and Literature Precedent .....	15
3	FLP Activation of Olefins and Alkynes .....	16
3.1	Boranes with Pendent Olefins .....	16
3.2	Activation of Dienes .....	17
3.3	Activation of Alkynes .....	18
4	FLPs in Ring-Opening Reactions .....	23
4.1	FLP Ring-Opening of THF .....	25
4.2	FLP Ring-Opening of Dioxane and Thioxane .....	27
4.3	FLP Ring-Opening and Contraction of Lactone and Lactide .....	27
4.4	FLP Ring-Opening of Cyclopropanes .....	28
5	FLP Activation of Greenhouse Gases .....	29
5.1	FLP Capture of CO <sub>2</sub> .....	29

---

D.W. Stephan (✉)  
Department of Chemistry, University of Toronto, 80 St. George Street, Toronto, ON,  
Canada M5S 3H6  
e-mail: [dstephan@chem.utoronto.ca](mailto:dstephan@chem.utoronto.ca)

5.2	FLPs in Stoichiometric Reduction of CO <sub>2</sub> .....	30
5.3	FLP Capture of N <sub>2</sub> O .....	33
5.4	FLP Capture of SO <sub>2</sub> .....	33
6	Additional Miscellaneous Reactions of FLPs .....	35
6.1	Heterolytic Cleavage of Disulfides .....	35
6.2	FLP Activation of Catechol Borane .....	35
6.3	Heterolytic NH Activation .....	36
6.4	Heterolytic CH Activation .....	37
6.5	Heterolytic CF Activation .....	37
7	Conclusion .....	38
	References .....	39

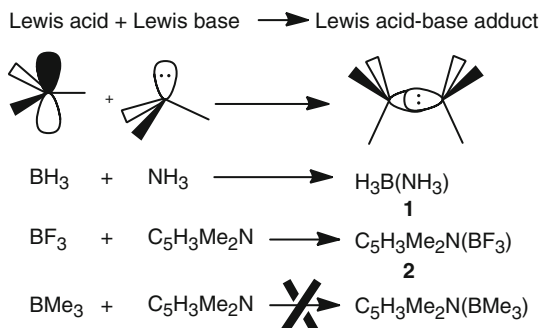
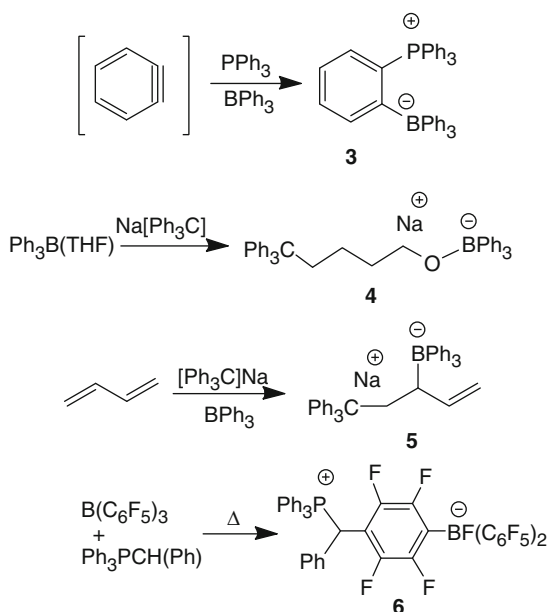
## Abbreviations

HOMO	Highest occupied molecular orbital
Idipp	((C <sub>6</sub> H <sub>3</sub> <i>i</i> Pr <sub>2</sub> N) <sub>2</sub> C <sub>3</sub> H <sub>2</sub> )
<i>t</i> Bu	( <i>t</i> BuN) <sub>2</sub> C <sub>3</sub> H <sub>2</sub>
LUMO	Lowest unoccupied molecular orbital
Me	Methyl = CH <sub>3</sub>
Mes	Mesityl = 2,4,6-trimethylphenyl
NHC	N-Heterocyclic carbene
Ph	Phenyl = C <sub>6</sub> H <sub>5</sub>
PMP	1,2,2,6,6-Pentamethylpiperidine
THF	tetrahydrofuran
TMP	2,2,6,6-Tetramethylpiperidine

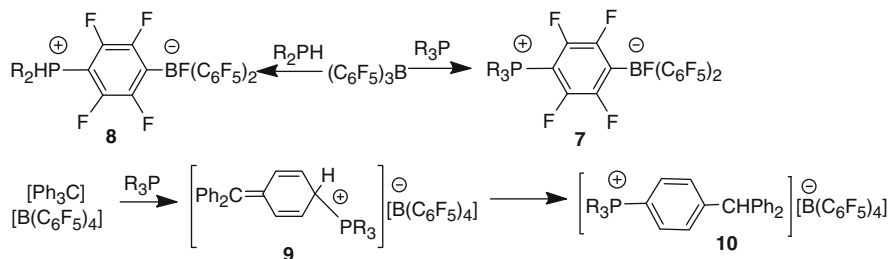
## 1 Introduction

The classification of molecules as electron donors and electron acceptors was first put forth by Gilbert Lewis in 1923 in his classic work entitled *Valence and the Structure of Atoms and Molecules* [1]. For this reason, such electron acceptors and donors are commonly referred to as “Lewis acids and bases.” An illustration of this concept, the combination of ammonia and borane to form the classical Lewis acid–base adduct H<sub>3</sub>B(NH<sub>3</sub>) **1**, is often a component of the undergraduate laboratory experience. Putting the concept of Lewis acidity and basicity in terms of molecular orbitals, Lewis acids are molecules that have a low lying LUMO while Lewis bases possess a high energy HOMO. This concept extends well beyond simple main group chemistry and indeed is now considered a fundamental axiom of our understanding of many reactions in inorganic, coordination and organic chemistry.

It was in 1942 that Brown and co-workers [2] described one of the first apparent exceptions to Lewis’ axiom when they reported that the combination of lutidine (2,6-dimethylpyridine) and BMe<sub>3</sub> failed to form a Lewis acid–base adduct. The authors noted that this stood in marked contrast to the analogous reaction of lutidine and BF<sub>3</sub> which resulted in the classical adduct (C<sub>5</sub>H<sub>3</sub>Me<sub>2</sub>N)BF<sub>3</sub> **2** (Scheme 1). The divergent behavior was attributed to the steric congestion resulting from the methyl groups on both the Lewis acid and base. This oddity was noted and left unexplored.

**Scheme 1** Reaction of Lewis acids and bases**Scheme 2** Non-conventional reactions of Lewis acids and bases

Subsequently other researchers discovered that such steric congestion between Lewis acids and bases can result in unexpected chemical ramifications. For example, Wittig and Benz [3] described how the combination of  $\text{PPh}_3$  and  $\text{BPh}_3$  in the presence of benzyne showed no evidence of the Lewis acid–base adduct but instead led to the *o*-phenylene-linked zwitterionic phosphonium-borate  $(\text{C}_6\text{H}_4)(\text{PPh}_3)(\text{BPh}_3)$  **3** (Scheme 2). Some years earlier, the corresponding reaction of trityl anion with  $(\text{THF})\text{BPh}_3$  led not to a facile base displacement reaction but rather to the attack of trityl on the borane-bound THF effecting ring-opening and formation of the salt  $\text{Na}[\text{Ph}_3\text{C}(\text{CH}_2)_4\text{OBPh}_3]$  **4** (Scheme 2) [4]. In related work in the 1960s, Tochtermann [5] described the addition of trityl anion and  $\text{BPh}_3$  to butadiene



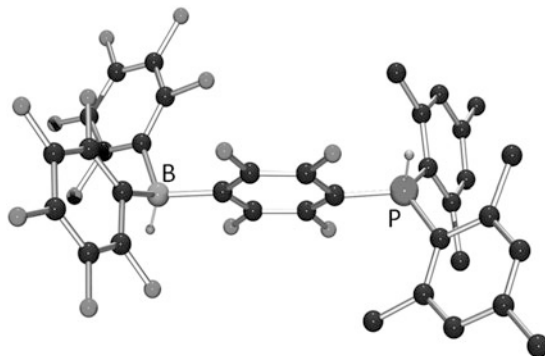
**Scheme 3** Synthesis of **7–10**

yielding  $\text{Na}[\text{Ph}_3\text{CCH}_2(\text{BPh}_3)\text{CHCH}_2]$  **5** (Scheme 2) despite expectations that the anion would either initiate anionic polymerization of the butadiene or form a Lewis acid–base adduct with the borane. The observation of this unusual reactivity resulting from this combination of a Lewis acid and base prompted Tochtermann [5] to dub this an “antagonistisches Paar”. In related chemistry, the reactions of sterically encumbered amines with a trityl cation did not yield an adduct but rather the trityl cation abstracts hydride from a carbon *alpha* to nitrogen affording an iminium cation [6]. Similarly, reactions of trityl cation with pyridine did not yield quaternization of N as expected on the basis of Lewis acid–base theory, but rather pyridine was thought to attack the carbon *para* to the carbocation [7] although this claim was disputed [8].

Other examples of the non-conventional behavior of Lewis acids and bases have continued to emerge. One such example emerged in the 1990s when Erker and co-workers [9] described the reactivity of  $\text{B}(\text{C}_6\text{F}_5)_3$  [10] and the ylide  $\text{Ph}_3\text{PC}(\text{H})\text{Ph}$ . Combination of this Lewis acid and base resulted in a classical Lewis acid–base adduct at room temperature; however, upon heating a rearrangement proceeds in which the ylide dissociates from boron and effects nucleophilic attack of the *para*-carbon with concurrent fluoride transfer to boron to give the zwitterionic salt  $\text{Ph}_3\text{PCH}(\text{Ph})(\text{C}_6\text{F}_4)\text{B}(\text{F})(\text{C}_6\text{F}_5)_2$  **6** (Scheme 2).

In subsequent work [11, 12], we described the reactions of sterically demanding tertiary phosphines with  $\text{B}(\text{C}_6\text{F}_5)_3$ . The steric congestion precludes the formation of a classical P–B dative bond. Instead these reactions afforded a series of zwitterions,  $\text{R}_3\text{P}(\text{C}_6\text{F}_4)\text{B}(\text{F})(\text{C}_6\text{F}_5)_2$  **7** ( $\text{R} = t\text{Bu}, i\text{Pr}, \text{Cy}$ ) (Scheme 3) resulting from the attack at the *para*-carbon of one of the fluoro-arene rings with concurrent migration of fluoride to boron. Related zwitterionic species can also be prepared from phosphine–borane adducts under thermal duress [13, 14]. In this fashion, tertiary and secondary phosphine–borane adducts rearrange to give the air and moisture stable zwitterions  $[\text{R}_3\text{P}(\text{C}_6\text{F}_4)\text{BF}(\text{C}_6\text{F}_5)_2]$  **7** ( $\text{R} = \text{Ph}, \text{Et}, \text{Cy}, n\text{Bu}, p\text{-CF}_3\text{C}_6\text{H}_4, o\text{-(MeO)C}_6\text{H}_4$ ) and  $[\text{R}_2\text{PH}(\text{C}_6\text{F}_4)\text{BF}(\text{C}_6\text{F}_5)_2]$  **8** ( $\text{R} = \text{C}_6\text{H}_2\text{Me}_3, t\text{Bu}, \text{Cp}, \text{Cy}, \text{R}_2 = t\text{Bu}(\text{Ph}), t\text{Bu}(\text{Mes})$ ) [13, 14].

In related chemistry, sterically unencumbered phosphines such as  $\text{PMe}_3$  react with trityl cation to give the classical Lewis acid–base phosphonium salt  $[\text{Ph}_3\text{C}(\text{PMe}_3)]\text{X}$ . However, sterically demanding tertiary phosphines cannot form P–C bonds between the phosphine and the central cationic carbon of the trityl



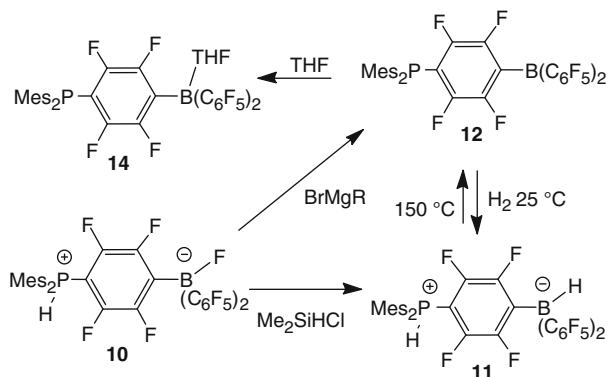
**Fig. 1** Molecular Structure of **11**

cation. Rather, attack at a *para*-carbon of a phenyl substituent generates the intermediate  $[\text{R}_3\text{P}(\text{C}_6\text{H}_5)\text{C}(\text{C}_6\text{H}_5)_2]^+$  **9**, which proceeds via hydride migration to the formerly cationic carbon, yielding the phosphonium cations of the form  $[\text{R}_3\text{P}(\text{C}_6\text{H}_4)\text{CH}(\text{C}_6\text{H}_5)_2]^+$  **10** (Scheme 3) [15]. In several cases the intermediate **9** has been isolated and spectroscopically characterized.

### 1.1 Discovering Metal-Free Hydrogen Activation

The above precedents illustrate that steric demands can have a dramatic impact on the course of the reaction depending on the different combinations of Lewis acids and bases utilized. In 2006 we became interested in the possibility of using zwitterionic species **8** as precursors to anionic phosphine ligands. Indeed, while preliminary work showed that treatment of such species with bases could result in deprotonation and the formation of anionic phosphine donors, it was some years later that we explored the utility of these zwitterions as ligand precursors for transition metal complexes [16]. We were distracted from this course of study by far more intriguing findings described below.

In the course of examining the reactivity of **8**, we discovered that **8** reacts cleanly with  $\text{Me}_2\text{Si}(\text{H})\text{Cl}$  to exchange hydride for fluoride yielding the phosphonium-hydridoborate salts  $[(\text{C}_6\text{H}_2\text{Me}_3)_2\text{P}(\text{H})(\text{C}_6\text{F}_4)\text{B}(\text{H})(\text{C}_6\text{F}_5)_2]$  (**11**) [12] (Fig. 1, Scheme 4). This species was shown to be remarkably robust and air stable despite containing protic and hydridic fragments. This latter aspect was surprising as we had anticipated loss of  $\text{H}_2$  and the subsequent oligomerization of the resulting phosphine-borane. Nonetheless, species **11** was shown to lose  $\text{H}_2$  upon heating up to  $150\text{ }^\circ\text{C}$ . Contrary to expectations, the resulting deep orange-red phosphino-borane  $\text{Me}_2\text{P}(\text{C}_6\text{F}_4)\text{B}(\text{C}_6\text{F}_5)_2$  **12** appeared to be monomeric in solution. It is interesting to note that related reactions of PH and BH fragments have been employed by Manners and co-workers to effect the loss of  $\text{H}_2$  from phosphine-borane adducts  $\text{R}_2\text{PH}(\text{BH}_3)$ . The products in these cases are not sterically encumbered and thus oligomerization via



**Scheme 4** Synthesis of **10–14**

dativative phosphorus–boron bonding affords cyclic and polymeric phosphinoboranes [17, 18]. Presumably the color of **12** arises from  $\pi$ -donation from phosphorus to the electron deficient arene and acceptance by boron, similar to that described for acetylene-based phosphino-borane  $\text{Ph}_2\text{PC}\equiv\text{CBMes}_2$  **13** [19, 20]. In addition, the monomeric nature of **12** is attributed to the sterically demanding substituents on phosphorus and boron. While **12** could not be crystallized in a fashion suitable for single-crystal X-ray diffraction studies, the structure of the corresponding THF adduct  $(\text{Mes})_2\text{P}(\text{C}_6\text{F}_4)\text{B}(\text{C}_6\text{F}_5)_2(\text{THF})$  **14** (Scheme 4) was crystallographically confirmed. Compound **12** was also generated by the reaction of **10** with a Grignard reagent [12].

The evolution of  $\text{H}_2$  from **11** was not surprising since the molecule contains both protic and hydridic hydrogens. However, given that this had to be driven thermally, we probed the reverse reaction and discovered that simply placing **12** under an atmosphere of  $\text{H}_2$  at  $25^\circ\text{C}$  resulted in the rapid and facile reformation of **11** [12]. This finding represents the first reversible activation of  $\text{H}_2$  by a non-metal system. Perhaps most surprising is the remarkably facile nature in which the hydrogen–hydrogen bond is heterolytically split to generate a hydride and proton. Moreover and perhaps most strikingly, this finding stands in sharp contrast to the generally held dogma of the day that the activation of dihydrogen requires the use of a transition metal species. In addition, it is also important to note that Lewis acid–base adducts were generally perceived as unreactive or thermodynamic “dead-ends” and well understood. Thus, combinations of Lewis acids and bases were not deemed worthy of further study. This discovery provides an important new dimension both in the chemistry of dihydrogen and main group systems.

In considering this reactivity, it appears that the key feature of **12** that allows for the activation of hydrogen is the unquenched Lewis acidity and Lewis basicity that permits the polarization of dihydrogen. It was indeed fortuitous that this study began with an examination of **11** whereas the analog where the  $\text{C}_6\text{H}_2\text{Me}_3$  groups are replaced by *t*Bu failed to liberate dihydrogen at  $150^\circ\text{C}$ . This suggests that the greater basicity of the phosphorus in this derivative inhibits proton release and thus

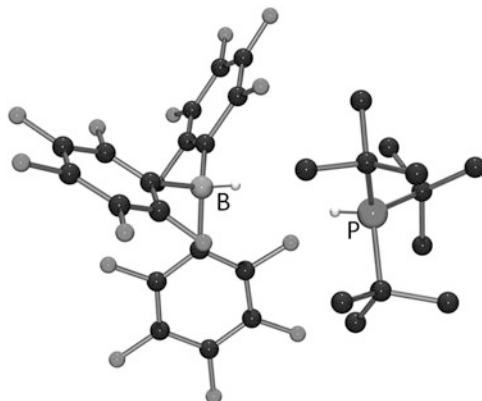
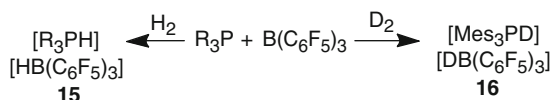


Fig. 2 Molecular structure of **15a**



Scheme 5 Synthesis of **15** and **16**

precludes protonation of the borohydride. However, the acidity of the phosphonium center for species **11** is sufficient to allow for dihydrogen release resulting in a bulky phosphine incapable of forming a classical Lewis acid–base adduct and thus is available to act in concert with the borane to split dihydrogen heterolytically.

Given that the steric congestion and basicity/acidity of the phosphine and borane were perceived as the critical factors for such reactivity, we were immediately prompted to examine the reactions of simple sterically encumbered phosphines and boranes with dihydrogen. Thus, bulky phosphines such as  $R_3P$  ( $R = tBu$ ,  $C_6H_2Me_3$ ) were combined with  $B(C_6F_5)_3$  [21] and shown to exhibit no evidence of adduct formation by multi-nuclear NMR studies. However, on exposure of these solutions to dihydrogen (1 atm) at room temperature, a spontaneous reaction afforded the precipitation of the phosphonium-hydridoborate salts  $[R_3PH][HB(C_6F_5)_3]$  **15** ( $R = tBu$  **15a**,  $Mes$  **15b**) (Fig. 2, Scheme 5). This heterolytic cleavage of dihydrogen was remarkably facile [21] and was confirmed with a crystallographic study of **15a**. While the structure of the salt is as anticipated, it does reveal that the cation and anion are oriented in the solid state with the BH and PH units towards each other, with a BH-HP separation of 2.75 Å (Fig. 2). In a similar fashion, the combination of  $Mes_3P$  and  $B(C_6F_5)_3$  reacts with dideuterium to give  $[Mes_3PD][DB(C_6F_5)_3]$  **16** (Scheme 5) [21]. Interestingly, in contrast to **11**, heating the salts **15** or **16** to 150 °C does not liberate dihydrogen or dideuterium, respectively.



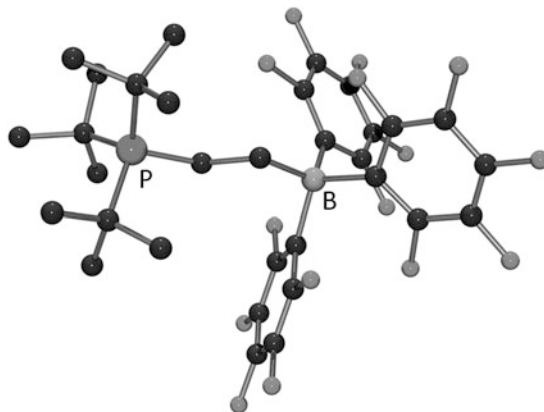
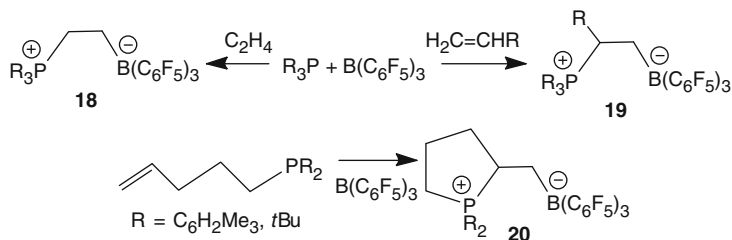


Fig. 3 Molecular structure of **18**

Probing the range of Lewis acidity and basicity was initially investigated via the reaction of dihydrogen with  $t\text{Bu}_3\text{P}$  and  $\text{BPh}_3$ . While the species  $[t\text{Bu}_3\text{PH}][\text{HBPh}_3]$  **17** was obtained, the low yield is attributable to the reduced Lewis acidity of the borane [21]. In a similar fashion, variation in the Lewis acidity and basicity as in the combinations of  $\text{Mes}_3\text{P}$  and  $\text{BPh}_3$ ,  $(\text{C}_6\text{F}_5)_3\text{P}$  and  $\text{B}(\text{C}_6\text{F}_5)_3$ , or  $t\text{Bu}_3\text{P}$  and  $\text{BMes}_3$  resulted in no apparent reaction with or without  $\text{H}_2$ . These observations further support the notion that while a critical aspect appears to be a combination of acid and base that do not form a strong adduct, there also appears to be a threshold of combined Lewis acidity and basicity that is necessary for dihydrogen activation.

## 1.2 Frustrated Lewis Pairs

We had come from a background in organometallic chemistry and thus our discovery of the ability of sterically encumbered phosphines and boranes to activate dihydrogen made us curious about the reactivity of such combinations with other small molecules. It was this curiosity that prompted the investigation of the reaction of the combination of  $t\text{Bu}_3\text{P}$  and  $\text{B}(\text{C}_6\text{F}_5)_3$  with ethylene. This reaction resulted in the immediate formation of the zwitterionic addition product  $[t\text{Bu}_3\text{P}(\text{C}_2\text{H}_4)\text{B}(\text{C}_6\text{F}_5)_3]$  **18** (Fig. 3, Scheme 6) [22]. Similarly, the terminal olefins propene or hexene gave the analogous products  $[t\text{Bu}_3\text{P}(\text{CH}(\text{R})\text{CH}_2\text{B}(\text{C}_6\text{F}_5)_3)]$  **19** ( $\text{R} = \text{CH}_3, \text{C}_4\text{H}_9$ ) (Scheme 6). In a related example, the phosphines incorporating a pendant olefinic fragment  $\text{CH}_2=\text{CH}(\text{CH}_2)_3\text{PR}_2$  ( $\text{R} = t\text{Bu}, \text{Mes}$ ) also reacted with  $\text{B}(\text{C}_6\text{F}_5)_3$  to give the cyclic phosphonium borate  $[\text{R}_2\text{PCH}(\text{C}_3\text{H}_6)\text{CH}_2\text{B}(\text{C}_6\text{F}_5)_3]$  **20** ( $\text{R} = t\text{Bu}, \text{Mes}$ ) (Scheme 6) [22]. In all of these additions, the boron added to the terminal carbon while the phosphorus added to the secondary carbon center.



**Scheme 6** Reactions of FLPs with olefins

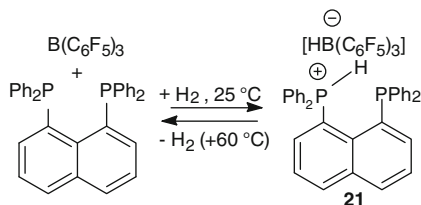
The reactivity of the combination of unquenched Lewis acids and bases above for dihydrogen and olefins is unprecedented. Moreover the requirement for steric congestion to frustrate the formation of a classical dative bond prompted us to describe the combinations of such bulky acids and bases as “frustrated Lewis pairs” (FLPs) [22]. Now, 6 years later, the term “frustrated Lewis pairs” has been accepted to describe the general situation where steric demands prevent the quenching of Lewis acidic and basic centers via adduct formation allowing them to act on a substrate.

### 1.3 Scope of Chapter

“Frustrated Lewis pairs” can be used to activate a variety of small molecules achieved with intermolecular and intramolecular combinations of Lewis acidic and basic centers. Moreover, the notion of FLPs has developed well beyond the initially discovered boron/phosphorus pairs, to include a range of main group elements and transition metals. In addition, while FLP chemistry began with reactions of dihydrogen and olefins, these substrates continue to be of much interest. Nonetheless, the range of substrates examined in FLP chemistry has also expanded dramatically. The contents of this chapter reflect this burgeoning breadth including intramolecular FLPs, metal-based FLPs, and all carbon based systems. While several reviews have detailed a broader discussion of the chemistry of FLPs [23–26], this first chapter of this volume of *Topics in Current Chemistry* is limited to a description of the discovery and current state of reactivity of intermolecular FLP systems specifically.

## 2 Heterolytic H<sub>2</sub> Activation by Intermolecular FLPs

The use of FLPs in the activation of dihydrogen has spurred the development of metal-free hydrogenation catalysts. A number of studies exploring the substrate scope and the impact of catalyst modification have been reported. In addition, elegant applications in asymmetric hydrogenations have also advanced the field.



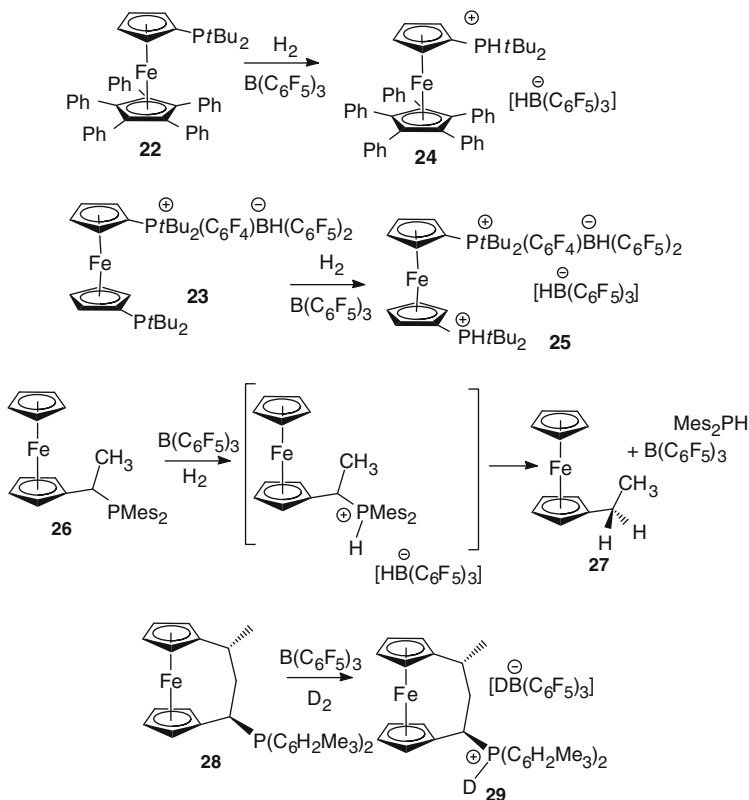
**Scheme 7** Reversible H<sub>2</sub> binding by **21**

The discussion of hydrogen activation in the present chapter is limited to intermolecular systems that effect dihydrogen activation. Discussion of work focused on the development and evaluation of hydrogenation catalysts as well as computational studies of the mechanism of dihydrogen activation are deferred to other chapters.

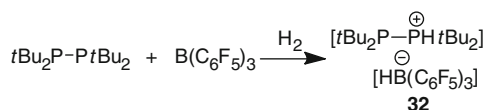
## 2.1 Phosphine/Borane FLPs

Shortly after our initial reports described above, Erker and co-workers [27] described the FLP derived from 1,8-bis(diphenylphosphino)-naphthalene [28] and B(C<sub>6</sub>F<sub>5</sub>)<sub>3</sub>. This diphosphine contains sterically crowded phosphorus donors and is structurally analogous to a proton sponge. Thus it acts as a base binding proton between the two phosphorus centers. The combination with the Lewis acid generates an FLP which reacts with dihydrogen to give the phosphonium hydridoborate salt [C<sub>10</sub>H<sub>6</sub>(PPh<sub>2</sub>)<sub>2</sub>H][HB(C<sub>6</sub>F<sub>5</sub>)<sub>3</sub>] **21** (Scheme 7) [27]. <sup>31</sup>P NMR spectral data for **21** show rapid proton exchange between the two phosphine sites which slows on cooling to low temperature. Similar to **15**, in the solid state the phosphonium cation and hydridoborate anion are oriented towards each other with a P–H...H–B approach of 2.08 Å. This salt liberates dihydrogen under mild conditions of heating to 60 °C [27], a feature that is attributable to the acidity of the cation.

In probing the impact of phosphine substituents, the reactions of ferrocenyl phosphines in FLP chemistry was also examined [29]. To this end the *mono*- and *bis*-ferrocenyl-phosphine derivatives (η<sup>5</sup>-C<sub>5</sub>H<sub>4</sub>PtBu<sub>2</sub>)Fe(C<sub>5</sub>Ph<sub>5</sub>) **22** and (η<sup>5</sup>-C<sub>5</sub>H<sub>4</sub>PtBu<sub>2</sub>(C<sub>6</sub>F<sub>4</sub>)BH(C<sub>6</sub>F<sub>5</sub>)<sub>2</sub>)Fe(η<sup>5</sup>-C<sub>5</sub>H<sub>4</sub>PtBu<sub>2</sub>) **23** were shown to react with dihydrogen in the presence of B(C<sub>6</sub>F<sub>5</sub>)<sub>3</sub> to give the respective phosphonium borate salts **24–25** (Scheme 8). The related ferrocene-phosphine derivative CpFe(C<sub>5</sub>H<sub>4</sub>CHMePMe<sub>2</sub>) **26** was shown by Erker and colleagues to react with B(C<sub>6</sub>F<sub>5</sub>)<sub>3</sub> and H<sub>2</sub>. The corresponding phosphonium borate salt was generated, however a further reaction results in the elimination of the borane adduct (Mes<sub>2</sub>PH)B(C<sub>6</sub>F<sub>5</sub>)<sub>3</sub> with hydride delivery to the ferrocenyl species generating CpFe(C<sub>5</sub>H<sub>4</sub>CH<sub>2</sub>Me) **27** (Scheme 8) [30, 31]. The closely related [3]ferrocenophane system **28** [31] reacts with B(C<sub>6</sub>F<sub>5</sub>)<sub>3</sub> and D<sub>2</sub> in a similar fashion to give the organometallic phosphonium/hydridoborate salt **29** (Scheme 8). In related chemistry zirconocene derivative (Mes<sub>2</sub>PC<sub>5</sub>H<sub>4</sub>)<sub>2</sub>ZrCl<sub>2</sub> **30** reacts in combination with



**Scheme 8** Phosphino-ferrocenes in FLP activation of dihydrogen

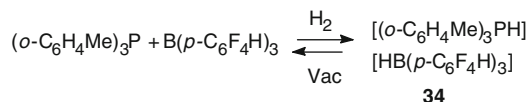


**Scheme 9** Reaction of the diphosphine  $t\text{Bu}_4\text{P}_2$  with  $\text{B}(\text{C}_6\text{F}_5)_3$  and  $\text{H}_2$

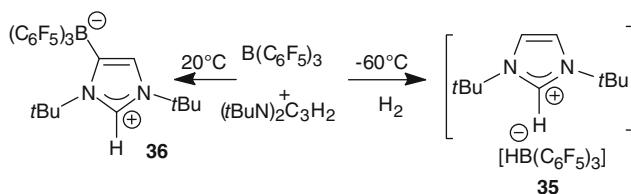
$\text{B}(\text{C}_6\text{F}_5)_3$  to split dihydrogen heterolytically under very mild conditions affording  $[(\text{Mes}_2\text{P}(\text{H})\text{C}_5\text{H}_4)_2\text{ZrCl}_2][\text{HB}(\text{C}_6\text{F}_5)_3]_2$  **31** [32, 33].

One unique variant in the phosphorus base that has been demonstrated is the use of the diphosphine  $t\text{Bu}_4\text{P}_2$ . This species in combination with  $\text{B}(\text{C}_6\text{F}_5)_3$  and  $\text{H}_2$  [34] leads to the generation of the salt  $[\text{tBu}_2\text{P}(\text{P}t\text{Bu}_2)][\text{HB}(\text{C}_6\text{F}_5)_3]$  **32** (Scheme 9).

One early variation in the Lewis acids partners involved the seemingly trivial modification of the borane to  $\text{B}(p\text{-C}_6\text{F}_4\text{H})_3$  **33** [35, 36]. This borane offers the advantage over  $\text{B}(\text{C}_6\text{F}_5)_3$  in that it is not susceptible to *para*-attack by Lewis bases. This feature permits the use of a broader range of phosphines in the formation of FLPs. Combination of **33** with  $\text{PR}_3$  ( $\text{R} = t\text{Bu}, \text{Cy}, o\text{-C}_6\text{H}_4\text{Me}$ ) under an atmosphere of  $\text{H}_2$  at 25 °C affords the phosphonium hydridoborates  $[\text{R}_3\text{PH}][\text{HB}(p\text{-C}_6\text{F}_4\text{H})_3]$  **34**



**Scheme 10** Reactions of  $\text{B}(\text{C}_6\text{F}_4\text{H})_3$  with phosphine and  $\text{H}_2$



**Scheme 11** Reactions of NHCs with  $\text{B}(\text{C}_6\text{F}_5)_3$

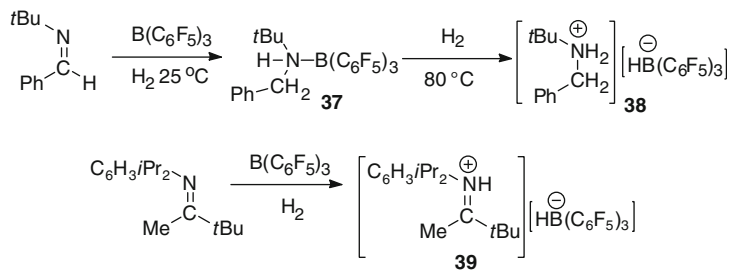
(Scheme 10). The salt  $[(o\text{-C}_6\text{H}_4\text{Me})_3\text{PH}][\text{HB}(p\text{-C}_6\text{F}_4\text{H})_3]$  was found to release  $\text{H}_2$  slowly by simple application of vacuum at  $25^\circ\text{C}$  [35, 36]. After 9 days the FLP was regenerated in 85% yield. On the other hand, loss of  $\text{H}_2$  was complete at  $80^\circ\text{C}$  in 12 h (Scheme 10). This observation stands in sharp contrast to the resistance to losing  $\text{H}_2$  by **15** and is attributed to the diminished Lewis acidity of  $\text{B}(p\text{-C}_6\text{F}_4\text{H})_3$ .

## 2.2 Carbene/Borane FLPs

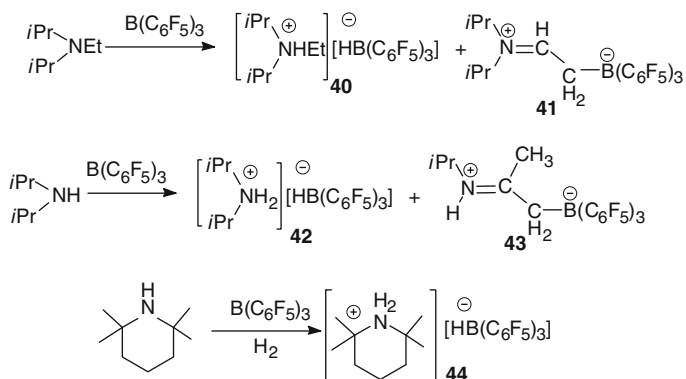
In 2007, Bertrand and coworkers [37] demonstrated the activation of  $\text{H}_2$  by alkylamino-carbenes (e.g.,  $i\text{Pr}_2\text{NtBu}$ ) affording the amine  $i\text{Pr}_2\text{NCH}_2\text{tBu}$ . This was attributed in part to the strong Lewis basicity and acidity localized at the carbene carbon. It is noteworthy that the analogous behavior does not proceed with N-heterocyclic carbenes (NHCs). However, combinations of sterically hindered NHCs and  $\text{B}(\text{C}_6\text{F}_5)_3$  were reported to effect the FLP activation of  $\text{H}_2$  simultaneously by the research groups of Stephan [38, 39] and Tamm [40]. In this work, it was shown that the NHC Idipp forms a strong adduct with  $\text{B}(\text{C}_6\text{F}_5)_3$ , but the combination of NHC  $\text{tBu}$  with  $\text{B}(\text{C}_6\text{F}_5)_3$  forms an FLP at low temperature. This pair reacts with  $\text{H}_2$  to give the imidazolium hydridoborate,  $[\text{tBuH}][\text{HB}(\text{C}_6\text{F}_5)_3]$  **35** (Scheme 11) resulting from heterolytic cleavage of  $\text{H}_2$ . Tamm and co-workers also showed that at room temperature the combination of  $\text{tBu}$  and  $\text{B}(\text{C}_6\text{F}_5)_3$  affords the “abnormal” carbene adduct  $\text{tBu}(\text{B}(\text{C}_6\text{F}_5)_3)$  **36** (Scheme 11).

## 2.3 Nitrogen Bases/Boranes FLPs

In early 2008 we reported that the stoichiometric reaction of the imine  $\text{tBuN}=\text{CPh}(\text{H})$  and  $\text{B}(\text{C}_6\text{F}_5)_3$  and  $\text{H}_2$  gives the amine–borane adduct  $\text{tBu}(\text{PhCH}_2)\text{NH}(\text{B}(\text{C}_6\text{F}_5)_3)$  **37**



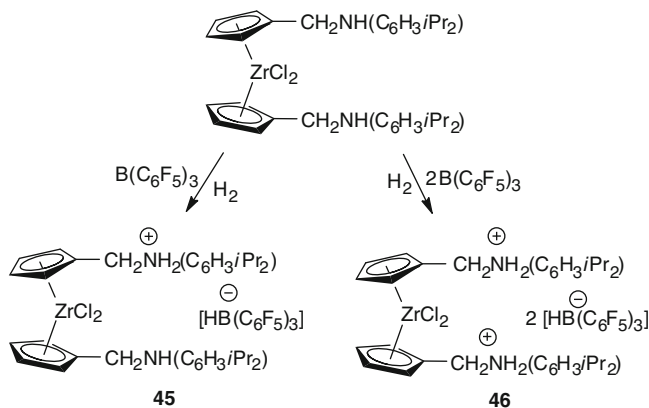
**Scheme 12** Reactions of imines with  $\text{B}(\text{C}_6\text{F}_5)_3$  and  $\text{H}_2$



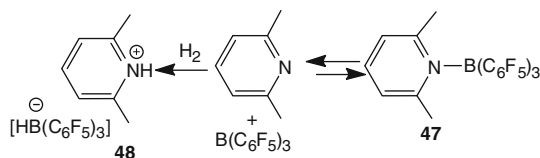
**Scheme 13** Reactions of amines with  $\text{B}(\text{C}_6\text{F}_5)_3$  and  $\text{H}_2$

(Scheme 12) [41]. Mechanistically this presumably proceeds via an FLP heterolytic cleavage of dihydrogen to give an iminium hydridoborate. This is followed by hydride transfer to the iminium carbon affording the amine-borane adduct. Further warming to  $80^\circ\text{C}$  for 1 h under  $\text{H}_2$  (4–5 atm) effects the thermal dissociation of the adduct and a further heterolytic activation of  $\text{H}_2$  affording  $[\text{tBuNH}_2(\text{CH}_2\text{Ph})][\text{HB}(\text{C}_6\text{F}_5)_3]$  **38** (Scheme 12). Interestingly the proposed reaction sequence is supported by the corresponding reaction of the highly sterically encumbered imine  $(\text{C}_6\text{H}_3/\text{iPr}_2)\text{N}=\text{CMe}(\text{tBu})$  with  $\text{B}(\text{C}_6\text{F}_5)_3$  under  $\text{H}_2$ . In this case, the activation of dihydrogen gives the iminium salt  $[(\text{C}_6\text{H}_3/\text{iPr}_2)\text{N}(\text{H})=\text{CMe}(\text{tBu})][\text{HB}(\text{C}_6\text{F}_5)_3]$  **39** (Scheme 12). Presumably the steric congestion precludes hydride transfer to the iminium carbon [41].

Rieger, Repo and co-workers [42] reported that combinations of the amine  $\text{iPr}_2\text{NEt}$  with  $\text{B}(\text{C}_6\text{F}_5)_3$  gave 50:50 mixtures of the salts  $[\text{iPr}_2\text{NHEt}][\text{HB}(\text{C}_6\text{F}_5)_3]$  **40** and  $\text{iPr}_2\text{N}=\text{CHCH}_2\text{B}(\text{C}_6\text{F}_5)_3$  **41** while the corresponding reaction of  $\text{iPr}_2\text{NH}$  gave  $[\text{iPr}_2\text{NH}_2][\text{HB}(\text{C}_6\text{F}_5)_3]$  **42** and  $\text{iPrNH}=\text{C}(\text{CH}_3)(\text{CH}_2)\text{B}(\text{C}_6\text{F}_5)_3$  **43** (Scheme 13). The former species **40** and **42** arise from the effective addition of dihydrogen while the latter species **41** and **43** arise from the dehydrogenation of the amines. On the other hand, exposure of mixtures of  $\text{iPr}_2\text{NH}$  or TMP with  $\text{B}(\text{C}_6\text{F}_5)_3$  and  $\text{H}_2$  gives the salts  $[\text{iPr}_2\text{NH}_2][\text{HB}(\text{C}_6\text{F}_5)_3]$  **42** and  $[\text{TMPH}][\text{HB}(\text{C}_6\text{F}_5)_3]$  **44**, respectively (Scheme 13).



**Scheme 14** Amino-borane reactions  $\text{H}_2$



**Scheme 15** Classical and FLP behavior of lutidine/ $\text{B}(\text{C}_6\text{F}_5)_3$

The corresponding mixtures with  $\text{BPh}_3$  resulted in no reaction, inferring the Lewis acidity is a key factor although Rieger *et al.* suggested that CF–HN interactions between the amine and borane were necessary for activation of  $\text{H}_2$  [42].

Similar to the metallocene-phosphine derivatives described above, Erker *et al.* described the reaction of the group 4 metallocene-amine derivative  $[(\text{C}_5\text{H}_4\text{CH}_2\text{NH}(\text{C}_6\text{H}_3i\text{Pr}_2))_2\text{ZrCl}_2]$  with  $\text{B}(\text{C}_6\text{F}_5)_3$  and  $\text{H}_2$  under ambient conditions (2 bar,  $25^\circ\text{C}$ ) to give the salts  $[(\text{C}_5\text{H}_4\text{CH}_2\text{NH}(\text{C}_6\text{H}_3i\text{Pr}_2))(\text{C}_5\text{H}_4\text{CH}_2\text{NH}_2(\text{C}_6\text{H}_3i\text{Pr}_2))\text{ZrCl}_2][\text{HB}(\text{C}_6\text{F}_5)_3]$  **45** and  $[(\text{C}_5\text{H}_4\text{CH}_2\text{NH}_2(\text{C}_6\text{H}_3i\text{Pr}_2))_2\text{ZrCl}_2][\text{HB}(\text{C}_6\text{F}_5)_3]_2$  **46** (Scheme 14) [32].

Pyridines form classical Lewis acid–base adducts with  $\text{B}(\text{C}_6\text{F}_5)_3$  [43, 44], although the early work of Brown [2] demonstrated that steric congestion can prevent adduct formation of lutidine and  $\text{BMe}_3$ . Building on this observation, we described reactions of the combination of 2,6-lutidine and  $\text{B}(\text{C}_6\text{F}_5)_3$ . The initial mixture presents as an equilibrium between the free Lewis acid and base and the corresponding adduct  $(2,6\text{-Me}_2\text{C}_5\text{H}_3\text{N})\text{B}(\text{C}_6\text{F}_5)_3$  **47** (Scheme 15) [45, 46]. Cooling the solution favors the adduct as evidenced by  $^{19}\text{F}$  NMR spectroscopy and indeed the adduct can be isolated and structurally characterized. The variable temperature data infer that  $\Delta\text{H}$  and  $\Delta\text{S}$  for this equilibrium are  $-42(1)$  kJ/mol and  $-131(5)$  J/mol K, respectively. The access to the free Lewis acid and base is also evidenced by the reaction of this mixture with  $\text{H}_2$  (1 atm, 2 h) which provides the pyridinium salt  $[2,6\text{-Me}_2\text{C}_5\text{H}_3\text{NH}][\text{HB}(\text{C}_6\text{F}_5)_3]$  **48** (Scheme 15) [45, 46]. This work emphasizes the relationship between a classical Lewis acid–base adduct and the

corresponding FLP. Rather than the previously held perception that classical and FLP reactivity are mutually exclusive reaction pathways, this work demonstrates that these reactivities are extremes of a continuum. This finding begs questions about the possible untapped reactivity of the vast number of known classical Lewis acid–base adducts. This exciting possibility as classical Lewis acid–base adducts stands in contrast to the previous perception of Lewis acid–base adducts as “thermodynamic dead-ends.”

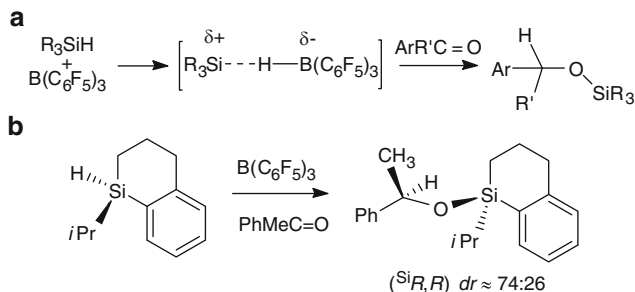
## 2.4 Mechanistic Considerations and Literature Precedent

The activation of dihydrogen by the FLP systems described above is challenging to explore experimentally due to the rapidity of the reaction. Indeed, efforts to monitor the activation in solution even at temperatures as low as  $-80\text{ }^{\circ}\text{C}$  were unsuccessful. Computational studies examining the mechanism of the activation of  $\text{H}_2$  have revealed the formation of an “encounter complex” intermediate and such studies are described by Rokob and Pápai [128] and Schirmer and Grimme [129].

In the context of experimental evidence regarding mechanistic questions, it is important to point out the insight provided by literature precedent. Indeed, it was in the late 1990s, almost 10 years prior to work on FLPs, that Piers and coworkers described the  $\text{B}(\text{C}_6\text{F}_5)_3$  catalyzed hydrosilylation of ketones and imines [47–50]. In the case of ketone hydrosilylation, Piers *et al.* showed conclusively that this reaction proceeds by activation of the silane by the strong Lewis acid  $\text{B}(\text{C}_6\text{F}_5)_3$  [51–55] rather than by Lewis acid activation of the carbonyl species [56, 57]. The “activated hydride” is then transferred from silicon to boron with concomitant addition of the carbonyl transient silicenium ion affording the hydrosilylation product [49, 50, 58–64]. Piers and coworkers also proposed similar mechanisms for the conversion of imines to amines and for hydrosilylation of silyl enol ethers [65], while Gevorgyan *et al.* [66–71] suggested that the hydrosilylation of olefins proceeds via a transient  $\beta$ -silyl-stabilized carbocation, to which hydride is delivered by  $[\text{HB}(\text{C}_6\text{F}_5)_3]^-$ . In subsequent work, Oestreich *et al.* [72–75] studied the  $\text{B}(\text{C}_6\text{F}_5)_3$ -mediated hydrosilylation of acetophenone with “Oestreich-silane,” an optically highly enriched chiral silane. In this fashion it was unambiguously demonstrated that the reaction proceeds with inversion of the configuration at silicon, thus ruling out involvement of a free silicenium ion. Thus, this observation is a consistent  $\text{S}_{\text{N}}2$ -type process (Scheme 16).

While these mechanistic aspects of hydrosilylation are particularly relevant to the mechanism of FLP-based hydrogenations described in the subsequent chapters in this volume (see below), the activation of silane by  $\text{B}(\text{C}_6\text{F}_5)_3$  clearly parallels the dihydrogen activation described herein. In this regard, it is also important to point out that Piers exploited the reaction of  $\text{B}(\text{C}_6\text{F}_5)_3$  with  $\text{Et}_3\text{SiH}$  to prepare  $\text{HB}(\text{C}_6\text{F}_5)_2$  [54, 55], suggesting the possibility of a related pathway for  $\text{B}(\text{C}_6\text{F}_5)_3/\text{H}_2$  activation. That being said, our efforts to directly detect a borane-dihydrogen interaction by NMR methods were unsuccessful.





**Scheme 16** Hydrosilylation of ketones mediated by B(C<sub>6</sub>F<sub>5</sub>)<sub>3</sub>

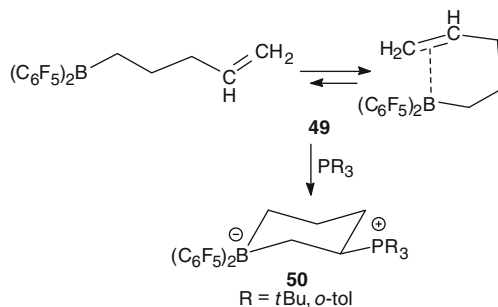
### 3 FLP Activation of Olefins and Alkynes

The initial report of the reactions of phosphines and boranes with simple olefins was the first to use the term “frustrated Lewis pairs.”<sup>[22]</sup> The reactions of related intermolecular FLPs with olefinic substrates have been expanded with a view to probing both mechanistic information and to broadening the synthetic utility. Similarly the extension of such additions to alkynes was also probed.

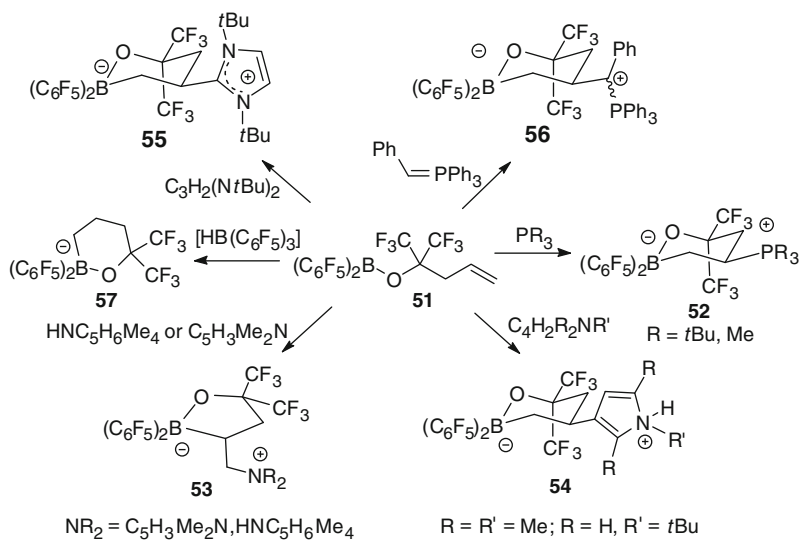
#### 3.1 Boranes with Pendent Olefins

The interactions of olefinic substrates and boranes have been probed employing the borane with a pendent olefinic fragment CH<sub>2</sub>=CH(CH<sub>2</sub>)<sub>n</sub>B(C<sub>6</sub>F<sub>5</sub>)<sub>2</sub> **49**. 2D <sup>1</sup>H-<sup>19</sup>F NOESY experiments were consistent with a weak “van der Waals complex”<sup>[76]</sup>. This species reacts with phosphines to effect phosphine-borane addition to the olefin affording cyclic phosphonium borates R<sub>3</sub>PCH<sub>2</sub>CH(CH<sub>2</sub>)<sub>n</sub>B(C<sub>6</sub>F<sub>5</sub>)<sub>2</sub> **50** (Scheme 17). The inference of a van der Waals interaction suggests a sequential reaction with phosphines. This stands in contrast to the theoretical studies by Pápai *et al.*<sup>[77]</sup> which conclude that the reaction of *t*Bu<sub>3</sub>P/B(C<sub>6</sub>F<sub>5</sub>)<sub>3</sub> and ethylene occurs via an antarafacial asynchronous concerted 1,2-addition process<sup>[78]</sup>. It is noteworthy that older matrix isolation studies<sup>[79]</sup> as well as computational studies<sup>[80, 81]</sup> have supported the notion of van der Waals interactions.

The generality of this reactivity is demonstrated with the electrophilic alkoxyborane, B(C<sub>6</sub>F<sub>5</sub>)<sub>2</sub>(OC(CF<sub>3</sub>)<sub>2</sub>CH<sub>2</sub>CHCH<sub>2</sub>) **51**<sup>[82]</sup>. This species reacts in a similar fashion with phosphines including *t*Bu<sub>3</sub>P or Me<sub>3</sub>P to give the phosphonium cyclic borate species B(C<sub>6</sub>F<sub>5</sub>)<sub>2</sub>(OC(CF<sub>3</sub>)<sub>2</sub>CH<sub>2</sub>CHCH<sub>2</sub>)(PR<sub>3</sub>) **52** (R = *t*Bu, Me). Moreover, addition of other nucleophiles such as 2,6-lutidine or 2,2,6,6-tetramethylpiperidine gave B(C<sub>6</sub>F<sub>5</sub>)<sub>2</sub>(OC(CF<sub>3</sub>)<sub>2</sub>CH<sub>2</sub>CHCH<sub>2</sub>)(NR<sub>2</sub>) **53** (NR<sub>2</sub> = C<sub>5</sub>H<sub>3</sub>Me<sub>2</sub>N, NHC<sub>5</sub>H<sub>6</sub>Me<sub>4</sub>). In contrast to **52**, the formation of **53** proceeds via addition of the nucleophile to the terminal carbon of the olefinic unit. The carbon-based nucleophiles, pyrroles, carbenes, and benzylidene triphenylphosphorane also give zwitterions B(C<sub>6</sub>F<sub>5</sub>)<sub>2</sub>(OC(CF<sub>3</sub>)<sub>2</sub>CH<sub>2</sub>CHCH<sub>2</sub>)(R<sup>+</sup>) **54–56** (Scheme 18) providing new C–C bonds. Hydride



**Scheme 17** “van der Waals complex” en route to cyclic phosphonium borates

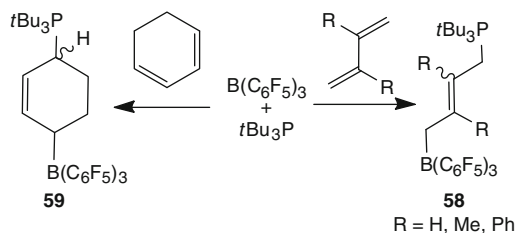


**Scheme 18** Reactions of **51**

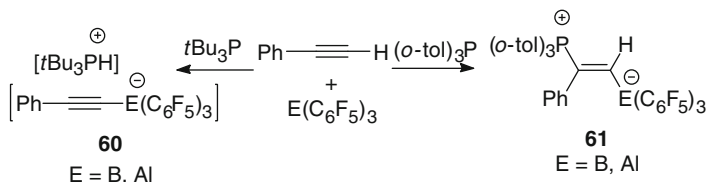
addition to the olefin is effected by reaction of **51** with PMP with a catalytic amount of  $B(C_6F_5)_3$  and  $H_2$ , affording  $[HPMP][B(C_6F_5)_2(OC(CF_3)_2CH_2CH_2CH_2)]$  (PMP = 1,2,2,6,6-pentamethylpiperidine) **57** (Scheme 18) [82].

### 3.2 Activation of Dienes

The reactions of FLPs with olefins also prompted us to probe the corresponding reactions with dienes. Combination of  $tBu_3P$  and  $B(C_6F_5)_3$  with butadiene, 2,3-diphenylbutadiene, 2,3-dimethylbutadiene, and 1,3-cyclohexadiene gave the corresponding 1,4-phosphonium borates **58** and **59** (Scheme 19) [35]. The isolated



**Scheme 19** Reactions of FLPs with dienes



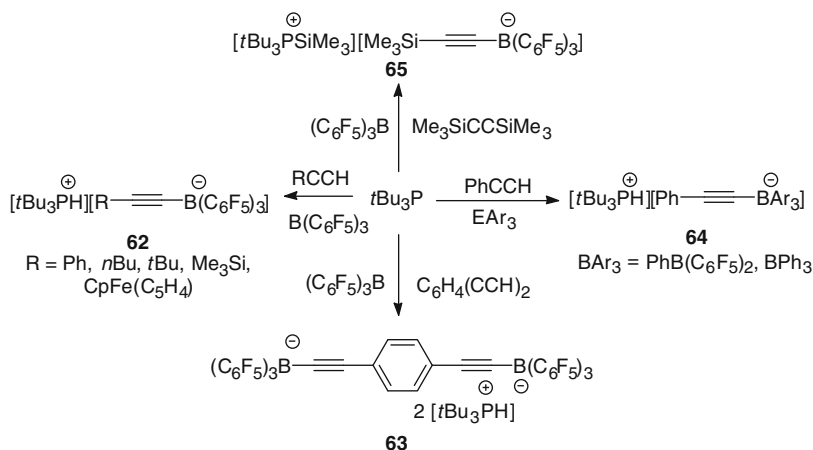
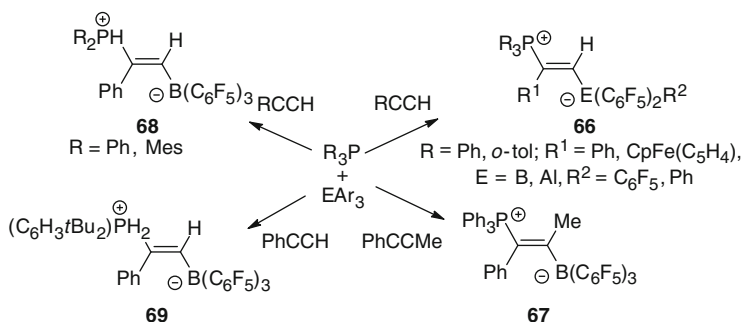
**Scheme 20** Reactions of alkynes with FLPs

yields in these cases were 50–60%, which suggested the possibility of byproducts that could arise from 1,2 addition. These minor species could not be isolated nor spectroscopically confirmed.

### 3.3 Activation of Alkynes

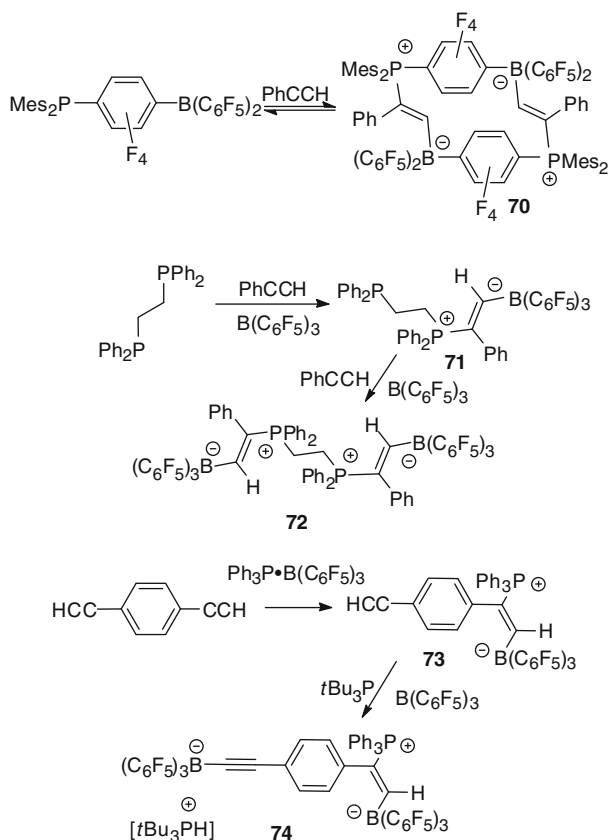
The reactions of FLPs with alkynes seemed like a logical extension given the reactivity with olefins. Thus, this aspect was also probed [83–85]. Our initial efforts described the reaction of  $\text{B}(\text{C}_6\text{F}_5)_3$  or  $(\text{PhMe})\text{Al}(\text{C}_6\text{F}_5)_3$  and  $t\text{Bu}_3\text{P}$  with  $\text{PhC}\equiv\text{CH}$ . These reactions resulted in deprotonation of the alkyne and isolation of the phosphonium alkynylborate salts  $[t\text{Bu}_3\text{PH}][\text{PhC}\equiv\text{CE}(\text{C}_6\text{F}_5)_3]$  **60** ( $\text{E} = \text{B, Al}$ ) (Scheme 20). Interestingly reduction of the basicity of the phosphine prompted an alternative reaction pathway. For example, the corresponding reactions using the less basic phosphine  $(\text{o-C}_6\text{H}_4\text{Me})_3\text{P}$  gave rise to the 1,2-addition products  $E$ - $(\text{o-C}_6\text{H}_4\text{Me})_3\text{PC}(\text{Ph})=\text{C}(\text{H})\text{E}(\text{C}_6\text{F}_5)_3$  ( $\text{E} = \text{B, Al}$ ) **61** (Scheme 20).

In a follow-up full paper [85] the generality of the scope of the reactions of FLPs with alkynes was broadened to include a variety of alkynes affording the salts  $[t\text{Bu}_3\text{PH}][\text{RC}\equiv\text{CB}(\text{C}_6\text{F}_5)_3]$  **62** ( $\text{R} = \text{Ph, } t\text{Bu, Me}_3\text{Si, CpFe}(\text{C}_5\text{H}_4)$ ) (Scheme 21). The analogous reaction of 1,4-diethynylbenzene with excess  $t\text{Bu}_3\text{P}/\text{B}(\text{C}_6\text{F}_5)_3$  gave  $[t\text{Bu}_3\text{PH}]_2[(\text{C}_6\text{F}_5)_3\text{BC}\equiv\text{C}(\text{C}_6\text{H}_4)\text{C}\equiv\text{CB}(\text{C}_6\text{F}_5)_3]$  **63** (Scheme 21), while the weaker Lewis acids  $\text{PhB}(\text{C}_6\text{F}_5)_2$  and  $\text{BPh}_3$  were shown to give the analogous deprotonation products  $[t\text{Bu}_3\text{PH}][\text{PhC}\equiv\text{CBAr}_3]$  **64**. Interestingly, the corresponding reaction of  $\text{Me}_3\text{SiC}\equiv\text{CSiMe}_3$  with  $t\text{Bu}_3\text{P}/\text{B}(\text{C}_6\text{F}_5)_3$  afforded  $[t\text{Bu}_3\text{PSiMe}_3][\text{Me}_3\text{SiC}\equiv\text{CB}(\text{C}_6\text{F}_5)_3]$  **65** (Scheme 21).

**Scheme 21** More reactions of alkynes with FLPs**Scheme 22** Generalized reactions of alkynes with FLPs

The alternative reaction pathway of addition to the alkyne was also observed for less basic phosphines for a variety of alkynes affording the species *trans*- $\text{R}_3\text{P}(\text{R}^1)\text{C}=\text{C}(\text{H})\text{EAr}_3$  **66** ( $\text{R} = \text{Ph}, o\text{-tol}$ ;  $\text{R}^1 = \text{Ph}, \text{CpFe}(\text{C}_5\text{H}_4)$ ,  $\text{EAr}_3 = \text{B}(\text{C}_6\text{F}_5)_3, \text{PhB}(\text{C}_6\text{F}_5)_2, \text{Al}(\text{C}_6\text{F}_5)_3$ ) (Scheme 22) [85]. It was perhaps surprising that even though  $\text{Ph}_3\text{P}$  forms the strong Lewis acid–base adduct  $\text{Ph}_3\text{P}\cdot\text{B}(\text{C}_6\text{F}_5)_3$ , the addition reactions with alkyne proceeds. In a similar fashion, variations in the alkyne, phosphine or borane afforded the species *trans*- $\text{Ph}_3\text{P}(\text{Ph})\text{C}=\text{C}(\text{Me})\text{B}(\text{C}_6\text{F}_5)_3$  **67**, *trans*- $\text{R}_2\text{PH}(\text{Ph})\text{C}=\text{C}(\text{H})\text{B}(\text{C}_6\text{F}_5)_3$  **68** ( $\text{R} = \text{Ph}, \text{Mes}$ ), and *trans*- $(\text{C}_6\text{H}_3t\text{Bu}_2)\text{PH}_2(\text{Ph})\text{C}=\text{C}(\text{H})\text{B}(\text{C}_6\text{F}_5)_3$  **69** (Scheme 22) [85]. Most recently, related addition reactions of phenylacetylene and  $\text{B}(\text{C}_6\text{F}_5)_3$  have been further extended to include the phosphinites and chlorophosphines,  $t\text{Bu}(\text{C}_{20}\text{H}_{12}\text{O}_2)\text{P}$ ,  $t\text{BuPCl}_2$ , and  $(\text{C}_6\text{H}_3(2,4\text{-}t\text{Bu}_2)\text{O})_3\text{P}$  [86].

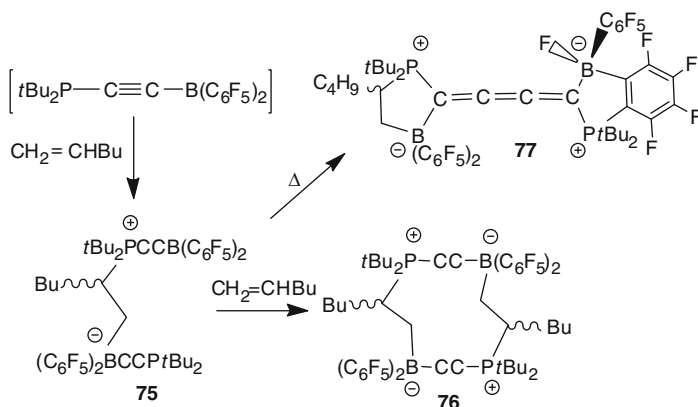
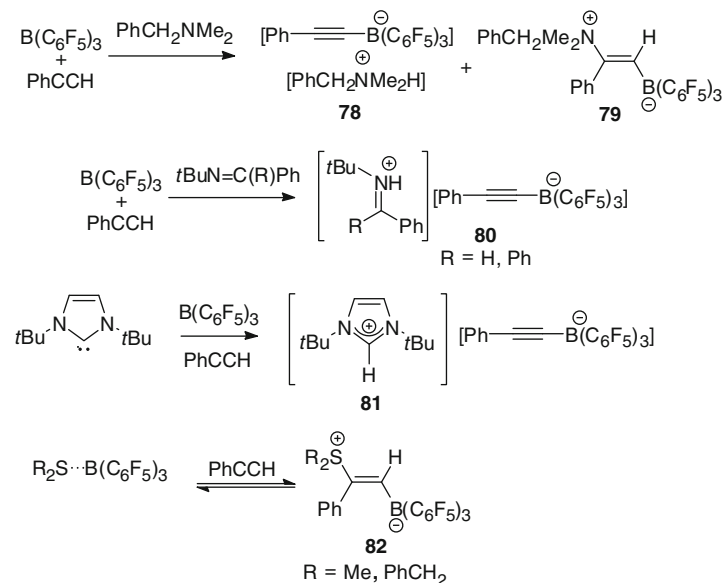
More elaborate structures are accessible using these FLP addition reactions. For example, employing our original phosphine–borane,  $\text{Mes}_2\text{PC}_6\text{F}_4\text{B}(\text{C}_6\text{F}_5)_2$ , the addition of phenylacetylene afforded the 2 + 2 macrocyclic species  $[(\text{H})\text{C}=\text{C}(\text{Ph})$



**Scheme 23** Reactions of alkynes with FLPs

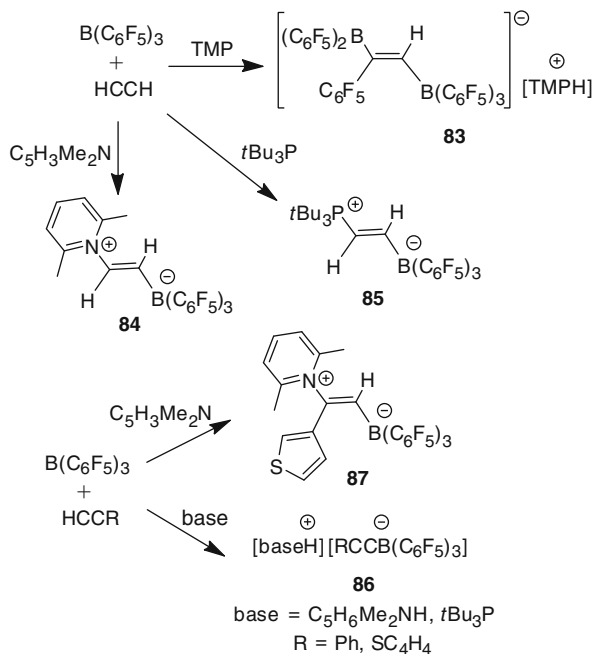
$\text{Mes}_2\text{PC}_6\text{F}_4\text{B}(\text{C}_6\text{F}_5)_2$  **70** (Scheme 23). A chain-like structure results from the reaction of  $\text{Ph}_2\text{PCH}_2\text{CH}_2\text{PPh}_2$  with alkyne and borane. In this fashion, the mono- and bis-addition products *trans*- $\text{Ph}_2\text{PCH}_2\text{CH}_2\text{PPh}_2(\text{Ph})\text{C}=\text{C}(\text{H})\text{B}(\text{C}_6\text{F}_5)_3$  **71** and *trans*- $(\text{CH}_2\text{PPh}_2(\text{Ph})\text{C}=\text{C}(\text{H})\text{B}(\text{C}_6\text{F}_5)_3)_2$  **72** were prepared (Scheme 23) [85]. On the other hand, employing differing phosphine-borane combinations allows the control of the reaction sequence. Thus initial reaction of 1,4-diethynylbenzene with  $\text{Ph}_3\text{P}\cdot\text{B}(\text{C}_6\text{F}_5)_3$  gave *trans*- $\text{HC}\equiv\text{CC}_6\text{H}_4\text{C}(\text{PPh}_3)=\text{C}(\text{H})\text{B}(\text{C}_6\text{F}_5)_3$  **73** via FLP addition. Subsequent reaction with  $t\text{Bu}_3\text{P}$  and  $\text{B}(\text{C}_6\text{F}_5)_3$  effected deprotonation of the remaining alkyne fragment affording the salt  $[\text{tBu}_3\text{PH}]^+[(\text{C}_6\text{F}_5)_3\text{BC}\equiv\text{CC}_6\text{H}_4\text{C}(\text{PPh}_3)=\text{C}(\text{H})\text{B}(\text{C}_6\text{F}_5)_3]^-$  **74** [85] demonstrating both avenues of FLP reactivity with alkynes in a single molecule.

In a related and more recent study, we have also reacted the alkynyl-linked phosphine borane  $t\text{Bu}_2\text{PC}\equiv\text{CB}(\text{C}_6\text{F}_5)_2$  with 1-hexene affording the species  $(t\text{Bu}_2\text{PC}\equiv\text{CB}(\text{C}_6\text{F}_5)_2)_2(\text{BuCH}_2\text{CH}_2)$  **75** [87]. In the presence of excess 1-hexene the dimeric species  $[(t\text{Bu}_2\text{PC}\equiv\text{CB}(\text{C}_6\text{F}_5)_2)(\text{BuCH}_2\text{CH}_2)]_2$  **76** was obtained (Scheme 24). Thermolysis of **75** at  $80^\circ\text{C}$  for 10 h was shown to give a rather unusual molecular rearrangement affording

**Scheme 24** Reactions of an alkyne-linked phosphine-borane**Scheme 25** Further reactions of alkynes and FLPs

two diastereomers of  $(t\text{Bu}_2\text{P})\text{C}_6\text{F}_4\text{BF}(\text{C}_6\text{F}_5)\text{C}_4\text{B}(\text{C}_6\text{F}_5)_2(\text{BuCH}_2\text{CH})(\text{PtBu}_2)$  **77** (Scheme 24) [88], a di-zwitterion incorporating discrete phosphonium-borate fragments and a cumulene linkage.

These FLP reactions with alkynes are not limited to phosphines as the bases. Indeed, nitrogen, carbon, and sulfur donors can be used. For example, reaction of  $\text{PhCH}_2\text{NMe}_2$  with  $\text{PhC}\equiv\text{CH}$  and  $\text{B}(\text{C}_6\text{F}_5)_3$  gave an 84:16 mixture of  $[\text{PhCH}_2\text{NMe}_2\text{H}] [\text{PhC}\equiv\text{CB}(\text{C}_6\text{F}_5)_3]$  **78** and  $\text{PhCH}_2\text{NMe}_2(\text{Ph})\text{C}=\text{C}(\text{H})\text{B}(\text{C}_6\text{F}_5)_3$  **79**, while the corresponding reaction of the imine  $(t\text{Bu})\text{N}=\text{CRPh}$  gave the salt  $[(t\text{Bu})\text{HN}=\text{CRPh}]$

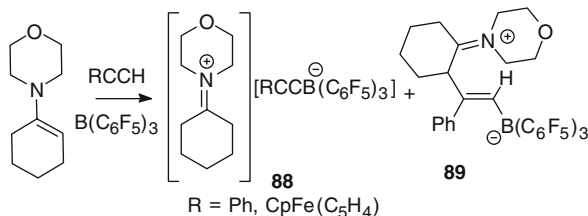


**Scheme 26** Berke's reactions of alkyne and FLPs

$[\text{PhC}\equiv\text{CB}(\text{C}_6\text{F}_5)_3]$  **80** (R = H, Ph) (Scheme 25) [85]. Similarly, the *N*-heterocyclic carbene *ItBu* reacts with  $\text{B}(\text{C}_6\text{F}_5)_3$  and  $\text{PhC}\equiv\text{CH}$  to effect deprotonation of the alkyne generating  $[\text{ItBuH}][\text{PhC}\equiv\text{CB}(\text{C}_6\text{F}_5)_3]$  **81**. In contrast, the softer sulfur donor  $\text{R}_2\text{S}$  reacts with borane and alkyne to give *trans*- $\text{R}_2\text{S}(\text{Ph})\text{C}=\text{C}(\text{H})\text{B}(\text{C}_6\text{F}_5)_3$  **82** (R = Me,  $\text{PhCH}_2$ ) (Scheme 25). The formation of these latter species was shown to be reversible, effecting exchange upon addition of a stronger donor.

Berke and coworkers [89] have also exploited these FLP reactions with alkynes to expand the breadth of systems. For example, reactions of  $\text{B}(\text{C}_6\text{F}_5)_3$  with TMP, *tBu*<sub>3</sub>P or lutidine and the alkynes  $\text{HC}\equiv\text{CH}$ ,  $\text{PhC}\equiv\text{CH}$  or  $\text{SC}_4\text{H}_3\text{C}\equiv\text{CH}$  gave either deprotonation or addition products [89]. In the case of the reactions involving  $\text{HC}\equiv\text{CH}$  and TMP the salt  $[\text{TMPH}][(\text{C}_6\text{F}_5)_2\text{BC}(\text{C}_6\text{F}_5)=\text{C}(\text{H})\text{B}(\text{C}_6\text{F}_5)_3]$  **83** was formed (Scheme 26). This finding pointed the way to the further elaboration of 1,1-carboborations by the Erker research group [90–92].

Lutidine and *tBu*<sub>3</sub>P gave principally the addition products  $(\text{C}_5\text{H}_3\text{Me}_2\text{N})\text{CH}=\text{CHB}(\text{C}_6\text{F}_5)_3$  **84** and  $\text{tBu}_3\text{PCH}=\text{CHB}(\text{C}_6\text{F}_5)_3$  **85** (Scheme 26), although minor amount of the corresponding salt of the anion  $[(\text{C}_6\text{F}_5)_2\text{BC}(\text{C}_6\text{F}_5)=\text{C}(\text{H})\text{B}(\text{C}_6\text{F}_5)_3]$ , analogous to **83**, was also seen in the latter case. The corresponding reactions of the alkynes  $\text{PhC}\equiv\text{CH}$  and  $\text{SC}_4\text{H}_3\text{C}\equiv\text{CH}$  afforded the deprotonation products  $[(\text{Base})\text{H}][\text{RC}\equiv\text{CB}(\text{C}_6\text{F}_5)_3]$  **86** (Base =  $\text{C}_5\text{H}_6\text{Me}_4\text{NH}$ , *tBu*<sub>3</sub>P, R = Ph,  $\text{SC}_4\text{H}_3$ ) (Scheme 26). The reaction of lutidine,  $\text{B}(\text{C}_6\text{F}_5)_3$ , and  $\text{PhC}\equiv\text{CH}$  gave the analogous product, whereas the corresponding combination including thiophene-alkyne afforded the olefinic addition product  $[(\text{SC}_4\text{H}_3)(\text{C}_5\text{H}_3\text{Me}_2\text{N})\text{C}=\text{C}(\text{H})\text{B}(\text{C}_6\text{F}_5)_3]$  **87** (Scheme 26) [89].



**Scheme 27** Reactions of an enamine with alkyne and B(C<sub>6</sub>F<sub>5</sub>)<sub>3</sub>

Since this work we have further applied these reactions employing a carbon based nucleophile derived from an enamine to effect C–C bond formation [84]. In this fashion, reaction of 1-morpholinocyclohexene, B(C<sub>6</sub>F<sub>5</sub>)<sub>3</sub> and phenylacetylene gave a mixture of the two products derived from deprotonation and addition pathways, [C<sub>6</sub>H<sub>9</sub>N(CH<sub>2</sub>CH<sub>2</sub>)<sub>2</sub>O][RC≡CB(C<sub>6</sub>F<sub>5</sub>)<sub>3</sub>] **88** (R = Ph, CpFe(C<sub>5</sub>H<sub>4</sub>)) and C<sub>6</sub>H<sub>9</sub>(2-PhC=C(H)B(C<sub>6</sub>F<sub>5</sub>)<sub>3</sub>)(N(CH<sub>2</sub>CH<sub>2</sub>)<sub>2</sub>O) **89** (Scheme 27). The corresponding reactions of ethynylferrocene gave only the analog of the deprotonation product **88**.

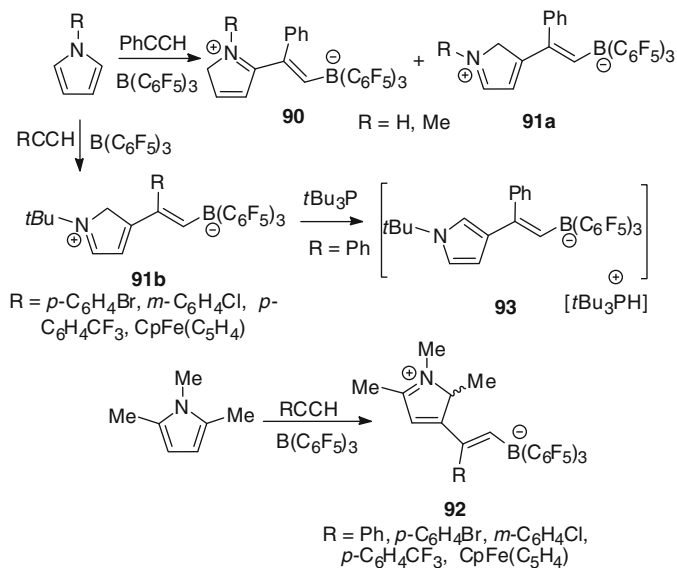
Pyrrole derivatives also provide carbon-based nucleophiles. Thus, reaction of pyrrole or methylpyrrole with phenylacetylene and B(C<sub>6</sub>F<sub>5</sub>)<sub>3</sub> gave the corresponding addition products, RNC<sub>4</sub>H<sub>4</sub>(2-PhC=C(H)B(C<sub>6</sub>F<sub>5</sub>)<sub>3</sub>) **90** (R = H, Me). The corresponding reaction of N-methylpyrrole gave a 3:2 mixture of the addition products in which substitution occurred at the 2- and 3- positions of the pyrroles **90** and **91a** [84]. Interestingly, substitution at the 2-position was avoided by the use of the bulky *N-tert*-butylpyrrole, as reaction with PhC≡CH and B(C<sub>6</sub>F<sub>5</sub>)<sub>3</sub> gave exclusively *t*BuNC<sub>4</sub>H<sub>4</sub>(3-PhC=C(H)B(C<sub>6</sub>F<sub>5</sub>)<sub>3</sub>) **91b** (Scheme 28). This reaction was also tolerant of variations in the aryl alkynes as well as modification of the Lewis acid to BPh(C<sub>6</sub>F<sub>5</sub>)<sub>2</sub> and the base to 1,2,5-trimethylpyrrole. In the latter case, the products MeNC<sub>4</sub>H<sub>2</sub>(2, 5-Me<sub>2</sub>)(3-RC=C(H)B(C<sub>6</sub>F<sub>5</sub>)<sub>3</sub>) **92** (R = Ph, *p*-C<sub>6</sub>H<sub>4</sub>Br, *m*-C<sub>6</sub>H<sub>4</sub>Cl, *p*-C<sub>6</sub>H<sub>4</sub>CF<sub>3</sub>, CpFe(C<sub>5</sub>H<sub>4</sub>)) (Scheme 28) were readily deprotonated with *t*Bu<sub>3</sub>P to give the salts [*t*Bu<sub>3</sub>PH][*t*BuNC<sub>4</sub>H<sub>3</sub>(PhC=C(H)B(C<sub>6</sub>F<sub>5</sub>)<sub>3</sub>)] **93** (Scheme 28).

Interestingly, the addition products above rearrange affording *t*BuNC<sub>4</sub>H<sub>4</sub>(3-RC=C(H)(C<sub>6</sub>F<sub>5</sub>)B(C<sub>6</sub>F<sub>5</sub>)<sub>2</sub>) **94** (R = Ph, CpFe(C<sub>5</sub>H<sub>4</sub>)) (Scheme 29) [84]. These species also react with Et<sub>3</sub>PO, which mediates proton transfer liberating the adduct Et<sub>3</sub>PO·B(C<sub>6</sub>F<sub>5</sub>)<sub>3</sub> and giving the corresponding vinyl pyrroles *t*BuNC<sub>4</sub>H<sub>3</sub>(3-RC=CH<sub>2</sub>) **95a** (R = Ph, *p*-C<sub>6</sub>H<sub>4</sub>Br, *m*-C<sub>6</sub>H<sub>4</sub>Cl, *p*-C<sub>6</sub>H<sub>4</sub>CF<sub>3</sub>) and MeNC<sub>4</sub>H<sub>2</sub>(2,5-Me<sub>2</sub>)(3-RC=CH<sub>2</sub>) **95b** (R = Ph, *p*-C<sub>6</sub>H<sub>4</sub>Br, *m*-C<sub>6</sub>H<sub>4</sub>Cl, *p*-C<sub>6</sub>H<sub>4</sub>CF<sub>3</sub>) (Scheme 29) [84].

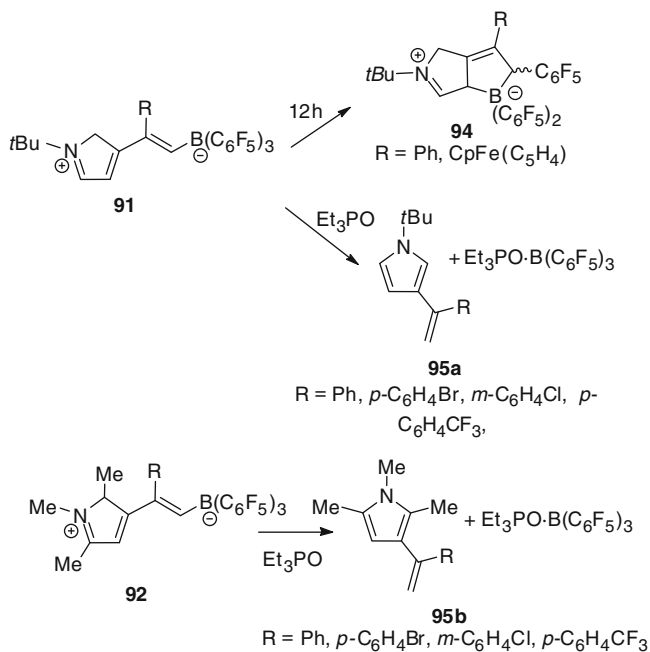
## 4 FLPs in Ring-Opening Reactions

FLPs can also be employed to effect the ring-opening of ethers, lactides, and cyclopropanes. Such reactions have appeared in the older literature, although of course these reactions were not described as FLP chemistry at that time. For example, in 1950 Wittig reported that the reaction of Ph<sub>3</sub>CNa with THF(BPh<sub>3</sub>) [4] effects ring-opening to give the borate anion [Ph<sub>3</sub>C(CH<sub>2</sub>)<sub>4</sub>OBPh<sub>3</sub>]<sup>−</sup> **96**

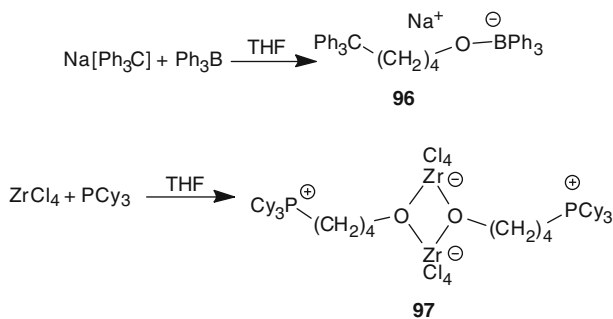




**Scheme 28** Reactions of pyrroles with alkynes and  $\text{B}(\text{C}_6\text{F}_5)_3$ .



**Scheme 29** Rearrangements of pyrrole-alkynes/ $\text{B}(\text{C}_6\text{F}_5)_3$  addition products

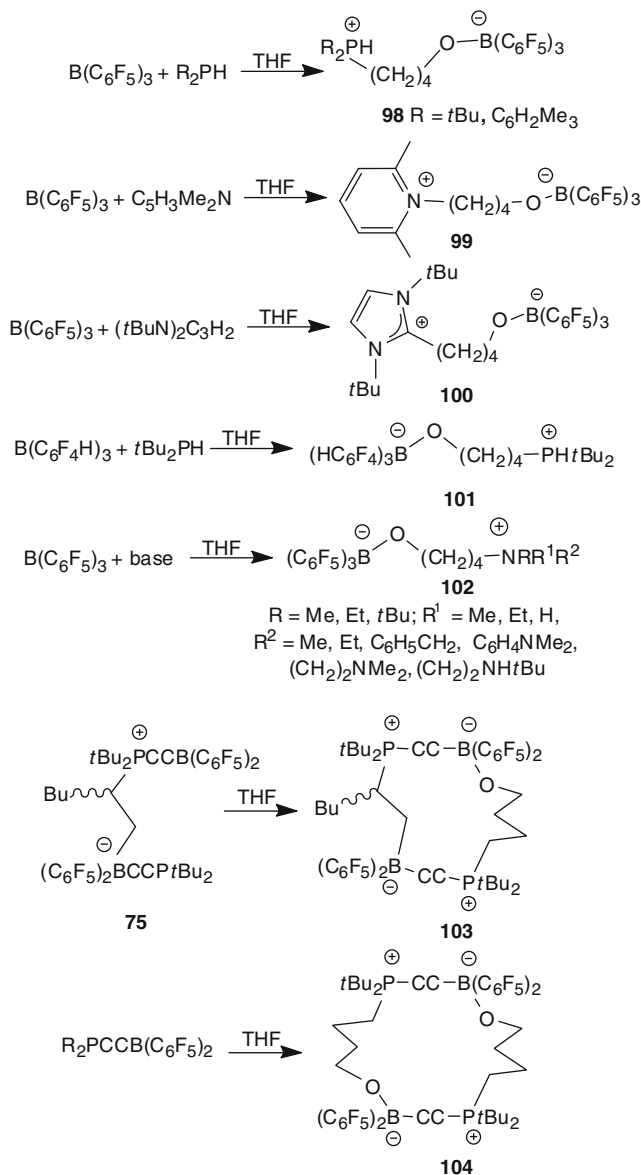


**Scheme 30** Examples of THF ring-openings with donors and acceptors

(Scheme 30). This could be regarded as the action of a Lewis acid and a Lewis base, an FLP, effecting the ring-opening of THF. In a similar sense, we described the action of  $\text{ZrCl}_4(\text{THF})_2$  with  $\text{PCy}_3$  on THF affording the di-zwitterionic dimer  $[\text{Cl}_4\text{Zr}(\mu\text{-O}(\text{CH}_2)_4\text{PCy}_3)]_2$  **97** (Scheme 30) [93]. Again, this ring-opening can be described as resulting from the action of sterically congested combinations of a Lewis acidic metal center and a bulky phosphine on THF. Indeed, similar ring-opening reactions are documented for a number of Lewis acids including U [94, 95], Sm [96], Ti [97], Zr [93, 98, 99], carborane [100], Te- [101, 102], and alane species [103], in combination with either N or P-based Lewis donors (Scheme 30).

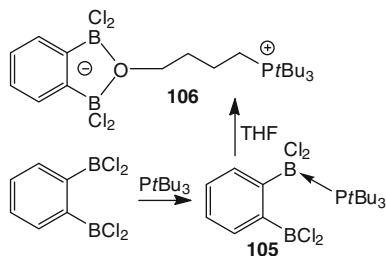
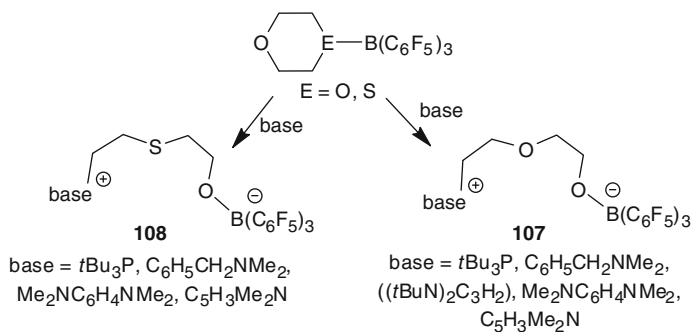
#### 4.1 FLP Ring-Opening of THF

More closely related to the FLP systems described above are the reactions of the FLP combinations of boranes, phosphines, and THF [104]. For example, the reactions of  $(\text{THF})\text{B}(\text{C}_6\text{F}_5)_3$  with sterically encumbered phosphines proceed to give the zwitterions  $\text{R}_2\text{PH}(\text{CH}_2)_4\text{OB}(\text{C}_6\text{F}_5)_3$  **98** ( $\text{R} = t\text{Bu}, \text{C}_6\text{H}_2\text{Me}$ ). In a similar fashion we also observed the reaction of lutidine/borane with THF yielded the zwitterionic species  $2,6\text{-Me}_2\text{C}_5\text{H}_3\text{N}(\text{CH}_2)_4\text{OB}(\text{C}_6\text{F}_5)_3$  **99** (Scheme 31) [46] while Tamm and coworkers observed the reactions of carbene/borane FLPs with THF affording  $[\text{tBu}(\text{CH}_2)_4\text{OB}(\text{C}_6\text{F}_5)_3]$  **100** (Scheme 31) [40]. These reactions have been generalized to some extent with the use of variations in the Lewis acids and bases. For example, reaction of  $t\text{Bu}_2\text{PH}$  and  $\text{B}(p\text{-C}_6\text{F}_4\text{H})_3$  in THF gives  $t\text{Bu}_2(\text{H})\text{P}(\text{CH}_2)_4\text{OB}(p\text{-C}_6\text{F}_4\text{H})_3$  **101** [105], while a series of amine bases react with a THF solution of  $\text{B}(\text{C}_6\text{F}_5)_3$  to give the THF-ring-opened species  $(\text{base})(\text{CH}_2)_4\text{OB}(\text{C}_6\text{F}_5)_3$  **102** ( $\text{base} = \text{C}_6\text{H}_5\text{CH}_2\text{NMe}_2, \text{Me}_2\text{NC}_6\text{H}_4\text{NMe}_2, \text{Me}_3\text{N}, \text{Et}_3\text{N}, \text{Me}_2\text{N}(\text{CH}_2)_2\text{NMe}_2, t\text{BuHN}(\text{CH}_2)_2\text{NH}t\text{Bu}$ ) (Scheme 31). The analogous reaction of  $(t\text{Bu}_2\text{PC}\equiv\text{CB}(\text{C}_6\text{F}_5)_2)_2(\text{BuCHCH}_2)$  **75** with THF yields the macrocyclic zwitterionic alkynylphosphonium borate  $(t\text{Bu}_2\text{PC}\equiv\text{CB}(\text{C}_6\text{F}_5)_2)(\text{BuCHCH}_2)(t\text{Bu}_2\text{PC}\equiv\text{CB}(\text{C}_6\text{F}_5)_2)(\text{O}(\text{CH}_2)_4)$  **103** (Scheme 31) [87], while reaction of the parent  $t\text{Bu}_2\text{PC}\equiv\text{CB}(\text{C}_6\text{F}_5)_2$ , with THF gives the macrocycle  $[(t\text{Bu}_2\text{PC}\equiv\text{CB}(\text{C}_6\text{F}_5)_2)(\text{O}(\text{CH}_2)_4)]_2$  **104** (Scheme 31).



**Scheme 31** THF ring-openings with FLPs

Most recently we have reported the reactions of the *bis*-borane 1,2- $\text{C}_6\text{H}_4(\text{BCl}_2)_2$  [106, 107] with  $\text{PtBu}_3$ . This results in the 1:1 adduct 1,2- $\text{C}_6\text{H}_4(\text{BCl}_2)_2 \cdot (\text{PtBu}_3)$  **105**. Despite the formation of this adduct, this species reacts with THF to effect ring-opening yielding 1,2- $\text{C}_6\text{H}_4(\text{BCl}_2)_2(\text{O}(\text{CH}_2)_4\text{PtBu}_3)$  **106** (Scheme 32). This species was confirmed to exhibit a unique bridging alkoxide between the boron centers [108].

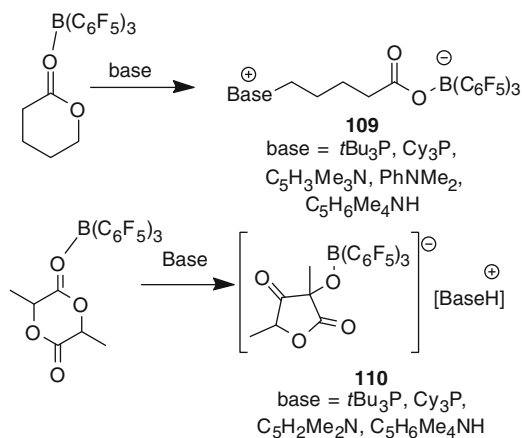
**Scheme 32** Reactions of **105****Scheme 33** Dioxane and thioxane ring-openings

## 4.2 FLP Ring-Opening of Dioxane and Thioxane

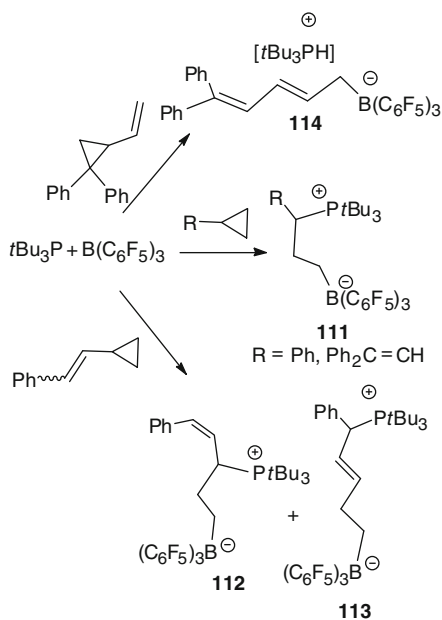
Other examples of ring-opening reactions are exhibited with the reactions of  $B(C_6F_5)_3$ , 1,4-dioxane, and an appropriate base. In this fashion the species  $(base)(CH_2)_2O(B(C_6F_5)_3)$  **107** (base =  $tBu_3P$ ,  $C_6H_5CH_2NMe_2$ ,  $(tBu)$ ,  $Me_2NC_6H_4NMe_2$ ,  $C_5H_3Me_2N$ ) were obtained (Scheme 33) [105]. Similarly ring-opening of thioxane gave ring-opened products  $(base)(CH_2)_2S(CH_2)_2O(B(C_6F_5)_3)$  **108** (base =  $tBu_3P$ ,  $C_6H_5CH_2NMe_2$ ,  $Me_2NC_6H_4NMe_2$ ,  $C_5H_3Me_2N$ ) (Scheme 33) [105].

## 4.3 FLP Ring-Opening and Contraction of Lactone and Lactide

The  $B(C_6F_5)_3$  adducts with  $\delta$ -valerolactone and *rac*-lactide react with phosphine or N-bases [109]. In the case of the lactone, ring-opening yields the zwitterionic species  $L(CH_2)_4CO_2B(C_6F_5)_3$  **109** (L =  $tBu_3P$ ,  $Cy_3P$ ,  $C_5H_3Me_3N$ ,  $PhNMe_2$ ,  $C_5H_6Me_4NH$ ) (Scheme 34). The corresponding reaction of *rac*-lactide leads to a ring-contraction giving the salts  $[LH][OCCHMeCO_2(CMe)OB(C_6F_5)_3]$  **110** (L =  $tBu_3P$ ,  $Cy_3P$ ,  $C_5H_3Me_2N$ ,  $C_5H_6Me_4NH$ ) (Scheme 34). This latter reaction results from deprotonation of lactide adduct, prompting ring contraction [109].



**Scheme 34** Reactions of lactone and lactide with FLPs



**Scheme 35** Ring-opening reactions of cyclopropanes

#### 4.4 FLP Ring-Opening of Cyclopropanes

Cyclopropanes also react with FLPs. For example the cyclopropanes PhC<sub>3</sub>H<sub>5</sub> and Ph<sub>2</sub>C=CCHC<sub>3</sub>H<sub>5</sub> are ring-opened in the presence of the FLP *t*Bu<sub>3</sub>P/B(C<sub>6</sub>F<sub>5</sub>)<sub>3</sub> affording the phosphonium borates *t*Bu<sub>3</sub>PCH(R)CH<sub>2</sub>CH<sub>2</sub>B(C<sub>6</sub>F<sub>5</sub>)<sub>3</sub> **111** (R = Ph, CH=CPh<sub>2</sub>) (Scheme 35) [110]. In contrast the corresponding reaction of the species

PhHC=CHCHC<sub>3</sub>H<sub>5</sub> gives rise to a 1:1.3 mixture of two ring-opened products **112** and **113** derived from 1,3 and 1,5 additions, respectively (Scheme 35) while analogous treatment of H<sub>2</sub>C=CHCHC<sub>3</sub>H<sub>3</sub>Ph<sub>2</sub> with B(C<sub>6</sub>F<sub>5</sub>)<sub>3</sub> and *t*Bu<sub>3</sub>P gave the salt [*t*Bu<sub>3</sub>PH][Ph<sub>2</sub>C=CHCH=CHCH<sub>2</sub>B(C<sub>6</sub>F<sub>5</sub>)<sub>3</sub>] **114**. These results suggest that sterically demanding substitution on the cyclopropanes inhibits attack by the base, resulting instead in deprotonation followed by rearrangement to the butadiene-borate anion [110].

## 5 FLP Activation of Greenhouse Gases

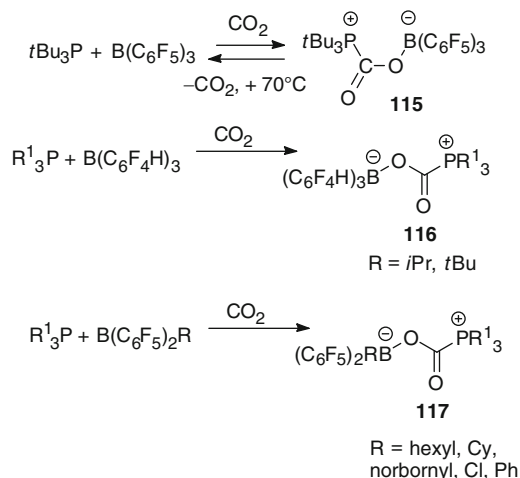
The ability of FLPs to react with small molecules prompted questions about the interactions of these combinations with CO<sub>2</sub>, N<sub>2</sub>O, and SO<sub>2</sub>. Each of these is a gas of some concern from an environmental standpoint and these new approaches to sequestration or to new reactivity patterns are of general interest.

### 5.1 FLP Capture of CO<sub>2</sub>

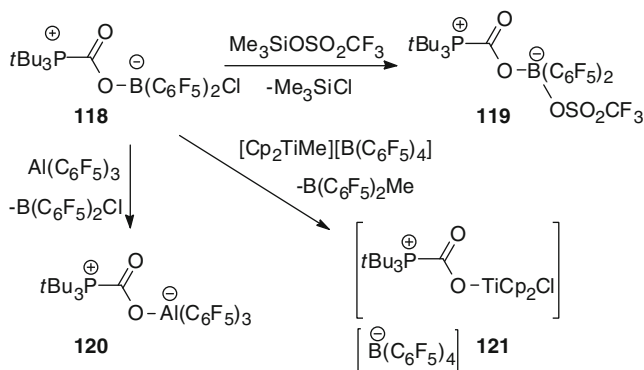
CO<sub>2</sub> is renowned as a greenhouse gas and thus strategies to capture it are of much interest. Therefore it was topical when it was found that the FLP *t*Bu<sub>3</sub>P/B(C<sub>6</sub>F<sub>5</sub>)<sub>3</sub> reacts with CO<sub>2</sub> to give the species *t*Bu<sub>3</sub>PCO<sub>2</sub>B(C<sub>6</sub>F<sub>5</sub>)<sub>3</sub> **115** (Scheme 36) [111]. This species evolves CO<sub>2</sub> above 70 °C. Subsequent treatment with either THF prompts loss of CO<sub>2</sub> and complexation of THF while exposure to H<sub>2</sub> also results in loss of CO<sub>2</sub> and activation of H<sub>2</sub>. While these observations suggest the binding of CO<sub>2</sub> by this FLP is weak, it is noteworthy that this species is significantly more stable than the corresponding system derived from the intramolecular FLP Me<sub>2</sub>PCH<sub>2</sub>CH<sub>2</sub>B(C<sub>6</sub>F<sub>5</sub>)<sub>2</sub>, (see below) [111]. Analogous reactions of other intermolecular FLPs have been extended to obtain the species R<sub>3</sub>P(CO<sub>2</sub>)B(C<sub>6</sub>F<sub>4</sub>H)<sub>3</sub> **116** (R = *i*Pr, *t*Bu) and *t*Bu<sub>3</sub>P(CO<sub>2</sub>)BR(C<sub>6</sub>F<sub>5</sub>)<sub>2</sub> **117** (R = hexyl, Cy, (norbornyl), Cl, Ph) [112].

In a similar fashion the species *t*Bu<sub>3</sub>P(CO<sub>2</sub>)B(C<sub>6</sub>F<sub>5</sub>)<sub>2</sub>Cl **118** was prepared and it proved sufficiently stable to react with Me<sub>3</sub>SiOSO<sub>2</sub>CF<sub>3</sub> to generate *t*Bu<sub>3</sub>P(CO<sub>2</sub>)B(C<sub>6</sub>F<sub>5</sub>)<sub>2</sub>(OSO<sub>2</sub>CF<sub>3</sub>) **119** [113]. Similarly, Lewis acid exchange reactions between **118** and Al(C<sub>6</sub>F<sub>5</sub>)<sub>3</sub> and [Cp<sub>2</sub>TiMe][B(C<sub>6</sub>F<sub>5</sub>)<sub>4</sub>] affording the products, *t*Bu<sub>3</sub>P(CO<sub>2</sub>)Al(C<sub>6</sub>F<sub>5</sub>)<sub>3</sub> **120** and [*t*Bu<sub>3</sub>P(CO<sub>2</sub>)TiCp<sub>2</sub>Cl][B(C<sub>6</sub>F<sub>5</sub>)<sub>4</sub>] **121** (Scheme 37) [113].

In an effort to effect stronger binding to CO<sub>2</sub>, the utility of *bis*-boranes in FLP activation of CO<sub>2</sub> was explored. To this end, O(B(C<sub>6</sub>F<sub>5</sub>)<sub>2</sub>)<sub>2</sub> was reacted with CO<sub>2</sub> and *Pt*Bu<sub>3</sub>. The product was formulated as O(B(C<sub>6</sub>F<sub>5</sub>)<sub>2</sub>)<sub>2</sub>(O<sub>2</sub>CP*t*Bu<sub>3</sub>) **122** (Scheme 38) [114] as the spectroscopic data were consistent with a symmetric structure. Nonetheless, an X-ray study revealed dissymmetric binding, consistent with rapid exchange of the B–O bonds in solution. In a similar fashion the *bis*-boranes Me<sub>2</sub>C=C(BR)<sub>2</sub> (R = Cl, C<sub>6</sub>F<sub>5</sub>) also reacted with CO<sub>2</sub> and *Pt*Bu<sub>3</sub> although



**Scheme 36** Reactions of CO<sub>2</sub> with FLPs

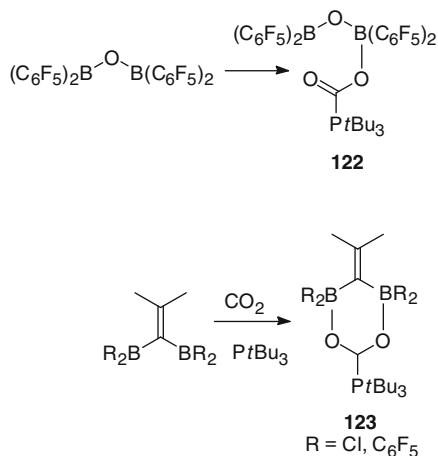
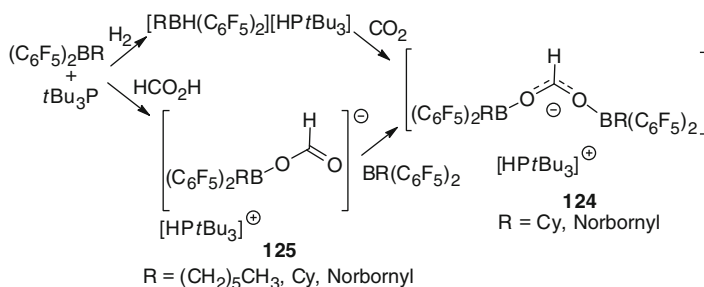


**Scheme 37** Reactions of **118** with FLPs

in these cases the symmetric cyclic products  $\text{Me}_2\text{C}=\text{C}(\text{BR}_2)_2(\text{O}_2\text{CP}t\text{Bu}_3)$  **123** (Scheme 38) were obtained [114]. Despite this chelation, all of these *bis*-borane derivatives lose CO<sub>2</sub> above 15 °C.

## 5.2 FLPs in Stoichiometric Reduction of CO<sub>2</sub>

In a communication Ashley and O'Hare [115] described the use of the FLP derived from TMP and B(C<sub>6</sub>F<sub>5</sub>)<sub>3</sub> in reaction with CO<sub>2</sub>/H<sub>2</sub>. Mass spectral data reveal that upon heating for 6 days at 160 °C, this mixture effects the conversion of CO<sub>2</sub> to

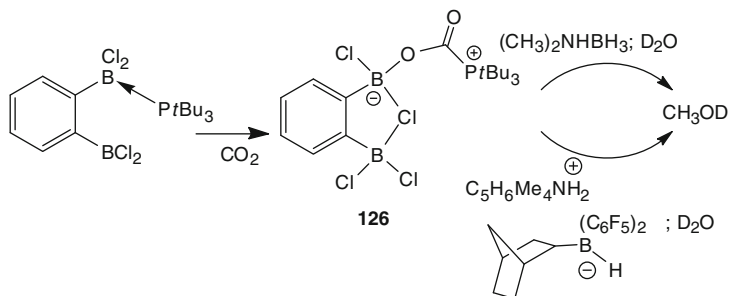
**Scheme 38** Reactions of CO<sub>2</sub> with *bis*-boranes**Scheme 39** Reductions of CO<sub>2</sub> with FLPs

methanol in 24% yield. This extremely important result of metal-free reduction of CO<sub>2</sub> has prompted a further examination of related systems.

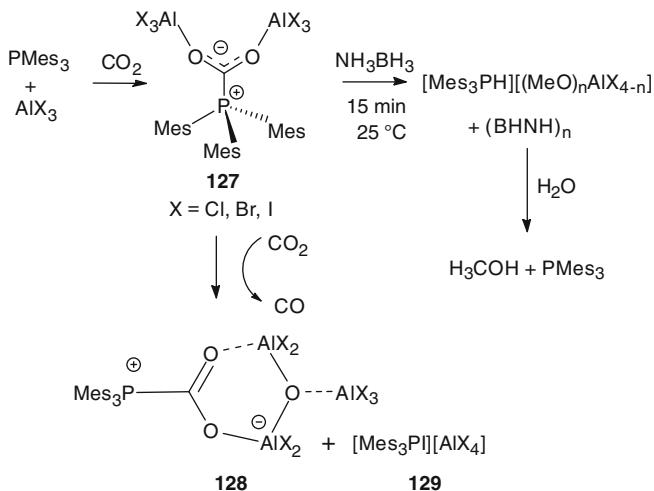
In the case of phosphine-borane FLPs the salts [tBu<sub>3</sub>PH][RBH(C<sub>6</sub>F<sub>5</sub>)<sub>2</sub>] (R = hexyl, Cy, norbornyl) were shown to react with CO<sub>2</sub> affording the formyl derivatives [tBu<sub>3</sub>PH][((C<sub>6</sub>F<sub>5</sub>)<sub>2</sub>BR)<sub>2</sub>(μ-HCO<sub>2</sub>)] **124**. This observation infers a pathway for the commencement of the reduction. The related formate derivative [tBu<sub>3</sub>PH][(C<sub>6</sub>F<sub>5</sub>)<sub>2</sub>BR(O<sub>2</sub>CH)] **125** was also obtained via the reaction of the corresponding phosphine/borane FLPs with formic acid (Scheme 39) [112]. Similar results have been reported using N-bases [116].

The *bis*-borane 1,2-C<sub>6</sub>H<sub>4</sub>(BCl<sub>2</sub>)<sub>2</sub> in combination with tBu<sub>3</sub>P acts as an FLP to bind CO<sub>2</sub>. This product formulated as 1,2-C<sub>6</sub>H<sub>4</sub>(BCl<sub>2</sub>)<sub>2</sub>(O<sub>2</sub>CPtBu<sub>3</sub>) **126** is remarkably stable [108]. It does not undergo loss of CO<sub>2</sub> even upon heating to 80 °C for 24 h. The stability prompted efforts to reduce the bound CO<sub>2</sub>. Treatment with the amine-borane Me<sub>2</sub>NHBH<sub>3</sub> for 15 min followed by quenching with D<sub>2</sub>O led to the generation of methanol-d<sub>1</sub> in 34% yield (Scheme 40). In a similar fashion, reaction





**Scheme 40** Reductions of CO<sub>2</sub> with *bis*-borane/phosphine FLPs



**Scheme 41** Reactions of AlX<sub>3</sub> and PMes<sub>3</sub> with CO<sub>2</sub>

with [C<sub>5</sub>H<sub>6</sub>Me<sub>4</sub>NH<sub>2</sub>][HB(C<sub>6</sub>F<sub>5</sub>)<sub>3</sub>] gave methanol in 15% yield after stirring for 24 h and subsequent treatment with D<sub>2</sub>O. Interestingly, modification of the ammonium borate salt to [C<sub>5</sub>H<sub>6</sub>Me<sub>4</sub>NH<sub>2</sub>][HB(C<sub>6</sub>F<sub>5</sub>)<sub>2</sub>(C<sub>7</sub>H<sub>11</sub>)] resulted in an increased yield of methanol to 57% after 1 h (Scheme 40) [108].

An alternative strategy to CO<sub>2</sub> reduction was uncovered by the study of the phosphine/alane FLPs derived from PMes<sub>3</sub> and AlX<sub>3</sub> (X = Cl, Br, I). Reaction with CO<sub>2</sub> afforded the facile formation of Mes<sub>3</sub>P(CO<sub>2</sub>)(AlX<sub>3</sub>)<sub>2</sub> **127** (Scheme 41) [117]. Subsequent treatment with H<sub>3</sub>NBH<sub>3</sub> effected the generation of Al-methoxide species which upon hydrolysis gave methanol in an overall yield of 50%.

An alternative reduction pathway was observed upon prolonged (18 h) exposure of **127** to CO<sub>2</sub>. In this case the reaction products were identified as Mes<sub>3</sub>P(CO<sub>2</sub>)(AlX<sub>2</sub>)<sub>2</sub>(OAlX<sub>3</sub>) **128**, [Mes<sub>3</sub>PX][AlX<sub>4</sub>] **129**, and CO (Scheme 41) [118]. The

liberation of CO was confirmed spectroscopically and by stoichiometric capture as a Ru complex.

### 5.3 FLP Capture of $N_2O$

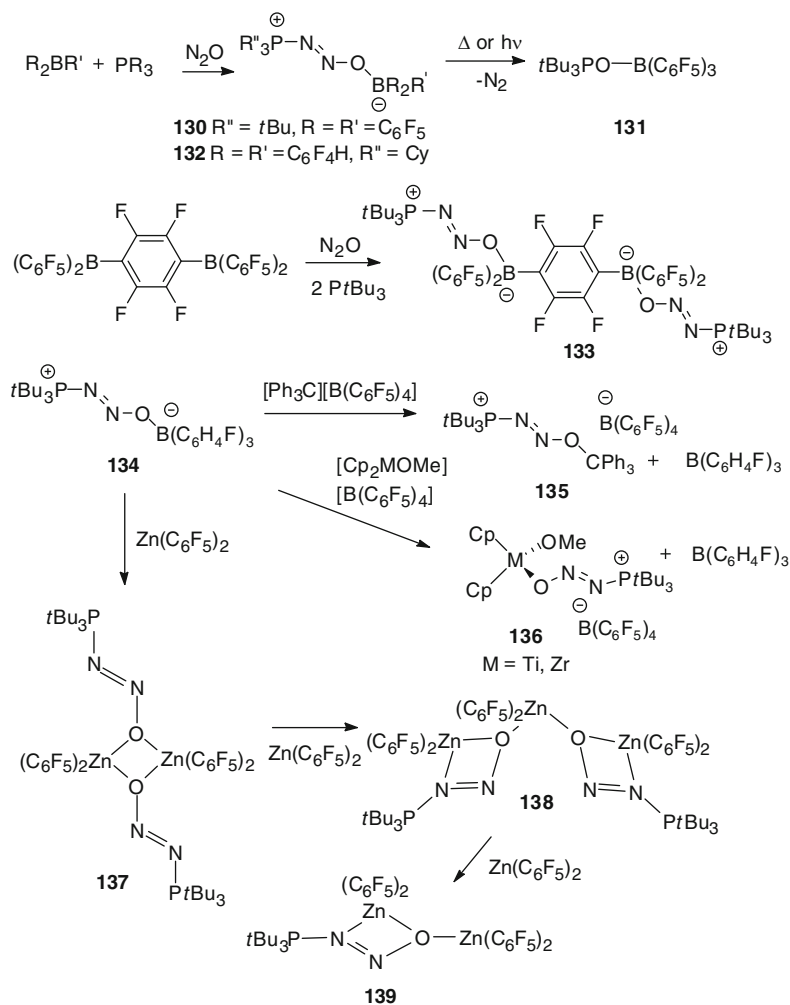
$N_2O$  is another greenhouse gas that is 300 times more potent than  $CO_2$ , albeit much less abundant. Thus it was of interest to find that the FLP derived from  $tBu_3P$  and  $B(C_6F_5)_3$  reacts with  $N_2O$  to give  $tBu_3P(NNO)B(C_6F_5)_3$  **130** (Scheme 42) [119]. The P–N=N–O–B is oriented such that the  $tBu_3P$  and  $OB(C_6F_5)_3$  fragment occupy *transoid* positions on the N=N double bond. The compound **130** evolves  $N_2$  on heating to 135 °C for 44 h resulting in the formation of  $(tBu_3P=O)B(C_6F_5)_3$  **131** (Scheme 42). In the same vein **131** is obtained from photolysis of **130** [119].

Efforts to modify the FLP system using less basic phosphines were unsuccessful. Indeed, one of the few alternative systems that was viable employed  $Cy_3P$  and  $B(C_6F_4-p-H)_3$  to capture  $N_2O$  affording  $Cy_3P(N_2O)B(C_6F_4-p-H)_3$  **132** (Scheme 42) [120]. This species was less stable than **130** as it lost  $N_2$  in a facile manner avoiding the phosphine oxide-borane adduct.

While the phosphine could not be varied dramatically,  $N_2O$  binding proved to be more tolerant of lesser Lewis acidic boranes including  $B(C_6F_5)_2R$  ( $R = Ph, Mes, OC_6F_5$ ) and  $BR_3$  ( $R = Ph, C_6F_4-p-H, C_6H_4-p-F$ ). Similarly, use of the *bis*borane  $(C_6F_5)_2B(C_6F_4)B(C_6F_5)_2$  with  $tBu_3P$  afforded the product  $C_6F_4[(C_6F_5)_2B(ON_2)PtBu_3]_2$  **133** (Scheme 42) [120]. The tolerance for weaker Lewis acids allows the use of  $tBu_3P(NNO)B(C_6H_4-p-F)_3$  **134** in exchange reactions. Thus treatment of **134** with  $B(C_6F_5)_3$  affords an alternative route to **130**. In the same vein reaction of **134** with  $[Ph_3C][B(C_6F_5)_4]$  afforded  $[tBu_3P(N_2O)CPh_3][B(C_6F_5)_4]$  **135** (Scheme 42). A mechanistic study of these exchange reactions provided the activation parameters  $\Delta H^\ddagger = 71.2(9) \text{ kJ mol}^{-1}$  and  $\Delta S^\ddagger = 32(3) \text{ J mol}^{-1} \text{ K}^{-1}$  [120]. These data are consistent with a B–O linkage that is weakened prior to the binding of the incoming Lewis acid. Similar exchange reactions allow the transfer to transition metal species. For example, reaction with  $[Cp_2ZrOMe][MeB(C_6F_5)_3]$  gave  $[tBu_3P(N_2O)ZrCp_2OMe][MeB(C_6F_5)_3]$  **136** (Scheme 42) [120]. Similarly, the Ti analog was prepared [120], while reaction of **134** with  $Zn(C_6F_5)_2$  [121] afforded the isolation of  $tBu_3PN_2OZn(C_6F_5)_2$  **137**,  $(tBu_3PN_2OZn(C_6F_5)_2)_2Zn(C_6F_5)_2$  **138**, and  $tBu_3PN_2O(Zn(C_6F_5)_2)_2$  **139**.

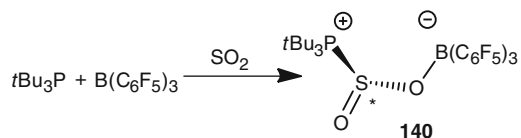
### 5.4 FLP Capture of $SO_2$

Another gas that is of environmental concern is  $SO_2$ . In probing ability of FLPs to capture such gases, the intermolecular FLP  $tBu_3P$  and  $B(C_6F_5)_3$  was shown to react with  $SO_2$  at room temperature to give the zwitterion  $tBu_3P(S(O)O)B(C_6F_5)_3$  **140** [122]. This compound structurally resembles the  $CO_2$  compound **115** in a general



**Scheme 42** Reactions of  $\text{N}_2\text{O}$  with FLPs

sense; however in contrast to the planar carbon atom in **115**, the sulfur center of **140** is pseudo-pyramidal (Scheme 43). Closely related intramolecular FLP derivatives have also been characterized (see below).



**Scheme 43** Reactions of intermolecular FLP with  $\text{SO}_2$

## 6 Additional Miscellaneous Reactions of FLPs

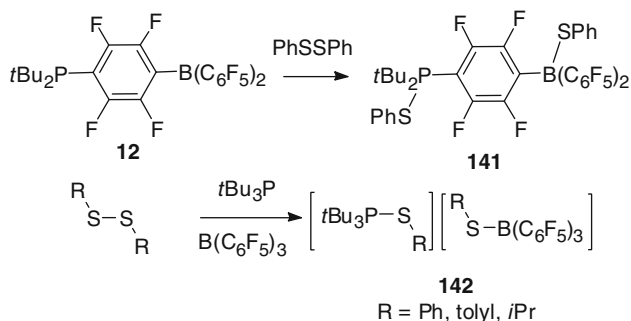
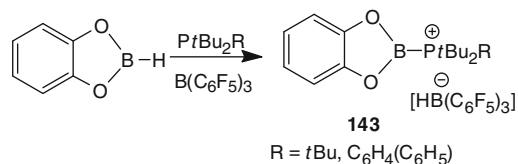
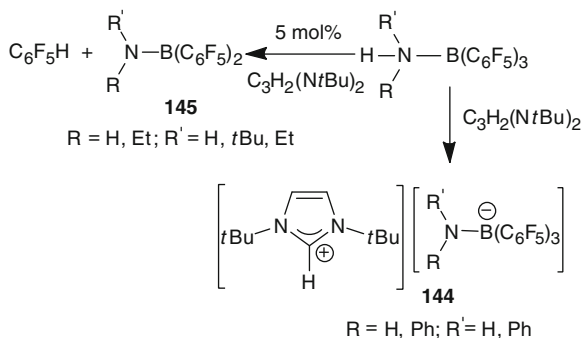
The study of FLPs has also revealed a variety of other reactions that result in the heterolytic activation of other bonds. In these cases the reactions have not been extensively studied but perhaps foreshadow other potential useful chemistry. Such reactions are described below.

### 6.1 Heterolytic Cleavage of Disulfides

The analogy between the heterolytic cleavage of  $\text{H}_2$  and that of disulfides prompted investigation of the reactions of FLPs with disulfides. To this end, diphenyl disulfide was reacted with **12** to afford the zwitterion phosphonium borate  $[\text{tBu}_2\text{P}(\text{SPh})(\text{C}_6\text{F}_4)\text{B}(\text{SPh})(\text{C}_6\text{F}_5)_2]$  **141** (Scheme 44).<sup>[123]</sup> In the same vein, the FLP  $t\text{Bu}_3\text{P}/\text{B}(\text{C}_6\text{F}_5)_3$  reacts with RSSR to give  $[\text{tBu}_3\text{P}(\text{SR})][(\text{RS})\text{B}(\text{C}_6\text{F}_5)_3]$  **142** ( $\text{R} = \text{Ph}, p\text{-tolyl}, i\text{Pr}$ ) (Scheme 44). In an interesting contrast, the reaction of  $\text{BnSSBn}$  yields a 1:1:1 mixture of  $t\text{Bu}_3\text{P}=\text{S}$ ,  $\text{Bn}_2\text{S}$ , and  $\text{B}(\text{C}_6\text{F}_5)_3$ , presumably a result of a further reaction of the corresponding salt  $[\text{tBu}_3\text{P}(\text{SBn})][(\text{BnS})\text{B}(\text{C}_6\text{F}_5)_3]$  <sup>[123]</sup>.

### 6.2 FLP Activation of Catechol Borane

Reaction of phosphine/borane FLPs with catecholborane were shown to prompt the formation of the salts  $[(\text{tBu}_2\text{RPBO}_2\text{C}_6\text{H}_4)][\text{HB}(\text{C}_6\text{F}_5)_3]$  **143** (Scheme 45) <sup>[124]</sup>. These reactions are thought to proceed via initial coordination of phosphine to catecholborane. Subsequent hydride abstraction results in the heterolytic cleavage. In this case, DFT computational studies infer that the three coordinate B cation ligated by O-donors <sup>[125]</sup> has a localized positive charge that resides on phosphorus atom, prompting the preferred description as a borylphosphonium cation rather than a phosphine stabilized borenium cation.

**Scheme 44** Heterolytic cleavage of disulfides**Scheme 45** B-H activation by an FLP**Scheme 46** N-H activation by an FLP

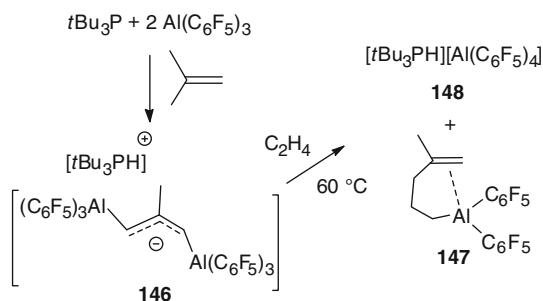
### 6.3 Heterolytic NH Activation

The combination of *It*Bu with (NH<sub>3</sub>)B(C<sub>6</sub>F<sub>5</sub>)<sub>3</sub> or (RR'NH)B(C<sub>6</sub>F<sub>5</sub>)<sub>3</sub> (R = H, R' = Ph, R' = R = Ph) results in the heterolytic cleavage of the N-H bond affording the imidazolium amidoborates [(*t*BuN)<sub>2</sub>C<sub>3</sub>H<sub>3</sub>][RR'NB(C<sub>6</sub>F<sub>5</sub>)<sub>3</sub>] **144** (Scheme 46) [38, 39]. The related reactions of alkylamine adducts (RR'NH)B(C<sub>6</sub>F<sub>5</sub>)<sub>3</sub> (R = H, R' = Et, *t*Bu, R' = R = Et) proceed in an analogous fashion, although the imidazolium cation protonates a fluoroarene ring liberating C<sub>6</sub>F<sub>5</sub>H and an amidoborane RR'NB(C<sub>6</sub>F<sub>5</sub>)<sub>2</sub> **145** (Scheme 46). This reaction allows for the

catalytic formation of the alkylamidoborane from the alkylamine adducts using 5 mol% of the NHC as catalyst [41]. It should be noted that NHCs do not react with amines on their own, in contrast to the reactivity of mono-amino carbenes described by Bertrand [37].

## 6.4 Heterolytic CH Activation

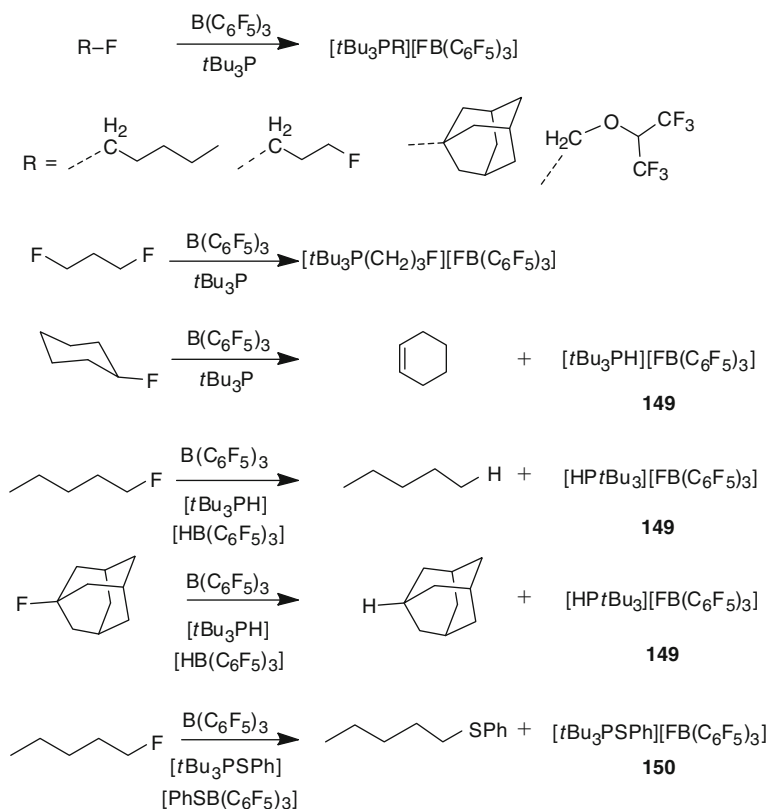
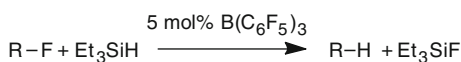
The FLP derived from  $t\text{Bu}_3\text{P}$  and  $\text{Al}(\text{C}_6\text{F}_5)_3$  reacts with isobutene to give the phosphonium salt  $[\text{tBu}_3\text{PH}][(\text{C}_6\text{F}_5)_3\text{Al}]_2((\text{CH}_2)_2\text{CMe})$  **146**, in which the planar allyl fragment links two Al centers via sigma interactions [126]. This is a very rare example of C–H activation by non-metal reagents under mild conditions. The species **146** reacts further with ethylene to give ethylene insertion in the Al–C bond, thus forming  $\text{CH}_2=\text{C}(\text{Me})(\text{CH}_2)_3\text{Al}(\text{C}_6\text{F}_5)_2$  **147** together with the byproduct  $[\text{tBu}_3\text{PH}][\text{Al}(\text{C}_6\text{F}_5)_4]$  **148** (Scheme 47) [126].



**Scheme 47** C–H activation by an FLP

## 6.5 Heterolytic CF Activation

The FLP derived from  $\text{B}(\text{C}_6\text{F}_5)_3$  and sterically demanding phosphines have been shown to activate alkylfluorides to give phosphonium fluoroborate salts (Scheme 48) [127]. In the same vein, treatment of  $\text{B}(\text{C}_6\text{F}_5)_3$ /alkylfluorides with the salts  $[\text{tBu}_3\text{PH}][\text{HB}(\text{C}_6\text{F}_5)_3]$  or  $[\text{tBu}_3\text{PSPPh}][\text{PhSB}(\text{C}_6\text{F}_5)_3]$  gives the alkane and the salt byproducts  $[\text{tBu}_3\text{PH}][\text{FB}(\text{C}_6\text{F}_5)_3]$  **149** or  $[\text{tBu}_3\text{PSPPh}][\text{FB}(\text{C}_6\text{F}_5)_3]$  **150**, respectively [127].  $\text{B}(\text{C}_6\text{F}_5)_3$  also catalyzes the conversion of fluoroalkanes to the analogous alkanes in the presence of  $\text{Et}_3\text{SiH}$  [127].

**Stoichiometric****Catalysis****Scheme 48** C–F activation by an FLP**7 Conclusion**

This chapter has reviewed the initial discovery of FLPs. Herein we have focused on intermolecular FLP systems that allow for three component reactions. These systems provide new strategies for the activation of a variety of small molecules, including  $\text{H}_2$ , olefins, alkynes, and greenhouse gases among others. Such activations have spurred much interest in the potential utility of metal-free systems. While commercial applications are perhaps for the future, the intriguing discovery challenges the commonly held chemistry dogma regarding the requirement of transition metals for small molecule activation. These findings have helped to stir interest in main group reactivity.

## References

1. Lewis GN (1923) Valence and the structure of atoms and molecules. Chemical Catalogue Company, Inc., New York
2. Brown HC, Schlesinger HI, Cardon SZ (1942) Studies in stereochemistry. I. Steric strains as a factor in the relative stability of some coordination compounds of boron. *J Am Chem Soc* 64:325
3. Wittig G, Benz E (1959) Über Das Verhalten Von Dehydrobenzol Gegenüber Nucleophilen Und Elektrophilen Reagenzien. *Chem Ber-Recl* 92:1999
4. Wittig G, Ruckert A (1950) Über Komplexbildung Mit Triphenylboron .2. Liebigs Ann Chem 566:101
5. Tochtermann W (1966) Structures and reactions of organic ate-complexes. *Angew Chem Int Ed* 5:351
6. Damico R, Broaddus CD (1966) Hydride transfer. Reactions of triphenylcarbonium fluoroborate and triphenylmethyl bromide with tertiary amines. *J Org Chem* 31:1607
7. Lankamp H, Nauta WT, Maclean C (1968) A new interpretation of monomer-dimer equilibrium of triphenylmethyl- and alkylsubstituted-diphenyl methyl-radicals in solution. *Tetrahedron Lett* 2:249
8. Okamoto Y, Shimakaw Y (1970) Synthesis, spectra, and reactions of N-triphenylmethylpyridinium salts – reaction of triphenylmethyl chloride with pyridine under high pressure. *J Org Chem* 35:3752
9. Doering S, Erker G, Fröhlich R, Meyer O, Bergander K (1998) Reaction of the Lewis acid tris(pentafluorophenyl)borane with a phosphorus ylide: competition between adduct formation and electrophilic and nucleophilic aromatic substitution pathways. *Organometallics* 17:2183
10. Massey AG, Park AJ (1964) Perfluorophenyl derivatives of the elements. 1. Tris(pentafluorophenyl)boron. *J Organomet Chem* 2:245
11. Welch GC, Cabrera L, Chase PA, Hollink E, Masuda JD, Wei PR, Stephan DW (2007) Tuning Lewis acidity using the reactivity of “frustrated Lewis pairs”: facile formation of phosphine-boranes and cationic phosphonium-boranes. *Dalton Trans* 3407
12. Welch GC, Juan RRS, Masuda JD, Stephan DW (2006) Reversible, metal-free hydrogen activation. *Science* 314:1124
13. Welch GC, Holtrichter-Roessmann T, Stephan DW (2008) Thermal rearrangement of phosphine-B(C<sub>6</sub>F<sub>5</sub>)<sub>3</sub> adducts. *Inorg Chem* 47:1904
14. Welch GC, Prieto R, Dureen MA, Lough AJ, Labeodan OA, Holtrichter-Roessmann T, Stephan DW (2009) Reactions of phosphines with electron deficient boranes. *Dalton Trans* 1559
15. Cabrera L, Welch GC, Masuda JD, Wei PR, Stephan DW (2006) Pyridine and phosphine reactions with [CPh<sub>3</sub>][B(C<sub>6</sub>F<sub>5</sub>)<sub>4</sub>]. *Inorg Chim Acta* 359:3066
16. Granville SL, Welch GC, Stephan DW (2012) Ni, Pd, Pt and Ru complexes of phosphine-borate ligands. *Inorg Chem* 51:4711
17. Clark TL, Rodezno JM, Clendenning SB, Aouba S, Brodersen PM, Lough AJ, Ruda HE, Manners I (2005) Rhodium-catalyzed dehydrocoupling of fluorinated phosphine-borane adducts: synthesis, characterization, and properties of cyclic and polymeric phosphinoboranes with electron-withdrawing substituents at phosphorus. *Chem Eur J* 11:4526
18. Jaska CA, Manners I (2004) Heterogeneous or homogeneous catalysis? Mechanistic studies of the rhodium-catalyzed dehydrocoupling of amine-borane and phosphine-borane adducts. *J Am Chem Soc* 126:9776
19. Yuan Z, Taylor NJ, Marder TB, Williams ID, Kurtz SK, Cheng LT (1990) Three coordinate phosphorus and boron as p-donor and p-acceptor moieties respectively, in conjugated organic molecules for nonlinear optics; crystal and molecular structures of E-PhCH=CHB(Mes)<sub>2</sub>, E-4-MeOC<sub>6</sub>H<sub>4</sub>CH=CHB(Mes)<sub>2</sub>, and E-Ph<sub>2</sub>PCH=CHB(Mes)<sub>2</sub> [Mes = 2,4,6-Me<sub>3</sub>C<sub>6</sub>H<sub>2</sub>]. *Chem Commun* 1489



20. Yuan Z, Taylor NJ, Sun Y, Marder TB, Williams ID, Cheng L-T (1993) Synthesis and second-order nonlinear optical properties of three coordinate organoboranes with diphenylphosphino and ferrocenyl groups as electron donors: crystal and molecular structures of (E)-DCH=CHB(Mes)<sub>2</sub> and DC≡C-B(Mes)<sub>2</sub> [D = P(C<sub>6</sub>H<sub>5</sub>)<sub>2</sub>, (η-C<sub>5</sub>H<sub>5</sub>)Fe(η-C<sub>5</sub>H<sub>4</sub>); Mes = 2,4,6-(CH<sub>3</sub>)<sub>3</sub>C<sub>6</sub>H<sub>2</sub>]. *J Organomet Chem* 449:27
21. Welch GC, Stephan DW (2007) Facile heterolytic cleavage of dihydrogen by phosphines and boranes. *J Am Chem Soc* 129:1880
22. McCahill JSJ, Welch GC, Stephan DW (2007) Reactivity of “frustrated Lewis pairs”: three-component reactions of phosphines, a borane, and olefins. *Angew Chem Int Ed* 46:4968
23. Stephan DW (2008) “Frustrated Lewis pairs”: a concept for new reactivity and catalysis. *Org Biomol Chem* 6:1535
24. Stephan DW (2009) Frustrated Lewis pairs: a new strategy to small molecule activation and hydrogenation catalysis. *Dalton Trans* 3129
25. Stephan DW (2010) Activation of dihydrogen by non-metal systems. *Chem Commun* 46:8526
26. Stephan DW, Erker G (2010) Frustrated Lewis pairs: metal-free hydrogen activation and more. *Angew Chem Int Ed* 49:46
27. Wang HD, Fröhlich R, Kehr G, Erker G (2008) Heterolytic dihydrogen activation with the 1,8-bis(diphenylphosphino)-naphthalene/B(C<sub>6</sub>F<sub>5</sub>)<sub>3</sub> pair and its application for metal-free catalytic hydrogenation of silyl enol ethers. *Chem Commun* 5966
28. Jackson RD, James S, Orpen AG, Pringle PG (1993) 1,8-Bis(diphenylphosphino)naphthalene – a rigid chelating, diphosphine analog of proton sponge. *J Organomet Chem* 458:C3
29. Ramos A, Lough AJ, Stephan DW (2009) Activation of H<sub>2</sub> by frustrated Lewis pairs derived from mono- and bis-phosphinoferrocenes and B(C<sub>6</sub>F<sub>5</sub>)<sub>3</sub>. *Chem Commun* 1118
30. Liptau P, Neumann M, Erker G, Kehr G, Fröhlich R, Grimme S (2004) Responsive iron neighboring group participation in amino-substituent-stabilized [3]ferrocenophane alpha-carbenium ions: a combined theoretical and experimental study. *Organometallics* 23:21
31. Huber DP, Kehr G, Bergander K, Fröhlich R, Erker G, Tanino S, Ohki Y, Tatsumi K (2008) Heterolytic cleavage of dihydrogen by frustrated Lewis pairs derived from alpha-(dimesitylphosphino)ferrocenes and B(C<sub>6</sub>F<sub>5</sub>)<sub>3</sub>. *Organometallics* 27:5279
32. Axenov KV, Kehr G, Fröhlich R, Erker G (2009) Catalytic hydrogenation of sensitive organometallic compounds by antagonistic N/B Lewis pair catalyst systems. *J Am Chem Soc* 131:3454
33. Unverhau K, Lübke G, Wibbeling B, Fröhlich R, Kehr G, Erker G (2010) Frustrated Lewis pair reactions at the [3]ferrocenophane framework. *Organometallics* 29:5320
34. Geier SJ, Gilbert TM, Stephan DW (2008) Activation of H<sub>2</sub> by phosphinoboranes R<sub>2</sub>PB(C<sub>6</sub>F<sub>5</sub>)<sub>2</sub>. *J Am Chem Soc* 130:12632
35. Ullrich M, Lough AJ, Stephan DW (2009) Reversible, metal-free, heterolytic activation of H<sub>2</sub> at room temperature. *J Am Chem Soc* 131:52
36. Ullrich M, Lough AJ, Stephan DW (2010) Dihydrogen activation by B(*p*-C<sub>6</sub>F<sub>4</sub>H)<sub>3</sub> and phosphines. *Organometallics* 29:3647
37. Frey GD, Lavallo V, Donnadiou B, Schoeller WW, Bertrand G (2007) Facile splitting of hydrogen and ammonia by nucleophilic activation at a single carbon center. *Science* 316:439
38. Chase PA, Gille AL, Gilbert TM, Stephan DW (2009) Frustrated Lewis pairs derived from N-heterocyclic carbenes and Lewis acids. *Dalton Trans* 7179
39. Chase PA, Stephan DW (2008) Hydrogen and amine activation by a frustrated Lewis pair of a bulky N-heterocyclic carbene and B(C<sub>6</sub>F<sub>5</sub>)<sub>3</sub>. *Angew Chem Int Ed* 47:7433
40. Holschumacher D, Bannenberg T, Hrib CG, Jones PG, Tamm M (2008) Heterolytic dihydrogen activation by a frustrated carbene-borane Lewis pair. *Angew Chem Int Ed* 47:7428
41. Chase PA, Jurca T, Stephan DW (2008) Lewis acid-catalyzed hydrogenation: B(C<sub>6</sub>F<sub>5</sub>)<sub>3</sub>-mediated reduction of imines and nitriles with H<sub>2</sub>. *Chem Commun* 1701

42. Sumerin V, Schulz F, Nieger M, Leskelä M, Repo T, Rieger B (2008) Facile heterolytic H<sub>2</sub> activation by amines and B(C<sub>6</sub>F<sub>5</sub>)<sub>3</sub>. *Angew Chem Int Ed* 47:6001
43. Piers WE (2005) The chemistry of perfluoroaryl boranes. *Adv Organomet Chem* 52:1
44. Focante F, Mercandelli P, Sironi A, Resconi L (2006) Complexes of tris(pentafluorophenyl) boron with nitrogen-containing compounds: synthesis, reactivity and metallocene activation. *Coord Chem Rev* 250:170
45. Geier SJ, Gille AL, Gilbert TM, Stephan DW (2009) From classical adducts to frustrated Lewis pairs: steric effects in the interactions of pyridines and B(C<sub>6</sub>F<sub>5</sub>)<sub>3</sub>. *Inorg Chem* 48:10466
46. Geier SJ, Stephan DW (2009) Lutidine/B(C<sub>6</sub>F<sub>5</sub>)<sub>3</sub>: at the boundary of classical and frustrated Lewis pair reactivity. *J Am Chem Soc* 131:3476
47. Roesler R, Har BJN, Piers WE (2002) Synthesis and characterization of (perfluoroaryl) borane-functionalized carbosilane dendrimers and their use as Lewis acid catalysts for the hydrosilation of acetophenone. *Organometallics* 21:4300
48. Parks DJ, Piers WE (1996) Tris(pentafluorophenyl)boron-catalyzed hydrosilation of aromatic aldehydes, ketones, and esters. *J Am Chem Soc* 118:9440
49. Blackwell JM, Sonmor ER, Scoccitti T, Piers WE (2000) B(C<sub>6</sub>F<sub>5</sub>)<sub>3</sub>-catalyzed hydrosilation of imines via silyliminium intermediates. *Org Lett* 2:3921
50. Blackwell JM, Foster KL, Beck VH, Piers WE (1999) B(C<sub>6</sub>F<sub>5</sub>)<sub>3</sub>-catalyzed silylation of alcohols: a mild, general method for synthesis of silyl ethers. *J Org Chem* 64:4887
51. Spence REvH, Piers WE, Sun YM, Parvez M, MacGillivray LR, Zaworotko MJ (1998) Mechanistic aspects of the reactions of bis(pentafluorophenyl)borane with the dialkyl zirconocenes Cp<sub>2</sub>ZrR<sub>2</sub> (R = CH<sub>3</sub>, CH<sub>2</sub>SiMe<sub>3</sub>, and CH<sub>2</sub>C<sub>6</sub>H<sub>5</sub>). *Organometallics* 17:2459
52. Spence REvH, Parks DJ, Piers WE, Macdonald MA, Zaworotko MJ, Rettig SJ (1995) Competing pathways in the reaction of bis(pentafluorophenyl)borane with bis(η<sup>5</sup>-cyclopentadienyl)dimethylzirconium – methane elimination versus methyl-hydride exchange and an example of pentacoordinate carbon. *Angew Chem Int Ed* 34:1230
53. Piers WE, Chivers T (1997) Pentafluorophenylboranes: from obscurity to applications. *Chem Soc Rev* 26:345
54. Parks DJ, Spence REvH, Piers WE (1995) Bis(pentafluorophenyl)borane – synthesis, properties, and hydroboration chemistry of a highly electrophilic borane reagent. *Angew Chem Int Ed* 34:809
55. Parks DJ, Piers WE, Yap GPA (1998) Synthesis, properties, and hydroboration activity of the highly electrophilic borane bis(pentafluorophenyl)borane, HB(C<sub>6</sub>F<sub>5</sub>)<sub>2</sub>. *Organometallics* 17:5492
56. Parks DJ, Piers WE, Parvez M, Atencio R, Zaworotko MJ (1998) Synthesis and solution and solid-state structures of tris(pentafluorophenyl)borane adducts of PhC(O)X (X = H, Me, OEt, N(*i*Pr)<sub>2</sub>). *Organometallics* 17:1369
57. Jacobsen H, Berke H, Döring S, Kehr G, Erker G, Fröhlich R, Meyer O (1999) Lewis acid properties of tris(pentafluorophenyl)borane. Structure and bonding in L–B(C<sub>6</sub>F<sub>5</sub>)<sub>3</sub> complexes. *Organometallics* 18:1724
58. Blackwell JM, Morrison DJ, Piers WE (2002) B(C<sub>6</sub>F<sub>5</sub>)<sub>3</sub> catalyzed hydrosilation of enones and silyl enol ethers. *Tetrahedron* 58:8247
59. Morrison DJ, Piers WE (2003) Weaker Lewis acid, better catalytic activity: dual mechanisms in perfluoroarylborane-catalyzed allylstannation reactions. *Org Lett* 5:2857
60. Morrison DJ, Blackwell JM, Piers WE (2004) Mechanistic insights into perfluoroaryl borane-catalyzed allylstannations: toward asymmetric induction with chiral boranes. *Pure Appl Chem* 76:615
61. Asao N, Ohishi T, Sato K, Yamamoto Y (2002) Lewis acid catalyzed stereoselective hydrosilylation of ketones under the control of sigma-pi chelation. *Tetrahedron* 58:8195
62. Chandrasekhar S, Chandrashekar G, Babu BN, Vijeender K, Reddy KV (2004) Reductive etherification of carbonyl compounds with alkyl trimethylsilyl ethers using polymethylhydro-siloxane (PMHS) and catalytic B(C<sub>6</sub>F<sub>5</sub>)<sub>3</sub>. *Tetrahedron Lett* 45:5497

63. Chandrasekhar S, Reddy CR, Babu BN (2002) Rapid defunctionalization of carbonyl group to methylene with polymethylhydrosiloxane-B(C<sub>6</sub>F<sub>5</sub>)<sub>3</sub>. *J Org Chem* 67:9080
64. Bach P, Albright A, Laali KK (2009) Influence of Lewis acid and solvent in the hydrosilylation of aldehydes and ketones with Et<sub>3</sub>SiH; tris(pentafluorophenyl)borane B(C<sub>6</sub>F<sub>5</sub>)<sub>3</sub> versus metal triflates [M(OTf)<sub>3</sub>; M = Sc, Bi, Ga, and Al] – mechanistic implications. *Eur J Org Chem* 1961
65. Piers WE, Marwitz AJV, Mercier LG (2011) Mechanistic aspects of bond activation with perfluoroarylboranes. *Inorg Chem* 50:12252
66. Gevorgyan V, Rubin M, Liu JX, Yamamoto Y (2001) A direct reduction of aliphatic aldehyde, acyl chloride, ester, and carboxylic functions into a methyl group. *J Org Chem* 66:1672
67. Gevorgyan V, Rubin M, Benson S, Liu JX, Yamamoto Y (2000) A novel B(C<sub>6</sub>F<sub>5</sub>)<sub>3</sub>-catalyzed reduction of alcohols and cleavage of aryl and alkyl ethers with hydrosilanes. *J Org Chem* 65:6179
68. Rubin M, Schwier T, Gevorgyan V (2002) Highly efficient B(C<sub>6</sub>F<sub>5</sub>)<sub>3</sub>-catalyzed hydrosilylation of olefins. *J Org Chem* 67:1936
69. Rubin M, Gevorgyan V (2001) B(C<sub>6</sub>F<sub>5</sub>)<sub>3</sub>-catalyzed allylation of secondary benzyl acetates with allylsilanes. *Org Lett* 3:2705
70. Imamura K, Yoshikawa E, Gevorgyan V, Sudo T, Asao N, Yamamoto Y (2001) Lewis acid-mediated intramolecular addition of silyl enol ethers to internal unactivated alkynes. *Can J Chem* 79:1624
71. Schwier T, Rubin M, Gevorgyan V (2004) B(C<sub>6</sub>F<sub>5</sub>)<sub>3</sub>-catalyzed allylation of propargyl acetates with allylsilanes. *Org Lett* 6:1999
72. Rendler S, Oestreich M, Butts CP, Lloyd-Jones GC (2007) Intermolecular chirality transfer from silicon to carbon: interrogation of the two-silicon cycle for Pd-catalyzed hydrosilylation by stereoisotopochemical crossover. *J Am Chem Soc* 129:502
73. Rendler S, Oestreich M (2008) Conclusive evidence for an SN<sub>2</sub>-Si mechanism in the B(C<sub>6</sub>F<sub>5</sub>)<sub>3</sub>-catalyzed hydrosilylation of carbonyl compounds: implications for the related hydrogenation. *Angew Chem Int Ed* 47:5997
74. Oestreich M, Rendler S (2005) “True” chirality transfer from silicon to carbon: asymmetric amplification in a reagent controlled palladium-catalyzed hydrosilylation. *Angew Chem Int Ed* 44:1661
75. Oestreich M (2007) Silicon-stereogenic silanes in asymmetric catalysis. *Synlett* 1629
76. Zhao X, Stephan DW (2011) Olefin-borane “van der Waals complexes”: intermediates in frustrated Lewis pair addition reactions. *J Am Chem Soc* 133:12448
77. Stirling A, Hamza A, Rokob TA, Pápai I (2008) Concerted attack of frustrated Lewis acid–base pairs on olefinic double bonds: a theoretical study. *Chem Commun* 3148
78. Guo Y, Li S (2008) A novel addition mechanism for the reaction of “frustrated Lewis pairs” with olefins. *Eur J Inorg Chem* 2501
79. Herrebout WA, van derVeken BJ (1997) Van der Waals complexes between unsaturated hydrocarbons and boron trifluoride: an infrared and ab initio study of ethene-BF<sub>3</sub> and propene-BF<sub>3</sub>. *J Am Chem Soc* 119:10446
80. Tarakeshwar P, Kim KS (1999) A theoretical investigation of benzene-AiX<sub>3</sub> and ethene-AiX<sub>3</sub> (X = H, F, Cl) interactions. *J Phys Chem A* 103:9116
81. Tarakeshwar P, Lee SJ, Lee JY, Kim KS (1999) Ab initio study of benzene-BX<sub>3</sub> (X = H, F, Cl) interactions. *J Phys Chem B* 103:184
82. Zhao X, Stephan DW (2012) Frustrated Lewis pair olefin addition reactions: P-, N-, C- and H-based nucleophilic additions to an olefin tethered to borane. *Chem Sci* 3:2123
83. Dureen MA, Stephan DW (2009) Terminal alkyne activation by frustrated and classical Lewis acid/phosphine pairs. *J Am Chem Soc* 131:8396
84. Dureen MA, Brown CC, Stephan DW (2010) Addition of enamines or pyrroles and B(C<sub>6</sub>F<sub>5</sub>)<sub>3</sub> “frustrated Lewis pairs” to alkynes. *Organometallics* 29:6422

85. Dureen MA, Stephan DW (2010) Deprotonation and addition reactions of frustrated Lewis pairs with alkynes. *Organometallics* 29:6594
86. Caputo CB, Geier SJ, Ouyang EY, Kreitner C, Stephan DW (2012) Chloro- and phenoxy-phosphines in frustrated Lewis pair additions to alkynes. *Dalton Trans* 41:237
87. Zhao X, Stephan DW (2011) Synthesis and reactions of zwitterionic alkynyl-phosphonium borates. *Chem Eur J* 17:6731
88. Zhao XX, Gilbert TM, Stephan DW (2010) C-C coupling by thermolysis of alkynyl phosphonium borates. *Chem Eur J* 16:10304
89. Jiang CF, Blacque O, Berke H (2010) Activation of terminal alkynes by frustrated Lewis pairs. *Organometallics* 29:125
90. Chen C, Kehr G, Fröhlich R, Erker G (2010) Carbon-carbon bond activation by 1,1-carboboration of internal alkynes. *J Am Chem Soc* 132:13594
91. Chen C, Fröhlich R, Kehr G, Erker G (2010) Remarkably variable reaction modes of frustrated Lewis pairs with non-conjugated terminal diacetylenes. *Chem Commun* 46:3580
92. Chen C, Eweiner F, Wibbeling B, Fröhlich R, Senda S, Ohki Y, Tatsumi K, Grimme S, Kehr G, Erker G (2010) Exploring the limits of frustrated Lewis pair chemistry with alkynes: detection of a system that favors 1,1-carboboration over cooperative 1,2-P/B-addition. *Chem Asian J* 5:2199
93. Breen TL, Stephan DW (1992) Substitution or nucleophilic-attack by phosphines on  $ZrCl_4(THF)_2$ . *Inorg Chem* 31:4019
94. Avens LR, Barnhart DM, Burns CJ, McKee SD (1996) Uranium-mediated ring opening of tetrahydrofuran. Crystal structure of  $Uf_2(OCH_2CH_2CH_2CH_2I)_2(Ph_3P=O)_2$ . *Inorg Chem* 35:537
95. Campello MPC, Domingos A, Santos I (1994) Uranium complexes with hydrotris(pyrazolyl) borate. *J Organomet Chem* 484:37
96. Evans WJ, Leman JT, Ziller JW, Khan SI (1996) Synthesis and reactivity of organosamarium diarylpycnitide complexes: cleavage reactions of group 15 E-E and E-C bonds by samarium (II). *Inorg Chem* 35:4283
97. Mommertz A, Leo R, Massa W, Harms K, Dehnicke K (1998) Synthesis of a titanoxacyclohexane ring by controlled ring opening of tetrahydrofuran. Crystal structures of  $[cyclo-(Ti(CH_2)_4O)\{Me_2Si(NrBu)_2\}]_2$ ,  $[TiCl\{Me_2Si(NrBu)_2\}]_3(\mu^3-O)(\mu^3-Cl)$ , and  $[Li_2(THF)_3\{Me_2Si(NrBu)_2\}]$ . *Z Anorg Allg Chem* 624:1647
98. Guo ZY, Bradley PK, Jordan RF (1992) THF ring-opening and hydrogen/deuterium exchange reactions of  $(C_5H_4Me)_2Zr(H)(THF)^+$ . Evidence for hydrogenolysis of zirconium-cyclopentadiene bonds. *Organometallics* 11:2690
99. Polamo M, Mutikainen I, Leskela M (1997) A tetrahydrofuran ring-opening product: trans-tetrachloro{4-[2-(phenylamino)pyridinio]butoxido-O}(tetrahydrofuran-O)zirconium(IV). *Acta Crystallogr C* 53:1036
100. GomezSaso M, Mullica DF, Sappenfield E, Stone FGA (1996) Reactions of nido-7,8- $C_2B_9H_{13}$  with pentacarbonyl(methyl)manganese: crystal structure of the charge-compensated complex  $[Mn(CO)_3\{v^5-7,8-C_2B_9H_{10}-10-O(CH_2)_4\}]$ . *Polyhedron* 15:793
101. Chivers T, Schatte G (2003) Cooperative THF ring-opening by  $B(C_6F_5)_3$  and a tellurium diimide dimer. *Eur J Inorg Chem* 3314
102. Kunnari SM, Oilunkaniemi R, Laitinen RS, Ahlgren M (2001) An unexpected tetrahydrofuran ring opening: synthesis and structural characterization of  $Ph_3PO(CH_2)_4TeBr_4$ . *J Chem Soc Dalton Trans* 3417
103. Campbell JP, Gladfelter WL (1997) Synthesis and structure of alkoxy- and (aryloxy)alanes. Observation of a ring-opening reaction involving tetrahydrofuran. *Inorg Chem* 36:4094
104. Welch GC, Masuda JD, Stephan DW (2006) Phosphonium-borate zwitterions, anionic phosphines, and dianionic phosphonium-dialkoxides via tetrahydrofuran ring-opening reactions. *Inorg Chem* 45:478
105. Birkmann B, Voss T, Geier SJ, Ullrich M, Kehr G, Erker G, Stephan DW (2010) Frustrated Lewis pairs and ring-opening of THF, dioxane, and thioxane. *Organometallics* 29:5310

106. Kaufmann D (1987) Borylation of arylsilanes. 2. Synthesis and reactions of silylated dihalogenphenylboranes. *Chem Ber-Recl* 120:901
107. Williams VC, Piers WE, Clegg W, Elsegood MRJ, Collins S, Marder TB (1999) New bifunctional perfluoroaryl boranes. Synthesis and reactivity of the ortho-phenylene-bridged diboranes 1,2-[B(C<sub>6</sub>F<sub>5</sub>)<sub>2</sub>]<sub>2</sub>C<sub>6</sub>X<sub>4</sub> (X = H, F). *J Am Chem Soc* 121:3244
108. Sgro MJ, Dömer J, Stephan DW (2012) Stoichiometric CO<sub>2</sub> reductions using a bis-borane-based frustrated Lewis pair. *Chem Commun* 48:7253–7255
109. Kreitner C, Geier SJ, Stanlake LJE, Caputo C, Stephan DW (2011) Ring openings of lactone and ring contractions of lactide by frustrated Lewis pairs. *Dalton Trans* 6771
110. Morton JGM, Dureen MA, Stephan DW (2010) Ring-opening of cyclopropanes by “frustrated Lewis pairs”. *Chem Commun* 46:8947
111. Mömming CM, Otten E, Kehr G, Fröhlich R, Grimme S, Stephan DW, Erker G (2009) Reversible metal-free carbon dioxide binding by frustrated Lewis pairs. *Angew Chem Int Ed* 48:6643
112. Peuser I, Neu RC, Zhao X, Ulrich M, Schirmer B, Tannert JA, Kehr G, Fröhlich R, Grimme S, Erker G, Stephan DW (2011) CO<sub>2</sub> and formate complexes of phosphine-borane frustrated Lewis pairs. *Chem Eur J* 17:9640
113. Neu RC, Ménard G, Stephan DW (2012) Exchange chemistry of tBu<sub>3</sub>P(CO<sub>2</sub>)B(C<sub>6</sub>F<sub>5</sub>)<sub>2</sub>Cl. *Dalton Trans*. doi:10.1039/C2DT30206C
114. Zhao X, Stephan DW (2011) Bis-boranes in the frustrated Lewis pair activation of carbon dioxide. *Chem Commun* 47:1833
115. Ashley AE, Thompson AL, O’Hare D (2009) Non-metal-mediated homogeneous hydrogenation of CO<sub>2</sub> to CH<sub>3</sub>OH. *Angew Chem Int Ed* 48:9839
116. Tran SD, Tronic TA, Kaminsky W, Heinekey DM, Mayer JM (2011) Metal-free carbon dioxide reduction and acidic C-H activations using a frustrated Lewis pair. *Inorg Chim Acta* 369:126
117. Menard G, Stephan DW (2010) Room temperature reduction of CO<sub>2</sub> to methanol by Al-based frustrated Lewis pairs and ammonia borane. *J Am Chem Soc* 132:1796
118. Ménard G, Stephan DW (2011) Stoichiometric Reduction of CO<sub>2</sub> to CO by Al-based frustrated Lewis pairs. *Angew Chem Int Ed* 51:8396
119. Otten E, Neu RC, Stephan DW (2009) Complexation of nitrous oxide by frustrated Lewis pairs. *J Am Chem Soc* 131:9918
120. Neu RC, Otten E, Lough A, Stephan DW (2011) The synthesis and exchange chemistry of frustrated Lewis pair-nitrous oxide complexes. *Chem Sci* 2:170
121. Neu RC, Otten E, Stephan DW (2009) Bridging binding modes of phosphine-stabilized nitrous oxide to Zn(C<sub>6</sub>F<sub>5</sub>)<sub>2</sub>. *Angew Chem Int Ed* 48:9709
122. Sajid M, Klose A, Birkmann B, Liang L, Kehr G, Lough AJ, Fröhlich R, Daniliuc C, Schirmer B, Grimme S, Stephan DW, Erker G (2012) Reactions of phosphorus/boron frustrated Lewis pairs with SO<sub>2</sub>. *Chem. Sci*. doi: 10.1039/C2SC21161K
123. Dureen MA, Welch GC, Gilbert TM, Stephan DW (2009) Heterolytic cleavage of disulfides by frustrated Lewis pairs. *Inorg Chem* 48:9910
124. Dureen MA, Lough A, Gilbert TM, Stephan DW (2008) B-H activation by frustrated Lewis pairs: borenium or boryl phosphonium cation? *Chem Commun* 4303
125. Piers WE, Bourke SC, Conroy KD (2005) Borinium, borenium, and boronium ions: synthesis, reactivity, and applications. *Angew Chem Int Ed* 44:5016
126. Ménard G, Stephan DW (2012) C-H activation of isobutylene using frustrated Lewis pairs: aluminum and boron  $\sigma$ -allyl complexes. *Angew Chem Int Ed* 51:4409
127. Caputo CB, Stephan DW (2012) Activation of alkyl C-F bonds by B(C<sub>6</sub>F<sub>5</sub>)<sub>3</sub>: stoichiometric and catalytic transformations. *Organometallics* 31:27
128. Rokob TA, Pápai I (2012) Hydrogen activation by frustrated Lewis pairs: Insights from computational studies. *Top Curr Chem* DOI: 10.1007/128\_2012\_399
129. Schirmer B, Grimme S (2012) Quantum chemistry of FLPs and their activation of small molecules: Methodological aspects. *Top Curr Chem* DOI: 10.1007/128\_2012\_389

# Intramolecular Frustrated Lewis Pairs: Formation and Chemical Features

Gerald Kehr, Sina Schwendemann, and Gerhard Erker

**Abstract** Intramolecular vicinal and geminal frustrated Lewis pairs (FLPs) featuring bulky substituents at phosphorus or nitrogen and strongly electron-withdrawing bulky pentafluorophenyl substituents at boron undergo a variety of addition and/or activation reactions with small molecules. A number of examples of such reactions are presented and discussed, among them the FLP activation of dihydrogen to give zwitterionic phosphonium (or ammonium)/hydridoborate zwitterions. Intramolecular FLPs also add to organic carbonyl compounds (including carbon dioxide), to alkenes and alkynes (including conjugated dienes, diynes or enynes), to heterocumulenes, to azides, and to nitric oxide.

**Keywords** FLP addition reactions · Small molecule activation · Synergistic reactions · Vicinal and geminal frustrated Lewis pairs

## Contents

1	Introduction .....	46
2	Vicinal Phosphorus/Boron FLPs and Their Reaction with Dihydrogen .....	47
3	Intramolecular N/B FLPs .....	55
4	FLP Reactions with $\pi$ -Systems and More .....	63
5	Geminal FLPs .....	74
6	Conclusions .....	76
	References .....	77

---

G. Kehr, S. Schwendemann, and G. Erker (✉)

Organisch-Chemisches Institut der Universität Münster, Corrensstr. 40, 48149 Münster, Germany  
e-mail: [erker@uni-muenster.de](mailto:erker@uni-muenster.de)

## Abbreviations

Bu	Butyl
CP	Cross polarization
DABCO	1,4-Diazabicyclo[2.2.2]octane
DEAD	Diethyl azodicarboxylate
DFT	Density functional theory
equiv.	Equivalent(s)
Et	Ethyl
FLP	Frustrated Lewis pair
gem.	Geminal
h	Hour(s)
HAA	Hydrogen atom abstraction
<i>i</i> -Pr	<i>iso</i> -Propyl
LA	Lewis acid
LB	Lewis base
MAS	Magic angle spinning
Me	Methyl
Mes	Mesityl, 2,4,6-trimethylphenyl
min	Minute(s)
NMR	Nuclear magnetic resonance
Ph	Phenyl
Pr	Propyl
r.t.	Room temperature
<i>s</i> -Bu	<i>sec</i> -Butyl
THF	Tetrahydrofuran
<i>t</i> -Bu	<i>tert</i> -Butyl
vic.	Vicinal

## 1 Introduction

Lewis acids (LA) and Lewis bases (LB) usually undergo strong adduct formation when brought together in solution. The ubiquitous Lewis acid/base adduct formation [1] is analogous to the neutralization reaction in Brønsted acid/base chemistry [2]. The resulting LA/LB adducts may have very interesting properties in themselves, e.g., as is found in the chemistry of ammonia borane ( $\text{H}_3\text{NBH}_3$ ) [3, 4], but they have lost the typical chemical features of their original components. Lewis acid/Lewis base adduct formation can effectively be hindered or even completely suppressed by steric and/or electronic means. Placing very bulky aryl or alkyl substituents at, e.g., phosphorus or nitrogen or even carbon based Lewis bases and combining them with, e.g., strongly electrophilic  $\text{R-B}(\text{C}_6\text{F}_5)_2$  type Lewis acids has often resulted in situations of co-existent pairs of active Lewis acids and Lewis bases in solution. Sometimes they appeared to be independent of each other,

sometimes they were found to be in equilibrium with their respective LA/LB adducts, sometimes they were weakly interacting. Such frustrated Lewis pairs (FLPs) [5–16] can, of course, show reactions of their separate LA and LB components, but they are special in that they have the potential to have the Lewis acid/Lewis base components reacting synergistically with added substrates. There are indications that weak interactions between the Lewis acid/Lewis base components of a frustrated Lewis pair might favor synergistic reaction behavior, maybe it is even mandatory in some cases. Intramolecular FLPs, where active Lewis acid and Lewis base components are closely connected by sufficiently flexible bridges, may be advantageous to introduce and control typical frustrated Lewis pair behavior. Here we report about a selection of intramolecular FLPs, mostly, but not exclusively, originating from our research group in Münster and our collaborating partners, which may serve to illustrate some of the remarkable and extraordinary features that such reactive bifunctional main group element compounds may exhibit.

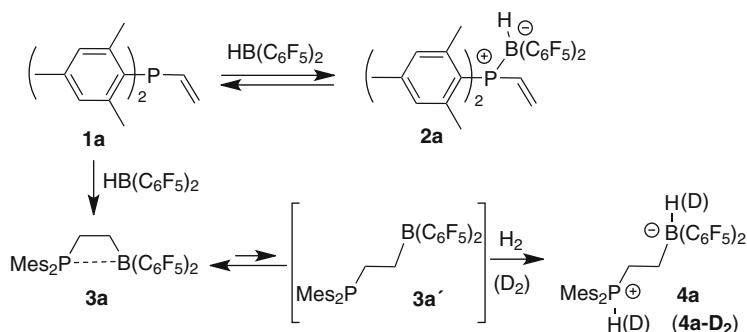
## 2 Vicinal Phosphorus/Boron FLPs and Their Reaction with Dihydrogen

We first reacted the bulky starting material dimesitylvinylphosphane (**1a**) with Piers' borane [HB(C<sub>6</sub>F<sub>5</sub>)<sub>2</sub>] [17–21]. The system forms a Lewis acid/Lewis base adduct (**2a**, Scheme 1) at low temperature. However, this has only a fleeting existence, since the **1a**/HB(C<sub>6</sub>F<sub>5</sub>)<sub>2</sub> reaction mixture undergoes a rapid hydroboration reaction of the vinyl substituent at room temperature with the usual anti-Markovnikov orientation to yield the intramolecular FLP **3a** [22].

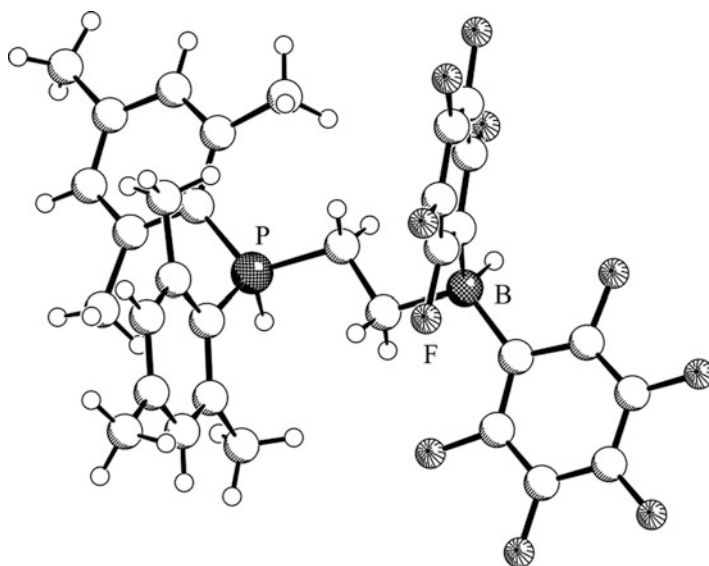
The spectroscopic data indicate that **3a** is a weakly interacting intramolecular FLP system. In solution it features NMR shifts of the heteronuclei [<sup>31</sup>P: δ 20.6, <sup>11</sup>B: δ 8.5, <sup>19</sup>F: δ -128.8 (*o*), -157.0 (*p*), -163.6 (*m*)] that are intermediate between a phosphane/phosponium, and borane/borate character. A detailed solid state MAS NMR analysis confirmed this [23]. Among other parameters the <sup>11</sup>B NMR quadrupolar coupling constant of **3a** pointed to a P...B interacting system with a boron center deviating only slightly from a trigonal planar BC<sub>3</sub> coordination sphere and a tentative P...B distance of ca. 2.2 Å. The DFT analysis of **3a** gave a similar result. According to this computational analysis the weak internal adduct **3a** equilibrated with a pair of open isomers **3a'** which were of slightly higher energy. One had the two functional groups oriented gauche to each other, whereas the other showed them in an anti-periplanar conformational arrangement [22].

Compound **3a** reacts rapidly with dihydrogen under mild conditions. It was one of the most active metal-free dihydrogen activations at the time when it was first studied. It splits dihydrogen at close to normal conditions (r.t., 1.5 bar H<sub>2</sub> pressure, pentane solution) within minutes. The pale yellow solution of **3a** turns colorless and the zwitterionic phosphonium/hydridoborate product **4a** precipitates from the solution. It was characterized by X-ray diffraction (Fig. 1) and by spectroscopy





**Scheme 1** Formation of the FLP **3a** and its reaction with dihydrogen

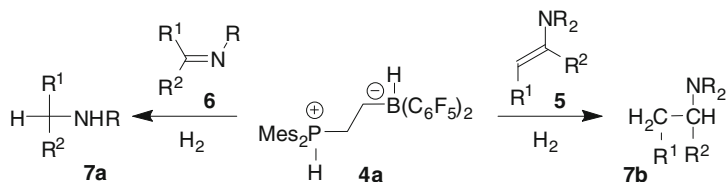
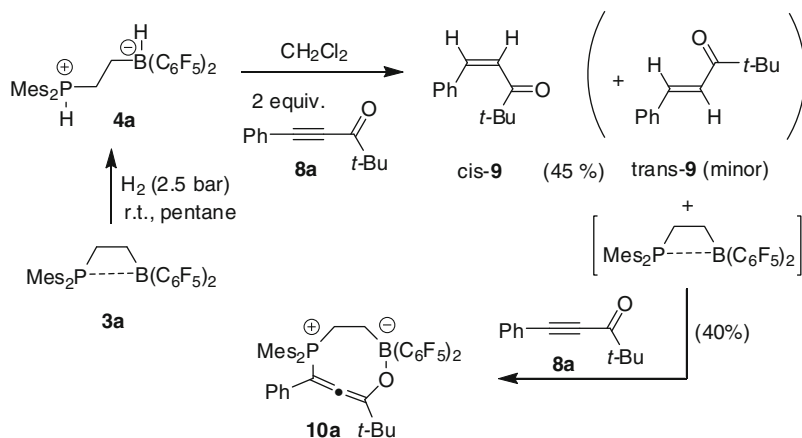


**Fig. 1** Molecular structure of the zwitterionic phosphonium/hydridoborate product **4a**

[ $^1\text{H}$  NMR:  $\delta$  7.87 ( $^1J_{\text{PH}} \sim 490$  Hz),  $^{31}\text{P}$ :  $\delta$   $-6.5$  [P–H],  $^{11}\text{B}$ :  $\delta$   $-20.1$  ( $^1J_{\text{BH}} \sim 90$  Hz) [B–H]]. The reaction was also carried out with dideuterium which confirmed the heterolytic dihydrogen splitting by observing the corresponding [B]–D and [P]–D signals in **4a-D<sub>2</sub>** (Scheme 1 and Fig. 1) [22].

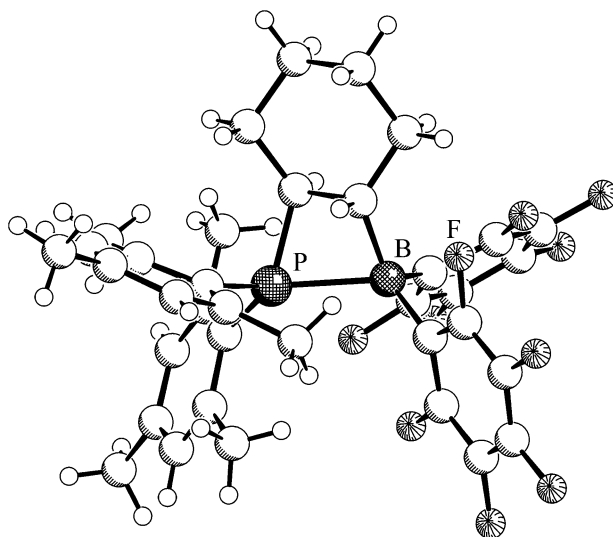
Compound **4a** is able to catalyze the hydrogenation of a variety of enamines **5** or imines **6** to the corresponding amine products **7** (Scheme 2) [24, 25] (Axenov, 2009, unpublished results).

Many FLPs have been shown to be quite reasonable catalysts for the metal-free catalytic hydrogenation of electron-rich unsaturated substrates such as enamines and dienamines (Scheme 2) [22, 24, 25] (Axenov, 2009, unpublished results), in addition to silyl enoethers [26], of a variety of imines and some aziridines [27–32].

Scheme 2  $H^+/H^-$  transfer from **4a**Scheme 3 Reaction of **4a** with ynone

D. W. Stephan recently showed that even the arene rings in some aniline derivatives can be hydrogenated by FLP systems to yield cyclohexylamines [33]. We showed that FLP catalyzed reactions can provide sufficiently mild conditions for reactions with rather sensitive organometallic substrates [14, 25, 34–38] (Axenov, 2009, unpublished results). All these developments posed the question of whether FLP induced hydrogenation of carbon–carbon double or triple bonds bearing strongly electron-withdrawing substituents could be achieved. For that purpose we treated the conjugated ynone **8a** with the zwitterionic  $H_2$ -activation product **4a**. We observed a rapid transfer of the  $H^+/H^-$  pair at room temperature with formation of the *cis*-enone *cis*-**9**. Unfortunately, in this case the liberated FLP **3a** reacted faster with the ynone substrate **8a** to give **10a** (Scheme 3). As a result, this FLP induced hydrogenation of the electron-poor carbon–carbon triple bond in **8a** remained stoichiometric [39].

We prepared a variety of analogs of the ethylene-bridged P/B FLP **3a** by hydroboration of a series of substituted dimesitylalkenylphosphanes with  $[HB(C_6F_5)_2]$ . The cyclohexenylphosphane derived FLP **3b** is a typical example [40]. Hydroboration of **1b** with Piers' borane gave the P/B FLP **3b** in good yield. Compound **3b** is chiral; it contains two chiral centers. Due to the fixed *cis*-[B]-H addition, the stereochemistry of the underlying hydroboration reaction, these chiral centers are dependent on each other. Only the *rac*-*trans*-diastereoisomer was formed. It is



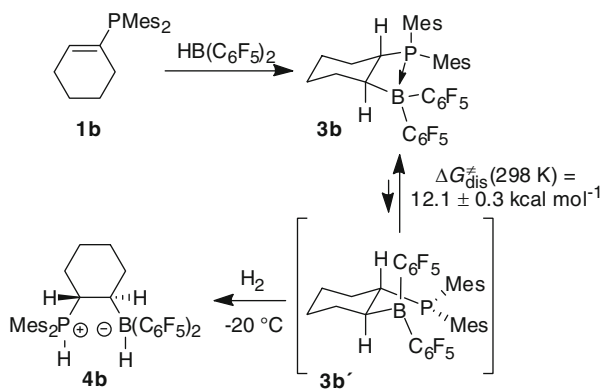
**Fig. 2** Molecular structure of the P/B FLP **3b**

characterized by having the bulky phosphanyl- and boryl-substituents *trans*-1,2-attached at the cyclohexane framework. Compound **3b** was characterized by X-ray diffraction (Fig. 2). In the crystal the cyclohexane ring of compound **3b** adopts a chair conformation with the C1-P and C2-B vectors oriented *trans*-bis-equatorially. There are two crystallographically independent molecules in the unit cell. Both show P...B interactions, although the P...B distance at 2.188(5) Å (molecule A) and 2.206(5) Å (molecule B) is at the long end of phosphane/borane interactions [41–47].

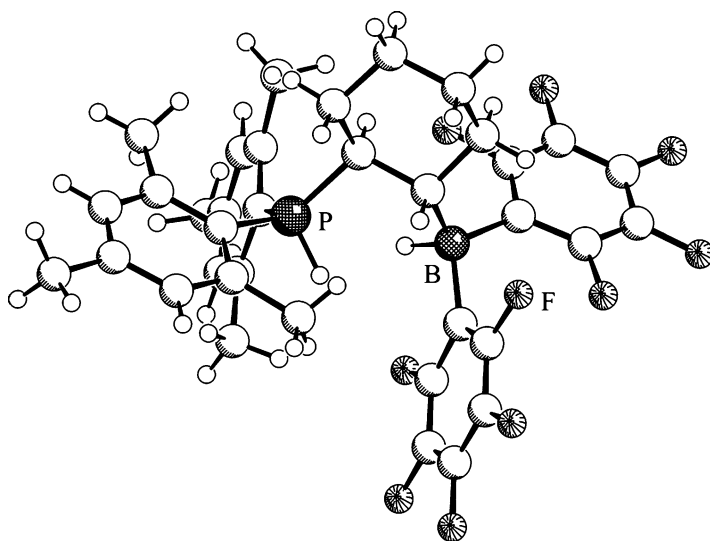
In solution we observed the  $^{19}\text{F}$  NMR signals corresponding to a pair of diastereotopic  $\text{C}_6\text{F}_5$  groups at boron at low temperatures, due to the tetracoordination at boron. Opening of the P–B linkage would result in the formation of a planar-tricoordinate boron center in the reactive intermediate **3b'**; its pair of  $\text{C}_6\text{F}_5$  substituents would, consequently, be homotopic. This feature allowed us to determine the activation energy of the reversible P–B bond cleavage in **3b** by temperature dependent dynamic  $^{19}\text{F}$  NMR spectroscopy. From the coalescence of the respective pairs of *ortho*-F resonances of the diastereotopic  $\text{C}_6\text{F}_5$  groups at boron we obtained the Gibbs activation energy of phosphane–borane dissociation in **3b** at  $\Delta G_{\text{dis}}^\ddagger$  (298 K) =  $12.1 \pm 0.3$  kcal mol $^{-1}$ . Thus, the FLP **3b** is a weak internal phosphane–borane adduct. It opens rapidly with a P–B bond dissociation energy of  $<12$  kcal mol $^{-1}$ .

Consequently, the FLP **3b** reacts very rapidly with dihydrogen.  $\text{H}_2$  is heterolytically cleaved by **3b** at  $-20$  °C with formation of the zwitterionic  $[\text{P}]^+\text{-H}/[\text{B}]^-\text{-H}$  product **4b** (Scheme 4 and Fig. 3) [40].

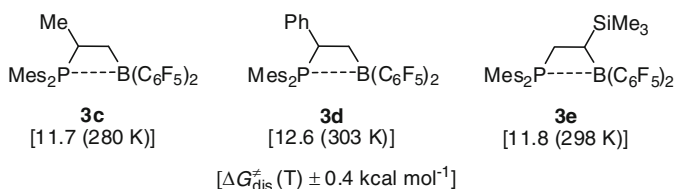
We prepared a variety of related bridge-substituted vicinal P/B FLPs analogously by hydroboration of the respective alkenyldimesitylphosphanes with Piers' borane  $[\text{HB}(\text{C}_6\text{F}_5)_2]$ , the compounds **3c–e** being typical examples (Scheme 5) [48]. Their NMR spectra indicated internal P–B coordination. Due to the presence of a chiral carbon center in the bridge, each of these compounds features pairs of



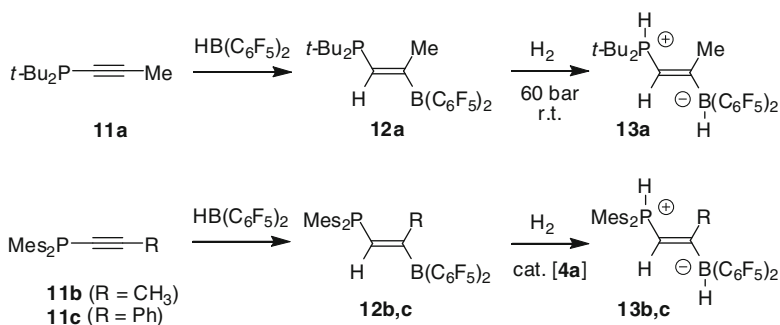
**Scheme 4** Formation of the FLP **3b** and its reaction with dihydrogen



**Fig. 3** Molecular structure of the H<sub>2</sub>-cleavage product **4b**



**Scheme 5** Examples of FLPs **3** and their activation barriers for P...B dissociation



**Scheme 6** Hydroboration of **11** with Piers' borane

diastereotopic  $C_6F_5$  substituents at boron. From the coalescence of their respective  $^{19}F$  NMR features we have determined the activation barrier of P–B bond dissociation ( $\Delta G_{dis}^\ddagger$ ) for each of these compounds (Scheme 5). They are similar in magnitude as found for **3b** (see above). Compound **3c** splits dihydrogen under our typical mild reaction conditions (2.5 bar  $H_2$ , r.t.), whereas the more bulky compounds **3d,e** were unreactive even at 60 bar  $H_2$  pressure at r.t. [48].

Hydroboration of di-*tert*-butylphosphinopropyne (**11a**) with  $[HB(C_6F_5)_2]$  gave the unsaturated FLP **12a**. It slowly splits dihydrogen under more forcing conditions (60 bar) to give the zwitterion **13a** (Scheme 6) [24]. The dimesitylphosphino-substituted FLPs **12b,c** were prepared analogously by hydroboration of the respective  $Mes_2P$ -substituted alkynes **11b,c**. These systems were themselves inert toward  $H_2$  under our typical conditions, but they rapidly accepted the  $H^+/H^-$  pair from the saturated FLP hydrogen activation product **4a**. This hydrogen transfer reaction was developed into a protocol for the formation of the products **13b,c** with dihydrogen catalyzed by the **3a/4a** FLP/FLP- $H_2$  pairs [24]. Both the products **13b,c** were characterized by X-ray diffraction (Fig. 4 for **13b**). The FLP **13b** was used as a selective catalyst for the hydrogenation of an enamine using ammonia borane ( $H_3NBH_3$ ) as a hydrogen source [49, 50].

The related unsaturated vicinal *cis*-FLPs **14** were prepared in different ways. Originally, such compounds were obtained by treatment of alkynylborates (e.g., **15**) with  $R_2PCl$  reagents [51–55]. The reaction proceeds with aryl migration from boron to the adjacent carbon atom and might be regarded as an early precursor of the 1,1-carboboration reaction [56, 57]. Grobe, Würthwein et al. [58] recently reported a remarkable related formation of an example of this by means of the intermediate formation of **16**. These *cis*-**14** systems do not seem reactive towards  $H_2$  but some of these bifunctional FLP-like compounds undergo interesting reactions with a variety of metal complexes (as do D. Bourissou's related phenylene-bridged FLP derivatives **17**) [59–62] (Scheme 7).

We have developed a convenient new synthetic pathway to the unsaturated P/B systems **14** by making use of the recently discovered advanced variants of the 1,1-carboboration reaction ([63]; see also [64–68]). For this purpose we treated,

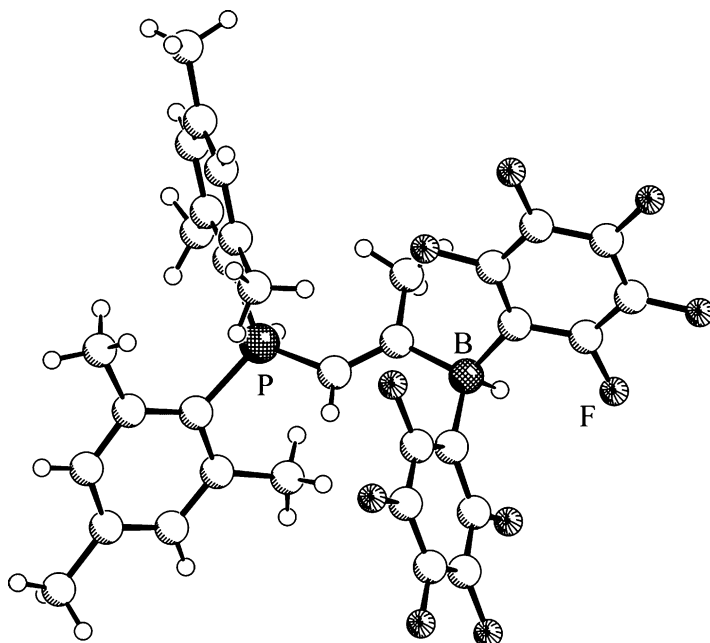
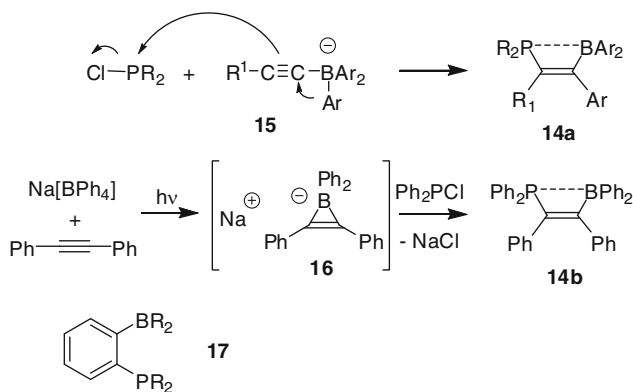
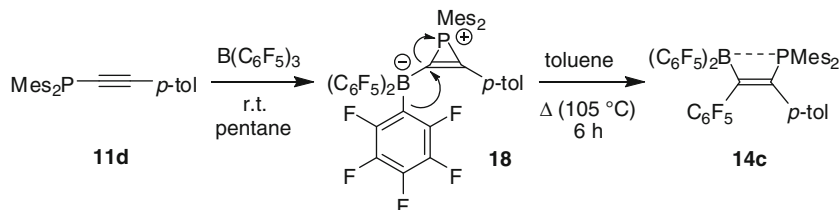


Fig. 4 Molecular structure of compound **13b**

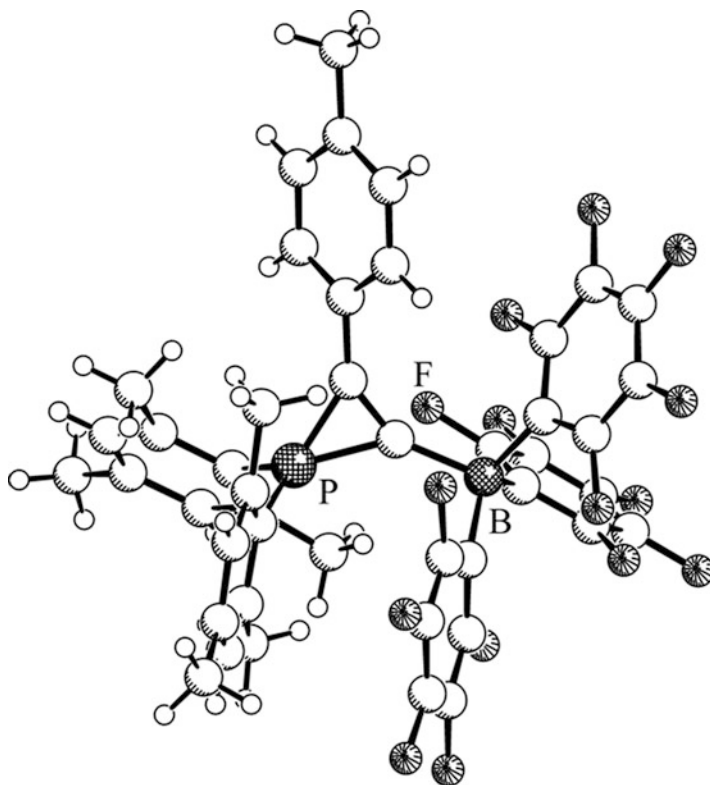


Scheme 7 Formation of the systems **14**

e.g., the dimesitylphosphinoacetylene derivative **11d** (Scheme 8) with  $\text{B}(\text{C}_6\text{F}_5)_3$  [69, 70] at room temperature in pentane. Under these conditions  $\text{B}(\text{C}_6\text{F}_5)_3$  adds to the alkyne and initiates migration of the  $\text{Mes}_2\text{P}$  moiety along the acetylenic carbon framework. After 30 min reaction time we isolated the product **18** [71]. The X-ray crystal structure analysis of **18** revealed the presence of the unsaturated cationic three-membered heterocycle to which the borate counter anion is bonded (Fig. 5).



**Scheme 8** Pathway to compound **14c**



**Fig. 5** A view of the molecular structure of the zwitterionic phosphonium-borate betaine **18**

This class of compounds exhibits very characteristic NMR features [71, 72]; compound **18** shows, e.g., a  $^{31}\text{P}$  NMR resonance at  $\delta -137.8$  and a  $^{11}\text{B}$  NMR signal at  $\delta -16.5$ . In the phosphonium-borate **18** the dimesitylphosphino group had migrated about half way across the acetylenic  $\text{C}\equiv\text{C}$  bond. Heating to  $105^\circ\text{C}$  was necessary to complete the 1,1-carboration reaction to eventually give the product **14c**. Compound **14c** shows heteronucleic NMR resonances at  $\delta 14.6$  ( $^{31}\text{P}$ ) and  $\delta 0$  ( $^{11}\text{B}$ ), respectively. The X-ray crystal structure analysis revealed a

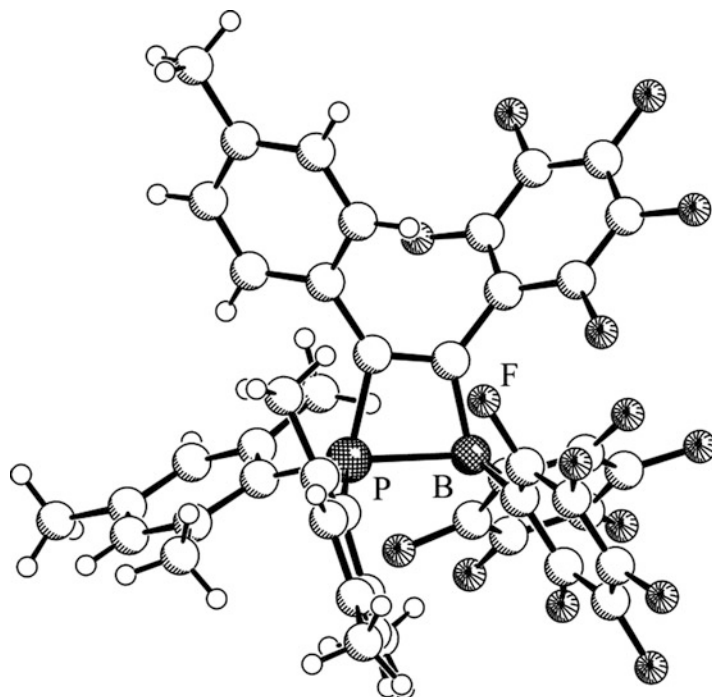


Fig. 6 Molecular structure of **14c**

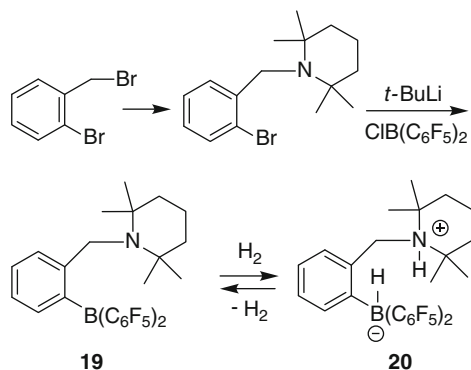
pronounced B–P interaction between the  $(\text{C}_6\text{F}_5)_2\text{B}$ - and  $\text{Mes}_2\text{P}$ -substituents which are *cis*-oriented at the bridging unsaturated  $\text{C}_2$ -framework (Fig. 6).

We prepared a variety of differently substituted P/B systems **14** by this advanced 1,1-carboboration method [73] and used them for an in depth analysis of the bonding between phosphorus and boron in such systems by solid state NMR techniques [23]. Both the  $^{11}\text{B}$  NMR isotropic chemical shifts and the nuclear electric quadrupolar coupling parameters were found to serve as sensitive experimental measures. In addition the large  $^{31}\text{P}$ - $^{11}\text{B}$  scalar spin–spin coupling of  $^1J \geq 50$  Hz, obtained from the  $^{31}\text{P}\{^1\text{H}\}$ -CPMAS NMR experiments, gave further evidence for the covalent P–B bonding component in such compounds.

### 3 Intramolecular N/B FLPs

Repo, Rieger et al. prepared the  $\text{C}_3$ -bridged N/B FLP **19** by a conventional route involving metalation. The N/B system **19** is an active frustrated Lewis pair that heterolytically cleaves dihydrogen to yield **20** ([74, 75]; see also [76]). The  $[\text{N}]^+\text{-H}/[\text{B}]^-\text{-H}$  zwitterion **20** was thoroughly characterized, including a neutron diffraction





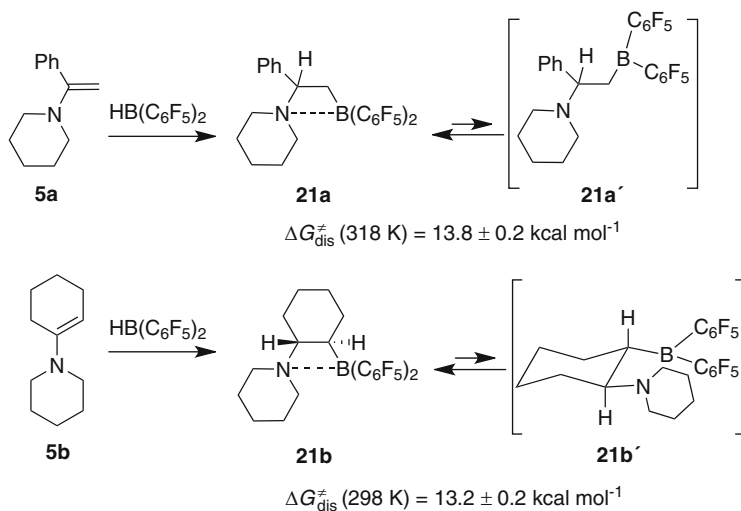
**Scheme 9** Formation of the N/B FLP **19** and its reaction with dihydrogen

study [77]. The system is special since it is one of the rare examples of reversible  $\text{H}_2$ -addition (and activation) by a frustrated Lewis pair [5, 26] (Scheme 9).

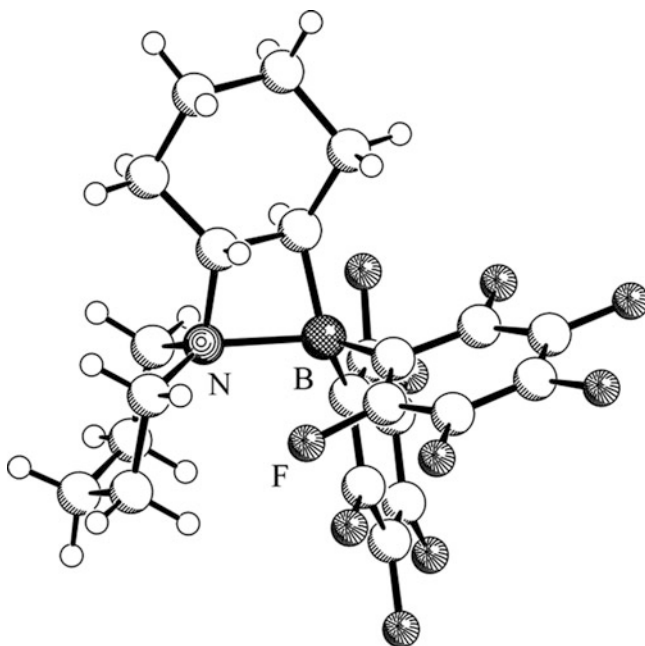
We prepared a series of vicinal N/B FLPs by enamine hydroboration [78]. A typical example is the reaction of the acetophenone derived enamine **5a** with  $[\text{HB}(\text{C}_6\text{F}_5)_2]$  which gave the phenyl substituted vicinal N/B FLP **21a** in good yield. Compound **21a** features a heterocyclic four-membered ring structure. The phenyl substituted bridge-carbon atom C1 is a chiral center. Therefore, we observed  $^1\text{H}/^{13}\text{C}$  NMR signals of the diastereotopic methylene groups of the piperidino substituent. The  $\text{C}_6\text{F}_5$  groups at boron are also diastereotopic in **21a** (at 298 K), which indicated N–B coordination. The related compound **21b** was obtained by  $[\text{HB}(\text{C}_6\text{F}_5)_2]$  hydroboration of the enamine piperidino cyclohexene (Scheme 10). The X-ray crystal structure analysis showed N–B coordination. Compound **21b** contains a heterocyclic four-membered ring structure (Fig. 7).

The N–B bond in compound **21a** is weak. This becomes evident from the dynamic  $^{19}\text{F}$  NMR spectra. The system shows signals of pairs of diastereotopic  $\text{C}_6\text{F}_5$  groups below ca. 320 K (Fig. 8). Warming leads to coalescence of both pairs of  $p\text{-C}_6\text{F}_5$  and  $m\text{-C}_6\text{F}_5$  signals, indicating rapid reversible N–B bond rupture and equilibration with the (invisible) reactive intermediate **21a'** on the  $^{19}\text{F}$  NMR time scale. From the dynamic  $^{19}\text{F}$  NMR spectra we estimate a barrier for the N–B opening in **21a** of  $\Delta G_{\text{dis}}^\ddagger$  (318 K) =  $13.8 \pm 0.2$  kcal mol $^{-1}$  (Fig. 8). A similar value was found for the ring opening process of the N/B FLP **21b** (Scheme 10).

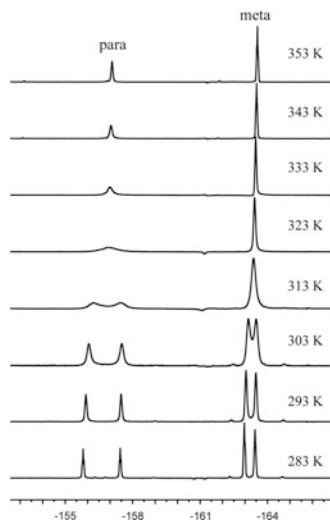
It appears that the intramolecular boron Lewis acid interaction with the *tert*-amine Lewis base in the FLPs **21** is slightly stronger than with the *tert*-phosphanes in **3**. However, the B–N bonds in the systems **21** must still be regarded as being weak (bond dissociation energies  $<13$  kcal mol $^{-1}$ ). These LA–LB bonds open and close rapidly. Both the N/B FLPs **21a** and **21b** react readily with dihydrogen to yield the ammonium/hydridoborate zwitterions **22a** and **22b**, respectively. Both were characterized by X-ray diffraction (**22a**, Fig. 9) and by spectroscopy [**22a**:  $^{11}\text{B}$  NMR:  $\delta$  –22.8 (d,  $^1J_{\text{BH}}$  ~80 Hz),  $^1\text{H}$  NMR:  $\delta$  3.08 (br, 1:1:1:1 q, [B]-H),  $\delta$  7.46 ([N]-H)] (Scheme 11).



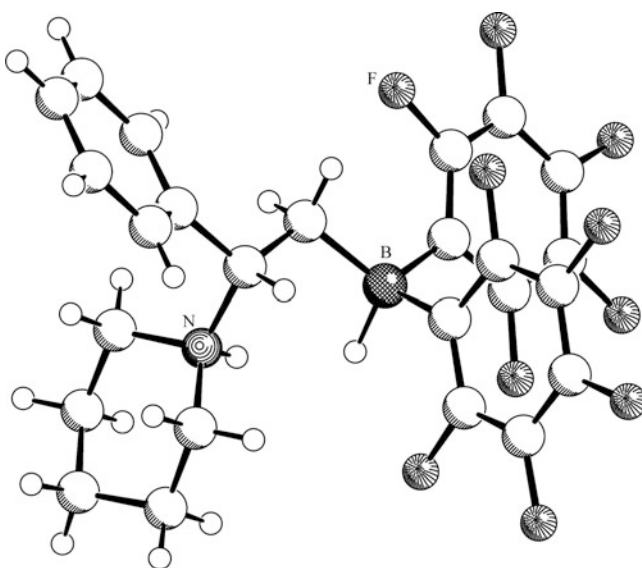
**Scheme 10** Formation and ring opening of the FLPs **21a** and **21b**



**Fig. 7** Molecular structure of the N/B FLP **21b** (N–B = 1.824(6) Å)



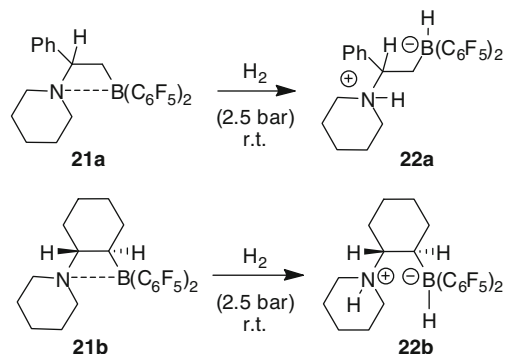
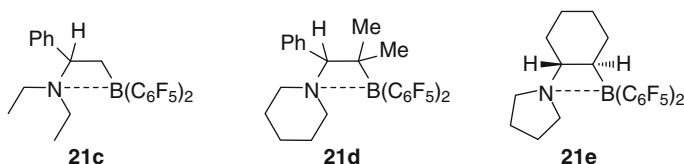
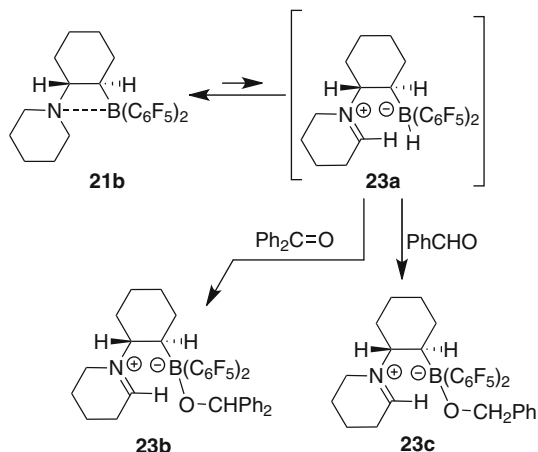
**Fig. 8** Temperature dependent dynamic  $^{19}\text{F}$  NMR spectra of the N/B FLP **21a**



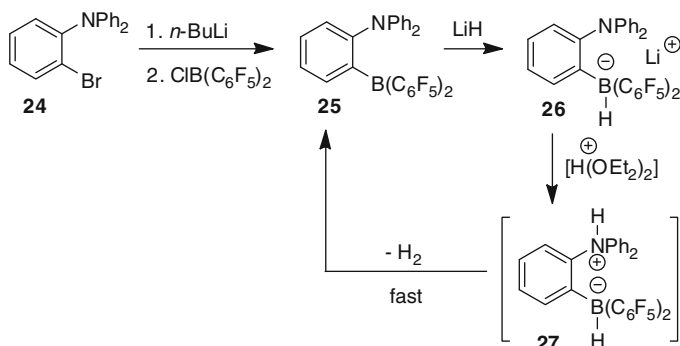
**Fig. 9** A view of the molecular structure of the ammonium/hydridoborate  $\text{H}_2$ -activation product **22a**

We prepared a variety of such vicinal N/B FLPs by means of the enamine hydroboration reaction (Scheme 12). The compounds **21c,d** did not react with dihydrogen under our typical conditions.

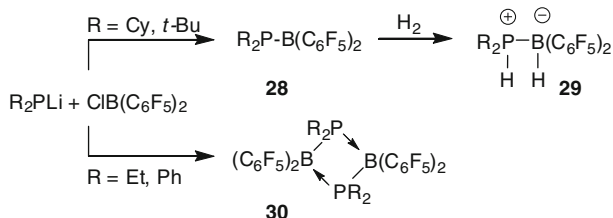
The nitrogen containing FLP **21b** shows a chemical peculiarity that appears upon its treatment with aldehydes or ketones. It is well known that  $\text{B}(\text{C}_6\text{F}_5)_3$  is able

**Scheme 11** Dihydrogen splitting with N/B FLPs **21a,b****Scheme 12** Examples of N/B FLPs **21****Scheme 13** Reactions of the FLP **21b** with organic carbonyl compounds

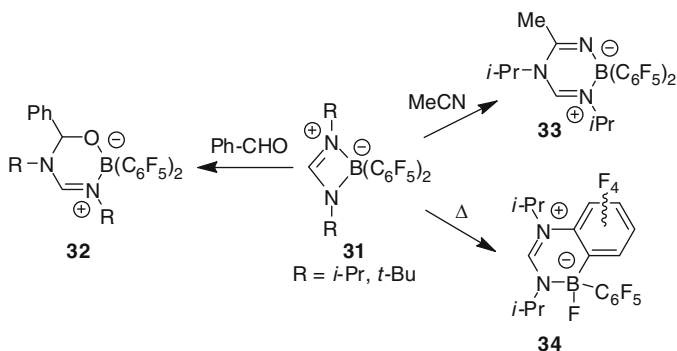
to abstract hydride anion from the  $\alpha$ -position of tertiary amines [37, 79–84]. In the case of the N/B FLP **21b** this could lead, e.g., to the formation of the iminium/hydridoborate zwitterion **23a** (Scheme 13). Without added reagents we did not observe its formation. However, added benzaldehyde or benzophenone



**Scheme 14** Generation of compound **27** and its loss of dihydrogen



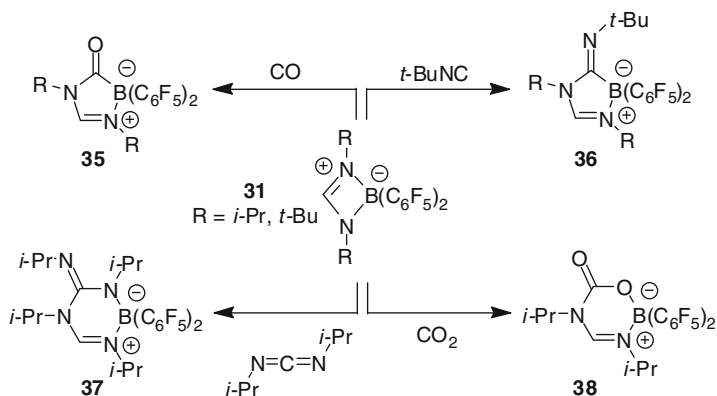
**Scheme 15** Phosphidoborane FLPs



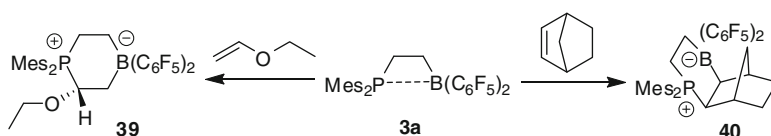
**Scheme 16** FLP behavior of a boron-amidinate

resulted in the formation of the respective trapping products, namely the zwitterionic systems **23b** and **23c**, respectively [78].

Previously, Piers reported the synthesis of a phenylene-bridged N/B system **25**. The separate addition of hydride followed by protonation may have generated the ammonium/hydridoborate system **27**, which was labile with regard to rapid H<sub>2</sub> elimination (Scheme 14) ([85]; see also [86]).



**Scheme 17** Reactions of the boron-amidinate **31**

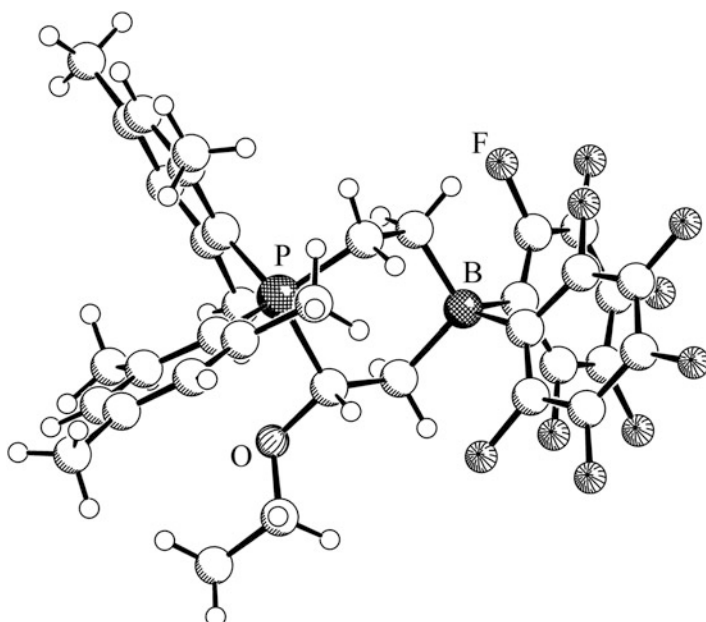


**Scheme 18** Olefin addition reactions to the FLP **3a**

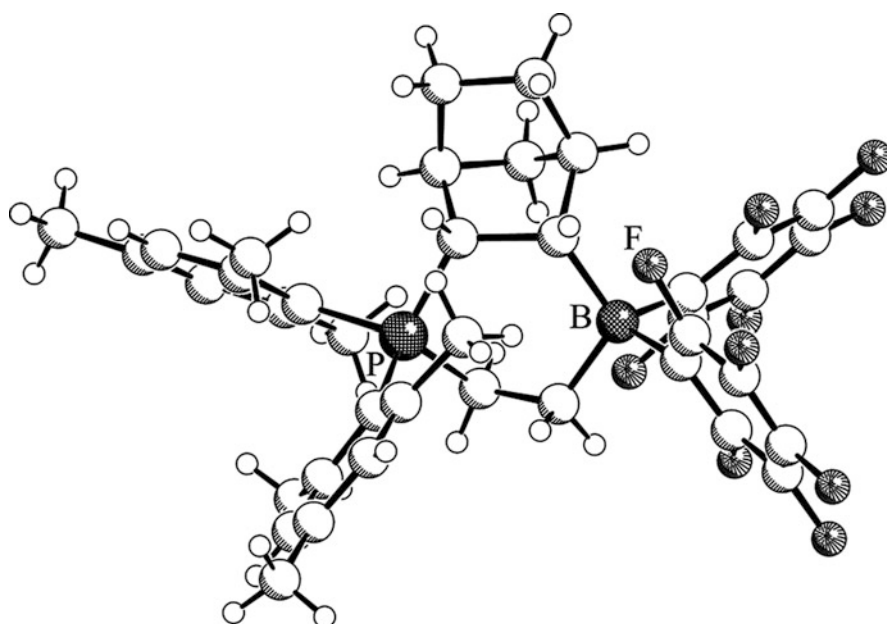
The monomeric phosphido-boranes  $\text{R}_2\text{P}-\text{B}(\text{C}_6\text{F}_5)_2$  **28** ( $\text{R}$  = cyclohexyl or *tert*-butyl) show a related FLP behavior. They react slowly at 60 °C with dihydrogen to give the phosphane–borane adducts  $\text{R}_2\text{HP}-\text{BH}(\text{C}_6\text{F}_5)_2$  **29**. In contrast, the dimeric phosphido–boranes  $[\text{R}_2\text{P}-\text{B}(\text{C}_6\text{F}_5)_2]_2$  **30** did not react with  $\text{H}_2$  under these conditions (Scheme 15) [87, 88].

Stephan and coworkers have recently shown that boron-amidinate  $\text{HC}(\text{RN})_2\text{B}(\text{C}_6\text{F}_5)_2$  **31** ( $\text{R}$  = *i*-Pr, *t*-Bu) react with benzaldehyde to give **32** ( $\text{R}$  = *i*-Pr, *t*-Bu). In addition, these species were also found to react with MeCN to give **33**. These reactions are thought to proceed via the ring opening of the boron-amidinate, although this could not be confirmed spectroscopically. However, this proposition was supported by thermolysis of the boron-amidinate which gave **34** (Scheme 16) [89].

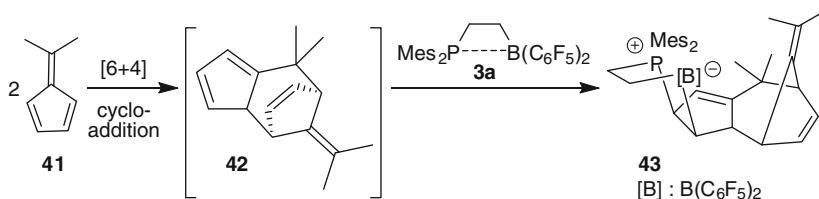
The systems **31** were also shown to insert CO and isonitriles into the B–N bond to yield the respective five-membered heterocycles **35** and **36**. Typically, **31** also reacts with a carbodiimide to give **37** and with carbon dioxide to yield the product **38** [89] (Scheme 17).



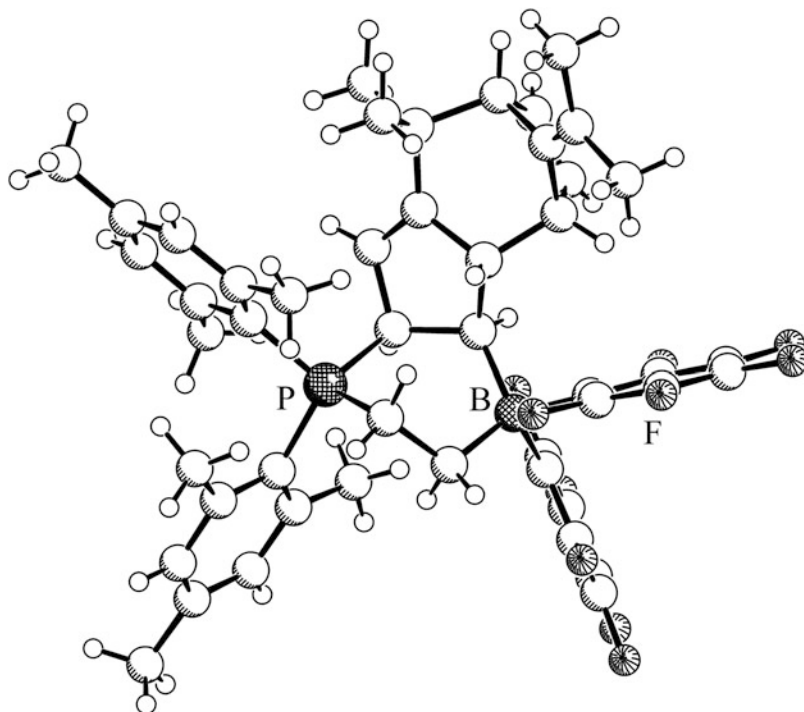
**Fig. 10** Molecular structure of compound 39



**Fig. 11** A view of the framework of the molecular structure of 40



**Scheme 19** Trapping of a fulvene dimer by FLP **3a**



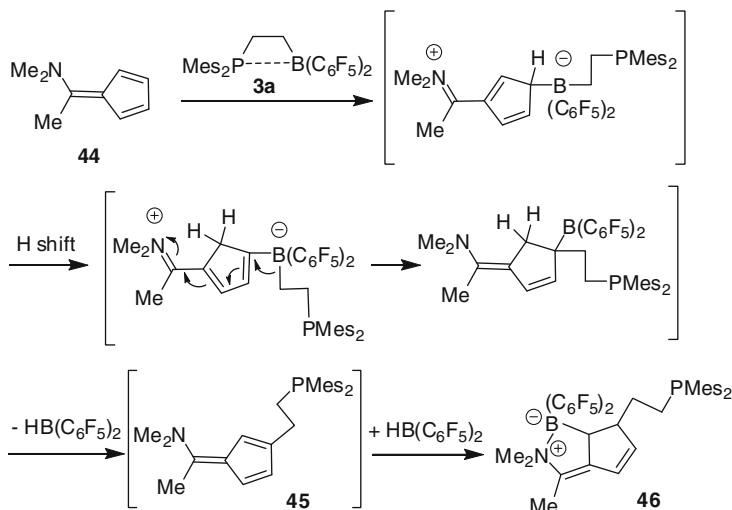
**Fig. 12** A projection of the framework structure of compound **43**

## 4 FLP Reactions with $\pi$ -Systems and More

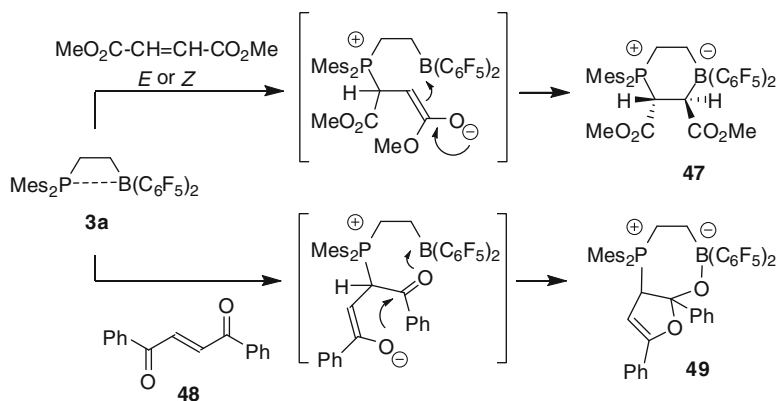
FLPs often add to olefinic carbon–carbon  $\pi$ -systems [7, 36, 38, 90–92]. A typical example is the reaction of the intramolecular FLP **3a** with ethylvinylether. The frustrated Lewis pair adds to the electron-rich carbon–carbon double bond regioselectively to yield the six-membered heterocyclic product **39** (Scheme 18) [90]. The product was characterized by X-ray diffraction (Fig. 10) and was shown to exhibit a typical chair-like conformation of the central framework [93].

The FLP **3a** adds cleanly to the norbornene C=C double bond to give selectively the *exo*-2,3-P/B addition product **40**. Although only this product was observed,





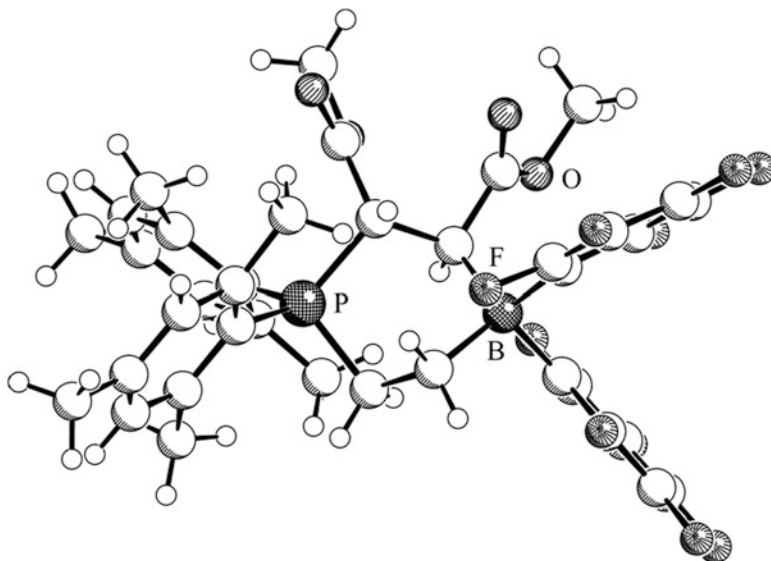
**Scheme 20** Reaction of an aminofulvene with FLP **3a**



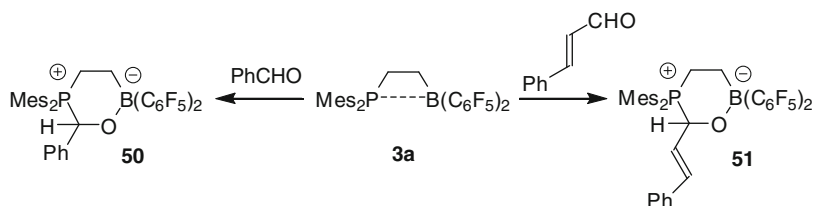
**Scheme 21** Reaction of FLP **3a** with activated alkenes

another possible rearranged product was calculated to be thermodynamically slightly favored. The selective formation of **40** without any of the typical norbornyl cation rearrangement products is in accord with the result of a computational study that indicated an asynchronous concerted 1,2-P/B FLP addition pathway of **3a** to norbornene from the *exo*-face (Fig. 11 for the structure of compound **40**) [90, 93].

A similar reaction was observed upon treatment of the FLP **3a** with 6,6-dimethylpentafulvene (**41**) in a 1:2 molar ratio. In this case the frustrated Lewis pair trapped the (otherwise unobserved) [6+4] fulvene dimer **42** by 1,2-P/B addition to one of its C=C double bonds (Scheme 19 and Fig. 12) to yield **43** [94].



**Fig. 13** A view of the molecular structure of compound **47**

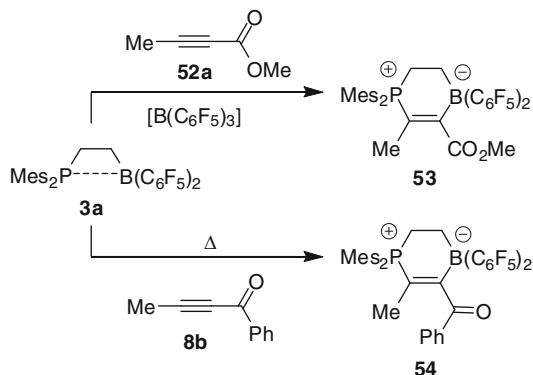


**Scheme 22** Reaction of FLP **3a** with aldehydes

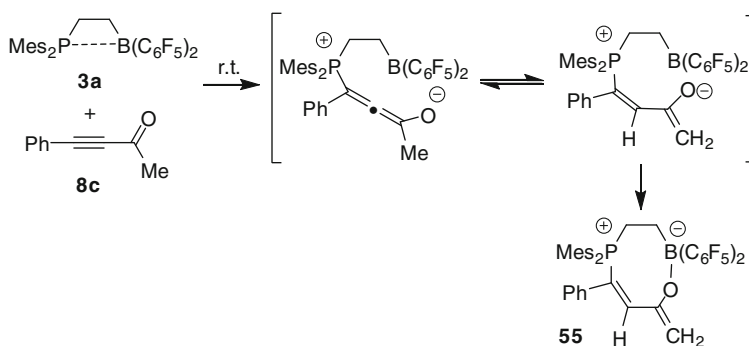
6-Dimethylamino-6-methylpentafulvene (**44**) undergoes a curious reaction with the FLP **3a** [95]. It readily forms the product **46** by a sequence that involves B–C bond cleavage. We had to assume that a retro-hydroboration reaction took place along the favored pathway (Scheme 20) that eventually was completed by addition of the in situ generated  $[\text{HB}(\text{C}_6\text{F}_5)_2]$  reagent to the substituted fulvene derivative **45**.

The FLP **3a** reacts with dimethylfumarate by 1,2-P/B addition to the activated carbon–carbon double bond to give the six-membered heterocycle **47** that features the pair of  $-\text{CO}_2\text{Me}$  substituents in *trans*-1,2-positions. The same product is obtained from the reaction of **3a** with dimethylmaleate, which indicates a conventional step-wise reaction mechanism (Scheme 21 and Fig. 13). A closely related reaction takes place upon treatment of **3a** with diphenylbutendione (**48**), only in this case O–B bond formation is favored over C–B bond formation in the second step to yield the product **49** (Scheme 21) [96].

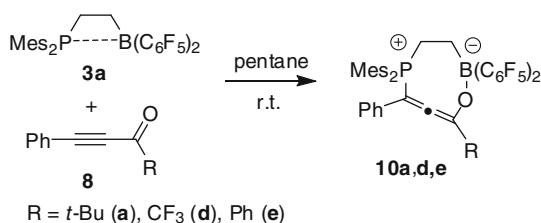
In the formation of the product **49** we see the involvement of the carbonyl functionality. This is often observed in FLP reactions. Typical examples are the 1,2-carbonyl addition reactions of **3a** to reactive aldehydes, such as benzaldehyde



**Scheme 23** Reaction of FLP **3a** with ynones



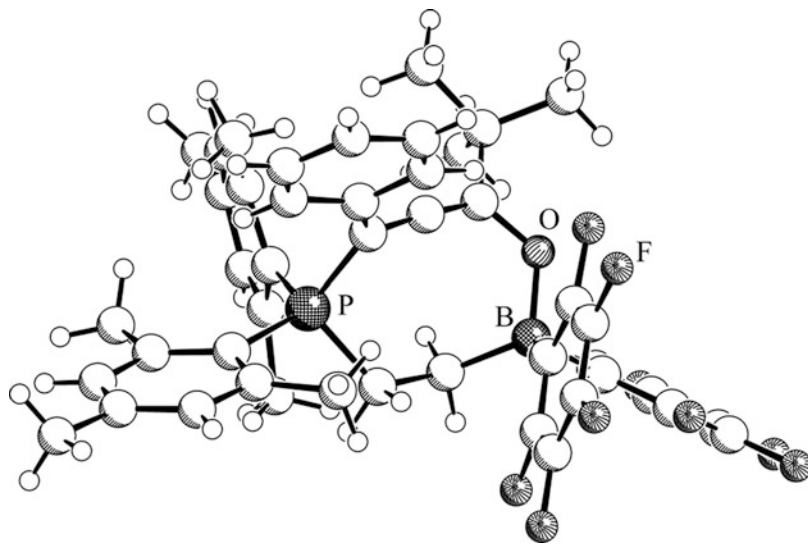
**Scheme 24** 1,4-Addition of FLP **3a** to the ynone **8c**



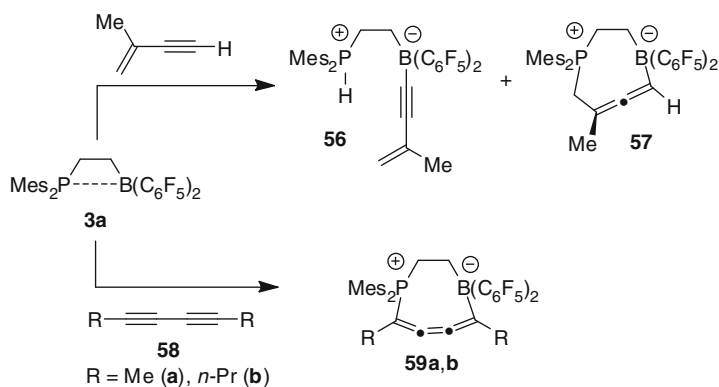
**Scheme 25** 1,4-Addition of FLP **3a** to non-enolizable conjugated ynones

(to give **50**) [97]. In a direct competition the addition of **3a** to the  $-\text{CH}=\text{O}$  group in *trans*-cinnamaldehyde forming compound **51** is strongly favored over any addition to the conjugated carbon–carbon double bond (Scheme 22) [90].

The situation which arises upon reacting the intramolecular P/B FLP **3a** with acetylenic esters **52** or conjugated ynones **8** is more subtle. The acetylenic ester **52a** itself was not reactive enough to allow for a clean product formation upon treatment with the intramolecular FLP **3a**. However, by preactivating **52a** with  $\text{B}(\text{C}_6\text{F}_5)_3$  the



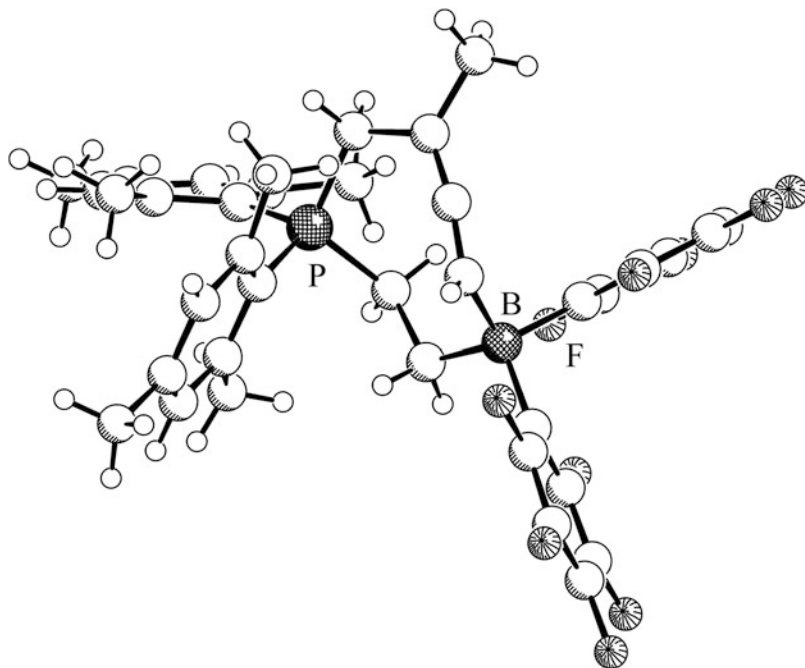
**Fig. 14** A view of the molecular structure of the product **10a** ( $R = t\text{-Bu}$ )



**Scheme 26** Cyclic cumulene formation from FLP **3a**

reaction proceeded to give the 1,2-addition product (**53**) of **3a** to the  $\text{C}\equiv\text{C}$  triple bond of the substrate **52a** [96]. The more reactive conjugated ynone **8b** did not require any extra activation to react with **3a**. It formed the six-membered addition product **54** when heated under reflux (Scheme 23) [39].

However, the formation of the six-membered products is an exception in the addition reaction of an intramolecular vicinal FLP to conjugated ynone substrates. Usually the formation of eight-membered heterocyclic compounds involving participation of the carbonyl oxygen atom is thermodynamically favored [39]. A typical example arose when the FLP **3a** was reacted at room temperature with the ynone **8c** to give the eight-membered addition product **55**. Apparently, **55** is



**Fig. 15** A view of the molecular structure of the eight-membered heterocyclic allene **57**

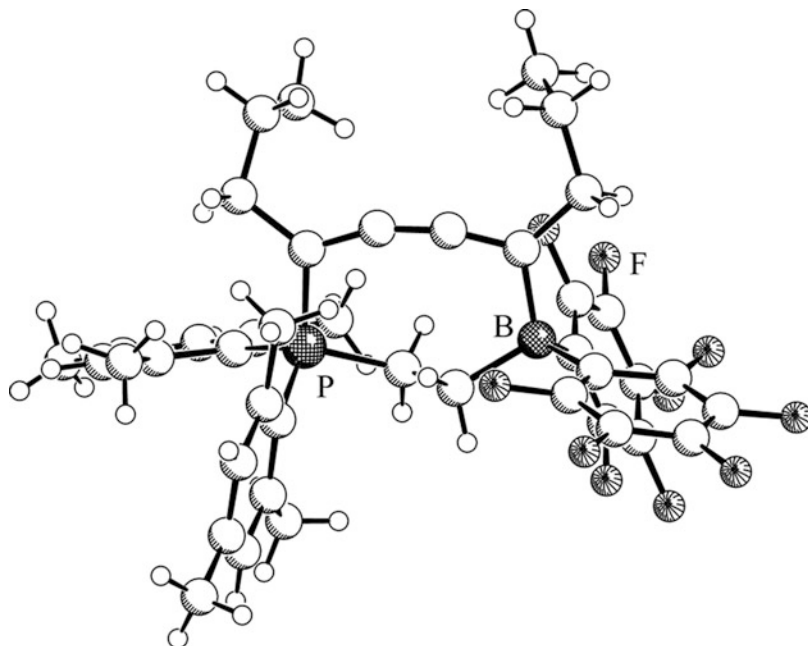
formed in a two step reaction sequence involving a tautomerization step before finally closing the medium sized ring by B–O bond formation (Scheme 24).

We also reacted a series of non-enolizable conjugated ynones **8a,d,e** with the intramolecular P/B FLP **3a**. They all directly gave the respective eight-membered heterocyclic allenic boron enolate products **10** (Scheme 25 and Fig. 14) [39].

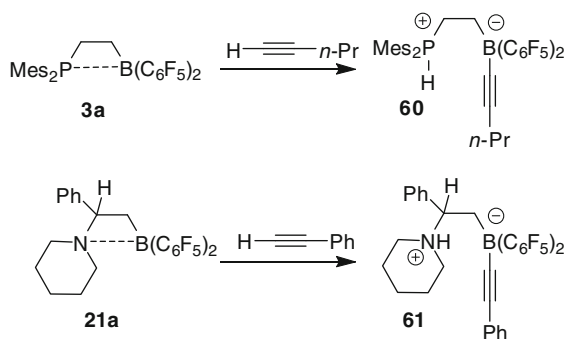
The chemistry of these compounds turned out to be important for our ongoing development of FLP-derived catalysts for the metal-free hydrogenation of electron-poor alkynes and alkenes [39].

Conjugated enynes seem to react similarly with FLPs [98, 99]. Treatment of 2-methyl-1,3-butenyne with  $\text{Mes}_2\text{PCH}_2\text{CH}_2\text{B}(\text{C}_6\text{F}_5)_2$  (**3a**) at room temperature gave a ca. 1:2 mixture of the products **56** and **57** (Scheme 26). Compound **56** is a very typical reaction product of FLPs with terminal acetylenes (for further examples see below). The medium ring-sized heterocyclic allene **57** is a remarkable compound, formed by a 1,4-FLP addition reaction to the conjugated  $\pi$ -system of the enyne reagent [98]. The X-ray crystal structure analysis of **57** (Fig. 15) revealed that this compound contains an almost regular allene unit – the angle between its substituents planes at the allene termini amounts to ca.  $75^\circ$ , i.e., not too far away from the  $90^\circ$  angle of an ideal allene structure. The central carbon atom of the cumulated C=C=C unit shows a typical allene  $^{13}\text{C}$  NMR resonance ( $\delta$  204.5 ppm).

A similar reaction took place when the intramolecular FLP **3a** was reacted with conjugated diynes **58a,b** (Scheme 26). We isolated the corresponding 1,4-FLP addition products **59a,b**. The X-ray crystal structure analysis of **59b** (Fig. 16)



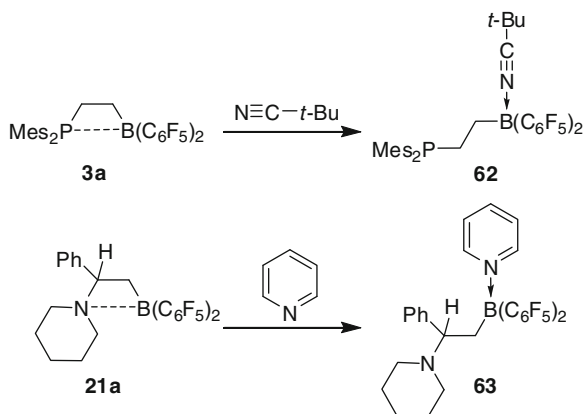
**Fig. 16** Molecular structure of the heterocyclic cumulene **59b**



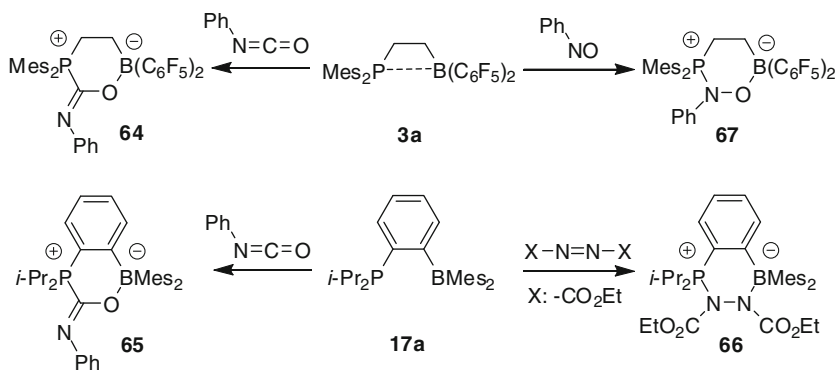
**Scheme 27** Reactions of FLPs with 1-alkynes

confirmed the formation of the substituted 1,2,3-butatriene substructure inside the strained eight-membered heterocyclic ring system. It exhibits some deviation of the C=C=C=C moiety from linearity featuring a pair of C–C–C angles of 161.1(2)° and 165.0(2)°. The P–CH<sub>2</sub>–CH<sub>2</sub>–B unit shows a dihedral angle of –129.8(2)°. This unit does not conformationally equilibrate at r.t. on the NMR time scale. Consequently, we observed pairs of diastereotopic C<sub>6</sub>F<sub>5</sub> substituents at boron and mesityl groups at phosphorus [98].

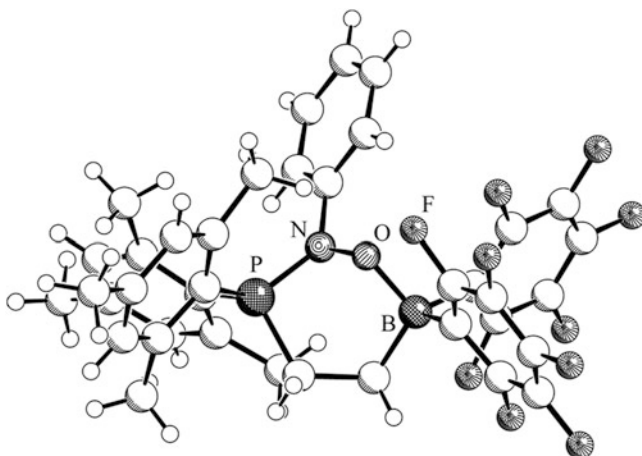
FLPs very often react with terminal acetylenes by means of deprotonation followed by boron–acetylide bond formation. The formation of compound **60** is a



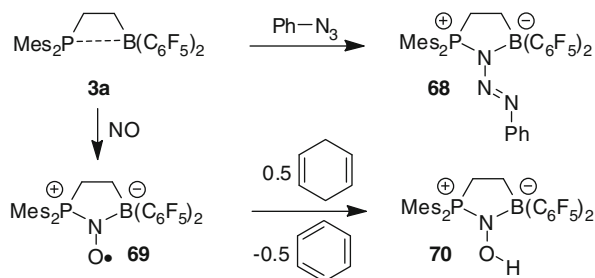
**Scheme 28** Reactions of FLPs with donor molecules



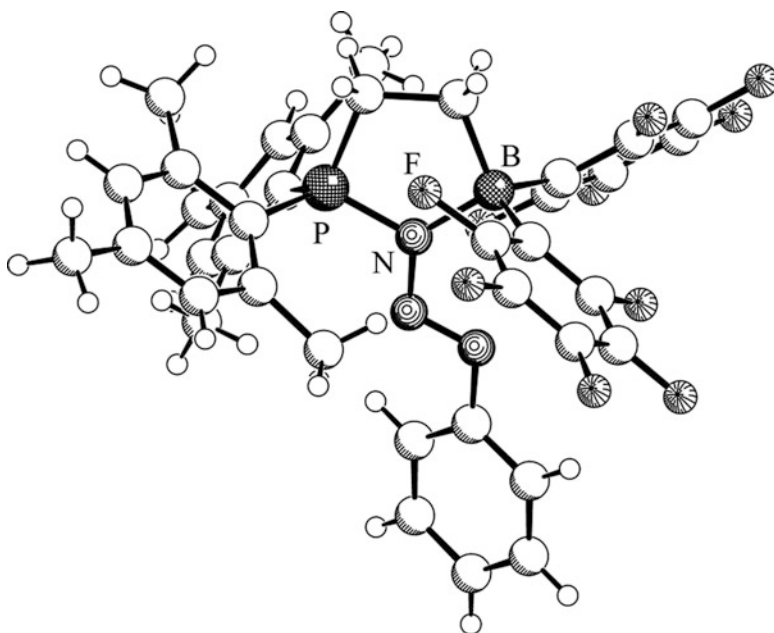
**Scheme 29** Various addition reactions to P/B FLPs



**Fig. 17** Molecular structure of the PhNO addition product **67**



**Scheme 30** Reactions of FLP **3a** with phenylazide and with nitric oxide



**Fig. 18** Molecular structure of compound **68**

typical example [90]. The N/B FLPs often undergo analogous  $\text{H}^+$  abstraction reactions with 1-alkynes, e.g., **21a**→**61** (Scheme 27) [78].

The FLP **3a** reacts with a variety of heteroatom containing substrates. Typical examples are the reactions with strong donor reagents such as nitriles (e.g., **62**), isonitriles, or pyridine. In all these cases the intramolecular  $\text{P} \cdots \text{B}$  interaction is lost with formation of the respective donor adducts to the borane functional group (Scheme 28) [97]. The N/B FLPs react similarly to form, e.g., **63** [78].

The heterocumulene phenylisocyanate adds to the intramolecular FLP **3a** via its reactive  $\text{C}=\text{O}$  functionality (**64**) [40, 97], as does the phenylene-bridged P/B system **17a** described by Bourissou et al. (**65**) (Scheme 29). The latter also adds to the  $-\text{N}=\text{N}-$  bond of DEAD ([59, 100]; see also [101]).



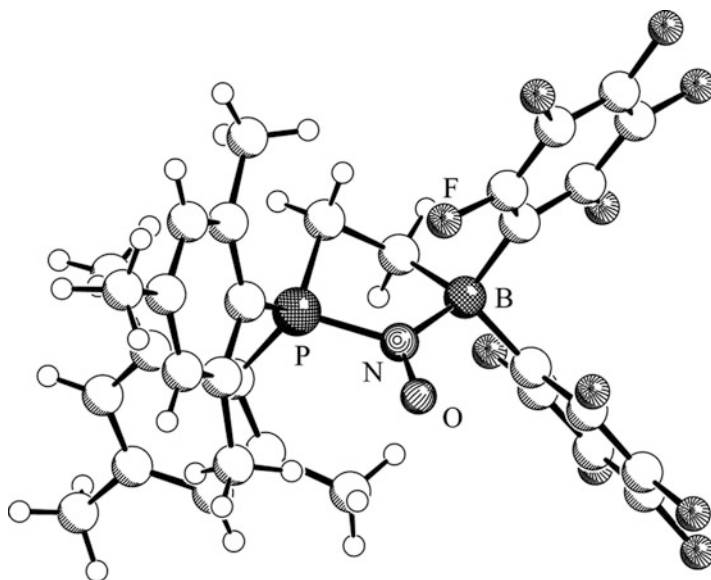
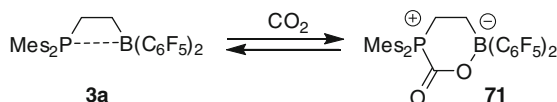


Fig. 19 Molecular structure of the FLPNO• aminoxyl radical **69**



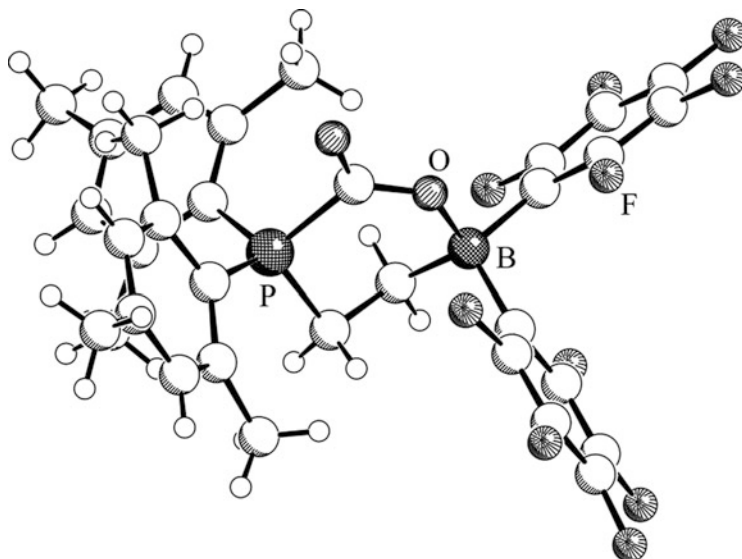
Scheme 31 Reactions of FLP **3a** with carbon dioxide

In a related study it was shown that  $\text{Mes}_2\text{PCH}_2\text{CH}_2\text{B}(\text{C}_6\text{F}_5)_2$  (**3a**) adds to the  $-\text{N}=\text{O}$  function of nitrosobenzene to yield the six-membered heterocyclic product **67** (Scheme 29 and Fig. 17) [97].

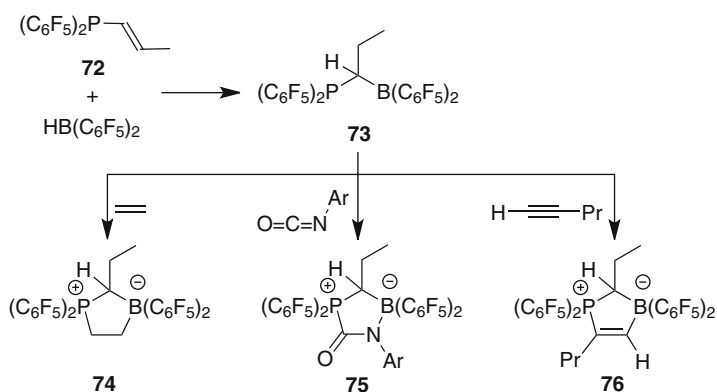
Some FLPs react cleanly with organic azides. The formation of the five-membered heterocyclic product **68** obtained by N,N-addition of **3a** to phenylazide is a typical example. In the crystal compound **68** features an alternating N–N=N bond sequence (1.374(2) Å/1.254(2) Å) (Scheme 30 and Fig. 18) [97].

The intramolecular FLP **3a** reacts readily with nitric oxide (NO) by N,N-addition to give the five-membered FLPNO• radical **69** in high yield. Compound **69** is the parent of a novel type of persistent aminoxyl radicals. It undergoes H-atom abstraction (HAA) reactions with a variety of hydrocarbon substrates to form the diamagnetic FLPNOH product **70** (Scheme 30). The FLPNO• radical **69** was characterized by X-ray diffraction (Fig. 19) [102, 103]. A detailed description of the chemistry of these new FLP derived nitroxide radicals is provided within this *Topics Curr. Chem.* volume by a separate contribution by T. W. Warren and G. Erker on “Radical Frustrated Lewis Pairs”.

There is great interest in the binding and chemical conversion of carbon dioxide. Frustrated Lewis pair chemistry has made some contributions to this field [104, 105]. We have observed that the intramolecular FLP **3a** is able to bind carbon dioxide rapidly under suitable conditions to form the 1,2-P/B addition product **71** (Scheme 31) [106].

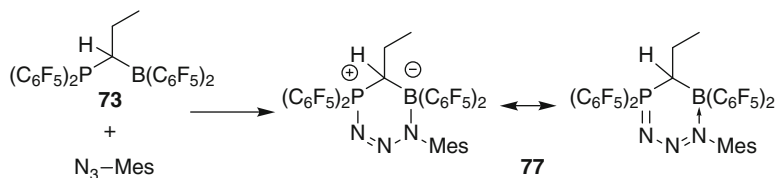


**Fig. 20** Molecular structure of the FLP-CO<sub>2</sub> addition product **71**

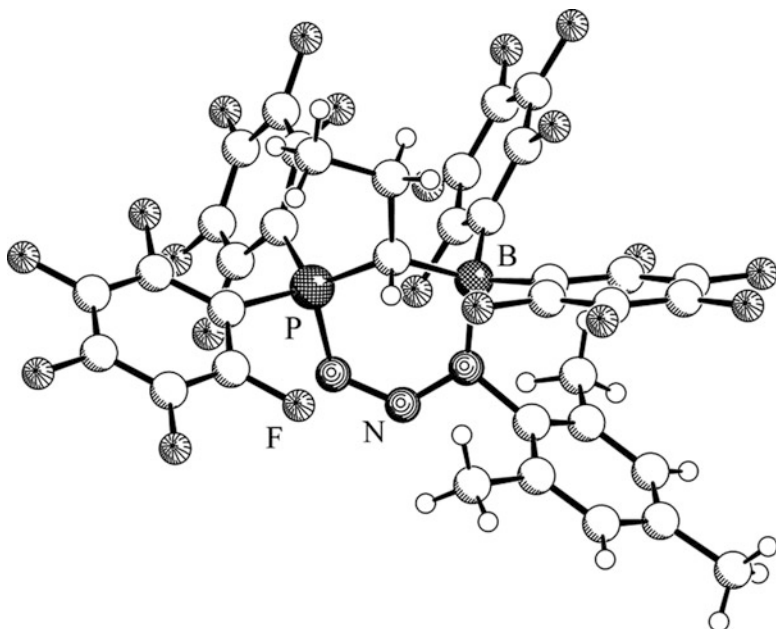


**Scheme 32** Formation and reactions of the geminal P/B FLP **73**

The compound precipitated in high yield as a white solid upon exposure of a pentane solution of **3a** to carbon dioxide at ambient temperature. When brought back into solution the adduct **71** rapidly lost CO<sub>2</sub> at temperatures above ca. -20 °C. Low temperature spectroscopy characterized the new compound (e.g., <sup>13</sup>C(C=O):δ 160.5 ppm). Crystallization at -36 °C gave single crystals of **71** suited for the X-ray crystal structure determination (Fig. 20). A detailed DFT analysis indicated that the addition reaction of the P/B FLP **3a** to a C=O bond of carbon dioxide is probably a concerted reaction. According to this analysis both the newly formed P-C and the B-O interactions have become almost equally established in the (rather symmetrical) transition state of this reaction [106].



**Scheme 33** Addition of mesitylazide to the geminal FLP **73**

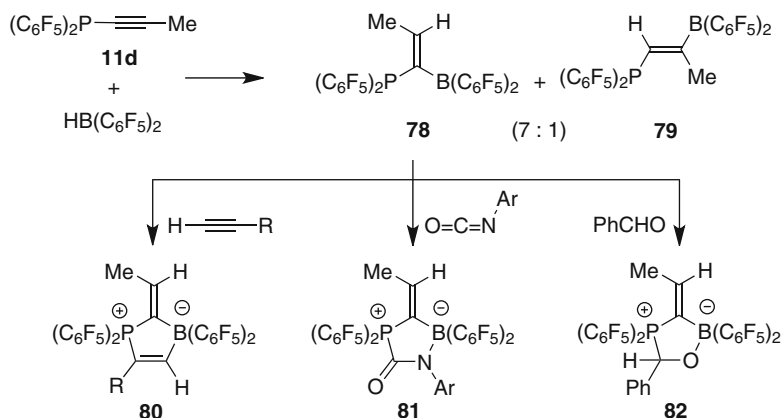


**Fig. 21** A view of the molecular structure of compound **77**

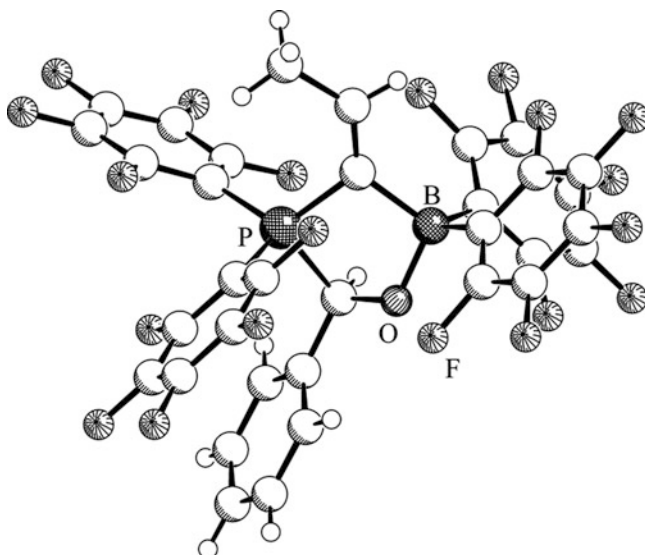
## 5 Geminal FLPs

In the literature one can find a variety of geminal P/B systems. Some of these were used as ligands in coordination chemistry (see for example [107–109]) whereas others were employed as Lewis acid catalysts [110, 111].

We have used weakly Lewis basic pentafluorophenyl substituted phosphane building blocks to construct electronically modified intramolecular FLPs. For that purpose we prepared the  $(\text{C}_6\text{F}_5)_2\text{P}$ -vinyl reagent and treated it with the  $\text{HB}(\text{C}_6\text{F}_5)_2$  hydroboration reagent. The ensuing hydroboration reaction proved to be regio-unselective, yielding a 2:1 mixture of the vicinal and geminal P/B-FLPs [112]. Introduction of a directing substituent resulted in regioselective geminal FLP formation. The  $(\text{C}_6\text{F}_5)_2\text{P}$ -propenyl (**72**) system added the  $\text{HB}(\text{C}_6\text{F}_5)_2$  reagent regioselectively to give the geminal FLP **73** in good yield (Scheme 32). NMR



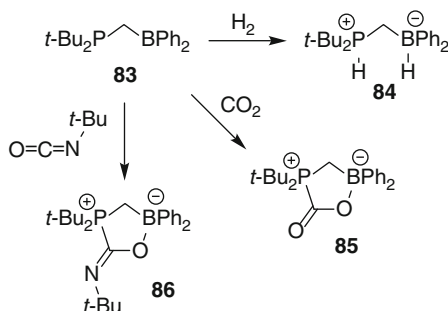
**Scheme 34** Formation and reactions of the geminal FLP **78**



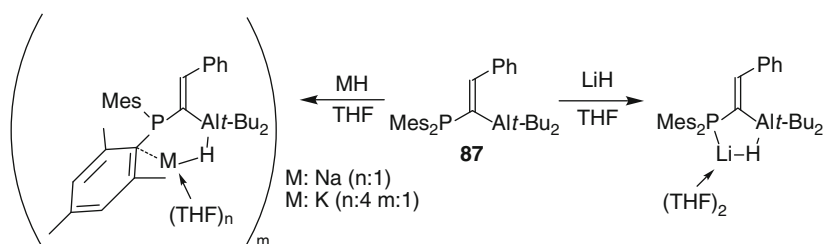
**Fig. 22** Molecular structure of compound **82**

spectroscopy indicated an open P/B FLP with no appreciable direct P...B interaction. This was evident from the  $^{11}\text{B}$  NMR resonance of **73** ( $\delta$  71) and its  $^{19}\text{F}$  NMR features ( $\Delta\delta_{\text{mp}} = 15.1$ ). Compound **73** did not activate dihydrogen under our typical conditions but reacted readily with a variety of unsaturated substrates by 1,2-addition, e.g., ethene, *p*-tolyl isocyanate, or 1-pentyne to yield **74**, **75**, and **76**, respectively [100–112].

The geminal P/B FLP **73** reacted with mesitylazide by 1,3-addition to give the six-membered heterocyclic product **77** (Scheme 33 and Fig. 21) [112]. The X-ray



**Scheme 35** Reactions of the FLP **83**



**Scheme 36** Metal hydride addition to compound **87**

crystal structure analysis revealed almost identical N1-N2 (1.304(3) Å) and N2-N3 (1.306(3) Å) bond lengths [113, 114].

Hydroboration of the electron deficient alkynyl phosphane **11d** with  $\text{HB}(\text{C}_6\text{F}_5)_2$  gave a 7:1 mixture of the products **78** and **79** [115]. The typical FLP reactivity of the non-internally coordinating major ( $\text{sp}^2$ ) $\text{C}_1$ -bridged compound **78** was probed from this mixture. It added cleanly to alkynes to give **80** and to aryl isocyanates affording **81** (Scheme 34). The addition product of, e.g., benzaldehyde **82** featured dynamic NMR spectra indicating reversible ring opening by P–C bond rupture (Scheme 34 and Fig. 22).

Lammertsma et al. prepared the  $\text{CH}_2$ -bridged P/B FLP **83** which contains phenyl substituents at boron [116]. This less Lewis acidic but markedly more Lewis basic FLP was able to activate dihydrogen affording **84**. It reacted with  $\text{CO}_2$  and added to the C=O bond of an isocyanate to give **85** and **86**, respectively (Scheme 35).

The FLP **87** even added alkali metal hydrides synergistically (Scheme 36) [117].

## 6 Conclusions

We started this work by studying P–B coordination and conformational behavior of intramolecular oligomethylene-linked phosphane/borane systems [42, 48] followed by the synthesis of the vicinal FLP  $\text{Mes}_2\text{PCH}_2\text{CH}_2\text{B}(\text{C}_6\text{F}_5)_2$  (**3a**). This system

turned out to be a very reactive frustrated Lewis pair that was able to react with a great variety of small molecules, often in a unique manner. The phosphane and the borane in this “archetypical” intramolecular FLP do interact but (as we have shown with the aid of its chiral derivatives) their interaction is weak. In addition a current DFT analysis by S. Grimme et al. has shown that the four-membered heterocyclic global minimum structure of **3a** rapidly opened to populate open local minimum structures of slightly higher energy content that have the C-P and C-B vectors either anti-periplanarly oriented or arranged in a gauche conformation. According to this calculation it is the reactive gauche type structure that undergoes the cooperative H–H activation reaction to yield the hydridoborate/phosphonium product [118–125]. This reaction has enabled us to develop protocols for metal-free FLP catalyzed hydrogenation reactions.

What is remarkable about FLP chemistry is that many such pairs of Lewis acids and Lewis bases, that have been prevented from neutralizing adduct formation by steric bulk or electronically, exhibit reactions where they act jointly with added substrates. A number of these reactions (e.g., hydrogen activation) are thermodynamically cooperative, some showing great kinetic preference by favoring concerted pathways (e.g., CO<sub>2</sub> addition and potentially FLP addition to some alkenes and to nitric oxide). This behavior, especially prone for the intramolecular FLPs, indicates that the typical FLP situation, characterized by the simultaneous presence of reactive free Lewis base and Lewis acid components in solution, bears the potential to find novel reactions in a rather simple way. From the exciting results FLP chemistry has furnished in the early stages of its development we are hopeful that this specific situation of having active non-quenched Lewis acids and bases co-existent in solution will result in discovering more such new reaction modes. We feel that intramolecular FLPs may play an important role in this forthcoming development.

**Acknowledgment** G. E. thanks his co-workers at Münster for their great contributions to this exciting field. We cordially thank the collaborating groups. For all of us it has been a pleasure to work together and discover new FLP reactions and FLP behavior. G. E. thanks the Deutsche Forschungsgemeinschaft, the Fonds der Chemischen Industrie, the Alexander von Humboldt-Stiftung, and the European Research Council for financial support.

## References

1. Lewis GN (1923) Valence and The Structure of Atoms and Molecules. Chemical Catalogue Company, New York
2. Brønsted JN (1923) Einige Bemerkungen über den Begriff der Säuren und Basen. Recl Trav Chim Pays-Bas 42:718–728
3. Stephens FH, Pons V, Baker TR (2007) Ammonia–borane: the hydrogen source *par excellence*? Dalton Trans 2613–2626
4. Hamilton CW, Baker TR, Staubitz A, Manners I (2009) B–N compounds for chemical hydrogen storage. Chem Soc Rev 38:279–293
5. Welch GC, San Juan RR, Masuda JD, Stephan DW (2006) Reversible, Metal-Free Hydrogen Activation. Science 314:1124–1126

- Welch GC, Stephan DW (2006) Facile Heterolytic Cleavage of Dihydrogen by Phosphines and Boranes. *J Am Chem Soc* 129:1880–1881
- McCahill JSJ, Welch GC, Stephan DW (2007) Reactivity of “Frustrated Lewis Pairs”: Three-Component Reactions of Phosphines, a Borane, and Olefins. *Angew Chem Int Ed* 46:4968–4971 (*Angew Chem* 119:5056–5059)
- Welch GC, Cabrera L, Chase PA, Hollink E, Masuda JD, Wel P, Stephan DW (2007) Tuning Lewis acidity using the reactivity of “frustrated Lewis pairs”: facile formation of phosphine-boranes and cationic phosphonium-boranes. *Dalton Trans* 3407–3414
- Stephan DW, Erker G (2010) Frustrated Lewis-Pairs: Metal-free Hydrogen Activation and More. *Angew Chem Int Ed* 49:46–76 (*Angew Chem* 122:50–81)
- Stephan DW (2008) “Frustrated Lewis pairs”: a concept for new reactivity and catalysis. *Org Biomol Chem* 6:1535–1539
- Stephan DW (2009) Frustrated Lewis pairs: a new strategy to small molecule activation and hydrogenation catalysis. *Dalton Trans* 3129–3136
- Stephan DW (2010) Activation of dihydrogen by non-metal systems. *Chem Commun* 46:8526–8533
- Erker G (2011) Frustrated Lewis pairs: Reactions with dihydrogen and other “small molecules”. *C R Chim* 4:831–841
- Erker G (2011) Organometallic frustrated Lewis pair chemistry. *Dalton Trans* 40:7475–7483
- Erker G (2011) Bio-Organometallic Chemistry, ansa-Metalloenes and Frustrated Lewis Pairs: Functional Group Chemistry at the Group 4 Bent Metalloenes. *Organometallics* 30:358–368
- Stephan DW (2012) “Frustrated Lewis pair” hydrogenations. *Org Biomol Chem* 10:5740–5746
- Parks DJ, Spence REH, Piers WE (1995) Bis(pentafluorophenyl)borane: Synthesis, Properties, and Hydroboration Chemistry of a Highly Electrophilic Borane Reagent. *Angew Chem Int Ed Engl* 34:809–811 (*Angew Chem* 107:895–897)
- Piers WE, Chivers T (1997) Pentafluorophenylboranes: from obscurity to applications. *Chem Soc Rev* 26:345–354
- Parks DJ, Piers WE, Yap GPA (1998) Synthesis, Properties, and Hydroboration Activity of the Highly Electrophilic Borane Bis(pentafluorophenyl)borane,  $\text{HB}(\text{C}_6\text{F}_5)_2$ . *Organometallics* 17:5492–5503
- Spence REH, Piers WE, Sun Y, Parvez M, MacGillivray LR, Zaworotko MJ (1998) Mechanistic Aspects of the Reactions of Bis(pentafluorophenyl)borane with the Dialkyl Zirconocenes  $\text{Cp}_2\text{ZrR}_2$  ( $\text{R} = \text{CH}_3, \text{CH}_2\text{SiMe}_3, \text{and } \text{CH}_2\text{C}_6\text{H}_5$ ). *Organometallics* 17:2459–2469
- Piers WE, Sun Y, Lee WM (1999) Zwitterionic metallocenes via reactions of organozirconocenes with highly electrophilic perfluorophenyl substituted boranes. *Top Catal* 7:133–143
- Spies P, Erker G, Kehr G, Bergander K, Fröhlich R, Grimme S, Stephan DW (2007) Rapid intramolecular heterolytic dihydrogen activation by a four-membered heterocyclic phosphane–borane adduct. *Chem Commun* 43:5072–5074
- Wiegand T, Eckert H, Ekkert O, Fröhlich R, Kehr G, Erker G, Grimme S (2012) New Insights into Frustrated Lewis Pairs: Structural Investigations of Intramolecular Phosphane–Borane Adducts by Using Modern Solid-State NMR Techniques and DFT Calculations. *J Am Chem Soc* 134:4236–4249
- Spies P, Schwendemann S, Lange S, Kehr G, Fröhlich R, Erker G (2008) Metal-Free Catalytic Hydrogenation of Enamines, Imines and Conjugated Phosphinoalkenylboranes. *Angew Chem Int Ed* 47:7543–7546 (*Angew Chem* 120:7654–7657)
- Schwendemann S, Tumay TA, Axenov KV, Peuser I, Kehr G, Fröhlich R, Erker G (2010) Metal-Free Frustrated Lewis Pair Catalyzed 1,4-Hydrogenation of Conjugated Metallocene Dienamines. *Organometallics* 29:1067–1069

26. Wang H, Fröhlich R, Kehr G, Erker G (2008) Heterolytic dihydrogen activation with the 1,8-bis(diphenylphosphino)naphthalene/B(C<sub>6</sub>F<sub>5</sub>)<sub>3</sub> pair and its application for metal-free catalytic hydrogenation of silyl enol ethers. *Chem Commun* 5966–5968
27. Chase PA, Jurca T, Stephan DW (2008) Lewis acid-catalyzed hydrogenation: B(C<sub>6</sub>F<sub>5</sub>)<sub>3</sub>-mediated reduction of imines and nitriles with H<sub>2</sub>. *Chem Commun* 1701–1703
28. Chen D, Wang Y, Klankermayer J (2010) Enantioselective Hydrogenation with Chiral Frustrated Lewis Pairs. *Angew Chem Int Ed* 49:9475–9478 (*Angew Chem* 122:9665–9668)
29. Geier SJ, Chase PA, Stephan DW (2010) Metal-free reductions of N-heterocycles *via* Lewis acid catalyzed hydrogenation. *Chem Commun* 46:4884–4886
30. Heiden ZM, Stephan DW (2011) Metal-free diastereoselective catalytic hydrogenations of imines using B(C<sub>6</sub>F<sub>5</sub>)<sub>3</sub>. *Chem Commun* 47:5729–5731
31. Ghattas G, Chen D, Pan F, Klankermayer J (2012) Asymmetric hydrogenation of imines with a recyclable chiral frustrated Lewis pair catalyst. *Dalton Trans* 41:9026–9028
32. Chase PA, Welch GC, Jurca T, Stephan DW (2007) Metal-Free Catalytic Hydrogenation. *Angew Chem Int Ed* 46:8050–8053, [9136] (*Angew Chem* 119:8196–8199 [9296])
33. Mahdi T, Heiden ZM, Grimme S, Stephan DW (2012) Metal-Free Aromatic Hydrogenation: Aniline to Cyclohexyl-amine Derivatives. *J Am Chem Soc* 134:4088–4091
34. Axenov KV, Kehr G, Fröhlich R, Erker G (2009) Catalytic Hydrogenation of Sensitive Organometallic Compounds by Antagonistic N/B Lewis Pair Catalyst Systems. *J Am Chem Soc* 131:3454–3455
35. Axenov KV, Kehr G, Fröhlich R, Erker G (2009) Functional Group Chemistry at the Group 4 Bent Metallocene Frameworks: Formation and “Metal-Free” Catalytic Hydrogenation of Bis(imino-Cp)zirconium Complexes. *Organometallics* 28:5148–5158
36. Sortais J-B, Voss T, Kehr G, Fröhlich R, Erker G (2009) 1,2-Olefin addition of a frustrated amine–borane Lewis pair. *Chem Commun* 7417–7418
37. Unverhau K, Lübke B, Wibbeling B, Fröhlich R, Kehr G, Erker G (2010) Frustrated Lewis Pair Reactions at the [3]Ferrocenophane Framework. *Organometallics* 29:5320–5329
38. Voss T, Sortais J-B, Fröhlich R, Kehr G, Erker G (2011) Alkene Addition of Frustrated P/B and N/B Lewis Pairs at the [3]Ferrocenophane Framework. *Organometallics* 30:584–594
39. Xu B-H, Kehr G, Fröhlich R, Wibbeling B, Schirmer B, Grimme S, Erker G (2011) Reaction of Frustrated Lewis Pairs with Conjugated Ynones–Selective Hydrogenation of the Carbon-Carbon Triple Bond. *Angew Chem Int Ed* 50:7183–7186 (*Angew Chem* 123:7321–7324)
40. Axenov K, Mömming CM, Kehr G, Fröhlich R, Erker G (2010) Structure and Dynamic Features of an Intramolecular Frustrated Lewis Pair. *Chem Eur J* 16:14069–14073
41. Jacobsen H, Berke H, Döring S, Kehr G, Erker G, Fröhlich R, Meyer O (1999) Lewis Acid Properties of Tris(pentafluorophenyl)borane. Structure and Bonding in L-B(C<sub>6</sub>F<sub>5</sub>)<sub>3</sub> Complexes. *Organometallics* 18:1724–1735
42. Spies P, Fröhlich R, Kehr G, Erker G, Grimme S (2008) Structural Importance of Secondary Interactions in Molecules: Origin of Unconventional Conformations of Phosphine-Borane Adducts. *Chem Eur J* 14:333–343
43. Bradley DC, Hursthouse MB, Motevalli M, Zheng DH (1991) The Preparation of 1:1 Phosphine: Triarylboron Complexes. The X-ray Crystal Structure of (C<sub>6</sub>F<sub>5</sub>)<sub>3</sub>B-PH<sub>3</sub>. *Chem Commun* 7–8
44. Lancaster SJ, Mountford AJ, Hughes DL, Schormann M, Bochmann M (2003) *Ansa*-metallocenes with B-N and B-P linkages: the importance of N-H...F-C hydrogen bonding in pentafluorophenyl boron compounds. *J Organomet Chem* 680:193–205
45. Denis J-M, Forintos H, Szelke H, Toupet L, Pham T-N, Madec P-J, Gaumont A-C (2003) B(C<sub>6</sub>F<sub>5</sub>)<sub>3</sub>-catalyzed formation of B-P bonds by dehydrocoupling of phosphine-boranes. *Chem Commun* 54–55
46. Chase PA, Parvez M, Piers WE (2006) Trimethylphosphine-tris(pentafluorophenyl)borane. *Acta Cryst E* 62:o5181–o5183
47. Welch GC, Holtrichter-Roessmann T, Stephan DW (2008) Thermal Rearrangement of Phosphine-B(C<sub>6</sub>F<sub>5</sub>)<sub>3</sub> Adducts. *Inorg Chem* 47:1904–1906



48. Spies P, Kehr G, Bergander K, Wibbeling B, Fröhlich R, Erker G (2009) Metal-free dihydrogen activation chemistry: structural and dynamic features of intramolecular P/B pairs. *Dalton Trans* 1534–1541
49. Spies P (2008) Von P-substituierten Zirconocenen zu metallfreier Wasserstoffaktivierung. Dissertation, Münster
50. Schwendemann S (2008) Hydrierungsreaktionen mit sterisch gehinderten Phosphan-Boran-Addukten. Diplomarbeit, Münster
51. Binger P, Köster R (1974) Organo-1,2-phosphaboretene. *J Organomet Chem* 73:205–210
52. Hagelee LA, Köster R (1977) Boron compounds XLIV: The influence of silicon on the formation of (Z/E)-tetrasubstituted ethylenes via 1-alkynylborates. *Synth React Inorg Met Org Chem* 7:53–67
53. Balueva AS, Erastov OA (1988) Synthesis of 3,4,6-borataoxaphosphoniacyclohexenes. *Russ Chem Bull* 37:151–153 (*Izv Akad Nauk SSSR Ser Khim* 163–165)
54. Grobe J, Martin R (1992) Alternativ-Liganden. XXIV Rhodium(I)-Komplexe mit P-Donor- und Sn- bzw. B-Akzeptor-Liganden. *Z Anorg Allg Chem* 607:146–152
55. Balueva AS, Nikonov GN (1993) Synthesis and properties of 1-diphenylboryl-2-diphenylphosphino-1,2-diphenylethene. *Russ Chem Bull* 42:341–343 (*Izv Akad Nauk Ser Khim* 378–380)
56. Wrackmeyer B (1995) 1,1-Organoboration of alkynylsilicon, -germanium, -tin and -lead compounds. *Coord Chem Rev* 145:125–156
57. Wrackmeyer B (2006) Metallacyclopentadienes and Related Heterocycles via 1,1-Organoboration of Alkyn-1-ylmetal Compounds. *Heteroat Chem* 17:188–208
58. Grobe J, Lütke-Brochtrup K, Krebs B, Läge M, Niemeyer H-H, Würthwein E-U (2006) Alternativ-Liganden, XXXVII. Phosphanliganden mit Bor als *Lewis*-acidem Zentrum: Synthese und Koordinationseigenschaften. *Z Naturforsch* 61b:882–895
59. Balueva AS, Nikonov GN, Arbizov BA, Musin RZ, Efremov YY (1991) Synthesis and some properties of *o*-borylphenylphosphine. *Russ Chem Bull* 40:2103–2105 (*Izv Akad Nauk SSSR Ser Khim* 2397–2399)
60. Bontemps S, Bouhadir G, Miqueu K, Bourissou D (2006) On the Versatile and Unusual Coordination Behavior of Ambiphilic Ligands *o*-R<sub>2</sub>P(Ph)BR'<sub>2</sub>. *J Am Chem Soc* 128:12056–12057
61. Fontaine F-G, Boudreau J, Thibault M-H (2008) Coordination Chemistry of Neutral (Ln)-Z Amphoteric and Ambiphilic Ligands. *Eur J Inorg Chem* 5439–5454
62. Bouhadir G, Amgoune A, Bourissou D (2010) Phosphine-Boranes and Related Ambiphilic Compounds: Synthesis, Structure, and Coordination to Transition Metals. *Adv Organomet Chem* 58:1–107
63. Kehr G, Erker G (2012) 1,1-Carboboration. *Chem Commun* 48:1839–1850
64. Chen C, Eweiner F, Wibbeling B, Fröhlich R, Senda S, Ohki Y, Tatsumi K, Grimme S, Kehr G, Erker G (2010) Exploring the Limits of Frustrated Lewis Pair Chemistry with Alkynes: Detection of a System that Favors 1,1-Carboboration over Cooperative 1,2-P/B-Addition. *Chem Asian J* 5:2199–2208
65. Chen C, Kehr G, Fröhlich R, Erker G (2010) Carbon–Carbon Bond Activation by 1,1-Carboboration of Internal Alkynes. *J Am Chem Soc* 132:13594–13595
66. Jiang C, Blacque O, Berke H (2010) Activation of Terminal Alkynes by Frustrated Lewis Pairs. *Organometallics* 29:125–133
67. Fan C, Piers WE, Parvez M, McDonald R (2010) Divergent Reactivity of Perfluoropentaphenylborole with Alkynes. *Organometallics* 29:5132–5139
68. Chen C, Voss T, Fröhlich R, Kehr G, Erker G (2011) 1,1-Carboboration of 1-Alkynes: A Conceptual Alternative to the Hydroboration Reaction. *Org Lett* 13:62–65
69. Massey AG, Park AJ, Stone FGA (1963) Tris(pentafluorophenyl)boron. *Proc Chem Soc* 212
70. Massey AG, Park AJ (1964) Perfluorophenyl derivatives of the elements I. Tris(pentafluorophenyl)boron. *J Organomet Chem* 2:245–250

71. Ekkert O, Kehr G, Fröhlich R, Erker G (2011) Phosphirenium-borate zwitterion: formation in the 1,1-carbo-boration reaction of phosphinylalkynes. *Chem Commun* 47:10482–10484
72. Möbus J, Bonnin Q, Ueda K, Fröhlich R, Itami K, Kehr G, Erker G (2012) The 1,1-Carbo-boration of Bis(alkynyl)phosphanes as a Route to Phosphole Compounds. *Angew Chem Int Ed* 51:1954–1957 (*Angew Chem* 124:1990–1993)
73. Ekkert O, Kehr G, Fröhlich R, Erker G (2011) P-C Bond Activation Chemistry: Evidence for 1,1-Carbo-boration Reactions Proceeding with Phosphorus-Carbon Bond Cleavage. *J Am Chem Soc* 133:4610–4616
74. Sumerin V, Schulz F, Atsumi M, Wang C, Nieger M, Leskelä M, Repo T, Pyykkö P, Rieger B (2008) Molecular Tweezers for Hydrogen: Synthesis, Characterization, and Reactivity. *J Am Chem Soc* 130:14117–14119
75. Sumerin V, Schulz F, Nieger M, Atsumi M, Wang C, Leskelä M, Pyykkö P, Repo T, Rieger B (2009) Experimental and theoretical treatment of hydrogen splitting and storage in boron–nitrogen systems. *J Organomet Chem* 694:2654–2660
76. Herrington TJ, Thom AJW, White AJP, Ashley AE (2012) Novel H<sub>2</sub> activation by a tris[3,5-bis(trifluoromethyl)phenyl]borane frustrated Lewis pair. *Dalton Trans* 41:9019–9022
77. Schulz F, Sumerin V, Heikkinen S, Pedersen B, Wang C, Atsumi M, Leskelä M, Repo T, Pyykkö P, Petry W, Rieger B (2011) Molecular Hydrogen Tweezers: Structure and Mechanism by Neutron Diffraction, NMR, and Deuterium Labeling Studies in Solid and Solution. *J Am Chem Soc* 133:20245–20257
78. Schwendemann S, Fröhlich R, Kehr G, Erker G (2011) Intramolecular frustrated N/B Lewis pairs by enamine hydroboration. *Chem Sci* 2:1842–1849
79. Millot N, Santini CC, Fenet B, Basset JM (2002) Formation and Characterization of Zwitterionic Stereoisomers from the Reaction of B(C<sub>6</sub>F<sub>5</sub>)<sub>3</sub> and NEt<sub>2</sub>Ph: (*E*)- and (*Z*)-[EtPhN<sup>+</sup>=CHCH<sub>2</sub>-B<sup>-</sup>(C<sub>6</sub>F<sub>5</sub>)<sub>3</sub>]. *Eur J Inorg Chem* 3328–3335
80. Liptau P, Neumann M, Erker G, Kehr G, Fröhlich R, Grimme S (2004) Responsive Iron Neighboring Group Participation in Amino-Substituent-Stabilized [3]ferrocenophane  $\alpha$ -Carbenium Ions: A Combined Theoretical and Experimental Study. *Organometallics* 23:21–25
81. Piers WE (2004) The Chemistry of Perfluoroaryl Boranes. *Adv Organomet Chem* 52:1–76
82. Focante F, Mercandelli P, Sironi A, Resconi L (2006) Complexes of tris(pentafluorophenyl)-boron with nitrogen-containing compounds: Synthesis, reactivity and metallocene activation. *Coord Chem Rev* 250:170–188
83. Sumerin V, Schulz F, Nieger M, Leskelä M, Repo T, Rieger B (2008) Facile Heterolytic H<sub>2</sub> Activation by Amines and B(C<sub>6</sub>F<sub>5</sub>)<sub>3</sub>. *Angew Chem Int Ed* 47:6001–6003 (*Angew Chem* 120:6090–6092)
84. Farrell JM, Heiden ZM, Stephan DW (2011) Metal-Free Transfer Hydrogenation Catalysis by B(C<sub>6</sub>F<sub>5</sub>)<sub>3</sub>. *Organometallics* 30:4497–4500
85. Roesler R, Piers WE, Parvez M (2003) Synthesis, structural characterization and reactivity of the amino borane 1-(NPh<sub>2</sub>)-2-[B(C<sub>6</sub>F<sub>5</sub>)<sub>2</sub>]C<sub>6</sub>H<sub>4</sub>. *J Organomet Chem* 680:218–222
86. Moebis-Sanchez S, Saffon N, Bouhadir G, Maron L, Bourissou D (2010) Hydrogen fluoride adduct of an amphiphilic phosphine–borane: NMR characterization and theoretical analysis of the bonding situation. *Dalton Trans* 39:4417–4420
87. Geier SJ, Gilbert TM, Stephan DW (2008) Activation of H<sub>2</sub> by Phosphinoboranes R<sub>2</sub>PB(C<sub>6</sub>F<sub>5</sub>)<sub>2</sub>. *J Am Chem Soc* 130:12632–12633
88. Geier SJ, Gilbert TM, Stephan DW (2011) Synthesis and Reactivity of the Phosphinoboranes R<sub>2</sub>PB(C<sub>6</sub>F<sub>5</sub>)<sub>2</sub>. *Inorg Chem* 50:336–344
89. Dureen MA, Stephan DW (2010) Reactions of Boron Amidinates with CO<sub>2</sub> and CO and Other Small Molecules. *J Am Chem Soc* 132:13559–13568
90. Mömning CM, Frömel S, Kehr G, Fröhlich R, Grimme S, Erker G (2009) Reactions of an Intramolecular Frustrated Lewis Pair with Unsaturated Substrates: Evidence for a Concerted Olefin Addition Reaction. *J Am Chem Soc* 131:12280–12289

91. Ullrich M, Seto KS-H, Lough AJ, Stephan DW (2009) 1,4-Addition reactions of frustrated Lewis pairs to 1,3-dienes. *Chem Commun* 2335–2337
92. Voss T, Chen C, Kehr G, Nauha E, Erker G, Stephan DW (2010) Cyclizations via Frustrated Lewis Pairs: Lewis Acid Induced Intramolecular Additions of Amines to Olefins and Alkynes. *Chem Eur J* 16:3005–3008
93. Mömming CM (2010) Reaktivität intramolekularer frustrierter LEWIS Paare: Fixierung kleiner Moleküle. Dissertation, Münster
94. Mömming CM, Kehr G, Fröhlich R, Erker G (2011) The frustrated Lewis pair induced formation of a pentafulvene [6+4] cycloaddition product. *Chem Commun* 47:2006–2007
95. Xu B-H, Mömming CM, Kehr G, Fröhlich R, Erker G (2012) Reaction of a 6-Dimethylaminopentafulvene with the  $\text{Mes}_2\text{PCH}_2\text{CH}_2\text{B}(\text{C}_6\text{F}_5)_2$  Frustrated Lewis Pair. *Chem Eur J* 18:1826–1830
96. Xu B-H, Adler Yanez RA, Nakatsuka H, Kitamura M, Fröhlich R, Kehr G, Erker G (2012) Reaction of Frustrated Lewis Pairs with Ketones and Esters. *Chem Asian J* 7:1347–1356
97. Mömming CM, Kehr G, Wibbeling B, Fröhlich R, Erker G (2010) Addition reactions to the intramolecular  $\text{mesityl}_2\text{P}-\text{CH}_2-\text{CH}_2-\text{B}(\text{C}_6\text{F}_5)_2$  frustrated Lewis pair. *Dalton Trans* 39:7556–7564
98. Mömming CM, Kehr G, Wibbeling B, Fröhlich R, Schirmer B, Grimme S, Erker G (2010) Formation of Cyclic Allene and Cumulene by Cooperative Addition of Frustrated Lewis Pairs to Conjugated Enynes and Diynes. *Angew Chem Int Ed* 49:2414–2417 (*Angew Chem* 122:2464–2467)
99. Feldhaus P, Schirmer B, Wibbeling B, Daniliuc CG, Fröhlich R, Grimme S, Kehr G, Erker G (2012) Frustrated Lewis pair addition to conjugated diynes: Formation of zwitterionic 1,2,3-butatriene derivatives. *Dalton Trans* 41:9135–9142
100. Moebs-Sanchez S, Bouhadir G, Saffon N, Maron L, Bourissou D (2008) Tracking reactive intermediates in phosphine-promoted reactions with ambiphilic phosphino-boranes. *Chem Commun* 3435–3437
101. Arbuzov BA, Nikonov GN, Balueva AS, Kamalov RM, Pudovik MA, Shagidullin RR, Plyamovatyi AK, Khadiullin RS (1991) Reaction of 1,2-borylphosphinoethene with phenyl isocyanate and the structure of the reaction products. *Russ Chem Bull* 40:2099–2102 (*Izv Akad Nauk SSSR Ser Khim* 2393–2396)
102. Cardenas AJP, Culotta BJ, Warren TH, Grimme S, Stute A, Fröhlich R, Kehr G, Erker G (2011) Capture of NO by a Frustrated Lewis Pair: A New Type of Persistent *N*-Oxyl Radical. *Angew Chem Int Ed* 50:7567–7571 (*Angew Chem* 123:7709–7713)
103. Sajid M, Stute A, Cardenas AJP, Culotta BJ, Hepperle JAM, Warren TH, Schirmer B, Grimme S, Studer A, Daniliuc CG, Fröhlich R, Petersen JL, Kehr G, Erker G (2012) *N,N*-Addition of Frustrated Lewis Pairs to Nitric Oxide: An Easy Entry to a Unique Family of Aminoxyl Radicals. *J Am Chem Soc* 134:10156–10168
104. Ashley AE, Thompson AL, O'Hare D (2009) Non-Metal-Mediated Homogeneous Hydrogenation of  $\text{CO}_2$  to  $\text{CH}_3\text{OH}$ . *Angew Chem Int Ed* 48:9839–9843 (*Angew Chem* 121:10023–10027)
105. Ménard G, Stephan DW (2010) Room Temperature Reduction of  $\text{CO}_2$  to Methanol by Al-Based Frustrated Lewis Pairs and Ammonia Borane. *J Am Chem Soc* 132:1796–1797
106. Mömming CM, Otten E, Kehr G, Fröhlich R, Grimme S, Stephan DW, Erker G (2009) Reversible Metal-Free Carbon Dioxide Binding by Frustrated Lewis Pairs. *Angew Chem Int Ed* 48:6643–6646 (*Angew Chem* 121:6770–6773)
107. Gloaguen Y, Alcaraz G, Pécharman A-F, Clot E, Vendier L, Sabo-Etienne S (2009) Phosphinoborane and Sulfidoborohydride as Chelating Ligands in Polyhydride Ruthenium Complexes: Agostic  $\sigma$ -Borane versus Dihydroborate Coordination. *Angew Chem Int Ed* 48:2964–2968 (*Angew Chem* 121:3008–3012)
108. Walker JM, Cox AM, Wang R, Spivak GJ (2010) Synthesis and Reactivity of  $[(\text{PhB}(\text{CH}_2\text{PPh}_2)_3-\kappa^3\text{P})\text{Ru}(\text{NCMe})_3]\text{PF}_6$  and Its Potential as a Transfer Hydrogenation Catalyst. *Organometallics* 29:6121–6124

109. Miller AJM, Labinger JA, Bercaw JE (2010) Homogeneous CO Hydrogenation: Ligand Effects on the Lewis Acid-Assisted Reductive Coupling of Carbon Monoxide. *Organometallics* 29:4499–4516
110. Schnurr A, Vitze H, Bolte M, Lerner H-W, Wagner M (2010) Rigid, Fluoroarene-Containing Phosphonium Borates and Boranes: Syntheses and Reactivity Studies. *Organometallics* 29:6012–6019
111. Schnurr A, Bolte M, Lerner H-W, Wagner M (2012) Cyclic Phosphonium Bis(fluoroaryl)-boranes – Trends in Lewis Acidities and Application in Diels-Alder Catalysis. *Eur J Inorg Chem* 112–120
112. Stute A, Kehr G, Fröhlich R, Erker G (2011) Chemistry of a geminal frustrated Lewis pair featuring electron withdrawing C<sub>6</sub>F<sub>5</sub> substituents at both phosphorus and boron. *Chem Commun* 47:4288–4290
113. Bebbington MWP, Bontemps S, Bouhadir G, Bourissou D (2007) Photoisomerizable Heterodienes Derived from a Phosphine Borane. *Angew Chem Int Ed* 46:3333–3336 (*Angew Chem* 119:3397–3400)
114. Kim Y, Hudnall TW, Bouhadir G, Bourissou D, Gabbai FP (2009) Azide ion recognition in water – CHCl<sub>3</sub> using a chelating phosphonium borane as a receptor. *Chem Commun* 3729–3731
115. Rosorius C, Kehr G, Fröhlich R, Grimme S, Erker G (2011) Electronic Control of Frustrated Lewis Pair Behavior: Chemistry of a Geminal Alkylidene-Bridged Per-pentafluorophenylated P/B Pair. *Organometallics* 30:4211–4219
116. Bertini F, Lyaskovskyy V, Timmer BJJ, de Kanter FJJ, Lutz M, Ehlers AW, Slootweg JC, Lammertsma K (2012) Preorganized Frustrated Lewis Pairs. *J Am Chem Soc* 134:201–204
117. Appelt C, Slootweg C, Lammertsma K, Uhl W (2012) A Phosphorus/Aluminum-Based Frustrated Lewis Pair as an Ion Pair Receptor: Alkali Metal Hydride Adducts and Phase-Transfer Catalysis. *Angew Chem Int Ed* 51:5911–5914 (*Angew Chem* 124:6013–6016)
118. Grimme S, Kruse H, Goerigk L, Erker G (2010) The Mechanism of Dihydrogen Activation by Frustrated Lewis Pairs Revisited. *Angew Chem Int Ed* 49:1402–1405 (*Angew Chem* 122:1444–1447)
119. Rokob TA, Hamza A, Stirling A, Soós T, Pápai I (2008) Turning Frustration into Bond Activation: A Theoretical Mechanistic Study on Heterolytic Hydrogen Splitting by Frustrated Lewis Pairs. *Angew Chem Int Ed* 47:2435–2438 (*Angew Chem* 123:12435–12439)
120. Guo Y, Li S (2008) Unusual Concerted Lewis Acid-Lewis Base Mechanism for Hydrogen Activation by a Phosphine-Borane Compound. *Inorg Chem* 47:6212–6219
121. Hamza A, Stirling A, Rokob TA, Pápai I (2009) Mechanism of Hydrogen Activation by Frustrated Lewis Pairs: A Molecular Orbital Approach. *Int J Quantum Chem* 109:2416–2425
122. Rajeev R, Sunoj RB (2009) On the Origin of Reversible Hydrogen Activation by Phosphine-Boranes. *Chem Eur J* 15:12846–12855
123. Rokob TA, Hamza A, Pápai I (2009) Rationalizing the Reactivity of Frustrated Lewis Pairs: Thermodynamics of H<sub>2</sub> Activation and the Role of Acid–Base Properties. *J Am Chem Soc* 131:10701–10710
124. Durfey BL, Gilbert TM (2011) Computational Studies of Lewis Acidities of Tris-(fluorophenyl)-Substituted Boranes: An Additive Relationship between Lewis Acidity and Fluorine Position. *Inorg Chem* 50:7871–7879
125. Lu Z, Cheng Z, Chen Z, Weng L, Li ZH, Wang H (2011) Heterolytic Cleavage of Dihydrogen by “Frustrated Lewis Pairs” Comprising Bis(2,4,6-tris(trifluoromethyl)phenyl)borane and Amines: Stepwise versus Concerted Mechanism. *Angew Chem Int Ed* 50:12227–12231 (*Angew Chem* 123:12435–12439)

# Frustrated Lewis Pair Mediated Hydrogenations

Douglas W. Stephan and Gerhard Erker

**Abstract** The development and use of *frustrated Lewis pairs* (FLPs) as both stoichiometric and catalytic reductants for the hydrogenation of a variety of organic substrate is described.

**Keywords** 1,1-Disubstituted olefins · Aromatic reductions · Aziridines · Enamines · Enones · Enynes · Frustrated Lewis pairs · Heterolytic cleavage of dihydrogen · Hydrogenation catalysis · Imines · Nitriles · Silyl enol ethers

## Contents

1	Introduction .....	86
2	Frustrated Lewis Pair Catalyzed Hydrogenations .....	86
2.1	Hydrogenation of Imines and Related Substrates .....	88
2.2	Hydrogenation of Silylenol Ether Substrates .....	93
2.3	Hydrogenation of Enamine Substrates .....	94
2.4	Hydrogenation of 1,1-Disubstituted Olefin Substrates .....	98
2.5	Hydrogenation of Electron-Poor Alkenes and Alkynes .....	101
2.6	Arene Hydrogenation .....	103
2.7	Transfer Hydrogenations .....	105
3	Conclusions .....	107
	References .....	108

---

D.W. Stephan  
Department of Chemistry, University of Toronto, 80 St. George Street,  
Toronto, ON, 69626, Canada  
e-mail: [dstephan@chem.utoronto.ca](mailto:dstephan@chem.utoronto.ca)

G. Erker  
Organisch-Chemisches Institut der Universität Münster, Corrensstrasse 40,  
48149 Münster, Germany  
e-mail: [erker@uni-muenster.de](mailto:erker@uni-muenster.de)

## Abbreviations

DABCO	1,4-Diazabicyclo[2.2.2]octane
dipp	2,6-Diisopropylphenyl = C <sub>6</sub> H <sub>3</sub> iPr <sub>2</sub>
Me	Methyl = CH <sub>3</sub>
Mes	Mesityl = 2,4,6-trimethylphenyl
<i>i</i> -Pr	Iso-propyl
Ph	Phenyl = C <sub>6</sub> H <sub>5</sub>
Et	Ethyl = C <sub>2</sub> H <sub>5</sub>
<i>t</i> -Bu	tert-butyl = C(CH <sub>3</sub> ) <sub>3</sub>
Pr	Propyl = C <sub>3</sub> H <sub>7</sub>
Cp	Cyclopentadienyl = (C <sub>5</sub> H <sub>5</sub> )-
Cy	Cyclohexyl = C <sub>6</sub> H <sub>11</sub>
TIBAL	Triisobutylaluminum = Al(CH(CH <sub>3</sub> ) <sub>2</sub> ) <sub>3</sub>

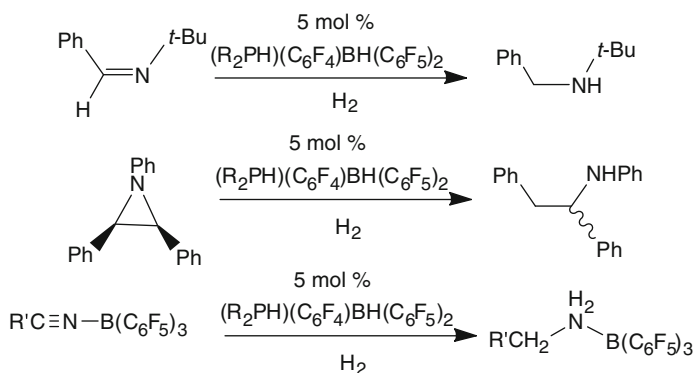
## 1 Introduction

Hydrogen activation and consequently catalytic hydrogenation of unsaturated organic substrates had been a domain of d- (and sometimes f-) block metal chemistry. Typically, catalytic hydrogenation of alkenes and alkynes or other more polar organic  $\pi$ -substrates is carried out heterogeneously using active noble metal surfaces often applied on inert supporting materials (such as Pd on charcoal) [1]. Alternatively, well defined molecular metal complexes, mostly but not exclusively from noble d-block metals, can be used for efficient catalytic hydrogenation. The *Wilkinson* catalyst [2] and the *Noyori* catalyst systems [3] are prominent examples which have led to the development of a great number and variety of metal complex catalysts for catalytic hydrogenation for various specific targets.

Before the advent of frustrated Lewis pair (FLP) chemistry [4], the cleavage and activation of dihydrogen by non-metallic systems had been rare [5–18]. The high activity of many FLPs to heterolytically split the H<sub>2</sub> molecule at mild conditions made it tempting to use these metal-free hydrogen activation systems catalytically. This has been achieved for a variety of substrates with relative ease, so that FLP chemistry has begun to branch out into active hydrogenation catalysis. Some aspects from the onset of this development and some features of the current state of FLP catalyzed hydrogenation will be presented and discussed in this account.

## 2 Frustrated Lewis Pair Catalyzed Hydrogenations

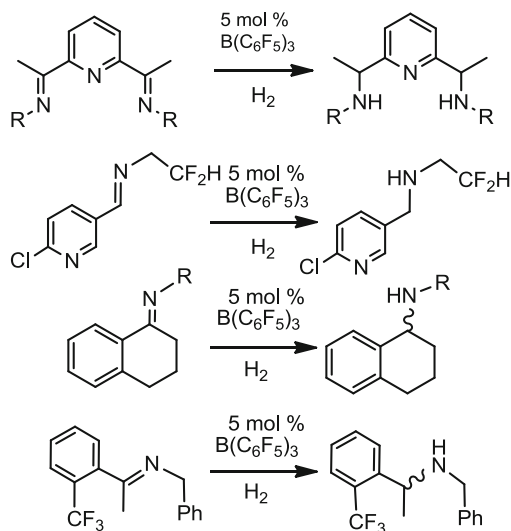
The discovery of the facile metal-free heterolytic cleavage of H<sub>2</sub> by FLPs prompted us to probe the utility of such activations in the catalytic reduction of organic substrates. Given that the hydrogen activation by FLPs is heterolytic in nature, we sought a polar substrate that would accept a proton and hydride in a consecutive fashion. In addition, in order to effect a catalytic reduction, it is necessary to destabilize the substrate-borane adduct.



**Scheme 1** Imine, aziridine, and protected nitrile hydrogenations by FLP catalysts (R = Mes **1**, *t*-Bu **2**)

**Table 1** Hydrogenation by aryl-linked phosphonium-borate FLP catalysts

	mol%	T °C	P atm	T h	Y
Catalyst = (C <sub>6</sub> H <sub>2</sub> Me <sub>3</sub> ) <sub>2</sub> PH(C <sub>6</sub> F <sub>4</sub> )BH(C <sub>6</sub> F <sub>5</sub> ) <sub>2</sub> <b>1</b> [19–21]					
PhCH=N <i>t</i> -Bu	5	80	1	1	79
PhCH=NSO <sub>2</sub> Ph	5	120	5	11	97
PhCH=NCHPh <sub>2</sub>	5	140	5	1	88
PhCH=NCH <sub>2</sub> Ph	5	120	5	48	5
PhCH=NCH <sub>2</sub> Ph(B(C <sub>6</sub> F <sub>5</sub> ) <sub>3</sub> )	5	120	5	46	57
MeC≡N(B(C <sub>6</sub> F <sub>5</sub> ) <sub>3</sub> )	5	120	5	24	75
PhC≡N(B(C <sub>6</sub> F <sub>5</sub> ) <sub>3</sub> )	5	120	5	24	84
(CH <sub>2</sub> CH <sub>2</sub> C≡N(B(C <sub>6</sub> F <sub>5</sub> ) <sub>3</sub> )) <sub>2</sub>	10	120	5	48	99
PhCHCHPhNPh	10	120	5	1.5	98
ClC <sub>5</sub> H <sub>3</sub> N(CH=NCH <sub>2</sub> CH <sub>2</sub> F)	5	124	120	4	54
ClC <sub>5</sub> H <sub>3</sub> N(CH=NCH <sub>2</sub> CH <sub>2</sub> F)	5	124	120	20	46
PhCH <sub>2</sub> CH <sub>2</sub> N((CH <sub>2</sub> ) <sub>2</sub> ) <sub>2</sub> C=NPh	5	117	120	20	26
C <sub>10</sub> H <sub>10</sub> =NCH <sub>2</sub> Ph	5	120	120	4	93
C <sub>10</sub> H <sub>10</sub> =NCH <sub>2</sub> Ph	5	120	120	20	100
C <sub>10</sub> H <sub>10</sub> =NCH <sub>2</sub> Pr	5	124	120	20	78
Catalyst = <i>t</i> -Bu <sub>2</sub> PH(C <sub>6</sub> F <sub>4</sub> )BH(C <sub>6</sub> F <sub>5</sub> ) <sub>2</sub> <b>2</b> [19]					
PhCH=N <i>t</i> -Bu	5	80	1	1	98
PhCH=NSO <sub>2</sub> Ph	5	120	5	16	87
ClC <sub>5</sub> H <sub>3</sub> N(CH=NCH <sub>2</sub> CH <sub>2</sub> F)	5	120	120	4	10
ClC <sub>5</sub> H <sub>3</sub> N(CH=NCH <sub>2</sub> CH <sub>2</sub> F)	5	117	120	20	10
PhCH <sub>2</sub> CH <sub>2</sub> N((CH <sub>2</sub> ) <sub>2</sub> ) <sub>2</sub> C=NPh	5	120	120	20	25
C <sub>10</sub> H <sub>10</sub> =NCH <sub>2</sub> Ph	5	120	120	4	90
C <sub>10</sub> H <sub>10</sub> =NCH <sub>2</sub> Ph	5	124	120	20	100
C <sub>10</sub> H <sub>10</sub> =NCH <sub>2</sub> Pr	5	124	120	20	100



**Scheme 2** FLP hydrogenations of several imine substrates

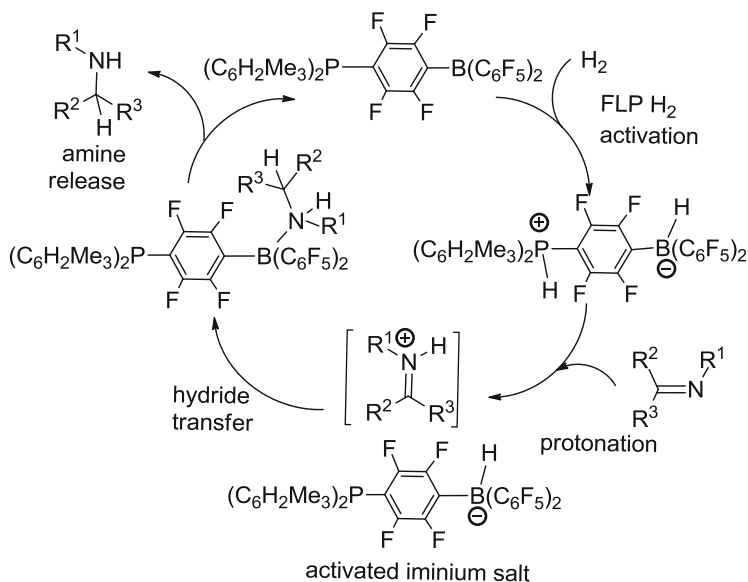
## 2.1 Hydrogenation of Imines and Related Substrates

We began with sterically encumbered imines. Indeed, in an initial report it was shown that several aldimines which incorporated sterically demanding substituents on nitrogen were shown to be hydrogenated effectively in the presence of 5 mol% of the phosphonium borate  $(R_2PH)(C_6F_4)BH(C_6F_5)_2$  ( $R = \text{Mes}$  **1**,  $t\text{-Bu}$  **2**) (Scheme 1, Table 1) at 80–120 °C under 1–5 atm of  $H_2$ . Under similar conditions, the aziridine  $\text{PhCHCHPhNPh}$  was also hydrogenated [19]. In general, the yields of these reductions were high although reaction times typically ranged from 1 to 24 h. Separation of the product amines from the catalyst was readily achieved via simple filtration through silica gel.

This strategy was also applied to the reductions of nitriles; however, in this case the “protecting group”  $B(C_6F_5)_3$  **3** was employed. Thus, treatment of nitrile adducts of **3** with  $H_2$  and the catalyst **1** resulted in slow reduction (24–48 h) to the corresponding amine adduct of  $B(C_6F_5)_3$  (Scheme 1). This strategy was effective as the borane **3** is more Lewis acidic than the borane center in **1**, and thus the nitrile does not exchange and inhibit the catalyst. While this strategy demonstrates the metal-free hydrogenation of nitriles, it is also true that the use of **3** as a protecting group is only feasible as a demonstration of principle.

More recently, this reduction strategy has been used to effect the reduction of simple diimines as well as pyridyldiimines. Using the aryl-linked phosphonium borate as catalyst, the corresponding diamines were readily obtained (Scheme 2) [22]. In a similar fashion, imine precursors to potential herbicides, the antidepressant sertraline, and precursors to anti-cancer and herbicide candidates were effectively reduced using this FLP strategy (Scheme 2, Table 1). In contrast, the imine precursor to the analgesic narcotic fentanyl was reduced in low yield.





**Scheme 3** Mechanism for FLP hydrogenation of imines

This ineffective reduction was attributed to catalyst deactivation by coordination of the amine center in the substrate to the boron center.

The mechanism of these metal-free imine reductions begins with protonation of the imine followed by hydride transfer from the hydridoborate to the iminium carbon (Scheme 3) [19]. This liberates the phosphine–borane for further reaction with  $\text{H}_2$  for the regeneration of the phosphonium–borate. Initial protonation of the imine is supported by the observation that reduction of the electron-rich imine  $t\text{-BuN}=\text{CPh}(\text{H})$  proceeds significantly faster than that of the electron-poor imine  $\text{PhSO}_2\text{N}=\text{CPh}(\text{H})$ . Moreover, reaction of the non-protic phosphonium–borate  $(\text{C}_y\text{P})(\text{C}_6\text{F}_4)\text{BH}(\text{C}_6\text{F}_5)_2$  [23] with imine leads to no reactions, affirming that imine does not insert into the B–H bond of the borohydride fragment.

In subsequent reports, the analogous reductions of sterically encumbered imines and aziridines were achieved using solely  $\text{B}(\text{C}_6\text{F}_5)_3$  **3** [24, 25] as the catalyst (Table 2). In these cases the substrate acts as the base partner in the FLP activation of hydrogen. It is noteworthy that electron-poor imines were hydrogenated very slowly; thus addition of a catalytic equivalent of  $\text{P}(\text{C}_6\text{H}_2\text{Me}_3)_3$  accelerated these reductions as the phosphine/borane combination effected the heterolytic cleavage of  $\text{H}_2$  more rapidly.

Mechanistically these phosphine-free heterolytic activations of  $\text{H}_2$  result from the substrate and borane acting as an FLP to generate the corresponding iminium cation and the borohydride  $[\text{HB}(\text{C}_6\text{F}_5)_3]$ . Subsequent hydride transfer liberates the borane for further  $\text{H}_2$  activation with the surplus substrate. Interestingly in the case

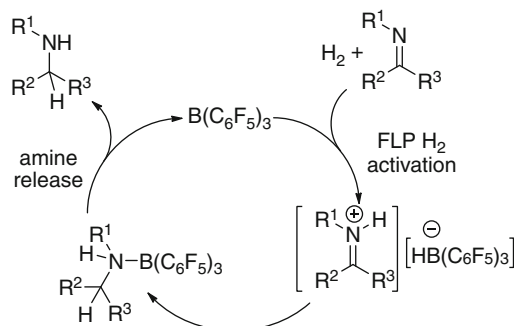
**Table 2** FLP hydrogenations catalyzed by  $B(C_6F_5)_3$  **3** [24–26]

	mol%	T °C	P atm	T h	Y
PhCH=N <i>r</i> -Bu	5	80	1	2	89
PhCH=NSO <sub>2</sub> Ph	5	120	5	41	94
PhCH=NCHPh <sub>2</sub>	5	120	5	1	99
PhCH=N(SO <sub>2</sub> C <sub>6</sub> H <sub>4</sub> Me)	10	80	10	22	7
PhCH=N(SO <sub>2</sub> C <sub>6</sub> H <sub>4</sub> Me)	10	80	20	22	97
PhCH=N(SO <sub>2</sub> C <sub>6</sub> H <sub>4</sub> Me)	10	100	20	22	91
PhCH=N(SO <sub>2</sub> C <sub>6</sub> H <sub>4</sub> Me)	10	100	30	22	99
C <sub>6</sub> H <sub>4</sub> CMe <sub>2</sub> CMe=N	10	100	40	22	0
C <sub>6</sub> H <sub>4</sub> CMe <sub>2</sub> CMe=N	10	140	20	22	21
C <sub>6</sub> H <sub>4</sub> CMe <sub>2</sub> CMe=N	10	140	40	22	53
Ph <sub>2</sub> C=N <i>r</i> -Bu	5	120	5	1	98
PhCMe=NC <sub>6</sub> H <sub>2</sub> Me <sub>3</sub>	5	120	5	8	94
PhCMe=NPh	2.5	80	10	22	19
PhCMe=NPh	5	80	10	22	68
PhCMe=NPh	10	80	10	22	99
PhCMe=NPh	10	50	10	22	29
PhCMe=NPh	5	80	20	22	99
PhCHCHPhNPh	5	120	5	2	95
C <sub>6</sub> H <sub>4</sub> CH=CHNMe	1	80	103	18	0
C <sub>6</sub> H <sub>4</sub> CH=CHNMe	10	80	103	18	98
C <sub>6</sub> H <sub>4</sub> CH=CMeNMe	1	80	103	18	21
C <sub>6</sub> H <sub>4</sub> CH=CMeNMe	10	80	103	18	98
C <sub>6</sub> H <sub>4</sub> CH=CPhNMe	1	80	103	18	37
C <sub>6</sub> H <sub>4</sub> CH=CPhNMe	10	80	103	18	91
C <sub>9</sub> H <sub>6</sub> N(2-Ph)	5	25	4	4	80
C <sub>9</sub> H <sub>6</sub> N(2-Me)	5	50	4	16	74
C <sub>9</sub> H <sub>6</sub> N(8-Me)	10	80	4	6	88
C <sub>13</sub> H <sub>9</sub> N(acridine)	5	25	4	2	80
C <sub>13</sub> H <sub>9</sub> N(phenanthroline)	5	25	4	3	84
(CH <sub>2</sub> =NMe) <sub>2</sub>	5	120	4	24	99
(CH <sub>2</sub> =Ndipp) <sub>2</sub>	5	120	4	24	99
(C <sub>5</sub> H <sub>3</sub> N)(MeC=N(C <sub>6</sub> H <sub>4</sub> -4- <i>i</i> Pr) <sub>2</sub> )	5	120	4	24	99
(C <sub>5</sub> H <sub>3</sub> N)(MeC=N(dipp) <sub>2</sub> )	5	120	4	24	99
(C <sub>5</sub> H <sub>3</sub> N)(MeC=NMe) <sub>2</sub>	5	120	4	24	99
ClC <sub>5</sub> H <sub>3</sub> N(CH=NCH <sub>2</sub> CH <sub>2</sub> F)	5	120	120	4	13
ClC <sub>5</sub> H <sub>3</sub> N(CH=NCH <sub>2</sub> CH <sub>2</sub> F)	5	120	120	20	31
C <sub>10</sub> H <sub>10</sub> =NCH <sub>2</sub> Pr	5	124	120	20	100
1-CF <sub>3</sub> C <sub>6</sub> H <sub>4</sub> (2-C(Me)=NCH <sub>2</sub> Ph)	2	117	120	16	95
PhC(Me)=NCH(Me) <i>r</i> -Bu	10	80	5	48	100
PhC(Me)=NCH(Me)C <sub>6</sub> H <sub>11</sub>	10	80	5	48	100
PhC(Me)=NCH(Me)Ph	10	80	5	48	72
PhC(Me)=NCH(Me)Ph	10	25	115	23	100
PhC(Et)=NCH(Me)Ph	10	80	5	48	100
PhC( <i>i</i> Pr)=NCH(Me)Ph	10	80	5	48	100
PhC(Et)=NCH(Et)	10	80	5	24	100
C <sub>7</sub> H <sub>7</sub> Me <sub>3</sub> =NCH <sub>2</sub> Ph	10	115	5	120	100

(continued)

**Table 2** (continued)

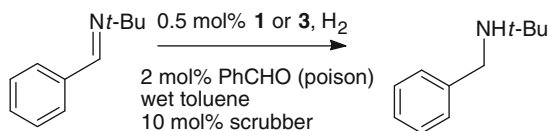
	mol%	T °C	P atm	T h	Y
C <sub>7</sub> H <sub>7</sub> Me <sub>3</sub> =NPh	10	115	5	120	92
C <sub>6</sub> H <sub>6</sub> Me( <i>i</i> -Pr)=NCH <sub>2</sub> Ph	10	115	5	120	100
C <sub>6</sub> H <sub>6</sub> Me( <i>i</i> -Pr)=NPh	20	115	5	120	100
C <sub>6</sub> H <sub>6</sub> Me( <i>i</i> -Pr)=NPh	10	115	5	120	66

**Scheme 4** Mechanism for FLP hydrogenation of imines by B(C<sub>6</sub>F<sub>5</sub>)<sub>3</sub> **3**

of the imine (C<sub>6</sub>H<sub>2</sub>Me<sub>3</sub>)N=C(Me)*t*-Bu, activation of H<sub>2</sub> led only to the isolation of the salt [(C<sub>6</sub>H<sub>2</sub>Me<sub>3</sub>)NH=C(Me)*t*-Bu][HB(C<sub>6</sub>F<sub>5</sub>)<sub>3</sub>], suggesting that hydride transfer to the iminium carbon was sterically inhibited [24]. These observations support a mechanism analogous to that proposed for the aryl-linked phosphonium borate catalysts (Scheme 4) and were also supported by the computational studies of Papai and co-workers [27].

The precise and detailed description of the mechanism of H<sub>2</sub> activation by these and other FLP systems has been examined computationally by the groups of Papai [27–31] and Grimme [32–34]. Both groups suggest the generation of an “encounter complex” where the Lewis acid and base are close to each other, but where adduct formation is sterically inhibited. The details of the geometry of the interaction of the encounter complexes with H<sub>2</sub> differ in the two models. In the Papai model the B-H<sub>2</sub>-P vector is linear, while in the Grimme model H<sub>2</sub> is “side-on” to B and the P is positioned so as to be an electron donor to the H<sub>2</sub> σ\* orbital. Further discussion of these studies is provided in the chapters from these respective authors.

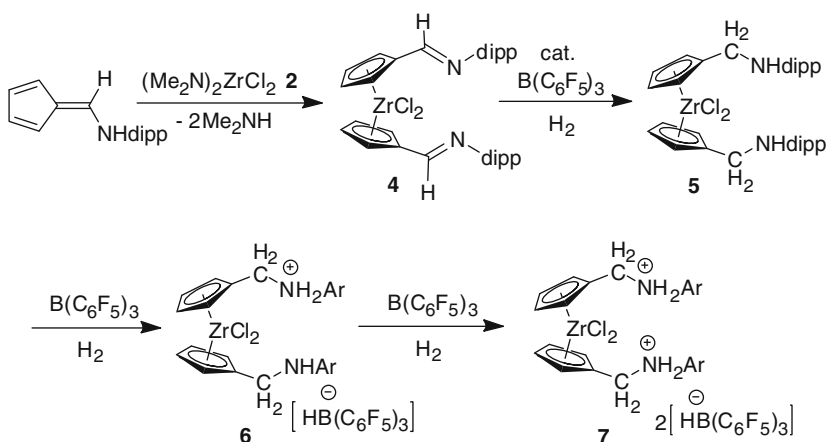
Evaluation of the functional group tolerance for these FLP hydrogenations using either phosphine-borane **1** or the borane **3** was probed by the performance of a standard imine hydrogenation in the presence of an equivalent of a function group surrogate. In this fashion, hydrogenation using the catalyst **1** or **3** was not inhibited by the presence of naphthalene, bulky ethers, *n*-hexyl acrylate, bulky amines, and alkyl and aryl halides [22]. In contrast, in the presence of PhNMe<sub>2</sub>, *t*-BuNH<sub>2</sub>, carbamates, ketones or aldehydes, and 2,4,6-Me<sub>3</sub>C<sub>6</sub>H<sub>2</sub>OH, these catalysts were not functional. Nonetheless, they tolerated the presence of 2,6-*t*-Bu<sub>2</sub>C<sub>6</sub>H<sub>3</sub>OH, suggesting that while steric encumbrance broadens the functional group tolerance,



Scrubber = TIBAL, Et<sub>3</sub>SiH, Me<sub>2</sub>SiHCl

Catalyst	Scrubber	Conversion
<b>1</b>	TIBAL	99%
<b>3</b>	TIBAL	68%
<b>3</b>	Et <sub>3</sub> SiH	100%
<b>3</b>	Me <sub>2</sub> SiHCl	100%

**Scheme 5** Imine hydrogenation in the presence of catalyst poison using a scrubber

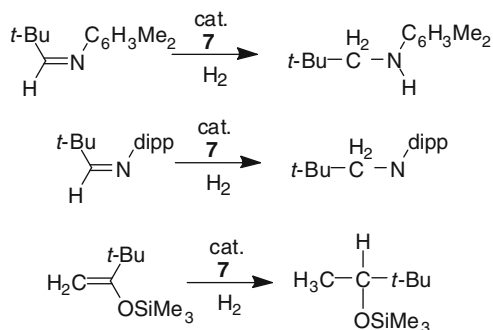


**Scheme 6** FLP reduction of organometallic imine complex and H<sub>2</sub> activation

these FLP reduction catalysts exhibit limited tolerance of polar substituents or sterically unencumbered donor functionalities.

In parallel optimizations, imine reductions were shown to be affected with as little as 0.1 mol% catalyst, although this required elevated temperature and hydrogen pressure (130 °C, 120 atm H<sub>2</sub>) [22]. The sensitivity of these metal-free hydrogenation catalysts to trace impurities such as water and aldehydes can be overcome by the use of an inexpensive scrubbing agent. In this fashion, hydrogenations of imine substrates proceed in high yields without the need for drying of solvent or gas, or the removal of trace aldehyde impurities (Scheme 5) [35]. In addition, these scrubbers are shown to regenerate aldehyde or water poisoned catalysts, increasing catalyst lifetime.

FLP reduction of imine functionalities has also been applied to sensitive organometallic substrates. Treatment of an *N*-dipp-aminofulvene with (Me<sub>2</sub>N)<sub>2</sub>ZrCl<sub>2</sub> resulted in NH deprotonation and formation of the group 4 metallocene Cp-rings **4** (Scheme 6). The pair of *N*-aryldimino substituents at the zirconocene Cp-rings were very efficiently hydrogenated by adding a catalytic amount of the Lewis acid **3**



**Scheme 7** Hydrogenations catalyzed by **7**

to the system followed by exposure to dihydrogen (rt, 2 bar). This resulted in reduction of the imine functional groups to the corresponding *N*-arylaminoethyl derivatives **5** [36, 37]. This reaction is one of many examples where the nitrogen atom of the imine functionality of the substrate initially serves itself as the Lewis base for the generation of the FLP for dihydrogen splitting.

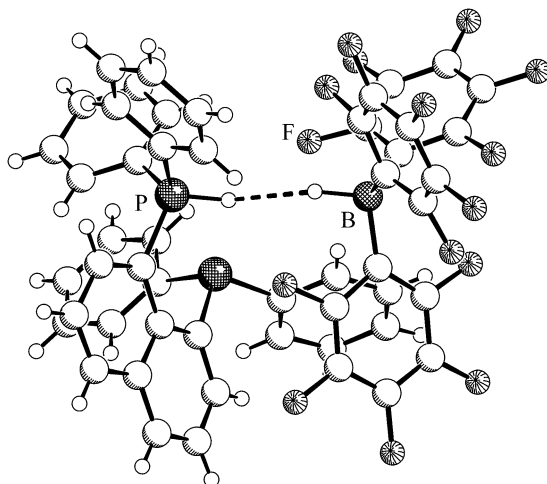
A number of other catalysts for the reduction of imines – among other substrates – have been explored by several other researchers [28, 38–41]. These developments are described in other chapters in this volume and thus are not reviewed here. In addition, further evolution of catalysts for asymmetric hydrogenations has emerged from the Klankermayer group [25, 42, 43]. This work is reviewed in the respective chapter.

## 2.2 Hydrogenation of Silylenol Ether Substrates

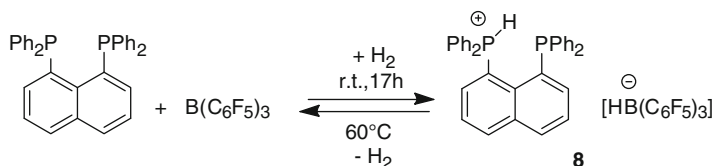
FLP hydrogenations are not limited to imines. In the presence of stoichiometric amounts of **3** the amine/borane FLPs reacted further with dihydrogen to yield the ammonium/hydridoborate product **6** and subsequently **7** (Scheme 6). The salt **7** is an efficient FLP catalyst for the hydrogenation of bulky organic imines as well as the reduction of a silylenolether to the corresponding silylated alcohol product (Scheme 7).

Related reductions are readily achieved using silylenol ethers as the substrates. For example, the FLP derived from 1,8-bis(diphenylphosphino)naphthalene and **3** has proved to be a suitable catalyst for this purpose [44]. This FLP slowly activates dihydrogen at ambient conditions to give the mono-phosphonium/hydrido borate salt **8** which features a B–H⋯H–P contact in the crystal (Fig. 1). The formation of **8** is a rare example of an FLP where the activation of H<sub>2</sub> is reversible [40, 45, 46] as **8** liberates H<sub>2</sub> to reform the FLP cleanly at elevated temperatures (60 °C) (Scheme 8).

This FLP system acts as a catalyst for the hydrogenation of silylenolethers [44]. The reaction of sufficiently sterically hindered silylenolethers proceeds to give the corresponding silylated alcohols with good substrate conversion and good yields of



**Fig. 1** Molecular structure of the phosphonium/hydrido borate salt **8**; B–H...H–P contact is 2.08 Å



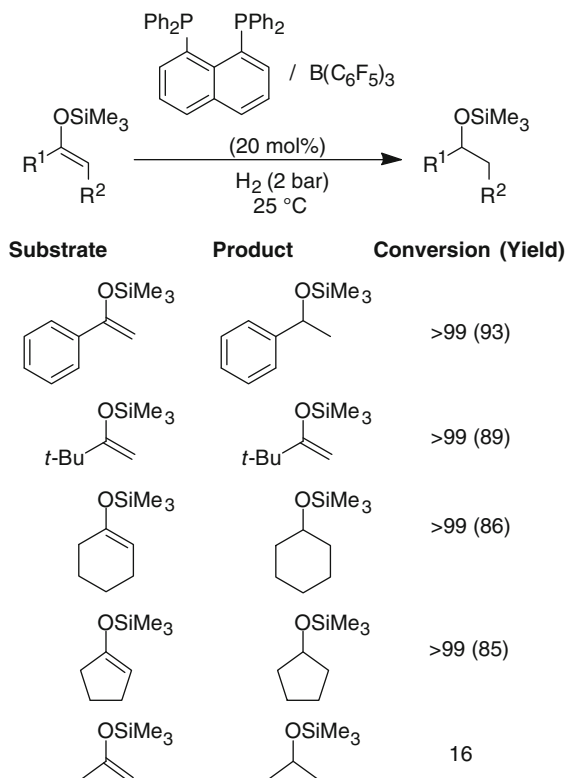
**Scheme 8** Reversible activation of H<sub>2</sub> by diphosphine/borane FLP **8**

the isolated products (Scheme 9). In cases where the steric bulk is insufficient, the reaction only proceeds in a stoichiometric fashion.

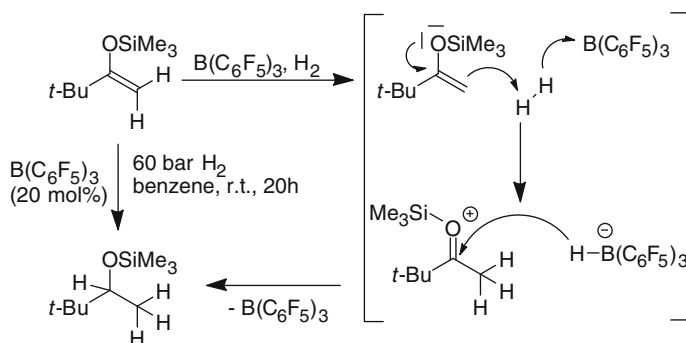
The slow background reaction in this system, in which the Lewis acid **3** alone effects the conversion of electron-rich silylenolethers to the respective silylated alcohol, becomes an efficient catalytic process at 60 bar H<sub>2</sub> pressure. In this fashion, the silylenolethers *t*-Bu(Me<sub>3</sub>SiO)C=CH<sub>2</sub>, C<sub>6</sub>H<sub>9</sub>(OCSiMe<sub>3</sub>) and C<sub>3</sub>H<sub>7</sub>(OCSiMe<sub>3</sub>) were quantitatively converted the corresponding saturated silyl ethers over a 20h period at room temperature employing 20 mol% **3** as the catalyst. These observations infer that the electron-rich silylenol ether substrate serves as the Lewis base in this FLP “self-catalyzed” hydrogenation reaction (Scheme 10) [47].

### 2.3 Hydrogenation of Enamine Substrates

The intramolecular FLP (Mes)<sub>2</sub>PCH<sub>2</sub>CH<sub>2</sub>B(C<sub>6</sub>F<sub>5</sub>)<sub>2</sub> **9** is a very active dihydrogen splitting reagent. It readily yields the phosphonium/hydrido borate zwitterion **10** when exposed to dihydrogen under mild conditions (Scheme 11) [32]. This FLP system is an active metal-free catalyst for the hydrogenation of imines and of

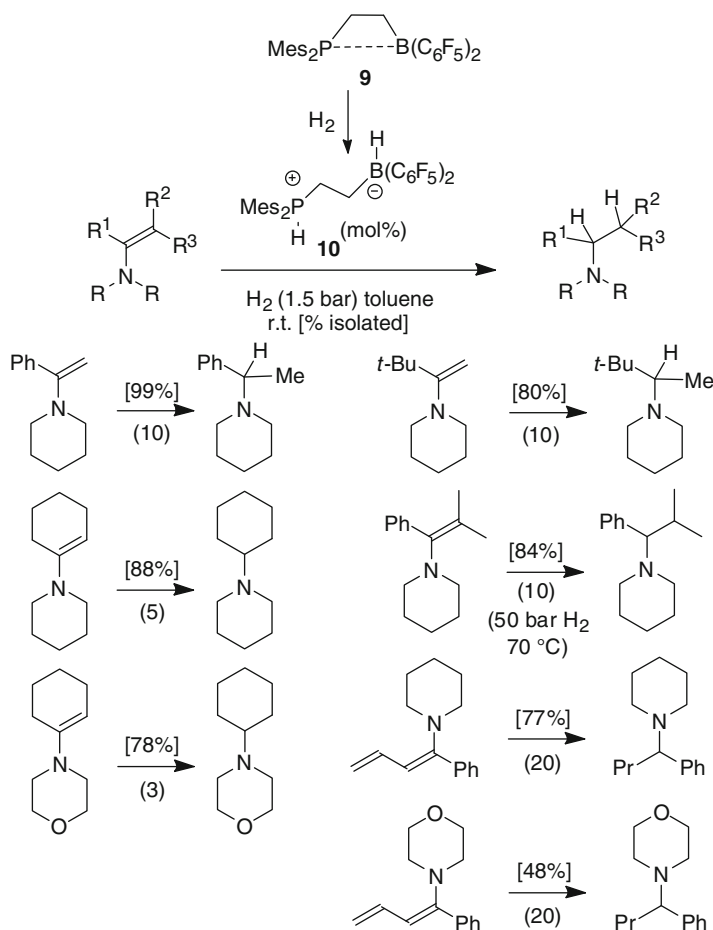


**Scheme 9** FLP hydrogenations of silylenol ethers



**Scheme 10** Proposed pathway for Lewis acid mediated hydrogenation of silylenol ethers

enamines (Scheme 11). A number of enamines were cleanly hydrogenated to their corresponding tertiary amines under homogeneous conditions with this FLP catalyst. In some cases good yields were obtained with less than 5 mol% of the catalyst system. Even tetra-substituted enamino-C=C double bonds could be hydrogenated, albeit under slightly more forcing reaction conditions. A few conjugated dienamine substrates were also fully hydrogenated to yield the saturated tertiary amines [20].

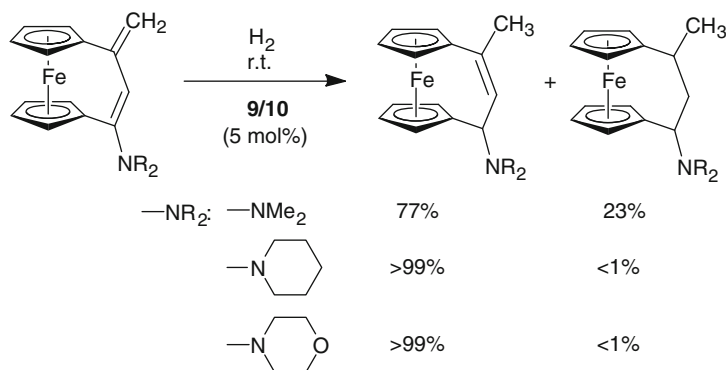


**Scheme 11** Catalytic hydrogenations of enamines by the FLP catalyst **9/10**

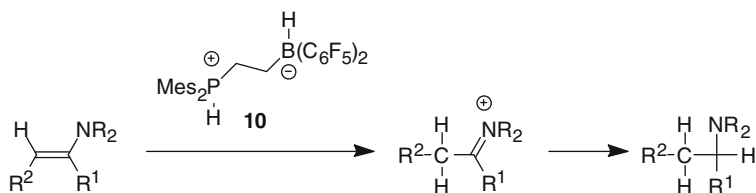
The catalytic hydrogenations of the ferrocenophane-derived dienamines by **9/10** are exceptional as they proceed predominantly or even exclusively to form the allylamine product, depending on the substitution at nitrogen. These products are derived from a 1,4-hydrogenation of the conformationally restricted conjugated dienamine unit (Scheme 12) [21].

These enamine hydrogenations by FLP catalysis are likely to proceed by a two-step reaction mechanism that is initiated by protonation to generate a reactive iminium ion intermediate that is then subsequently reduced by hydride transfer from the hydrido borate anion (Scheme 13). This view was supported by a series of experiments using the [3]-ferrocenophane derived conjugated dienamine [21]. Treatment with HCl in ether resulted in selective protonation at the 4-position of the dienamine unit to give the conjugated iminium salt (Scheme 14). Anion exchange with  $\text{Ag}[\text{BF}_4]$  yielded the corresponding  $\text{BF}_4$  salt. Analogous treatment of the [3]-ferrocenophane conjugated dienamine with the zirconocene bound

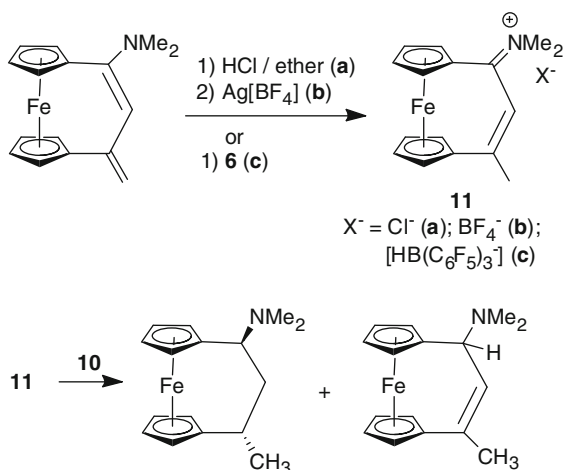




**Scheme 12** Catalytic hydrogenation of ferrocenophane-derived dienamines by **9/10**



**Scheme 13** Proposed sequence of proton/hydride transfer to enamine by an FLP



**Scheme 14** Reactions of [3]ferrocenophane conjugated dienamine

ammonium/hydrido borate salt **6** gave an iminium salt with an  $[\text{HB}(\text{C}_6\text{F}_5)_3]^-$  anion, **11**. This latter species **11** was characterized by X-ray diffraction (Fig. 2). Subsequent treatment of the iminium salt ( $\text{X}^- = \text{BF}_4^-$ ) with the FLP derived hydrogen activation product **10** (70 °C, 20 min) eventually gave a ca. 70:30 mixture of the allylamine and fully hydrogenated product, similar to that derived from the catalytic hydrogenation described above.

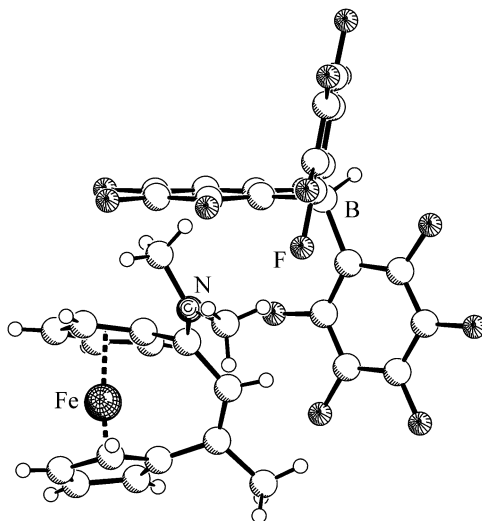
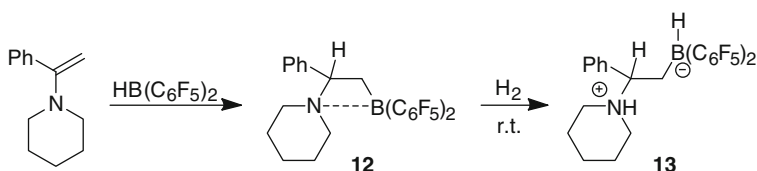


Fig. 2 Molecular structure of the salt **11**

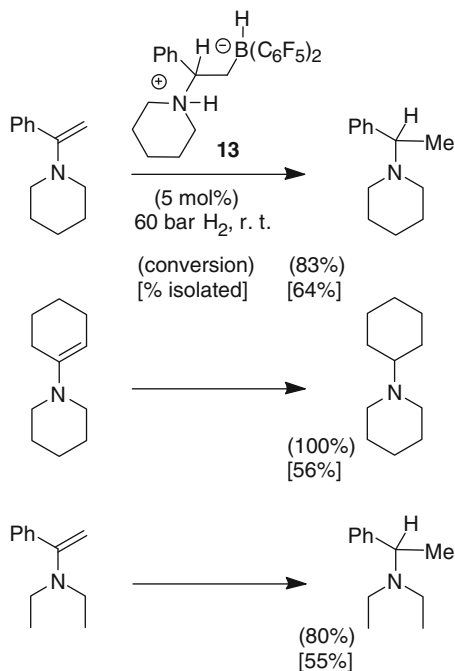


Scheme 15 Synthesis and reaction amine-borane FLP with  $H_2$

Intramolecular vicinal amine/borane FLPs can be obtained by hydroboration of a variety of enamines with *Piers'* borane  $[HB(C_6F_5)_2]$  [48–51]. Some of the systems split dihydrogen under mild conditions to give the respective ammonium/hydroborate borate zwitterions (Scheme 15). The system **12/13** is a typical example. This system also acts as a catalyst for the reduction of enamines. At 60 bar  $H_2$  pressure, a series of enamines were hydrogenated to the respective tertiary amines at room temperature in the presence of 5 mol% of this N/B FLP hydrogenation catalyst (Scheme 16) [51].

## 2.4 Hydrogenation of 1,1-Disubstituted Olefin Substrates

Seeking to broaden further the scope of FLP hydrogenations, a study was initiated employing **3** in combination with the weakly basic phosphine  $(C_6F_5)_2P$  [52]. Spectroscopic examination of a 1:1 mixture inferred no reaction at 25 °C. Exposure of this FLP to  $H_2$  (5 bar) gave no changes in the NMR spectra at room temperature; however, at –80 °C the  $^{31}P\{^1H\}$  NMR signal shifts significantly to lower field,



**Scheme 16** Catalytic enamine reduction by **12/13**

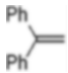
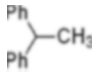
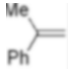
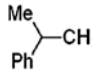
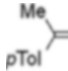
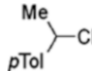
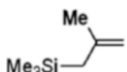
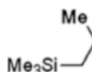
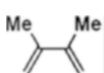
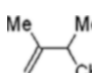
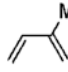
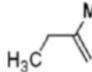
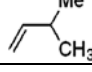
consistent with the formation of the phosphonium species  $[(\text{C}_6\text{F}_5)_2\text{PH}_2]^+$ . The corresponding  $^{11}\text{B}$  and  $^{19}\text{F}$  NMR spectra were consistent with the formation of the phosphonium-borate salt  $[(\text{C}_6\text{F}_5)_2\text{PH}_2][\text{HB}(\text{C}_6\text{F}_5)_3]$  **14**. On warming back to room temperature the NMR spectra were consistent with the reformation of the FLP, demonstrating a remarkably low barrier to the reversible activation of  $\text{H}_2$ .

The facility of the reversible loss of  $\text{H}_2$  is attributable in part to the acidity of the cation of **14**. Thus, 20 mol% mixture of  $(\text{C}_6\text{F}_5)_2\text{PH}_2/\mathbf{3}$  were exposed to 1,1-diphenylethene under 5 bar of  $\text{H}_2$  at room temperature, leading to the formation of saturated product 1,1-diphenylethane in quantitative yield (Table 3).<sup>1</sup> In a similar fashion, this reaction was not effected using the phosphine  $(\text{C}_6\text{F}_5)_2\text{PH}_2$ , presumably a result of the low nucleophilicity of this phosphine. On the other hand,  $(2,6\text{-C}_6\text{H}_3\text{Cl}_2)_3\text{P}$  and  $(\text{C}_{10}\text{H}_7)_3\text{P}$  were also effective [52].

A series of substrates were probed including 2-phenylpropene, 2-tolylpropene, and 2-neosilylpropene (Table 3). In the case of 2,3-dimethylbutadiene, heating to  $50\text{ }^\circ\text{C}$  afforded a 99% yield of 2,3-dimethylbutene, while the reduction of 2-methylbutadiene produced a mixture of 3-methylbutene and 2-methylbutene in a 10:1 ratio [52].

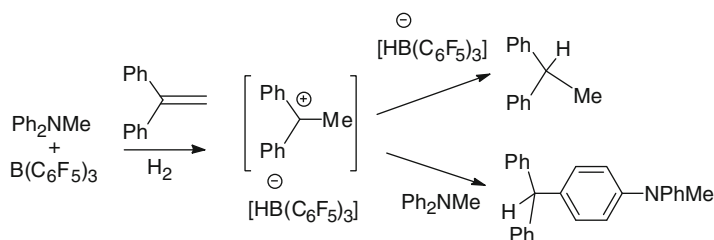
<sup>1</sup> No reaction was observed when **3a** was reacted with **1** or **2** and **1/2** in the absence of hydrogen.

**Table 3** Catalytic olefin hydrogenations by FLPs<sup>a</sup>

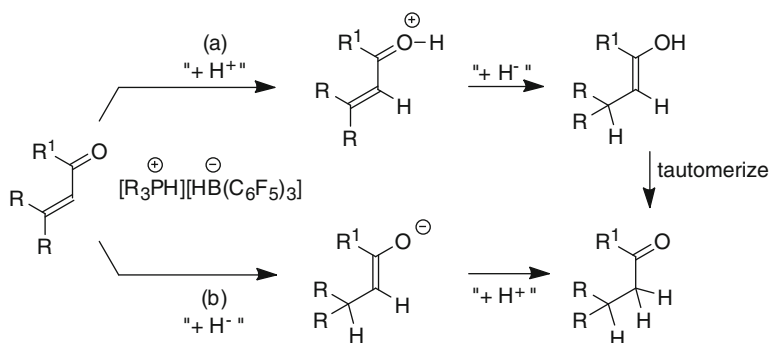
Olefin	Lewis base	Time [h]	Product	Yield [%]
	(C <sub>6</sub> F <sub>5</sub> ) <sub>2</sub> P	24		99
	(2,6-C <sub>6</sub> H <sub>3</sub> Cl <sub>2</sub> ) <sub>3</sub> P	24		99
	(C <sub>10</sub> H <sub>7</sub> ) <sub>3</sub> P <sup>b</sup>	12		95
	(C <sub>10</sub> H <sub>7</sub> ) <sub>3</sub> P <sup>b</sup>	240		96
	(C <sub>10</sub> H <sub>7</sub> ) <sub>3</sub> P	96		85
	(C <sub>10</sub> H <sub>7</sub> ) <sub>3</sub> P	12		95
	(C <sub>10</sub> H <sub>7</sub> ) <sub>3</sub> P	240		90
	(C <sub>10</sub> H <sub>7</sub> ) <sub>3</sub> P	240		82
				8

<sup>a</sup>Reactions were on 0.1 mmol scale in CD<sub>2</sub>Cl<sub>2</sub> (0.5 mL, 0.2 M) using 20 mol% Lewis base and **3**; yields were determined by <sup>1</sup>H NMR spectroscopy

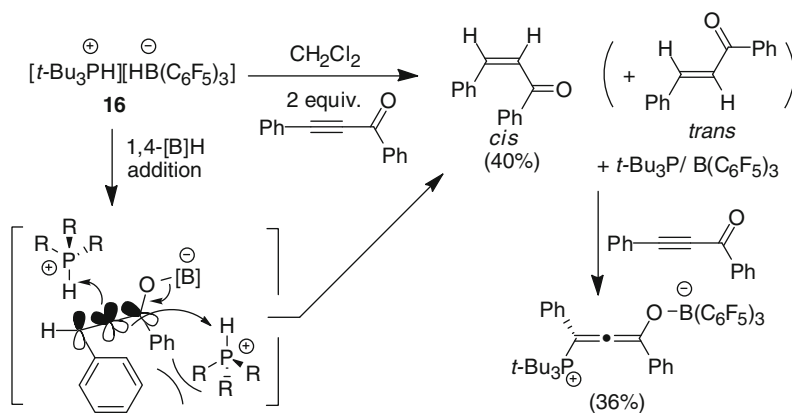
<sup>b</sup>Reactions were performed at 50 °C

**Scheme 17** Competition experiment using Ph<sub>2</sub>NMe to capture the transient carbocation

The mechanism of these FLP-catalyzed reductions of simple olefinic bonds is thought to involve protonation of the olefin generating a carbocation to which hydride transfer occurs. The intermediacy of the carbocation was confirmed with a competition experiment in which the cation was scavenged by the arylamine Ph<sub>2</sub>NMe. Thus, combination of 1,1-diphenylethene and 1.2 equiv of Ph<sub>2</sub>NMe with 20 mol% **3** resulted in the formation of 69% yield of 1,1-diphenylethane, and 31% yield of Ph<sub>2</sub>MeC(C<sub>6</sub>H<sub>4</sub>)NMePh (Scheme 17). In contrast, use of *p*Tol<sub>2</sub>NMe proved to be a superior Lewis base for the hydrogenation of 1,1-diphenylethylene. In this case, catalyst loadings could be reduced to 5 mol% [52].



**Scheme 18** Possible mechanisms of enone reduction by an FLP

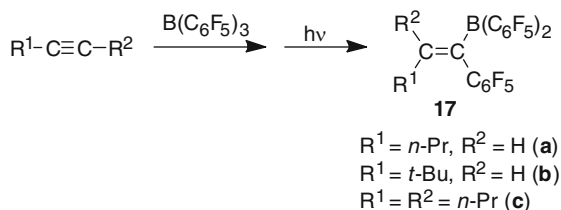


**Scheme 19** Reduction of ynones by an FLP

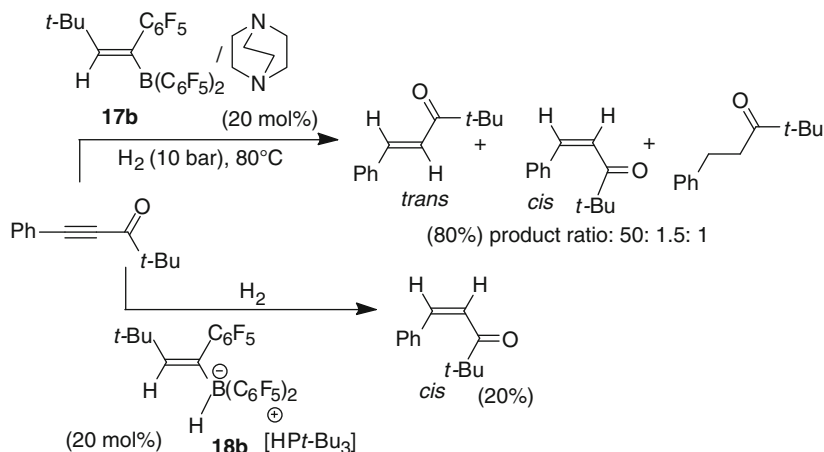
## 2.5 Hydrogenation of Electron-Poor Alkenes and Alkynes

In considering the catalytic hydrogenation of  $\alpha,\beta$ -unsaturated enones or ynones there are, a priori, two mechanistic options. The reaction could be proton induced (Scheme 18a) where the electrophilicity of the enone (or ynone) is further enhanced by protonation of the carbonyl oxygen, thus facilitating hydride attack at the “Michael position.” Alternatively, it might be that the electrophilic enone (or ynone) reactivity might itself be sufficient for addition of the hydride nucleophile at the  $\beta$ -position (Scheme 18b), followed by proton transfer.

To probe this question, the  $[\text{t-Bu}_3\text{PH}][\text{HB}(\text{C}_6\text{F}_5)_3]$  salt **16**, generated from **3**/ $\text{t-Bu}_3\text{P}$  FLP [53] and  $\text{H}_2$ , was treated with the conjugated ynone  $\text{PhC}\equiv\text{CC}(\text{O})\text{Ph}$  [54]. This led to reduction of the  $\text{C}\equiv\text{C}$  triple bond affording the corresponding *cis*-enone and a minor amount of the *trans*-isomer (Scheme 19). The latter product was shown to be the product of an acid catalyzed isomerisation of *cis*-isomer.



**Scheme 20** Synthesis of alkenylboranes

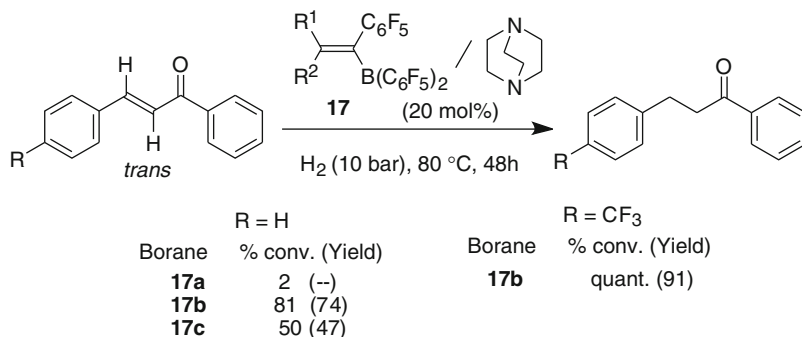


**Scheme 21** Hydrogenation of ynones with DABCO/**17b** or **18b** FLPs

The preferential formation of the *cis*-enone is rationalized by protonation of an allenic boron enolate intermediate by the bulky [*t*-Bu<sub>3</sub>PH]<sup>+</sup> phosphonium cation from the less hindered side (Scheme 19). The *cis*-enone was obtained in 40% stoichiometric yield. This results from the sequestration of the FLP **3**/*t*-Bu<sub>3</sub>P FLP by the relatively fast reaction of the liberated FLP with the ynone substrate to give the phosphonium allenic boron enolate, *t*-Bu<sub>3</sub>P C(Ph)=C=C(Ph)OB(C<sub>6</sub>F<sub>5</sub>)<sub>3</sub> (Scheme 19).

To effect catalytic ynone hydrogenation, use of a less Lewis acidic borane component of the FLP is envisioned as this would make trapping of the α,β-unsaturated ketone less favorable. To this end, a series of very bulky alkenylboranes (**17a–c**) were prepared by 1,1-carboboration of acetylenes (Scheme 20) [55–60]. In some cases, subsequent photolytic *E/Z*-olefin isomerization was required to obtain a single product.

The FLP derived from **17b**/*t*-Bu<sub>3</sub>P activated H<sub>2</sub> rapidly to form the salt **18b**. This was able to transfer stoichiometrically the H<sup>+</sup>/H<sup>−</sup> pair cleanly to the ynone PhC≡CC(O)*t*Bu to yield the corresponding *cis*-enone. However, increasing the H<sub>2</sub> pressure and reaction temperature and changing the Lewis base to DABCO achieved the catalytic hydrogenation of the ynone (Scheme 21). Interestingly these conditions yielded the *trans*-enone as the major product although some of the



**Scheme 22** Hydrogenation of enones

*cis*-isomer and a small amount of the saturated ketone were also observed. Soos et al. had described a related example of a terpene derived enone hydrogenation with the related (Mes)B(C<sub>6</sub>F<sub>5</sub>)<sub>2</sub>/DABCO catalyst [28].

The **17b**/DABCO and **17c**/DABCO FLP systems are also good catalysts for the hydrogenation of the conjugated enone PhCH=CHC(O)Ph (Scheme 22) affording a good yield of the saturated ketone. The yield of hydrogenation product was improved for the substrate *p*-(CF<sub>3</sub>)C<sub>6</sub>H<sub>4</sub>CH=CHC(O)Ph while the corresponding –OMe substituted substrate was not hydrogenated under these conditions [61].

In the case of the closely related FLP derived from the *n*-propyl substituted alkenylborane, **17a**/DABCO system only gave a small of the hydrogenation of the enone, PhCH=CHC(O)Ph. Nonetheless, the FLP derived from **17a**/*t*-Bu<sub>3</sub>P cleanly splits H<sub>2</sub>; however in this case a second molar equivalent of H<sub>2</sub> was consumed effecting the hydrogenation of the alkenylborane C=C double bond. The product, the saturated hydridoborate/phosphonium derivative **19** (Fig. 3, Scheme 23) [61], is a rare example of a hydrogenation of an alkenylborane [62].

## 2.6 Arene Hydrogenation

The FLP activation of H<sub>2</sub> is readily achieved by the combination of the amine *t*-BuNHPh/**3** under H<sub>2</sub> (4 atm) at 25 °C for 12 h, affording the salt [*t*-BuNH<sub>2</sub>Ph][HB(C<sub>6</sub>F<sub>5</sub>)<sub>3</sub>] **20** [63]. However, on prolonged heating at 110 °C for 96 h under H<sub>2</sub>, the *N*-bound phenyl ring is reduced yielding [*t*-BuNH<sub>2</sub>Cy][HB(C<sub>6</sub>F<sub>5</sub>)<sub>3</sub>] **21** (Scheme 24). In a similar fashion, hydrogenation with an equivalent of **3** of *i*-PrNHPh afforded [*i*-PrNH<sub>2</sub>Cy][HB(C<sub>6</sub>F<sub>5</sub>)<sub>3</sub>] while hydrogenation of PhCyNH or Ph<sub>2</sub>NH gave [Cy<sub>2</sub>NH<sub>2</sub>][HB(C<sub>6</sub>F<sub>5</sub>)<sub>3</sub>]. In a similar fashion, *i*-PrNH(2-MeC<sub>6</sub>H<sub>4</sub>), *i*-PrNH(4-RC<sub>6</sub>H<sub>4</sub>) (R = Me, OMe), *i*-PrNH(3-MeC<sub>6</sub>H<sub>4</sub>), and *i*-PrNH(3,5-Me<sub>2</sub>C<sub>6</sub>H<sub>3</sub>) (Table 4) were reduced with **3** under H<sub>2</sub> (4 atm) at 110 °C gave the corresponding products [*i*-PrNH<sub>2</sub>(2-MeC<sub>6</sub>H<sub>10</sub>)][HB(C<sub>6</sub>F<sub>5</sub>)<sub>3</sub>], [*i*-PrNH<sub>2</sub>(4-RC<sub>6</sub>H<sub>10</sub>)][HB(C<sub>6</sub>F<sub>5</sub>)<sub>3</sub>] (R = Me, OMe), [*i*-PrNH<sub>2</sub>(3-MeC<sub>6</sub>H<sub>10</sub>)][HB(C<sub>6</sub>F<sub>5</sub>)<sub>3</sub>], and [*i*-PrNH<sub>2</sub>(3,5-Me<sub>2</sub>C<sub>6</sub>H<sub>9</sub>)][HB

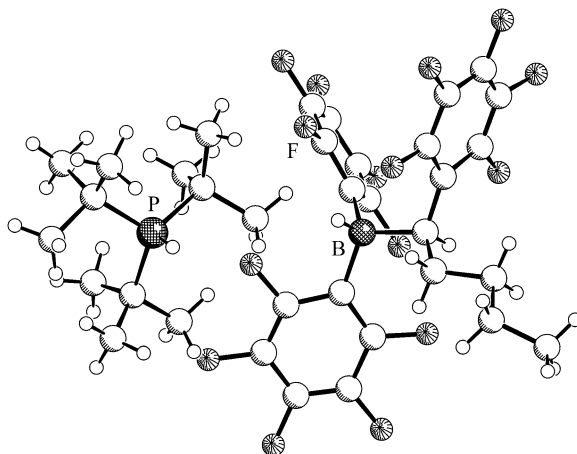
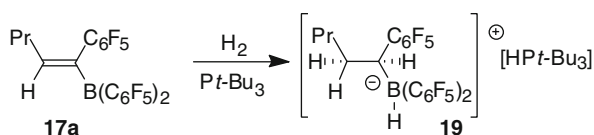


Fig. 3 A view of the molecular structure of compound **19**

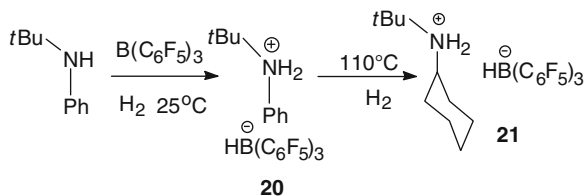


Scheme 23 Reaction of **17a**/Pt-Bu<sub>3</sub> with H<sub>2</sub>

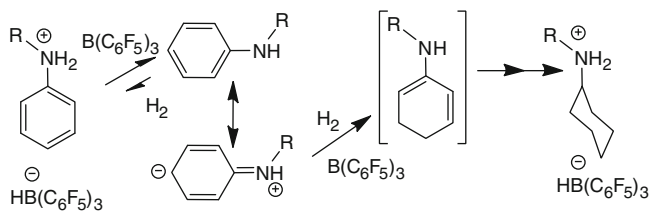
(C<sub>6</sub>F<sub>5</sub>)<sub>3</sub>] (Table 4). The yields ranged from 61 to 82% [63]. The corresponding treatment of *cis*-1,2,3-triphenylaziridine with **3** at 110 °C for 96 h yielded the salt [CyNH<sub>2</sub>CHPhCH<sub>2</sub>Ph][HB(C<sub>6</sub>F<sub>5</sub>)<sub>3</sub>] [63], in which only the *N*-bound phenyl ring is reduced. Similarly, the imines PhN=CMePh and (Me<sub>2</sub>C=N)<sub>2</sub>C<sub>6</sub>H<sub>4</sub> are reduced to [PhCH(Me)NH<sub>2</sub>Cy][HB(C<sub>6</sub>F<sub>5</sub>)<sub>3</sub>] and [(*i*-PrNH<sub>2</sub>)<sub>2</sub>C<sub>6</sub>H<sub>10</sub>][HB(C<sub>6</sub>F<sub>5</sub>)<sub>3</sub>]<sub>2</sub>, respectively (Table 4).

These unique reductions were also probed via computational studies. They suggest that the FLP activation of H<sub>2</sub> by amine *t*-BuNHPh and **3** is energetically 9.7 kcal/mol lower than the FLP. This relatively low barrier yields equilibrium conditions at elevated temperatures allowing for the amine to rotate attaining a van der Waals complex in which the *para*-carbon of the arene ring is proximal to boron. This provides an activation barrier of 8.7 kcal/mol, and thus a net free activation enthalpy (i.e., relative to the FLP) of 23.8 kcal/mol to the transient species [*t*-BuNHC<sub>6</sub>H<sub>6</sub>][HB(C<sub>6</sub>F<sub>5</sub>)<sub>3</sub>] which undergoes subsequent hydrogenation to effect the complete arene reduction (Scheme 25) [63].



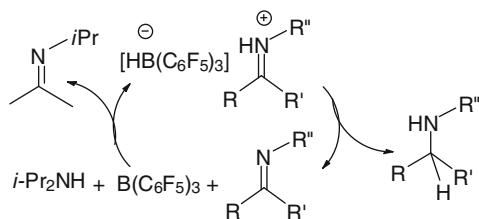
**Scheme 24** Hydrogenation of *tert*-butylaniline**Table 4** Aniline hydrogenations

Aniline	Product cation	<i>t</i> (h)	Y %
<i>t</i> -BuNHPh	[ <i>t</i> -BuNH <sub>2</sub> Cy] <sup>+</sup>	96	30
<i>i</i> -PrNHPh	[ <i>i</i> -PrNH <sub>2</sub> Cy] <sup>+</sup>	36	93
CyNHPh	[Cy <sub>2</sub> NH <sub>2</sub> ] <sup>+</sup>	36	88
Ph <sub>2</sub> NH	[Cy <sub>2</sub> NH <sub>2</sub> ] <sup>+</sup>	96	65
<i>i</i> -PrNH(2-MeC <sub>6</sub> H <sub>4</sub> )	[ <i>i</i> -PrNH <sub>2</sub> (2-MeC <sub>6</sub> H <sub>10</sub> )] <sup>+</sup>	36	77
<i>i</i> -PrNH(4-MeC <sub>6</sub> H <sub>4</sub> )	[ <i>i</i> -PrNH <sub>2</sub> (4-MeC <sub>6</sub> H <sub>10</sub> )] <sup>+</sup>	36	73
<i>i</i> -PrNH(4-MeOC <sub>6</sub> H <sub>4</sub> )	[ <i>i</i> -PrNH <sub>2</sub> (4-MeOC <sub>6</sub> H <sub>10</sub> )] <sup>+</sup>	36	61
<i>i</i> -PrNH(3-MeC <sub>6</sub> H <sub>4</sub> )	[ <i>i</i> -PrNH <sub>2</sub> (3-MeC <sub>6</sub> H <sub>10</sub> )] <sup>+</sup>	36	82
<i>i</i> -PrNH(3,5-Me <sub>2</sub> C <sub>6</sub> H <sub>3</sub> )	[ <i>i</i> -PrNH <sub>2</sub> (3,5-Me <sub>2</sub> C <sub>6</sub> H <sub>9</sub> )] <sup>+</sup>	72	48
PhN(C <sub>2</sub> H <sub>2</sub> Ph <sub>2</sub> )	[CyNH <sub>2</sub> (CH(Ph)CH <sub>2</sub> Ph)] <sup>+</sup>	96	50
PhN=C(Me)Ph	[CyNH <sub>2</sub> CH(Me)Ph] <sup>+</sup>	96	57
(Me <sub>2</sub> C=N) <sub>2</sub> C <sub>6</sub> H <sub>4</sub>	[( <i>i</i> -PrNH <sub>2</sub> ) <sub>2</sub> C <sub>6</sub> H <sub>10</sub> ] <sup>2+</sup>	72	64

**Scheme 25** Proposed reaction pathways to anilinium and cyclohexylammonium salts

## 2.7 Transfer Hydrogenations

Transfer hydrogenations of imines are also possible employing an FLP approach. Indeed, **3** is known to activate amines [64], and has recently been shown to effect the catalytic racemization of a chiral amine [65]. Extending this strategy to a bimolecular process, catalytic hydrogen transfer from *i*-Pr<sub>2</sub>NH to imines, enamines and N-heterocycles can be effected, although the catalyst loading varied from 1 to 20 mol%. The proposed catalytic cycle is illustrated in Scheme 26 (Table 5).



**Scheme 26** Proposed catalytic cycle for transfer hydrogenation

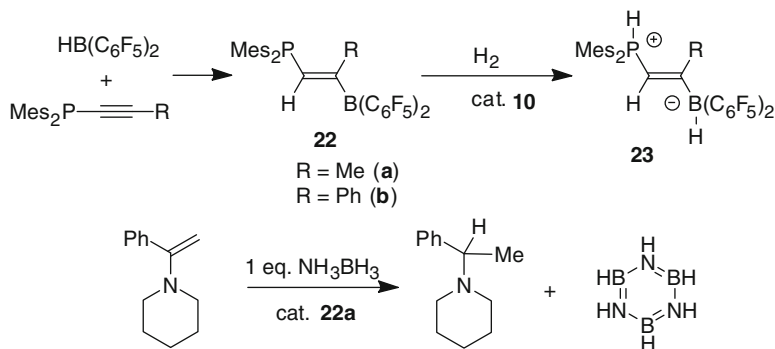
**Table 5** B(C<sub>6</sub>F<sub>5</sub>)<sub>3</sub> catalyzed transfer hydrogenations<sup>a</sup>

Substrate	Product	Cat. (mol%)	Yield (%)
PhCH=N <i>t</i> -Bu	PhCH <sub>2</sub> NH <i>t</i> -Bu	1	70
PhCH=N <i>t</i> -Bu	PhCH <sub>2</sub> NH <i>t</i> -Bu	5	98
PhCH=NC <sub>6</sub> H <sub>3</sub> Me <sub>2</sub>	PhCH <sub>2</sub> NHC <sub>6</sub> H <sub>3</sub> Me <sub>2</sub>	20	98
PhCH=NPh	PhCH <sub>2</sub> NHPh	20	98
PhC(Me)=NPh	PhC(Me)HNHPh	20	37
		20	90 <sup>b</sup>
C <sub>5</sub> H <sub>10</sub> NC <sub>6</sub> H <sub>9</sub>	C <sub>5</sub> H <sub>10</sub> NC <sub>6</sub> H <sub>11</sub>	20	98
		20	98
		20	56
		20	27

<sup>a</sup>24 h at 100 °C; yields determined by <sup>1</sup>H-NMR spectroscopy

<sup>b</sup>Mixture of diastereomers

The unsaturated intramolecular FLPs Z-Mes<sub>2</sub>PCH=CRB(C<sub>6</sub>F<sub>5</sub>)<sub>2</sub> **22** (R = Me, Ph) were readily available by HB(C<sub>6</sub>F<sub>5</sub>)<sub>2</sub> hydroboration of the corresponding phosphinoacetylene. While this FLP did not activate H<sub>2</sub>, treatment with a catalytic amount of **10** effected transfer of H<sup>+</sup>/H<sup>-</sup> pair affording the vicinal phosphonium/hydroborate zwitterions **23** (Scheme 27) [20]. Despite the inability of **22** to activate H<sub>2</sub>, it does act as an effective catalyst for the transfer of hydrogen from ammonia



**Scheme 27** Transfer hydrogenation of an enamine using ammonia borane

borane to an enamine as treatment of the enamine  $\text{Ph}(\text{NC}_5\text{H}_{10})\text{C}=\text{CH}_2$  with  $\text{H}_3\text{NBH}_3$  in the presence of ca. 16 mol% of **22a** resulted in the formation of the corresponding tertiary amine with concurrent formation of borazine (Scheme 27).

### 3 Conclusions

In the century since the discoveries of hydrogenations by Sabatier, the field has evolved to one of the most important reactions used in chemistry. The onset of organometallic chemistry and development of homogeneous catalysts in the 1960s were major landmarks in this field. The recent discovery of the FLP approach to metal-free heterolytic cleavage of  $\text{H}_2$  may also be viewed as a turning point. In the 5 years since the first report of FLP hydrogenations, the scope of substrates has broadened dramatically as has the studies of catalyst variations. To date, imines, aziridines, enamines, silyl enol ethers, diimines, metallocene derivatives and nitrogen-based heterocycles, olefins, and arene rings have been reduced employing this metal-free approach. It is clear that this is an exciting time and undoubtedly new developments of FLP systems will continue to emerge being driven by the potential for applications in academic and industrial settings.

**Acknowledgement** The authors thank their coworkers and their collaborating groups for their valuable contributions to the work described in this article. G.E. thanks the Deutsche Forschungsgemeinschaft, the Fond der Chemischen Industrie, the Alexander von Humboldt-Stiftung and the European Research Council for financial support. D.W.S. thanks NSERC of Canada for financial support and the award of a Canada Research Chair In addition, D.W.S. thanks the Killam Foundation and the Alexander von Humboldt-Stiftung for the award of Senior Research Fellowships.

## References

1. Mozingo R (1946) Palladium catalysts. *Org Synth* 26:77
2. Osborn JA, Jardine FH, Young JF, Wilkinso G (1966) Preparation and properties of tris (triphenylphosphine)halogenorhodium(1) and some reactions thereof including catalytic homogeneous hydrogenation of olefins and acetylenes and their derivatives. *J Chem Soc A* 1711
3. Noyori R (2002) Asymmetric catalysis: science and opportunities (Nobel Lecture). *Angew Chem Int Ed* 41:2008
4. Stephan DW, Erker G (2010) Frustrated Lewis pairs: metal-free hydrogen activation and more. *Angew Chem Int Ed* 49:46. doi:10.1002/anie.200903708
5. Dewitt EJ, Trapasso LE, Ramp FL (1961) Homogeneous hydrogenation catalyzed by boranes. *J Am Chem Soc* 83:4672
6. Ramp FL, Dewitt EJ, Trapasso LE (1962) Homogeneous hydrogenation catalyzed by boranes. *J Org Chem* 27:4368
7. Siskin M (1974) Strong acid chemistry. 2. Catalytic-hydrogenation of aromatics in hydrogen fluoride-tantalum pentafluoride and related strong acid systems. *J Am Chem Soc* 96:3641
8. Wristers J (1975) Strong acid-catalyzed hydrogenation of aromatics. *J Am Chem Soc* 97:4312
9. Yalpani M, Lunow T, Köster R (1989) Reduction of polycyclic arenes by BH-boranes. 2. Borane catalyzed hydrogenation of naphthalenes to tetralins. *Chem Ber* 122:687
10. Yalpani M, Köster R (1990) Partial hydrogenation – from anthracene to coronene. *Chem Ber* 123:719
11. Yalpani M, Koster R, Haenel MW (1990) Reductions of polycyclic arenes by B–H boranes. 4. Coal-tar hydrogenation catalyzed by B–H boranes. *Erdol Kohle Erdgas P* 43:344
12. Kötting C, Sander W (1999) Insertion of difluorovinylidene into hydrogen and methane. *J Am Chem Soc* 121:8891
13. Sander W, Kötting C (1999) Reactions of difluorovinylidene – a super-electrophilic carbene. *Chem Eur J* 5:24
14. Sander W, Hubert R, Kraka E, Grafenstein J, Cremer D (2000) 4-Oxo-2,3,5,6-tetrafluorocyclohexa-2,5-dienylidene – a highly electrophilic triplet carbene. *Chem Eur J* 6:4567
15. Haenel MW, Narangerel J, Richter UB, Rufinska A (2006) The first liquefaction of high-rank bituminous coals by preceding hydrogenation with homogeneous borane or iodine catalysts. *Angew Chem Int Ed* 45:1061. doi:10.1002/anie.200502614
16. Frey GD, Lavallo V, Donnadiu B, Schoeller WW, Bertrand G (2007) Carbenes reacting like metals, oxidative addition of H<sub>2</sub> and NH<sub>3</sub>. *Science* 316:439
17. Bettinger HF, Filthaus M, Neuhaus P (2009) Insertion into dihydrogen employing the nitrogen centre of a borylnitrene. *Chem Commun* 2186. doi:10.1039/B817270f
18. Bettinger HF, Filthaus M, Bornemann H, Oppel IM (2008) Metal-free conversion of methane and cycloalkanes to amines and amides by employing a borylnitrene. *Angew Chem Int Ed* 47:4744. doi:10.1002/anie.200705936
19. Chase PA, Welch GC, Jurca T, Stephan DW (2007) Metal-free catalytic hydrogenation. *Angew Chem Int Ed* 46:8050. doi:10.1002/anie.200702908
20. Spies P, Schwendemann S, Lange S, Kehr G, Fröhlich R, Erker G (2008) Metal-free catalytic hydrogenation of enamines, imines, and conjugated phosphinoalkenylboranes. *Angew Chem Int Ed* 47:7543. doi:10.1002/anie.200801432
21. Schwendemann S, Tumay TA, Axenov KV, Peuser I, Kehr G, Fröhlich R, Erker G (2010) Metal-free frustrated Lewis pair catalyzed 1,4-hydrogenation of conjugated metallocene dienamines. *Organometallics* 29:1067. doi:10.1021/Om900963p
22. Stephan DW, Greenberg S, Graham TW, Chase P, Hastie JJ, Geier SJ, Farrell JM, Brown CC, Heiden ZM, Welch GC, Ullrich M (2011) Metal-free catalytic hydrogenation of polar substrates by frustrated Lewis pairs. *Inorg Chem* 50:12338
23. Welch GC, Prieto R, Dureen MA, Lough AJ, Labeodan OA, Holtrichter-Rossmann T, Stephan DW (2009) Reactions of phosphines with electron deficient boranes. *Dalton Trans* 1559. doi:10.1039/B814486a

24. Chase PA, Jurca T, Stephan DW (2008) Lewis acid-catalyzed hydrogenation: B(C<sub>6</sub>F<sub>5</sub>)<sub>3</sub>-mediated reduction of imines and nitriles with H<sub>2</sub>. *Chem Commun* 1701. doi:10.1039/B718598g
25. Chen DJ, Klankermayer J (2008) Metal-free catalytic hydrogenation of imines with tris(perfluorophenyl) borane. *Chem Commun* 2130. doi:10.1039/B801806e
26. Geier SJ, Chase PA, Stephan DW (2010) Metal-free reductions of N-heterocycles via Lewis acid catalyzed hydrogenation. *Chem Commun* 46:4884. doi:10.1039/C0cc00719f
27. Rokob TA, Hamza A, Papai I (2009) Rationalizing the reactivity of frustrated Lewis pairs: thermodynamics of H<sub>2</sub> activation and the role of acid–base properties. *J Am Chem Soc* 131:10701. doi:10.1021/Ja903878z
28. Eros G, Mehdi H, Papai I, Rokob TA, Kiraly P, Tarkanyi G, Soos T (2010) Expanding the scope of metal-free catalytic hydrogenation through frustrated Lewis pair design. *Angew Chem Int Ed* 49:6559. doi:10.1002/anie.201001518
29. Rokob TA, Hamza A, Stirling A, Papai I (2009) On the mechanism of B(C<sub>6</sub>F<sub>5</sub>)<sub>3</sub>-catalyzed direct hydrogenation of imines: inherent and thermally induced frustration. *J Am Chem Soc* 131:2029. doi:10.1021/Ja809125r
30. Rokob TA, Hamza A, Stirling A, Soos T, Papai I (2008) Turning frustration into bond activation: a theoretical mechanistic study on heterolytic hydrogen splitting by frustrated Lewis pairs. *Angew Chem Int Ed* 47:2435. doi:10.1002/anie.200705586
31. Stirling A, Hamza A, Rokob TA, Papai I (2008) Concerted attack of frustrated Lewis acid–base pairs on olefinic double bonds: a theoretical study. *Chem Commun* 3148. doi:10.1039/B804662j
32. Spies P, Erker G, Kehr G, Bergander K, Fröhlich R, Grimme S, Stephan DW (2007) Rapid intramolecular heterolytic dihydrogen activation by a four-membered heterocyclic phosphane–borane adduct. *Chem Commun* 5072. doi:10.1039/B710475h
33. Grimme S, Kruse H, Goerigk L, Erker G (2010) The mechanism of dihydrogen activation by frustrated Lewis pairs revisited. *Angew Chem Int Ed* 49:1402. doi:10.1002/anie.200905484
34. Mömming CM, Fromel S, Kehr G, Fröhlich R, Grimme S, Erker G (2009) Reactions of an intramolecular frustrated Lewis pair with unsaturated substrates: evidence for a concerted olefin addition reaction. *J Am Chem Soc* 131:12280. doi:10.1021/Ja903511s
35. Thomson JW, Hatnean JA, Hastie JJ, Pasternak A, Stephan DW, Chase PA (2012) Scrubbers for metal-free hydrogenation catalysts (submitted)
36. Axenov KV, Kehr G, Fröhlich R, Erker G (2009) Functional group chemistry at the Group 4 bent metallocene frameworks: formation and "metal-free" catalytic hydrogenation of bis(imino-Cp)zirconium complexes. *Organometallics* 28:5148. doi:10.1021/Om9004093
37. Axenov KV, Kehr G, Fröhlich R, Erker G (2009) Catalytic hydrogenation of sensitive organometallic compounds by antagonistic N/B Lewis pair catalyst systems. *J Am Chem Soc* 131:3454. doi:10.1021/Ja8100006
38. Jiang CF, Blacque O, Berke H (2009) Metal-free hydrogen activation and hydrogenation of imines by 1,8-bis(dipentafluorophenylboryl)naphthalene. *Chem Commun* 5518. doi:10.1039/B909620e
39. Eros G, Nagy K, Mehdi H, Papai I, Nagy P, Kiraly P, Tarkanyi G, Soos T (2012) Catalytic hydrogenation with frustrated Lewis pairs: selectivity achieved by size-exclusion design of Lewis acids. *Chem Eur J* 18:574. doi:10.1002/chem.201102438
40. Sumerin V, Schulz F, Atsumi M, Wang C, Nieger M, Leskela M, Repo T, Pykko P, Rieger B (2008) Molecular tweezers for hydrogen: synthesis, characterization, and reactivity. *J Am Chem Soc* 130:14117. doi:10.1021/Ja806627s
41. Sumerin V, Schulz F, Nieger M, Leskela M, Repo T, Rieger B (2008) Facile heterolytic H<sub>2</sub> activation by amines and B(C<sub>6</sub>F<sub>5</sub>)<sub>3</sub>. *Angew Chem Int Ed* 47:6001. doi:10.1002/anie.200800935
42. Chen D, Leich V, Pan F, Klankermayer J (2012) Enantioselective hydrosilylation with chiral frustrated Lewis pairs. *Chem Eur J* 18:5184. doi:10.1002/chem.201200244
43. Chen DJ, Schmitkamp M, Francio G, Klankermayer J, Leitner W (2008) Enantioselective hydrogenation with racemic and enantiopure binap in the presence of a chiral ionic liquid. *Angew Chem Int Ed* 47:7339. doi:10.1002/anie.200801995

44. Wang HD, Fröhlich R, Kehr G, Erker G (2008) Heterolytic dihydrogen activation with the 1,8-bis(diphenylphosphino)-naphthalene/ $B(C_6F_5)_3$  pair and its application for metal-free catalytic hydrogenation of silyl enol ethers. *Chem Commun* 5966. doi:10.1039/B813286k
45. Welch GC, Juan RRS, Masuda JD, Stephan DW (2006) Reversible, metal-free hydrogen activation. *Science* 314:1124. doi:10.1126/science.1134230
46. Sumerin V, Schulz F, Nieger M, Atsumi M, Wang C, Leskela M, Pyykko P, Repo T, Rieger B (2009) Experimental and theoretical treatment of hydrogen splitting and storage in boron–nitrogen systems. *J Organomet Chem* 694:2654. doi:10.1016/j.jorganchem.2009.03.023
47. Spannhoff K (2010) C1-Verbrückte Diphosphine in Organometallchemie und frustrierten Lewis-Paaren, doctoral dissertation: Universität Münster
48. Parks DJ, Spence REVH, Piers WE (1995) Bis(pentafluorophenyl)borane – synthesis, properties, and hydroboration chemistry of a highly electrophilic borane reagent. *Angew Chem Int Ed Engl* 34:809
49. Parks DJ, Piers WE, Yap GPA (1998) Synthesis, properties, and hydroboration activity of the highly electrophilic borane bis(pentafluorophenyl)borane,  $HB(C_6F_5)_2$ . *Organometallics* 17:5492
50. Spence REV, Piers WE, Sun YM, Parvez M, MacGillivray LR, Zaworotko MJ (1998) Mechanistic aspects of the reactions of bis(pentafluorophenyl)borane with the dialkyl zirconocenes  $Cp_2ZrR_2$  ( $R = CH_3, CH_2SiMe_3, \text{ and } CH_2C_6H_5$ ). *Organometallics* 17:2459
51. Schwendemann S, Fröhlich R, Kehr G, Erker G (2011) Intramolecular frustrated N/B Lewis pairs by enamine hydroboration. *Chem Sci* 2:1842. doi:10.1039/C1sc00124h
52. Greb L, Ono-Burgos P, Schirmer B, Breher F, Grimme S, Stephan DW, Paradies J (2012) Metal-free catalytic olefin hydrogenations: low temperature  $H_2$ -activation by frustrated Lewis pairs. *Angew Chem Int Ed Engl* 51:10164–10168
53. Welch GC, Stephan DW (2007) Facile heterolytic cleavage of dihydrogen by phosphines and boranes. *J Am Chem Soc* 129:1880. doi:10.1021/Ja067961j
54. Xu BH, Kehr G, Fröhlich R, Wibbeling B, Schirmer B, Grimme S, Erker G (2011) Reaction of frustrated Lewis pairs with conjugated ynones-selective hydrogenation of the carbon–carbon triple bond. *Angew Chem Int Ed* 50:7183. doi:10.1002/anie.201101051
55. Chen C, Eweiner F, Wibbeling B, Fröhlich R, Senda S, Ohki Y, Tatsumi K, Grimme S, Kehr G, Erker G (2010) Exploring the limits of frustrated Lewis pair chemistry with alkynes: detection of a system that favors 1,1-carboboration over cooperative 1,2-P/B-addition. *Chem Asian J* 5:2199. doi:10.1002/asia.201000189
56. Chen C, Kehr G, Fröhlich R, Erker G (2010) Carbon–carbon bond activation by 1,1-carboboration of internal alkynes. *J Am Chem Soc* 132:13594. doi:10.1021/Ja106365j
57. Chen C, Voss T, Fröhlich R, Kehr G, Erker G (2011) 1,1-Carboboration of 1-alkynes: a conceptual alternative to the hydroboration reaction. *Org Lett* 13:62. doi:10.1021/Ol102544x
58. Kehr G, Erker G (2012) 1,1-Carboboration. *Chem Commun (Cambridge, UK)* 48:1839. doi:10.1039/c1cc15628d
59. Wrackmeyer B (1995) 1,1-Organoboration of alkynylsilicon, -germanium, -tin and -lead compounds. *Coord Chem Rev* 145:125
60. Wrackmeyer B (2006) Metallacyclopentadienes and related heterocycles via 1,1-organoboration of alkyne-1-ylmetal compounds. *Heteroat Chem* 17:188. doi:10.1002/Hc.20222
61. Reddy JS, Xu B, Mahdi T, Kehr G, Fröhlich R, Stephan DW, Erker G (2012) Alkenylboranes derived frustrated Lewis pairs: metal-free catalytic hydrogenation reactions of electron-deficient alkenes. *Organometallics*. doi:10.1021/om3006068
62. Ganic A, Pfaltz A (2012) Iridium-catalyzed enantioselective hydrogenation of alkenylboronic esters. *Chem Eur J* 18:6724. doi:10.1002/chem.201200246
63. Mahdi T, Heiden ZM, Grimme S, Stephan DW (2012) Metal-free aromatic hydrogenation: aniline to cyclohexyl-amine derivatives. *J Am Chem Soc* 134:4088. doi:10.1021/Ja300228a
64. Millot N, Santini CC, Fenet B, Basset JM (2002) Formation and characterization of zwitterionic stereoisomers from the reaction of  $B(C_6F_5)_3$  and  $NEt_2Ph$ : (E)- and (Z)- $[EtPhN=CHCH_2B(C_6F_5)_3]$ . *Eur J Inorg Chem* 3328
65. Farrell JM, Heiden ZM, Stephan DW (2011) Metal-free transfer hydrogenation catalysis by  $B(C_6F_5)_3$ . *Organometallics* 30:4497. doi:10.1021/Om2005832

# Amine-Borane Mediated Metal-Free Hydrogen Activation and Catalytic Hydrogenation

Victor Sumerin, Konstantin Chernichenko, Felix Schulz, Markku Leskelä, Bernhard Rieger, and Timo Repo

**Abstract** The use of frustrated Lewis pairs (FLPs) as hydrogenation catalysts is attracting increasing attention as one of the most modern and rapidly growing areas of organic chemistry, with many research groups around the world working on this subject. Since the pioneering studies of the groups of Stephan and Piers on the Lewis acid–base pairs, which do not react irreversibly with each other and act as a trap for small molecules, numerous FLPs for hydrogen activation have been reported. Among others, intra- and intermolecular systems based on phosphines, organic carbenes, amines as Lewis bases, and boranes or alanes as Lewis acids were studied. This review presents a progression from the first observation of the facile heterolytical cleavage of hydrogen gas by amines and  $B(C_6F_5)_3$  to highly active non-metal catalysts for both enantioselective and racemic hydrogenation of unsaturated nitrogen-containing compounds and also internal alkynes.

**Keywords** Amines · Aminoboranes · Boranes · FLP · Homogeneous catalysis · Hydrogenation · Organocatalysis

---

V. Sumerin  
Borealis Polymers Oy, P.O. Box 330,06101 Porvoo, Finland

K. Chernichenko · M. Leskelä · T. Repo (✉)  
Department of Chemistry, University of Helsinki, P.O. Box 55,00014 Helsinki, Finland  
e-mail: [timo.repo@helsinki.fi](mailto:timo.repo@helsinki.fi)

F. Schulz  
Clariant Produkte (Deutschland) GmbH, Waldheimer Straße 13, 83052 Bruckmühl, Germany

B. Rieger (✉)  
WACKER-Lehrstuhl für Makromolekulare Chemie, Technische Universität München,  
Lichtenbergstraße 4, 85747 Garching bei München, Germany  
e-mail: [rieger@tum.de](mailto:rieger@tum.de)

## Contents

1	Introduction .....	113
2	Pioneering Studies .....	113
3	Hydrogen Activation by Amines and Boranes .....	115
4	Hydrogenation by Amines and Boranes .....	123
5	Hydrogen Activation by Intramolecular <i>ansa</i> -Aminoboranes .....	129
6	Catalytic Hydrogenation of Unsaturated Nitrogen-Containing Compounds by Intramolecular <i>ansa</i> -Ammonium Borates .....	139
7	Enantioselective Hydrogenation of Unsaturated Nitrogen-Containing Compounds by Intramolecular <i>ansa</i> -Aminoboranes .....	145
8	Catalytic Hydrogenation of Unactivated Triple C–C Bonds by Intramolecular <i>ansa</i> - Aminoboranes .....	149
9	Conclusions .....	151
	References .....	152

## Abbreviations

1D NOE	One-dimensional nuclear Overhauser effect spectroscopy
2D NOESY	Two-dimensional nuclear Overhauser effect spectroscopy
9-BBN	9-Borabicyclo[3.3.1]nonane
BCF	Tris(pentafluorophenyl)borane
Bn	Benzyl
Bu	Butyl
d	Day(s)
DABCO	1,4-Diazabicyclo[2.2.2]octane
DFT	Density functional theory
DHB	Dihydrogen bond
DMDPP	<i>trans</i> -2,6-Dimethyl-2,6-diphenylpiperidine
ee	Enantiomer excess
equiv.	Equivalent(s)
Et	Ethyl
FLP	Frustrated Lewis pair
FT-IR	Fourier transform infrared spectroscopy
h	Hour(s)
<i>i</i> Pr	Isopropyl
<i>I</i> Bu	1,3-Di- <i>tert</i> -butylimidazolin-2-ylidene
LAB	Lewis acid–base
Me	Methyl
Mes	Mesityl 2,4,6-trimethylphenyl (not methanesulfonyl)
min	Minute(s)
MTBE	Methyl <i>tert</i> -butyl ether
NHC	<i>N</i> -Heterocyclic carbene
NMR	Nuclear magnetic resonance
Np	Naphthyl
<i>o</i> -Tol	<i>o</i> -Methylphenyl



Ph	Phenyl
PMP	<i>p</i> -Methoxyphenyl
Pr	Propyl
RT	Room temperature
<i>t</i> Bu	<i>tert</i> -Butyl
THF	Tetrahydrofuran
TMP	2,2,6,6-Tetramethylpiperidine
TMS	Trimethylsilyl
Tos	Tosyl 4-toluenesulfonyl
TRIP	3,3'-Bis(2,4,6-triisopropylphenyl)-1,1'-binaphthyl-2,2'-diyl hydrogenphosphate

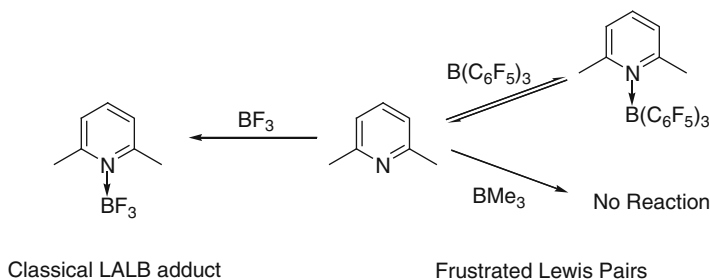
## 1 Introduction

During the past century, hydrogen activation and hydrogenation of unsaturated compounds under mild conditions was an exclusive prerogative of transition metals [1–3]. While there are countless synthetic and enzymatic complexes which contain a transition metal at their reactive core and that are able to cleave dihydrogen and catalytically reduce organic substrates, the H–H bond activation solely by non-metals under mild conditions was unknown until recently [4, 5]. In 2005–2007 different main group systems capable of hydrogen activation were reported and the “frustrated Lewis pairs (FLPs)” concept was introduced (Scheme 1) [6–9]. According to this concept, steric and/or electronic properties of the Lewis acid and the Lewis base prevent the irreversible classical Lewis acid–base (LAB) adduct formation. Recently, several metal-free FLP catalysts for the direct metal-free catalytic hydrogenation of imines, enamines, nitrogen-containing heterocycles, and non-terminal alkynes were developed.

Compared to traditional transition metal catalysts and enzymes, these systems offer many advantages related to catalyst selectivity, functional-group tolerance, environmental sustainability, cost-efficiency, and the fine purification of the final products [10–12]. This review concentrates on hydrogen activation and catalytic hydrogenation by intra- and inter-molecular amine-borane FLPs. The capabilities and limitations of such systems are described and compared to each other.

## 2 Pioneering Studies

Like many other organocatalytic methods, the FLP concept took a long time to mature. Remarkably, the first example of an unusual LAB pair, comprising amine and borane, dates back to 1942, when Brown and co-workers reported that



**Scheme 1** Classical versus frustrated Lewis pairs

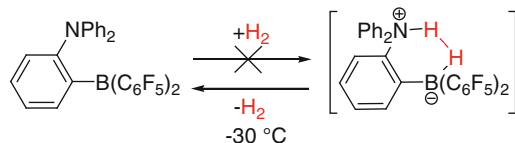


**Scheme 2** Reversible hydrogen activation by Stephan's "frustrated" phosphinoborane [6]

2,6-lutidine reacts with  $\text{BF}_3$  to give a stable classical LAB adduct in quantitative yield, but does not react with  $\text{BMe}_3$  even at low temperature (Scheme 1) [13]. Moreover, the subsequent reactivity of unusual LAB pairs with other molecules had already been discovered by Wittig and co-workers in the 1950s. For instance, they showed that a mixture of tritylsodium ( $\text{Ph}_3\text{CNa}$ ) with triphenylborane ( $\text{Ph}_3\text{B}$ ) can attack suitable substrates like tetrahydrofuran, 2,3-dimethylbutadiene, and carbon monoxide nucleophilically and electrophilically at the same time to form new organosodium compounds [14–18]. However, as with other metal-free catalytic transformations, FLPs required a key discovery – reversible hydrogen activation by a nonmetal system based on bulky phosphinoborane in 2006 – to boost the research activity in this field (Scheme 2) [6].

The key to the successful heterolytic cleavage of  $\text{H}_2$  under mild conditions by Stephan's phosphinoborane is the use of the LAB pair with correctly matched electronic and steric properties. While steric repulsion is sufficient to preclude the formation of the phosphine-borane adduct, the Lewis acidity of the boron and the Lewis basicity of the phosphorus atoms are high enough to favor thermodynamically the formation of a hydrogenated product at room temperature. When the reaction is almost thermodynamically neutral, facile hydrogen liberation takes place at elevated temperature [19]. In an analogous fashion, later, mixtures of sterically demanding phosphines and  $\text{B}(\text{C}_6\text{F}_5)_3$  were also shown to cleave  $\text{H}_2$  heterolytically. However, the resulting phosphonium-borates  $[\text{R}_3\text{PH}][\text{HB}(\text{C}_6\text{F}_5)_3]$  ( $\text{R} = t\text{Bu}, o\text{-MeC}_6\text{H}_4, \text{Mes}$ ) were more stable and did not release hydrogen even upon heating at 150 C [7].

Looking back now, 3 years before Stephan's "frustrated" phosphinoborane, there was an important prerequisite for the discovery of FLPs. In 2003 Roesler and Piers published "synthesis, structural characterization and reactivity of the



**Scheme 3** Piers' aminoborane and ammonium borate [20]

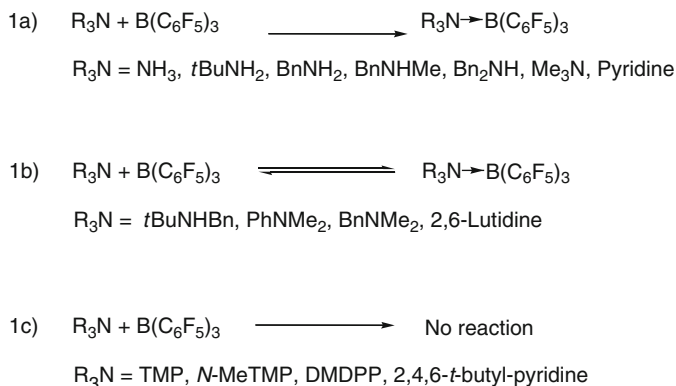
amino borane 1-(NPh<sub>2</sub>)-2-[B(C<sub>6</sub>F<sub>5</sub>)<sub>2</sub>]C<sub>6</sub>H<sub>4</sub>", invited paper in *Journal of Organometallic Chemistry*, which is a specialized journal and as a result their work was not recognized at that time. In this article, they described the first "frustrated" intramolecular LAB system, where the active Lewis acidic boron and Lewis basic nitrogen centers were located close to each other and did not form a classical LAB adduct due to the steric hindrance of the bulky amine and borane moieties and the high strain energy of the corresponding four-membered ring [20].

Roesler and Piers also predicted that such a "Lewis acid/Lewis base trap" would be suitable for the reversible activation of H<sub>2</sub> (Scheme 3). Specifically, they not only speculated that ammonium borate *o*-Ph<sub>2</sub>NH<sup>+</sup>-C<sub>6</sub>H<sub>4</sub>-[HB(C<sub>6</sub>F<sub>5</sub>)<sub>2</sub>]<sup>-</sup> might be a "dihydrogen storage device, able to release H<sub>2</sub> upon heating or during a chemical reaction, regenerating" aminoborane *o*-Ph<sub>2</sub>N-C<sub>6</sub>H<sub>4</sub>-B(C<sub>6</sub>F<sub>5</sub>)<sub>2</sub>, but also suggested that strong N-H<sup>δ+</sup>...<sup>δ-</sup>H-B dihydrogen bond (DHB) interactions would play a key role in this process. Unfortunately, Piers' aminoborane was unable to cleave H<sub>2</sub> due to another important observation made in this paper: the significantly reduced basicity of the amino group, which "would have to be significantly higher in order to thermodynamically favor the formation of a dihydrogen adduct over the elimination of hydrogen". Although the hydrogenated system was never characterized, attempts to generate ammonium borate in situ led to spontaneous liberation of dihydrogen gas even at low temperature.

Nevertheless, their "frustrated" aminoborane was extremely sensitive to moisture and acids or, in other words, was able to activate H<sub>2</sub>O and HCl forming zwitterionic products. Recently, analogous properties of ammonium and phosphonium boranes were found to be essential for the selective receptors for cyanide and fluoride ions in water at neutral pH [21–23]. Moreover, as we showed recently, a simple replacement of the diphenylamino moiety by the more electron-donating dimethylamino group led to aminoborane *o*-Me<sub>2</sub>N-C<sub>6</sub>H<sub>4</sub>-B(C<sub>6</sub>F<sub>5</sub>)<sub>2</sub>, which is indeed able to activate reversibly hydrogen gas [24].

### 3 Hydrogen Activation by Amines and Boranes

The FLP concept states that steric and/or electronic properties of the corresponding Lewis acid and Lewis base should be appropriate to preclude the irreversible LAB adduct formation [25]. Indeed, the first examples of FLP systems, which were able to cleave hydrogen in a facile manner, consisted of extremely bulky phosphines and



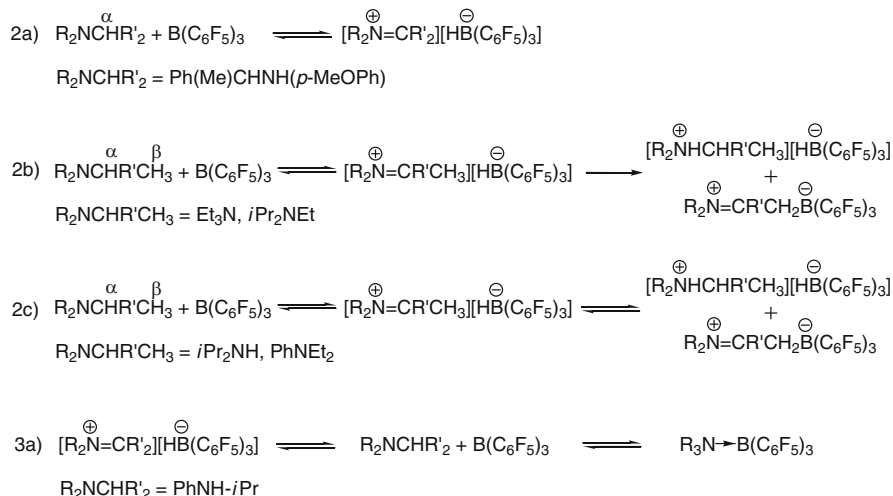
**Scheme 4** LAB interactions between amines and  $B(C_6F_5)_3$

tris(pentafluorophenyl)borane [6, 7]. This was due to the fact that less sterically hindered phosphines can react with  $B(C_6F_5)_3$  forming stable LAB adducts or can undergo nucleophilic substitution of the *para*-fluorine atom, giving intramolecular phosphonium-borates [26]. Thus, there are only a few commercially available bulky phosphines, such as  $Me_3P$ , *o*-Tol $_3P$ ,  $tBu_3P$ , that can be used for hydrogen activation in combination with highly Lewis acidic boranes [7, 27]. Even then, in some cases, despite the seeming simplicity of such FLPs, the mechanistic picture is rather complex and includes the in situ formation of phosphinoboranes  $p\text{-}R_2PC_6F_4B(C_6F_5)_2$ , which can further catalyze phosphonium-borate formation, for example  $[tBu_3PH][HB(C_6F_5)_3]$  [28].

A logical development of the FLP systems, but still significant, was the implementation of bulky amines as Lewis basic components [29]. Since the carbon–nitrogen bond is shorter than the carbon–phosphorus bond, a much broader variety of sterically hindered amines is readily and commercially available. Furthermore, in contrast to bulky phosphines, such amines are air-stable and inexpensive.

Similarly to non-bulky phosphines and  $B(C_6F_5)_3$ , the binary mixtures of amines and boranes can undergo different transformations depending on their steric, electronic, and chemical properties [30–33]. These transformations can be classified into two categories: the classical LAB adduct formation and the abstraction of an  $\alpha$ -hydride from an amine by the Lewis acidic  $B(C_6F_5)_3$  (Schemes 4 and 5). In the first case, whilst sterically accessible amines and pyridines react with boranes forming stable LAB adducts (Scheme 4, 1a), the reactions of more sterically hindered amines or pyridines with  $B(C_6F_5)_3$  are fully reversible either at room or elevated temperature (Scheme 4, 1b). In addition, no interaction between the most bulky amines and  $B(C_6F_5)_3$  can be detected via NMR spectroscopy, even at low temperature (Scheme 4, 1c). Generally, in this case the steric effects prevail over electronic effects.

However, if the steric effects are large enough to prevent irreversible LAB adduct formation, then, depending on their electronic properties, amines and anilines that contain an aliphatic chain with  $\alpha$ - or  $\alpha$ - and  $\beta$ -protons next to each

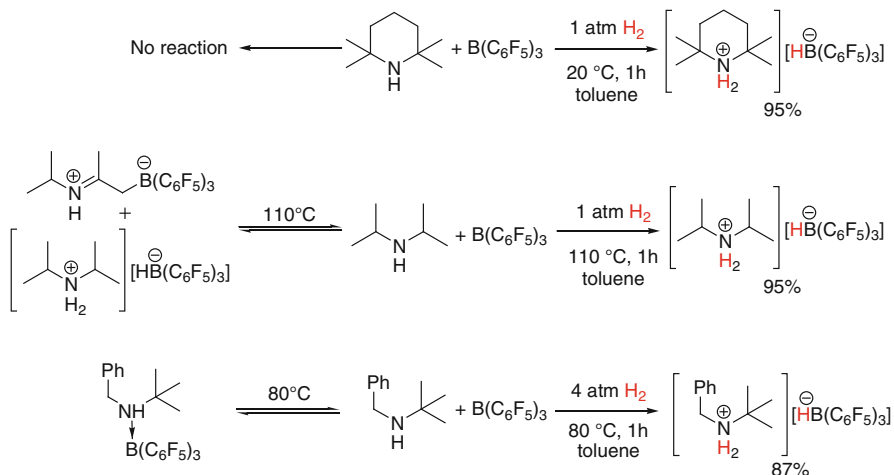


**Scheme 5** LAB interactions between amines and  $B(C_6F_5)_3$

other (like Me, Bn or Et, *n*-Pr, *i*Pr groups) may exhibit completely different reactivities towards tris(pentafluorophenyl)borane. In this case, the reaction of various amines with  $B(C_6F_5)_3$  results in an  $\alpha$ -hydride abstraction by the Lewis acidic borane from an amine, followed by the reversible formation of iminium borohydride (Scheme 5, 2a). The racemization of enantioenriched amines catalyzed by  $B(C_6F_5)_3$  is an example of this type of reaction [34, 35]. When both  $\alpha$  and  $\beta$  protons are present in the alkyl chain of an amine, the reaction can proceed further to produce, in either an irreversible or a reversible manner, a mixture of zwitterion iminium borate and ammonium borohydride (Scheme 5, 2b and 2c). In some cases, as with *N*-isopropylaniline and  $B(C_6F_5)_3$ , both LAB adduct formation and abstraction of an  $\alpha$ -hydride pathways were observed (Scheme 5, 3a).

The above examples demonstrate a wide range of possible interactions between amines and  $B(C_6F_5)_3$ . Nevertheless, in most of the cases (1b, 2a, 2c, 3a) the free amine and tris(pentafluorophenyl)borane are in equilibrium with the products of the reaction or do not react with each other at all (1c), and can be used in the subsequent activation of small molecules.

The first examples of hydrogen activation by intermolecular amine-borane based FLP systems were reported in 2008 by us and others (Scheme 6) [29, 36]. Specifically, the facile heterolytic cleavage of  $H_2$  was readily achieved by the cooperative action of the Lewis basic 2,2,6,6-tetramethylpiperidine, diisopropylamine, and *tert*-butylbenzylamine with Lewis acidic tris(pentafluorophenyl)borane at 20°C, 100°C, and 80°C, respectively, to afford the corresponding  $[R_2NH_2]^+[HB(C_6F_5)_3]^-$  products (Scheme 6). Since less bulky diisopropylamine or *tert*-butylbenzylamine react with  $B(C_6F_5)_3$  to give a mixture of iminium borate and ammonium borohydride or the LAB adduct, the higher temperatures were required in order to shift equilibria toward the free amines and borane. The more sterically hindered



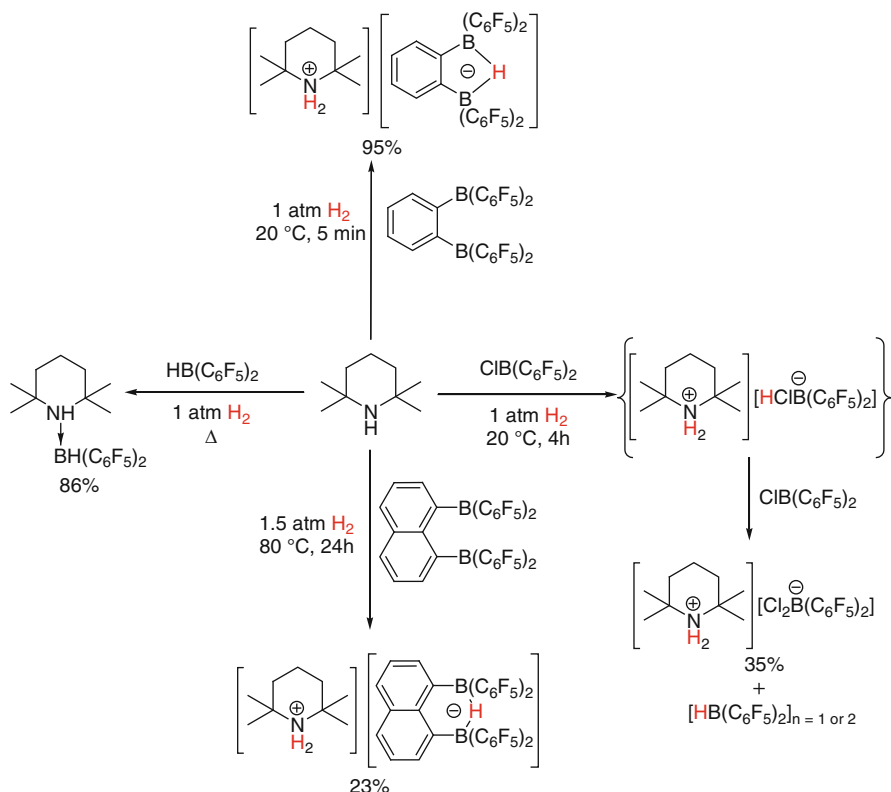
**Scheme 6** Hydrogen activation by bulky amines and  $B(C_6F_5)_3$  [29, 36]

2,2,6,6-tetramethylpiperidine without  $\alpha$ -protons does not react with  $B(C_6F_5)_3$  even at low temperature, meaning that the TMP/ $B(C_6F_5)_3$  system is capable of splitting  $H_2$  at temperature as low as  $-80^\circ C$  [37].

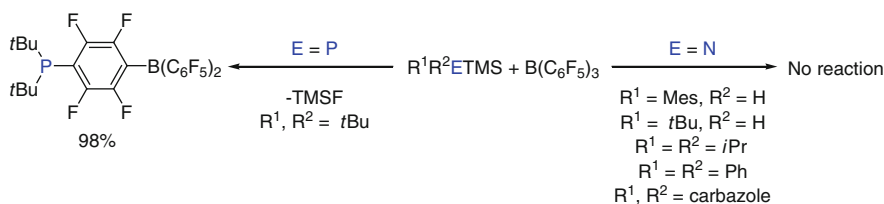
Later, hydrogen activation by the FLPs of TMP and different boranes was also studied (Scheme 7). Similar to the reaction with  $B(C_6F_5)_3$ , bis(pentafluorophenyl) chloroborane  $ClB(C_6F_5)_2$  reacted with TMP under an atmosphere of  $H_2$  to yield initially  $[TMPH]^+[ClHB(C_6F_5)_2]^-$ , which was not stable in the presence of  $ClB(C_6F_5)_2$  and dismutates subsequently into  $[TMPH]^+[Cl_2B(C_6F_5)_2]^-$  and  $HB(C_6F_5)_2$  [37]. While, in combination with more Lewis acidic 1,2-bis(pentafluorophenylboryl) benzene  $[(C_6F_5)_2B]_2C_6H_4$  an almost quantitative yield of the hydrogenated product was achieved in less than 5 min instead of 1 h with  $B(C_6F_5)_3$ , the reaction with more bulky 1,8-bis(dipentafluorophenylboryl)naphthalene required prolonged heating at  $80^\circ C$  and gave a low product yield (unpublished results) [38]. Even at elevated temperatures the less sterically hindered Piers' bis(pentafluorophenyl)borane  $HB(C_6F_5)_2$  reacted with TMP to give a very stable LAB adduct [37].

In order to extend the family of FLPs based on amines and borane, we investigated the behavior of simple *N*-trimethylsilyl protected amines as Lewis bases in combination with  $B(C_6F_5)_3$  [39]. The usage of TMS substituted amines has a couple of advantages. First, most *N*-TMS-amines are bulky enough and should not form stable adducts with  $B(C_6F_5)_3$ . Second, they are easily synthesized or commercially available.

In contrast to bulky *P*-TMS-phosphines that undergo nucleophilic aromatic substitution reaction of the *para*-fluorine atom, the less nucleophilic *N*-TMS-amines do not react with  $B(C_6F_5)_3$  (Scheme 8). Exposing toluene solutions of *N*-TMS-amines and  $B(C_6F_5)_3$  to an atmosphere of  $H_2$  (1.5 atm) showed different reactivity of such FLPs. Whilst less Lewis basic trimethylsilyldiphenylamine or trimethylsilylcarbazole together with tris(pentafluorophenyl)borane did not react with  $H_2$  at  $110^\circ C$ , more basic  $MesNHTMS$ ,  $tBuNHTMS$ , or  $iPr_2NTMS$  and  $B(C_6F_5)_3$  cleaved hydrogen even at



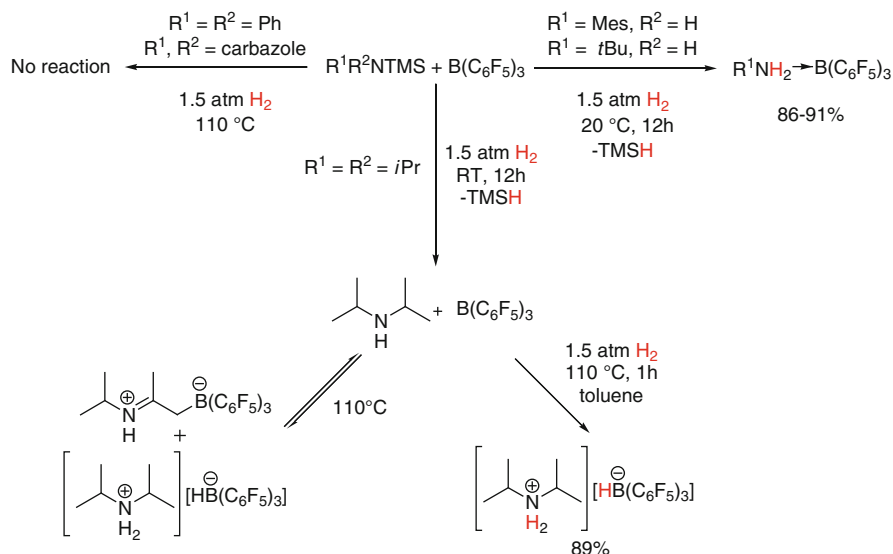
**Scheme 7** Hydrogen activation by TMP and boranes (unpublished results) [37, 38]



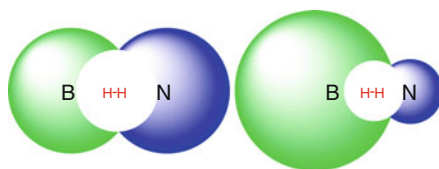
**Scheme 8** Interactions between bulky *N*-TMS-amines and *P*-TMS-phosphines with  $B(C_6F_5)_3$  [39]

room temperature in a facile manner (Scheme 9). In addition to the previous study on the influence of Lewis acidity on the hydrogen activation (Scheme 7), this finding suggests that the Lewis basicity of the amine should also be high enough to favor thermodynamically the cleavage of the  $H_2$  bond.

Based on real-time NMR studies we assumed that hydrogen splitting by MesNHTMS, *t*BuNHTMS, and *i*Pr<sub>2</sub>NTMS in combination with  $B(C_6F_5)_3$  resulted in *N*-TMS-ammonium borohydrides. However, the formed salts were not stable and



**Scheme 9** Hydrogen activation by bulky TMS-amines and  $\text{B}(\text{C}_6\text{F}_5)_3$  [39]

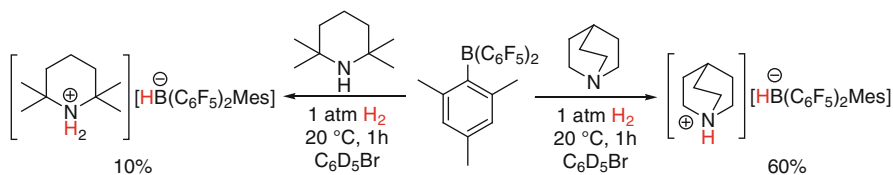


**Scheme 10** Relative steric hindrance phenomenon in hydrogen activation by amines and boranes

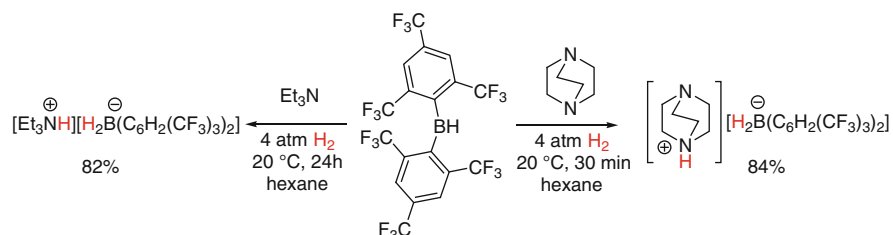
spontaneously liberated TMSH gas (bp = 6.7°C). The stable LAB adducts were formed as the ultimate reaction products in the cases of mesitylaniline and *tert*-butylamine. The reaction of more bulky diisopropyltrimethylsilylamine and  $\text{B}(\text{C}_6\text{F}_5)_3$  with  $\text{H}_2$  afforded the expected 1:1 mixture of the salt  $[i\text{Pr}_2\text{NH}_2]^+[\text{HB}(\text{C}_6\text{F}_5)_3]^-$  and the zwitterion  $i\text{PrN}^+\text{H}=\text{C}(\text{CH}_3)\text{CH}_2\text{B}^-(\text{C}_6\text{F}_5)_3$ . As described earlier, the two former compounds are in an equilibrium with the free diisopropylamine and  $\text{B}(\text{C}_6\text{F}_5)_3$  at 110°C, and can further split hydrogen upon heating (Scheme 9).

In 2010 Soós and co-workers demonstrated that steric hindrance required for  $\text{H}_2$  activation in FLPs is a complementary phenomenon (Scheme 10) [40, 41]. They found that further increase of the steric bulk of the *ortho*-substituted aryl groups of the active boron center leads to Lewis acids with a remarkably high tolerance to the nature of the corresponding Lewis bases. Thus, in contrast to  $\text{B}(\text{C}_6\text{F}_5)_3$  (Schemes 4 and 5), even non-bulky amines with  $\alpha$ - and  $\beta$ -protons next to each other can be used as a Lewis basic part of FLPs in combination with more sterically hindered  $\text{MesB}(\text{C}_6\text{F}_5)_2$ . For instance, FLP consisting of quinuclidine or DABCO and  $\text{MesB}(\text{C}_6\text{F}_5)_2$  showed faster  $\text{H}_2$  splitting than the bulky TMP/ $\text{MesB}(\text{C}_6\text{F}_5)_2$  system (Scheme 11).





**Scheme 11** Hydrogen activation by amines and  $\text{MesB}(\text{C}_6\text{F}_5)_2$  [40]

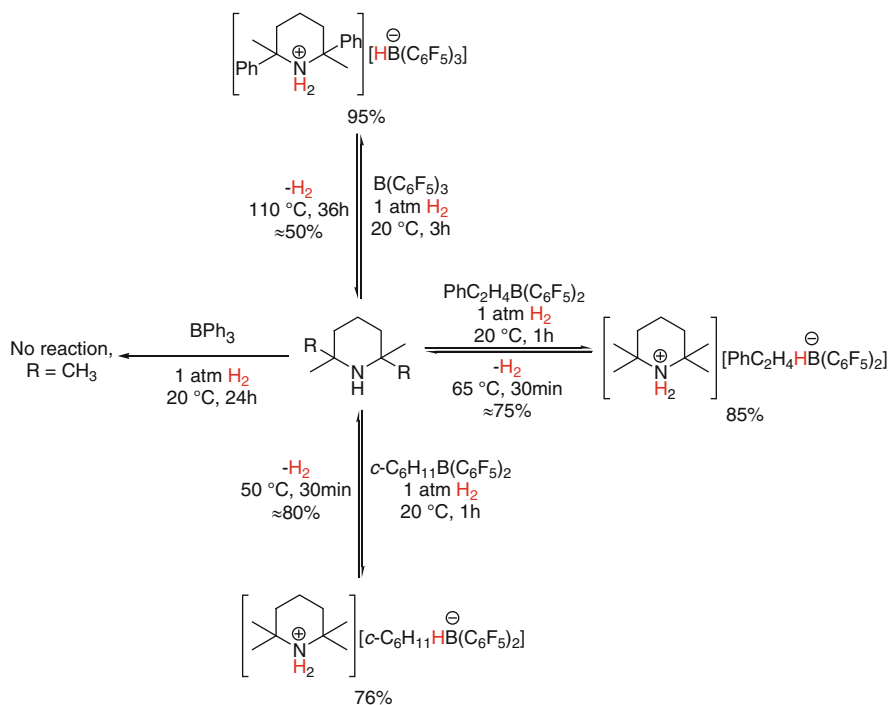


**Scheme 12** Hydrogen activation by amines and  $(2,4,6\text{-(CF}_3)_3\text{C}_6\text{H}_2)_2\text{BH}$  [42]

More recently, Li and Wang et al. also reported that the secondary borane with extremely bulky and electron-withdrawing 2,4,6-tris(trifluoromethyl)phenyl groups, together with simple sterically benign amines, can activate hydrogen under mild conditions (Scheme 12) [42].

Unfortunately, none of the amine-borane FLP systems described above was able to liberate hydrogen upon heating. However, as it was shown by us and others to facilitate the hydrogen release reaction, the activation of  $\text{H}_2$  by FLP should be almost thermodynamically neutral [19, 43–45]. Thus, the FLP systems derived from less Lewis basic amines and  $\text{B}(\text{C}_6\text{F}_5)_3$  or less Lewis acidic boranes and TMP can heterolytically cleave hydrogen under ambient conditions to form ammonium borohydrides, which can liberate hydrogen at higher temperatures (Scheme 13).

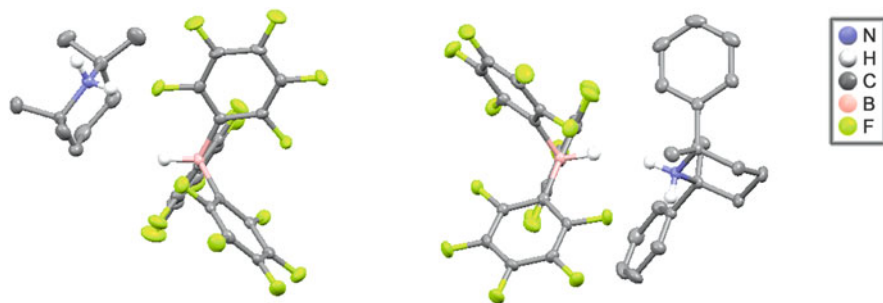
While the main factor for the reversible hydrogen activation by intermolecular amine-borane FLP systems was shown to be the reduced Lewis acidity of the boron center, the changes in the Lewis basicity of amines turned out to be of secondary importance. Specifically, the ammonium borohydrides prepared from TMP and cyclohexylbis(pentafluorophenyl)borane or 1-phenyl-2-[bis(pentafluorophenyl)boryl]ethane, exhibiting 15% and 10% lower acidity than  $\text{B}(\text{C}_6\text{F}_5)_3$ , easily liberate hydrogen at  $50^\circ\text{C}$  or  $65^\circ\text{C}$ , respectively [44]. In contrast to that, the hydrogen release reaction from the hydrogenated FLP system based on  $\text{B}(\text{C}_6\text{F}_5)_3$  and *trans*-2,6-dimethyl-2,6-diphenylpiperidine, which is about 15% less basic than TMP, required a higher temperature and longer time ( $110^\circ\text{C}$  and 36 h) to yield 50% of the free amine and borane [43]. Moreover, if the Lewis acidity of the borane is too low, the corresponding FLP, for instance triphenylborane ( $\text{BPh}_3$ ) and 2,2,6,6-tetramethylpiperidine, may not form a stable ammonium borohydride [29].



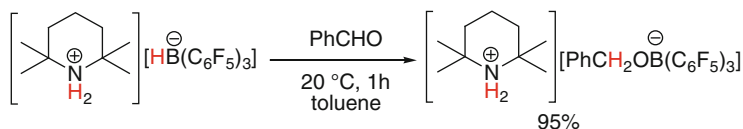
**Scheme 13** Reversible hydrogen activation by amines and boranes [29, 43, 44]

The structures of different ammonium borohydrides were determined by X-ray diffraction crystallography. It was found that the ammonium and borohydride ions in these compounds are usually connected by a network of N–H⋯F and C–H⋯F hydrogen bonds (Fig. 1, left). Additionally, a strong N–H⋯H–B dihydrogen bond the length of which is less than 2.0 Å can be present (Fig. 1, right) [36, 43, 44]. However, the ability to liberate hydrogen by intermolecular ammonium borohydrides was shown to correlate mainly with the strength of the B–H and N–H bonds rather than with a close interaction between the protonic and hydridic hydrogen atoms [44].

All of these results support the idea that the reversible hydrogen activation requires amines and boranes with fine-tuned steric and electronic properties. First, the steric constraints between the Lewis acid and Lewis base and their electronic properties must be sufficient to provide at least the equilibrium amounts of free amine and borane. Second, the power of the FLP, which depends on the basicity of the Lewis base and the acidity of the Lewis acid counterparts, should be high enough to favor thermodynamically the formation of a hydrogenated product at mild temperature, but not too high to facilitate hydrogen liberation at elevated temperature. Although the detailed mechanisms of hydrogen activation solely by boranes or by FLPs have been investigated in some detail, they are still a subject of debate and not the focus of this review [19, 42, 46–53].



**Fig. 1** X-ray structures of [TMPH]<sup>+</sup>[HB(C<sub>6</sub>F<sub>5</sub>)<sub>3</sub>]<sup>-</sup> (left) and [DMDPPH]<sup>+</sup>[HB(C<sub>6</sub>F<sub>5</sub>)<sub>3</sub>]<sup>-</sup> (right) [29, 43]



**Scheme 14** Stoichiometric reduction of benzaldehyde by [TMPH]<sup>+</sup>[HB(C<sub>6</sub>F<sub>5</sub>)<sub>3</sub>]<sup>-</sup> [29]

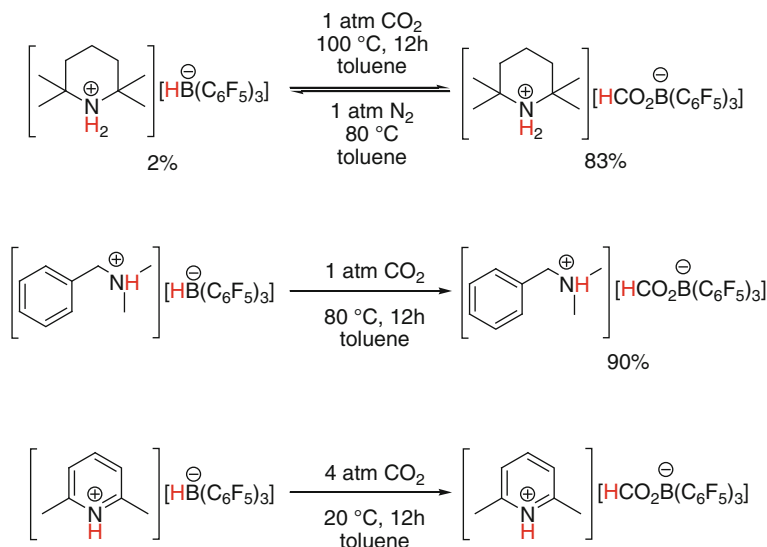
## 4 Hydrogenation by Amines and Boranes

The subsequent reactivity of ammonium borohydrides obtained through hydrogen activation by amine-borane FLP systems was investigated. In a preliminary experiment, benzaldehyde was selectively and rapidly reduced at room temperature to a product with the molecular formula [TMPH]<sup>+</sup>[PhCH<sub>2</sub>OB(C<sub>6</sub>F<sub>5</sub>)<sub>3</sub>]<sup>-</sup> in 95% yield by employing [TMPH]<sup>+</sup>[HB(C<sub>6</sub>F<sub>5</sub>)<sub>3</sub>]<sup>-</sup> as a stoichiometric reducing agent (Scheme 14) [29].

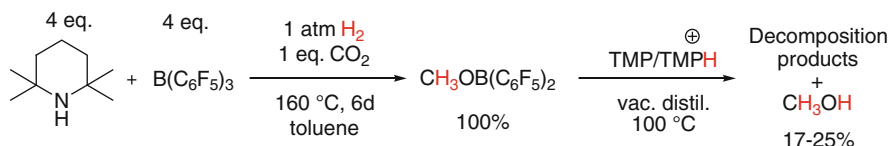
Later, different ammonium borohydrides were also successfully applied in the stoichiometric fixation of CO<sub>2</sub>, which is a promising C1 feedstock for the production of many chemicals (Scheme 15) [31, 54, 55]. Moreover, because the zwitterionic *N*-heterocyclic carbene adduct with CO<sub>2</sub> was recently considered as the key intermediate in the deoxygenative hydrosilylation of CO<sub>2</sub> by diphenylsilane to CH<sub>3</sub>OH upon workup, this initial finding foreshadowed the potential of ammonium borohydrides to act as CO<sub>2</sub> activator for its further reduction [56].

Indeed, a procedure for the in situ quantitative hydrogenation of CO<sub>2</sub> to methoxy-(bis(pentafluorophenyl))borane with a four times excess of the TMP/B(C<sub>6</sub>F<sub>5</sub>)<sub>3</sub> pair was reported by O'Hare and co-workers (Scheme 16) [54]. Unfortunately, further cleavage of the B–O bond was rather difficult due to the high bond energy of the B–O bond (560–790 kJ/mol) which makes it hard to break, and the desired methanol product was obtained in very low yield (Scheme 16) [57].

More recently, Piers et al. demonstrated that a tandem catalyst, based on [TMPH]<sup>+</sup>[HB(C<sub>6</sub>F<sub>5</sub>)<sub>3</sub>]<sup>-</sup> together with B(C<sub>6</sub>F<sub>5</sub>)<sub>3</sub> and in the presence of excess of triethylsilane as a reducing and deoxygenative agent, can convert carbon dioxide



**Scheme 15** CO<sub>2</sub> fixation by ammonium and lutidinium borohydrides [31, 54, 55]



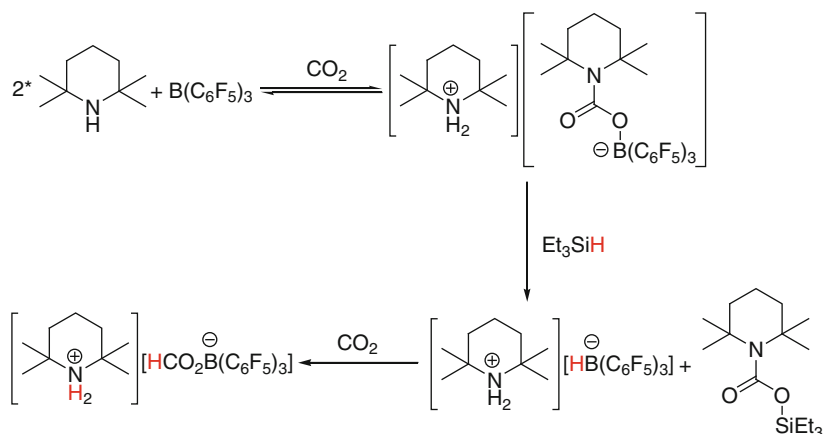
**Scheme 16** Reduction of CO<sub>2</sub> to methanol by TMP/B(C<sub>6</sub>F<sub>5</sub>)<sub>3</sub> FLP [54]

directly to methane under mild conditions [58]. The TMP/B(C<sub>6</sub>F<sub>5</sub>)<sub>3</sub> FLP reacts with CO<sub>2</sub> (2–4 atm) in the presence of Et<sub>3</sub>SiH at 56 °C in C<sub>6</sub>D<sub>5</sub>Br to afford ammonium borohydride [TMPH]<sup>+</sup>[HB(C<sub>6</sub>F<sub>5</sub>)<sub>3</sub>]<sup>−</sup> which further reacts with CO<sub>2</sub> to give the previously reported ammonium formateborate [TMPH]<sup>+</sup>[HCO<sub>2</sub>B(C<sub>6</sub>F<sub>5</sub>)<sub>3</sub>]<sup>−</sup> (Scheme 17).

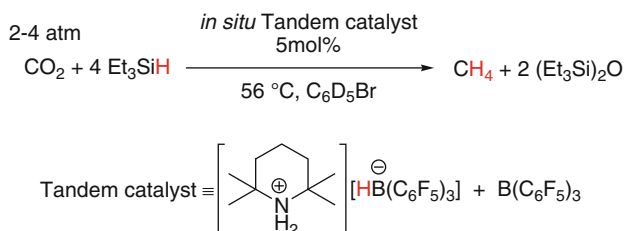
Further addition of a catalytic amount of B(C<sub>6</sub>F<sub>5</sub>)<sub>3</sub> to the reaction mixture results in the immediate and complete conversion of ammonium formateborate back into the starting ammonium borohydride and the appearance of CH<sub>4</sub> along with 2 equiv. of (Et<sub>3</sub>Si)<sub>2</sub>O as the final reaction products (Scheme 18).

Whilst the reduction of carbonyl compounds by FLPs is still rather limited, simple tris(pentafluorophenyl)borane, 1,8-bis(dipentafluorophenyl)naphthalene, and others were recently shown to catalyze the direct hydrogenation of bulky imines, anilines, and quinolines (Table 1) (unpublished results) [36, 59–62].

The initiation step in this transformation involves heterolytic splitting of H<sub>2</sub> by the imino-borane FLP to generate an iminium borohydride, which can be further reduced by nucleophilic attack of a hydride ion on the iminium carbon atom to afford the corresponding amine in the form of an LAB adduct with B(C<sub>6</sub>F<sub>5</sub>)<sub>3</sub>.



**Scheme 17** Formation of the key ammonium formatoborate intermediate [58]



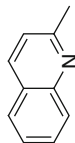
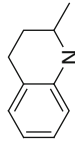
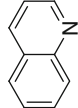
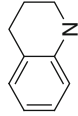
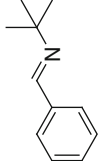
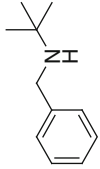
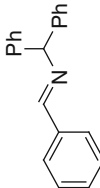
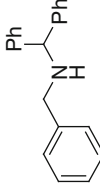
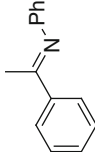

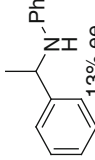
**Scheme 18** Catalytic deoxygenative hydrosilylation of CO<sub>2</sub> [58]

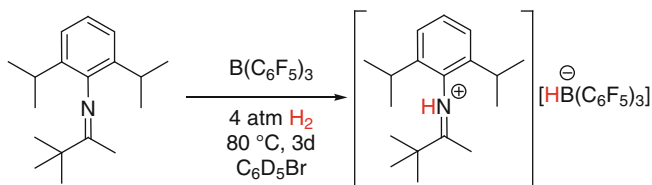
In some cases, if the starting imine is too bulky for the nucleophilic attack, an intermediate iminium borohydride can be isolated (Scheme 19) [36]. Moreover, as discussed above, the addition of a hydride ion to the iminium double bond is a reversible reaction and the same intermediate iminium borohydride is responsible for the racemization of enantioenriched amines catalyzed by B(C<sub>6</sub>F<sub>5</sub>)<sub>3</sub> (Scheme 5).

The main disadvantage of perfluorophenylboranes as catalysts for the reduction of unsaturated nitrogen-containing compounds is their strong sensitivity to the nature of the substrates. Therefore, only sterically hindered (Table 1, entries 1, 2, 5–9) and low-basic (Table 1, entries 3–6, 9) imines and quinolines can be catalytically reduced. Both of these factors facilitate dissociation of the LAB adducts between borane and the final amine, which inhibits borane's catalytic activity. For instance, the stoichiometric reaction between *t*BuN=C(H)Ph and B(C<sub>6</sub>F<sub>5</sub>)<sub>3</sub> under hydrogen at room temperature gives a stable LAB adduct of *tert*-butylbenzylamine and trispentafluorophenylborane (Scheme 20). However, heating of the toluene solution of *N-tert*-butylbenzaldimine in the presence of only 5 mol% of B(C<sub>6</sub>F<sub>5</sub>)<sub>3</sub> under 1 atm of H<sub>2</sub> at 80°C leads to the rapid formation of *tert*-butylbenzylamine in an almost quantitative yield (Table 1, entry 1) due to the fast thermal dissociation of the B–N bond forming free borane at elevated temperatures.

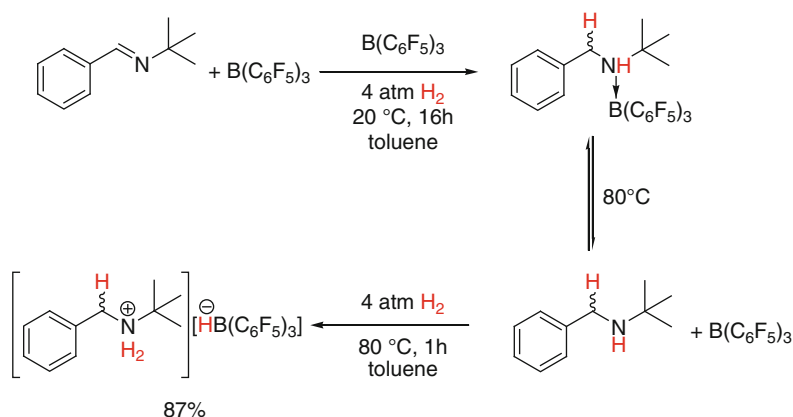
**Table 1** Catalytic hydrogenation of imines and quinolines by boranes

Entry	Substrate	Catalyst	Conditions	Amine	Conv. (%)
1		5 mol% B(C <sub>6</sub> F <sub>5</sub> ) <sub>3</sub>	1 atm H <sub>2</sub> , 80°C, 2 h		89 [36]
2		5 mol% B(C <sub>6</sub> F <sub>5</sub> ) <sub>3</sub>	5 atm H <sub>2</sub> , 120°C, 1 h		99 [36]
3		5 mol% B(C <sub>6</sub> F <sub>5</sub> ) <sub>3</sub>	5 atm H <sub>2</sub> , 120°C, 41 h		98 [36]
4		10 mol% B(C <sub>6</sub> F <sub>5</sub> ) <sub>3</sub>	30 atm H <sub>2</sub> , 100°C, 15 h		99 [36]
5		5 mol% B(C <sub>6</sub> F <sub>5</sub> ) <sub>3</sub>	20 atm H <sub>2</sub> , 80°C, 15 h		99 [36]
6		5 mol% B(C <sub>6</sub> F <sub>5</sub> ) <sub>3</sub>	4 atm H <sub>2</sub> , 25°C, 1 h		80 [59]

7		10 mol% MesB(C <sub>6</sub> F <sub>4</sub> H) <sub>2</sub>	4 atm H <sub>2</sub> , 105°C, 17 h		99 [60]
8		10 mol% MesB(C <sub>6</sub> F <sub>4</sub> H) <sub>2</sub>	4 atm H <sub>2</sub> , 105°C, 17 h		99 [60]
9		10 mol% (C <sub>6</sub> F <sub>5</sub> ) <sub>2</sub> B B(C <sub>6</sub> F <sub>5</sub> ) <sub>2</sub>	15 atm H <sub>2</sub> , 120°C, 1 h		99 (unpublished results)
10		5 mol% (C <sub>6</sub> F <sub>5</sub> ) <sub>2</sub> B B(C <sub>6</sub> F <sub>5</sub> ) <sub>2</sub>	15 atm H <sub>2</sub> , 120°C, 1 h		99 (unpublished results)
11		10 mol%  (C <sub>6</sub> F <sub>5</sub> ) <sub>2</sub> B	20 atm H <sub>2</sub> , 65°C, 15 h	 13% ee	99 [61]



**Scheme 19** Hydrogen activation by bulky imine and  $\text{B(C}_6\text{F}_5)_3$  [36]



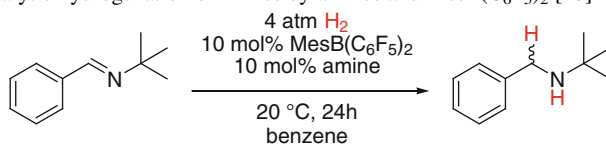
**Scheme 20** Ammonium borohydride formation via hydrogen activation by imine and  $\text{B(C}_6\text{F}_5)_3$  [36]

Since both free amine and borane are also present in the reaction mixture during catalytic hydrogenation, they can compete with the imine-borane FLP in the cleavage of  $\text{H}_2$  to form an ammonium borohydride (Scheme 20), which can act as a reducing agent in the subsequent transfer hydrogenation of imine. Additionally, because the corresponding amines are more basic than starting imines, the rate of the hydrogen activation by amine-borane FLPs is higher than those for imine-borane FLPs.

Indeed, recently, Soós and co-workers confirmed that the addition of a catalytic amount of a properly chosen amine to borane accelerates the hydrogenation of imines (Table 2) [40, 41]. Specifically, they showed that intermolecular amine-borane FLPs with well-matched steric and electronic properties are highly active hydrogenation catalysts even at room temperature (Table 3).

However, despite the significantly improved activity of the new amine-borane FLPs, a strong substrate limitation is still the major drawback of these catalytic systems [35]. For instance, even with a mixture of sterically hindered borane  $\text{MesB(C}_6\text{F}_5)_2$  and quinuclidine as a catalyst, only 49% conversion of non-bulky imine  $\text{PhCH}_2\text{N}=\text{C(H)Ph}$  to dibenzylamine was achieved (Table 3, entry 5).



**Table 2** Catalytic hydrogenation of imines by amines and MesB(C<sub>6</sub>F<sub>5</sub>)<sub>2</sub> [40]

Entry	Amine	Conv. (%) <sup>a</sup>
1		0
2		5
3		2
4		48
5		100

<sup>a</sup>Determined by GC analysis

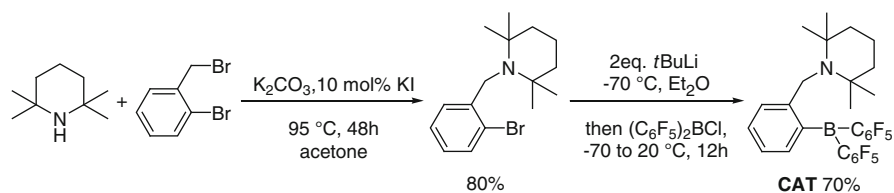
## 5 Hydrogen Activation by Intramolecular *ansa*-Aminoboranes

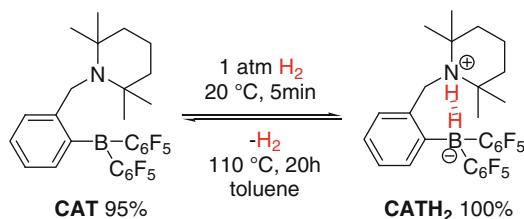
After our initial discovery of the first intermolecular TMP/B(C<sub>6</sub>F<sub>5</sub>)<sub>3</sub> FLP system for hydrogen activation under ambient conditions, we designed intramolecular *ansa*-aminoborane *o*-N-TMPCH<sub>2</sub>C<sub>6</sub>H<sub>4</sub>B(C<sub>6</sub>F<sub>5</sub>)<sub>2</sub> where active B and N centers are located close to each other [63]. We also developed an effective and common procedure for the preparation of such dual Lewis acid–base systems using commercially available 2-bromobenzyl bromide, amine, and (C<sub>6</sub>F<sub>5</sub>)<sub>2</sub>BCl (Scheme 21).

The first step of the synthesis was N-alkylation of TMP with *o*-bromobenzyl bromide in the presence of K<sub>2</sub>CO<sub>3</sub> as a base and 10 mol% of KI as a catalyst to produce 1-(2-bromobenzyl)-2,2,6,6-tetramethylpiperidine in 80% yield. The corresponding intermediate product readily underwent halogen–lithium exchange with *tert*-butyllithium at –70 °C in diethyl ether, after which a pre-cooled solution of (C<sub>6</sub>F<sub>5</sub>)<sub>2</sub>BCl was added to give the crude product **CAT** in 70% yield as a bright

**Table 3** Catalytic transfer hydrogenation of imines and enamines by amines with  $\text{MesB}(\text{C}_6\text{F}_5)_2$  [40]

Entry	Substrate	Amine	Conv. (%) <sup>a</sup>
1			75
2			98
3			73
4			92
5			49
6			16

<sup>a</sup>Determined by  $^1\text{H}$  NMR spectroscopy**Scheme 21** Synthesis of *ansa*-aminoborane CAT [63]



**Scheme 22** Reversible hydrogen activation by *ansa*-aminoborane CAT [63]

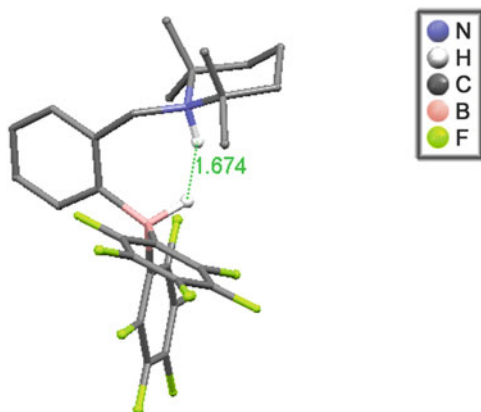
yellow oil. In the next step, the *ansa*-aminoborane CAT reacted rapidly with H<sub>2</sub> at room temperature and 1 atm pressure to give the *ansa*-ammonium borate CATH<sub>2</sub> in almost quantitative yield in 5 min (Scheme 22). In contrast to the starting *ansa*-aminoborane CAT, CATH<sub>2</sub> is an air- and moisture-stable solid compound. Therefore, this method allowed successful preparation of CATH<sub>2</sub> in good yield on a gram scale.

The possibility of hydrogen gas liberation from CATH<sub>2</sub> was also examined. When a toluene solution of *ansa*-ammonium borate CATH<sub>2</sub> (0.1 M) was refluxed at 110°C in a closed system under reduced pressure for 3 h, a 50% conversion of CATH<sub>2</sub> was observed. An extension of the reaction time up to 20 h resulted in almost quantitative recovery of the starting *ansa*-aminoborane CAT, exemplifying the first non-metal FLP-based system able to activate hydrogen reversibly through an intramolecular mechanism.

To gain further insight into the mechanism of reversible hydrogen activation by intramolecular *ansa*-aminoborane CAT, the structure of the corresponding *ansa*-ammonium borate CATH<sub>2</sub> was studied by X-ray, neutron-diffraction and thermogravimetric mass spectroscopic experiments in the solid state and by NMR and FT-IR in solution. Additionally, the structure, reaction path, and energetics were studied theoretically [64].

The neutron diffraction data of *ansa*-ammonium borate CATH<sub>2</sub> showed the presence of C–H...F (2.36 and 2.82 Å) hydrogen bonds and a strong, partially covalent, dihydrogen bond interaction N–H...H–B of 1.67 Å between the ammonium cation and borohydride anion (Fig. 2) [65]. Ab initio DFT calculations performed by ourselves and others on the PBE/6-31G(d) and the M05-2X/6-31G(d) levels of theory for geometry optimizations in solution and gas phase, respectively, were in good agreement with the neutron diffraction results [19, 63]. However, the values found for the intramolecular N–H...H–B dihydrogen bond distance were significantly shorter (1.51 and 1.53 Å, Table 4).

Since both hydrogen activation and liberation occurred in organic solvents and in solid state studies, multinuclear solution NMR experiments of CATH<sub>2</sub> and its deuterated isotopomers were performed [64]. It could be shown that, in contrast to the B–H hydride, the N–H proton can be exchanged easily in solution. These experiments also showed that no rotation of H<sub>2</sub> within the molecule takes place even at elevated temperatures. Dilution, variable temperature, and 2D NOESY NMR measurements of *ansa*-ammonium borate CATH<sub>2</sub> in CD<sub>2</sub>Cl<sub>2</sub> solution



**Fig. 2** Crystal structure of *ansa*-ammonium borate **CATH<sub>2</sub>** determined by neutron diffraction [64]

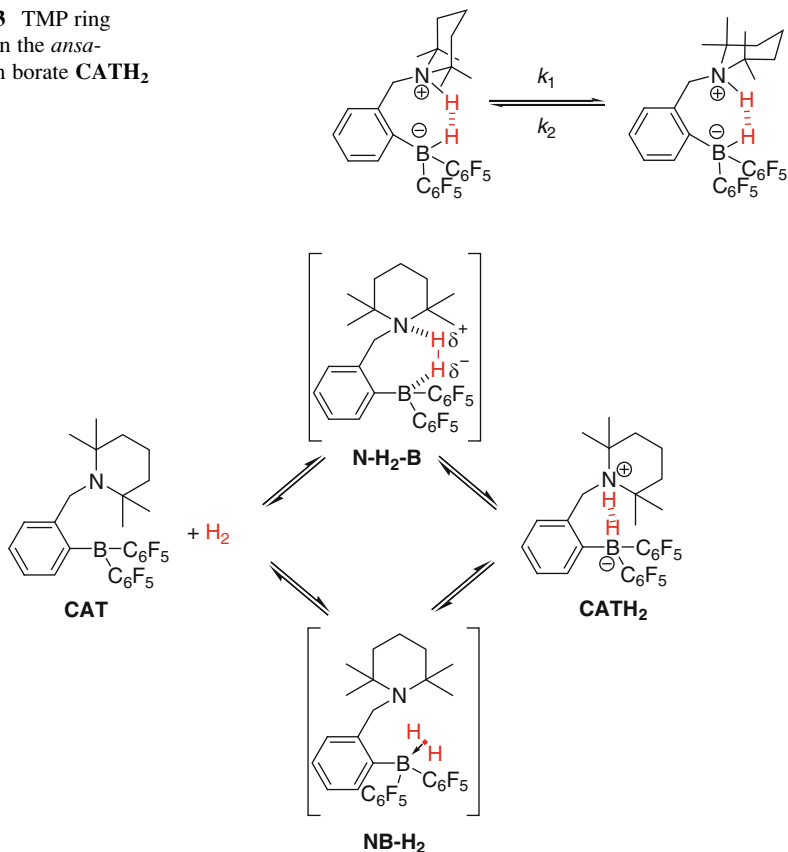
**Table 4** Comparison of the structural data of *ansa*-ammonium borate **CATH<sub>2</sub>** obtained by different methods [19, 63, 64]

Property	Neutron diffraction [64]	X-ray [63]	PBE/6-31G(d) with PCM model (in C <sub>6</sub> H <sub>6</sub> ) [63]	M05-2X/6-31G(d) (in gas phase) [19]
$d(\text{NH-HB})$ (Å)	1.67	1.78	1.51	1.53
$d(\text{N-H})$ (Å)	1.03	0.94	1.06	1.04
$d(\text{B-H})$ (Å)	1.24	1.19	1.24	1.23
$d(\text{N-B})$ (Å)	3.35	3.36	3.34	3.25
$\psi(\angle \text{N-H}\cdots\text{H})$ (°)	154.9	154.2	150.3	159.7
$\theta(\angle \text{B-H}\cdots\text{H})$ (°)	123.1	125.2	132.5	122.9

showed that it consists of two conformers which are in dynamic equilibrium (Scheme 23). Both of them have the N–H proton in an axial position and differ only in the orientation of the axial methyl groups adjacent to the nitrogen center. Based on the chemical NMR shifts of N–H and CH<sub>2</sub> groups and the X-ray crystal structure of **CATH<sub>2</sub>**, the more stable conformer was assumed to have the methyl groups in an axial position pointed away from the N–H group. Thus, the subsequent conformer equilibrium was shifted to the right side with  $k_1:k_2 \approx 9:1$  (Scheme 23).

To determine the intramolecular N–H $\cdots$ H–B dihydrogen bond distance in CD<sub>2</sub>Cl<sub>2</sub> solution <sup>1</sup>H NMR T<sub>1</sub> relaxation and selective 1D NOE measurements were carried out. These independent experiments showed that the DHB length is very close to the value determined in the solid state by neutron diffraction in the range of approximately 1.6–1.8 Å and becomes even shorter at elevated temperatures. Therefore, the NMR data gave strong evidence that the structure of *ansa*-ammonium borate **CATH<sub>2</sub>** in solution is similar to that in the solid state, which was also supported by independent FT-IR measurements.

**Scheme 23** TMP ring inversion in the *ansa*-ammonium borate **CATH<sub>2</sub>** [64]



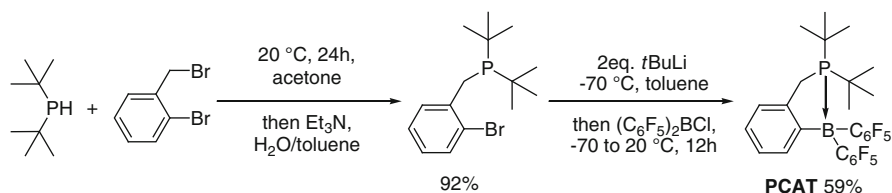
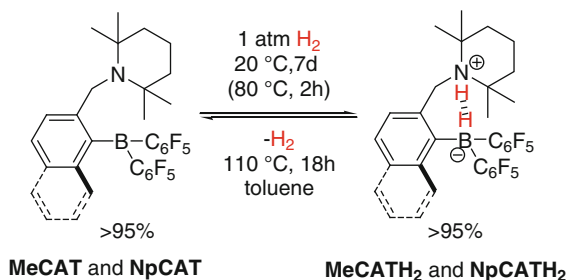
**Scheme 24** Possible intermediates in hydrogen activation by *ansa*-aminoborane **CAT** [64]

Although our theoretical calculations support the synchronous mechanism for the hydrogen activation with **N-H<sub>2</sub>-B** as an intermediate, the formation of a  $\sigma$ -complex between borane and hydrogen **NB-H<sub>2</sub>** cannot be ruled out at this point (Scheme 24). Further experimental studies are needed to favor one of the mechanisms.

As a continuation of our work, we proposed that the reduction of Lewis acidity of the active boron center of *ansa*-aminoboranes should not only lower the temperature needed for hydrogen liberation but should also lead to an increase in their catalytic activity in hydrogenation reactions, which will be discussed in the next section. In this respect, the new *ansa*-aminoboranes **MeCAT** and **NpCAT**, with more sterically hindered and electron donating benzyl bridges between Lewis acid and base, were synthesized in a similar manner as the original *ansa*-aminoborane **CAT** (Scheme 21) (unpublished results) [43].

While the time required for the splitting of hydrogen by **MeCAT** and **NpCAT** dramatically increased compared to the *ansa*-aminoborane **CAT** (1 week instead of

**Scheme 25** Reversible hydrogen activation by *ansa*-aminoboranes **MeCAT** and **NpCAT** (unpublished results) [43]



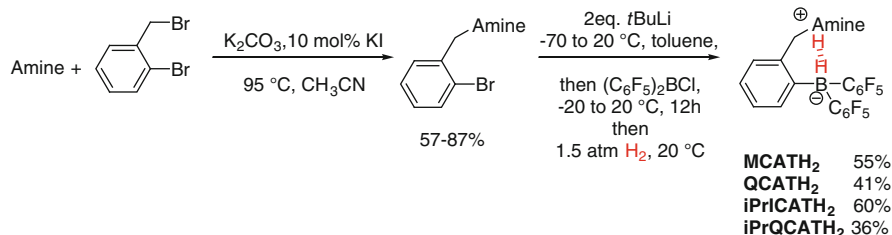
**Scheme 26** Synthesis of *ansa*-phosphinoborane **PCAT** (unpublished results)

a few minutes), the corresponding *ansa*-ammonium borates **MeCATH<sub>2</sub>** and **NpCATH<sub>2</sub>** were losing hydrogen gas only slightly faster than **CATH<sub>2</sub>** upon heating (Schemes 22 and 25). Thus, in contrast to intermolecular phosphine-borane and amine-borane systems, the further reduction of the Lewis acidity of the borane moiety turned out to be of minor importance in the case of the *ansa*-aminoboranes [27, 44].

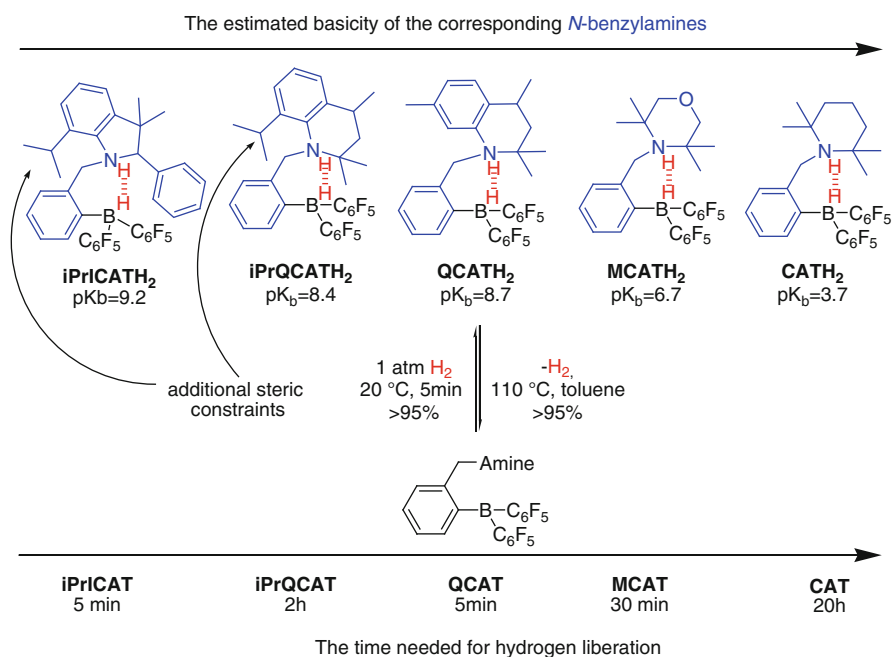
After unsuccessful efforts to decrease the time needed for the hydrogen liberation from *ansa*-ammonium borate systems by modification of the Lewis acidic component, systematic studies on the Lewis basic amine moiety were performed by us. At first, the TMP moiety in the *ansa*-aminoborane **CAT** was replaced by a bulky secondary di-*tert*-butylphosphine (Scheme 26). The corresponding *ansa*-phosphinoborane **PCAT**, which was synthesized by a standard two-step procedure in 54% total yield, exists as a stable intramolecular LAB adduct and cannot cleave H<sub>2</sub> even at elevated temperature (unpublished results) [66].

During further investigations a general approach for the modification of *ansa*-ammonium borates was considered: basicity of the nitrogen atom can be reduced to facilitate proton transfer by weakening the N–H bond. The corresponding *ansa*-ammonium borates containing less basic amine moieties than TMP – **MCATH<sub>2</sub>**, **QCATH<sub>2</sub>**, **iPrQCATH<sub>2</sub>**, and **iPrICATH<sub>2</sub>** – were synthesized on a gram scale by a standard three-step procedure from readily or commercially available starting materials (Scheme 27) [34].

Interestingly, lowering the basicity of the starting amines had no significant effect on the rate of hydrogen activation, but dramatically decreased the temperature and the time required for hydrogen liberation. While the original *ansa*-ammonium borate **CATH<sub>2</sub>** system liberated H<sub>2</sub> almost quantitatively only after 20 h at 110 °C

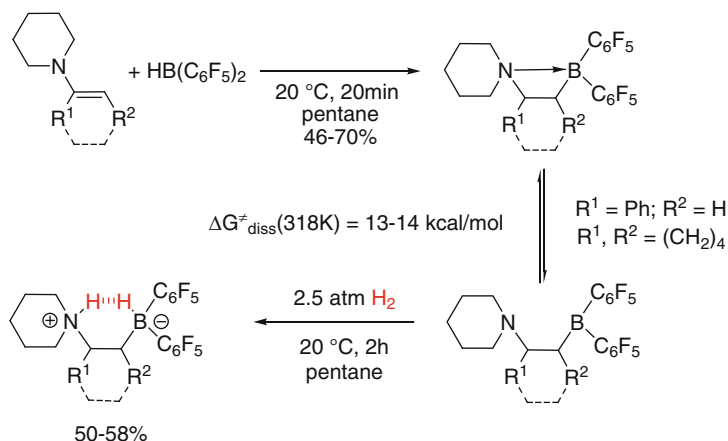


**Scheme 27** Synthesis of the new *ansa*-ammonium borates [34]



**Scheme 28** The effect of the basicity of amine moiety on the reversible H<sub>2</sub> activation by *ansa*-aminoboranes [34]

(Schemes 22 and 28), under the same conditions **MCATH<sub>2</sub>**, produced with less basic 3,3,5,5-tetramethylmorpholine instead of TMP, released hydrogen in less than 30 min. Furthermore, the *ansa*-ammonium borates **QCATH<sub>2</sub>** and **iPrICATH<sub>2</sub>**, containing amine moieties with even lower basicity than former ones, slowly decomposed in solution even at room temperature and can be quantitatively converted to starting *ansa*-aminoboranes **QCAT** and **iPrICAT** after 5–10 min at 110 °C. Thereby, new *ansa*-ammonium borates exhibited excellent kinetics (a few minutes) for the hydrogen activation and liberation. This is believed to be mainly due to a rare combination of steric, electronic, and thermodynamic effects, which were tuned by a simple modification of the amine moieties.



**Scheme 29** Synthesis of *ansa*-aminoboranes by the hydroboration of enamines [67]

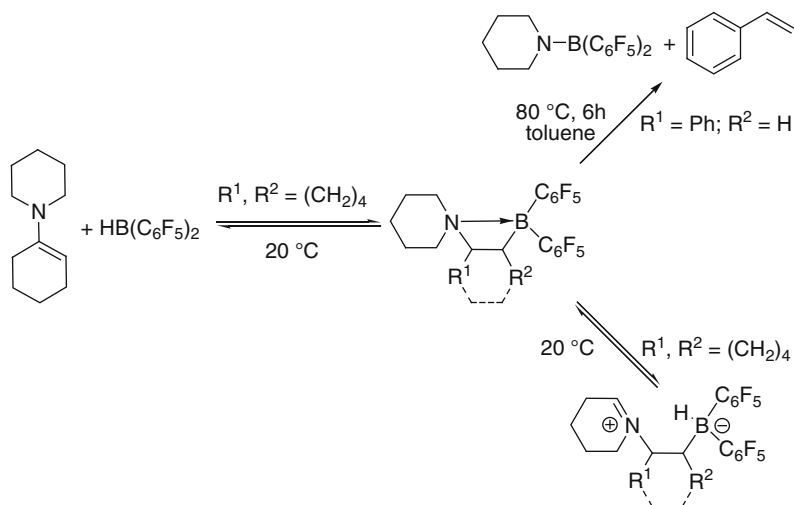
A different approach for the synthesis of *ansa*-aminoboranes by hydroboration of enamines with Piers' bis(pentafluorophenyl)borane  $\text{HB}(\text{C}_6\text{F}_5)_2$  was recently developed by Erker and co-workers [67]. The corresponding  $\text{C}_2$ -bridged *ansa*-aminoboranes were isolated in good yields of 46–70% as intramolecular LAB adducts. Some of these four-membered *ansa*-aminoboranes with correctly matched electronic and steric properties can dissociate to the “unquenched” Lewis pairs and subsequently activate hydrogen to form *ansa*-ammonium borates (Scheme 29).

In contrast to the previously reported *ansa*-aminoboranes with benzyl bridges between Lewis acid and Lewis base centers, Erker's *ansa*-aminoboranes undergo different reversible transformations even at room temperature and fully decompose upon heating (Scheme 30). The above-mentioned side reactions considerably limit further applications of  $\text{C}_2$ -bridged *ansa*-aminoboranes.

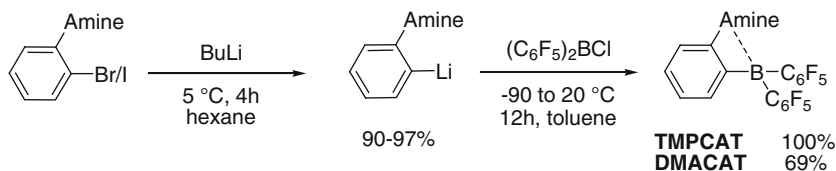
Recently we also reported new  $\text{C}_2$ -bridged *ansa*-aminoboranes with a 1,2-phenylene fragment between the N and B active centers [24]. The *ansa*-aminoboranes **TMPCAT** and **DMACAT** were prepared in high yield by the standard procedure from *o*-*N,N*-dialkylaminophenyllithiums and bis(pentafluorophenyl)chloroborane (Scheme 31). While dimethylamine-based **DMACAT** exists as an intramolecular LAB adduct, in **TMPCAT** Lewis acidic and Lewis basic centers remain “unquenched” due to the steric hindrance between the bulky 2,2,6,6-tetramethylpiperidine and bis(pentafluorophenyl)borane moieties.

Both **TMPCAT** and **DMACAT** activated hydrogen under mild conditions and gave the corresponding *ansa*-ammonium borates in almost quantitative yields. However, *ansa*-aminoborane **TMPCAT** was much more reactive towards hydrogen than **DMACAT** and formed the *ansa*-ammonium borate **TMPCATH<sub>2</sub>** instantly upon exposure to hydrogen (Scheme 32). On the other hand, all attempts to dehydrogenate **TMPCATH<sub>2</sub>** back to the starting *ansa*-aminoborane were unsuccessful and only trace amounts of **TMPCAT** could be detected by  $^{19}\text{F}$  NMR, while *ansa*-ammonium borate **DMACATH<sub>2</sub>** containing a less basic dimethylamine moiety was able to release hydrogen even at room temperature.





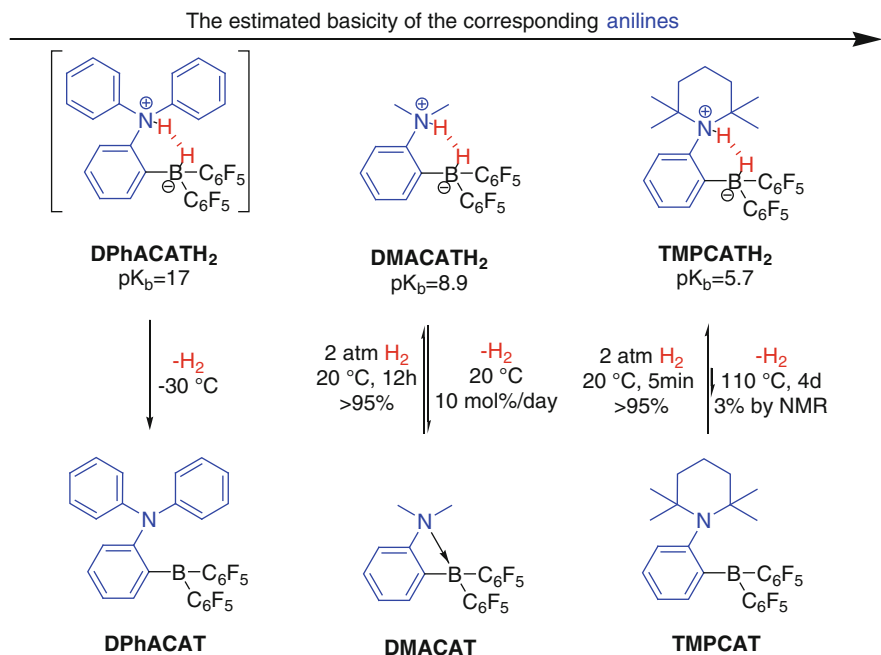
**Scheme 30** Possible side reactions of Erker's *ansa*-aminoboranes [67]



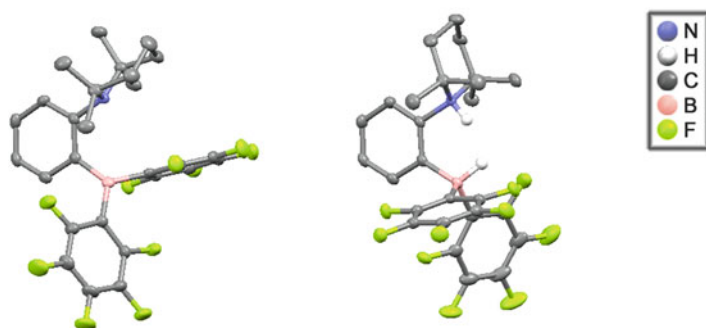
**Scheme 31** Synthesis of *ansa*-aminoboranes **TMPCAT** and **DMACAT** [24]

The exceptional stability of **TMPCATH<sub>2</sub>** ( $\text{p}K_{\text{b}} = 5.7$ ) compared to the “more basic” **CATH<sub>2</sub>** ( $\text{p}K_{\text{b}} = 3.7$ ) with an additional  $\text{CH}_2$  group between active centers can be explained by the fact that the formation of the six-membered  $\text{H-B-C}_2\text{-N-H}$  pseudo-ring is thermodynamically more favorable than the respective  $\text{H-B-C}_3\text{-N-H}$  seven-membered ring. The comparison of the structures of *ansa*-aminoborane **TMPCAT** and *ansa*-ammonium borate **TMPCATH<sub>2</sub>** in a solid state, revealed that hydrogen activation results in a minor change in the geometry of the  $\text{B-C=C-N}$  frame (Fig. 3). Thus the rigid geometry of **TMPCAT** is optimal for the activation of hydrogen.

These new results on the effect of the basicity of amine moiety on the stability of *ansa*-ammonium borates are in a good agreement with those obtained by Piers for the first *ansa*-aminoborane **DPhACAT** (Schemes 3 and 32) [20]. Specifically, while **DPhACAT** was unable to activate hydrogen due to the significantly reduced basicity of the diphenylamino group, in situ generated *ansa*-ammonium borate **DPhACATH<sub>2</sub>** was not detected even at low temperatures and only liberation of hydrogen was observed.

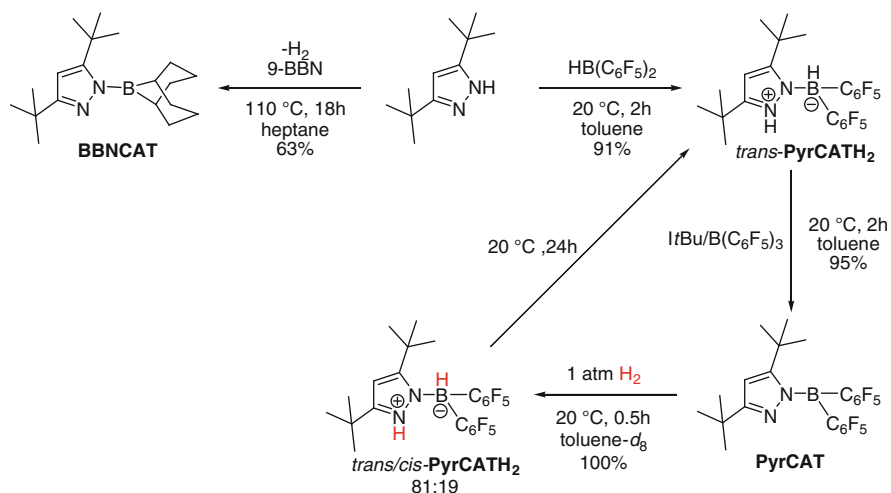


**Scheme 32** The effect of the basicity of amine moiety on the reversible H<sub>2</sub> activation by *ansa*-aminoboranes [24]



**Fig. 3** Crystal structures of *ansa*-aminoborane **TMPCAT** and *ansa*-ammonium borate **TMPCATH<sub>2</sub>** determined by X-ray [24]

Another example of intramolecular *ansa*-aminoboranes able to cleave hydrogen heterolytically is pyrazolylboranes recently reported by Tamm et al. (Scheme 33) [68]. They showed that the direct reaction of the bulky 3,5-di-*tert*-butyl-1*H*-pyrazole with secondary boranes leads to the corresponding pyrazolylboranes and pyrazoliumborates depending on the Lewis acidity of the borane. Thus, while highly Lewis acidic Piers' bis(pentafluorophenyl)borane HB(C<sub>6</sub>F<sub>5</sub>) reacted with 3,5-di-*tert*-butyl-1*H*-pyrazole to afford pyrazolium-borate *trans*-**PyrCATH<sub>2</sub>** in high yield, the reaction



**Scheme 33** Synthesis of pyrazolylboranes and pyrazolium-borates [68, 69]

with less Lewis acidic 9-borabicyclo[3.3.1]nonane (9-BBN) proceeded with evolution of H<sub>2</sub> and gave pyrazolylborane **BBNCAT** as a final product [69]. Since 3,5-di-*tert*-butyl-1H-pyrazole is much more basic than the *N*-phenyl-2,2,6,6-tetramethylpiperidine moiety in **TMPCATH<sub>2</sub>**, the corresponding pyrazolium-borate *trans*-**PyrCATH<sub>2</sub>** can even be sublimed at 100 °C/0.05 mbar without noticeable decomposition. However, the dehydrogenation of *trans*-**PyrCATH<sub>2</sub>** to pyrazolylborane **PyrCAT** was successfully achieved only by employing extremely reactive carbene-borane FLP consisting of 1,3-di-*tert*-butylimidazolin-2-ylidene (ItBu) and B(C<sub>6</sub>F<sub>5</sub>)<sub>3</sub> [19, 70]. In contrast to **BBNCAT**, the obtained pyrazolylborane **PyrCAT** could easily react with hydrogen under mild conditions to give a mixture of *trans* and *cis* isomers (81:19) of **PyrCATH<sub>2</sub>** in almost quantitative yield.

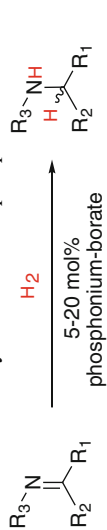
## 6 Catalytic Hydrogenation of Unsaturated Nitrogen-Containing Compounds by Intramolecular *ansa*-Ammonium Borates

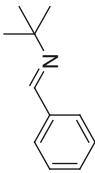
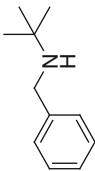

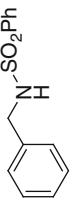
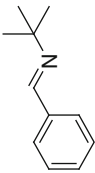
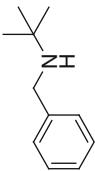
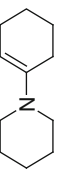
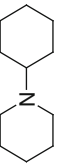
While the hydrogenation of unactivated alkenes and alkynes without transition metals is still rather limited (see Chap. 8), boranes (see Chap. 4) and phosphinoboranes were recently shown to catalyze the direct hydrogenation of bulky imines and enamines under mild conditions (Table 5) [71, 72].

The main disadvantages of boranes and phosphinoboranes as metal-free catalysts for hydrogenation are their low substrate tolerance and low activity. For instance, only sterically hindered (Table 5, entries 1, 2, 5, 7, 8) and low-basic (Table 5, entries 3, 6) unsaturated nitrogen-containing compounds can be

**Table 5** Catalytic hydrogenation of imines and enamines by intramolecular phosphonium-borates

Entry	Substrate	Catalyst	Conditions	Amine	Conv. (%)
1		5 mol% Mes. <sup>⊕</sup> PH 	5 atm H <sub>2</sub> , 80°C, 1 h		79 [71]
2			5 atm H <sub>2</sub> , 140°C, 1 h		88 [71]
3		C <sub>6</sub> F <sub>5</sub> <sup>⊖</sup> BH <sub>2</sub> <sup>⊕</sup> C <sub>6</sub> F <sub>5</sub>	5 atm H <sub>2</sub> , 120°C, 10.5 h		97 [71]
4			5 atm H <sub>2</sub> , 120°C, 48 h		5 [71]



5		5 mol% tBu <sup>+</sup> PH <sup>-</sup> tBu F F F F C <sub>6</sub> F <sub>5</sub> <sup>-</sup> BH <sup>+</sup> C <sub>6</sub> F <sub>5</sub>	5 atm H <sub>2</sub> , 80°C, 1 h		98 [71]
6			5 atm H <sub>2</sub> , 120°C, 16 h		87 [71]
7		20 mol% Mes <sup>+</sup> PH <sup>-</sup> Mes C <sub>6</sub> F <sub>5</sub> <sup>-</sup> BH <sup>+</sup> C <sub>6</sub> F <sub>5</sub>	2.5 atm H <sub>2</sub> , 20°C, 0.8 h		87 [72]
8		5 mol% C <sub>6</sub> F <sub>5</sub> <sup>-</sup> BH <sup>+</sup> C <sub>6</sub> F <sub>5</sub>	2.5 atm H <sub>2</sub> , 20°C, 20 h		88 [72]

catalytically hydrogenated with 5–20 mol% of phosphonium-borates. Both of these above-mentioned factors facilitate dissociation of the LAB adducts between the catalyst and the substrate/product or fully prevent their formation. The unsaturated nitrogen-containing compounds that do not fulfill the required criteria, for instance the sterically open imine from benzaldehyde and benzylamine, can only be reduced stoichiometrically with such systems (Table 5, entry 4).

As a continuation of our investigations on the intramolecular *ansa*-aminoboranes, we examined the reduction of unsaturated nitrogen-containing compounds with the original **CATH<sub>2</sub>** and later with its low basic analogues: **MCATH<sub>2</sub>**, **QCATH<sub>2</sub>**, **iPrICATH<sub>2</sub>**, **iPrQCATH<sub>2</sub>** (Table 6) [34, 63]. Among previously reported non-metal systems for catalytic hydrogenation based on the bis(perfluorophenyl)boranyl moiety (Table 5) the *ansa*-ammonium borates have shown high activity and high substrate tolerance in the hydrogenation of a wide range of imines, enamines, and quinolines.

These results (Table 6) further support a proposed mechanism for the catalytic hydrogenation by FLPs in which any one, or more, of the equilibrium steps may be the rate-determining step, depending on the structure of both substrates and catalysts (Scheme 34).

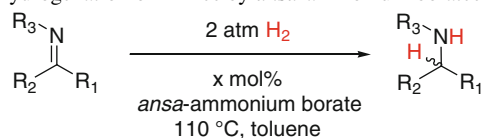
First, *ansa*-aminoboranes **MeCAT** and **NpCAT** with decreased Lewis acidity showed extremely low activity in the hydrogenation of imines, due to the longer time required for the splitting of dihydrogen compared to **CAT** (1 week instead of a few minutes; Scheme 34, Stage I).

Second, the “less basic” *ansa*-ammonium borates **MCATH<sub>2</sub>**, **QCATH<sub>2</sub>**, **iPrICATH<sub>2</sub>**, and **iPrQCATH<sub>2</sub>** showed higher catalytic activity than the original **CATH<sub>2</sub>** due to a facilitated proton transfer. Full conversions were achieved with lower catalyst loadings and/or shorter reaction times and/or lower temperatures. Thus the proton-transfer equilibrium seems to be a primary and rate controlling step in the reduction of bulky *N*-arylketimines and quinolines (Scheme 34, Stage II and Table 6, entries 16–25 and 31–35).

Third, when both the starting unsaturated nitrogen-containing compound and the catalyst are bulky enough (e.g., *N*-benzyl- $\alpha$ -methylbenzylamine and **iPrQCATH<sub>2</sub>**; Table 6, entry 10), the nucleophilic attack of a hydride ion to the protonated double bond can also be suppressed and becomes the rate-limiting step (Scheme 34, Stage III and Table 6, entries 10, 20, 25).

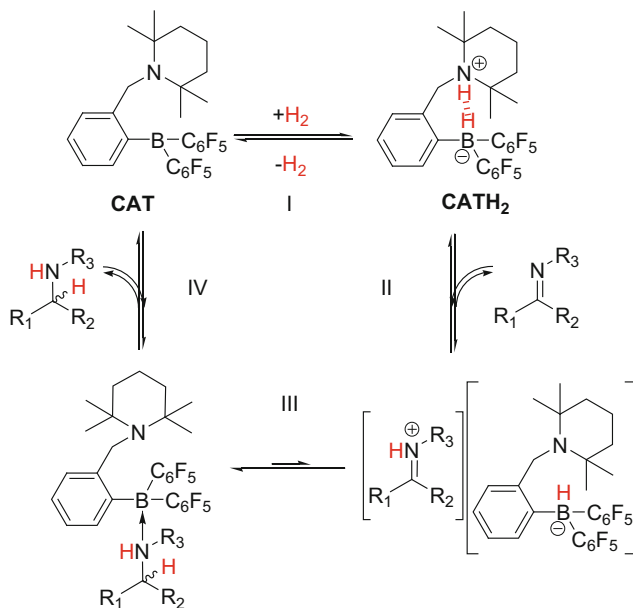
Finally, the inhibition of the catalyst activity by LAB adduct formation seems to be a rate-determining step in the reduction of non-bulky imines (Scheme 34, Stage IV and Table 6, entries 3, 26–29, 31–32). While generally more active *ansa*-ammonium borates **MCATH<sub>2</sub>**, **QCATH<sub>2</sub>**, and **iPrICATH<sub>2</sub>** could provide only a stoichiometric reduction of non-bulky phenylacetone-*N*-methylimine (Table 6, entries 26–29), the more sterically hindered **iPrQCATH<sub>2</sub>**-catalyzed hydrogenation gave the corresponding amine in 82% yield (Table 6, entry 30).

Further optimization of the reaction conditions for the hydrogenation of bulky unsaturated nitrogen-containing compounds revealed (Table 7) that the best results can be obtained by using 1 mol% of **QCATH<sub>2</sub>** as a catalyst in toluene and hexane at 80°C (2.5 h) or Et<sub>2</sub>O at 50°C (1 h), respectively (Table 7, entries 4, 5, 10).

**Table 6** Catalytic hydrogenation of imines by *ansa*-ammonium borates [34, 63]

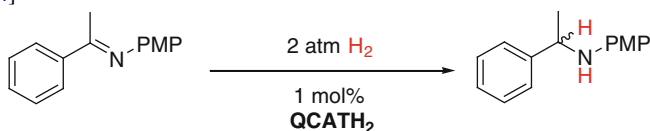
Entry	Substrate	Catalyst	mol%	Time (h)	Conv. (%)
1		CATH <sub>2</sub>	4	20	100
2		MCATH <sub>2</sub>	1	12	100
3		QCATH <sub>2</sub>	1	12	15
4		iPrICATH <sub>2</sub>	1	12	100
5		iPrQCATH <sub>2</sub>	1	12	12
6		CATH <sub>2</sub>	4	6	100
7		MCATH <sub>2</sub>	1	12	100
8		QCATH <sub>2</sub>	1	5	100
9		iPrICATH <sub>2</sub>	2	12	100
10		iPrQCATH <sub>2</sub>	4	12	52
11		CATH <sub>2</sub>	4	12	100
12		MCATH <sub>2</sub>	2	12	100
13		QCATH <sub>2</sub>	2	12	100
14		iPrICATH <sub>2</sub>	2	12	100
15		iPrQCATH <sub>2</sub>	4	12	100
16		CATH <sub>2</sub>	4	12	37
17		MCATH <sub>2</sub>	1	40	70
18		QCATH <sub>2</sub>	1	3	100 <sup>a</sup>
19		iPrICATH <sub>2</sub>	2	12	100
20		iPrQCATH <sub>2</sub>	4	12	80
21		CATH <sub>2</sub>	4	12	4
22		MCATH <sub>2</sub>	4	12	4
23		QCATH <sub>2</sub>	4	40	21
24		iPrICATH <sub>2</sub>	4	12	15
25		iPrQCATH <sub>2</sub>	4	12	4
26		CATH <sub>2</sub>	4	12	4
27		MCATH <sub>2</sub>	4	12	4
28		QCATH <sub>2</sub>	4	12	4
29		iPrICATH <sub>2</sub>	4	12	4
30		iPrQCATH <sub>2</sub>	4	12	82
31		CATH <sub>2</sub>	4	12	4
32		MCATH <sub>2</sub>	4	12	4
33		QCATH <sub>2</sub>	4	40	80
34		iPrICATH <sub>2</sub>	4	12	100
35		iPrQCATH <sub>2</sub>	4	12	97

<sup>a</sup>80°C



**Scheme 34** Proposed mechanism for the catalytic hydrogenation of imines by *ansa*-ammonium borates [34]

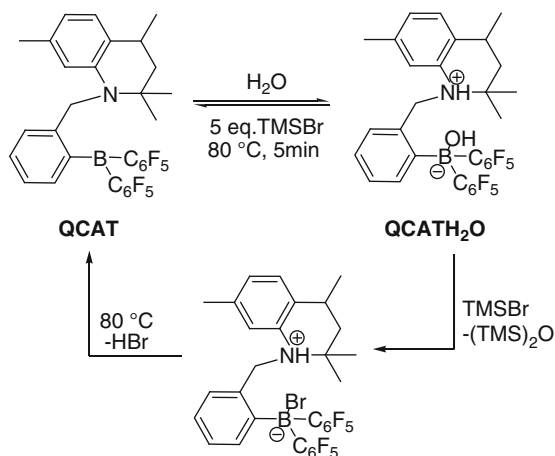
**Table 7** Optimization of the conditions for catalytic hydrogenation by *ansa*-ammonium borate QCATH<sub>2</sub> [34]



Entry	Solvent	Time (h)	Temperature (°C)	Conv. (%)
1	CH <sub>2</sub> Cl <sub>2</sub>	2.5	60	51
2	Et <sub>2</sub> O	2.5	60	100
3	CDCl <sub>3</sub>	2.5	80	92
4	Hexane	2.5	80	100
5	Toluene	2.5	80	99
6	THF	2.5	80	42
7	Toluene	1	25	31
8	Et <sub>2</sub> O	1	25	17
9	Toluene	1	50	89
10	Et <sub>2</sub> O	1	50	97



**Scheme 35** Regeneration of *ansa*-aminoborane **QCAT** from hydrated adduct **QCATH<sub>2</sub>O** [34]



The sensitivity of FLPs towards traces of water is a well known fact [7, 20, 29]. The presence of accidental  $\text{H}_2\text{O}$  in the reaction mixture poisons the *ansa*-aminoborane FLP catalyst via adduct formation; the same hydrated adduct is also formed during the quenching of the reaction mixture (Scheme 35). Therefore the dehydration of *ansa*-ammonium borates, containing the highly energetic boron–oxygen bonds, is a key transformation in the catalyst recovery procedure. Surprisingly, after the benzene solution of **QCATH<sub>2</sub>O** was treated with an excess of  $\text{TMSBr}$  (5 equiv.) at  $80^\circ\text{C}$  for 5 min and then evaporated under vacuum, *ansa*-aminoborane **QCAT** was isolated in almost quantitative yield. This procedure was successful mainly because the Si–O bond is even more stable than the B–O bond. However, this protocol is not applicable to the recovery of **CAT** from the corresponding water adduct, since the decreased basicity of the amine part plays a key role, facilitating elimination of  $\text{HBr}$  upon heating.

As a result of the above-mentioned observations, the hydrogenation of a model compound, *N*-(4-methoxy)phenyl-1-phenylethylideneamine, by *ansa*-ammonium borate **QCATH<sub>2</sub>** (1 mol%) was scaled up to gram quantities (5.632 g) giving the corresponding amine in 97% isolated yield. Moreover, 80% of the catalyst **QCATH<sub>2</sub>** was recovered by a simple extraction of the acidic solution with toluene followed by dehydration with  $\text{TMSBr}$  at  $80^\circ\text{C}$  and hydrogen activation at room temperature.

## 7 Enantioselective Hydrogenation of Unsaturated Nitrogen-Containing Compounds by Intramolecular *ansa*-Aminoboranes

The enantioselective hydrogenation of unsaturated nitrogen-containing compounds catalyzed by FLP systems is a less developed topic and until recently was possible only by the asymmetric hydrogenation of *N*-arylimine with 3-pinanyl-bis(perfluorophenyl)borane and tris(*tert*-butyl)phosphonium/chiral-alkyl-bis

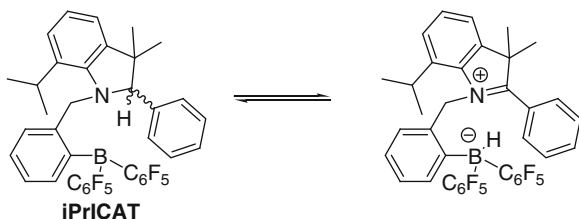
**Table 8** Enantioselective catalytic hydrogenation of *N*-arylketimines by chiral-borane and phosphonium-chiral-borate

Entry	Substrate	Catalyst	Conditions	Conv. (%)	ee (%)
1		10 mol% 	20 atm H <sub>2</sub> , 65°C, 15 h	>99	13 [61]
2		5 mol%	25 atm H <sub>2</sub> , 65°C, 15 h	95	79 [73]
3			25 atm H <sub>2</sub> , 65°C, 15 h	96	81 [73]
4			25 atm H <sub>2</sub> , 65°C, 15 h	>99	81 [73]
5			25 atm H <sub>2</sub> , 65°C, 15 h	37	74 [73]

(perfluorophenyl)hydroborate (Table 8) [61, 73]. The phosphonium-chiral-borate catalyzed the hydrogenation of different *N*-arylketimines giving the corresponding amines in good yields and good enantioselectivities (Table 8, entries 2–5). However, in contrast to achiral systems based on triarylboranes (unpublished results) [36, 59, 60, 71], higher pressure of hydrogen (25 atm) were required in the case of chiral-alkyl-bis(perfluorophenyl)borane-based FLP, probably to prevent retrohydroboration see [74].

Since, in contrast to boranes, a much broader variety of chiral amines is readily and commercially available, chiral *ansa*-ammonium borates are promising candidates for asymmetric hydrogenation. Indeed, we demonstrated that *ansa*-ammonium borates with chiral-amine moieties can also be used as catalysts for the asymmetric hydrogenation of unsaturated nitrogen-containing compounds [34]. The standard procedure for the preparation of chiral *ansa*-ammonium borates **Q**\*CATH<sub>2</sub>, and **iPr**\*CATH<sub>2</sub> from the corresponding enantiopure secondary

**Scheme 36** Racemization of the enantiopure **iPrI\*CAT** [34]

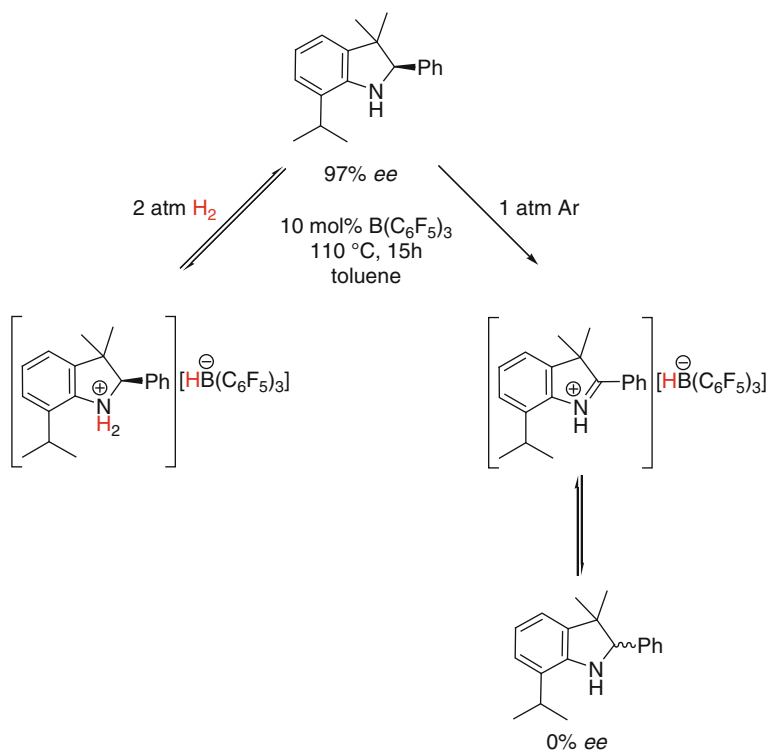


amines was applied (Scheme 27). Unfortunately, in the case of chiral-7-isopropyl-3,3-dimethyl-2-phenylindoline the racemic *ansa*-ammonium borate **iPrICATH<sub>2</sub>** was obtained as a final product (Scheme 36). A possible mechanism for the racemization of *ansa*-aminoborane **iPrICAT** involves the abstraction of an  $\alpha$ -hydride from the amine fragment by the Lewis acidic borane moiety and formation of the intramolecular iminium borohydride (Scheme 37).

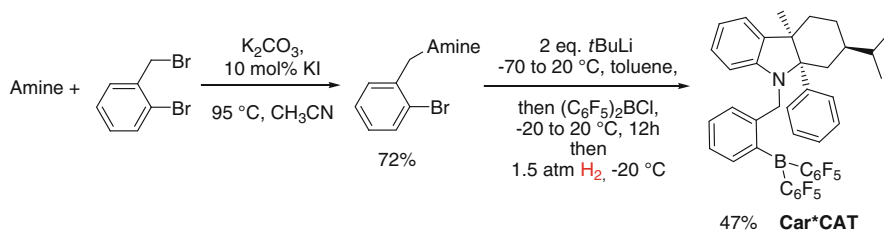
Later, a similar racemization phenomenon was also observed for intermolecular FLP systems consisting of catalytic amounts of  $\text{B}(\text{C}_6\text{F}_5)_3$  and chiral amines (Scheme 38) [34, 35]. Interestingly, heating of the chiral 7-isopropyl-3,3-dimethyl-2-phenylindoline with 10 mol% of  $\text{B}(\text{C}_6\text{F}_5)_3$  at 110°C and 1 atm of argon led to full racemization in 15 h. However, no racemization occurred under an atmosphere of  $\text{H}_2$  but otherwise identical conditions.

Therefore, only amines with a chiral tertiary carbon atom adjacent to the nitrogen atom can be applied in the backbone of chiral *ansa*-ammonium borates. For this reason, another enantiopure *ansa*-aminoborane **Car\*CAT** based on 4a,9a-substituted-2,3,4,4a,9,9a-hexahydro-1*H*-carbazole skeleton was prepared according to the standard procedure in 34% total yield (Scheme 38). However, because the starting hexahydrocarbazole had the lowest basicity in the series of investigated amines, the equilibrium in hydrogen activation between **Car\*CAT** and **Car\*CATH<sub>2</sub>** is shifted to the left and the corresponding *ansa*-ammonium borate could not be isolated even at low temperature.

The asymmetric hydrogenation of nitrogen-containing compounds with chiral *ansa*-ammonium borate **Q\*CATH<sub>2</sub>** and *ansa*-aminoborane **Car\*CAT** was investigated (Table 9). While the enantiopure *ansa*-ammonium borate **Q\*CATH<sub>2</sub>** exhibited the same unprecedentedly high activity as its racemic version (Table 9), hydrogenation with “low basic” *ansa*-aminoborane **Car\*CAT** resulted in low to moderate conversions (Table 9, entry 4). In all cases the best ees were obtained in MTBE as a solvent at room temperature (Table 9, entries 3, 7, 10). Although the achieved enantioselectivities were low with both *ansa*-ammonium borate **Q\*CATH<sub>2</sub>** and *ansa*-aminoborane **Car\*CAT**, these experiments clearly proved the feasibility of using chiral amines as a part of intramolecular FLP systems for the chiral induction during catalytic hydrogenation. The highest ees achieved with **Q\*CATH<sub>2</sub>** are in the range of about 35–40% (er ~70:30). This is remarkable, taking into account the large distance between the chiral center at the 4-position of the tetrahydroquinoline moiety and the active stereogenic boron center.



**Scheme 37** Interactions of chiral 7-isopropyl-3,3-dimethyl-2-phenylindoline with  $\text{B(C}_6\text{F}_5)_3$  under an atmosphere of hydrogen or nitrogen [34]



**Scheme 38** Synthesis of enantiopure *ansa*-aminoborane **Car\*CAT** [34]

**Table 9** Enantioselective catalytic hydrogenation by *ansa*-ammonium borate **Q\*CATH<sub>2</sub>** and *ansa*-aminoborane **Car\*CAT** [34]

Entry	Substrate	Catalyst	Solvent	Time (h)	Temp. (°C)	Conv. (%)	ee (%)
1		<b>Q*CATH<sub>2</sub></b>	Et <sub>2</sub> O	1	60	100	12
2			Et <sub>2</sub> O	1	20	100	19
3		MTBE	1	20	100	26	
4		<b>Car*CAT</b>	Et <sub>2</sub> O	20	60	35	17
5		<b>Q*CATH<sub>2</sub></b>	Et <sub>2</sub> O	1	60	100	21
6			Et <sub>2</sub> O	12	20	100	31
7		MTBE	12	20	100	35	
8		<b>Q*CATH<sub>2</sub></b>	Et <sub>2</sub> O	1	60	100	18
9			Et <sub>2</sub> O	12	20	100	31
10		MTBE	12	20	100	37	

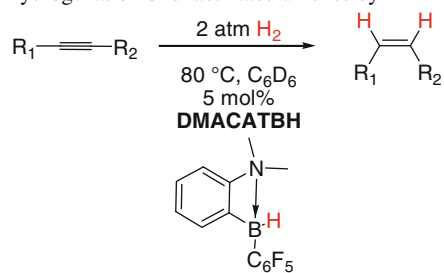
## 8 Catalytic Hydrogenation of Unactivated Triple C–C Bonds by Intramolecular *ansa*-Aminoboranes

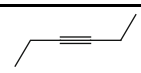
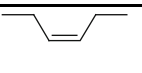
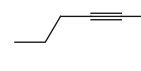
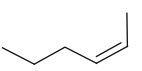
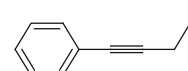
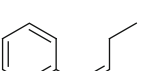
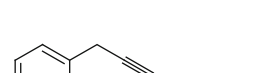
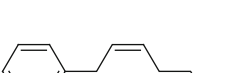
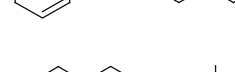


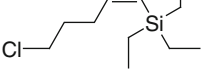
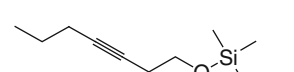
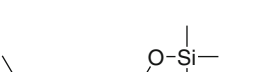

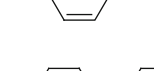
The metal-free hydrogenation of unactivated alkenes (220–235°C and 68–170 atm of H<sub>2</sub>) [75, 76], polycyclic aromatic hydrocarbons (170–200°C and 25–100 atm of H<sub>2</sub>) [77, 78] and coal (280–350°C and 148–247 atm of H<sub>2</sub>) [79] under harsh reaction conditions with simple trialkylboranes, tetraalkyldiborane and boron triiodide is well known. Until recently, due to the heterolytic nature of onium borohydrides, there were only a few examples of 1,4-conjugated hydrogenation of enone, ynone, dienes, and styrenes catalyzed by FLPs [40, 80, 81].

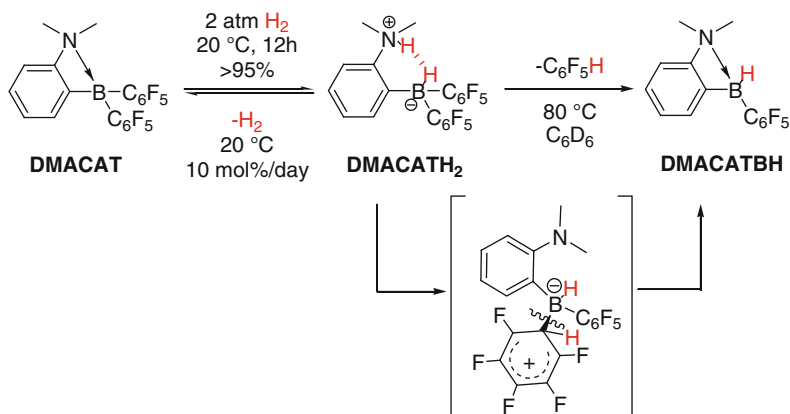
A breakthrough in this area was the recent discovery by us that *ansa*-aminohydroborane **DMACATBH** can hydrogenate internal alkynes even under mild conditions at 2 atm hydrogen pressure and 80°C (Table 10) [82].

The *ansa*-aminohydroborane **DMACATBH** was prepared by heating of either **DMACAT** at 80°C under 2 atm of hydrogen or **DMACATH<sub>2</sub>** under an atmosphere of argon via hydrogenolysis of the B–C bond (Scheme 39).

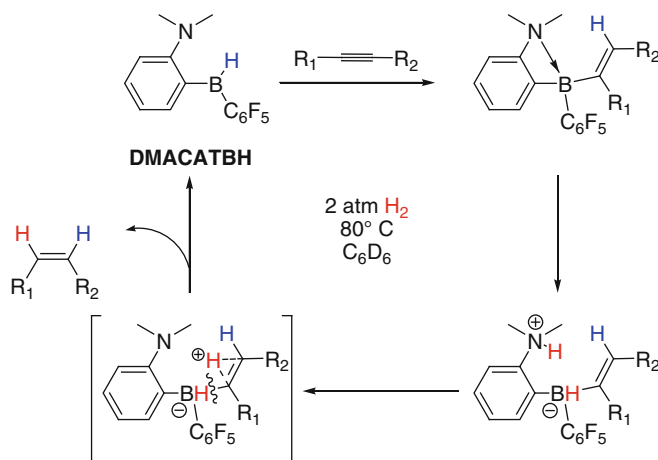
The mechanisms of hydrogenation of alkynes by **DMACATBH** have been investigated in some detail. It involves the sequence of hydroboration followed by hydrogen activation and hydrogenolysis of the B–C bond accompanied by the liberation of alkene (Scheme 40).

**Table 10** Catalytic hydrogenation of unactivated alkenes by **DMACATBH** [81]

Entry	Substrate	Time (h)	Product	Yield (%)
1		3		100
2		3		80
3		3		100
4		3		78
5		3		100
6		3		100
7		3		100
8		3 9		52 100



Scheme 39 Synthesis of DMACATBH [81]



Scheme 40 Proposed mechanism for the catalytic hydrogenation of unactivated alkenes by DMACATBH [81]

## 9 Conclusions

The use of FLPs as metal-free hydrogenation catalysts is a rapidly expanding field in modern organic chemistry. Since the pioneering studies on the reversible hydrogen activation by phosphinoboranes, numerous FLP systems for hydrogenation have been reported. Among others the *ansa*-aminoborane concept is one of the most promising for further elaboration with the aim of obtaining industrially applicable catalysts. Specifically, this approach allows the performance of hydrogenation of unsaturated nitrogen-containing compounds and internal alkynes under mild conditions with low catalyst loadings. Furthermore, recently the first example of

the enantioselective hydrogenation with chiral *ansa*-ammonium borates was demonstrated. Given the wide range of *ansa*-aminoboranes with different structures and properties, we anticipate new transformations will arise in the near future. Therefore over the next few years, many new exciting developments within this field are expected.

## References

1. De Vries JG, Elsevier CJ (2008) The handbook of homogeneous hydrogenation. Wiley-VCH, Weinheim
2. Tye JW, Darensbourg Y, Hall MB (2006) The activation of dihydrogen. In: Tolman WB (ed) Activation of small molecules. Wiley-VCH, Weinheim
3. Beller M, Bolm C (2004) Transition metals for organic synthesis. Wiley-VCH, Weinheim
4. Spikes GH, Gettinger JC, Power PP (2005) Facile activation of dihydrogen by an unsaturated heavier main group compound. *J Am Chem Soc* 127:12232–12233
5. Kenward AL, Piers WE (2007) Heterolytic H<sub>2</sub> activation by non-metals. *Angew Chem Int Ed* 47:38–41
6. Welch GC, Juan RRS, Masuda JD, Stephan DW (2006) Reversible, metal-free hydrogen activation. *Science* 314:1124–1126
7. Welch GC, Stephan DW (2007) Facile heterolytic cleavage of dihydrogen by phosphines and boranes. *J Am Chem Soc* 129:1880–1881
8. Frey GD, Lavallo V, Donnadiou B, Schoeller WW, Bertrand G (2007) Facile splitting of hydrogen and ammonia by nucleophilic activation at a single carbon center. *Science* 316:439–441
9. Welch GC, Cabrera L, Chase PA, Hollink E, Masuda JD, Wei P, Stephan DW (2007) Tuning Lewis acidity using the reactivity of “frustrated Lewis pairs”: facile formation of phosphine-boranes and cationic phosphonium-boranes. *Dalton Trans* 3407–3414
10. Garrett CE, Prasad K (2004) The art of meeting palladium specifications in active pharmaceutical ingredients produced by Pd-catalyzed reactions. *Adv Synth Catal* 346:889–900
11. Barbaras D, Brozio J, Johannsen I, Allmendinger T (2009) Removal of heavy metals from organic reaction mixtures: preparation and application of functionalized resins. *Org Process Res Dev* 13:1068–1079
12. List B (2007) Special issue: “organocatalysis”. *Chem Rev* 107:5413–5883
13. Brown HC, Schlesinger HI, Cardon SZ (1942) Studies in stereochemistry. I. Steric strains as a factor in the relative stability of some coordination compounds of boron. *J Am Chem Soc* 64:325–329
14. Wittig G, Rückert A (1950) Über komplexbildung mit triphenylbor (II. Mitt.). *Liebigs Ann Chem* 566:101–113
15. Wittig G, Bub O (1950) Über komplexbildung mit triphenyl-aluminium. *Liebigs Ann Chem* 566:113–127
16. Wittig G, Schloeder H (1955) Über die addition des trityl-natriums an butadiene in gegenwart von triphenyl-bor. *Liebigs Ann Chem* 592:38–53
17. Tochtermann W (1966) Structures and reactions of organic ate-complexes. *Angew Chem Int Ed* 5:351–371
18. Wittig G, Gonsior L, Vogel H (1965) Über die struktur und hydrolyse eines aus tritylnatrium, triphenylbor und kohlenmonoxyd gebildeten komplexsalzes. *Liebigs Ann Chem* 688:1–13
19. Rokob TA, Hamza A, Pápai I (2009) Rationalizing the reactivity of frustrated Lewis pairs: thermodynamics of H<sub>2</sub> activation and the role of acid–base properties. *J Am Chem Soc* 131:10701–10710



20. Roesler R, Piers WE, Parvez M (2003) Synthesis, structural characterization and reactivity of the amino borane 1-(NPh<sub>2</sub>)-2-[B(C<sub>6</sub>F<sub>5</sub>)<sub>2</sub>]C<sub>6</sub>H<sub>4</sub>. *J Organomet Chem* 680:218–222
21. Chiu C-W, Gabbai FP (2006) Fluoride ion capture from water with a cationic borane. *J Am Chem Soc* 128:14248–14249
22. Hudnall TW, Gabbai FP (2007) Ammonium boranes for the selective complexation of cyanide or fluoride ions in water. *J Am Chem Soc* 129:11978–11986
23. Hudnall TW, Kim Y-M, Bebbington MWP, Bourissou D, Gabbai FP (2008) Fluoride ion chelation by a bidentate phosphonium/borane Lewis acid. *J Am Chem Soc* 130:10890–10891
24. Chernichenko K, Nieger M, Leskelä M, Repo T (2012) Hydrogen activation by 2-boryl-N,N-dialkylanilines: a revision of Piers' ansa-aminoborane. *Dalton Trans* 41:9029–9032
25. Lindqvist M, Sarnela N, Sumerin V, Chernichenko K, Leskelä M, Repo T (2012) Heterolytic dihydrogen activation by B(C<sub>6</sub>F<sub>5</sub>)<sub>3</sub> and carbonyl compounds. *Dalton Trans* 41:4310–4312
26. Welch GC, Holtrichter-Roessmann T, Stephan DW (2008) Thermal rearrangement of phosphine-B(C<sub>6</sub>F<sub>5</sub>)<sub>3</sub> adducts. *Inorg Chem* 47:1904–1906
27. Ullrich M, Lough AJ, Stephan DW (2009) Reversible, metal-free, heterolytic activation of H<sub>2</sub> at room temperature. *J Am Chem Soc* 131:52–53
28. Marwitz AJV, Dutton JL, Mercier LG, Piers WE (2011) Dihydrogen activation with <sup>t</sup>Bu<sub>3</sub>P/B(C<sub>6</sub>F<sub>5</sub>)<sub>3</sub>: a chemically competent indirect mechanism via in situ-generated *p*-<sup>t</sup>Bu<sub>2</sub>P–C<sub>6</sub>F<sub>4</sub>–B(C<sub>6</sub>F<sub>5</sub>)<sub>2</sub>. *J Am Chem Soc* 133:10026–10029
29. Sumerin V, Schulz F, Nieger M, Leskelä M, Repo T, Rieger B (2008) Facile heterolytic H<sub>2</sub> activation by amines and B(C<sub>6</sub>F<sub>5</sub>)<sub>3</sub>. *Angew Chem Int Ed* 47:6001–6003
30. Focante F, Mercandelli P, Sironi A, Resconi L (2006) Complexes of tris(pentafluorophenyl) boron with nitrogen-containing compounds: synthesis, reactivity and metallocene activation. *Coord Chem Rev* 250:170–188
31. Voss T, Mahdi T, Otten E, Fröhlich R, Kehr G, Stephan DW, Erker G (2012) Frustrated Lewis pair behavior of intermolecular amine/B(C<sub>6</sub>F<sub>5</sub>)<sub>3</sub> pairs. *Organometallics* 31:2367–2378
32. Mountford AJ, Lancaster SJ, Coles SJ, Horton PN, Hughes DL, Hursthouse MB, Light ME (2005) Intra- and intermolecular N–H···F–C hydrogen-bonding interactions in amine adducts of tris(pentafluorophenyl)borane and -alane. *Inorg Chem* 44:5921–5933
33. Millot N, Santini CC, Fenet B, Basset JM (2002) Formation and characterization of zwitterionic stereoisomers from the reaction of B(C<sub>6</sub>F<sub>5</sub>)<sub>3</sub> and NEt<sub>2</sub>Ph: (E)- and (Z)-[EtPhN<sup>+</sup>=CHCH<sub>2</sub>–B–(C<sub>6</sub>F<sub>5</sub>)<sub>3</sub>]. *Eur J Inorg Chem* 3328–3335
34. Sumerin V, Chernichenko K, Nieger M, Leskelä M, Rieger B, Repo T (2011) Highly active metal-free catalysts for hydrogenation of unsaturated nitrogen-containing compounds. *Adv Synth Catal* 353:2093–2110
35. Farrell JM, Heiden ZM, Stephan DW (2011) Metal-free transfer hydrogenation catalysis by B(C<sub>6</sub>F<sub>5</sub>)<sub>3</sub>. *Organometallics* 30:4497–4500
36. Chase PA, Jurca T, Stephan DW (2008) Lewis acid-catalyzed hydrogenation: B(C<sub>6</sub>F<sub>5</sub>)<sub>3</sub>-mediated reduction of imines and nitriles with H<sub>2</sub>. *Chem Commun* 1701–1703
37. Jiang C, Blacque O, Fox T, Berke H (2011) Heterolytic cleavage of H<sub>2</sub> by frustrated B/N Lewis pairs. *Organometallics* 30:2117–2124
38. Schulz F, Sumerin V, Leskelä M, Repo T, Rieger B (2010) Frustrated Lewis pairs: reactivities of TMS protected amines and phosphines in the presence of B(C<sub>6</sub>F<sub>5</sub>)<sub>3</sub>. *Dalton Trans* 39:1920–1922
39. Erős G, Mehdi H, Pápai I, Rokob TA, Király P, Tárkányi G, Soós T (2010) Expanding the scope of metal-free catalytic hydrogenation through frustrated Lewis pair design. *Angew Chem Int Ed* 49:6559–6563
40. Soós T (2011) Design of frustrated Lewis pair catalysts for metal-free and selective hydrogenation. *Pure Appl Chem* 83:667–675
41. Lu Z, Cheng Z, Chen Z, Weng L, Li ZH, Wang H (2011) Heterolytic cleavage of dihydrogen by “frustrated Lewis pairs” comprising bis(2,4,6-tris(trifluoromethyl)phenyl)borane and amines: stepwise versus concerted mechanism. *Angew Chem Int Ed* 50:12227–12231

42. Sumerin V, Schulz F, Nieger M, Atsumi M, Wang C, Leskelä M, Pyykkö P, Repo T, Rieger B (2009) Experimental and theoretical treatment of hydrogen splitting and storage in boron–nitrogen systems. *J Organomet Chem* 694:2654–2660
43. Jiang C, Blaque O, Fox T, Berke H (2011) Reversible, metal-free hydrogen activation by frustrated Lewis pairs. *Dalton Trans* 40:1091–1097
44. Pyykkö P, Wang C (2010) Theoretical study of H<sub>2</sub> splitting and storage by boron–nitrogen-based systems: a bimolecular case and some qualitative aspects. *Phys Chem Chem Phys* 12:149–155
45. Fan C, Mercier LG, Piers WE, Tuononen HM, Parvez M (2010) Dihydrogen activation by antiaromatic pentaarylboroles. *J Am Chem Soc* 132:9604–9606
46. Rajeev R, Sunoj RB (2009) On the origin of reversible hydrogen activation by phosphino-boranes. *Chem Eur J* 15:12846–12855
47. Rokob TA, Hamza A, Stirling A, Soós T, Pápai I (2008) Turning frustration into bond activation: a theoretical mechanistic study on heterolytic hydrogen splitting by frustrated Lewis pairs. *Angew Chem Int Ed* 47:2435–2438
48. Kim HW, Rhee YM (2009) Dispersion-oriented soft interaction in a frustrated Lewis pair and the entropic encouragement effect in its formation. *Chem Eur J* 15:13348–13355
49. Grimme S, Kruse H, Goerigk L, Erker G (2010) The mechanism of dihydrogen activation by frustrated Lewis pairs revisited. *Angew Chem Int Ed* 49:1402–1405
50. Guo Y, Li S (2008) Unusual concerted Lewis acid–Lewis base mechanism for hydrogen activation by a phosphine-borane compound. *Inorg Chem* 47:6212–6219
51. Hamza A, Stirling A, Rokob TA, Pápai I (2009) Mechanism of hydrogen activation by frustrated Lewis pairs: a molecular orbital approach. *Int J Quant Chem* 109:2416–2425
52. Nikonov GI, Vyboishchikov SF, Shirobokov OG (2012) Facile activation of H–H and Si–H bonds by boranes. *J Am Chem Soc* 134:5488–5491
53. Ashley AE, Thompson AL, O'Hare D (2009) Non-metal-mediated homogeneous hydrogenation of CO<sub>2</sub> to CH<sub>3</sub>OH. *Angew Chem Int Ed* 48:9839–9843
54. Tran SD, Tronic TA, Kaminsky W, Heinekey DM, Mayer JM (2011) Metal-free carbon dioxide reduction and acidic C–H activations using a frustrated Lewis pair. *Inorg Chim Acta* 369:126–132
55. Riduan SN, Zhang Y, Ying JY (2009) Conversion of carbon dioxide into methanol with silanes over *N*-heterocyclic carbene catalysts. *Angew Chem Int Ed* 48:3322–3325
56. Cotton FA, Wilkinson G, Murillo CA, Bochmann M (1999) *Advanced inorganic chemistry*, 6th edn. Wiley, New York
57. Berkefeld A, Piers WE, Parvez M (2010) Tandem frustrated Lewis pair/tris (pentafluorophenyl)borane-catalyzed deoxygenative hydrosilylation of carbon dioxide. *J Am Chem Soc* 132:10660–10661
58. Geier SJ, Chase PA, Stephan DW (2010) Metal-free reductions of *N*-heterocycles via Lewis acid catalyzed hydrogenation. *Chem Commun* 4884–4886
59. Chen D, Klankermayer J (2008) Metal-free catalytic hydrogenation of imines with tris (perfluorophenyl)borane. *Chem Commun* 2130–2131
60. Mahdi T, Heiden ZM, Grimme S, Stephan DW (2012) Metal-free aromatic hydrogenation: aniline to cyclohexyl-amine derivatives. *J Am Chem Soc* 134:4088–4091
61. Erős G, Nagy K, Mehdi H, Pápai I, Nagy P, Király P, Tárkányi G, Soós T (2012) Catalytic hydrogenation with frustrated Lewis pairs: selectivity achieved by size-exclusion design of Lewis acids. *Chem Eur J* 18:574–585
62. Sumerin V, Schulz F, Atsumi M, Wang C, Nieger M, Leskelä M, Repo T, Pyykkö P, Rieger B (2008) Molecular tweezers for hydrogen: synthesis, characterization, and reactivity. *J Am Chem Soc* 130:14117–14119
63. Schulz F, Sumerin V, Heikkinen S, Pedersen B, Wang C, Atsumi M, Leskelä M, Repo T, Pyykkö P, Petry W, Rieger B (2011) Molecular hydrogen tweezers: structure and mechanisms by neutron diffraction, NMR, and deuterium labeling studies in solid and solution. *J Am Chem Soc* 133:20245–20257

64. Grabowski SJ, Sokalski WA, Leszczynski J (2007) Wide spectrum of H · · H interactions: van der Waals contacts, dihydrogen bonds and covalency. *Chem Phys* 337:68–76
65. Heiden ZM, Schedler M, Stephan DW (2011) Synthesis and reactivity of *o*-benzylphosphino- and *o*- $\alpha$ -methylbenzyl(*N,N*-dimethyl)amine-boranes. *Inorg Chem* 50:1470–1479
66. Schwendemann S, Fröhlich R, Kehr G, Erker G (2011) Intramolecular frustrated N/B Lewis pairs by enamine hydroboration. *Chem Sci* 2:1842–1849
67. Theuergarten E, Schlüns D, Grunenberg J, Daniliuc CG, Jones PG, Tamm M (2010) Intramolecular heterolytic dihydrogen cleavage by a bifunctional frustrated pyrazolylborane Lewis pair. *Chem Commun* 8561–8563
68. Yalpani M, Boese R, Köster R (1990) Pyrazole-organoboranes, VI. Monomeric and dimeric 9-pyrazolyl-9-borabicyclo[3.3.1]nonanes. *Chem Ber* 123:1275–1283
69. Holschumacher D, Bannenberg T, Hrib CG, Jones PG, Tamm M (2008) Heterolytic dihydrogen activation by a frustrated carbene–borane Lewis pair. *Angew Chem Int Ed* 47:7428–7432
70. Chase PA, Welch GC, Jurca T, Stephan DW (2007) Metal-free catalytic hydrogenation. *Angew Chem Int Ed* 46:8050–8053
71. Spies P, Schwendemann S, Lange S, Kehr G, Fröhlich R, Erker G (2008) Metal-free catalytic hydrogenation of enamines, imines, and conjugated phosphinoalkenylboranes. *Angew Chem Int Ed* 47:7543–7546
72. Chen D, Wang Y, Klankermayer J (2010) Enantioselective hydrogenation with chiral frustrated Lewis pairs. *Angew Chem Int Ed* 49:9475–9478
73. Parks DJ, Piers WE, Yap GPA (1998) Synthesis, properties, and hydroboration activity of the highly electrophilic borane bis(pentafluorophenyl)borane, HB(C<sub>6</sub>F<sub>5</sub>)<sub>2</sub>. *Organometallics* 17:5492–5503
74. DeWitt EJ, Ramp FL, Trapasso LE (1961) Homogeneous hydrogenation catalyzed by boranes. *J Am Chem Soc* 83:4672
75. Ramp FL, DeWitt EJ, Trapasso LE (1962) Homogeneous hydrogenation catalyzed by boranes. *J Org Chem* 27:4368–4372
76. Yalpani M, Lunow T, Köster R (1989) Reduction of polycyclic arenes by boranes. II. Borane catalyzed hydrogenation of naphthalenes to tetralins. *Chem Ber* 122:687–693
77. Yalpani M, Köster R (1990) Partial hydrogenation: from anthracene to coronene. *Chem Ber* 123:719–724
78. Haenel MW, Narangerel J, Richter U-B, Rufinska A (2006) The first liquefaction of high-rank bituminous coals by preceding hydrogenation with homogeneous borane or iodine catalysts. *Angew Chem Int Ed* 45:1061–1066
79. Xu B-H, Kehr G, Fröhlich R, Wibbeling B, Schirmer B, Grimme S, Erker G (2011) Reaction of frustrated Lewis pairs with conjugated ynone-selective hydrogenation of the carbon–carbon triple bond. *Angew Chem Int Ed* 50:7183–7186
80. Greb L, Oña-Burgos P, Schirmer B, Grimme S, Stephan DW, Paradies J (2012) Metal-free catalytic olefin hydrogenation: low-temperature H<sub>2</sub> activation by frustrated Lewis pairs. *Angew Chem Int Ed*. doi:10.1002/anie.201204007
81. Chernichenko K, Nieger M, Leskelä M, Repo T (2012) *Angew Chem Int Ed* (submitted)
82. Jiang C, Blacque O, Berke H (2009) Metal-free hydrogen activation and hydrogenation of imines by 1,8-bis(dipentafluorophenylboryl)naphthalene. *Chem Commun* 5518–5520

# Hydrogen Activation by Frustrated Lewis Pairs: Insights from Computational Studies

Tibor András Rokob and Imre Pápai

**Abstract** Sterically encumbered Lewis acid–base pairs, the so-called frustrated Lewis pairs, can split dihydrogen heterolytically and act as transition metal free catalysts for the hydrogenation of unsaturated compounds. Here we review the results from our quantum chemical calculations aimed at the understanding of this remarkable class of reactions and we put them into the context of related works from other research groups. The thermodynamics of the H<sub>2</sub> splitting reaction is discussed first; the role of acid–base properties, intramolecular cooperativity, and other factors is assessed, employing an energy partitioning scheme and also in the light of the latest experimental findings. The mechanism of hydrogen cleavage is then examined, and an overview about the applicability of our reactivity model involving synergistic electron transfers between H<sub>2</sub> and preorganized Lewis acid/base centers is given. Finally, insights about catalytic cycles in FLP-mediated hydrogenations are summarized, pinpointing the diversity of the involved elementary steps and their possible sequences.

**Keywords** Catalysis · Dihydrogen · Lewis acid–base reaction · Quantum chemistry · Reaction mechanism

## Contents

1	Introduction .....	159
2	Computational Approaches .....	160
3	Thermodynamics of H <sub>2</sub> Cleavage .....	162
3.1	Types of FLPs and Scope of the Study .....	162
3.2	Overall Free Energies .....	165

---

T.A. Rokob and I. Pápai (✉)

Institute of Organic Chemistry, Research Centre for Natural Sciences, Hungarian Academy of Sciences, Pusztaszeri út 59-67, 1025 Budapest, Hungary  
e-mail: [papai@chemres.hu](mailto:papai@chemres.hu)

3.3	Partitioning of the Reaction Free Energy .....	167
3.4	Tuning the Overall Free Energy: Are Acid and Base Strengths Decisive? .....	171
3.5	Related Studies in the Literature .....	173
4	The Mechanism and the Notion of Frustration .....	174
4.1	The Prototypical <i>t</i> -Bu <sub>3</sub> P/B(C <sub>6</sub> F <sub>5</sub> ) <sub>3</sub> + H <sub>2</sub> Reaction .....	175
4.2	Proposed Reactivity Model .....	180
4.3	Theoretical Studies of Other D/A + H <sub>2</sub> Reactions .....	183
4.4	Dihydrogen Activation with Linked FLPs .....	190
4.5	On the Elusive Nature of Reaction Intermediates: Can We Detect Frustrated Complexes? .....	193
5	Hydrogenation of Double Bonds .....	196
5.1	Hydrogenation of Imines with B(C <sub>6</sub> F <sub>5</sub> ) <sub>3</sub> .....	196
5.2	Hydrogenation of Quinolines with B( <i>p</i> -C <sub>6</sub> F <sub>4</sub> H) <sub>2</sub> Mes .....	200
5.3	Related Studies in the Literature .....	202
6	Summary and Outlook .....	203
	References .....	205

## Abbreviations

A	Acceptor (Lewis acid)
Ar	Aryl
Cy	Cyclohexyl
D	Donor (Lewis base)
D/A	Intermolecular (nonlinked) donor–acceptor pair
D~A	Intramolecular (covalently linked) donor–acceptor compound
D...A	Noncovalent donor–acceptor complex
D–A	Dative donor–acceptor adduct
DFT	Density functional theory
Et	Ethyl
FLP	Frustrated Lewis pair
HOMO	Highest occupied molecular orbital
<i>i</i> -Pr	<i>iso</i> -Propyl
IRC	Intrinsic reaction coordinate
LUMO	Lowest unoccupied molecular orbital
Me	Methyl
Mes	Mesityl (2,4,6-trimethylphenyl)
NMR	Nuclear magnetic resonance
PES	Potential energy surface
Ph	Phenyl
<i>t</i> -Bu	<i>tert</i> -Butyl
TM	Transition metal

## 1 Introduction

The propensity of bulky Lewis acid–base pairs to avoid dative bond formation was described about 70 years ago [1]. Untypical or unexpected reaction pathways were observed with these “antagonistic pairs” [2, 3] due to the coexistence of strong, unquenched acidic and basic centers. Nevertheless, a new field of research, now called “frustrated Lewis pair” (FLP) chemistry [4], was born only recently when a series of milestone experiments revealed that bulky Lewis pairs can activate various small molecules or bonds [5]. In particular, they are capable of reversible hydrogen activation under mild conditions [6].

The activation of hydrogen has been the realm of transition metals (TMs), and catalytic hydrogenation, a significant synthetic transformation of both industrial and academic interest, is typically carried out by homogeneous or heterogeneous TM-containing catalysts [7]. Due to the presence of the partially filled *d*-orbitals, TMs are indeed particularly well suited for the cleavage of H<sub>2</sub> [8]. However, they are usually expensive, and their traces remaining in the products present toxicological and environmental concerns. On the other hand, certain main-group compounds can also react readily with H<sub>2</sub>. Recently discovered examples include (alkyl)(amino)carbenes [9], unsaturated ArEEAr molecules and Ar<sub>2</sub>E carbene analogues with E = Ge or Sn [10], (amido)(boryl)silylenes [11], organocalcium derivatives [12], and antiaromatic boroles [13], and the range has been notably extended by FLPs [14]. By now, a series of frustrated pairs have been shown to exhibit H<sub>2</sub> activation, and many of them have been successfully applied in TM-free catalytic hydrogenation procedures [15, 16]. Nevertheless, hydrogen activation is intriguing not only because of its potential use in developing cleaner synthetic procedures. The cleavage of such an inert molecule under mild conditions is in itself a fascinating ramification of Lewis acid–base chemistry.

Breakthroughs in a research field may stem from serendipitous discoveries, but very often, understanding contributes significantly to the development of new or better approaches. In order to advance metal-free hydrogen activation and hydrogenation chemistry it is desirable to attain more knowledge about the atomistic details of the reactions and to rationalize factors affecting the kinetics and the thermodynamics of both cleavage and transfer of H<sub>2</sub>. The primary sources of information along these lines are, of course, experimental analyses, quantitative ones in particular. However, due to the spectacular development in both methodology and computer power, contemporary computational chemistry has reached a level where it can provide useful and reliable complementary information. There are still numerous known pitfalls and problematic systems, and the free energy data for molecules of 50–100 atoms in solution are rarely of “chemical accuracy” (having errors below 1 kcal/mol), but computational chemistry offers several advantages that can contribute significantly to the understanding. For instance, reaction heats and other thermodynamical properties can be calculated on the basis of computed energetics, providing a direct link to experimentally observable quantities. The atomistic level of description and the possibility of arbitrary modifications of the

investigated systems or partitioning of the computed energetic data allow easy identification of the reactivity-determining factors. Valuable information regarding the reaction mechanism can also be obtained from thorough examination of alternative reaction pathways, including the computational identification of key reaction intermediates and transition states. The computed free energy diagrams can then be used to judge the feasibility of the envisioned mechanistic pathways and to plan new experiments.

We initiated several computational studies on FLP H<sub>2</sub> activation with the goal of providing explanations, trends, predictions, and analogies to establish a solid background for the rational design of improved FLP catalysts [17–25]. In the present chapter we summarize our findings, divided into three main sections covering three aspects of this intriguing reactivity: the thermodynamics of heterolytic H<sub>2</sub> splitting, the mechanism of H<sub>2</sub> activation, and the mechanism of catalytic hydrogenation. Although we focus primarily on our own contributions, we present them in the context of achievements disclosed by other research groups, being aware that most of them are discussed in detail in other chapters of this book. Herein, we wish to give a critical overview of the currently available results of theoretical works and also to bring out some unresolved issues and possible new research directions. A brief and general description of computational approaches is provided prior to the discussion of the results.

## 2 Computational Approaches

The majority of contemporary theoretical studies aimed at the understanding of chemical reactivity explore the potential energy surface (PES) as a function of nuclear coordinates, a concept brought into existence by the Born–Oppenheimer approximation. By locating the minima and identifying the connecting first-order saddle points, one obtains structures of the intermediates and transition states together with the corresponding (“electronic”) potential energies. To address the effects of finite temperature in the simplest way, free energies are then calculated by treating the species as rigid rotors and the internal motions as harmonic oscillators. Solvent models based on a continuum representation can provide estimates of solvation free energies, thereby linking the gas-phase and solution-phase free energy data. Ideal behavior in both gas phase and solution is typically assumed. We also employed this approach in most of our investigations.

The first component of this protocol is the approximate method used to calculate electronic energies. For systems as large as a typical FLP, density functional theory (DFT) offers an efficient and reasonably accurate choice in general; however, the exchange–correlation functional must be selected carefully. In mechanistic studies, it must reliably describe relative energies of intermediates with fully formed, well localized bonds and transition states with partially broken, more delocalized ones in order to estimate activation barriers accurately. Hybrid functionals, which combine the nonlocal Hartree–Fock-type exchange with semilocal approximated exchange

and correlation, are therefore typically chosen. Characteristic for FLPs is the importance of the interactions among the bulky substituents, a significant component of which is dispersion. An appropriate treatment for this type of weak interaction is only provided by more recent density functionals [26]. For example, the M05/M06 families [27], nonlocal van der Waals density functionals [28], and Grimme's dispersion correction [29], applicable to a variety of older and newer functionals, were reported to yield acceptable results. In most cases, we utilized the M05-2X functional.

As the energy changes slowly in the vicinity of a stationary point, geometry optimizations are often carried out at a lower, cheaper level of theory. In contrast, the subsequent single-point energy computations may involve more expensive approaches. For instance, larger basis sets can be used for the DFT calculations, and wave function methods can also be considered. The SCS-MP2 method [30], based on a physically motivated scaling of the MP2 components, was found to be quite robust, and we applied it to obtain some of the results discussed in the present chapter.

Having the stationary points on the PES and their energies in hand, one can proceed to the calculation of free energies. Admittedly, the commonly utilized rigid rotor, harmonic oscillator model does not perform particularly well when the PES has several close-lying minima separated by tiny barriers, such as in the case of internal rotations [31, 32]. General experience, however, shows that the relative free energy data obtained are accurate enough to characterize trends and understand mechanisms. This is supposedly due to a favorable cancellation of errors.

The investigated reactions occur in condensed phase, and solvents can have profound effects on the reaction free energy profiles. The solvent is often modeled as a polarizable continuum, which usually provides acceptable results in the absence of direct participation of solvent molecules in the chemical reaction and very strong, specific solute–solvent binding [33–37]. Particularly for apolar solvents and uncharged solutes, nonelectrostatic contributions to the solvation can be large, and continuum solvation models typically contain some more or less empirical terms to account for them. In our earlier works we employed the IEF-PCM/UA0 [38] formulation of the continuum model. Later, when it became widely available, we switched to the more accurate SMD [39] scheme. While many important aspects of solvation are correctly grasped by these methods, their limited accuracy must be kept in mind.

As discussed, free energies determined by the above approach, which we might term as “static” quantum chemistry, suffer from larger uncertainties because of the thermal motions, entropies, and interactions with the solvent. These phenomena may be better addressed by a statistical sampling of the PES at finite temperature with explicit solvent molecules. To this end, Monte Carlo techniques or molecular dynamics can be applied. In both cases, a much larger number of points on the PES are involved than with “static” approaches, and much more efficient methods for the calculation of the energy are necessary. Empirical force fields may be a good choice for nonreactive systems; for the description of reactivity, force fields with various corrections or cheap DFT techniques can be chosen. In one of our works [25], which is to our knowledge the first study going beyond “static”



quantum chemistry in the field of FLPs, we employed molecular dynamics and a custom force field with an empirical correction to describe the energy contribution of incipient dative bonding.

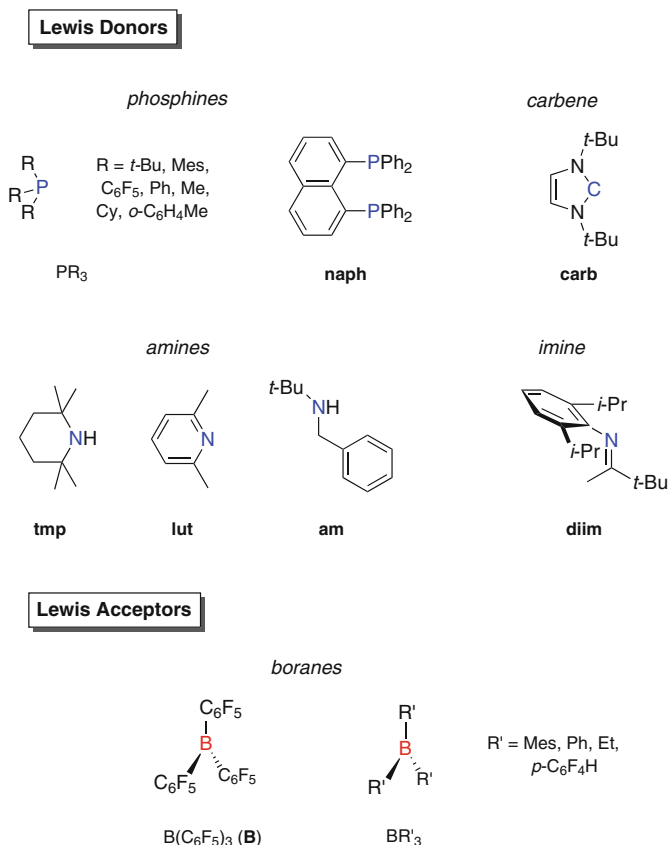
### 3 Thermodynamics of H<sub>2</sub> Cleavage

Steric hindrance of dative bond formation has been known for quite long time, but in connection with proton and hydride bound to Lewis bases and acids, evolution, and not cleavage, of hydrogen was typically observed (e.g., in borohydride hydrolysis [40]). Why does thermodynamics prefer H<sub>2</sub> splitting with FLPs? In their early study [41], the Stephan group highlighted the role of cumulative strength of the acidic and basic components to allow breaking of the H–H bond, and indeed, typical reactive pairs feature multiple electron-donating alkyl or alkylaryl substituents on the donor and fluorinated, electron-withdrawing substituents on the acceptor center. Nevertheless, neither a large number of alkyl groups nor the fluorine atoms seem to be indispensable in light of later results [42, 43]. The requirement for the complete absence of the dative bond, originally considered as a key to FLP behavior, can also be dropped in some cases (for early examples see [44, 45]). In addition, Repo, Rieger et al. came to the conclusion that it is the favorable electrostatic interaction between the charged fragments of the zwitterionic products that can “pay for the loss of the strong Heitler–London covalent bond of H<sub>2</sub>” [46]. It thus seems that H<sub>2</sub> cleavage capability results from a delicate balance of various properties, which is worth examining.

Failure of H<sub>2</sub> cleavage may, of course, originate from unfavorable kinetics as well. In the field of FLPs, this was first demonstrated by Erker and coworkers, who prepared the phosphinoborane compounds *trans*-Mes<sub>2</sub>P–CH=CR–B(C<sub>6</sub>F<sub>5</sub>)<sub>2</sub> (R = Me or Ph), which are unreactive toward H<sub>2</sub> but readily accept the H<sup>+</sup> and H<sup>–</sup> from other systems [47]. Nevertheless, several studies in the literature confirm that investigation of thermodynamic properties of hydrogen activating or releasing systems can unfold important details about the reactivity-determining factors [48, 49]. In an effort to understand these factors better, we undertook and published a computational study on the thermodynamics of the hydrogen splitting process by various FLPs [20]. Besides predictions of the overall reaction energies, the theoretical approach allowed us to address directly the importance of all contributions suggested to be important for H<sub>2</sub> cleavage and to highlight some aspects that may be exploited in the rational design of related new compounds. This section summarizes the most important findings from our 2009 study.

#### 3.1 Types of FLPs and Scope of the Study

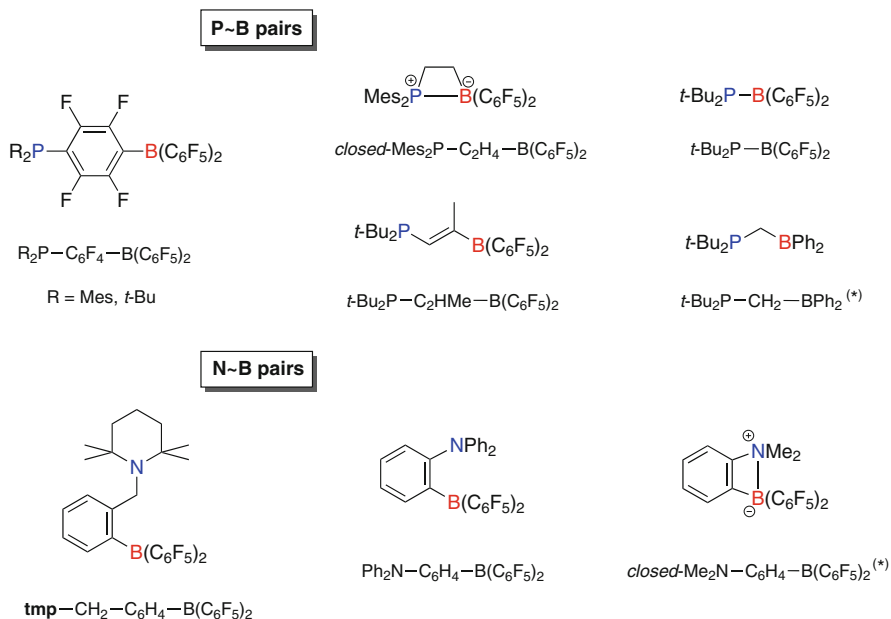
Starting from the phosphine/borane combinations disclosed in the seminal papers of this field [6, 41, 50], the range of FLPs has been notably extended by now. Many of the reported systems are simple pairs of separate donor and acceptor molecules



**Fig. 1** Components of the investigated intermolecular Lewis acid–base pairs

(D/A pairs; also referred to as *intermolecular* or *nonlinked* FLPs). It was demonstrated in several studies that the “classical” Lewis reactivity (dative bond formation) is not mutually exclusive with FLP behavior, so among the intermolecular “FLPs,” a number of dative D–A adducts can also be found. The other class of FLPs consists of *intramolecular* or *linked* pairs, where the donor and acceptor centers are connected by a covalent backbone (denoted as D~A here). For some of these compounds, intramolecular dative bonds were also observed, leading to heterocyclic structures, which we denote by *closed*-D~A.

In our 2009 investigations we included a large set of Lewis pairs for which experiments clearly indicated either hydrogenated product formation or the absence of any reaction with H<sub>2</sub> [4, 6, 41, 44–47, 50–58]. This list has now been extended by two items that further illustrate some of the conclusions we drew at that time [43, 59]. The involved components of intermolecular D/A or D~A pairs are shown in Fig. 1. From the impressive list of FLP donors applied in the literature, we included a representative series with various donor atoms (P,N,C), various levels of steric

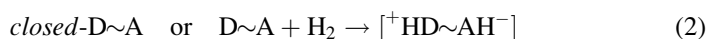


**Fig. 2** Covalently linked Lewis pairs under study. Molecules added to the list of originally investigated systems are marked with an *asterisk*

encumbrance (e.g., Me<sub>3</sub>P vs Mes<sub>3</sub>P), and with substituents having various electronic effects (e.g., (C<sub>6</sub>F<sub>5</sub>)<sub>3</sub>P vs Ph<sub>3</sub>P). A much narrower range of compounds has been reported on the acceptor side; so far, almost all hydrogen-activating systems employ boranes. We studied the most often utilized tris(pentafluorophenyl)borane, B(C<sub>6</sub>F<sub>5</sub>)<sub>3</sub>, together with a small set of other symmetric triaryl- and trialkylboranes. In addition, we carried out calculations for a series of linked donor–acceptor systems (D~A) including phosphinoborane and aminoborane compounds with various tethers having length of 0, 1, 2, 3, or 4 atoms (see Fig. 2). Intramolecular dative bonds were only observed for the CH<sub>2</sub>–CH<sub>2</sub>-linked Mes<sub>2</sub>P–C<sub>2</sub>H<sub>4</sub>–B(C<sub>6</sub>F<sub>5</sub>)<sub>2</sub> molecule, and the *ortho*-phenylene-linked Me<sub>2</sub>N–C<sub>6</sub>H<sub>4</sub>–B(C<sub>6</sub>F<sub>5</sub>)<sub>2</sub>, whose observed forms with four-membered heterocycles will be referred to as *closed*-Mes<sub>2</sub>P–C<sub>2</sub>H<sub>4</sub>–B(C<sub>6</sub>F<sub>5</sub>)<sub>2</sub> and *closed*-Me<sub>2</sub>N–C<sub>6</sub>H<sub>4</sub>–B(C<sub>6</sub>F<sub>5</sub>)<sub>2</sub>, respectively. Furthermore, for the directly linked *t*-Bu<sub>2</sub>P–B(C<sub>6</sub>F<sub>5</sub>)<sub>2</sub> compound, weak π overlap between the adjacent phosphorus lone pair and boron empty orbital was revealed by computations, and it is also apparent from the X-ray geometry showing planar P and B centers as well as an unusually short P–B bond [58]. Nevertheless, this compound retains sufficient Lewis acidic and basic character to react directly with H<sub>2</sub>; therefore, we consider it for the moment as containing no dative bond.

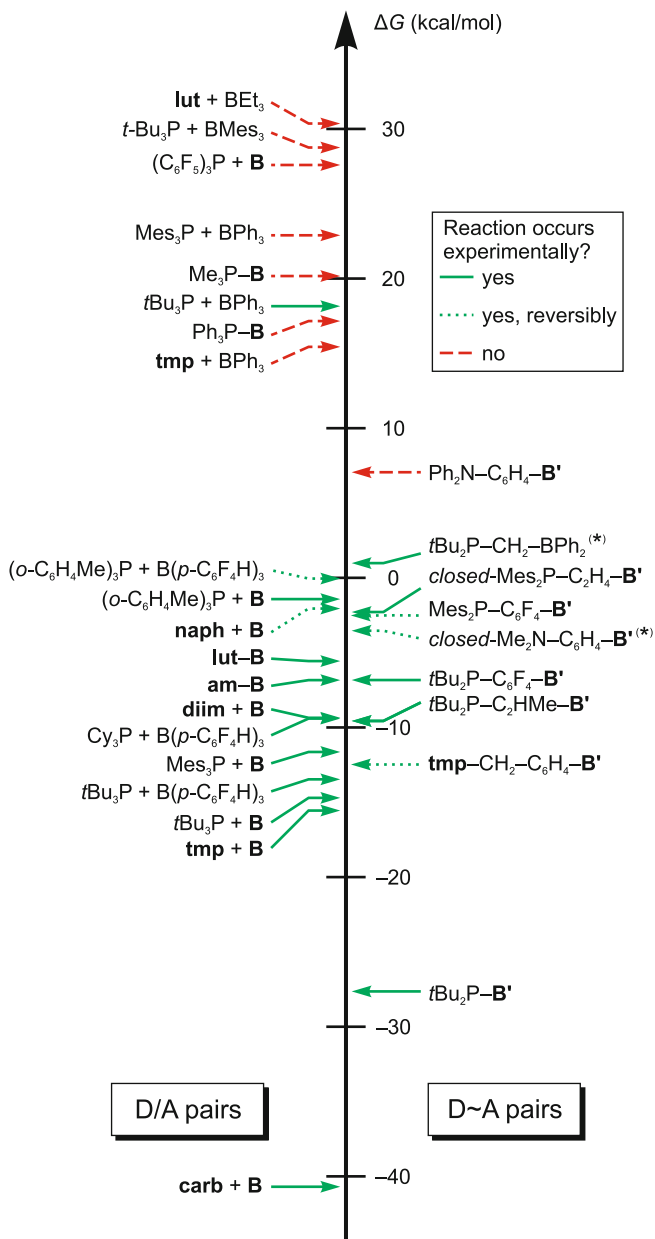
### 3.2 Overall Free Energies

In order to investigate the thermodynamic feasibility of the H<sub>2</sub> cleavage reaction with various D/A and D~A systems, we calculated the overall solution-phase Gibbs free energies ( $\Delta G$ ) at 25 °C of the H<sub>2</sub> activation reaction using the M05-2X functional. We chose a single solvent for all calculations to make the identification of trends easier; toluene was selected, as most of the experiments had employed this medium. The experimentally found stable forms (datively bound or unbound) of the Lewis acid–base systems and molecular H<sub>2</sub> were considered as reactants, and the product was treated as a solvated cation–anion pair [DH]<sup>+</sup>[HA]<sup>−</sup> or a single zwitterionic species [<sup>+</sup>HD~AH<sup>−</sup>]. In other words, we considered the following reactions:



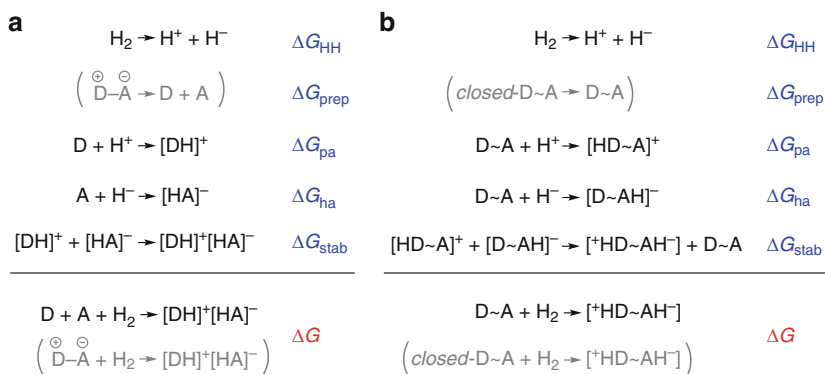
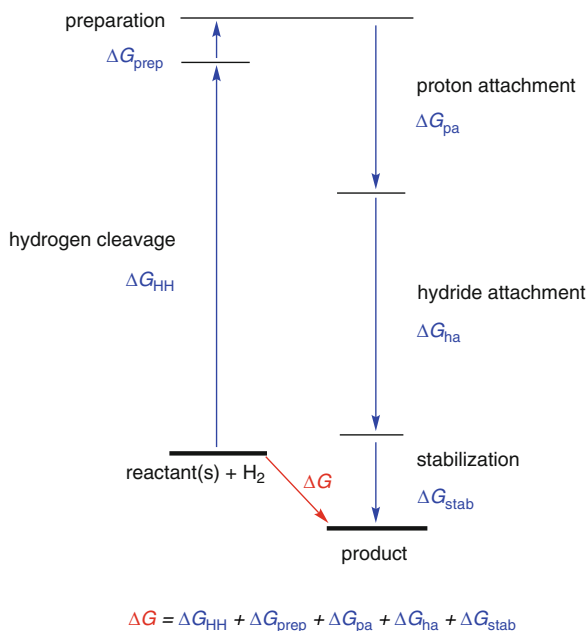
The computed solution-phase  $\Delta G$  data for all examined Lewis pairs are presented on an energy scale in Fig. 3. Apparently the calculated free energies cover a remarkably wide range (from −40 to +30 kcal/mol). All systems that were shown to be unreactive experimentally are characterized by positive  $\Delta G$  values typically above +10 kcal/mol, which suggests that it is the thermodynamically unfavorable nature of these reactions that hampers the isolation of the H<sub>2</sub> cleavage product. Accordingly, for all reactive systems but one, we obtained free energy values near to or in some cases well below zero. For the reactive *t*-Bu<sub>3</sub>P + BPh<sub>3</sub> pair, however, the calculated  $\Delta G = +18.2$  kcal/mol is quite high and, more importantly, it falls into a region of several nonreactive systems. In spite of the possible uncertainties of the computed solvent-phase free energies, consideration of the qualitative agreement for all other systems and also for the trends (see below) suggests that revisiting the experimental data might be necessary in this particular case.

Reversibility of the H<sub>2</sub> binding was observed for some of the treated FLPs, that is, H<sub>2</sub> is lost and the original FLP is reformed upon exposure to heat or/and reduced pressure. One expects that reversible FLP/H<sub>2</sub> systems are slightly exergonic in the direction of H<sub>2</sub> uptake at standard conditions, and this is indeed what we found. However, it is also apparent that we cannot distinguish between reversible and nonreversible systems on the basis of the calculated  $\Delta G$  values. This fact may be explained by different reaction barriers as well as the nonequilibrium conditions leading to H<sub>2</sub> expulsion, neither of which was taken into account in our present theoretical approach. Nevertheless, uncertainties of the computational protocol may also mask small but relevant differences in  $\Delta G$ .



**Fig. 3** Calculated Gibbs free energies for the hydrogen splitting reactions of Lewis pairs. Notation used for borane units: **B** = B(C<sub>6</sub>F<sub>5</sub>)<sub>3</sub>, **B'** = B(C<sub>6</sub>F<sub>5</sub>)<sub>2</sub>. Molecules added to the list of originally investigated systems are marked with an *asterisk*

**Fig. 4** Thermodynamic cycle of hydrogen splitting by Lewis pairs



**Fig. 5** Substeps of the  $\text{H}_2$  cleavage reaction according to the thermodynamic cycle in Fig. 4, for inter- (a) and intra-molecular (b) FLPs

### 3.3 Partitioning of the Reaction Free Energy

As noted before, computational chemistry provides the possibility of dividing a reaction and its free energy into hypothetical, but chemically meaningful steps and contributions. Accordingly, we constructed a decomposition scheme for the  $\text{H}_2$  activation that delivers information about each influencing factor mentioned in the introduction. The thermodynamic cycle used in our study is presented in Fig. 4, and the corresponding substeps of the hydrogenation reactions of D/A and D~A Lewis pairs are shown in Fig. 5.

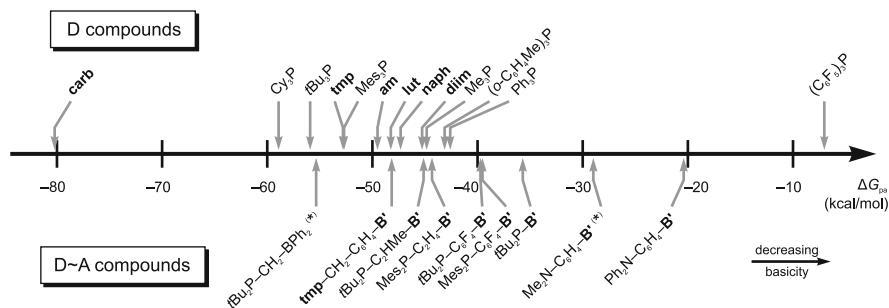
The first step of our thermodynamic cycle is the *heterolytic cleavage of dihydrogen* into  $\text{H}^+$  and  $\text{H}^-$  ions in toluene. For all FLPs, this step corresponds to a free energy change of  $\Delta G_{\text{HH}} = +128.8$  kcal/mol. The high positive value reflects the thermodynamic stability of the H–H bond, which must be compensated for in a favorable cleavage reaction.

For most of the examined systems, steric congestion leads to the complete absence of the dative bond between the Lewis centers in equilibrium, so the cleavage of  $\text{H}_2$  is the only step uphill in free energy. However, the active sites of the Lewis donor and acceptor may also be quenched, and an additional amount of free energy ( $\Delta G_{\text{prep}}$ ) is required to break the intra- or intermolecular dative bonds, so that the base and acid become *prepared* to receive the  $\text{H}^+$  and  $\text{H}^-$  ions. These dative bonds are typically strained, and five out of the six bound systems in our study possess  $\Delta G_{\text{prep}}$  values ranging between +3 and +12 kcal/mol. Only the sterically less crowded  $\text{Me}_3\text{P}$  forms stronger dative bonds with  $\text{B}(\text{C}_6\text{F}_5)_3$ , reaching a  $\Delta G_{\text{prep}}$  value of  $\sim 23$  kcal/mol. It is important to note that this free energy in itself is determined by a balance of steric bulkiness and acid/base strength of the reactants, and further decomposition might be considered. Nevertheless, taking into account the small number of datively bound pairs in our study, we simply took  $\Delta G_{\text{prep}}$  as the next contribution to the overall free energy.

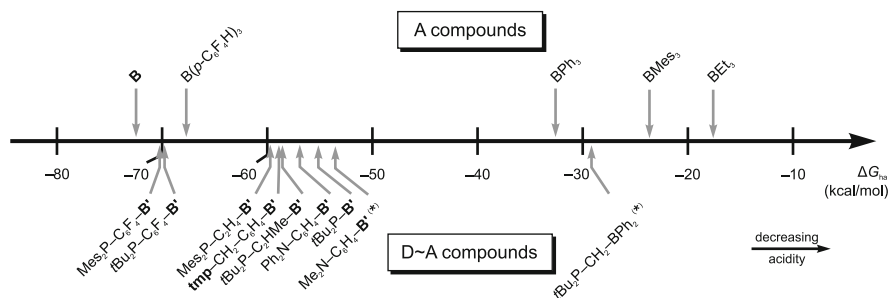
The following two terms of the partitioning were chosen to be the Gibbs free energies of the *attachment of a proton* ( $\Delta G_{\text{pa}}$ ) and a *hydride* ( $\Delta G_{\text{ha}}$ ) ion to the donor or acceptor molecules as well as to the neutral ambiphilic D~A compounds. These values account for the energy stored in the newly formed chemical bonds (D–H and A–H) and measure the Lewis donor and acceptor strength of the FLP. From the numerous methods available in the literature for the quantification of Lewis basicity or acidity, these may not be the easiest to measure experimentally, but they are readily amenable to computational determination and most directly linked to the potential of the Lewis components to act in the heterolytic hydrogen splitting reaction.

The computed  $\Delta G_{\text{pa}}$  and  $\Delta G_{\text{ha}}$  values for the compounds of interest are shown in Figs. 6 and 7, respectively; more negative values correspond to stronger donor/acceptor centers. The acidity/basicity ranges are very wide; e.g., for basicity, an interval of  $\sim 70$  kcal/mol is covered, which roughly corresponds to 50  $\text{pK}_a$  units. Nevertheless, the trends correspond to chemical intuition, and most of the data can be interpreted simply by considering that electron-donating substituents increase donor and decrease acceptor strength; electron-withdrawing substituents, such as fluorines, act the opposite way.

For intermolecular systems, the final, *stabilization* step corresponds to the formation of the product ion pair from the separated  $[\text{DH}]^+$  and  $[\text{HA}]^-$  ions (see Fig. 5a). The free energy  $\Delta G_{\text{stab}}$  associated with this step is simply the binding free energy of the ion pair. For the intramolecular pairs, the last step of the thermodynamic cycle is the somewhat counterintuitive reaction of the ionic  $[\text{HD}\sim\text{A}]^+$  and  $[\text{D}\sim\text{AH}]^-$  species that yields the zwitterionic  $[\text{H}^+\text{D}\sim\text{AH}^-]$  product and a neutral D~A molecule (see Fig. 5b). The free energy of this step ( $\Delta G_{\text{stab}}$ ) measures how much the Lewis acidity is enhanced upon protonation of the basic site, or



**Fig. 6** Calculated Gibbs free energies of proton attachment to the Lewis donors. Notation used for borane units:  $\mathbf{B}' = \text{B}(\text{C}_6\text{F}_5)_2$ . Molecules added to the list of originally investigated systems are marked with an *asterisk*

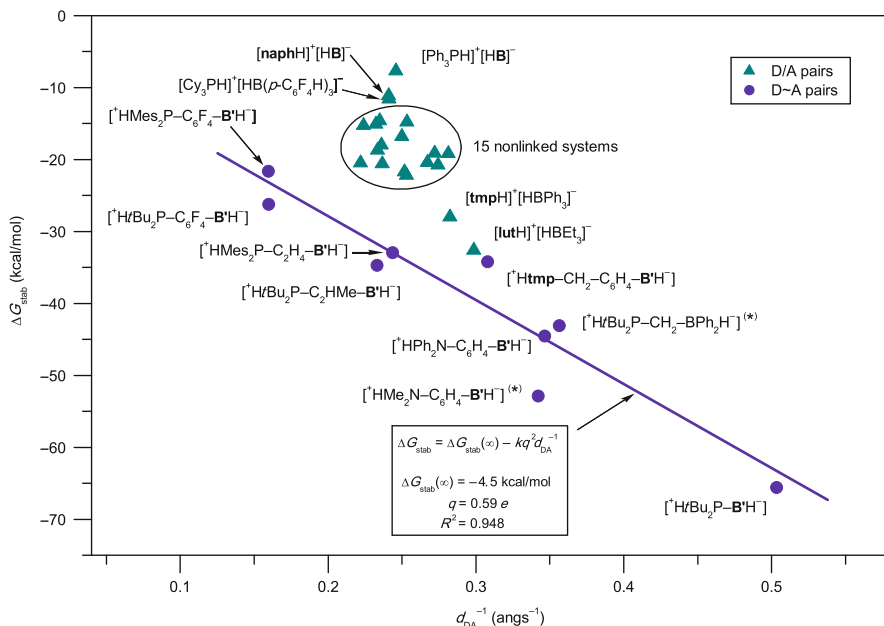


**Fig. 7** Calculated Gibbs free energies of hydride attachment to the Lewis acceptors. Notation used for borane units:  $\mathbf{B} = \text{B}(\text{C}_6\text{F}_5)_3$ ,  $\mathbf{B}' = \text{B}(\text{C}_6\text{F}_5)_2$ . Molecules added to the list of originally investigated systems are marked with an *asterisk*

equivalently, how much the Lewis basicity increases due to hydride binding to the acidic site.  $\Delta G_{\text{stab}}$  thereby quantifies the effect of intramolecular acid–base cooperativity on the thermodynamics of the reaction.

In order to explore the relationship between the molecular structure and  $\Delta G_{\text{stab}}$  and to assess the significance of electrostatics, a plot of the calculated data as a function of the reciprocal of the distance of the donor and acceptor atoms in the product ( $d_{\text{DA}}^{-1}$ ) is provided in Fig. 8. It is apparent from these results that the vast majority of the intermolecular systems can be characterized by a stabilization free energy lying in a fairly narrow range between  $-14$  and  $-24$  kcal/mol. The modest variation of this term can be associated with the structural similarity of the  $[\text{DH}]^+[\text{HA}]^-$  ion pairs, bearing singly charged donor/acceptor centers shielded by bulky apolar groups. No clear correlations between  $\Delta G_{\text{stab}}$  and  $d_{\text{DA}}^{-1}$  or between  $\Delta G_{\text{stab}}$  and the  $\text{H}\cdots\text{H}$  distance can be observed, which suggests that several factors (electrostatics, dihydrogen bond, steric effects, solvation, etc.) may be equally important in determining the binding strength.





**Fig. 8** Calculated stabilization Gibbs free energies of the products of the hydrogen splitting reactions, plotted as a function of the reciprocal of the distance of the donor and acceptor atoms in the product ( $d_{\text{DA}}^{-1}$ ). Linear fit of linked systems corresponds to the Coulomb interaction of  $q$  point charges at distance  $d_{\text{DA}}$ . Notation used for borane units: **B** =  $\text{B}(\text{C}_6\text{F}_5)_3$ , **B'** =  $\text{B}(\text{C}_6\text{F}_5)_2$ . Molecules added to the list of originally investigated systems are marked with an *asterisk*, and they were not included in the fit

Linked systems tend to have more favorable stabilization free energies than intermolecular pairs in general, which can partly be attributed to the difference in the stoichiometry of the stabilization step (see Fig. 5). This step of the thermodynamic cycle involves entropy loss for intermolecular systems due to ion association, whereas the number of molecules does not vary in the stabilization step of linked pairs. In the present partitioning, this step accounts for the different entropy changes of the overall reactions, which represents a fundamental difference between the two families of FLPs. Namely, the fact that three molecules must be brought together to form the product implies an entropic penalty on the nonlinked systems, as compared to the linked pairs. We note that in the present partitioning, FLPs that form strained dative adducts on the reactant side bear a favorable entropy contribution in the preparation step and an unfavorable one in the stabilization step, and, considering the overall entropy, they resemble the linked class more closely.

As is apparent from Fig. 8, the  $\Delta G_{\text{stab}}$  values of linked FLPs vary in a broader energy interval than those of the D/A pairs, and their trends are consistent with a simple electrostatic interpretation, corresponding to the interaction of  $\sim \pm 0.6$  charges located on the donor and acceptor atoms (see Fig. 8). The shortest donor–acceptor distances, and thereby the most negative  $\Delta G_{\text{stab}}$  values, are provided by the

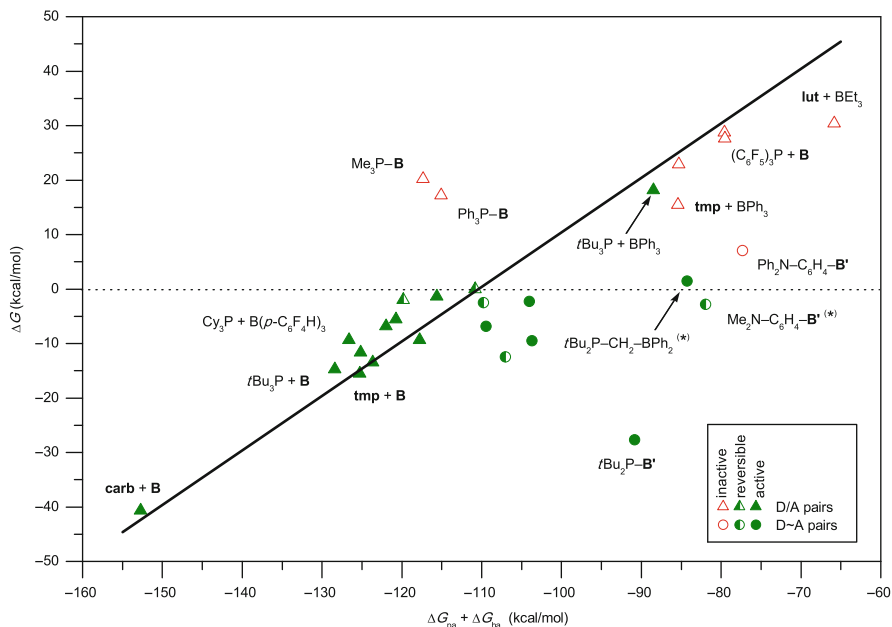
“zero-atom linker” in  $t\text{-Bu}_2\text{P-B}(\text{C}_6\text{F}_5)_2$ , the *ortho*-phenylene bridge as in  $[\text{HPh}_2\text{N-C}_6\text{H}_4\text{-B}(\text{C}_6\text{F}_5)_2\text{H}^-]$  and  $[\text{HMe}_2\text{N-C}_6\text{H}_4\text{-B}(\text{C}_6\text{F}_5)_2\text{H}^-]$ , and the methylene group in  $[\text{H}t\text{-Bu}_2\text{P-CH}_2\text{-BPh}_2\text{H}^-]$ . The stabilizing effect is gradually reduced with increasing intramolecular  $d_{\text{DA}}$  separations, reaching a value comparable to nonlinked systems for the  $\text{C}_6\text{F}_4$ -linked products. One can conclude from these results that the intramolecular distance of the active sites has a significant and well-defined effect on acid–base cooperativity, and the variations in this term can easily exceed those found in the ion pair binding energies of intermolecular pairs.

### 3.4 Tuning the Overall Free Energy: Are Acid and Base Strengths Decisive?

In order to create an FLP thermodynamically allowed to form the hydrogenated product, it is sufficient to ensure that the  $\text{H}_2$  uptake has *negative* reaction free energy. However, the design of hydrogenation catalysts imposes a slightly different and stricter requirement: the free energy needs to be *close to zero* (but not necessary below it). The reason is that a too positive value would not allow formation of the reactive intermediate in sufficient concentration, while a too negative free energy would make the hydrogen transfer to the substrate disfavored. This line of thinking has been fruitful in the design of transition metal based complexes that produce or oxidize  $\text{H}_2$  [49], and it has also been considered as a criterion in the computational design of FLP catalysts [60]. This design principle requires fine control over the reaction free energy; we therefore think it is instructive to consider how the above discussed terms combine and what are their relative importances.

From the above analysis of the individual contributions, it is clear that all three negative terms are essential to balance the energy demand of H–H splitting and to obtain hydrogenation processes with  $\Delta G$  around zero. Acid–base properties show the largest diversity in this series of compounds although the stabilization free energies may exhibit significant variations for the linked systems. In order to correlate the cumulative acid–base strength of Lewis pairs with the thermodynamics of  $\text{H}_2$  splitting reactions, we show the plot of the overall reaction free energies as a function of  $\Delta G_{\text{pa}} + \Delta G_{\text{ha}}$  (Fig. 9).

The figure clearly demonstrates that, for most of the intermolecular systems studied here, the absence of the dative bond and the near invariance of the ion pair binding energy infer a decisive role for donor–acceptor strength in determining the thermodynamic feasibility of  $\text{H}_2$  activation. Among these systems, a  $\Delta G_{\text{pa}} + \Delta G_{\text{ha}}$  value somewhat below  $-110$  kcal/mol leads to slightly exergonic hydrogen activation; many combinations of bulky P and N donors with strong Lewis acids ( $\text{B}(\text{C}_6\text{F}_5)_3$  or  $\text{B}(p\text{-C}_6\text{F}_4\text{H})_3$ ) can be found in this region. The results point out that, together with the strongest bases, e.g., **tmp**,  $t\text{-Bu}_3\text{P}$ , and particularly the carbene **carb**, considerable reduction in the acidity of the acceptor can be carried out while still fulfilling the requirements for a good hydrogenation catalyst. We note here that



**Fig. 9** Overall Gibbs free energy of the reactions plotted as a function of the cumulative acid–base strength. The straight line corresponds to a perfect correlation between  $\Delta G$  and  $\Delta G_{\text{pa}} + \Delta G_{\text{ha}}$ , drawn assuming  $\Delta G_{\text{prep}} = 0$  and the mean  $\Delta G_{\text{stab}}$  of the nonlinked systems ( $-18.4$  kcal/mol). Notation used for borane units:  $\mathbf{B} = \text{B}(\text{C}_6\text{F}_5)_3$ ,  $\mathbf{B}' = \text{B}(\text{C}_6\text{F}_5)_2$ . Molecules added to the list of originally investigated systems are marked with an *asterisk*

in a hydrogen transfer reaction to a given unsaturated substrate, the relationships among the acidity and basicity of the Lewis components and the substrate may determine whether proton or hydride is transferred first, or they are transferred in a concerted way [61] (besides steric effects [62]). Consideration of whether a particular FLP- $\text{H}_2$  system has a larger propensity to donate the proton or the hydride first may thus contribute to the successful design of catalysts for a specific substrate class.

For the intermolecular pairs, significant deviations from the correlation between  $\Delta G$  and  $\Delta G_{\text{pa}} + \Delta G_{\text{ha}}$  can be attributed either to the formation of dative bonds (e.g.,  $\text{Me}_3\text{P}-\text{B}(\text{C}_6\text{F}_5)_3$  and  $\text{Ph}_3\text{P}-\text{B}(\text{C}_6\text{F}_5)_3$ ) or to unusually large ion pair binding energies (e.g., **lut** +  $\text{BEt}_3$  and **tmp** +  $\text{BPh}_3$ ). Notably, for the datively bound  $\text{Me}_3\text{P}-\text{B}(\text{C}_6\text{F}_5)_3$  and  $\text{Ph}_3\text{P}-\text{B}(\text{C}_6\text{F}_5)_3$  systems, the cumulative acid–base strengths are comparable to those obtained for reactive pairs, but the  $\Delta G_{\text{prep}}$  terms shift these systems into the endergonic range.

As noted before, the entropic cost associated with the hydrogen splitting in linked systems is smaller compared to nonlinked pairs. Lower cumulative acid–base strength is thus generally sufficient to render a linked system thermodynamically feasible. Indeed, we find all reactive D~A systems between  $-110$  and  $-80$  kcal/mol on the  $\Delta G_{\text{pa}} + \Delta G_{\text{ha}}$  scale. Due to the large variations in the

$\Delta G_{\text{stab}}$  components, discussed in the previous section, no clear correlation between the overall free energy and the cumulative acid–base strength can be established for the investigated linked pairs. This feature provides an additional degree of freedom to control the thermodynamics of  $\text{H}_2$  splitting reactions. It is interesting to note in this regard that the unreactive nature of the  $\text{Ph}_2\text{N}-\text{C}_6\text{H}_4-\text{B}(\text{C}_6\text{F}_5)_2$  system indeed stems from the low basicity of the N atom as pointed out by Piers et al. [57] but, despite the unfavorable acid–base properties, the calculated  $\Delta G = +7.1$  kcal/mol is surprisingly low owing to unusually high stabilization free energy. In fact, a small increase in base strength was sufficient, and the dimethyl derivative prepared later (*closed*- $\text{Me}_2\text{N}-\text{C}_6\text{H}_4-\text{B}(\text{C}_6\text{F}_5)_2$  [59]) does react with hydrogen. Notably, the tuning of the basicity also had an effect on the preparation step as a weak dative bond is observed here; moreover, the stabilization free energy also increased (see Fig. 8), for which there seems to be no simple rationalization within the present scheme. Further investigations may provide explanation via uncovering the overlooked subtle interplay among the various terms and the details of intramolecular cooperation.

The importance of large intramolecular stabilization provided by short covalent linkers is also borne out by the data on the methylene-linked *t*- $\text{Bu}_2\text{P}-\text{CH}_2-\text{BPh}_2$  pair. This compound, prepared by Slootweg, Lammertsma, and coworkers [43], is capable of cleaving hydrogen despite the absence of the fluorine atoms and the resulting low acidity of the boron center. This molecule also exemplifies that the FLP design strategy presented by Wang and coworkers, comprising the use of  $\text{CH}_2$  or similar groups between the donor and acceptor centers [63, 64], leads not only to favorable kinetics but also enhances the exergonicity of the hydrogen activation reaction as compared to nonlinked pairs or longer linkers.

### 3.5 Related Studies in the Literature

A handful of computational studies addressing the thermodynamic factors of hydrogen cleavage have been published by various authors. Nyhlén and Privalov carried out a detailed study on the substituent effects in  $\text{H}_2$  activation by  $\text{R}_2\text{P}-\text{BR}'_2$  compounds [65]. The main focus of this work was to understand the relationship between the structure and the activation barrier, but the reaction exothermicities were also reported. The trends of the latter were not analyzed, however.

To our knowledge, a thermochemical cycle for heterolytic hydrogen cleavage by Lewis pairs first appeared as supplementary material to a paper of Repo, Rieger, and coworkers [46]. These authors highlighted that the estimated magnitude of electrostatic interaction in the product ion pair or zwitterion is comparable to the energy required for the *homolytic* dissociation of  $\text{H}_2$ , and formulated the “Coulomb pays for Heitler–London” hypothesis as a driving force. While this might be a good order-of-magnitude estimate in the absence of a solvent, its significance is limited because the *heterolytic* dissociation relevant to FLPs (see Figures 4 and 5) is more endothermic, and the energy gained from the newly formed chemical bonds is far

from being negligible. This fact was admitted in a related later study on the energetics of the dimethyl-diphenylpyridine + B(C<sub>6</sub>F<sub>5</sub>)<sub>3</sub> pair, where the possibility of stabilization of the product ion pairs due to oligomerization or crystallization was also discussed [66].

Concurrently with our thermodynamic study, an independent investigation was reported by Gao, Wu, and Mo [67], in which they employed a very similar energy partitioning to understand the reactivity difference between the H<sub>3</sub>P–B(CF<sub>3</sub>)<sub>3</sub> and *t*-Bu<sub>3</sub>P + B(C<sub>6</sub>F<sub>5</sub>)<sub>3</sub> pairs. Solvation and entropic effects were not considered, but many of their conclusions are completely parallel to ours. A follow-up paper from the same authors appeared later [68], extending the discussion to various phosphine/borane combinations. The same approach was adopted by Jia and coworkers in their studies about lutidine/borane [69] and phosphine/borane pairs [70].

The effect of tuning FLPs via changing steric effects or acid/base strength has also been investigated from the experimental side. Several studies have been devoted to the understanding of substituent effects on adduct formation as well as on feasibility and reversibility of hydrogen activation, e.g., by varying phosphines and boranes [71], amines [72], amines and boranes [73], carbenes [74], and pyridines [75]. Important information can also be obtained from studies that simply encompass a wide range of compounds, e.g., phosphines [76], pyridines and boranes [77], and amines [78]. In some cases, computations were invoked besides the experimental work to help rationalize the observed trends [74, 75]. Synthesis and calculations on *i*-Pr<sub>2</sub>N–B(C<sub>6</sub>F<sub>5</sub>)<sub>2</sub> allowed interpretation of the reactivity difference from the related phosphinoboranes [79]. Phosphine/borane FLPs with decreased basicity on the donor side have been synthesized, where the absence of the dative bond stems not from steric but rather from electronic effects; these pairs do not activate H<sub>2</sub> but do show FLP-type reactivity toward other substrates [80, 81]. Last but not least, as a practical application of FLP tuning, more active hydrogenation catalysts have been synthesized following the principle that decreased basicity makes the transfer of hydrogen to the substrate thermodynamically more favored [82].

## 4 The Mechanism and the Notion of Frustration

H<sub>2</sub> is very inert, does not react with Lewis acids or bases separately, and the absence of any detectable intermediate in the FLP + H<sub>2</sub> system opens a wide field for speculations about the actual reactive species in this process. In general, mechanistic hypotheses can be tested experimentally by identifying the reaction intermediates and carrying out kinetic and isotope labeling studies; however, such explorations in the field of H<sub>2</sub> activation by FLPs are often challenging because of several technical difficulties. The reactant H<sub>2</sub> is gaseous; it has low solubility in typical solvents; reactions are often diffusion-controlled, and a precise control over the concentration of H<sub>2</sub> might be hard to realize. Many of the reactions are rapid, and in some of them, even a third phase is involved because the product precipitates. The chemical complexity is often large; the presence of side reactions might make it difficult to

decide whether a particular intermediate detected in the solution is mechanistically relevant, and multiple pathways for H<sub>2</sub> activation can be operative in parallel. Most of the discovered FLPs are air and moisture sensitive, and the influence of trace amounts of oxygen or water can be large. It is therefore not surprising that, despite the very early efforts to come up with mechanistic proposals and verify them, there are only a few clear-cut conclusions from experiments.

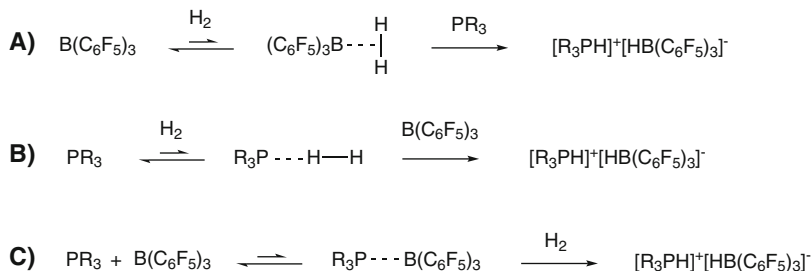
On the other hand, reaction intermediates can be identified computationally even if they are high energy species and form in too low concentrations to be observable. The suggested mechanistic pathways can be compared directly by exploring the involved elementary steps and deriving free energy diagrams for different reaction routes. The characterization of the reactive intermediates and the rate-determining transition states provide complementary mechanistic information to formulate simple reactivity models, which might be useful for further development.

In what follows in this section, we first review the results published for the *t*-Bu<sub>3</sub>P/B(C<sub>6</sub>F<sub>5</sub>)<sub>3</sub> + H<sub>2</sub> system, a prototype reaction investigated by us [17, 21] and by several other research groups. The reactivity model we proposed from our studies [17, 21] and its relationship to other H<sub>2</sub> activation modes is discussed next. The basic messages from the large body of theoretical mechanistic studies of other D/A + H<sub>2</sub> reactions as well as of reactions with linked FLPs are presented, too, including our own contributions [19, 23, 24]. Finally, we address the elusive nature of intermediates involved in these reactions and summarize the results of our first attempt to apply dynamic theoretical models to rationalize the reactivity [25].

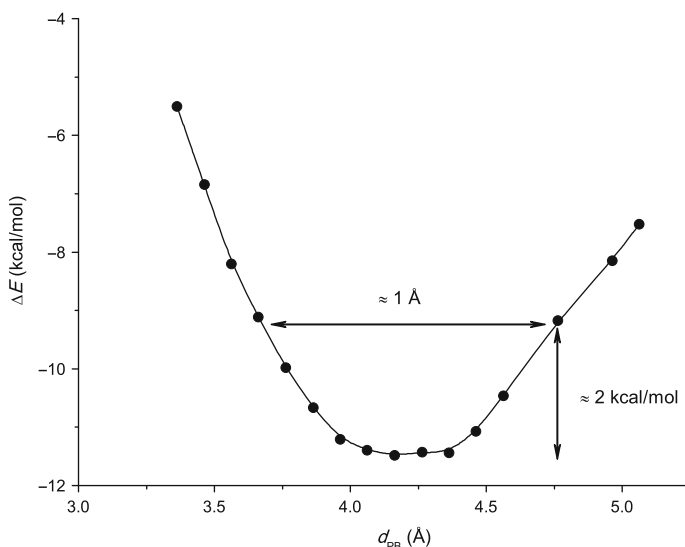
#### 4.1 The Prototypical *t*-Bu<sub>3</sub>P/B(C<sub>6</sub>F<sub>5</sub>)<sub>3</sub> + H<sub>2</sub> Reaction

The reactivity of simple bimolecular phosphine/borane pairs towards H<sub>2</sub> was explored by Welch and Stephan [41]. Among the investigated systems, the R<sub>3</sub>P/B(C<sub>6</sub>F<sub>5</sub>)<sub>3</sub> pairs with bulky R = *t*-Bu and R = Mes groups were shown to react rapidly with H<sub>2</sub> under mild conditions, resulting in the [R<sub>3</sub>PH]<sup>+</sup>[HB(C<sub>6</sub>F<sub>5</sub>)<sub>3</sub>]<sup>-</sup> products. Our initial computational analysis focused on the identification of possible intermediates in these reactions [17].

Considering the *t*-Bu<sub>3</sub>P/B(C<sub>6</sub>F<sub>5</sub>)<sub>3</sub> system, we first examined the two putative reaction pathways outlined by Welch and Stephan, which involve the coordination of H<sub>2</sub> either to the donor or to the acceptor molecule followed by subsequent proton or hydride abstraction processes (mechanism A and B in Fig. 10). By analogy to transition metal chemistry, the side-on coordination of H<sub>2</sub> to the borane seemed plausible; however, no experimental evidence was found for the existence of (C<sub>6</sub>F<sub>5</sub>)<sub>3</sub>B⋯H<sub>2</sub> adducts even at low temperatures. The potential energy curves derived by a combined use of DFT and wave function quantum chemical methods pointed to unfavorable interactions for both side-on and end-on approaches of H<sub>2</sub> to borane B(C<sub>6</sub>F<sub>5</sub>)<sub>3</sub>, and the *t*-Bu<sub>3</sub>P⋯H<sub>2</sub> interaction was found to be repulsive as well. Based upon these results, we proposed pathways A and B to be excluded from the possible mechanisms of the H<sub>2</sub> activation process.



**Fig. 10** Investigated reaction mechanisms for H<sub>2</sub> activation with *t*-Bu<sub>3</sub>P/B(C<sub>6</sub>F<sub>5</sub>)<sub>3</sub>

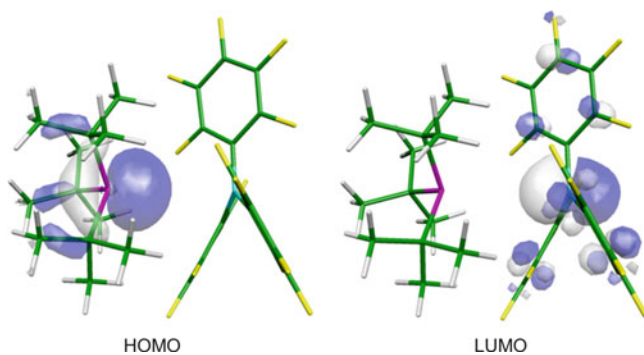
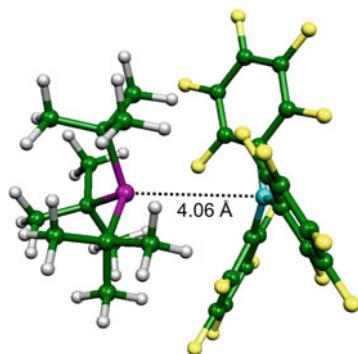


**Fig. 11** Interaction energy of *t*-Bu<sub>3</sub>P and B(C<sub>6</sub>F<sub>5</sub>)<sub>3</sub> as a function of P–B distance

Although not observed experimentally in related NMR measurements, we assumed that secondary interactions between the phosphine and borane molecules may lead to weakly bound complexes with properly oriented active centers, which can then act as reactive intermediates in the reaction with H<sub>2</sub> (mechanism C in Fig. 10). This idea was confirmed computationally [17].

The envisioned *t*-Bu<sub>3</sub>P⋯B(C<sub>6</sub>F<sub>5</sub>)<sub>3</sub> complex was first identified by DFT calculations with B3LYP and the 6-31G(d) basis set, but bearing in mind that the B3LYP functional performs poorly for dispersion interactions, we derived a potential energy curve with respect to the P–B distance ( $d_{\text{PB}}$ ) of the approaching *t*-Bu<sub>3</sub>P and B(C<sub>6</sub>F<sub>5</sub>)<sub>3</sub> molecules at the SCS-MP2/cc-pVTZ level (see Fig. 11). The potential energy curve exhibits a minimum around  $d_{\text{PB}} = 4.2$  Å, and a very similar structure has been obtained via full geometry optimizations at the M05-2X/6-31G(d) level of DFT [21] (see Fig. 12). This particular configuration of the *t*-Bu<sub>3</sub>P⋯B(C<sub>6</sub>F<sub>5</sub>)<sub>3</sub>

**Fig. 12** Structure of the frustrated  $t\text{-Bu}_3\text{P}\cdots\text{B}(\text{C}_6\text{F}_5)_3$  complex

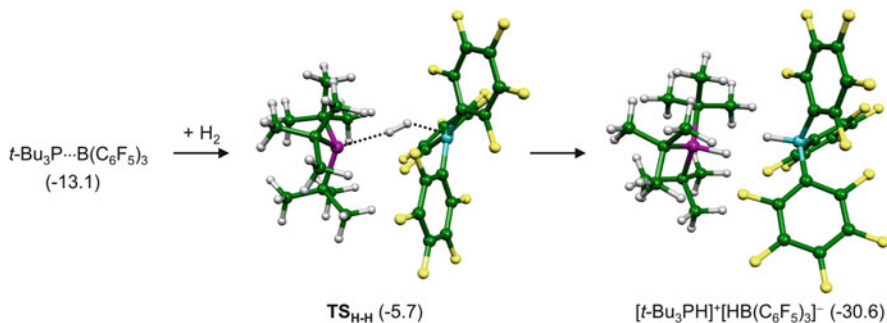


**Fig. 13** Frontier orbitals of the frustrated  $t\text{-Bu}_3\text{P}\cdots\text{B}(\text{C}_6\text{F}_5)_3$  complex

system has been termed “frustrated complex” [17], implying that the frontier orbitals of the P and B centers are aligned for dative bond formation, but their overlap is prevented by the steric congestion of the FLP members (see Fig. 13). In this arrangement, the donor/acceptor centers are preorganized for simultaneous interaction with an  $\text{H}_2$  molecule, which appears to be an important ingredient of the activation process. The loosely bound preorganized  $t\text{-Bu}_3\text{P}\cdots\text{B}(\text{C}_6\text{F}_5)_3$  adduct is often referred to as the “encounter complex” in the literature.

The bonding in the frustrated complex can be characterized as a combination of dispersion interactions and multiple  $\text{C}\text{--}\text{H}\cdots\text{F}$  hydrogen bonds, which give rise to appreciable stabilization. The association energy of the adduct is predicted to be in the 8–19 kcal/mol range depending on the applied methodology [17, 21, 83–86]. Quantum chemical methods that account for dispersion interactions reasonably well give 12–15 kcal/mol for interaction energy [17, 21, 85, 86]. Due to the



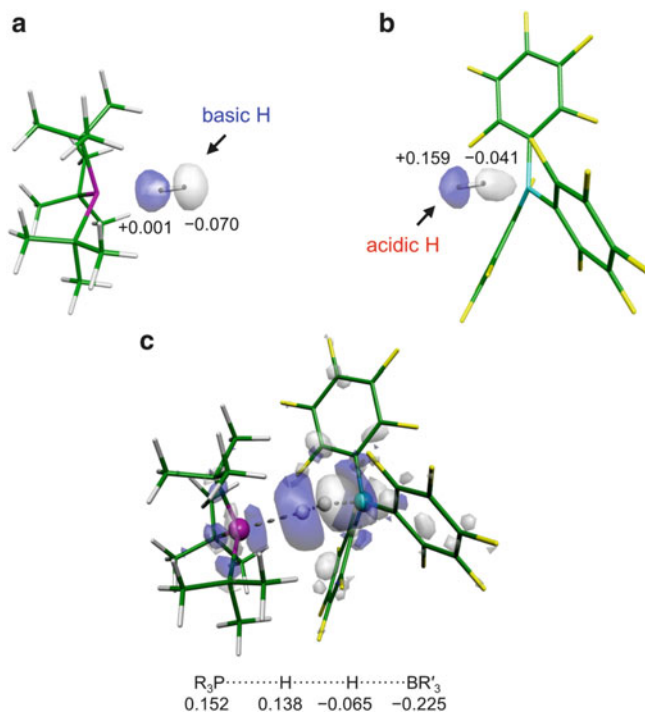


**Fig. 14** The transition state of  $\text{H}_2$  cleavage and the product ion-pair identified at the M05-2X/6-31G(d) level [21]. Relative energies (in kcal/mol; with respect to separated reactants) are given in *parentheses*

dominance of weak, nondirectional, long-range forces, the frustrated complex is structurally flexible. This is apparent from the shape of the computed P–B potential energy curve (Fig. 12), but a high degree of flexibility has also been revealed for displacements perpendicular to the borane axis [85]. In the equilibrium structure of  $t\text{-Bu}_3\text{P}\cdots\text{B}(\text{C}_6\text{F}_5)_3$ , the borane molecule remains planar, pointing to negligible electron transfer in this configuration. At shorter P–B distances, a partial dative bond formed via the overlap of P and B frontier orbitals could be identified; a weak overlap was proposed to contribute to the enthalpic stabilization already at the equilibrium geometry of the frustrated  $t\text{-Bu}_3\text{P}\cdots\text{B}(\text{C}_6\text{F}_5)_3$  complex [85].

Considering the flexible nature of the frustrated complex, one expects that it can easily open up, allowing the small hydrogen molecule to interact with both active centers of the phosphine/borane pair, which may initiate an activation process. The potential energy surface has been explored in this region, and transition states associated with the H–H bond cleavage have been located at various levels of theory (first via B3LYP/6-31G(d) optimizations [17] and later by using the M05-2X/6-31G(d) [21] and B97D/TZVPP' [86] methods). The performance of these DFT methods for noncovalent interactions is quite different, which leads to somewhat different structural parameters for loosely bound systems. For instance, the position of the  $\text{H}_2$  molecule entering the reactive region of the frustrated complex (i.e., the shape of the  $\text{P}\cdots\text{H}\cdots\text{B}$  unit of the transition state) was shown to be sensitive to the applied functional [86]. Nevertheless, the located transition states at all mentioned levels of theory share the same structural features (see  $\text{TS}_{\text{H-H}}$  in Fig. 14):

1. The  $\text{H}_2$  molecule interacts with both active centers of the FLP.
2. The H–H bond is only slightly elongated with respect to the free  $\text{H}_2$ , corresponding to an early transition state for the bond cleavage.
3. The  $\text{H}_2$  molecule is nearly aligned with the  $\text{P}\cdots\text{B}$  axis of the complex, and the  $\text{P}\cdots\text{H}\cdots\text{B}$  unit of the transition state is slightly bent.
4. The borane unit of the transition state is notably pyramidalized, pointing to the importance of electron transfer processes already in this initial phase of the reaction.

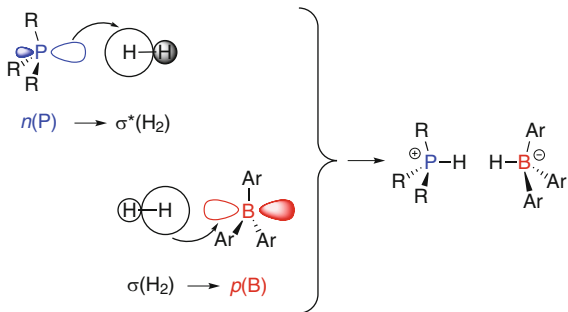


**Fig. 15** Electron density difference maps calculated for (a)  $t\text{-Bu}_3\text{P}\cdots\text{H}_2$ , (b)  $(\text{C}_6\text{F}_5)_3\text{B}\cdots\text{H}_2$  and (c)  $\text{TS}_{\text{H-H}}$ . Gray and blue surfaces, drawn with a cutoff of 0.0025 au (a and b) or 0.001 au (c), indicate gain and loss of electron density with respect to the isolated  $\text{H}_2$  plus the donor (a), acceptor (b), donor–acceptor complex (c). Atomic and fragment charges shown in part (c) were obtained from natural population analysis

The identified transition state represents only a small energy barrier for the heterolytic  $\text{H}_2$  splitting and the formation of the  $[t\text{-Bu}_3\text{PH}]^+[\text{HB}(\text{C}_6\text{F}_5)_3]^-$  product ion-pair is highly exothermic. The optimized structure of the phosphonium-hydridoborate ion pair is consistent with the X-ray data [41]. Due to the flexibility of the frustrated complex, the energy barrier arises predominantly from the distortion of the individual reactants and the work required to bring the  $\text{H}_2$  molecule into close contact with the acid/base centers. It is important to point out, however, that entropy provides a major contribution to the free energy barrier of the reaction as both reaction steps (i.e., the preassociation of the  $t\text{-Bu}_3\text{P}/\text{B}(\text{C}_6\text{F}_5)_3$  partners and the reaction of  $\text{H}_2$  with the frustrated complex) are entropically disfavored.

In addition to structural and energetic information, quantum chemical calculations provided valuable insight into the electronic rearrangements associated with the  $\text{H}_2$  splitting process [17, 21]. As a starting point, it is useful to examine the  $t\text{-Bu}_3\text{P}\cdots\text{H}_2$  and  $(\text{C}_6\text{F}_5)_3\text{B}\cdots\text{H}_2$  binary systems at the geometries corresponding to the  $\text{TS}_{\text{H-H}}$  transition state. The electron density difference maps shown in Fig. 15a, b indicate that both binary interactions lead to the polarization of the hydrogen

**Fig. 16** MO representation of electron donations in the  $t\text{-Bu}_3\text{P}/\text{B}(\text{C}_6\text{F}_5)_3 + \text{H}_2$  system



molecule with the same polarization pattern. In both cases, the interacting Lewis site induces the opposite Lewis property at the closer end of the  $\text{H}_2$  molecule, reducing the repulsion between the molecules. In turn, the opposite end of the  $\text{H}_2$  molecule obtains the same Lewis function as the interacting Lewis center. It thus appears that the  $\text{H}_2$  molecule, which in itself is a very poor Lewis acid and base, relays the Lewis property of the center involved in the binary interaction. In the reactive, ternary system ( $\text{TS}_{\text{H-H}}$ ), the  $\text{H}_2$  molecule interacts simultaneously with the Lewis acidic and basic centers of the frustrated complex. Both sites induce polarization of  $\text{H}_2$  in the same direction, which thus leads to reduced repulsion on both sides of the molecule and to a shift of electron density in the  $t\text{-Bu}_3\text{P} \rightarrow \text{B}(\text{C}_6\text{F}_5)_3$  direction. This partial electron transfer can be identified clearly on the electron density difference map, and it is also corroborated by the computed atomic and fragment charges of the transition state (see Fig. 15c). The cooperative nature of the phosphine/ $\text{H}_2$  and  $\text{H}_2$ /borane interactions has also been confirmed by an analysis of two- and three-body contributions to the interaction energy and electron density difference [87].

In terms of the MO formalism [17, 21], the electron transfer identified by the electron density analysis takes place via synergistic  $t\text{-Bu}_3\text{P} \rightarrow \sigma^*(\text{H}_2)$  and  $\sigma(\text{H}_2) \rightarrow \text{B}(\text{C}_6\text{F}_5)_3$  donations (see Fig. 16), which actually correspond to two concerted Lewis acid–base reactions between the reacting partners, and they both weaken the  $\text{H-H}$  bond. In this reaction, the  $\text{H}_2$  molecule acts as a bridge between the phosphine and borane fragments and enables an electron transfer that was hindered sterically in the frustrated complex, so that the formation of two new dative bonds ( $\text{P-H}$  and  $\text{B-H}$ ) can begin.

## 4.2 Proposed Reactivity Model

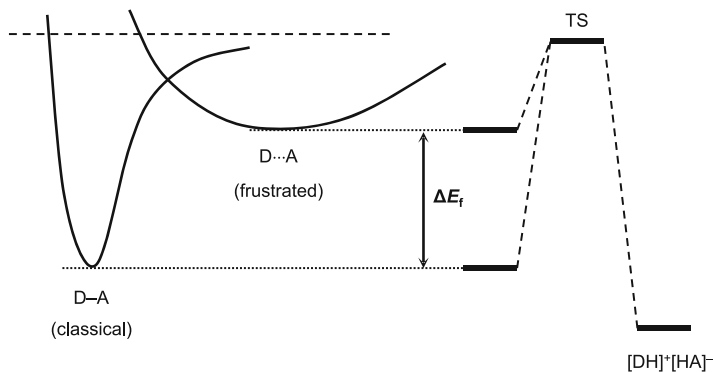
By the conceptualization of the results obtained for the prototypical  $t\text{-Bu}_3\text{P}/\text{B}(\text{C}_6\text{F}_5)_3 + \text{H}_2$  system, we proposed a general mechanistic model for  $\text{H}_2$  activation processes by intermolecular FLPs [17]. The reactivity model is actually a refined version of mechanism C depicted in Fig. 10, and it involves the following features:

1. The preassociation of the Lewis acidic and basic components gives rise to “frustrated complex” configurations with intermolecular arrangements similar to classical Lewis donor–acceptor adducts, but having a much looser structure and containing no dative bond. This flexibility provides a range of optimal acid–base distances for bifunctional cooperativity.
2. Simultaneous interaction of H<sub>2</sub> with both active centers of this preorganized ambiphilic system is feasible, leading to bond activation and ultimately to heterolytic bond cleavage in a bimolecular, low-barrier process.
3. Electron transfer occurs already at the initial phase of the reaction via cooperative D → σ\*(H<sub>2</sub>) and σ(H<sub>2</sub>) → A donations, which is analogous in its physical nature to the hindered D–A dative bond formation and thereby represents the release of frustration. The H<sub>2</sub> molecule acts as a bridge by sacrificing its σ bond, and a thermodynamically favored cleavage product can form.

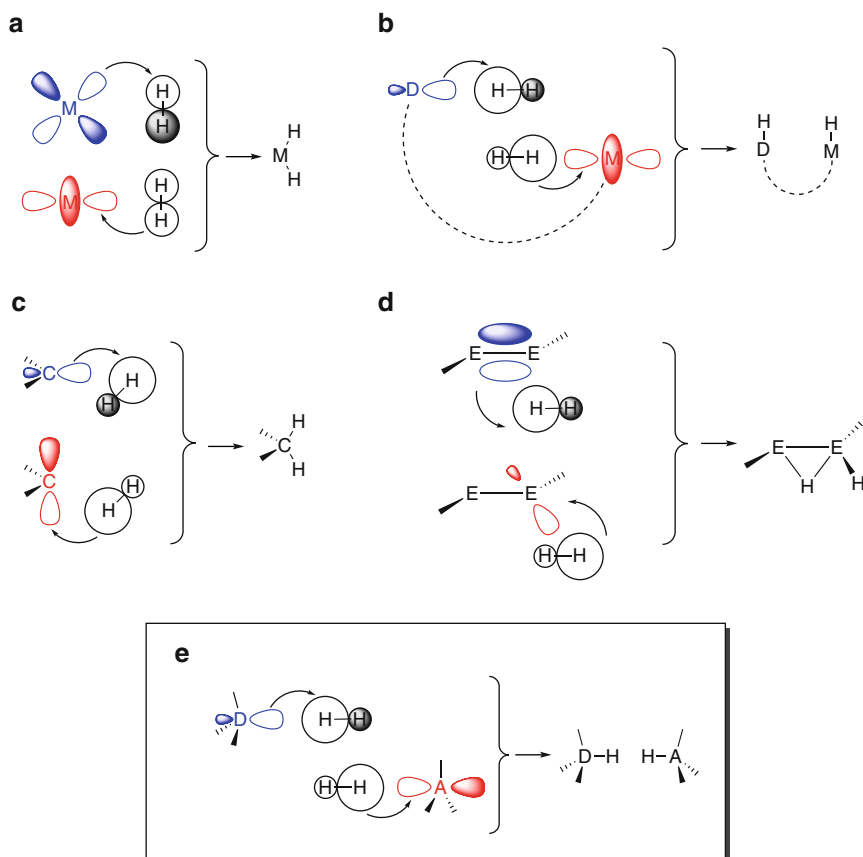
Although this reactivity model was originally formulated for H<sub>2</sub> activation, computational studies revealed very similar mechanism for the reaction of *t*-Bu<sub>3</sub>P/B(C<sub>6</sub>F<sub>5</sub>)<sub>3</sub> with olefins [18, 83, 88]. In this latter reaction, however, borane–olefin interactions give an additional contribution to the preorganization of the reacting molecules to an arrangement favorable for cooperative interactions. Such interactions have been detected even experimentally in a tethered alkenylborane [89]. For this reason, the transition state of the concerted addition reaction can also be derived from the weakly bound borane⋯olefin adduct reacting with the phosphine molecule.

In Sects. 3.3–3.4 we discussed how the absence or weakness of the donor–acceptor dative bond can contribute to the favorable free energy of the hydrogen splitting reaction. From this point of view, frustration not only involves steric effects but also implies an energized state, a strain, which increases the exothermicity of the reaction (Fig. 17). Importantly, this reactant-state destabilization influences the barrier analogously. The extent of destabilization as compared to a hypothetical classical Lewis pair having the same intrinsic acid–base properties, which we may call “frustration energy” ( $\Delta E_f$ ), lowers the activation energy, thus providing an example of “steric assistance” to a chemical reaction [90]. The simple qualitative picture of FLP-type H<sub>2</sub> activation shown in Fig. 17 was also supported by a computational study reported by Mo et al. [67].

The present reactivity model can be paralleled with H<sub>2</sub> activation modes of other systems described previously [21] (see Fig. 18). The common feature of various H<sub>2</sub> splitting mechanisms is the synergism of electron transfer processes that always involve electron donation to the σ\*(H<sub>2</sub>) orbital and electron acceptance from the σ(H<sub>2</sub>) orbital. However, the mechanisms differ in the way the three interacting partners (H<sub>2</sub>, donor, and acceptor) are positioned in the H–H splitting transition state. The donor and the acceptor sites may be located on the same atom (transition metal centers and singlet carbenes, Fig. 18a, c), or on two separated active centers (bifunctional metal–ligand systems and FLPs, Fig. 18b, e), but an occupied bonding orbital can also act as a donor partner (such as in ArEEAr molecules, Fig. 18d [91]). For single centers, the cooperativity is provided naturally, and the character of the



**Fig. 17** The role of frustration in the mechanistic proposal.  $\Delta E_f$  represents the energy benefit of frustration that lowers the barrier and increases the exothermicity of heterolytic H–H bond cleavage



**Fig. 18** Schematic representation of various  $H_2$  splitting mechanisms: single transition metal centers (a), metal–ligand bifunctional systems (b), singlet carbenes (c), multiply bonded heavier main-group systems (d), and frustrated Lewis pairs (e)

splitting process (homolytic or heterolytic) is determined by the symmetry of the donor/acceptor orbitals. For separated active centers, however, a particular structural preorganization is required to ensure the synergistic electron transfer processes. Intermolecular FLPs represent a fascinating example, where the orbital preorganization is provided by purely secondary interactions. Intramolecular FLPs, on the other hand, can benefit from the presence of a covalent linker between the donor and acceptor centers.

The mechanistic model proposed for intermolecular FLPs has been widely applied to rationalize the reactivity of other bulky D/A pairs towards heterolytic H<sub>2</sub> splitting [19, 23, 24, 53, 66, 69, 92–94], and the MO-based picture of H<sub>2</sub> activation has also been used as a general principle to design computationally new hydrogenation catalysts [60, 62–64, 95–97]. However, an interesting alternative mechanistic proposal has been reported by Grimme et al. [86, 98] which emphasizes the role of the electric field induced by the active centers of the frustrated complex. According to this model, the reactivity of FLPs can be rationalized without involving specific FLP/H<sub>2</sub> orbitals, because the H<sub>2</sub> activation occurs as a result of polarization by the strong electric field in the cavity of the frustrated complex. This reactivity model represents a novel principle of small molecule activation, and highlights the unique position of FLP chemistry more than its analogies with related systems. In our view, further studies might be useful to assess the relevance of the electric field model and the extent of its applicability in guiding the design of new compounds. An insightful analysis of the orbital and electric field effects in the activation of H<sub>2</sub> with small (not frustrated) Lewis acid/base pairs has recently been reported by Camaioni et al. [99], who concluded that the electric field alone is insufficient to split the H–H bond.

### 4.3 Theoretical Studies of Other D/A + H<sub>2</sub> Reactions

Stephan's landmark discoveries shed light on the potential of using bulky Lewis pairs as metal-free hydrogenation catalysts and motivated further studies to broaden the scope of FLPs. In addition to simple phosphine/borane pairs, a series of different intermolecular FLPs have been described and found to cleave H<sub>2</sub> efficiently. These systems include a variety of P-, N-, O-, and C-based donors usually combined with B(C<sub>6</sub>F<sub>5</sub>)<sub>3</sub>, but successful modifications to the borane have been introduced as well. Some of these reactions were examined computationally, and the results gave more information on the mechanistic details as well as on the concept of frustration. In this section, we summarize these contributions.

#### 4.3.1 N/C/O Donors: A Wide Range of Similar Reactions

Tamm and coworkers published a joint experimental–theoretical study on the heterolytic hydrogen splitting by the carbene/borane pair **carb**/B(C<sub>6</sub>F<sub>5</sub>)<sub>3</sub> [53]. In accordance with an independent experimental work of Stephan et al. [54], they

found that this pair is also capable of hydrogen activation, yielding an amidinium hydridoborate salt. A noncovalent, preorganized complex of the Lewis components [**carb**...B(C<sub>6</sub>F<sub>5</sub>)<sub>3</sub>] was identified computationally with an association energy of  $\Delta E = -10.9$  kcal/mol. The transition state of hydrogen splitting was also located and showed similar characteristics to that described for the *t*-Bu<sub>3</sub>P/B(C<sub>6</sub>F<sub>5</sub>)<sub>3</sub> + H<sub>2</sub> reaction. The calculations predicted very low energy barrier for the H–H cleavage ( $\Delta E^\ddagger = +1.1$  kcal/mol with respect to **carb**...B(C<sub>6</sub>F<sub>5</sub>)<sub>3</sub> + H<sub>2</sub>). In a computational study reported by Wang et al. [94], the reactivity of carbene/borane pairs (including **carb**/B(C<sub>6</sub>F<sub>5</sub>)<sub>3</sub>) was paralleled with that of *t*-Bu<sub>3</sub>P/B(C<sub>6</sub>F<sub>5</sub>)<sub>3</sub>. Despite the large difference in the basicity of carbenes and phosphines, very similar activation barriers were found, which is in qualitative agreement with experimental observations.

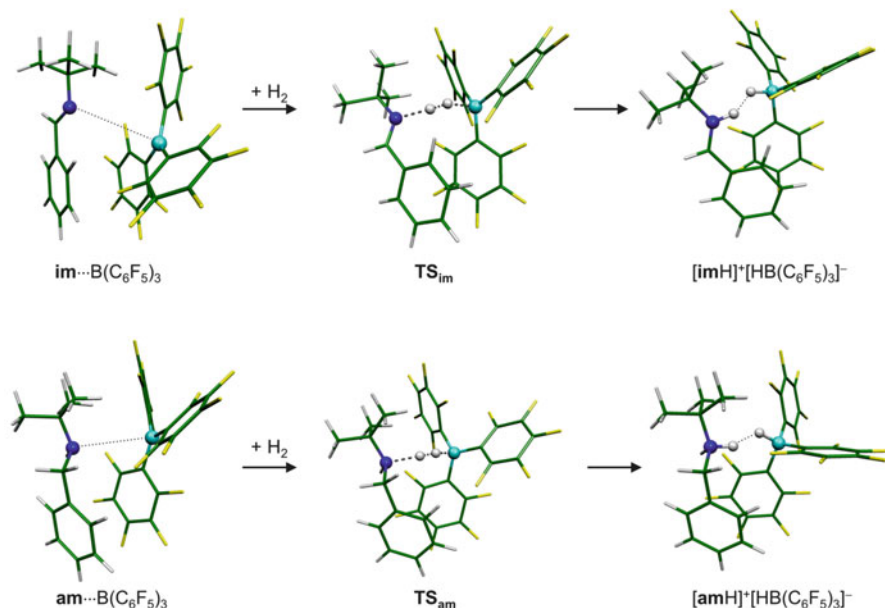
In their calculations, Privalov et al. addressed the possibility of hydrogen cleavage via carbonyl/borane pairs [93]. The authors identified the corresponding transition state of H<sub>2</sub> activation, in which the carbonyl oxygen atom and the boron center serve as a Lewis base and acid, respectively. Despite the relatively low basicity of the carbonyl oxygen, the H<sub>2</sub> splitting and the reduction of C=O bonds were predicted to be feasible at elevated temperatures. These predictions were later verified experimentally by Repo et al., who reported direct hydrogenation of aromatic carbonyl compounds in the presence of stoichiometric B(C<sub>6</sub>F<sub>5</sub>)<sub>3</sub> [100].

The mechanism of H<sub>2</sub> splitting by an amine/borane pair, namely by the combination of *trans*-2,6-dimethyl-2,6-diphenylpiperidine (**dmdpp**) with B(C<sub>6</sub>F<sub>5</sub>)<sub>3</sub>, has been examined computationally by Pyykkö and Wang [66]. This intermolecular FLP is capable of reversible H<sub>2</sub> activation as demonstrated earlier by Sumerin et al. [101]. The calculations indicated that this reaction takes place via an early transition state correlating to a weakly bound **dmdpp**...B(C<sub>6</sub>F<sub>5</sub>)<sub>3</sub> intermediate on the reactant side. The Morokuma energy decomposition analysis carried out for the located transition state pointed to the importance of orbital interactions in the H<sub>2</sub> activation process.

The metal-free hydrogenation of the phenyl ring in *N*-phenyl amines represents another remarkable application of the FLP concept [42]. These reduction processes occur at 110 °C in the presence of an equivalent of B(C<sub>6</sub>F<sub>5</sub>)<sub>3</sub> and yield the corresponding *N*-cyclohexylammonium hydridoborate salts. Related computations carried out for the *t*-BuNHPh/B(C<sub>6</sub>F<sub>5</sub>)<sub>3</sub> + H<sub>2</sub> reaction revealed that a van der Waals complex having the *para*-carbon of the aniline moiety preorganized with the boron center, stabilized by  $\pi$  stacking interaction, is able to cleave H<sub>2</sub> heterolytically in a low-energy-barrier step. It was noted that the located transition state is more advanced than usually observed for analogous reactions.

### 4.3.2 Imine/Borane and Amine/Borane Pairs: Two Consecutive Hydrogen Activations

As a part of our theoretical investigation [19] of the mechanism of borane catalyzed imine reduction [44, 102], we explored the H<sub>2</sub> splitting reaction pathway for the hydrogenation of imine *t*-BuN=CHPh (**im**). Experimentally, the hydrogen



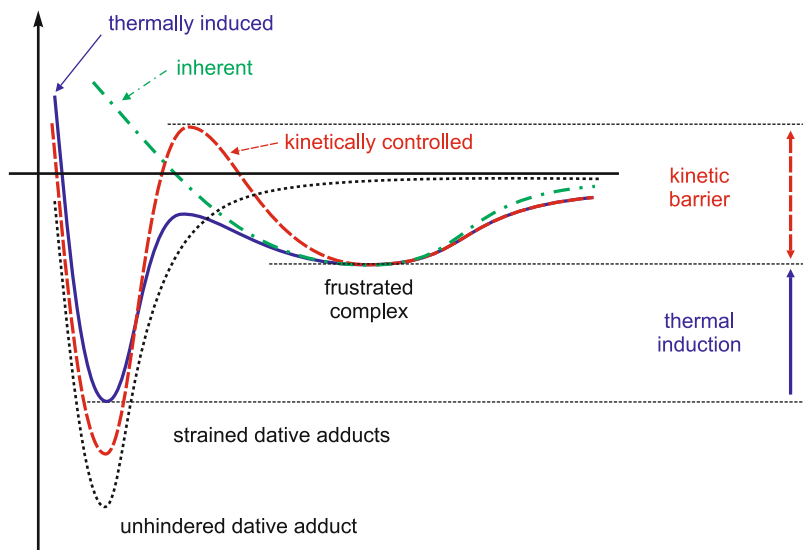
**Fig. 19** Stationary points along the hydrogen splitting processes by the **im**/ $\text{B}(\text{C}_6\text{F}_5)_3$  and **am**/ $\text{B}(\text{C}_6\text{F}_5)_3$  pairs

activation by the stoichiometric **im**/ $\text{B}(\text{C}_6\text{F}_5)_3$  mixture proceeds similarly to the  $t\text{-Bu}_3\text{P}/\text{B}(\text{C}_6\text{F}_5)_3 + \text{H}_2$  system in that room temperature and ambient pressure are sufficient to induce the reaction [44]. However, the expected iminium hydridoborate product cannot be isolated in this reaction as hydride transfer occurs rapidly, and the resulting amine  $t\text{-BuNH-CH}_2\text{Ph}$  (**am**) forms a classical Lewis adduct with  $\text{B}(\text{C}_6\text{F}_5)_3$ . The role of iminium hydridoborate as an intermediate was confirmed in a separate experiment where the bulkier imine  $2,6\text{-}(i\text{-Pr})_2\text{C}_6\text{H}_3\text{-N}=\text{C}(\text{Me})t\text{-Bu}$  (**diim**) was found to produce the salt  $[\text{diimH}]^+[\text{HB}(\text{C}_6\text{F}_5)_3]^-$  under identical conditions, with the hydride transfer step being apparently blocked [44].

The transition state of the  $\text{H}_2$  splitting process induced by the **im**/ $\text{B}(\text{C}_6\text{F}_5)_3$  pair is depicted in Fig. 19 along with the optimized structures of the corresponding frustrated complex and the ion pair product. The structure of the preorganized **im**... $\text{B}(\text{C}_6\text{F}_5)_3$  complex is stabilized by various types of noncovalent interactions including  $\pi$  stacking. Although formed in an entropically unfavored process, this species reacts rapidly with  $\text{H}_2$  through transition state  $\text{TS}_{\text{im}}$ , which represents only a modest energy barrier for the H–H bond cleavage.

The room temperature final product of the **im** +  $\text{B}(\text{C}_6\text{F}_5)_3 + \text{H}_2$  reaction, the covalent **am**– $\text{B}(\text{C}_6\text{F}_5)_3$  adduct, is still capable of hydrogen activation at elevated temperature. The computed reaction pathway of  $\text{H}_2$  splitting by the **am**/ $\text{B}(\text{C}_6\text{F}_5)_3$  pair is analogous to that of the **im**/ $\text{B}(\text{C}_6\text{F}_5)_3 + \text{H}_2$  system (see Fig. 19). Nevertheless, the energy minimum of this system is the strained but datively bound **am**– $\text{B}(\text{C}_6\text{F}_5)_3$  adduct, with a binding energy of  $\Delta E = -26.7$  kcal/mol. As a result





**Fig. 20** Systems showing inherent, thermally induced, and kinetically controlled frustration

of the dative bond formation, higher activation energy is needed to reach the transition state of  $H_2$  splitting than with **im**, which is in full agreement with the experimental finding that the formation of the ammonium hydridoborate product occurs only at  $80\text{ }^\circ\text{C}$  [44]. We note that similar pathways have been described in a parallel study reported by Privalov [92].

### 4.3.3 Classifying Frustrated Systems

Based on the characteristics of a wider range of acid/base pairs, the qualitative picture of FLP type reactivity could be refined as illustrated in Fig. 20 [19, 103, 104]. The figure suggests a classification of Lewis acid–base pairs in terms of the shape of the associated  $\Delta E(d_{AD})$  potential energy curves. Bulky Lewis pairs having their global energy minima at their reactive forms (i.e., frustrated complexes) can be termed as *inherently frustrated* systems. The datively bound forms of these D/A pairs are either completely absent (as in the case of  $t\text{-Bu}_3\text{P/B}(\text{C}_6\text{F}_5)_3$ ), or the minimum corresponding to the dative adduct lies above the frustrated complex. Classical Lewis pairs represent the other extreme class on this scale; they are characterized by a single low-lying energy minimum corresponding to the stable, unhindered dative adduct. In between, systems that exhibit both a frustrated complex form and a lower-lying, strained but datively bound global minimum can be regarded as showing *thermally induced frustration*. In these systems, the reactive  $\text{D}\cdots\text{A}$  states of the pairs are accessible only via thermal activation of the strained dative adducts.

Thermally induced frustration is thus a consequence of “intermediate” steric bulk, allowing the formation of classical adducts that are, however, far less stable than for the unhindered systems. This situation is not uncommon among the investigated FLP systems as several D/A pairs exhibiting datively bound states and showing FLP-type reactivity have been reported [45, 72, 76, 78, 100, 105]. As pointed out by Geier and Stephan, classical Lewis acid–base and FLP-type reactivities are not mutually exclusive [45].

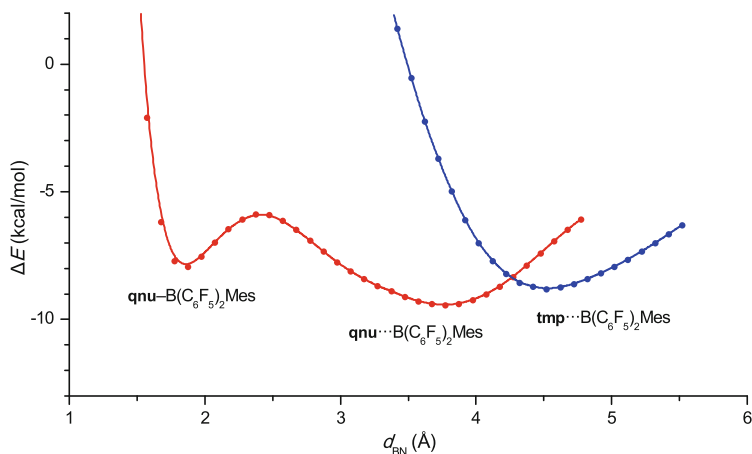
Alcarazo et al. have recently described another specific class of Lewis pairs that require low temperatures to avoid quenching of the FLP components and preserve their reactivity [103]. These systems feature an appreciable barrier separating the dative adduct and the weakly bound reactive forms, and they can be regarded to be frustrated due to *kinetic control* (the authors of [103] suggested the term “kinetically induced frustration”).

Kwon, Kim, and Rhee showed that the possibility of weak dative bond formation between the Lewis acceptor (A) and the solvent (S) can lead to *solvent-assisted frustration* [104]. In this case, a classical Lewis D/A pair is turned into an FLP not by destabilizing the D–A bond but due to a stabilization of the dissociated D + A state via an A–S bonding. Together with a noncovalent D···A–S interaction, this effect results in an effective potential energy curve similar to the case of thermally induced frustration.

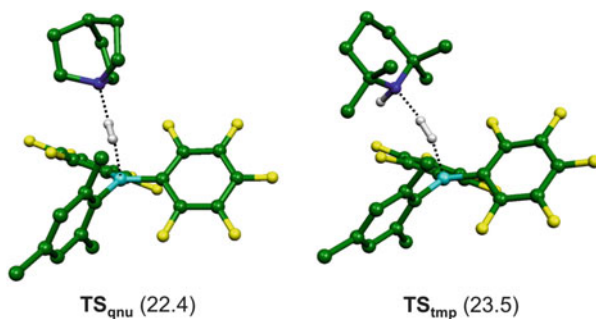
#### 4.3.4 Tuning Frustrated Complex Geometry and Barrier Height by Steric Effects

Soós et al. introduced a new FLP design concept to increase the functional-group tolerance in metal-free catalytic hydrogenation [23]. Mesityl borane  $\text{B}(\text{C}_6\text{F}_5)_2\text{Mes}$  was selected as a Lewis acid with enhanced shielding of the boron center to exclude addition reactions with unsaturated functionalities while retaining the capability of reaction with the small  $\text{H}_2$  molecule. The optimization of the Lewis base component of the pair revealed that, among the tested N-based donors, only compact and relatively basic amines, such as quinuclidine (**qnu**) and 1,4-diazabicyclo[2.2.2]octane (DABCO), were able to cleave  $\text{H}_2$  when combined with  $\text{B}(\text{C}_6\text{F}_5)_2\text{Mes}$ . These new FLPs, however, could be used as efficient hydrogenation catalysts with unprecedented orthogonal reactivity and chemoselectivity.

In order to rationalize the reactivity trend observed for the investigated amine/borane pairs, computations have been carried out for the **qnu**/ $\text{B}(\text{C}_6\text{F}_5)_2\text{Mes} + \text{H}_2$  and **tmp**/ $\text{B}(\text{C}_6\text{F}_5)_2\text{Mes} + \text{H}_2$  reactions (**tmp** = 2,2,6,6-tetramethylpiperidine) [23]. The  $\Delta E(d_{\text{BN}})$  potential energy curves computed for the **qnu**/ $\text{B}(\text{C}_6\text{F}_5)_2\text{Mes}$  and **tmp**/ $\text{B}(\text{C}_6\text{F}_5)_2\text{Mes}$  pairs indicated that the small quinuclidine base affords favorable interaction with the borane in a broad  $d_{\text{BN}}$  range, and the datively bound form could also be identified on the potential energy surface with binding energy comparable to that of the **qnu**··· $\text{B}(\text{C}_6\text{F}_5)_2\text{Mes}$  frustrated complex (see Fig. 21). In contrast, the intermolecular forces become repulsive at a rather large B–N distance in **tmp**/ $\text{B}(\text{C}_6\text{F}_5)_2\text{Mes}$ , which hampers the cooperative base  $\rightarrow \sigma^*(\text{H}_2)$  and  $\sigma(\text{H}_2) \rightarrow$  borane



**Fig. 21** Potential energy curves illustrating the interactions of borane  $B(C_6F_5)_2Mes$  with bases **qnu** and **tmp**

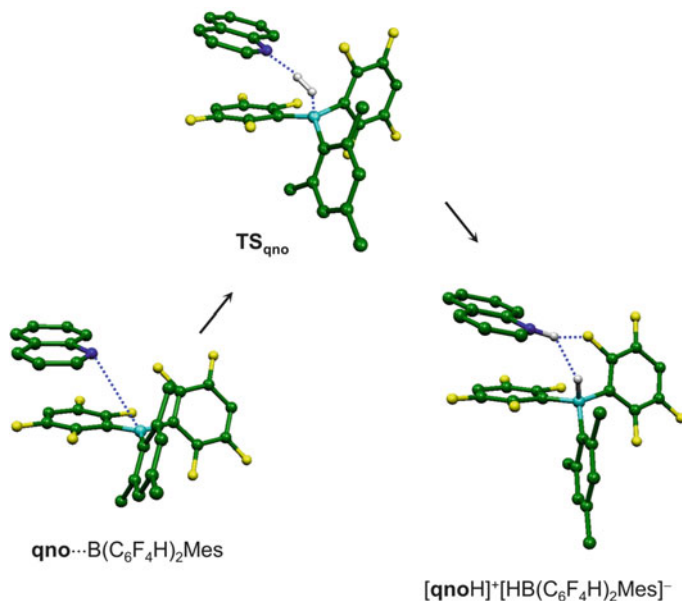


**Fig. 22** Transition states identified for the heterolytic  $H_2$  splitting via the **qnu**/ $B(C_6F_5)_2Mes$  and **tmp**/ $B(C_6F_5)_2Mes$  pairs. Solution-phase Gibbs free energies (in kcal/mol) with respect to the separated reactants are given in parentheses

donations and leads to reduced reactivity. This trend is indeed reflected in the computed activation barriers of heterolytic  $H_2$  splitting (see Fig. 22). These results underline that the accessible  $d_{BN}$  range can be fine-tuned by steric effects around the donor/acceptor centers and also emphasize that even the activation of  $H_2$ , the smallest possible molecule, may be hindered by steric overcrowding. Similar effects might be responsible for the missing reactivity of the *trans*- $Mes_2P-CH=CR-B(C_6F_5)_2$  FLPs toward  $H_2$  [47].

#### 4.3.5 Flat Donors Offer Multiple $H_2$ Activation Pathways

As a further exploitation of the size-exclusion design principle, Soós and co-workers investigated the partial hydrogenation of quinoline (**qno**) [24]. Borane  $B(C_6F_5)_2Mes$  was found to catalyze the reaction, and the replacement of *para*-fluorine atoms



**Fig. 23** A possible pathway for hydrogen activation by the **qno**/**B**(*p*-**C**<sub>6</sub>**F**<sub>4</sub>**H**)<sub>2</sub>**Mes** pair

with hydrogens gave substantial improvement in the catalytic performance, presumably due to the enhanced stability of the catalyst. The new mesityl borane **B**(*p*-**C**<sub>6</sub>**F**<sub>4</sub>**H**)<sub>2</sub>**Mes** was successfully applied in metal-free hydrogenation of various quinoline derivatives and showed excellent functional group tolerance in these reactions.

As part of our continued collaboration with this group, we examined the mechanism of these processes via DFT calculations and explored the H<sub>2</sub> splitting reaction for the **qno**/**B**(*p*-**C**<sub>6</sub>**F**<sub>4</sub>**H**)<sub>2</sub>**Mes** pair [24]. A selected pathway is depicted in Fig. 23. The role of  $\pi$  stacking interactions in the formation of the **qno**...**B**(*p*-**C**<sub>6</sub>**F**<sub>4</sub>**H**)<sub>2</sub>**Mes** reactive species and the cooperative nature of the hydrogen activation are apparent from the optimized structures of the stationary points. Importantly, we found that a variety of reaction pathways exist, differing in the relative position of the FLP components in the corresponding frustrated complexes and leading to different [**qnoH**]<sup>+</sup>[**HB**(*p*-**C**<sub>6</sub>**F**<sub>4</sub>**H**)<sub>2</sub>**Mes**]<sup>-</sup> ion-pair conformers. The relative energies of the identified transition states are within 0.5 kcal/mol which means that, for certain FLPs, a multitude of competing reaction channels contribute to product formation, and a single transition state may not fully reflect the inherent flexibility of these systems.

#### 4.3.6 Stepwise Hydrogen Activation

The D/A + H<sub>2</sub> reactions we have discussed so far were all interpreted in terms of the concerted action of Lewis acid/base centers. Interestingly, a stepwise mechanism

involving an intermediate formed via side-on coordination of  $H_2$  to a borane was proposed to be operative in reactions reported by Li, Wang, and coworkers [106].

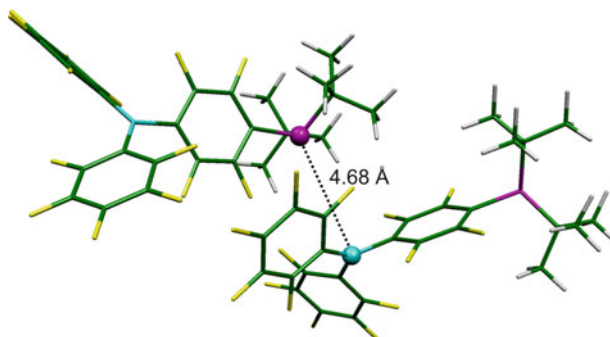
These authors synthesized a new borane  $BAr^F_2H$  with two bulky, electron deficient aryl groups ( $Ar^F = 2,4,6-(CF_3)_3C_6H_2$ ). At elevated temperature ( $50\text{ }^\circ\text{C}$ ) the deuterated analogue  $BAr^F_2D$  was shown to undergo H/D exchange with  $H_2$ . DFT calculations identified a borane- $(\eta^2-H_2)$  complex as an intermediate in the H/D exchange process. This species was also proposed to be an intermediate in the  $Et_3N/BAr^F_2H + H_2$  reaction, which affords  $[Et_3NH]^+[HBAr^F_2H]^-$ . In the latter reaction the coordination of  $H_2$  was predicted to be the rate-determining step since the corresponding transition state was found to be clearly higher in energy than that of the subsequent  $H_2$  splitting step. In contrast, the analogous reaction with the DABCO base was found to occur in a single step via the concerted mechanism. This dramatic change in the reaction mechanism is surprising, and it was attributed to different steric demands of the Lewis donors. However, the unexpectedly large barrier for the dissociation of  $H_2$  from the borane- $(\eta^2-H_2)\cdots NEt_3$  complex and the large activation free energy difference between the two donors, inconsistent with experimental results, remain unexplained, suggesting that further studies might be necessary to understand fully the details of this intriguing stepwise pathway.

We note that a borane- $(\eta^2-H_2)$  complex was also found to be a reaction intermediate in a model reaction ( $PH_3/B(CF_3)_3 + H_2$ ) studied computationally by Gao et al. [67], but the analogous complex with borane  $B(C_6F_5)_3$  could be identified neither in calculations [17] nor in experiments [41]. Furthermore, the diaryl borane  $B(C_6F_5)_2H$  undergoes exchange reaction with  $H_2$  as well, but calculations do not indicate involvement of a  $\eta^2-H_2$  complex [107]. On the other hand, the dihydrogen activation of antiaromatic pentaarylboroles can take place via the  $\eta^2-H_2$  coordination to the boron center as revealed by DFT calculations; however, attempts to identify this intermediate by low-temperature NMR experiments were unsuccessful in this case either [13].

## 4.4 Dihydrogen Activation with Linked FLPs

### 4.4.1 The Curious Case of the $C_6F_4$ Linker

In the first linked phosphinoboranes investigated in the FLP context by Stephan et al. ( $t\text{-Bu}_2P-C_6F_4-B(C_6F_5)_2$  and  $Mes_2P-C_6F_4-B(C_6F_5)_2$ ), the phosphorus and boron centers are linked by a large and rigid  $C_6F_4$  (perfluoro-1,4-phenylene) moiety, which makes a direct intramolecular cooperation of the P and B atoms in these systems impossible. However, the experimentally observed kinetics of hydrogen loss from the corresponding phosphonium borate [ $^+HMe_2P-C_6F_4-B(C_6F_5)_2H^-$ ] is first-order, which led Stephan and coworkers to formulate a mechanism involving proton or hydride migration, followed by  $H_2$  elimination from the adjacent B-C or P-C atoms [6]. For the hydrogen activation, the reversed sequence of steps,



**Fig. 24** Frustrated complex formed by the association of two  $t\text{-Bu}_2\text{P-C}_6\text{F}_4\text{-B(C}_6\text{F}_5)_2$  molecules

i.e., cleavage over the B–C or P–C bonds and consecutive  $\text{H}^+/\text{H}^-$  shifts, was considered [6, 108].

In our preliminary investigations, we found these migration intermediates to lie very high in energy, but we were able to identify frustrated complexes formed from two phosphinoborane molecules (Fig. 24). We therefore suggested that hydrogen splitting may proceed via a mechanism similar to nonlinked pairs, involving intermolecular cooperation of the phosphorus and boron centers [17].

A detailed computational analysis of this system was reported by Guo and Li [109], who concluded that the migration channels are unfavorable. They found the intermolecular pathway feasible via a concerted mechanism involving simultaneous phosphorus  $\rightarrow \sigma^*(\text{H}_2)$  and  $\sigma(\text{H}_2) \rightarrow$  boron electron donations, which is practically identical to the mechanism proposed for  $t\text{-Bu}_3\text{P/B(C}_6\text{F}_5)_3 + \text{H}_2$  [17]. As the authors pointed out, this mechanism interprets the observed bimolecular exchange process, which was anticipated by Stephan et al. [6] to rationalize the scrambling of deuterium labels when a mixture of  $[\text{}^+\text{HMes}_2\text{P-C}_6\text{F}_4\text{-B(C}_6\text{F}_5)_2\text{H}^-]$  and  $[\text{}^+\text{DMes}_2\text{P-C}_6\text{F}_4\text{-B(C}_6\text{F}_5)_2\text{D}^-]$  was heated. On the other hand, the observed first-order kinetics of hydrogen loss is seemingly inconsistent with this bimolecular process.

The intramolecular reaction pathway for this reversible hydrogen activation process was later re-examined by Rajeev and Sunoj in a theoretical study [110]. The authors used a simplified model ( $\text{Me}_2\text{P-C}_6\text{F}_4\text{-B(CF}_3)_2$ ) to represent the FLP and explored possible  $\text{H}_2$  addition and elimination reaction routes. The energetically most favored hydrogen activation pathway that yields the phosphonium borate species corresponded to heterolytic  $\text{H}_2$  addition across the C–B bond followed by a cascade of 1,2-proton migration steps. Although the overall energy barrier of this pathway was predicted to be rather high (35.6 kcal/mol relative to the reactants), the authors concluded that this mechanism is feasible. However, this activation energy is clearly inconsistent with the observed high reaction rate, particularly if the entropic cost of the  $\text{H}_2$  addition step is also taken into account. Additional experimental and theoretical investigations are therefore necessary to provide deeper understanding of the reaction mechanism.

#### 4.4.2 Intramolecular Cooperation

While the  $C_6F_4$  linker of the first covalently tethered frustrated pairs excludes intramolecular cooperation of the P and B centers in  $H_2$  splitting, the short alkyl chain in  $Mes_2P-C_2H_4-B(C_6F_5)_2$ , prepared by Erker et al. [50], possesses significant flexibility, allowing the preorganization of active centers. Although the most stable form of this linked Lewis pair is the datively bound four-membered heterocycle, the computations indicate that the reactive open forms should be readily accessible even at room temperature [86]. The  $H_2$  activation was shown to occur via an early transition state in a concerted but asynchronous reaction (the BH bond is formed slightly earlier than the PH bond). The similar chemical behavior of the  $Mes_2P-C_2H_4-B(C_6F_5)_2$  and  $t-Bu_3P/B(C_6F_5)_3$  FLPs was interpreted in terms of the similar electric field strengths provided by these compounds [86].

Intramolecular cooperativity of the active centers was also assumed for the heterolytic  $H_2$  splitting by the methyl-*ortho*-phenyl-linked aminoborane compound **tmp**- $CH_2-C_6H_4-B(C_6F_5)_2$ , synthesized by Repo, Rieger, and coworkers [46]. Computational investigations confirmed the possibility of intramolecular hydrogen activation via the identification of the corresponding transition state. The reaction mechanism was later examined by various isotopic labeling techniques, but no direct evidence could be obtained for the intramolecular mechanism [111]. The reaction of this “molecular tweezer” with HD gas gave all four possible isotopomers of the zwitterionic product, which was interpreted as a result of intermolecular proton exchange occurring after the intramolecular  $H_2$  activation process. No kinetic isotope effect could be observed in these experiments, which was associated with the early nature of the computed transition state. Indeed, the Gibbs free energy barriers predicted for the two reaction routes toward the  $[^+Htmp-CH_2-C_6H_4-B(C_6F_5)_2D^-]$  and  $[^+Dttmp-CH_2-C_6H_4-B(C_6F_5)_2H^-]$  products were almost identical [111].

The “directly linked” phosphinoboranes, such as  $t-Bu_2P-B(C_6F_5)_2$  [58], represent another class of FLPs that are capable of intramolecular hydrogen splitting. As mentioned earlier in this chapter, the experimental geometry and a theoretical analysis both point to some  $\pi$ -type overlap between the phosphorus lone pair  $n(P)$  and the borane  $p$  orbital, but it is limited, and the centers retain sufficient Lewis acidic and basic character to react with  $H_2$  directly [58]. In the transition state, which was located later by Privalov [112], the approach of hydrogen is asymmetric, with end-on-like interaction with the phosphine and side-on-like with the borane moiety. This topology is consistent with the expected  $n(P) \rightarrow \sigma^*(H_2)$  and  $\sigma(H_2) \rightarrow p(B)$  donations, and it appears to be a general characteristic of transition states in FLP +  $H_2$  reactions. Privalov et al. also carried out a detailed analysis of the substituent effects on the barrier [65] and concluded that decreasing the  $\pi$  interaction between  $n(P)$  and  $p(B)$  via geometrical constraints or placing electron-withdrawing substituents on the borane facilitates the reaction.

The  $\pi$ -type overlap between the donor and acceptor sites can be precluded while maintaining the advantageous coplanar orientation of the frontier orbitals by using a simple  $CH_2$  linker between the active sites. This design strategy was proposed in a computational study by Wang et al. [63], who also examined other short linker units

to reach an optimal orientation of donor/acceptor orbitals for cooperative H<sub>2</sub> activation [64]. Wang's group later designed several other metal-free catalysts computationally [60, 62, 95–97], which are presented in a separate chapter of this book.

Inspired by these computational studies, Tamm and coworkers synthesized a frustrated pyrazolylborane Lewis pair [113]. Although the structural analysis showed a notable deviation from the ideal orientation of donor/acceptor sites, the new N-linked FLP was found to activate hydrogen rapidly and could be used as a metal-free catalyst for the hydrogenation of imines. Related computations located the transition state associated with the H–H bond cleavage, which is consistent with the cooperative mechanism [113].

A methylene-bridged FLP, namely the phosphinoborane *t*-Bu<sub>2</sub>P–CH<sub>2</sub>–BPh<sub>2</sub>, could also be synthesized as reported by Slootweg, Lammerstma et al. [43]. As noted by the authors, this geminal FLP is ideally preorganized for small molecule activation. The concerted action of active sites in the heterolytic H<sub>2</sub> splitting process was borne out by the structure of the computed transition state. As discussed above, this linker also has beneficial effects on the exothermicity of the reaction, which allows the utilization of nonfluorinated aryl substituents on boron.

#### 4.5 *On the Elusive Nature of Reaction Intermediates: Can We Detect Frustrated Complexes?*

The computational studies presented in the previous sections provided useful information on possible mechanistic pathways in FLP-mediated hydrogen activation processes. Most of the results emerging from these theoretical contributions are consistent with a mechanistic picture that involves reactive intermediates preorganized for cooperative interaction with H<sub>2</sub> (or generally with a small molecule). In the case of intermolecular FLPs, the reactive species are formed by the preassociation of FLP components into weakly bound complexes with properly oriented active centers (frustrated complexes). For a large number of pairs, the structure with ideally oriented, nonquenched donor/acceptor centers does not represent the global energy minimum of the system. Some degree of thermal activation might then be required to access the reactive frustrated configurations. Synergistic electron transfer processes with the involvement of both Lewis centers and the H<sub>2</sub> molecule acting as a bridge were identified to play an important role in the actual cleavage reactions.

On the experimental side, there is only very limited evidence available that could be used as an argument for or against this mechanistic view. There are a few observations mentioned in the literature indicative of noncovalent interactions between the donor and acceptor molecules. For instance, the color of the Mes<sub>3</sub>P/B(C<sub>6</sub>F<sub>5</sub>)<sub>3</sub> and **tmp**/B(C<sub>6</sub>F<sub>5</sub>)<sub>3</sub> mixtures is thought to arise from such intermolecular association [41, 55]. For the latter system, an observed NMR chemical shift of the

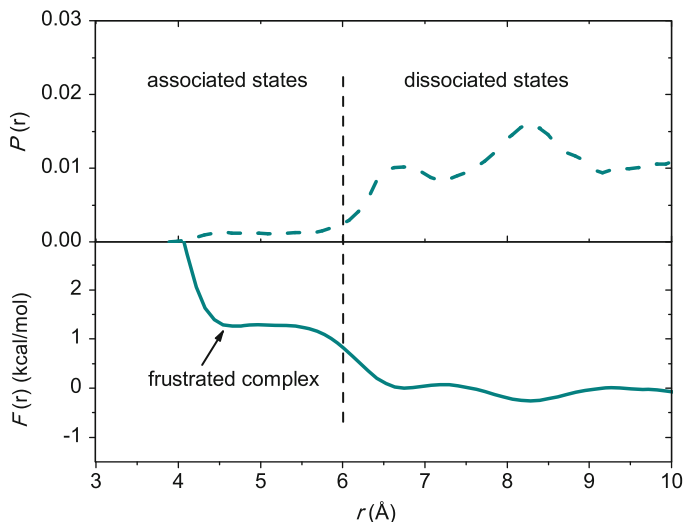


NH group was related to intermolecular N–H...F hydrogen bonding interactions [55]. In a recent experimental mechanistic study, Piers and coworkers attempted to identify weakly bound complexes in the mixture of *t*-Bu<sub>3</sub>P and B(C<sub>6</sub>F<sub>5</sub>)<sub>3</sub>, but the yellow color of the solution turned out to arise from the phosphinoborane *t*-Bu<sub>2</sub>P–C<sub>6</sub>F<sub>4</sub>–B(C<sub>6</sub>F<sub>5</sub>)<sub>2</sub> formed in detectable quantities in the mixture, and not from phosphine–borane interactions as originally thought [114]. They further confirmed this fact by a time-dependent DFT calculation of the UV–vis spectrum of the frustrated complex, which does not show any red-shifted absorption band with respect to the free B(C<sub>6</sub>F<sub>5</sub>)<sub>3</sub>. In another set of experiments, the same group prepared a selectively labeled ion pair, the [*t*-Bu<sub>3</sub>PH]<sup>+</sup>[DB(C<sub>6</sub>F<sub>5</sub>)<sub>3</sub>]<sup>−</sup> species, and expected to access the *t*-Bu<sub>3</sub>P...B(C<sub>6</sub>F<sub>5</sub>)<sub>3</sub> encounter complex states by heating the solution to 100 °C [115]. As no H/D exchange was observed in the labeled ion pair, the authors concluded that they failed to reach the frustrated complex species in this experiment, which, however, does not prove its nonexistence. The intermediacy of ternary complexes formed between various intermolecular N/B Lewis pairs and H<sub>2</sub> was probed experimentally by Berke et al., but the variable temperature NMR measurements did not provide any sign of such transient intermediates [72]. It thus appears that so far no conclusive experimental evidence exists for or against the assumed reactive intermediates in D/A + H<sub>2</sub> reactions.

One of the reasons why observing weakly bound species in solution phase is difficult is their low concentration. Although secondary intermolecular forces provide significant enthalpic stabilization in these complexes, the entropic cost of association can overcompensate the exothermicity, and solvent effects may also favor the dissociated states. With the aim of estimating the concentration of frustrated complexes in solution phase, we have recently performed classical molecular dynamics (MD) simulations on extended models that involve the explicit treatment of solvent molecules [25]. This approach allowed us to incorporate entropic contributions and solvent effects in a straightforward manner, which had not been addressed in previous studies. In principle, the free energy of association can be estimated in static quantum chemical calculation as well, but those predictions are expected to be less accurate for flexible, solvated systems.

The model we employed in our MD study included a single pair of *t*-Bu<sub>3</sub>P and B(C<sub>6</sub>F<sub>5</sub>)<sub>3</sub> and over one thousand toluene molecules in a periodically repeated cubic cell. The MD simulations were carried out by using an improved force field that accounts for stabilizing short-range direct P–B interactions as well. The umbrella sampling MD technique was used to monitor the probability of finding the *t*-Bu<sub>3</sub>P/B(C<sub>6</sub>F<sub>5</sub>)<sub>3</sub> pair at a certain distance in toluene at room temperature. The probability distribution  $P(r)$  and the related Helmholtz free energy variation  $F(r)$  as functions of the distance between the P and B atoms ( $r$ ) are depicted in Fig. 25.

It is apparent from the obtained free energy curve that the association of the *t*-Bu<sub>3</sub>P and B(C<sub>6</sub>F<sub>5</sub>)<sub>3</sub> molecules in toluene is thermodynamically disfavored. All configurations that can be considered as associated states (herein defined as  $r < 6$  Å) lie at least 1 kcal/mol above the dissociation limit. Although considerable interaction energies are predicted for the *t*-Bu<sub>3</sub>P/B(C<sub>6</sub>F<sub>5</sub>)<sub>3</sub> pair in gas phase, configurations corresponding to the frustrated complex species (those with



**Fig. 25** Free energy curve  $F(r)$  and probability distribution  $P(r)$  as functions of the P–B distance ( $r$ ), computed from MD simulations for  $t\text{-Bu}_3\text{P}/\text{B}(\text{C}_6\text{F}_5)_3$  in toluene

$r \sim 4.5 \text{ \AA}$ ) do not represent a minimum on the free energy curve. This is actually due to the entropic penalty related to limited conformational freedom as compared to those with larger  $r$  separations. The free energy of the system decreases gradually in the  $5.6 \text{ \AA} < r < 6.5 \text{ \AA}$  region, which can be attributed to solvent effects. At these separations, the  $t\text{-Bu}_3\text{P}$  and  $\text{B}(\text{C}_6\text{F}_5)_3$  molecules are still in contact, but some of the bulky substituents are more accessible for the solvent molecules, providing beneficial contributions to the overall free energy.

The calculated probability distribution presented in Fig. 25 approaches zero in the  $r < 6 \text{ \AA}$  region, suggesting that only a small fraction of the  $t\text{-Bu}_3\text{P}/\text{B}(\text{C}_6\text{F}_5)_3$  is in associated form in toluene. On the basis of the  $P(r)$  function, we estimate that about 2% of the total amount of phosphine and borane dissolved in toluene are in associated states. The relative concentration of the reactive, preorganized states (i.e., frustrated complexes) is estimated to be about 0.5%, which is typical of reactive intermediates, but it is rather low to be detectable by standard spectroscopic techniques. The shape of the calculated free energy curve points to a smooth transition between active and inactive forms of FLPs. This feature points to an elusive nature of frustrated complexes, which renders their spectroscopic identification even more difficult. Reaction intermediates identified as ternary complexes preceding the  $\text{H}_2$  activation transition states lie extremely high in free energy; therefore, the spectroscopic observation of these latter states is quite unlikely even at low temperatures.

## 5 Hydrogenation of Double Bonds

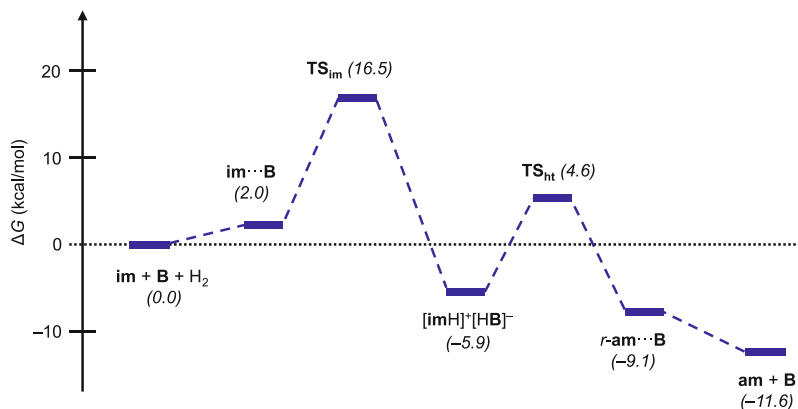
Saturation of C=C, C=N, or C=O double bonds is a key step in numerous synthetic processes both in research laboratories and in industry. Direct reactions of olefins, imines, and carbonyl compounds with H<sub>2</sub> can provide the products at a very high level of atom economy; however, catalysts are necessary in practice as neither of these double bonds is reactive toward H<sub>2</sub> under practical conditions. Transition metal based systems are commonly applied for this purpose, but recently FLPs have been shown to be emerging, viable alternatives [15, 16]. In the above sections we have discussed in detail the thermodynamic and mechanistic aspects of H<sub>2</sub> splitting by FLPs; now we turn our attention to the equally important, subsequent step, the actual hydrogenation to the substrate. In general, the cleavage products H<sup>+</sup> and H<sup>-</sup> may be transferred to the substrate simultaneously, or the transfer of one of them can initiate a two-step hydrogenation [61]. The necessity of some substrate coordination/activation step or side reactions, such as catalyst quenching, can complicate the mechanism.

Like in the case of H<sub>2</sub> cleavage, detailed experimental mechanistic studies are scarce. Computational chemistry can be of great help by creating a full map of the potential or free energy surface and describing all elementary steps of a catalytic cycle, from which the factors affecting the efficiency of the catalysts can be inferred. We carried out theoretical investigations on two systems, hydrogenation of imines with the Lewis acid B(C<sub>6</sub>F<sub>5</sub>)<sub>3</sub> [19] and hydrogenation of quinolines with B(*p*-C<sub>6</sub>F<sub>4</sub>H)<sub>2</sub>Mes [24], and summarize here the most important findings of the original studies.

### 5.1 Hydrogenation of Imines with B(C<sub>6</sub>F<sub>5</sub>)<sub>3</sub>

Shortly after the first reports on FLP-catalyzed hydrogenation by the linked systems R<sub>2</sub>P-C<sub>6</sub>F<sub>4</sub>-B(C<sub>6</sub>F<sub>5</sub>)<sub>2</sub> [56], independent studies from the Stephan [44] and Klankermayer [102] groups revealed that catalytic hydrogenation of bulky imines can be accomplished using solely B(C<sub>6</sub>F<sub>5</sub>)<sub>3</sub> as catalyst. Experiments oriented toward mechanistic understanding uncovered the following:

- At room temperature, the substrate imine can function as the basic partner in the H<sub>2</sub> cleavage, and a rapid hydride transfer step follows to complete the reduction. The produced amine-borane dative adduct can still cleave H<sub>2</sub> at elevated temperature, yielding an ammonium hydridoborate salt. These suppositions were corroborated by stoichiometric experiments [44], described previously in Sect. 4.3.2 of this chapter.
- The dissociation of the amine-borane adduct contributes to the determination of the turnover frequency because the elevated temperature needed for the catalysis was only required to break the amine-borane dative bond in the stoichiometric experiments, while the H<sub>2</sub> activation and reduction of the imine proceeded at room temperature [44].



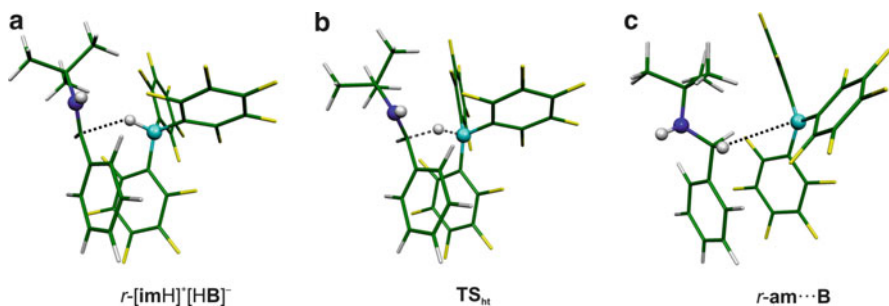
**Fig. 26** Solution-phase Gibbs free energy profile at  $T = 80\text{ }^{\circ}\text{C}$  for catalytic cycle 1. Borane  $\text{B}(\text{C}_6\text{F}_5)_3$  is denoted as **B**

- The  $\text{H}_2$  cleavage also takes part in the determination of the turnover frequency. Early experiments showed that electron-deficient imines were found to react more slowly [44], and later a quantitative study revealed linear relationship between the turnover frequency and  $\text{H}_2$  pressure [116].
- The hydridoborate was confirmed to be involved in the selectivity-determining step as chiral boranes were found to provide the amine products enantioselectively [102].

On the basis of the early experimental results, a catalytic cycle was suggested [44]. Hydrogen splitting by the frustrated imine–borane system was proposed to yield an ion pair consisting of an activated iminium ion and a hydridoborate ion. An amine–borane dative adduct is then formed in the hydride transfer step. Thermal dissociation of this adduct delivers the amine and regenerates the free borane, which can enter the cycle again. This cycle bears analogy to the  $\text{B}(\text{C}_6\text{F}_5)_3$ -catalyzed hydrosilylation of carbonyl compounds, where the  $\text{H}\text{--}\text{Si}$  bond is heterolytically cleaved, with the  $\text{C}=\text{O}$  group accepting the silyl cation and the borane being transformed into a hydridoborate [117–121].

We described our results from the investigation of the FLP-type hydrogen cleavage by the  $t\text{-BuN}=\text{CHPh}$  (**im**) imine and the corresponding  $t\text{-BuNH}\text{--}\text{CH}_2\text{Ph}$  (**am**) amine in combination with  $\text{B}(\text{C}_6\text{F}_5)_3$  in Sect. 4.3.2. Both pairs were found to provide easily iminium or ammonium hydridoborate ion pairs. Here, we will focus on understanding the reduction steps and the catalytic cycle. Conclusions similar to ours have also been obtained in the already mentioned parallel study of Privalov [92].

To monitor the kinetic and thermodynamic feasibility of the reaction steps involved in the catalytic reduction of **im**, solvent phase Gibbs free energy data were calculated at  $T = 80\text{ }^{\circ}\text{C}$ , which were employed in the experiments. The main steps and the free energy profile of the catalytic cycle suggested by Stephan and coworkers [44] (hereafter referred to as cycle 1) are depicted in Fig. 26. The starting point of the cycle and the zero level of the energy scale is the free **im** +  $\text{B}(\text{C}_6\text{F}_5)_3$



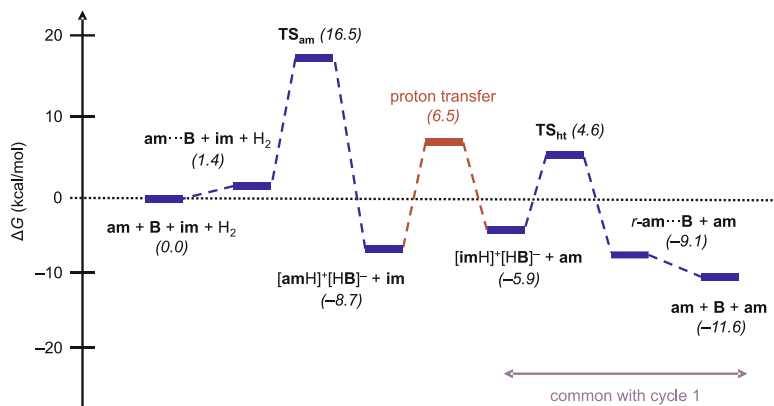
**Fig. 27** Optimized structures of the stationary points for the hydride transfer step: rearranged iminium hydridoborate ion pair (a), transition state of hydride transfer (b), and weakly bound amine–borane product complex (c). Borane  $B(C_6F_5)_3$  is denoted as **B**

pair with  $H_2$ . The first chemical transformation is the hydrogen cleavage, which is proposed to proceed via the  $im \cdots B(C_6F_5)_3$  frustrated complex and the cooperative transition state for the hydrogen splitting,  $TS_{im}$ , lying at a free energy of 16.5 kcal/mol with respect to the reactants. Overall, this step leads to the formation of the  $[imH]^+[HB(C_6F_5)_3]^-$  ion pair and is exergonic.

Activated hydrogen being available in  $[imH]^+[HB(C_6F_5)_3]^-$ , subsequent reduction of the iminium by the hydridoborate can easily occur. An internal rearrangement of the  $[imH]^+[HB(C_6F_5)_3]^-$  ion pair gives an isomer ( $r-[imH]^+[HB(C_6F_5)_3]^-$ , not shown in the energy profile) wherein the B–H bond points toward the unsaturated carbon atom of iminium (Fig. 27a). The hydride transfer in  $r-[imH]^+[HB(C_6F_5)_3]^-$  occurs via  $TS_{ht}$  (Fig. 27b) with a rather low activation free energy (10.5 kcal/mol with respect to the more stable form of the ion pair). This step is exergonic as well and yields an adduct of the neutral amine and borane, bound by secondary interactions ( $r-am \cdots B(C_6F_5)_3$ , Fig. 27c). Thermodynamically favored dissociation of this weak adduct regenerates the free borane and completes the catalytic cycle.

Considering the free energy profile shown in Fig. 26, it is apparent that the hydrogen splitting represents the rate limiting step in this cycle or, more precisely [122], the turnover frequency is determined by the states  $im + B(C_6F_5)_3 + H_2$  and  $TS_{im}$ , leading to an estimated activation free energy of 16.5 kcal/mol. Importantly, as the reaction proceeds and **am** develops in considerable amounts, the free  $B(C_6F_5)_3$  catalyst is quenched in the stable amine–borane dative adduct. This implies that the turnover determining intermediate will be the  $am-B(C_6F_5)_3$  datively bound off-cycle species, and the free energy required to dissociate the  $am-B(C_6F_5)_3$  dative bond (7.0 kcal/mol) must be included in the barrier. Thus, the overall activation free energy of the cycle is estimated to be 23.5 kcal/mol. This value is consistent with the required higher temperature for the reaction.

The experimental results for the stoichiometric reaction pointed out that the amine–borane pair  $am + B(C_6F_5)_3$  is able to cleave dihydrogen at elevated temperatures. We envisioned that this process may also play a role in the catalytic hydrogenation of **im**. In Fig. 28 we present the calculated free energy profile for a catalytic pathway that can be associated with the amine–borane  $H_2$

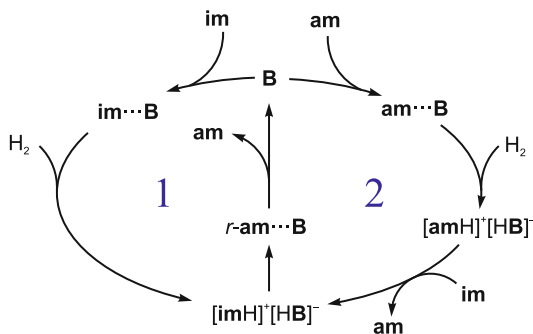


**Fig. 28** Solution-phase Gibbs free energy profile at  $T = 80\text{ }^{\circ}\text{C}$  for catalytic cycle 2. The barrier for the proton exchange step (shown in red) was estimated from a PES scan calculation. Borane  $\text{B}(\text{C}_6\text{F}_5)_3$  is denoted as **B**

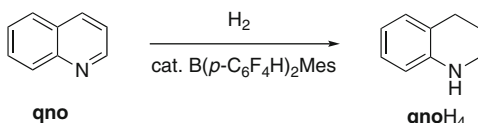
cleavage (cycle 2). After passing through the amine–borane frustrated complex  $\text{am}\cdots\text{B}(\text{C}_6\text{F}_5)_3$  and the hydrogen cleavage transition state  $\text{TS}_{\text{am}}$ , the first stable intermediate in this cycle is the ammonium hydridoborate compound  $[\text{amH}]^+[\text{HB}(\text{C}_6\text{F}_5)_3]^-$ . The activation free energy of this step is almost identical to that predicted for the imine–borane pair, pointing to competing reaction channels in  $\text{H}_2$  activation. We found that a subsequent proton exchange between the ammonium ion and the imine molecule is feasible in a ternary  $\text{im}\cdots[\text{amH}]^+[\text{HB}(\text{C}_6\text{F}_5)_3]^-$  complex, ultimately producing the free amine and the iminium hydridoborate ion pair  $[\text{imH}]^+[\text{HB}(\text{C}_6\text{F}_5)_3]^- + \text{am}$ . Although the proton activation of imine in terms of the  $[\text{amH}]^+[\text{HB}(\text{C}_6\text{F}_5)_3]^- + \text{im} \rightarrow [\text{imH}]^+[\text{HB}(\text{C}_6\text{F}_5)_3]^- + \text{am}$  reaction is slightly endergonic, the subsequent hydride transfer (via  $\text{TS}_{\text{ht}}$ ) and the dissociation of the  $r\text{-am}\cdots\text{B}(\text{C}_6\text{F}_5)_3$  species (already described for cycle 1) provide significant stabilization along the reaction pathway and render the overall reduction process thermodynamically feasible as well.

The above computational results point out that cycle 1 proposed by Stephan et al. [44] can be extended by cycle 2, based on  $\text{H}_2$  splitting via the amine–borane pair, followed by its transfer to the imine. The two catalytic cycles share the reduction and product dissociation steps, and they are therefore interconnected, as illustrated in Fig. 29. The catalysis starts necessarily on cycle 1, i.e., with imine-mediated heterolytic  $\text{H}_2$  cleavage, but as soon as the amine product appears in notable amounts, cycle 2 represents a competing reaction pathway. On the basis of the *product* participating in the catalysis, we originally termed this route as autocatalytic but, in more precise terminology [123], this is an example of autoinductive catalysis, where the product is involved in a new catalytic cycle with the original catalyst ( $\text{B}(\text{C}_6\text{F}_5)_3$ ) still being necessary. However, with respect to cycle 1, we note here that the participation of the *substrate* in hydrogen activation qualifies neither as an autocatalytic nor as an autoinductive process, in contrast to Privalov’s

**Fig. 29** Interconnected catalytic cycles for imine hydrogenation. Borane  $B(C_6F_5)_3$  is denoted as **B**



**Fig. 30** Partial metal-free reduction of unsubstituted quinoline



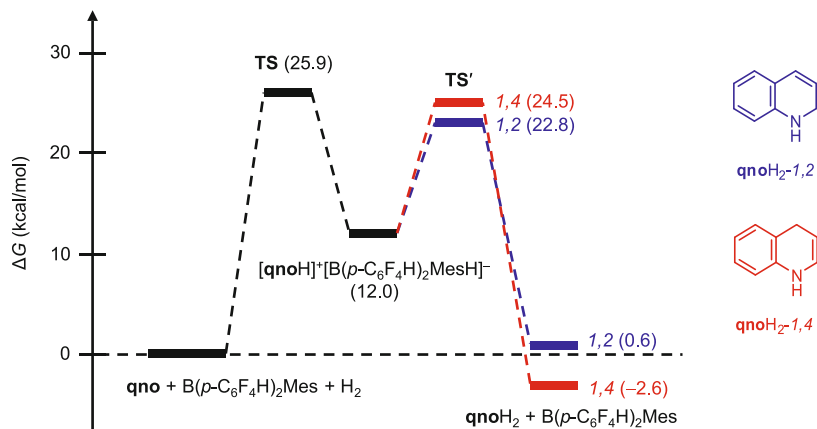
classification [92]. Cycle 2 can also be regarded as a prototype of a more general FLP-catalyzed hydrogenation, where the **am**/ $B(C_6F_5)_3$  pair cleaves  $H_2$  and transfers it to the **im** substrate, without the involvement of the latter in the hydrogen activation process.

## 5.2 Hydrogenation of Quinolines with $B(p-C_6F_4H)_2Mes$

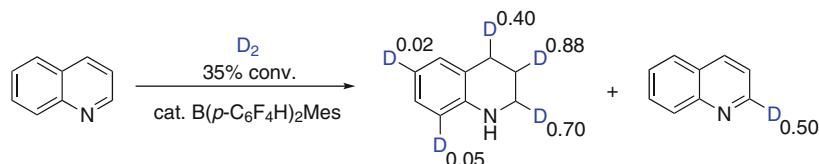
Closely related to the above reaction is the partial hydrogenation of quinolines to 1,2,3,4-tetrahydro-quinolines using electron-deficient boranes. Stephan et al. reported such reactivity of  $B(C_6F_5)_3$  [124], but in this case only quinolines with bulky substituents can be employed. The Soós group showed that tuning the steric factors around the borane, together with some reduction in the Lewis acidity and increase in stability, can lead to the  $B(p-C_6F_4H)_2Mes$  catalyst, capable of partial reduction of various quinolines, including the unsubstituted base compound (**qno**; see Fig. 30) [24].

The catalytic cycle of the reduction process is expected to start with FLP hydrogen activation, followed by a hydride transfer step. Experimental attempts to detect any intermediates were unsuccessful; combined theoretical calculations and deuterium labeling studies were therefore applied to elucidate the mechanism. As the first steps seem to have a rate-determining role, the computational efforts were devoted to the understanding of the beginning of the reduction.

Results from the exploration of hydrogen cleavage by the **qno**/ $B(p-C_6F_4H)_2Mes$  pair were described in Sect. 4.3.5. Here we only recall that several close-lying isomers for the hydrogen cleavage transition state and the  $[qnoH]^+[HB(p-C_6F_4H)_2Mes]^-$  ion pair could be identified, pointing to a variety of competing  $H_2$  activation channels.



**Fig. 31** Solution-phase Gibbs free energy profile ( $T = 25\text{ }^{\circ}\text{C}$ ) computed for the partial reduction of quinoline



**Fig. 32** Results of one of the isotopic labeling experiments

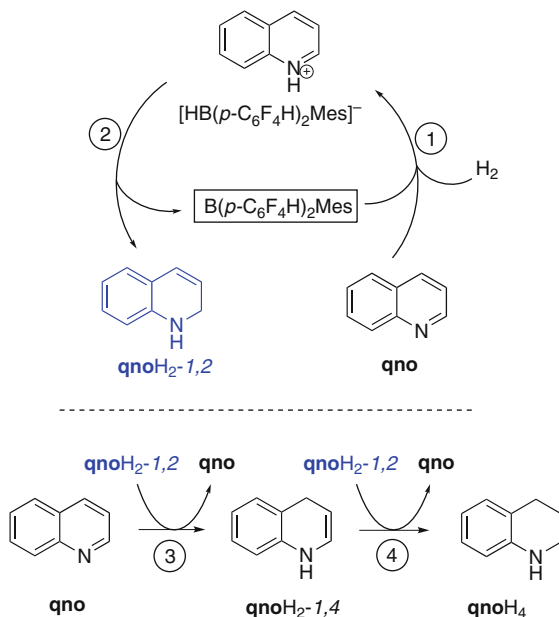
Importantly, the hydrogen cleavage yielding this ion pair was found to be thermodynamically unfavorable; the computed solution-phase  $\Delta G$  of 12.0 kcal/mol indicates that the ion pair would only form in small concentration even if a pre-equilibrium were established (see Fig. 31).

In principle, the subsequent hydride transfer step can occur at both the 2- and 4-positions of the protonated quinoline to result in 1,2- and 1,4-dihydroquinolines (**qnoH<sub>2</sub>-1,2** and **qnoH<sub>2</sub>-1,4**). The relative stabilities of the hydride transfer transition states indicate that the formation of **qnoH<sub>2</sub>-1,2** is kinetically favored, which can be easily rationalized by considering that the charge separation occurring in the **[qnoH]<sup>+</sup>[HB(p-C<sub>6</sub>F<sub>4</sub>H)<sub>2</sub>Mes]<sup>-</sup>** ion pair on the pathway toward the **qnoH<sub>2</sub>-1,4** species represents notable destabilization with respect to the 1,2-addition route. The neutralization of the ion pair via hydride transfer to either position leads to significant energy gain, and the overall reduction of **qno** to both **qnoH<sub>2</sub>-1,2** and **qnoH<sub>2</sub>-1,4** species is essentially neutral in free energy. Our results thus suggest that quinoline and borane can heterolytically cleave H<sub>2</sub> and generate the 1,2-hydrogenated **qnoH<sub>2</sub>** isomer in a kinetically controlled step.

Our collaborators carried out a series of isotopic labeling experiments. In one of these attempts, quinoline was reduced with D<sub>2</sub> using the catalyst B(p-C<sub>6</sub>F<sub>4</sub>H)<sub>2</sub>Mes until 35% conversion was reached (Fig. 32). Deuterium enrichment in the 2- but not in the 4-position of the starting material suggests that it is indeed the



**Fig. 33** Proposed mechanism for catalytic metal-free hydrogenation of quinolines. Numbers within the circles correspond to steps discussed in the text



1,2-hydrogenated product that forms after H<sub>2</sub> activation, in line with the computational results. This species can then function as a reducing agent and transfer H<sub>2</sub> to quinoline or other partially reduced quinolines, which also explains the unequal distribution of deuterium in the qnoH<sub>4</sub> product.

1,2-Dihydroquinolines are known to be quite stable against additional hydride attack, but they easily undergo disproportionation to qno and qnoH<sub>4</sub> with the intermediacy of 1,4-dihydroquinolines [125]. On the basis of this reactivity pattern and further labeling experiments, a catalytic cycle was formulated, consisting of the following key steps (see Fig. 33): (1) quinoline and borane cleave H<sub>2</sub> heterolytically to generate the [qnoH]<sup>+</sup>[HB(p-C<sub>6</sub>F<sub>4</sub>H)<sub>2</sub>Mes]<sup>-</sup> intermediate; (2) this intermediate forms the qnoH<sub>2</sub>-1,2 organohydride in a step that is kinetically favored over the reduction to qnoH<sub>2</sub>-1,4; (3) quinoline is reduced by qnoH<sub>2</sub>-1,2 to afford qnoH<sub>2</sub>-1,4 (in a possibly H<sup>+</sup> or Lewis acid catalyzed step); (4) in the last step, the half-reduced qnoH<sub>2</sub>-1,4 is fully saturated again by the strong reducing agent qnoH<sub>2</sub>-1,2.

### 5.3 Related Studies in the Literature

As ramifications of the B(C<sub>6</sub>F<sub>5</sub>)<sub>3</sub>-catalyzed imine hydrogenations, we would like to direct the reader's attention to two experimental papers from the Stephan group. First, this kind of hydrogenation was later shown to provide modest to excellent diastereoselectivities in the reduction of chiral ketimines [126]. Apparently, the bulkiness of the hydride donor [HB(C<sub>6</sub>F<sub>5</sub>)<sub>3</sub>]<sup>-</sup> and the chiral center near to the imine carbon atom lead

to preferential attack from one of the diastereotopic faces, although the sense of diastereoselection was not easily interpretable. Second, the key steps of the hydrogenation can be combined in a different way in a reaction where  $\text{B}(\text{C}_6\text{F}_5)_3$  was shown to act as an imine/amine transfer hydrogenation catalyst [127].

In the FLP context, theoretical studies about various hydrogenation processes have been published. We have already mentioned Privalov's parallel work on imine hydrogenation via  $\text{B}(\text{C}_6\text{F}_5)_3$  [92]. He also reported an investigation of direct imine reduction catalyzed by the linked system  $\text{R}_2\text{P}-\text{C}_6\text{F}_4-\text{B}(\text{C}_6\text{F}_5)_2$ , confirming the two-step, proton-first mechanism [128] suggested from experiments [56]. A more complicated situation arises in the reduction of FLP-bound  $\text{CO}_2$  by ammonia-borane, reported experimentally by Stephan et al. [129] and studied computationally by Paul et al. [130], where a combination of stepwise and concerted reduction steps leads to the final methanol product.

A bolder application of computational chemistry is to analyze hitherto undiscovered molecules and reaction pathways with the aim of providing new ideas for experimental realization. The findings in Privalov's study [112] on the possibility of the conversion of alcohols to oxo compounds by  $\text{R}_2\text{P}-\text{BR}'_2$  phosphinoboranes still wait for experimental confirmation. A paper by the same research group showed that the catalytic reduction of carbonyl moieties via  $\text{B}(\text{C}_6\text{F}_5)_3$  should be feasible [93]; as discussed previously, experiments later confirmed that carbonyl/borane pairs can indeed cleave  $\text{H}_2$ , but side reactions not considered in the theoretical work still hamper the construction of catalytic systems [100]. Li, Zou, and coworkers envisioned that the dehydrogenation of ammonia-borane could be catalyzed by FLPs and confirmed computationally that this process should be feasible using the linked **tmp**- $\text{CH}_2-\text{C}_6\text{H}_4-\text{B}(\text{C}_6\text{F}_5)_2$  as catalyst [131]. In a parallel experimental study, Miller et al. revealed that  $\text{NH}_3\text{BH}_3$  can in fact react with a stoichiometric amount of the *t*- $\text{Bu}_3\text{P}/\text{B}(\text{C}_6\text{F}_5)_3$  pair to yield the dehydrogenated product [132].

Wang and coworkers have been perhaps the most active in the computational design of FLP catalysts. We have already mentioned their works on the  $\text{CH}_2$ -linked or similar intramolecular FLPs [63, 64]. Another paper from this group deals with ways of mimicking the electronic effects of transition metal pincer catalysts [96]. FLP systems have been engineered for the catalytic hydrogenation of imines [60, 62] and computed to be active for the reduction of ketones [95]. A simpler analogue was probed in the catalytic reduction of alkenes, imines, ketones, and silyl enol ethers [97]. Some of these highly optimized compounds seem to present a significant challenge for synthesis; nevertheless, experiments show that the design principles are successful in practice [43, 113].

## 6 Summary and Outlook

Within its only 6 years of existence, the field of FLP chemistry has undergone remarkable development. The range of FLP systems and explored reactions has grown significantly, and our understanding of this intriguing chemistry has also deepened. Hand in hand with experiments, computational studies provided insight

into many aspects of the sometimes surprising chemical behavior. We begin to see how thermodynamics controls FLP reactivity and to which extent this is determined by acid–base strength. We have an idea why it is difficult to detect the actual species reacting with  $H_2$ , and why it is reactive enough to break the strong H–H bond, approaching the activity of transition metal complexes. We have started to explore the intertwined catalytic cycles of FLP-mediated hydrogenations. Nevertheless, a number of new questions have also emerged from these studies, and many old ones have remained unanswered; here, we mention a couple of these open problems.

More and more pairs are discovered that are quenched in equilibrium and still react with  $H_2$ . In these systems, the acid–base properties affect both the dative bond strength and  $H^+/H^-$  binding. The overall effect on thermodynamics is therefore supposed to be more complex and may be worthy of more detailed study, in order to see where the boundary of classical and frustrated behavior can be pushed. Still in the realm of thermodynamics, the reversibility of  $H_2$  activation should be, to a first approximation, related to the  $\Delta G$  values, but our computations did not allow a clear-cut distinction on their basis. It remains to be seen whether more accurate thermodynamics or kinetic data, such as forward/backward free energy barriers, can explain the observed behavior.

Considering the mechanism of  $H_2$  cleavage, the cooperative Lewis acid/base mechanism was found to be in agreement with experiments and provides links to other  $H_2$  activating systems. Nevertheless, the proposed alternative, electric field based model comprises a conceptually different picture of bond activation; its limits of validity and usefulness still need to be explored. In any case, cooperative action of the acidic and basic components of an intermolecular FLP seems necessary, and so far no experimental evidence confirms the existence of the reactive, preorganized frustrated complexes. Here, more detailed computational studies on the dynamics of frustrated complex formation/dissociation and on its reaction with  $H_2$  can also uncover further aspects that might be expedient in FLP design. In contrast to all these mechanistic considerations, a stepwise mechanism was predicted for one particular FLP, but we do not know yet the factors determining the stepwise or concerted nature of the cleavage and whether these mechanisms imply different design principles. Finally, and more specifically, seemingly contradicting pieces of data are available for the  $H_2$  activation mechanism by the  $C_6F_4$ -linked systems, which would be interesting to clear up, not only because it is the first compound of its kind but also because it is one of the most active  $H_2$  cleavage systems.

In FLP-mediated hydrogenation catalysis we saw good correspondence between the data from theory and experiments. However, the scope of the investigated systems is limited, and there are still points not fully understood. An important example is the sense of diastereoselectivity in the hydrogenation of bulky imines; as selective catalysis is an important development goal today and easily realized via transition metal systems, further insight into the selectivity-determining step with FLPs would be essential.

In short, computational chemistry has been able to provide answers to a number of puzzling mechanistic questions in the field of FLPs, but a series of fascinating

problems are still ahead. Numerous laboratories around the world, including ours, are working to garner further insight and to complement the ongoing experimental efforts. It will be intriguing to see what directions the development will take, and how the lessons learned here will prove useful in other branches of chemistry.

**Acknowledgements** Our results presented here were obtained in a common effort with a number of outstanding colleagues, whose names are indicated on the original papers. We gratefully thank all of them for their valuable and enthusiastic contributions. Financial support from the Hungarian Scientific Research Fund (OTKA, grant K-81927) is acknowledged.

## References

1. Brown HC, Schlesinger HI, Cardon SZ (1942) Studies in stereochemistry. I. Steric strains as a factor in the relative stability of some coordination compounds of boron. *J Am Chem Soc* 64:325
2. Wittig G, Benz E (1959) Über das Verhalten von Dehydrobenzol gegenüber nucleophilen und elektrophilen Reagenzien. *Chem Ber* 92:1999
3. Tochtermann W (1966) Structures and reactions of organic ate-complexes. *Angew Chem Int Ed* 5:351
4. Welch GC, Cabrera L, Chase PA, Hollink E, Masuda JD, Wei P, Stephan DW (2007) Tuning Lewis acidity using the reactivity of “frustrated Lewis pairs”: facile formation of phosphine-boranes and cationic phosphonium-boranes. *Dalton Trans* 3407
5. Stephan DW (2008) “Frustrated Lewis pairs”: a concept for new reactivity and catalysis. *Org Biomol Chem* 6:1535
6. Welch GC, San Juan RR, Masuda JD, Stephan DW (2006) Reversible, metal-free hydrogen activation. *Science* 314:1124
7. Special issue (1–2) on catalytic hydrogenation (2003) *Adv Synth Catal* 345:1–323
8. Kubas GJ (2007) Fundamentals of H<sub>2</sub> binding and reactivity on transition metals underlying hydrogenase function and H<sub>2</sub> production and storage. *Chem Rev* 107:4152
9. Frey GD, Lavallo V, Donnadiou B, Schoeller WW, Bertrand G (2007) Facile splitting of hydrogen and ammonia by nucleophilic activation at a single carbon center. *Science* 316:439
10. Power PP (2011) Interaction of multiple bonded and unsaturated heavier main group compounds with hydrogen, ammonia, olefins, and related molecules. *Acc Chem Res* 44:627
11. Protchenko AV, Birj Kumar KH, Dange D, Schwarz AD, Vidovic D, Jones C, Kaltsoyannis N, Mountford P, Aldridge S (2012) A stable two-coordinate acyclic silylene. *J Am Chem Soc* 134:6500
12. Spielmann J, Buch F, Harder S (2008) Early main-group metal catalysts for the hydrogenation of alkenes with H<sub>2</sub>. *Angew Chem Int Ed* 47:9434
13. Fan C, Mercier LG, Piers WE, Tuononen HM, Parvez M (2010) Dihydrogen activation by antiaromatic pentaarylboroles. *J Am Chem Soc* 132:9604
14. Stephan DW, Erker G (2010) Frustrated Lewis pairs: metal-free hydrogen activation and more. *Angew Chem Int Ed* 49:46
15. Stephan DW (2012) “Frustrated Lewis pair” hydrogenations. *Org Biomol Chem* 10:5740
16. Stephan DW, Greenberg S, Graham TW, Chase P, Hastie JJ, Geier SJ, Farrell JM, Brown CC, Heiden ZM, Welch GC, Ullrich M (2011) Metal-free catalytic hydrogenation of polar substrates by frustrated Lewis pairs. *Inorg Chem* 50:12338
17. Rokob TA, Hamza A, Stirling A, Soós T, Pápai I (2008) Turning frustration into bond activation: a theoretical mechanistic study on heterolytic hydrogen splitting by frustrated Lewis pairs. *Angew Chem Int Ed* 47:2435

18. Stirling A, Hamza A, Rokob TA, Pápai I (2008) Concerted attack of frustrated Lewis acid–base pairs on olefinic double bonds: a theoretical study. *Chem Commun* 3148
19. Rokob TA, Hamza A, Stirling A, Pápai I (2009) On the mechanism of  $B(C_6F_5)_3$ -catalyzed direct hydrogenation of imines: inherent and thermally induced frustration. *J Am Chem Soc* 131:2029
20. Rokob TA, Hamza A, Pápai I (2009) Rationalizing the reactivity of frustrated Lewis pairs: thermodynamics of  $H_2$  activation and the role of acid–base properties. *J Am Chem Soc* 131:10701
21. Hamza A, Stirling A, Rokob TA, Pápai I (2009) Mechanism of hydrogen activation by frustrated Lewis pairs: a molecular orbital approach. *Int J Quantum Chem* 109:2416
22. Rokob TA (2009) Computational studies on small molecule activation via cooperative Lewis pairs. Dissertation, Eötvös Loránd University
23. Erős G, Mehdi H, Pápai I, Rokob TA, Király P, Tárkányi G, Soós T (2010) Expanding the scope of metal-free catalytic hydrogenation through frustrated Lewis pair design. *Angew Chem Int Ed* 49:6559
24. Erős G, Nagy K, Mehdi H, Pápai I, Nagy P, Király P, Tárkányi G, Soós T (2012) Catalytic hydrogenation with frustrated Lewis pairs: selectivity achieved by size-exclusion design of Lewis acids. *Chem Eur J* 18:574
25. Bakó I, Stirling A, Bálint S, Pápai I (2012) Association of frustrated phosphine–borane pairs in toluene: molecular dynamics simulations. *Dalton Trans* 41:9023
26. Grimme S (2011) Density functional theory with London dispersion corrections. *Comput Mol Sci* 1:211
27. Zhao Y, Truhlar DG (2008) Density functionals with broad applicability in chemistry. *Acc Chem Res* 41:157
28. Vydrov OA, Van Voorhis T (2010) Nonlocal van der Waals density functional: the simpler the better. *J Chem Phys* 133:244103
29. Grimme S, Antony J, Ehrlich S, Krieg H (2010) A consistent and accurate ab initio parametrization of density functional dispersion correction (DFT-D) for the 94 elements H–Pu. *J Chem Phys* 132:154104
30. Grimme S (2003) Improved second-order Møller–Plesset perturbation theory by separate scaling of parallel- and antiparallel-spin pair correlation energies. *J Chem Phys* 118:9095
31. Pfäendner J, Yu X, Broadbelt LJ (2007) The 1-D hindered rotor approximation. *Theor Chem Acc* 118:881
32. Lin CY, Izgorodina EI, Coote ML (2008) How accurate are approximate methods for evaluating partition functions for hindered internal rotations? *J Phys Chem A* 112:1956
33. Mennucci B (2012) Polarizable continuum model. *Comput Mol Sci* 2:386
34. Tomasi J, Mennucci B, Cammi R (2005) Quantum mechanical continuum solvation models. *Chem Rev* 105:2999
35. Cramer CJ, Truhlar DG (2008) A universal approach to solvation modeling. *Acc Chem Res* 41:760
36. Klamt A, Mennucci B, Tomasi J, Barone V, Curutchet C, Orozco M, Luque FJ (2009) On the performance of continuum solvation methods. A comment on “Universal approaches to solvation modeling”. *Acc Chem Res* 42:489
37. Cramer CJ, Truhlar DG (2009) Reply to comment on “A universal approach to solvation modeling”. *Acc Chem Res* 42:493
38. Tomasi J, Mennucci B, Cancès E (1999) The IEF version of the PCM solvation method: an overview of a new method addressed to study molecular solutes at the QM ab initio level. *J Mol Struct (Theochem)* 464:211
39. Marenich AV, Cramer CJ, Truhlar DG (2009) Universal solvation model based on solute electron density and on a continuum model of the solvent defined by the bulk dielectric constant and atomic surface tensions. *J Phys Chem B* 113:6378
40. Liu BH, Li ZP (2009) A review: Hydrogen generation from borohydride hydrolysis reaction. *J Power Sources* 187:527

41. Welch GC, Stephan DW (2007) Facile heterolytic cleavage of dihydrogen by phosphines and boranes. *J Am Chem Soc* 129:1880
42. Mahdi T, Heiden ZM, Grimme S, Stephan DW (2012) Metal-free aromatic hydrogenation: aniline to cyclohexyl-amine derivatives. *J Am Chem Soc* 134:4088
43. Bertini F, Lyaskovskyy V, Timmer BJJ, de Kanter FJJ, Lutz M, Ehlers AW, Slootweg JC, Lammertsma K (2012) Preorganized frustrated Lewis pairs. *J Am Chem Soc* 134:201
44. Chase PA, Jurca T, Stephan DW (2008) Lewis acid-catalyzed hydrogenation: B(C<sub>6</sub>F<sub>5</sub>)<sub>3</sub>-mediated reduction of imines and nitriles with H<sub>2</sub>. *Chem Commun* 1701
45. Geier SJ, Stephan DW (2009) Lutidine/B(C<sub>6</sub>F<sub>5</sub>)<sub>3</sub>: at the boundary of classical and frustrated Lewis pair reactivity. *J Am Chem Soc* 131:3476
46. Sumerin V, Schulz F, Atsumi M, Wang C, Nieger M, Leskelä M, Repo T, Pykkö P, Rieger B (2008) Molecular tweezers for hydrogen: synthesis, characterization, and reactivity. *J Am Chem Soc* 130:14117
47. Spies P, Schwendemann S, Lange S, Kehr G, Fröhlich R, Erker G (2008) Metal-free catalytic hydrogenation of enamines, imines, and conjugated phosphinoalkenylboranes. *Angew Chem Int Ed* 47:7543
48. Staubitz A, Besora M, Harvey JN, Manners I (2008) Computational analysis of amine–borane adducts as potential hydrogen storage materials with reversible hydrogen uptake. *Inorg Chem* 47:5910
49. DuBois MR, DuBois DL (2009) The roles of the first and second coordination spheres in the design of molecular catalysts for H<sub>2</sub> production and oxidation. *Chem Soc Rev* 38:62
50. Spies P, Erker G, Kehr G, Bergander K, Fröhlich R, Grimme S, Stephan DW (2007) Rapid intramolecular heterolytic dihydrogen activation by a four-membered heterocyclic phosphane–borane adduct. *Chem Commun* 5072
51. Wang H, Fröhlich R, Kehr G, Erker G (2008) Heterolytic dihydrogen activation with the 1,8-bis(diphenylphosphino)naphthalene/B(C<sub>6</sub>F<sub>5</sub>)<sub>3</sub> pair and its application for metal-free catalytic hydrogenation of silyl enol ethers. *Chem Commun* 5966
52. Ullrich M, Lough AJ, Stephan DW (2009) Reversible, metal-free, heterolytic activation of H<sub>2</sub> at room temperature. *J Am Chem Soc* 131:52
53. Holschumacher D, Bannenberg T, Hrib CG, Jones PG, Tamm M (2008) Heterolytic dihydrogen activation by a frustrated carbene–borane Lewis pair. *Angew Chem Int Ed* 47:7428
54. Chase PA, Stephan DW (2008) Hydrogen and amine activation by a frustrated Lewis pair of a bulky *N*-heterocyclic carbene and B(C<sub>6</sub>F<sub>5</sub>)<sub>3</sub>. *Angew Chem Int Ed* 47:7433
55. Sumerin V, Schulz F, Nieger M, Leskelä M, Repo T, Rieger B (2008) Facile heterolytic H<sub>2</sub> activation by amines and B(C<sub>6</sub>F<sub>5</sub>)<sub>3</sub>. *Angew Chem Int Ed* 47:6001
56. Chase PA, Welch GC, Jurca T, Stephan DW (2007) Metal-free catalytic hydrogenation. *Angew Chem Int Ed* 46:8050. Corrigendum: Chase PA, Welch GC, Jurca T, Stephan DW (2007) Metal-free catalytic hydrogenation. *Angew Chem Int Ed* 46:9136
57. Roesler R, Piers WE, Parvez M (2003) Synthesis, structural characterization and reactivity of the amino borane 1-(NPh<sub>2</sub>)-2-[B(C<sub>6</sub>F<sub>5</sub>)<sub>2</sub>]C<sub>6</sub>H<sub>4</sub>. *J Organomet Chem* 680:218
58. Geier SJ, Gilbert TM, Stephan DW (2008) Activation of H<sub>2</sub> by phosphinoboranes R<sub>2</sub>P–B(C<sub>6</sub>F<sub>5</sub>)<sub>2</sub>. *J Am Chem Soc* 130:12632
59. Chernichenko K, Nieger M, Leskelä M, Repo T (2012) Hydrogen activation by 2-boryl-*N*, *N*-dialkylanilines: a revision of Piers' ansa-aminoborane. *Dalton Trans* 41:9029
60. Zhao L, Li H, Lu G, Wang ZX (2010) Computational design of metal-free catalysts for catalytic hydrogenation of imines. *Dalton Trans* 39:4038
61. Berke H (2010) Conceptual approach to the reactivity of dihydrogen. *ChemPhysChem* 11:1837
62. Zhao L, Li H, Lu G, Huang F, Zhang C, Wang ZX (2011) Metal-free catalysts for hydrogenation of both small and large imines: a computational experiment. *Dalton Trans* 40:1929

63. Wang ZX, Lu G, Li HX, Zhao L (2010) Encumbering the intramolecular  $\pi$  donation by using a bridge: a strategy for designing metal-free compounds to hydrogen activation. *Chin Sci Bull* 55:239
64. Lu G, Li H, Zhao L, Huang F, Wang ZX (2010) Computationally designed metal-free hydrogen activation site: reaching the reactivity of metal–ligand bifunctional hydrogenation catalysts. *Inorg Chem* 49:295
65. Nyhlén J, Privalov T (2009) “Frustration” of orbital interactions in Lewis base/Lewis acid adducts: a computational study of  $H_2$  uptake by phosphanylboranes  $R_2P=BR'_2$ . *Eur J Inorg Chem* 2759
66. Pyykkö P, Wang C (2010) Theoretical study of  $H_2$  splitting and storage by boron–nitrogen-based systems: a bimolecular case and some qualitative aspects. *Phys Chem Chem Phys* 12: 149
67. Gao S, Wu W, Mo Y (2009) The B–H...H–P dihydrogen bonding in ion pair complexes  $[(CF_3)_3BH^-][HPH_{3-n}(Me)_n^+]$  ( $n = 0-3$ ) and its implication in  $H_2$  elimination and activation reactions. *J Phys Chem A* 113:8108
68. Gao S, Wu W, Mo Y (2011) Steric and electronic effects on the heterolytic  $H_2$ -splitting by phosphine-boranes  $R_3B/PR'_3$  ( $R = C_6F_5, Ph$ ;  $R' = C_6H_2Me_3, tBu, Ph, C_6F_5, Me, H$ ): a computational study. *Int J Quantum Chem* 111:3761
69. Wu D, Jia D, Liu L, Zhang L, Guo J (2010) Reactivity of 2,6-lutidine/ $BR_3$  and pyridine/ $BR_3$  Lewis pairs ( $R = F, Me, C_6F_5$ ): a density functional study. *J Phys Chem A* 114:11738
70. Wu D, Jia D, Liu A, Liu L, Guo J (2012) Theoretical study on the reactivity of Lewis pairs  $PR_3/B(C_6F_5)_3$  ( $R = Me, Ph, tBu, C_6F_5$ ). *Chem Phys Lett* 541:1
71. Neu RC, Ouyang EY, Geier SJ, Zhao X, Ramos A, Stephan DW (2010) Probing substituent effects on the activation of  $H_2$  by phosphorus and boron frustrated Lewis pairs. *Dalton Trans* 39:4285
72. Jiang C, Blacque O, Fox T, Berke H (2011) Heterolytic cleavage of  $H_2$  by frustrated B/N Lewis pairs. *Organometallics* 30:2117
73. Jiang C, Blacque O, Fox T, Berke H (2011) Reversible, metal-free hydrogen activation by frustrated Lewis pairs. *Dalton Trans* 40:1091
74. Kronig S, Theuergarten E, Holschumacher D, Bannenberg T, Daniliuc CG, Jones PG, Tamm M (2011) Dihydrogen activation by frustrated carbene–borane Lewis pairs: an experimental and theoretical study of carbene variation. *Inorg Chem* 50:7344
75. Geier SJ, Gille AL, Gilbert TM, Stephan DW (2009) From classical adducts to frustrated Lewis pairs: steric effects in the interactions of pyridines and  $B(C_6F_5)_3$ . *Inorg Chem* 48:10466
76. Ullrich M, Lough AJ, Stephan DW (2010) Dihydrogen activation by  $B(p-C_6F_4H)_3$  and phosphines. *Organometallics* 29:3647
77. Caputo CB, Geier SJ, Winkelhaus D, Mitzel NW, Vukotic VN, Loeb SJ, Stephan DW (2012) Reactions of substituted pyridines with electrophilic boranes. *Dalton Trans* 41:2131
78. Voss T, Mahdi T, Otten E, Fröhlich R, Kehr G, Stephan DW, Erker G (2012) Frustrated Lewis pair behavior of intermolecular amine/ $B(C_6F_5)_3$  pairs. *Organometallics* 31:2367
79. Robertson APM, Whittell GR, Staubitz A, Lee K, Lough AJ, Manners I (2011) Experimental and theoretical studies of the potential interconversion of the amine–borane  $iPr_2NH \cdot BH(C_6F_5)_2$  and the aminoborane  ${}^1Pr_2N=B(C_6F_5)_2$  involving hydrogen loss and uptake. *Eur J Inorg Chem* 5279
80. Stute A, Kehr G, Fröhlich R, Erker G (2011) Chemistry of a geminal frustrated Lewis pair featuring electron withdrawing  $C_6F_5$  substituents at both phosphorus and boron. *Chem Commun* 47:4288
81. Rosorius C, Kehr G, Fröhlich R, Grimme S, Erker G (2011) Electronic control of frustrated Lewis pair behavior: chemistry of a geminal alkylidene-bridged per-pentafluorophenylated P/B pair. *Organometallics* 30:4211
82. Sumerin V, Chernichenko K, Nieger M, Leskelä M, Rieger B, Repo T (2011) Highly active metal-free catalysts for hydrogenation of unsaturated nitrogen-containing compounds. *Adv Synth Catal* 353:2093

83. Guo Y, Li S (2008) A novel addition mechanism for the reaction of “frustrated Lewis pairs” with olefins. *Eur J Inorg Chem* 2501
84. Gille AL, Gilbert TM (2008) Donor–acceptor dissociation energies of group 13–15 donor–acceptor complexes containing fluorinated substituents: approximate Lewis acidities of  $(F_3C)_3M$  vs  $(F_5C_6)_3M$  and the effects of phosphine steric bulk. *J Chem Theory Comput* 4:1681
85. Kim HW, Rhee YM (2009) Dispersion-oriented soft interaction in a frustrated Lewis pair and the entropic encouragement effect in its formation. *Chem Eur J* 15:13348
86. Grimme S, Kruse H, Goerigk L, Erker G (2010) The mechanism of dihydrogen activation by frustrated Lewis pairs revisited. *Angew Chem Int Ed* 49:1402
87. Mück-Lichtenfeld C, Grimme S (2012) Theoretical analysis of cooperative effects of small molecule activation by frustrated Lewis pairs. *Dalton Trans* 41:9111
88. Mömning CM, Frömel S, Kehr G, Fröhlich R, Grimme S, Erker G (2009) Reactions of an intramolecular frustrated Lewis pair with unsaturated substrates: evidence for a concerted olefin addition reaction. *J Am Chem Soc* 131:12280
89. Zhao X, Stephan DW (2011) Olefin–borane “van der Waals complexes”: intermediates in frustrated Lewis pair addition reactions. *J Am Chem Soc* 133:12448
90. Brown HC (1956) Chemical effects of steric strains. *J Chem Soc* 1248
91. Zhao LL, Huang F, Lu G, Wang ZX, Schleyer PvR (2012) Why the mechanisms of digermynes and distannynes reactions with  $H_2$  differ so greatly. *J Am Chem Soc* 134:8856
92. Privalov T (2009) The role of amine– $B(C_6F_5)_3$  adducts in the catalytic reduction of imines with  $H_2$ : a computational study. *Eur J Inorg Chem* 2229
93. Nyhlén J, Privalov T (2009) On the possibility of catalytic reduction of carbonyl moieties with tris(pentafluorophenyl)borane and  $H_2$ : a computational study. *Dalton Trans* 5780
94. Li HX, Zhao LL, Lu G, Mo YR, Wang ZX (2010) Insight into the relative reactivity of “frustrated Lewis pairs” and stable carbenes in activating  $H_2$  and  $CH_4$ : a comparative computational study. *Phys Chem Chem Phys* 12:5268
95. Li HX, Zhao LL, Lu G, Wang ZX (2010) Catalytic metal-free ketone hydrogenation: a computational experiment. *Dalton Trans* 39:5519
96. Lu G, Li HX, Zhao LL, Huang F, Wang ZX (2011) Designing metal-free catalysts by mimicking transition-metal pincer templates. *Chem Eur J* 17:2038
97. Zhao LL, Lu G, Huang F, Wang ZX (2012) A computational experiment to study hydrogenations of various unsaturated compounds catalyzed by a rationally designed metal-free catalyst. *Dalton Trans* 41:4674
98. Schirmer B, Grimme S (2010) Electric field induced activation of  $H_2$  – can DFT do the job? *Chem Commun* 46:7942
99. Camaioni DM, Ginovska-Pangovska B, Schenter GK, Kathmann SM, Autrey T (2012) Analysis of the activation and heterolytic dissociation of  $H_2$  by frustrated Lewis pairs:  $NH_3/BX_3$  ( $X = H, F, \text{ and } Cl$ ). *J Phys Chem A* 116:7228
100. Lindqvist M, Sarnela N, Sumerin V, Chernichenko K, Leskelä M, Repo T (2012) Heterolytic dihydrogen activation by  $B(C_6F_5)_3$  and carbonyl compounds. *Dalton Trans* 41:4310
101. Sumerin V, Schulz F, Nieger M, Atsumi M, Wang C, Leskelä M, Pyykkö P, Repo T, Rieger B (2009) Experimental and theoretical treatment of hydrogen splitting and storage in boron–nitrogen systems. *J Organomet Chem* 694:2654
102. Chen D, Klankermayer J (2008) Metal-free catalytic hydrogenation of imines with tris(perfluorophenyl)borane. *Chem Commun* 2130
103. Palomas D, Holle S, Inés B, Bruns H, Goddard R, Alcarazo M (2012) Synthesis and reactivity of electron poor allenes: formation of completely organic frustrated Lewis pairs. *Dalton Trans* 41:9073
104. Kwon HJ, Kim HW, Rhee YM (2011) On the mechanism of irreversible carbon dioxide binding with a frustrated Lewis pair: solvent-assisted frustration and transition-state entropic encouragement. *Chem Eur J* 17:6501



105. Jiang C, Stephan DW (2012) Phosphinimine–borane combinations in frustrated Lewis pair chemistry. *Dalton Trans.* doi:10.1039/c2dt30720k
106. Lu Z, Cheng Z, Chen Z, Weng L, Li ZH, Wang H (2011) Heterolytic cleavage of dihydrogen by “frustrated Lewis pairs” comprising bis(2,4,6-tris(trifluoromethyl)phenyl)borane and amines: stepwise versus concerted mechanism. *Angew Chem Int Ed* 50:12227
107. Nikonov GI, Vyboishchikov SF, Shirobokov OG (2012) Facile activation of H–H and Si–H bonds by boranes. *J Am Chem Soc* 134:5488
108. Kubas GJ (2006) Breaking the H<sub>2</sub> marriage and reuniting the couple. *Science* 314:1096
109. Guo Y, Li S (2008) Unusual concerted Lewis acid–Lewis base mechanism for hydrogen activation by a phosphine–borane compound. *Inorg Chem* 47:6212
110. Rajeev R, Sunoj RB (2009) On the origin of reversible hydrogen activation by phosphine–boranes. *Chem Eur J* 15:12846
111. Schulz F, Sumerin V, Heikkinen S, Pedersen B, Wang C, Atsumi M, Leskelä M, Repo T, Pyykkö P, Petry W, Rieger B (2011) Molecular hydrogen tweezers: structure and mechanisms by neutron diffraction, NMR, and deuterium labeling studies in solid and solution. *J Am Chem Soc* 133:20245
112. Privalov T (2009) On the possibility of conversion of alcohols to ketones and aldehydes by phosphinoboranes R<sub>2</sub>PBR'R'': a computational study. *Chem Eur J* 15:1825
113. Theuergarten E, Schlüns D, Grunenberg J, Daniliuc CG, Jones PG, Tamm M (2010) Intramolecular heterolytic dihydrogen cleavage by a bifunctional frustrated pyrazolylborane Lewis pair. *Chem Commun* 46:8561
114. Marwitz AJV, Dutton JL, Mercier LG, Piers WE (2011) Dihydrogen activation with <sup>t</sup>Bu<sub>3</sub>P/B(C<sub>6</sub>F<sub>5</sub>)<sub>3</sub>: a chemically competent indirect mechanism via in situ-generated *p*-<sup>t</sup>Bu<sub>2</sub>P–C<sub>6</sub>F<sub>4</sub>–B(C<sub>6</sub>F<sub>5</sub>)<sub>2</sub>. *J Am Chem Soc* 133:10026
115. Piers WE, Marwitz AJV, Mercier LG (2011) Mechanistic aspects of bond activation with perfluoroarylboranes. *Inorg Chem* 50:12252
116. Jiang C, Blacque O, Berke H (2009) Metal-free hydrogen activation and hydrogenation of imines by 1,8-bis(dipentafluorophenylboryl)naphthalene. *Chem Commun* 5518
117. Blackwell JM, Sonmor ER, Scoccitti T, Piers WE (2000) B(C<sub>6</sub>F<sub>5</sub>)<sub>3</sub>-catalyzed hydrosilation of imines via silyliminium intermediates. *Org Lett* 2:3921
118. Rendler S, Oestreich M (2008) Conclusive evidence for an S<sub>N</sub>2-Si mechanism in the B(C<sub>6</sub>F<sub>5</sub>)<sub>3</sub>-catalyzed hydrosilylation of carbonyl compounds: implications for the related hydrogenation. *Angew Chem Int Ed* 47:5997
119. Parks DJ, Blackwell JM, Piers WE (2000) Studies on the mechanism of B(C<sub>6</sub>F<sub>5</sub>)<sub>3</sub>-catalyzed hydrosilation of carbonyl functions. *J Org Chem* 65:3090
120. Chen D, Leich V, Pan F, Klankermayer J (2012) Enantioselective hydrosilylation with chiral frustrated Lewis pairs. *Chem Eur J* 18:5184
121. Hog DT, Oestreich M (2009) B(C<sub>6</sub>F<sub>5</sub>)<sub>3</sub>-catalyzed reduction of ketones and imines using silicon-stereogenic silanes: stereoinduction by single-point binding. *Eur J Org Chem* 5047
122. Kozuch S, Shaik S (2011) How to conceptualize catalytic cycles? The energetic span model. *Acc Chem Res* 44:101
123. Blackmond DG (2009) An examination of the role of autocatalytic cycles in the chemistry of proposed primordial reactions. *Angew Chem Int Ed* 48:386
124. Geier SJ, Chase PA, Stephan DW (2010) Metal-free reductions of *N*-heterocycles via Lewis acid catalyzed hydrogenation. *Chem Commun* 46:4884
125. Mani NS, Chen P, Jones TK (1999) Addition of Grignard reagents to quinolinium salts: evidence for a unique redox reaction between a 1,4- and a 1,2-dihydroquinoline. *J Org Chem* 64:6911
126. Heiden ZM, Stephan DW (2011) Metal-free diastereoselective catalytic hydrogenations of imines using B(C<sub>6</sub>F<sub>5</sub>)<sub>3</sub>. *Chem Commun* 47:5729
127. Farrell JM, Heiden ZM, Stephan DW (2011) Metal-free transfer hydrogenation catalysis by B(C<sub>6</sub>F<sub>5</sub>)<sub>3</sub>. *Organometallics* 30:4497

128. Privalov T (2009) Hydrogenation of imines by phosphonium borate zwitterions: a theoretical study. *Dalton Trans* 1321
129. Ménard G, Stephan DW (2010) Room temperature reduction of CO<sub>2</sub> to methanol by Al-based frustrated Lewis pairs and ammonia borane. *J Am Chem Soc* 132:1796
130. Roy L, Zimmerman PM, Paul A (2011) Changing lanes from concerted to stepwise hydrogenation: the reduction mechanism of frustrated Lewis acid–base pair trapped CO<sub>2</sub> to methanol by ammonia–borane. *Chem Eur J* 17:435
131. Guo Y, He X, Li Z, Zou Z (2010) Theoretical study on the possibility of using frustrated Lewis pairs as bifunctional metal-free dehydrogenation catalysts of ammonia–borane. *Inorg Chem* 49:3419
132. Miller AJM, Bercaw JE (2010) Dehydrogenation of amine–boranes with a frustrated Lewis pair. *Chem Commun* 46:1709

# Quantum Chemistry of FLPs and Their Activation of Small Molecules: Methodological Aspects

Birgitta Schirmer and Stefan Grimme

**Abstract** We discuss methodological aspects of the computation of structures and energies of three common FLPs which are able to activate dihydrogen under ambient conditions. The effect of London dispersion corrections by the DFT-D3 scheme and solvent as well as rovibrational corrections to yield free reaction enthalpies in solutions are described. Common density functionals of semi-local, hybrid, and double-hybrid type as well as (SCS-)MP2 wave function based methods with very large AO basis sets are investigated. It is found that reliable structures (in comparison to X-ray data) are already obtained using relatively cheap DFT methods like TPSS-D3/TZ. The variations between different density functionals for electronic reaction energies are small to moderate (1–2 kcal/mol which is about 10% of the H<sub>2</sub> was addition energy). Dispersion corrections are found to be essential for accurate thermochemistry. Computed free H<sub>2</sub> reaction enthalpies in the gas phase are close to zero while values computed in common solvents with the COSMO-RS continuum solvation model are strongly exergonic (about –10 kcal/mol in CH<sub>2</sub>Cl<sub>2</sub>). This new finding emphasizes the important role of the solvent for FLP chemistry involving zwitterionic species. According to our results the future for reliable quantum chemistry of FLP processes is bright.

**Keywords** (SCS-)MP2 · Calculations · DFT · FLP · Free enthalpy calculations · H<sub>2</sub>-activation · London dispersion · Solvent effects

---

B. Schirmer  
Organisch-Chemisches Institut, Westfälische Wilhelms-Universität Münster, Corrensstr 40,  
48153 Münster, Germany

S. Grimme (✉)  
Mulliken Center for Theoretical Chemistry, Institut für Physikalische und Theoretische Chemie,  
Universität Bonn, Beringstr. 4, 53115 Bonn, Germany  
e-mail: [grimme@thch.uni-bonn.de](mailto:grimme@thch.uni-bonn.de)

## Contents

1	Introduction .....	214
2	Example Systems .....	215
3	Geometry Optimizations .....	217
4	Electronic Energy Calculations .....	220
5	Thermal Corrections in the Gas Phase .....	224
6	Solvation Effects .....	225
7	Conclusions .....	227
	References .....	228

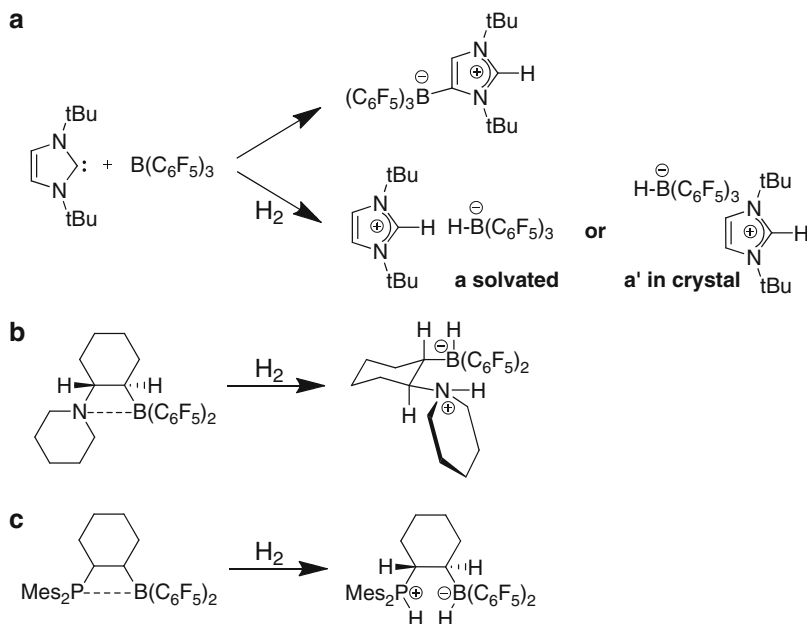
## 1 Introduction

Activation reactions have always been a major point of interest to the chemical community, but lately some change has happened in this field. The discovery of Frustrated Lewis Pairs (FLPs) some years ago [1] shifted some attention from metal-mediated to metal-free activation reactions. Various FLPs and even more possible substrates were discussed, discovered, and invented by several groups all over the world [2]. Of course it did not take long until the quantum chemical community also became interested in this aspiring topic.

Since then, several dozens of studies have been published discussing geometries, energies, orbital interactions, suggesting new mechanistic pathways, and proving why (or why not) a reaction would be possible in experiment. As one may expect, the theoretical approaches were as manifold as the studies, some suggesting M05-2X as a good Density Functional Theory (DFT) method for these systems [3, 4], some relying on “good old” B3LYP/6-31G\* [5–7], some stressing the importance of dispersion effects [8], and some preferring wave function based methods like MP2 [9, 10]. Also, there seemed to be no consensus on whether it would be necessary to include statistical thermodynamic corrections or solvent effects or even on which method would be appropriate for a decent geometry optimization of molecular structures.

For this reason we decided to have a closer look at the various methodological aspects of quantum chemical studies on FLPs and their prototypical reactions. We would like to give the reader some suggestions on how to produce accurate quantum chemical *ab initio* results for structures and thermodynamic properties. Mechanistic aspects as well as theoretical bonding analyses will not be considered (for a recent theoretical study of cooperative phenomena in FLP reactions see [11]).

For this purpose we chose three sample FLP reactions from the literature which shall be introduced shortly in the next section. Afterwards, we will show how to calculate step by step accurate free reaction enthalpy ( $\Delta G$ ) values starting from, for example, experimental X-ray structures. We will initially study the computation of characteristic bond distances, will then have a closer look at electronic energies, (statistical) thermal corrections yielding  $\Delta G_{\text{gas}}$ , and will finally discuss the importance of solvation leading to accurate  $\Delta G_{\text{solution}}$  values. We concentrate here on equilibrium properties, which seems to be appropriate when discussing many FLP systems because the corresponding reaction barriers are small (thermodynamic control).



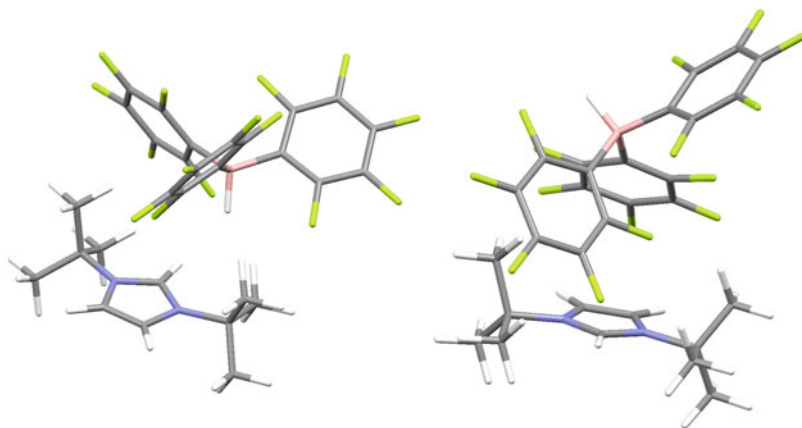
**Scheme 1** Structures of the three selected example systems

## 2 Example Systems

We selected three different example FLP systems from the literature which shall now be introduced (Scheme 1).

The first system – from now on dubbed **a** – was synthesized by the group of Matthias Tamm in 2008 [12]. It consists of the commonly used Lewis acid (LA)  $B(C_6F_5)_3$  (=BCF) and an *N*-heterocyclic carbene as Lewis basic part. These compounds have been shown to activate different molecules successfully, especially  $H_2$ , provided that the substituents on the nitrogen atoms are chosen to be sufficiently large and bulky [12]. For this combination a crystal structure of an adduct was obtained which shows an unexpected orientation – the boron compound has added to one of the carbons in the double bond of the heterocycle while the hydrogen which was originally occupying this position has moved to the carbene-carbon. This leads to a negative charge on the boron atom and a positive charge in the heterocycle where it is delocalized over the carbon and the two nitrogens. This “abnormal” adduct was reasoned to be a dead-end for further activation reactions due to its high thermodynamic stability and hence a second “classical” adduct was suggested. Since a crystal structure of this thermodynamically less stable adduct could not be obtained, we decided not to include it in this study.

Upon addition of  $H_2$  the hydrogenation product is formed which also exhibits an untypical orientation. The X-ray structure shows that the two fragments of the



**Fig. 1** TPSS-D3 optimized structures of systems **a** (from X-ray) and **a'** (suggested structure in solution)

zwitterionic complex are oriented towards each other in such a way that the newly added hydrogens face opposite directions. In this case, we suggest a different structure **a'** in which the hydrogen atoms face each other and which can be reasoned to originate directly from the hydrogenation reaction. Probably this structure exists in solution and only rearranges to the observed conformer in the crystal where packing as well as long-range electrostatic effects play a role. Both structures are shown in Fig. 1.

The second system we chose to investigate was presented by the group of Gerhard Erker in 2011 [13]. This FLP **b** was made via a hydroboration reaction of the enamine piperidino-cyclohexene with  $\text{HB}(\text{C}_6\text{F}_5)_2$ . X-ray analysis reveals that it consists of a chair-shaped cyclohexene ring to which the boron and nitrogen components are bound in adjacent equatorial positions. The bond between them closes a strained four-membered ring which is annellated to the cyclohexane ring. Interestingly, this compound bears two chiral centers on the carbons directly connected to B and N. Their orientation is dictated by the procedure in which the compound was made and is therefore fixed for this system. Upon reaction with  $\text{H}_2$  the B–N bond opens and a zwitterionic hydrogenation product is formed in which the hydrogen atoms originating from  $\text{H}_2$  point towards each other.

One year earlier the same group suggested another FLP [14] which will serve as our third example in this study. Compound **c** resembles **b** in that it also contains a chair-shaped cyclohexane ring to which a  $\text{B}(\text{C}_6\text{F}_5)_2$  moiety is bound. In contrast to **b**, the Lewis base part in this FLP is a phosphane with two large mesityl substituents. A weak bond between LA and LB can also be observed here as well as the chirality on the C1 and C2 atoms as explained for structure **b**. The behavior upon addition of gaseous  $\text{H}_2$  is also as expected – the four-membered ring opens and the zwitterionic hydrogenation product forms.

### 3 Geometry Optimizations

The first and maybe most important prerequisite to get realistic computational results is, of course, a good molecular structure. Since we explicitly chose systems for which crystal structures are available, we already have good starting points. Although this is by no means mandatory and one could start the modeling from scratch, it is clear that many of the functional FLPs often contain large groups with some flexibility which would require systematic conformational searches.

Due to the size of the systems, wave function based methods are usually not feasible for geometry optimization and density functional theory (DFT) is the method of choice. Our experience over the years in dozens of applications has shown that structures computed with the (dispersion-corrected) meta-GGA functional TPSS-D3 [15, 16] compare very well with experimental data. This also holds for non-covalently bound systems [16, 17]. For complicated cases, for example transition metal complexes, TPSS has also been found to perform very well [18].

Another point of discussion and important aspect in terms of computing time as well as accuracy is the choice of a decent atomic orbital (AO) basis set. To investigate the effect of the basis set size on the accuracy of the geometry we optimized all tested FLP-structures with three different Gaussian-AO basis sets: the split-valence double zeta basis set def-SV(P), the bigger triple zeta basis set def2-TZVP, and the large quadruple zeta basis set def2-QZVP as implemented in the TURBOMOLE 6.3 suite of programs [19, 20]. The latter basis provides results very close to the Complete Basis Set (CBS) limit for many properties with semi-local or hybrid density functionals.

These geometry optimizations were all carried out twice, first with the plain density functional and then including the atom-pair wise D3 London dispersion correction recently developed in our group [16, 17]. This enables us to discuss the effect of dispersion on the quality of the resulting structures. Both calculations used the experimental crystal structure as a starting point.

The D3-dispersion correction was constructed to correct for the asymptotically incorrect behavior of most commonly available density functionals in an easily applicable way and at almost no additional computational costs. This is achieved by calculating a dispersion term which is added to the energy from the density functional calculation. The general formula used for this is

$$E_{disp}^{DFT-D3(BJ)} = -\frac{1}{2} \sum_{A \neq B} \sum_{n=6,8} s_n \frac{C_n^{AB}}{R_{AB}^n + f_{damp}(R_{AB}^0)^n}$$

in which the sum is over all atom pairs in the system,  $C_n^{AB}$  is the  $n$ th-order dispersion coefficient for each atom pair  $AB$ , and  $R_{AB}$  is the distance between these two atoms, while  $s_n$  is a global scaling factor depending on the functional. The damping function  $f_{damp}$  is necessary to avoid near-singularities for small values of  $R$  and

**Table 1** Geometry data for structure **a** (bond lengths  $r$  in Å, angle  $\alpha$  in degree)

Property	Without dispersion correction			With D3 correction			X-ray data
	def-SV(P)	def2-TZVP	def2-QZVP	def-SV(P)	def2-TZVP	Def2-QZVP	
$r(\text{B-Ring})$	1.670	1.665	1.665	1.657	1.652	1.651	1.650
$\alpha(\text{NCN})$	109.9	109.9	109.9	109.5	109.4	109.4	110.0
$r(\text{C}^+-\text{H})$	1.085	1.074	1.072	1.084	1.073	1.072	— <sup>a</sup>
$r(\text{C}=\text{C})$	1.380	1.372	1.372	1.378	1.371	1.371	1.350

<sup>a</sup>H-bond lengths are not correctly obtained in X-ray structure measurements

**Table 2** Geometry data for structure **b** (bond lengths  $r$  in Å, dihedral angle  $\theta$  in degree)

Property	Without dispersion correction			With D3 correction			X-ray data
	def-SV(P)	def2-TZVP	def2-QZVP	def-SV(P)	def2-TZVP	def2-QZVP	
$r(\text{N-B})$	1.875	1.866	1.867	1.820	1.810	1.812	1.824
$r(\text{N-Ring})$	1.523	1.524	1.524	1.519	1.519	1.519	1.508
$r(\text{B-Ring})$	1.645	1.640	1.640	1.644	1.639	1.638	1.634
$r(\text{B-R}_1)$	1.628	1.627	1.628	1.621	1.621	1.621	1.615
$r(\text{B-R}_2)$	1.640	1.639	1.639	1.632	1.631	1.631	1.634
$\theta(\text{NCCB})$	−29.7	−29.8	−29.9	−29.3	−29.3	−29.4	−28.2

**Table 3** Geometry data for structure **c** (bond lengths  $r$  in Å, dihedral angle  $\theta$  in degree)

Property	Without dispersion correction			With D3 correction			X-ray data
	def-SV(P)	def2-TZVP	def2-QZVP	def-SV(P)	def2-TZVP	def2-QZVP	
$r(\text{P-B})$	2.278	2.286	2.290	2.168	2.158	2.161	2.206
$r(\text{P-Ring})$	1.887	1.871	1.870	1.873	1.855	1.854	1.841
$r(\text{B-Ring})$	1.645	1.638	1.638	1.648	1.643	1.642	1.623
$r(\text{P-Mes}_1)$	1.862	1.850	1.849	1.845	1.832	1.832	1.820
$r(\text{P-Mes}_2)$	1.886	1.873	1.873	1.871	1.858	1.858	1.856
$r(\text{B-R}_1)$	1.664	1.645	1.645	1.639	1.641	1.641	1.643
$r(\text{B-R}_2)$	1.617	1.616	1.617	1.611	1.611	1.611	1.613
$\theta(\text{PCCB})$	40.7	41.1	41.0	39.7	40.0	40.0	38.3

double-counting-effects of correlation at medium distances. The formula by Becke and Johnson (BJ) [21], which is applied consistently throughout this study, reads

$$f_{damp}(R_{AB}^0)^n = a_1 R_{AB}^0 + a_2$$

$$\text{with } R_{AB}^0 = \sqrt{\frac{C_8^{AB}}{C_6^{AB}}}$$

and fit parameters  $a_1$  and  $a_2$

and leads to a constant contribution to the correlation energy from each spatially close pair of atoms (for example in a bond). The Minnesota functionals (M05-2X and M06-2X) proved incompatible with this dispersion correction because they



already include short-range dispersion terms (see e.g. [22]). For these, a slightly different version of D3 published earlier and including a different kind of damping is more appropriate. Whenever this so-called “zero-damping” variant is used in this study, it will be marked separately (by the tag D3(zero)); in all other cases the Becke-Johnson damping is applied.

Tables 1, 2, and 3 summarize the calculated and measured structural data for compounds **a** to **c**.

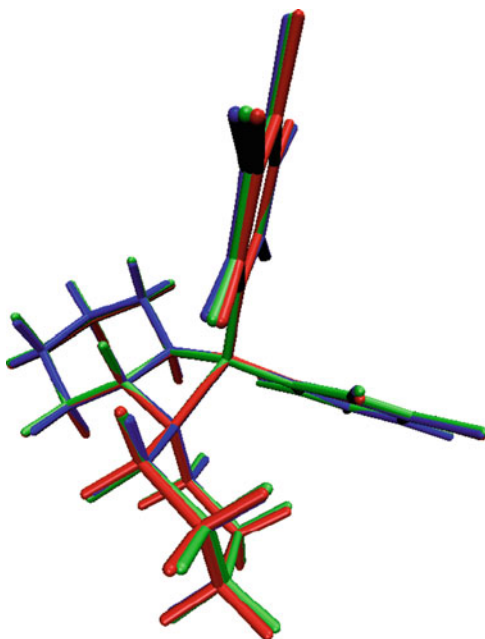
For all systems the general trend holds that the bond lengths decrease with an increase of the basis set size, while bond angles and dihedral angles do not seem to be influenced much. Within one set of calculations (with or without D3 correction) the difference between TZ and QZ basis sets is rather small (on average 0.001 Å and 0.05°) compared to the difference between DZ and TZ (about 0.008–0.013 Å and 0.08–0.3°). Therefore we can conclude that for most cases a triple zeta basis set should yield sufficiently converged structures, and within much shorter computation times.

Comparing the two sets of calculations with one another, it is first observed that the bond lengths from the calculations with D3 are always shorter than without. This effect is most pronounced for the long, more flexible bonds. In particular, for the most interesting bonds between LA and LB this shrinking effect of the dispersion correction on the bond length ranges from 0.013 Å for system **a** to a large value of 0.130 Å for system **c**. The dispersion effect for bond angles is smaller and differences between values with and without dispersion correction of only about 0.5° are observed. For dihedrals the effect is a little more pronounced but still small, leading to deviations of 0.3–1.1° between dispersion corrected and non-dispersion corrected values. It should be noted that the values computed with dispersion correction are still closer to the experimental values than the non-corrected values, leading to remaining deviations of only about 1.1° (**b**) to 1.8° (**c**). These effects on the geometry are almost independent from the basis set size and up to two orders of magnitude bigger than the basis set effects discussed above.

If we now compare these theoretical data to the experimentally observed geometries from X-ray diffraction we find significantly smaller deviations for the dispersion corrected values. A very impressive example is structure **c** where the deviation from the X-ray structure drops from about –0.028 Å for the non-dispersion corrected bond lengths to –0.003 Å for the dispersion corrected values. C–H bonds are not taken into account here as they cannot be accurately measured by X-ray diffraction and are usually assigned too short values. Their lengths are generally accepted to be more realistic in DFT calculations.

Figure 2 also visualizes the effect of the dispersion correction on the optimized structure of system **b** and shows the good congruence with the experimentally determined crystal structure of the system. According to visual inspection of this figure there seems to be no advantage when applying dispersion corrections but one has to keep in mind that, especially the bulky groups are significantly influenced by neighboring molecules (crystal packing). More realistic comparisons between theory and experiment should hence be undertaken using periodic DFT-D3 calculations as discussed recently [23].

**Fig. 2** Overlay of the X-ray structure (*blue*), the TPSS-D3-optimized structure (*green*) and the TPSS (without D3) optimized structure (*red*) of FLP **b**



These results prove that the inclusion of dispersion effects is crucial for systems like FLPs, which are largely influenced by non-covalent interactions between their large substituents. Similar observations were recently made in a combined DFT-D3/NMR study of the B–P distances in some FLPs [24]. Since the effect of the dispersion correction could be shown to be up to two orders of magnitude bigger than the basis set effect, we highly recommend its use as the default in all DFT investigations of large systems as already recently noted for the computation of thermodynamic properties [25].

## 4 Electronic Energy Calculations

Next, we would like to discuss the calculation of accurate reaction energies. For this purpose we chose the activation reaction of  $H_2$  as depicted in Scheme 1.

Single point calculations have been carried out with various methods on the basis of TPSS-D3/def2-TZVP optimized structures. For the GGA functional PBE (0% Fock-exchange) [26], the widely used hybrid GGA functional B3LYP (20% Fock-exchange) [27, 28], and the double-hybrid functional B2PLYP (53% Fock-exchange and 27% perturbative correlation energy) [29], the TURBOMOLE 6.3 [20] code has been used, while the calculations with the hybrid GGA functional PW6B95 (28% Fock-exchange) [30] were carried out with a modified version of TURBOMOLE 5.7 [31]. All these functionals were enhanced with the afore-mentioned

**Table 4** Electronic reaction energies for the activation of H<sub>2</sub> in kcal/mol

Method	System a	System a'	System b	System c
TPSS-D3(opt)/TZ	-10.3	-11.8	-12.9	-10.9
TPSS-D3(opt)/QZ	-10.3	-12.3	-13.6	-11.6
TPSS(opt)	-14.1	-15.6	-14.4	-12.8
PBE-D3	-12.2	-13.5	-15.8	-10.8
B3LYP-D3	-13.5	-14.6	-15.5	-12.5
PW6B95-D3	-11.7	-13.5	-13.9	-9.4
M05-2X	-12.6	-13.8	-15.7	-11.7
M06-2X	-11.0	-12.7	-14.8	-9.9
M06-2X-D3 <sup>a</sup>	-11.2	-13.2	-14.8	-10.1
B2PLYP-D3	-10.3	-11.3	-13.4	-9.4
<b>B2PLYP-D3/CBS<sup>b</sup></b>	<b>-11.3</b>	<b>-12.5</b>	<b>-14.8</b>	<b>-10.7</b>
MP2/TZ	-2.3	-2.6	-8.3	-2.0
MP2/QZ	-4.3	-5.2	-11.3	-4.7
MP2/CBS	-5.9	-7.1	-13.2	-6.5
SCS-MP2/TZ	-4.7	-5.7	-9.1	-4.2
SCS-MP2/QZ	-6.6	-8.1	-11.8	-6.8
SCS-MP2/CBS	-7.9	-9.7	-13.6	-8.4

<sup>a</sup>D3 with zero-damping, compare text for details

<sup>b</sup>Corrected B2PLYP-D3 means B2PLYP-D3/TZ + 0.27\*Δ(MP2/CBS-MP2/TZ); compare text for details

D3-dispersion correction [16, 17]. For the meta-hybrid GGA functionals M05-2X (56% Fock-exchange) [32, 33] and M06-2X (54% Fock-exchange) [34] the GAUSSIAN09 program package was used [35]. These functionals are supposed to describe at least medium-range dispersion effects, but as parameters for M06-2X in the zero-damping version of D3 exist, we also included results for this combination of methods. For comparison we also added the energy values originating from the geometry optimizations with TPSS and TPSS-D3. All these calculations were carried out using the large Gaussian-AO def2-TZVP basis set.

As an example of commonly used wave function methods we included triple zeta, quadruple zeta, and CBS(TQ) extrapolated [36] values for MP2 [37] and SCS-MP2 [38] (all computed with TURBOMOLE 6.3). All TURBOMOLE calculations were converged to 10<sup>-7</sup> for the energy and 10<sup>-5</sup> for the gradient; for GAUSSIAN calculations the *tight* criterion was used. For the DFT calculations the *m4* and *fine* grids were used, respectively.

Table 4 summarizes the results of these investigations.

Since CCSD(T) calculations [39–41] are not feasible due to the size of the systems under consideration, we mainly discuss the differences between the tested methods. From previous experience for huge thermodynamic benchmark sets [25] it is known that double-hybrids like B2PLYP-D3 should yield the best results closely followed by PW6B95-D3 and M06-2X. For the non-metallic main-group systems studied herein, SCS-MP2/CBS is also expected to perform well.

We first note that the bare reaction energy for all four systems is similar and falls for each quantum chemical method in a rather small range with differences of only 2–5 kcal/mol. All values are negative (exothermic) and, for example, for our optimization method TPSS-D3 we obtain values for **a**, **a'**, **b**, and **c** of –10.3, –11.8, –12.9, and –10.9 kcal/mol, respectively. This already shows that even a wide range of different computational methods provide qualitatively consistent results.

The dispersion corrected TPSS-D3 method which was already used to optimize the underlying geometries leads to a deviations between 0.2 kcal/mol (system **c**) and 1.9 kcal/mol (system **b**) relative to the reference energies calculated at B2PLYP-D3/CBS level (as estimated by adding the TZ-CBS difference at the MP2 level to the corresponding B2PLYP/TZ result, i.e.,  $E(\text{B2PLYP-D3/CBS}) = E(\text{B2PLYP-D3/TZ}) + 0.27 \times [E(\text{MP2/CBS}) - E(\text{MP2/TZ})]$ ; the factor of 0.27 represents the amount of non-local perturbative correlation in B2PLYP). In comparison, the corresponding non-dispersion corrected TPSS energies are about 3 kcal/mol off for systems **a**, **a'**, and **c**, while only system **b** shows a surprisingly small energy deviation of 0.4 kcal/mol. Tentatively, this can be explained by the nature of this system – **b** does not contain any large substituents like phenyl rings which exhibit a larger amount of non-covalent interactions to their neighbors. These results clearly indicate, once more, that for reaction energies dispersion interactions also play an important role and should not be neglected when aiming at “chemical accuracy” (about 1 kcal/mol). How good the performance of TPSS-D3 really is shows a direct comparison with the B2PLYP-D3 values: for system **a** both methods yield the same value of –10.3 kcal/mol, while system **c** shows the biggest difference between the two methods with –9.4 kcal/mol for B2PLYP-D3 and –10.9 kcal/mol for TPSS-D3. Thus, TPSS-D3 can be seen as a computationally cheaper alternative to the double-hybrid functional B2PLYP-D3 for the calculation of reaction energies of FLPs.

The other tested functionals also show a reasonably high accuracy with PW6B95-D3 being almost as good as TPSS-D3. M06-2X is only slightly behind those two. As this functional from the Minnesota functional family does already account for medium-range dispersion interactions, its performance was tested with and without D3 (zero) dispersion correction. As expected, the effect of long-range (London) dispersion, which is added by the D3 correction, is only small changing the energies from –11.0 to –11.2 kcal/mol for system **a** (reference: –11.3 kcal/mol) or from –9.9 to –10.1 kcal/mol for system **c** (reference: –10.7 kcal/mol). The earlier version M05-2X, which has often been used for the quantum chemical description of FLP chemistry [3, 4], performs only slightly worse than its successor. PBE-D3 is on the same level of accuracy and even B3LYP-D3, the “worst” functional tested here, can still provide reasonably accurate reaction energies with a deviation of about 2 kcal/mol from the reference.

A surprisingly bad performance is exhibited by MP2 which shows deviations of about 5 kcal/mol from the DFT values for all systems except **b**, where the deviation is only 1 kcal/mol. SCS-MP2 significantly improves upon MP2 and results in acceptable deviations of 2–3 kcal/mol. Notable (but not unexpected) is the much

**Table 5** Electronic reaction energies in kcal/mol for the association of FLP **a** from its components (NHC + B(C<sub>6</sub>F<sub>5</sub>)<sub>3</sub>)

Method	Association energy
TPSS-D3(opt)/TZ	-41.9
TPSS-D3(opt)/QZ	-41.5
TPSS(opt)	-24.9
PBE-D3	-41.5
B3LYP-D3	-40.5
PW6B95-D3	-43.7
M05-2X	-41.5
M06-2X	-44.0
M06-2X-D3 <sup>a</sup>	-46.6
B2PLYP-D3	-45.1
<b>B2PLYP-D3/CBS<sup>b</sup></b>	<b>-47.5</b>
MP2/TZ	-61.2
MP2/QZ	-66.1
MP2/CBS	-69.9
SCS-MP2/TZ	-50.0
SCS-MP2/QZ	-47.8
SCS-MP2/CBS	-47.6

<sup>a</sup>D3 with zero-damping, compare text for details

<sup>b</sup>B2PLYP-D3/CBS means B2PLYP-D3/TZ + 0.27\*Δ(MP2/CBS-MP2/TZ), compare text for details

stronger basis set dependence of the two MP2 type methods compared to that of DFT (cf. the TPSS-D3 values at TZ and QZ levels). The difference between triple zeta and CBS treatments is roughly 5 kcal/mol and larger basis sets improve the results in all cases.

In summary only SCS-MP2 together with CBS extrapolation can be recommended as an alternative to DFT for FLPs. The fact that an accurate and robust description of FLP thermochemistry can already be achieved with medium-sized TZ basis sets and even semi-local functionals like TPSS-D3 is the main reason for widespread acceptance of DFT in chemistry.

Up to here we have exclusively discussed the hydrogen activation reaction energy but functional FLPs also have other properties – most notable is the “frustration,” that is, an existing but not too strong bond between LA and LB. For the case **a** we finally want to investigate the performance of the above theoretical methods for the computation of the association energy in the gas phase.

The first conclusion from Table 5 is that the association of the NHC and B(C<sub>6</sub>F<sub>5</sub>)<sub>3</sub> in the gas phase is highly exothermic with values of about -40 to -50 kcal/mol (depending on the method). While the TPSS-D3 results on triple and quadruple zeta levels are rather similar, the non-dispersion corrected TPSS value is higher by more than 16 kcal/mol. This highlights the effect of dispersion interactions between the Lewis acid and the Lewis base part in this intermolecular FLP and clearly shows how big the error in the total reaction energy can become if dispersion interactions are neglected.

Taking again the B2PLYP-D3/CBS value of -47.5 kcal/mol as reference, all tested density functionals perform more or less well. M06-2X-D3(zero) yields the

smallest deviation (0.9 kcal/mol), closely followed by B2PLYP-D3, M06-2X (without dispersion correction) and PW6B95-D3 which are all up to 4 kcal/mol too high. The largest deviation among the tested functionals is found for B3LYP-D3 with an association energy value of  $-40.5$  kcal/mol, resulting in an unacceptable deviation from the reference of 7.2 kcal/mol.

As discussed for the reaction with dihydrogen, the computed association energy is also much more basis set dependent at MP2 and SCS-MP2 levels than for DFT. The change from TZ to QZ basis set amounts to several kcal/mol and hence CBS extrapolation seems mandatory. Although counterpoise corrections for BSSE would be possible in this intermolecular case, this does not hold for intramolecular FLPs and many reactions, so that, in general, we recommend for (SCS-)MP2 the CBS extrapolation which diminishes this source of error. In passing we note that the SCS-MP2/CBS [42] value ( $-47.6$  kcal/mol) agrees extremely well with the DFT results and that MP2/CBS (as usual) strongly overestimates the interaction (by about 22.5 kcal/mol).

## 5 Thermal Corrections in the Gas Phase

Up to this point we have only considered electronic energies mainly to test the variations and differences between the methods. However, these values are not physically observable and cannot be directly compared to experimental data. Thus, the computation of enthalpies and free enthalpies is required which is useful to explain or predict the outcome of experiments. Focusing again on the activation of  $\text{H}_2$  by our example systems we calculated the statistical thermal correction terms of translational, rotational, and vibrational origin (including vibrational zero-point energies) which are added to the electronic reaction energies to yield  $\Delta H_{\text{gas}}$  and  $\Delta G_{\text{gas}}$  at 298 K.

First we tried to stick to DFT for the harmonic frequency calculations, but numerical problems leading to artificial imaginary modes prohibited the use of these results. For other, less problematic cases, highly converged DFT-calculations (energy: up to  $10^{-9}$   $E_{\text{h}}$ ) on a big grid (e.g.,  $m5$ ) may also lead to reasonable results. Still, special attention needs to be paid to methyl rotations and lattice vibrations of the molecule which lead to additional imaginary modes and therefore to frequencies which cannot be used for the calculation of thermal corrections.

Instead, we decided to switch to the semi-empirical PM6-D3H method [43–45] which has been shown to yield reliable and sufficiently accurate vibrational frequencies.

As can be seen from Table 6, the correction terms for  $\Delta H$  and  $\Delta G$  are all positive. The reason for this is comparatively simple – when going from the FLP and  $\text{H}_2$  to the hydrogenated FLP the number of particles is reduced from two to one (in the case of  $\mathbf{a/a'}$  from three to two). This leads to a significant decrease in the entropy contribution and therefore to a more positive  $\Delta G$ .

**Table 6** Thermal corrections in the gas phase at 298 K in kcal/mol

Method	System <b>a</b>	System <b>a'</b>	System <b>b</b>	System <b>c</b>
Corr. to $\Delta H$	2.8	2.4	2.6	3.8
Corr. to $\Delta G$	9.5	10.2	10.3	12.0
$\Delta H_{\text{gas}}$ B2PLYP-D3/CBS	-8.7	-10.2	-12.2	-6.9
$\Delta G_{\text{gas}}$ B2PLYP-D3/CBS	-2.0	-2.3	-4.4	1.3

**Table 7** (Free) enthalpies of solvation and final (free) enthalpies in solution for the solvent pentane at 298 K

Method	System <b>a</b>	System <b>a'</b>	System <b>b</b>	System <b>c</b>
$\Delta H_{\text{solv}}$	-2.8	-1.2	-3.2	-1.9
$\Delta G_{\text{solv}}$	-8.6	-7.2	-9.0	-7.8
$\Delta H_{\text{solution}}$ B2PLYP-D3/CBS	-11.1	-11.3	-15.4	-8.8
$\Delta G_{\text{solution}}$ B2PLYP-D3/CBS	-11.4	-9.5	-13.5	-6.5

The  $\Delta G$  contribution varies only little from 9.5 to 12 kcal/mol for the four systems, which is a typical value for bimolecular reactions (for the hydrogenation of **a** the associated FLP is taken as reference, not the separate LA and LB as in the other cases).

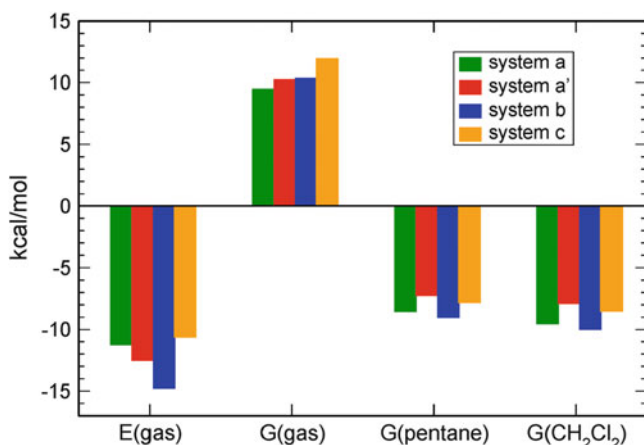
When the thermal corrections are added to the B2PLYP-D3/CBS electronic reaction energies (which we consider exclusively in the following), small  $\Delta G_{\text{gas}}$  values for the total activation reaction between -3.1 and 2.5 kcal/mol are obtained. This is an important result as it shows that the reaction under gas phase equilibrium conditions is rather unfavorable and unlikely to occur efficiently. Unpublished calculations for other FLP/ $\text{H}_2$  reactions (including the original system from D. Stephan) indicate that this is a general property and that the stabilization of the formed ion pair by solvation is essential (see below).

## 6 Solvation Effects

All calculations presented above were gas phase calculations, whereas all of the corresponding experiments are carried out in solution. To investigate further the effect of solvation on the reaction (free) enthalpy we applied the COSMO-RS solvation model [46] to our gas phase optimized structures, focusing on the two commonly used solvents dichloromethane and pentane. This procedure yields (free) enthalpies of solvation  $\Delta H_{\text{solv}}$  and  $\Delta G_{\text{solv}}$  for reactants and products which are added to the gas phase  $\Delta G_{\text{gas}}$  and  $\Delta H_{\text{gas}}$  values from the last section in order to get the final  $\Delta H_{\text{solution}}$  and  $\Delta G_{\text{solution}}$  values for the reaction in solution, which corresponds to experimental observables. These data are summarized in Tables 7 and 8. For a thorough discussion of the performance of current solvation models the reader is referred to [45] and [47–49].

**Table 8** (Free) enthalpies of solvation and final (free) enthalpies in solution for the solvent dichloromethane at 298 K

Method	System a	System a'	System b	System c
$\Delta H_{\text{solv}}$	-3.9	-2.0	-4.6	-2.8
$\Delta G_{\text{solv}}$	-9.5	-7.9	-10.0	-8.5
$\Delta H_{\text{solution}}$ B2PLYP-D3/CBS	-12.6	-12.1	-16.8	-9.7
$\Delta G_{\text{solution}}$ B2PLYP-D3/CBS	-11.6	-10.2	-14.4	-7.2

**Fig. 3** H<sub>2</sub> activation reaction energies (B2PLYP-D3/CBS) and free enthalpies in the gas phase and for two common solvents. Note the cancellation effect between entropic and solvation contributions

The first observation is that the difference between the effects of the two solvents is rather small. Although dichloromethane is significantly more polar than pentane, their  $\Delta G_{\text{solv}}$  values differ only by up to 1 kcal/mol. This is already in qualitative agreement with experimental observations that FLP reactions are only weakly influenced by the choice of solvent. A second and very important finding is that the (free) enthalpies of solvation presented here are of about the same size as the gas phase thermal corrections presented in the last section but have a different sign. The two effects almost cancel for our example reactions so that the COSMO-RS treatment brings the total  $\Delta G_{\text{solution}}$  results back down to values between  $-6$  and  $-14$  kcal/mol in both solvents (compare Fig. 3).

According to these data, the activation reaction for **a** and **b** is essentially irreversible under the experimental conditions (298 K) while **c** is a borderline case with a  $\Delta G_{\text{solution}}$  value of about  $-7$  kcal/mol. In this context it seems important to mention that aggregation and even the formation of microcrystals of the ion-pairs might occur in reality which is of course beyond the capabilities of a reasonable theoretical treatment. The enthalpies are much less influenced by the COSMO-RS corrections ( $\Delta H_{\text{solv}}$  values range between 1 and 4 kcal/mol) which demonstrates



that the increase of the solvent entropy during the formation of the product complex represents a significant driving force of the reaction.

The mentioned cancelation effect between entropy and solvation can of course not be expected to be quantitative and it is not recommended to approximate  $\Delta G_{\text{solution}}$  by  $\Delta E_{\text{gas}}$  even though the numerical values are similar (for a recent discussion of this problem – including dispersion effects – see [50–53]). Instead we suggest using the above procedure to compute all relevant terms as accurately as possible in order to get reliable and physically reasonable results.

## 7 Conclusions

In this study we tried to shed some light on the different quantum chemical methodologies that are available for the study of the energetics and structures of FLP systems and give some advice about which factors to consider in order to produce accurate and reliable geometries, reaction energies, and (free) enthalpies.

Three different sample FLP systems have been selected from the literature including some of the most often found types of Lewis bases, a carbene, a phosphane, and an amine. Detailed studies of the structures of  $\text{H}_2$  addition products in comparison to X-ray data revealed TPSS-D3/def2-TZVP as a good and affordable first-principles method to generate accurate geometries. The substantial effect of London dispersion correction could once more be proved and we very strongly recommend the use of D3 or similarly accurate dispersion corrections schemes as a default in DFT.

An investigation of different density functional- and MP2-type methods shows that FLP thermochemistry is not very sensitive to the specific choice of the method. Approaches which perform well in standard thermochemical benchmarks also yield rather similar reaction energies here. We can recommend PW6B95-D3 and TPSS-D3 as somewhat cheaper alternatives to B2PLYP-D3 and also note that the M06-2X method performs well. As a non-DFT method the SCS-MP2 approach yields reaction energy values close to those from DFT, whereas MP2 shows a very poor performance with deviations on the order of 5 kcal/mol and cannot be recommended. A big disadvantage of both MP2 based methods is (not unexpectedly) the relatively strong dependence of the results on the size of the basis set. While for DFT methods triple-zeta quality AO sets are sufficient and the improvement gained when going to quadruple zeta basis sets is only small (typically <1 kcal/mol change), for (SCS-)MP2 extrapolation to the CBS limit is mandatory.

Thermal corrections in the gas phase and in solution could be shown to almost cancel for the systems under consideration since their contributions were of about the same size but of different sign. Adding gas phase thermal corrections to electronic energies alone would have left some doubt in the feasibility of reactions yielding positive values or values just slightly below zero. This study has very clearly shown that the FLP activation reaction of  $\text{H}_2$  under ambient equilibrium conditions is significantly driven by the solvation of the formed ion pair. Although it seems trivial that solvent effects should be included in quantum chemical studies when aiming for

accurate free reaction enthalpy values in the condensed phase (for recent COSMO-RS studies of ionic reactions in polar solvents see [54]), this does not seem to be standard in many published studies in the field. The same holds for the application of London dispersion corrections when using standard density functionals like B3LYP for which these are essential even to get qualitatively correct results. In summary, the future for DFT-D3/COSMO-RS based simulations of the structure and thermochemistry of FLPs and related systems seems bright.

**Acknowledgement** Financial support from the DFG/SNF Forschergruppe 1175 “Unconventional Approaches to the Activation of Dihydrogen” is gratefully acknowledged.

## References

1. Welch GC, San Juan RR, Masuda JD, Stephan DW (2006) Reversible, metal-free hydrogen activation. *Science* 314:1124
2. Stephan DW, Erker G (2010) Frustrated Lewis pairs: metal-free hydrogen activation and more. *Angew Chem Int Ed* 49:46–76
3. Rokob TA, Hamza A, Stirling A, Pápai I (2009) On the mechanism of  $B(C_6F_5)_3$ -catalyzed direct hydrogenation of imines: inherent and thermally induced frustration. *J Am Chem Soc* 131:2029–2036
4. Lu G, Li H, Zhao L, Huang F, Wang ZX (2010) Computationally designed metal-free hydrogen activation site: reaching the reactivity of metal–ligand bifunctional hydrogenation catalysts. *Inorg Chem* 49:295–301
5. Jiang C, Blacque O, Fox T, Berke H (2011) Heterolytic cleavage of  $H_2$  by frustrated B/N Lewis pairs. *Organometallics* 30:2117–2124
6. Fan C, Mercier LG, Piers WE, Tuononen HM, Parvez M (2010) Dihydrogen activation by antiaromatic pentaarylboroles. *J Am Chem Soc* 132:9604–9606
7. Nyhlén J, Privalov T (2009) On the possibility of catalytic reduction of carbonyl moieties with tris(pentafluorophenyl) borane and  $H_2$ : a computational study. *Dalton Trans* 29:5780–5786
8. Grimme S, Kruse H, Goerigk L, Erker G (2010) The mechanism of dihydrogen activation by frustrated Lewis pairs revisited. *Angew Chem Int Ed* 49:1402–1405
9. Guo Y, Li S (2008) A novel addition mechanism for the reaction of “frustrated Lewis pairs” with olefins. *Eur J Inorg Chem* 16:2501–2505
10. Pyykkö P, Wang C (2010) Theoretical study of  $H_2$  splitting and storage by boron–nitrogen-based systems: a bimolecular case and some qualitative aspects. *Phys Chem Chem Phys* 12:149–155
11. Mück-Lichtenfeld C, Grimme S (2012) Theoretical analysis of cooperative effects of small molecule activation by frustrated Lewis pairs. *Dalton Trans* 41:9111–9118
12. Holschumacher D, Bannenberg T, Hrib CG, Jones PG, Tamm M (2008) Heterolytic dihydrogen activation by a frustrated carbene–borane Lewis pair. *Angew Chem Int Ed* 47:7428–7432
13. Schwendemann S, Fröhlich R, Kehr G, Erker G (2011) Intramolecular frustrated N/B Lewis pairs by enamine hydroboration. *Chem Sci* 2:1842–1849
14. Axenov KV, Mömning CM, Kehr G, Fröhlich R, Erker G (2010) Structure and dynamic features of an intramolecular frustrated Lewis pair. *Chem Eur J* 16:14069–14073
15. Staroverov VN, Scuseria GE, Tao J, Perdew JP (2003) Comparative assessment of a new nonempirical density functional: molecules and hydrogen-bonded complexes. *J Chem Phys* 119:12129–12137
16. Grimme S, Antony J, Ehrlich S, Krieg H (2010) A consistent and accurate *ab initio* parametrization of density functional dispersion correction (DFT-D) for the 94 elements H–Pu. *J Chem Phys* 132:154104

17. Grimme S, Ehrlich S, Goerigk L (2011) Effect of the damping function in dispersion corrected density functional theory. *J Comput Chem* 32:1456–1465
18. Bühl M, Kabrede H (2006) Geometries of transition-metal complexes from density-functional theory. *J Chem Theory Comput* 2:1282–1290
19. Weigend F, Ahlrichs R (2005) Balanced basis sets of split valence, triple zeta valence and quadruple zeta valence quality for H to Rn: design and assessment of accuracy. *Phys Chem Chem Phys* 7:3297–3305
20. Ahlrichs R et al (2011) TURBOMOLE, version 6.3, Universität Karlsruhe 2011, see <http://www.turbomole.com>
21. Becke AD, Johnson ER (2005) Exchange-hole dipole moment and the dispersion interaction. *J Chem Phys* 122:154104
22. Goerigk L, Kruse H, Grimme S (2011) Benchmarking density functional methods against the S66 and S66x8 datasets for non-covalent interactions. *ChemPhysChem* 12:3421–3433
23. Möllmann J, Grimme S (2010) Importance of London dispersion effects for the packing of molecular crystals: a case study for intramolecular stacking in a bis-thiophene derivative. *Phys Chem Chem Phys* 12:8500–8504
24. Wiegand T, Eckert H, Ekkert O, Fröhlich R, Kehr G, Erker G, Grimme S (2012) New insights into frustrated Lewis pairs: structural investigations of intramolecular phosphane–borane adducts by using modern solid-state NMR techniques and DFT calculations. *J Am Chem Soc* 134:4236–4249
25. Goerigk L, Grimme S (2011) A thorough benchmark of density functional methods for general main group thermochemistry, kinetics, and noncovalent interactions. *Phys Chem Chem Phys* 13:6670–6688
26. Perdew JP, Burke K, Ernzerhof M (1996) Generalized gradient approximation made simple. *Phys Rev Lett* 77:3865–3868
27. Becke AD (1993) Density-functional thermochemistry. III. The role of exact exchange. *J Chem Phys* 98:5648–5652
28. Lee C, Yang W, Parr RG (1988) Development of the Colle-Salvetti correlation-energy formula into a functional of the electron density. *Phys Rev B* 37:785–789
29. Grimme S (2006) Semiempirical hybrid density functional with perturbative second-order correlation. *J Chem Phys* 124:034108
30. Zhao Y, Truhlar DG (2005) Design of density functionals that are broadly accurate for thermochemistry, thermochemical kinetics, and nonbonded interactions. *J Phys Chem A* 109:5656–5667
31. Ahlrichs R et al (2006) TURBOMOLE, version 5.7, Universität Karlsruhe 2006, see <http://www.turbomole.com>
32. Zhao Y, Schultz NE, Truhlar DG (2006) Design of density functionals by combining the method of constraint satisfaction with parametrization for thermochemistry, thermochemical kinetics, and noncovalent interactions. *J Chem Theory Comput* 2:364–382
33. Zhao Y, Truhlar DG (2008) Density functionals with broad applicability in chemistry. *Acc Chem Res* 41:157–167
34. Zhao Y, Truhlar DG (2008) The M06 suite of density functionals for main group thermochemistry, thermochemical kinetics, noncovalent interactions, excited states, and transition elements: two new functionals and systematic testing of four M06-class functionals and 12 other functionals. *Theor Chem Acc* 120:215–241
35. Frisch MJ et al (2009) Gaussian 09, Rev. A.02. Gaussian Inc., Pittsburgh, PA
36. Halkier A, Helgaker T, Jørgensen P, Klopper W, Koch H, Olsen J, Wilson AK (1998) Basis-set convergence in correlated calculations on Ne, N<sub>2</sub>, and H<sub>2</sub>O. *Chem Phys Lett* 286:243–252
37. Møller C, Plesset MS (1934) Note on an approximation treatment for many-electron systems. *Phys Rev* 46:618–622
38. Grimme S (2003) Improved second-order Møller–Plesset perturbation theory by separate scaling of parallel- and antiparallel-spin pair correlation energies. *J Chem Phys* 118:9095–9102

39. Crawford TD, Schaefer HF III (2000) An introduction to coupled cluster theory for computational chemists. In: Lipkowitz KB, Boyd DB (eds) *Reviews in computational chemistry*. Wiley-VCH, New York
40. Pople JA, Head-Gordon M, Raghavachari K (1987) Quadratic configuration interaction. A general technique for determining electron correlation energies. *J Chem Phys* 87:5968
41. Lee TJ, Rendell AP, Taylor PR (1990) Comparison of the quadratic configuration interaction and coupled-cluster approaches to electron correlation including the effect of triple excitations. *J Phys Chem* 94:5463–5468
42. Neese F (2012) ORCA - an ab initio, density functional and semiempirical program package, version 2.9. University of Bonn, Bonn
43. Stewart JJP (2007) Optimization of parameters for semiempirical methods V: modification of NDDO approximations and application to 70 elements. *Mol Model* 13:1173–1213
44. MOPAC2009, Stewart computational chemistry, version 11.052W, available at <http://OpenMOPAC.net>
45. Grimme S (2012) Supramolecular binding thermodynamics by dispersion-corrected density functional theory. *Chem Eur J* 18(32):9955–9964
46. Grimme S (2012) Comment on: “On the accuracy of DFT methods in reproducing ligand substitution energies for transition metal complexes in solution: the role of dispersive interactions” by H. Jacobsen and L. Cavallo. *Chemphyschem* 13:1407–1409
47. Cramer CJ, Truhlar DG (2008) A universal approach to solvation modeling. *Acc Chem Res* 41:760–768
48. Klamt A, Mennucci B, Tomasi J, Barone V, Curutchet C, Orozco M, Luque FJ (2009) On the performance of continuum solvation methods. A comment on “Universal approaches to solvation modeling”. *Acc Chem Res* 42:489–492
49. Cramer CJ, Truhlar DG (2009) Reply to comment on “a universal approach to solvation modeling”. *Acc Chem Res* 42:493–497
50. Klamt A, Schüürmann G (1993) COSMO: a new approach to dielectric screening in solvents with explicit expressions for the screening energy and its gradient. *J Chem Soc Perkin Trans* 2:799–805
51. Klamt A (1995) Conductor-like screening model for real solvents: a new approach to the quantitative calculation of solvation phenomena. *J Phys Chem* 99:2224–2235
52. Eckert F, Klamt A (2002) Fast solvent screening via quantum chemistry: COSMO-RS approach. *AIChE J* 48:369
53. Eckert F, Klamt A (2010) COSMOtherm, Version C2.1, Release 01.11. COSMOlogic GmbH & Co. KG, Leverkusen
54. Deglmann P, Schenk S (2012) Thermodynamics of chemical reactions with COSMO-RS: the extreme case of charge separation or recombination. *J Comput Chem* 33:1304–1320

# Computational Design of Metal-Free Molecules for Activation of Small Molecules, Hydrogenation, and Hydroamination

Zhi-Xiang Wang, Lili Zhao, Gang Lu, Haixia Li, and Fang Huang

**Abstract** Hydrogen activation is a key step in hydrogenation reactions which are widely used in both laboratory synthesis and the chemical industry. Traditionally, it was often considered that only transition metal complexes/systems are able to activate hydrogen and to catalyze hydrogenations. This view has been changed recently; more and more metal-free molecules/systems have been found capable of activating hydrogen. Among these developments, the frustrated Lewis pairs (FLPs) are of particular significance, not only because they exhibit high reactivity toward hydrogen as well as other small molecules, but also because some of them can perform direct catalytic hydrogenations, which pave the way to the development of cheaper and greener hydrogenation catalysts. Inspired by the FLP principle, we used quantum mechanics computations to design molecules for H<sub>2</sub>, CH<sub>4</sub>, and NH<sub>3</sub> activation and catalysts for hydrogenation of imines, ketones, and alkenes. While our designed molecules are awaiting experimental preparation, the active sites in our designed molecules anticipated the features appeared in the compounds synthesized later by experimentalists. This chapter reviews our computational explorations to enrich FLP chemistry.

**Keywords** Bifunctional reactivity · DFT calculations · Frustrated Lewis pairs · Metal-free catalyst design · Metal-free hydrogen activation · Metal-free hydrogenation

## Contents

1 Introduction .....	232
2 General Principles for Facile Hydrogen Activation .....	234

---

Z.-X. Wang (✉), L. Zhao, G. Lu, H. Li, and F. Huang  
School of Chemistry and Chemical Engineering, University of Chinese Academy of Sciences,  
Beijing 100049, People's Republic of China  
e-mail: [zxwang@gucas.ac.cn](mailto:zxwang@gucas.ac.cn)

3	Computational Design of Metal-Free Molecules for Activations of Small Molecules ...	235
3.1	$\pi$ -FLP Strategy for H <sub>2</sub> Activation .....	235
3.2	Fine Tuning the $\pi$ -FLP Active Site for Enhanced Reactivity Toward H <sub>2</sub> .....	239
3.3	Further Fine Tuning the $\pi$ -FLP Active Site for Methane Activation .....	240
3.4	Designing Metal-Free Molecules for H <sub>2</sub> Activation by Mimicking TM Pincer Catalysts .....	242
4	Computational Design of Metal-Free Catalysts .....	245
4.1	Designing Metal-Free Catalyst for Hydrogenation of Small Imine .....	245
4.2	Catalytic Hydrogenations of Both Small and Large Imines .....	248
4.3	Catalytic Hydrogenations of Bulky Ketones .....	249
4.4	Catalytic Hydrogenations of Various Unsaturated Compounds .....	251
4.5	Catalytic Intramolecular Hydroaminations of Non-activated Aminoalkenes .....	255
5	Concluding Remarks .....	258
	References .....	259

## Abbreviations

DFT	Density functional theory
FLP	Frustrated Lewis pair
HOMO	Highest occupied molecular orbital
LUMO	Lowest unoccupied molecular orbital
MLBHC	Metal-ligand bifunctional hydrogenation catalyst
TM	Transition metal
ZPE	Zero point energy

## 1 Introduction

The hydrogen molecule is small but plays an important role in chemistry. Hydrogen activation not only is an important chemical process (e.g., its involvement in catalytic hydrogenation) but also enriches our understanding of the reactivity of unsaturated compounds [1, 2]. The mechanisms whereby many transition metal (TM) complexes cleave dihydrogen readily have long been known [3–8]. In contrast, hydrogen activation by main group compounds *under mild conditions* was unknown until 2005 [9], when Power and coworkers discovered that, unlike acetylenes, the heavier germanium congener [e.g., Ar'GeGeAr', Ar' = C<sub>6</sub>H<sub>3</sub>-2,6-(C<sub>6</sub>H<sub>3</sub>-2,6-*i*Pr<sub>2</sub>)<sub>2</sub>] can react with H<sub>2</sub> at 25 °C and 1 atm. Since then more similar compounds [e.g., ArSnSnAr, Ar = Ar' or Ar\*; Ar\* = C<sub>6</sub>H<sub>2</sub>-2,6-(C<sub>6</sub>H<sub>2</sub>-2,4,6-*i*Pr<sub>3</sub>)<sub>2</sub>-3,5-*i*Pr<sub>2</sub>] were found to react with H<sub>2</sub> facilely [10]. The heavier congeners of carbene, GeAr<sub>2</sub> (Ar = Ar' or Ar\*), and SnAr'<sub>2</sub>, were found capable of hydrogen activation [11, 12]. Bertrand revealed in 2007 that stable (alkyl)(amino)carbenes can activate hydrogen and ammonia just like TM complexes [13]. Earlier examples of TM-free hydrogen activation involved transient main-group species generated by extreme methods (e.g., laser ablation) [14–16] and TM-free hydrogenation under

forcing conditions (135 bar and 210 °C) [17, 18]. Radom and coworkers employed quantum chemistry computations to help understand TM-free H<sub>2</sub> activation/hydrogenation [19–22] and to design TM-free catalysts for the transformation of CO<sub>2</sub> into methanol [23, 24].

Hydrogenations are widely used in both laboratory synthesis and the chemical industry [25]. Because direct addition of H<sub>2</sub> to unsaturated bonds is symmetry-forbidden, hydrogenation using H<sub>2</sub> as hydrogen source, known as direct hydrogenation, requires catalysts that can be heterogeneous (e.g., Raney-nickel catalyst) [26–29] or homogeneous TM catalysts (e.g., metal-ligand bifunctional hydrogenation catalysts, MLBHCs) [25]. Alternatively, main group hydrides (e.g., NaBH<sub>4</sub> and LiAlH<sub>4</sub>) [20] or hydride surrogates (e.g., isopropanol and Hantzsch ester) [30–36] can serve as hydrogen sources to carry out stoichiometric transfer hydrogenation. The cost of the noble TMs (e.g., Pt, Pd, Ru, Rh, Ir, and Os), the contamination of heavy TMs in direct hydrogenation, and the need for stoichiometric hydrogen sources and waste remediation in transfer hydrogenations have encouraged chemists to develop cheaper and greener catalysts to perform direct catalytic hydrogenation. To overcome the disadvantages in conventional hydrogenation, efforts have been directed to develop hydrogenation catalysts using readily available TMs (e.g., Fe) [37–45]. Another promising approach is to develop TM-free or even metal-free hydrogenation catalysts, which is relevant to the present chapter.

To perform catalytic hydrogenation, the hydrogen activation step must be reversible or nearly reversible. A breakthrough was made by Stephan and coworkers who discovered in 2006 that phosphino-borane (C<sub>6</sub>H<sub>2</sub>Me<sub>3</sub>)<sub>2</sub>P(C<sub>6</sub>F<sub>4</sub>)B(C<sub>6</sub>F<sub>5</sub>)<sub>2</sub> can activate H<sub>2</sub> reversibly under mild conditions [46]. The experimental discovery opened the area of so-called frustrated Lewis pair (FLP) chemistry and triggered more and more similar systems, generally termed FLPs [47–49]. According to the centers of Lewis acids and bases of FLPs, the known FLPs can be classified into phosphorus/boron [50–65], nitrogen/boron [65–77], carbon/boron (where carbon is the carbon center of stable N-heterocyclic carbenes) [78–81], and phosphorus/aluminum FLPs [82]. Some FLPs have been shown capable of performing catalytic hydrogenations [47–49]. In addition to activating H<sub>2</sub>, some FLPs also exhibit novel reactivity toward small molecules such as NH<sub>3</sub> [78], N<sub>2</sub>O [83], THF [64, 84], C<sub>2</sub>H<sub>4</sub> [85], CO<sub>2</sub> [86], terminal alkyne [63], and 1,3-dienes [87]. FLP chemistry has also been broadened to organometallics, elucidating the reversible dehydrogenation/hydrogenation of nitrogen heterocycles catalyzed by Ir-complex [88] and developing TM-containing FLPs [77]. The experimental developments of FLP chemistry have been timely reviewed by Stephan and coworkers [47, 48], Stephan and Erker [49], and Piers [89], respectively, and the experimentalists of the book will further review their studies insightfully and extensively.

The novel reactivity of FLPs has attracted computational chemists to unveil the origins of FLP reactivity [90–102] and the mechanisms of the reactions catalyzed by FLPs [103–106]. Fascinated by FLP chemistry, we were interested in using computational chemistry as an “experimental tool” to make predictions. On the basis of the FLP principle, we designed metal-free molecules for hydrogen [107–109], methane [110], and ammonia [111] activations and catalysts for

hydrogenation of imines [112–114], ketones [114, 115], and alkenes [114]. As we noticed that several computational chemists are also the contributors of the book, to avoid repetition we will limit the scope of this chapter to the studies from our group [107–115] with a focus on computational design.

## 2 General Principles for Facile Hydrogen Activation

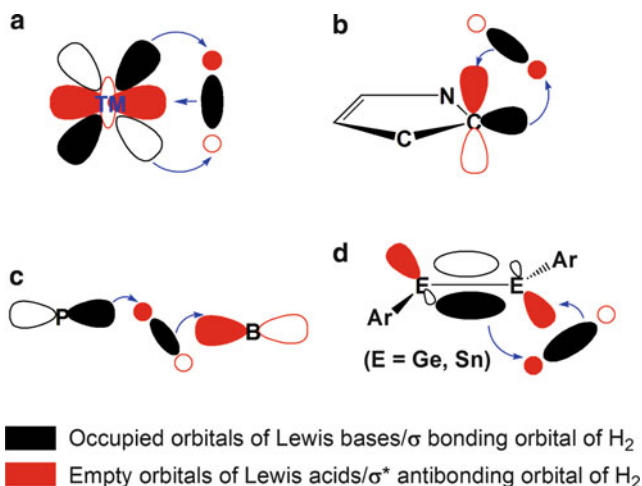
In general, when an electron-deficient Lewis acid attacks the H–H bond, the vacant orbital of the Lewis acid interacts with the H–H  $\sigma$ -bonding orbital, which weakens the H–H bond by reducing the  $\sigma$ -bonding electrons. When an electron-rich Lewis base attacks the H–H bond, the lone pair orbital of the Lewis base interacts with the H–H  $\sigma^*$ -antibonding orbital, which weakens the H–H bond by giving electrons to the H–H  $\sigma^*$ -antibonding orbital. If a system combines the two effects to operate cooperatively, the system would possess both Lewis acid and base catalytic effects and thus exhibit high reactivity toward  $H_2$ . Essentially, the various hydrogen activation systems, including both TM and TM-free ones, share the same general principle but differ in the manner of how to allow both effects to operate cooperatively.

For the TM-mediated hydrogen activation [7], as illustrated by Scheme 1a, the H–H  $\sigma$ -bonding orbital interacts with the empty  $d_z^2$  orbital of the TM center and meanwhile the occupied  $d_{xy}$  orbital interacts with the H–H  $\sigma^*$ -antibonding orbital (i.e., the back-donation), resulting in facile H–H bond cleavage. Interestingly, the single TM-center plays both Lewis acid and base roles. In this regard, the metal-free (alkyl)(amino) stable carbenes activate hydrogen similarly [13]. The carbene carbon serves as both Lewis acid and base center; the lone pair on the carbene carbon functions as a Lewis base to donate electrons and the empty  $p_\pi$  orbital as a Lewis acid to accept electrons (Scheme 1b) [13].

The well-known metal–ligand bifunctional hydrogenation catalysts have separate Lewis acid and base active sites [25]. Similarly, as represented by the prototypical FLP,  $tBu_3P/B(C_6F_5)_3$  (Scheme 1c), FLPs have distinguishable Lewis acid and base components [50]. Because Lewis acids and bases prefer to form stable Lewis acid/base adducts, sterically demanding substituents are required to prevent formations of stable Lewis acid/base adducts. The Lewis acids and bases in FLPs can either be two separate molecules (e.g.,  $tBu_3P/B(C_6F_5)_3$ ) [50] or be grafted into a single molecule (e.g.,  $Mes_2PCH_2CH_2B(C_6F_5)_2$ ,  $TMPN-CH_2C_6H_4B(C_6F_5)_2$  ( $TMPN = 2,2,6,6$ -tetramethylpiperidine)) [69, 116]. Pápai's [90] and Li's [91] groups proposed that the synergic catalytic effects of Lewis acids and bases are the origins of the high reactivity of FLPs, but the study by Grimme–Erker joint group called attention to the electric field created by the Lewis acid/base pairs [99]. The systematic computational study by Pápai's group emphasized the profound effects of the Lewis acidity and basicity of FLPs on the FLP reactivity [95].

Power and coworkers attributed the facile hydrogen activation by the heavier alkyne congeners (e.g.,  $Ar'EEAr'$ ,  $E = Ge$  and  $Sn$ ) to the synergic interaction





**Scheme 1** Orbital interactions to operate Lewis acid/base bifunctional reactivity cooperatively

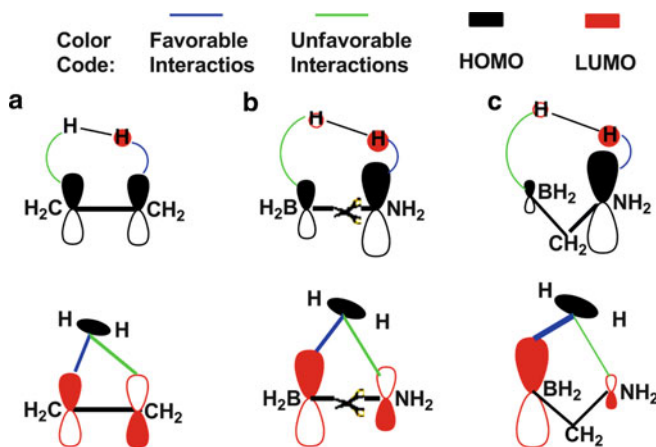
between the occupied  $\pi$ -orbital of E–E bond with H–H  $\sigma^*$ -antibonding orbital and that between the empty  $n_+$  orbital of  $Ar'EEAr'$  with H–H  $\sigma$ -bonding orbital (Scheme 1d) [117, 118]. Previous computational study using models of experimental compounds suggested that the heavier alkyne analogs ( $Ar'GeGeAr'$  in particular) may have significant diradical character responsible for their high reactivity [119], but our recent study on the experimental digermynes and distannynes showed that they have no substantive diradical character [120], and the differences between the reactions of  $Ar'EEAr'$  ( $E = Ge$  and  $Sn$ ) with  $H_2$  can be ascribed to the higher reactivity of the key intermediate  $Ar'GeGeH_2Ar'$  than that of its counterpart ( $Ar'SnSnH_2Ar'$ ) due to the inert lone pair effect [120].

### 3 Computational Design of Metal-Free Molecules for Activations of Small Molecules

#### 3.1 $\pi$ -FLP Strategy for $H_2$ Activation

Hydrogen activation is the crucial step in catalytic hydrogenation [25]. To design hydrogenation catalysts we first need to find an active site with electronic structure capable of cleaving H–H bonds. In terms of the frontier molecular orbital (FMO) theory, Scheme 2 illustrates our thinking of how to find the active site.

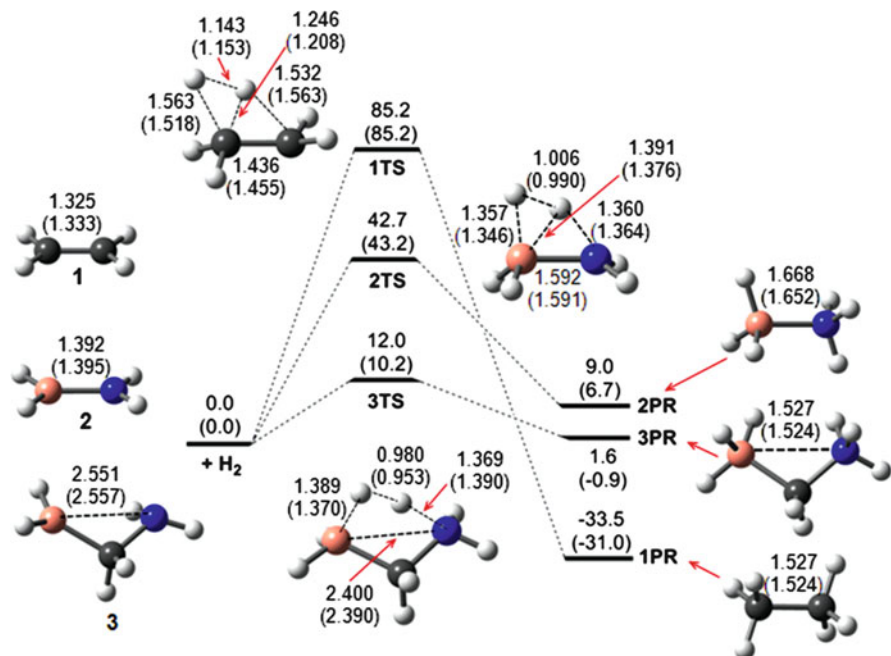
The addition of  $H_2$  to ethylene (**1**) is a symmetry-forbidden reaction. Because the symmetries of HOMO and LUMO of **1** do not match those of LUMO and HOMO of  $H_2$ , respectively,  $H_2$  cannot interact with **1** effectively, resulting in a very high activation barrier. We viewed the FMO interaction picture from another angle,



**Scheme 2** Schematic illustrations of how to enhance the favorable and weaken the unfavorable interactions in the two pairs of FMO interactions. Note that the width of arcs or lines qualitatively represent the magnitude of the interactions. From  $C_2H_4$  to  $BH_2NH_2$  to  $BH_2CH_2NH_2$ , the favorable interactions increase and the unfavorable interactions decrease

considering each of the two pairs of FMO interactions including both favorable (blue arcs or lines in Scheme 2a) and unfavorable (green arcs or lines) interactions. Due to the symmetric features of **1**, the favorable and unfavorable interactions in either pairs of FMO interactions cancel each other, resulting in a very high barrier. Along this line of thinking, to reduce the activation barrier we need to enhance the favorable interactions and weaken the unfavorable ones. This can be fulfilled by isoelectronic replacement of CC in **1** with BN, giving  $BH_2NH_2$  (**2**). Because the HOMO and LUMO of **2** are dominated by the nitrogen and boron  $p_\pi$  atomic orbitals, respectively (Scheme 2b), the favorable interactions are enhanced and the unfavorable ones weakened. It can be expected that **2** has a lower activation barrier than **1**. However, there exists a  $\pi$  donation from nitrogen to boron in **2**; the boron  $p_\pi$  atomic orbital and the nitrogen  $p_\pi$  lone pair still have substantial contributions to the HOMO and LUMO of **2**, respectively. To lower the activation barrier further, we insert a  $-CH_2-$  linkage to the B–N bond of **2** to prevent the electron donation, giving  $BH_2CH_2NH_2$  (**3**). Because the  $-CH_2-$  linkage in **3** precludes the intramolecular  $\pi$  donation from nitrogen to boron, the contribution of boron  $p_\pi$  atomic orbital to the **3** HOMO and that of nitrogen  $p_\pi$  atomic orbital to the **3** LUMO are further reduced, and thus the favorable interactions are further enhanced and the unfavorable ones further weakened. Therefore, the activation barrier by **3** is expected to be greatly reduced.

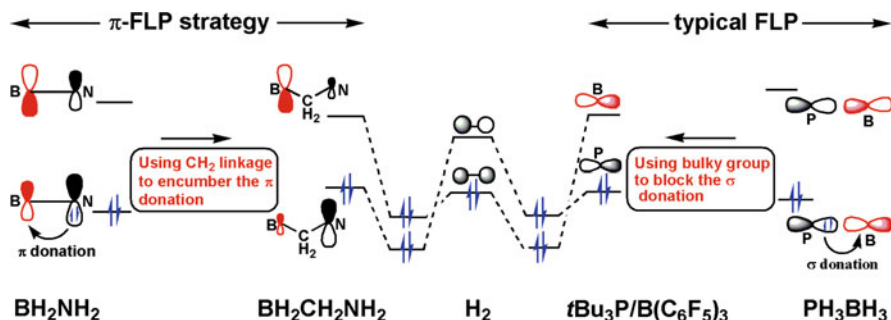
Figure 1 shows the computed energetic and geometric results for the hydrogen activations by **1**, **2**, and **3**. In accordance with the FMO analyses, the activation energies drop significantly and sequentially. The  $H_2$  activation energies by **1**, **2**, and **3** are 85.2, 42.7, and 12.0 kcal/mole at the M05-2X/6-311++G(d,p) + ZPE(zero point energy) level, respectively, which are close to the 85.2, 43.2, and 10.2 kcal/



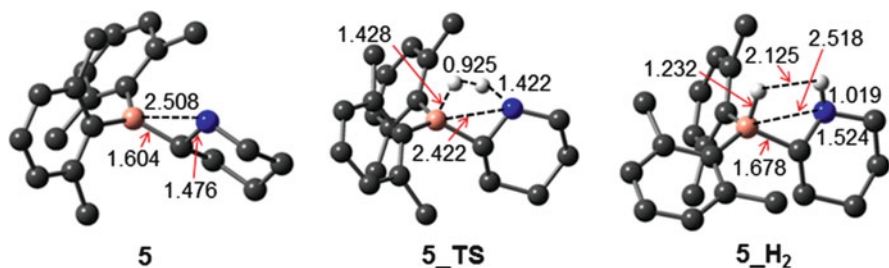
**Fig. 1** Energetic and geometric results for the H<sub>2</sub> activations by **1**, **2**, and **3**. The geometries with key bond lengths in Å were optimized at the M05-2X/6-311++G(d,p) level, and the relative energies (in kcal/mole) were obtained at the M05-2X/6-311++G(d,p) + ZPE level. The bond lengths in the parentheses were obtained at the MP2/aug-cc-pVTZ level and the energetic values in the parentheses at the CCSD(T)/aug-cc-pVTZ//MP2/aug-cc-pVTZ + ZPE(MP2) level

mole predicted at the CCSD(T)/aug-cc-pVTZ//MP2/aug-cc-pVTZ + ZPE(MP2) level. Therefore, the CH<sub>2</sub> linkage is very effective to prevent the  $\pi$ -donation. The hydrogen activation barrier by BH<sub>2</sub>CH<sub>2</sub>NH<sub>2</sub> (**3**) is also less than the 17.3 kcal/mole by BH<sub>2</sub>PH<sub>2</sub> (**4**) [107] whose derivative, R<sub>2</sub>PB(C<sub>6</sub>F<sub>5</sub>)<sub>2</sub> (R = Cy, *t*Bu), has been experimentally demonstrated capable of H<sub>2</sub> activation [53]. The hydrogen activation barrier of *t*Bu<sub>2</sub>PB(C<sub>6</sub>F<sub>5</sub>)<sub>2</sub> was reported to be 28.0 kcal/mole by Privalov et al. at the B3LYP/6-31+G(d) + ZPE level [105]. In terms of the ZPE-corrected energies, the active site in **3** shows potential for reversible hydrogen activation which is desired for designing hydrogenation catalysts.

The facile H<sub>2</sub> activation by **3** also follows the general principle discussed in Sect. 2. The function of the -CH<sub>2</sub>- linkage is to prevent the  $\pi$  electron donation from nitrogen to boron, thereby preserving the reactivity of Lewis acidic boron and Lewis basic nitrogen centers, respectively. The strategy is similar to FLP but differs in constructing the active site. Scheme 3 shows the difference between **3** and the prototypical *t*Bu<sub>3</sub>P/B(C<sub>6</sub>F<sub>5</sub>)<sub>3</sub> FLP. While the active site of *t*Bu<sub>3</sub>P/B(C<sub>6</sub>F<sub>5</sub>)<sub>3</sub> FLP is constructed by blocking the  $\sigma$  bonding in the Lewis acid/base adduct (PH<sub>3</sub>BH<sub>3</sub>), the -CH<sub>2</sub>- linkage in **3** prevents the intramolecular  $\pi$  donation in **2**. Because of



**Scheme 3** Comparisons of the  $\text{BH}_2\text{CH}_2\text{NH}_2$   $\pi$ -FLP and the typical  $t\text{Bu}_3\text{P}/\text{B}(\text{C}_6\text{F}_5)_3$  FLP



**Fig. 2** Optimized structures of **5**, **5<sub>TS</sub>**, and **5<sub>H<sub>2</sub></sub>** at M05-2X/6-311++G(d,p) level

the difference, we have termed our strategy “ $\pi$ -FLP” in the following for the convenience of description.

The model **3** has a low  $\text{H}_2$  activation barrier (12.0 kcal/mole), but it is experimentally impracticable, because its reactivity can be quenched by dimerization, isomerization to more stable isomer, or formation of stable complexes with solvent molecules (e.g., THF) [107]. To preserve its reactivity, proper chemical scaffolds need to be constructed to protect the active site. Molecule **5** (see Fig. 2) is such an example among many possible variations after excluding possible deactivations [107].

Table 1 lists the energetic results of the **5** +  $\text{H}_2$  reaction in the different solvents, and the optimized structures of **5**, **5<sub>TS</sub>** (activation transition state), and **5<sub>H<sub>2</sub></sub>** (product) are displayed in Fig. 2. As compared in Table 1, the solvents have no apparent effects on the activation barrier but can stabilize the product by several kcal/mole, which can be attributed to the zwitterionic product due to the heterolytic  $\text{H}_2$  cleavage. Because ideal gas phase model computations often overestimate the entropic penalty for entropically unfavorable reactions in solvents [112, 121–126], we considered the hydrogen activations to be nearly reversible, which is desirable for design of metal-free hydrogenation catalysts. Interestingly, as the experimental FLPs often used perfluorophenyl substituted boron-site to enhance the Lewis

**Table 1** M05-2X/6-311++G(d,p) free energy and enthalpy results (in kcal/mole) for the H<sub>2</sub> activation by **5** in the gas phase (GAS), toluene (TOL), THF, and DMSO

Molecule <b>5</b>	Transition states		Products	
	$\Delta G^\ddagger$	$\Delta H^\ddagger$	$\Delta G$	$\Delta H$
Gas phase	26.1	14.8	8.2	-1.9
TOL ( $\epsilon = 2.38$ )	27.0	14.8	6.4	-4.4
THF ( $\epsilon = 7.58$ )	26.7	14.5	4.0	-6.8
DMSO ( $\epsilon = 46.7$ )	27.4	15.2	3.5	-7.3

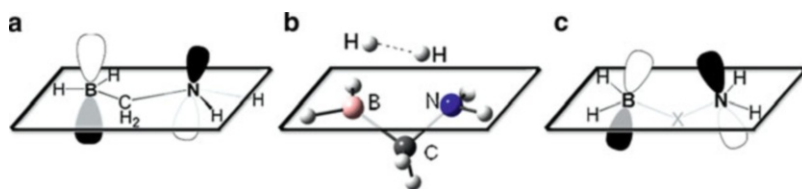
acidity [47–49], **5** has a weaker Lewis acidic site ( $-\text{B}(2,6\text{-Me-C}_6\text{H}_3)_2$ ) but still has high reactivity toward H<sub>2</sub>, which can be attributed to the optimal bifunctional active site ( $>\text{BCH}_2\text{N}<$ ) that allows H<sub>2</sub> to interact with the active site more efficiently.

### 3.2 Fine Tuning the $\pi$ -FLP Active Site for Enhanced Reactivity Toward H<sub>2</sub>

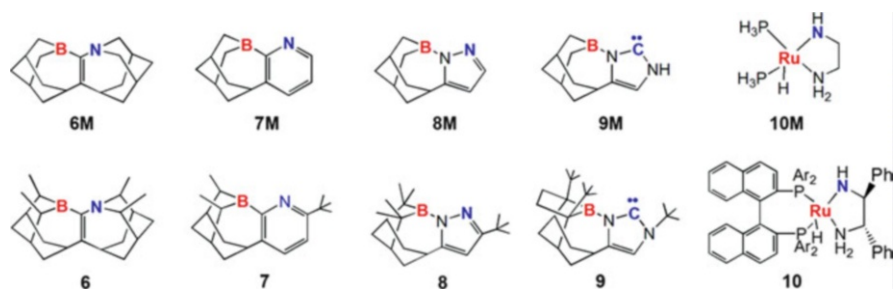
Reversible hydrogen activation is crucial for catalytic hydrogenation. It is desired to make hydrogen activation as reversible as possible. Analyzing the HOMO and LUMO of BH<sub>2</sub>CH<sub>2</sub>NH<sub>2</sub> model (**3**), we speculated that the reactivity of  $\pi$ -FLP active site could be further improved by tuning the construction of the active site [108].

Scheme 4 illustrates our reasoning for tuning the active site. In BH<sub>2</sub>CH<sub>2</sub>NH<sub>2</sub> the boron vacant p <sub>$\pi$</sub>  orbital is nearly perpendicular to the defined BCN plane and the nitrogen p <sub>$\pi$</sub>  lone pair tilts to the plane (Scheme 4a); the orientation of the two orbitals is not optimal to perform bifunctional reactivity. In the transition state (Scheme 4b), the dihydrogen tends to be coplanar with the B...N axis, implying that a transition state with dihydrogen and B...N in the same plane could lower the barrier by relieving the strain. We hypothesized that an active site in which the two orbitals are in the same plane and face to face (Scheme 4c) could be a better active site. To implement such an active site, we embedded the active site in proper molecular frameworks [108]. As exemplified by **6M–7M** in Scheme 5, such an active site can be enforced by utilizing the planarization of sp<sup>2</sup> carbon. The bridging nitrogen atoms in **8M** and **9M** are not sp<sup>2</sup> hybridized, but the planarization due to aromaticity of the five-membered rings can also hold such an active site.

**6M–9M** possess the optimal active sites, but the active sites can be deactivated by intermolecular dimerization. To avoid the issue the molecules **6–9** were designed. The energetic results for the reactions of **6–9** with H<sub>2</sub> are compared with those of the model (**10M**) of the experimental MLBHC (**10**) [127–139] in Table 2. The metal-free **6** and **7** have kinetics and thermodynamics for reversibility comparable with those of **10M**. The molecules **8** and **9** have lower activation barriers than **10M**, but their reactions with H<sub>2</sub> are somewhat too exothermic (in particular **9**), implying that the active sites in **8** and **9** are probably unsuitable for hydrogenation catalyst design.



**Scheme 4** Idea to construct more reactive active sites for H<sub>2</sub> activation



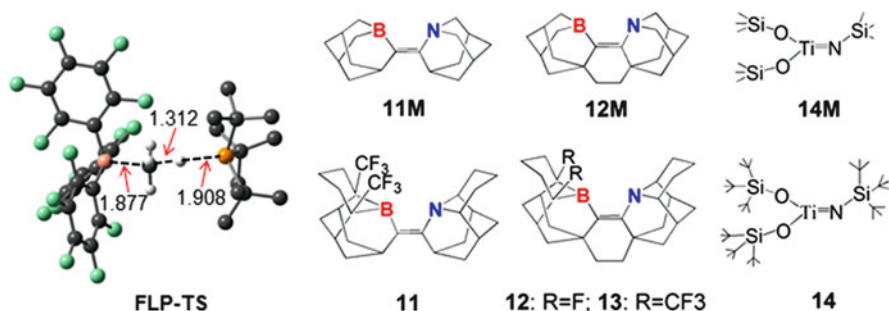
**Scheme 5** Designed models/molecules with desired hydrogen activation sites

**Table 2** M05-2X(IEFPCM, solvent=toluene)/6-311++G(d,p)//M05-2X/6-311++G(d,p) free energy and enthalpy results (in kcal/mole) for the H<sub>2</sub> activations in toluene by **6–9**, compared with those of the model (**10M**) of the MLBHC (**10**)

Solvents	Transition states		Products	
	$\Delta G^\ddagger$	$\Delta H^\ddagger$	$\Delta G$	$\Delta H$
<b>6</b>	13.5	3.8	−2.7	−11.8
<b>7</b>	15.4	5.8	−7.8	−16.7
<b>8</b>	15.4	5.9	−12.7	−22.6
<b>9</b>	15.5	5.4	−32.9	−43.0
<b>10M</b>	17.2	7.8	−5.1	−14.4

### 3.3 Further Fine Tuning the $\pi$ -FLP Active Site for Methane Activation

It is more difficult to activate methane than H<sub>2</sub> [1, 2, 140]. In addition to H<sub>2</sub>, FLPs were found to have high reactivity toward other small molecules (e.g., NH<sub>3</sub> [78], N<sub>2</sub>O [83], THF [64, 84], C<sub>2</sub>H<sub>4</sub> [85], CO<sub>2</sub> [86], terminal alkyne [63], and 1,3-dienes [87]), but there has been no experimental or computational study to show that FLP can activate methane. To evaluate the reactivity of FLPs toward methane, the methane activation transition state by *t*Bu<sub>3</sub>P/B(C<sub>6</sub>F<sub>5</sub>)<sub>3</sub> FLP was located (**FLP-TS** in Scheme 6). Because the CH<sub>3</sub> moiety hampers effective interaction of the boron vacant orbital with the C–H  $\sigma$  bonding orbital of methane, the FLP cannot perform its Lewis acidic reactivity optimally. Consistently, the methane activation barrier



**Scheme 6** M05-2X/6-31+G(d,p) optimized geometry of the transition state (**FLP-TS**) and our designed metal-free models/molecules for methane activation

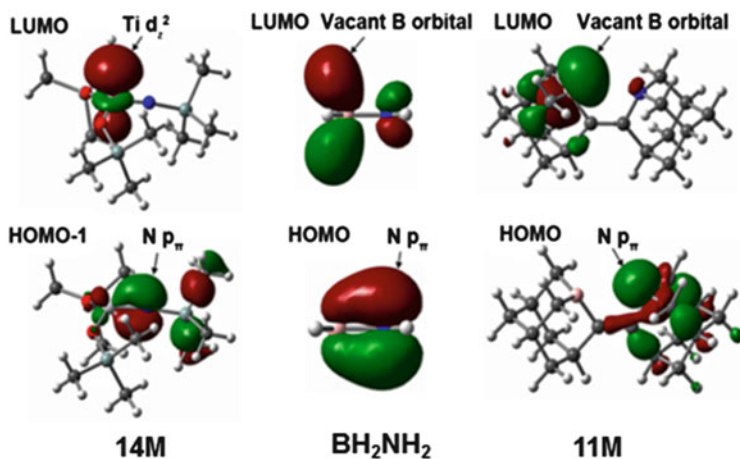
( $\Delta G_{sol}^{\ddagger} = 38.3$  kcal/mole, solvent = cyclohexane) was predicted to be much higher than the 13.4 kcal/mole of hydrogen activation [110]. On the basis of the fact that a side-on attack was adopted in the methane activation by TM complex, we reasoned that our  $\pi$ -FLP active site could be structurally suitable for methane activation. Based on **6M** (see Scheme 5), **11M** and **12M** were designed under the considerations that the long B...N distance can further prevent the possible electron donation from nitrogen to boron as in **6M**, and the enlarged active sites could benefit methane activation, because methane is larger than hydrogen [110].

On the basis of **11M** and **12M** models, more molecules were designed after excluding possible dimerizations [110]. The molecules **11–13** in Scheme 6 are representative. The use of CF<sub>3</sub> and F substituents is to enhance the Lewis acidic reactivity of the boron center. **14M** is the model of the TM complex **14** (*t*Bu<sub>3</sub>SiO)<sub>2</sub>Ti=NSi*t*Bu<sub>3</sub>) that was experimentally shown to be able to activate methane via 1,2-addition [141, 142]. As compared in Table 3, the methane activations by **11–13** have barriers comparable with/or lower barriers than that by the TM complex model (**14M**). The reactions of **11–13** with methane are nearly reversible, implying that such active sites could be based to develop catalysts for methane utilization.

The methane activation mechanism by **11–13** is similar to that by TM complex (e.g., **14M**). Their active sites are composed of electron deficient centers (boron in **11–13** and Ti in **14**) and electron rich center (i.e., N) to exert the Lewis acidic/basic reactivity cooperatively. However, the Ti- and N-centers in **14M** are bound together directly, while the N- and B-centers in **11M** are separated by linkages. To gain insight into the difference, the two orbitals of **11M**, **14M**, and **2** (BH<sub>2</sub>NH<sub>2</sub>) contributing to the Lewis acidic/basic reactivity, respectively, are compared in Fig. 3. For **14M**, the LUMO is dominated by Ti  $d_z^2$  atomic orbital and the HOMO-1 by the nitrogen  $p_\pi$  lone pair. Because the two atomic orbitals ( $d_z^2$  and  $p_\pi$ ) are not symmetrically compatible, the nitrogen lone pair electrons cannot be donated to the electron deficient Ti-center, which maintains the Lewis acidity of the center. In contrast, the vacant boron orbital and nitrogen lone pair orbital have the same symmetry ( $p_\pi$ ) in BH<sub>2</sub>NH<sub>2</sub>, allowing them to interact with each other, which weakens both the Lewis acidity of boron center and the basicity

**Table 3** M05-2X(IEFPCM, solvent=cyclohexane)/6-311++G(2d,p)//M05-2X/6-31G(d,p) free energy and enthalpy results (in kcal/mole) for the methane activation

Molecules	Transition states		Products	
	$\Delta G^\ddagger$	$\Delta H^\ddagger$	$\Delta G$	$\Delta H$
<b>11</b>	22.4	10.4	-1.9	-13.6
<b>12</b>	20.0	7.7	-4.5	-16.7
<b>13</b>	20.2	8.1	-5.2	-17.4
<b>14M</b>	22.3	11.3	-11.4	-21.4



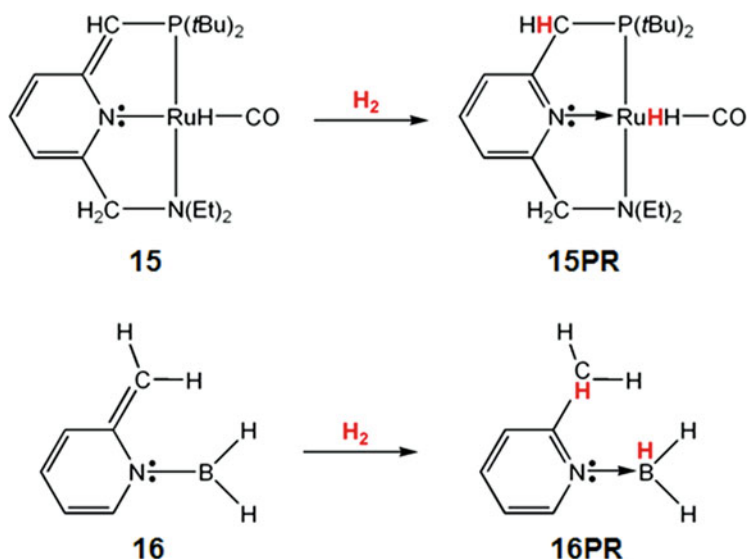
**Fig. 3** Two critical MOs for the Lewis acid and Lewis base centers of TM-complex model (**14M**),  $\text{BH}_2\text{NH}_2$  and our designed molecule (**11M**)

of nitrogen center. When the B- and N-centers are separated by linkages as exemplified by **11M**, the interaction between the vacant boron orbital and nitrogen lone pair is spatially prohibited. It can be concluded that the principles of methane activation by the TM complex (e.g., **14**) and by our designed metal-free molecules are the same, but the ways to preserve the effective acid/base active sites are different; the former uses incompatible atomic orbital symmetries to prevent the donor-acceptor interaction between the bound Ti and N atoms, and thus maintain Lewis acidity of Ti center, while the latter uses space to prevent the donor-acceptor interaction between B and N atoms, and thus maintain the Lewis acidity of B center.

### 3.4 Designing Metal-Free Molecules for $\text{H}_2$ Activation by Mimicking TM Pincer Catalysts

As discussed in Sect. 2,  $\text{H}_2$  activations by metal-free molecules and TM complexes essentially share the same principle, using the reactivity of Lewis acids/bases cooperatively, which inspired to hypothesize that one may design metal-free molecules based on known transition metal complexes. In our exploration, the

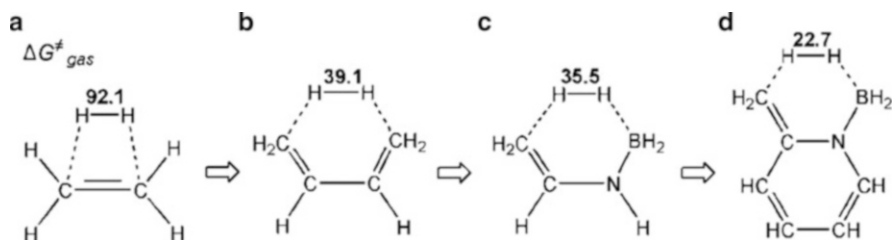




**Scheme 7** Mimicking the electronic effects of TM pincer catalysts

TM-pincer catalyst (e.g., **15** in Scheme 7), developed by Milstein's group [143–149], was chosen as a template. The catalyst **15** or its analogs have shown great reactivity toward various  $\sigma$ -bonds such as H–H [143, 144], C–H [145], N–H [149], and O–H [146, 150] bonds. The reactivity of these TM complexes originates from their novel electronic effects, including the following. (1) H<sub>2</sub> activation is a formal [4+2] cycloaddition involving the two electrons of the C=C bond, the two nitrogen lone pair electrons, and the two  $\sigma$  electrons of the H–H bond. The aromatic effect due to the involvement of six electrons can stabilize the activation transition state and thus facilitates H–H bond breaking. (2) The nonaromatic six-membered ring in **15** gains aromaticity gradually during the H<sub>2</sub> addition and becomes an aromatic pyridine ring in the product (**15PR**). The aromatization effect can facilitate H–H bond breaking. (3) The Ru center and the sp<sup>2</sup> C of the arm have Lewis acidic/basic catalytic effects, respectively, contributing to H–H bond cleavage. To mimic these electronic effects, the metal-free counterpart **16** of the TM complex (**15**) was designed [109]. Needless to say, the metal-free counterpart **16** can mimic the electronic effects of **15** in hydrogen activation.

Scheme 8 shows the individual contributions of these electronic effects to H<sub>2</sub> activation in terms of the barriers heights at the M05-2X/6-311++G(2d,p)//M05-2X/6-31(d,p) + ZPE level. The 93.9 kcal/mole barrier for the symmetry-forbidden [2+2] addition of H<sub>2</sub> to ethylene (Scheme 8a) is lowered dramatically to 39.1 kcal/mole due to the six electron aromatic stabilization in the transition state for the 1,4-addition of H<sub>2</sub> to *syn*-butadiene (Scheme 8b) [109]. The replacement of a C=C bond with the isoelectronic N–B bond (Scheme 8c) lowers the barrier by



**Scheme 8** Individual contributions of electronic effects computed at the M05-2X/6-311++G(2d, p)//M05-2X/6-31G(d,p) + ZPE level. The energy results are in kcal/mole

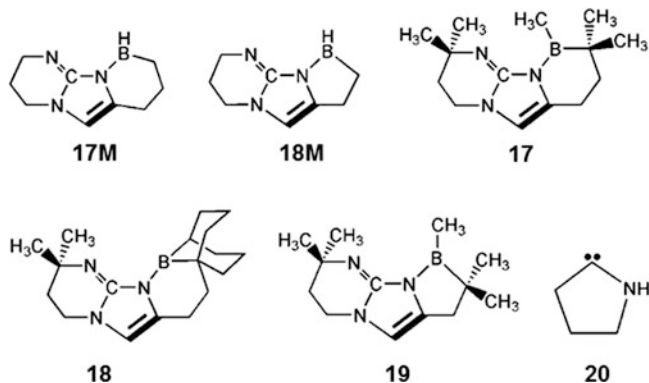
**Table 4** Free energy results (in kcal/mole) at M05-2X(IEFPCM, solvent=cyclohexane)/6-311++G(2d,p)//M05-2X/6-31G\*\*

Molecules	Transition states ( $\Delta G^\ddagger$ )	Products ( $\Delta G$ )
<b>15</b>	23.9	-2.2
<b>16</b>	20.7	-23.8
<b>17M</b>	24.0	-5.6
<b>18M</b>	29.2	-6.3
<b>17</b>	26.6	-1.3
<b>18</b>	26.6	-3.1
<b>19</b>	31.2	-2.8
<b>20</b>	35.8	-45.1
<i>t</i> Bu <sub>2</sub> P-B(C <sub>6</sub> F <sub>5</sub> ) <sub>2</sub>	31.2	-23.6

an additional 3.6 kcal/mole. The small decrease can be attributed to the weakened Lewis acidity of the boron center due to the electron donation from nitrogen. The aromatization effect utilized in Scheme 8d lowers the barrier to 22.7 kcal/mole, a 12.8 kcal/mole decrease relative to Scheme 8c.

Although the hydrogen activation free energy barrier (20.7 kcal/mole) by **16** is less than the 23.9 kcal/mole by **15** (Table 4), the activation by **16** is highly exergonic by -23.8 kcal/mole compared with the -2.2 kcal/mole of the experimental TM complex (**15**). In terms of reversibility, the model **16** is thermodynamically unsuitable for catalyst design. To achieve reversible hydrogen activation, we designed the models **17M** and **18M** (Scheme 9) by tuning these electronic effects [109], which have kinetics and thermodynamics suitable for reversible hydrogen activation (Table 4).

The models (**17M** and **18M**) may undergo dimerization or trimerization, resulting in deactivation. To avoid the issue, **17-19** were constructed on the basis of **17M** and **18M**. As compared in Table 4, the activation barriers of **17-19** are higher than that of **15**, but these could still be experimentally accessible. Note that the barriers are lower than those of the two experimental TM-free systems (a model for mono(amino) stable carbene (**20**), and *t*Bu<sub>2</sub>P-B(C<sub>6</sub>F<sub>5</sub>)<sub>2</sub>) at the same computational level. As for reversible activation, **17-19** are comparable to the TM complex **15** [109].



**Scheme 9** Schematic drawings of 17M–20

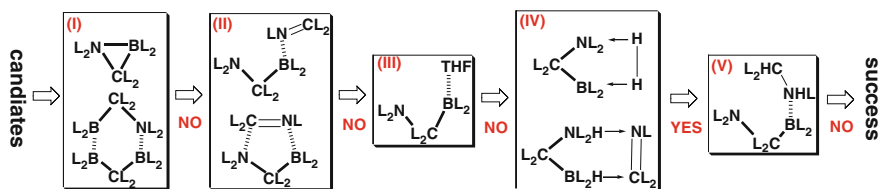
## 4 Computational Design of Metal-Free Catalysts

### 4.1 Designing Metal-Free Catalyst for Hydrogenation of Small Imine

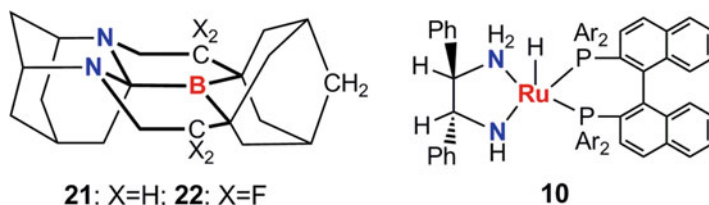
Hydrogen activation is an important process, but realizations of hydrogenation are of more practical use [25]. On the basis of the  $\pi$ -FLP strategy, we proceeded to design hydrogenation catalysts by choosing the hydrogenation of small imine  $\text{MeN}=\text{CMe}_2$  (**im1**) to amine (**am1**) as our target [112]. Note that the substrates in the FLP-based hydrogenations should be sterically demanding enough to avoid forming catalysis-quenching adducts with the Lewis acids in FLPs [59, 67].

In general, a homogeneous catalyst can be viewed as a molecule possessing the right electronic and geometric structures. The electronic structure is a prerequisite, determining whether a molecule has the potential to catalyze the desired reactions. The geometric structure ensures that the electronic structure acts properly. We have shown  $\pi$ -FLP strategy is effective to activate  $\text{H}_2$  [107–109]. To perform catalytic imine hydrogenation we need to construct appropriate chemical scaffolds to protect the  $\pi$ -FLP active site from deactivations. Based on the electronic structures of  $\pi$ -FLP active site and the imine substrate, a set of five criteria (Scheme 10) was devised to guide the catalyst design.

Criterion I excludes formation of intermolecular dimer and intramolecular adduct. Criterion II avoids forming tight adducts with imine substrates. Two types of adducts are possible: one is the conventional Lewis acid–base adduct and the other is the addition product with a five-membered ring. If hydrogenation reactions are carried out in the solvents containing electron-rich atoms such as O and N, there is a concern that the catalysts may form stable adducts with solvent molecules. We used THF as a representative to examine if a candidate can form adduct with THF (Criterion III). It should be pointed out that Criterion III is not



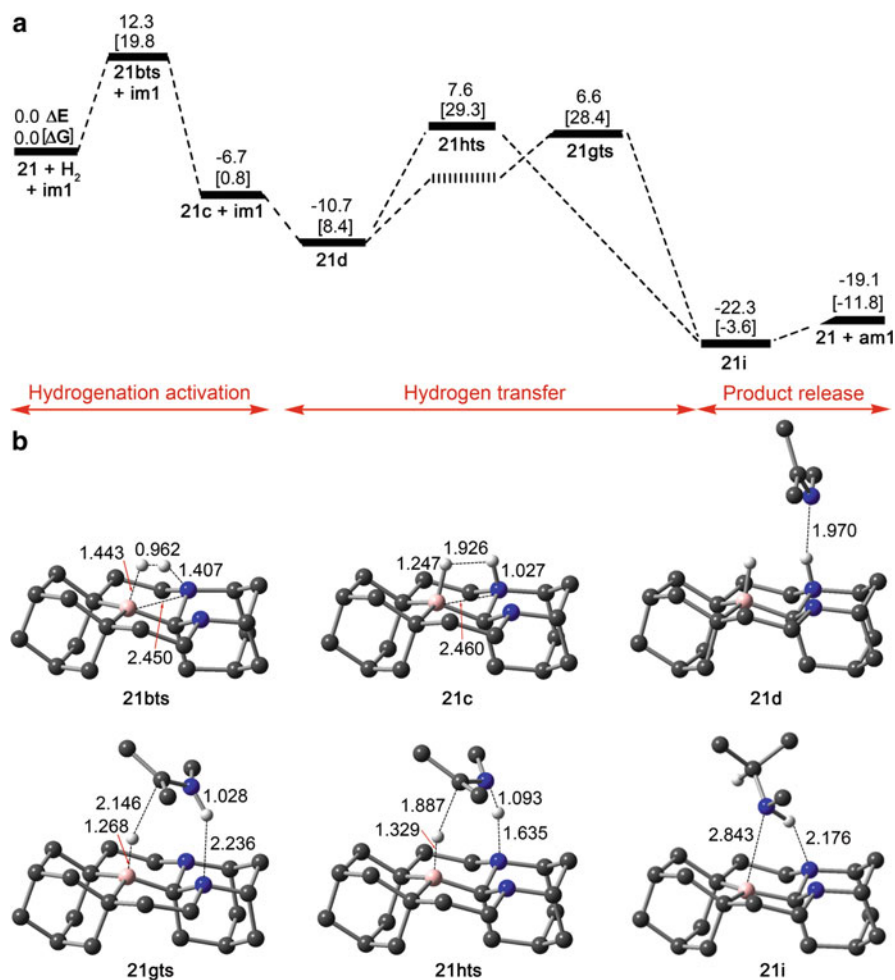
**Scheme 10** Five criteria for catalyst design



**Scheme 11** Computational designed metal-free catalysts (**21–22**) and experimental used MLBHCs (**10**)

always necessary because hydrogenation can be performed in the solvents (e.g., toluene) without electron-rich atoms. Criterion IV requires both hydrogen activation and hydride transfer steps to be kinetically and thermodynamically feasible. Criterion V ensures that the reduced product (e.g., amine) can be readily released and the catalyst can be liberated and reused in the next catalytic cycle. In short, Criteria I–III and V prevent the side reactions and Criterion IV ensures the desired hydrogenation occurs favorably. All the criteria are equally important and a failure in passing any of the criteria causes the disqualification of a candidate. The difference between a computational rationalization and a de novo design is that the former often focuses on the main reaction channels, whereas the later must consider all possible side reactions to avoid the desired reactions from being overtaken by side reactions. Our experience tells that it is not so difficult to meet Criteria I–III and V because we can always increase the steric effects to avoid forming the various complexes. The challenge lies in maintaining a balance between preventing the undesired reactions and simultaneously facilitating the desired reactions.

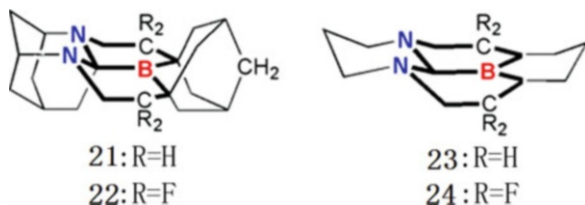
On the basis of the five criteria, the catalysts (**21** and **22**, Scheme 11) were obtained by trial and error, and they can pass the five criteria [112]. As compared in Scheme 11, the designed metal-free catalysts resemble the well-known MLBHCs (e.g., **10**) [127–139]; the electron-deficient B-center is equivalent to the unsaturated Ru-center and both use the electron-rich N-center as the proton acceptor. Furthermore, they also have similar hydrogenation mechanisms including hydrogen activation and hydrogen transfer. The difference lies in that hydrogen activation by the metal-free catalysts occurs via the B–C–N linkage, while the activation by the MLBHCs takes place through the direct Ru–N bond.



**Fig. 4** (a) Energy profile and optimized structures for the MeN=CMe<sub>2</sub> hydrogenation by **21** at M05-2X(IEFPCM, solvent=THF)/6-311++G(2d,p)//M05-2X/6-31G(d,p) level. (b) Optimized structures of the stationary points, along with the key bond distances in Å. Trivial hydrogen atoms are omitted for clarity

Figure 4 shows the geometric and energetic results for the **21**-catalyzed hydrogenation of MeN=CMe<sub>2</sub> (**im1**) to amine MeNH-CHMe<sub>2</sub> (**am1**). Considering that the ideal gas phase model computations often overestimate the entropic penalty for entropically unfavorable reactions in solvents [112, 121–126], the energetics indicates that **21** could act as a catalyst to mediate the transformation of imine (**im1**) to amine (**am1**). For the **im1** hydrogenation by **22**, because the C–H...F hydrogen bond interactions, the barriers for hydrogen transfer step are lower [112].

**Scheme 12** Schematic drawings of **21–24**

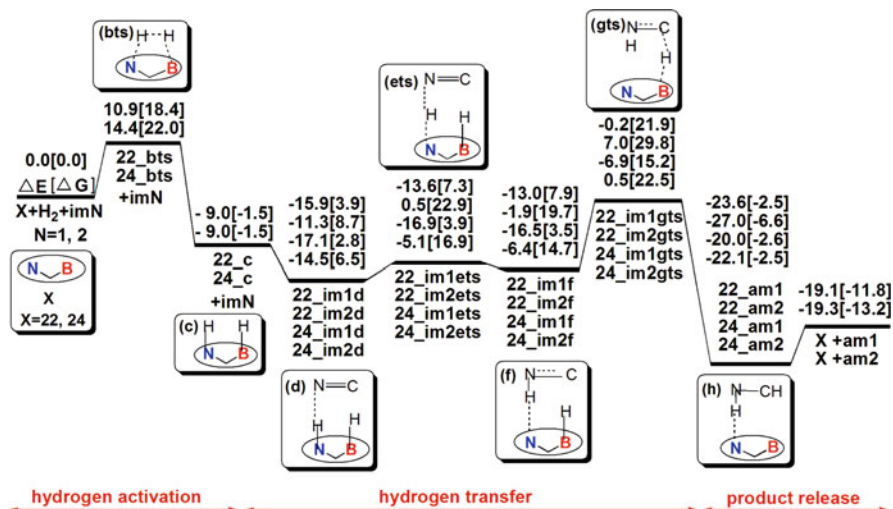


## 4.2 Catalytic Hydrogenations of Both Small and Large Imines

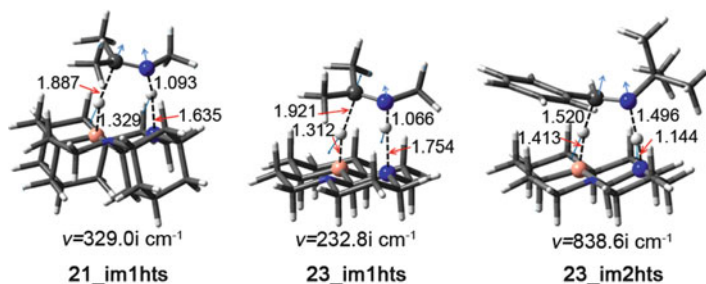
The catalysts **21** and **22** (Scheme 11) were designed using the hydrogenation of the small imine ( $\text{MeN}=\text{CMe}_2$ , **im1**) as a target [112]. It is unknown whether they are able to hydrogenate bulky imines. Note that the catalytic effect of a catalyst is closely related to the substrates. Even for the same class of substrates, the performance of a catalyst can be very different. For example, the experimental system (e.g.,  $(\text{C}_6\text{H}_2\text{Me}_3)_2\text{P}(\text{C}_6\text{F}_4)\text{B}(\text{C}_6\text{F}_5)_2$ ) can only catalyze the hydrogenation of sterically more demanding imines but perform stoichiometric hydrogenation of small imines [59]. On the basis of the previous experimental and computational studies, we selected  $t\text{BuN}=\text{C}(\text{H})\text{Ph}$  (**im2**) as a representative of large imines to assess the energetics of the **21**- and **22**-catalyzed hydrogenations of bulky imines [113]. As expected, the computed energetics indicates that **21** and **22** have higher hydrogen transfer barriers in **im2** than in **im1** hydrogenation [113].

To improve the catalysis in hydrogenating large imines, we truncated the two lower  $\text{CH}(\text{CH}_2)_3$  fragments in **21** and **22**, giving **23** and **24** (see Scheme 12) [113] which were found to have improved kinetics for the hydrogenation of the bulky  $t\text{BuN}=\text{C}(\text{H})\text{Ph}$  (**im2**) compared to **21** and **22**. As compared in Fig. 5, **24** catalyzes **im2** hydrogenation with more favorable kinetics than **22**. In terms of barriers in both hydrogen activation and hydrogen transfer steps, the **im1** hydrogenations catalyzed by **23** and **24** are energetically more favorable than the hydrogenations by **21** and **22** [113]. In addition, because of the less complex construction of **23** and **24** compared to **21** and **22**, the former molecules (**23** and **24**) were recommended for experimental realizations and could be suitable for hydrogenation of both small and large imines.

Interestingly, comparing the hydrogen transfer steps in the eight hydrogenations (**imN/X**,  $\text{N} = 1, 2$ ;  $\text{X} = \mathbf{21-24}$ ), it was observed that the mechanism for the hydrogen transfer step in the catalytic cycles depends on the steric effect between the catalysts and substrates [113]. The hydrogen transfer mechanism can be switched from stepwise in the case of large steric effect to concerted in the case of small steric effect. For examples, among the eight hydrogenations (**im1-im2/21-24**), the steric effect between **im1** and **23** is least and the hydrogen transfer in **im1/23** takes place via a concerted mechanism (see **23\_im1hts** in Fig. 6). For the hydrogenations (**im2/21**, **im2/22**, **im2/24**, **im1/22**, and **im1/24**) which have relatively large steric effects, the hydrogen transfer steps take place via a stepwise mechanism. For the **im1/21** and **im2/23** hydrogenations, the steric effect is



**Fig. 5** Energy profile in THF (in kcal/mole) and the structures of the stationary points in the catalytic cycle for 22- and 24-mediated hydrogenation of im1 and im2. The values in the square brackets are free energies (in kcal/mole)



**Fig. 6** M05-2x/6-31G(d,p) optimized structures of 21\_im1hts, 23\_im1hts, and 23\_im2hts (bond distance in Å) and the vibration vector corresponding to the imaginary frequencies

expected to be between the above two cases – both stepwise and concerted pathways can be located [113] (the transition states, 21\_im1hts and 23\_im2hts, for the concerted pathways in im1/21 and im2/23 are given in Fig. 6), but stepwise is more energetically favorable.

### 4.3 Catalytic Hydrogenations of Bulky Ketones

Ketone hydrogenation is another class of important reactions [25]. In comparison with imine hydrogenation, two issues may complicate FLP-based ketone hydrogenation. First, like imine hydrogenations catalyzed by  $\text{B}(\text{C}_6\text{F}_5)_3$ , if ketone

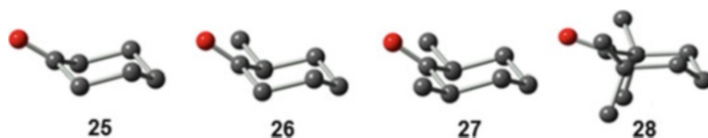


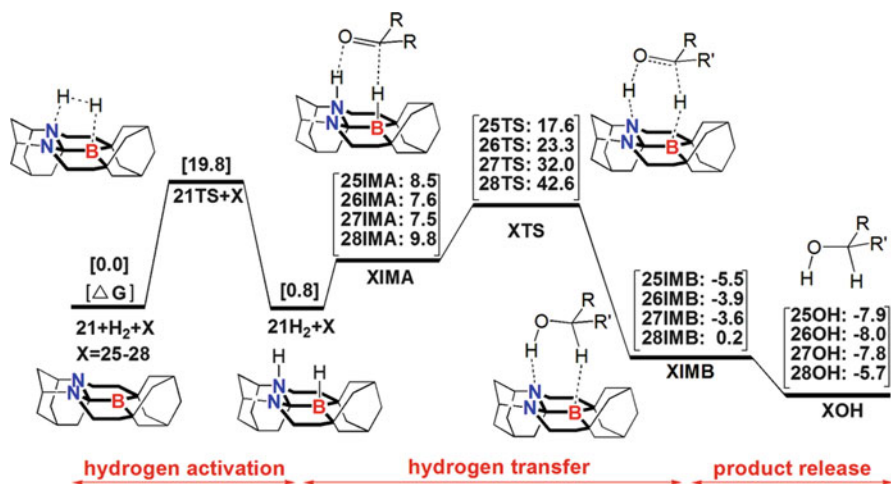
Fig. 7 Four ketones used to explore the catalytic reactions with catalyst **21**

substrates are required to play a Lewis base role to break H–H bond, ketones may not be Lewis basic enough to form FLPs to activate hydrogen, which could be one of the reasons for the lack of experimental FLPs combining a Lewis acid and an oxygen-centered Lewis base. Experimentally, Stephan and coworkers observed that the proton transfer from the phosphonium center to the oxygen atom of ketones is more difficult than to the nitrogen atom of imines [59]. Computationally, the study by Privalov's group indicated the hydrogen activation by benzophenone/ $B(C_6F_5)_3$  FLP is endergonic by 18.8 kcal/mole [151], while the hydrogen activation by the imine ( $tBuN=C(H)Ph$ )/ $B(C_6F_5)_3$  FLP conducted by Papái's group is exothermic by 27.1 kcal/mole [104]. Second, ketones are easier to form Lewis acid–base adducts with the Lewis acids than imines because of the exposed oxygen atom of the ketone C=O double bond. The formations of such adducts can disable the reactivity of FLPs. In addition, experimental studies have shown that FLPs can also undergo 1,2-additions to carbonyl groups [49, 61]. We envisioned that small ketones could also form Lewis adducts with our designed catalysts, and thus use the more sterically demanding cyclohexanone (**25**, Fig. 7) and its derivatives (**26–28**) as ketone representatives to examine whether the catalyst (**21**) can complete the catalytic cycle of ketone hydrogenation with feasible energetics [115].

It was confirmed that these ketones and their reduced alcohols cannot form stable complexes with **21** [115]. In addition to the side reactions considered in Criteria I–III and V (Scheme 10), another possible side reaction in ketone hydrogenation was considered; the catalyst may break the O–H bond of the alcohol products to form stable alkoxide complexes which prevent the release of the alcohol products [139, 152, 153]. We also confirmed that these side reactions cannot occur in these ketone hydrogenations [115]. Figure 8 shows the energetic results (free energy) for the hydrogenations of **25–28** catalyzed by **21**, which indicate the catalyst **21** could be effective for the hydrogenations of bulky ketones (**25–27**), but the hydrogen transfer barrier in the hydrogenation of **28** is too high.

With regard to our designed catalysts (**21–22**, Scheme 11), as well as **23** and **24** (Scheme 12), while they are awaiting experimental synthesis we envision that the catalysts could have the following advantages. (1) Similar to the MLBHC-catalyzed hydrogenation, the hydrogen activation step takes place separately without the involvement of the substrate (e.g., imine), in contrast to the  $B(C_6F_5)_3$ -mediated imine hydrogenation in which the substrate functions as the Lewis base of FLP to activate hydrogen. This feature can benefit the hydrogen addition to the double bonds which lack strong Lewis basic center. (2) Like the hydrides of MLBHCs, the two activated hydrogen atoms in the hydrides of the catalysts lie closely on the



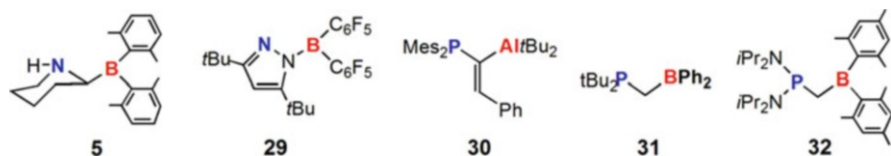


**Fig. 8** Free energy profiles in THF (in kcal/mole) and the structures of the stationary points in the catalytic cycle for **21**-mediated hydrogenations of **25–28**

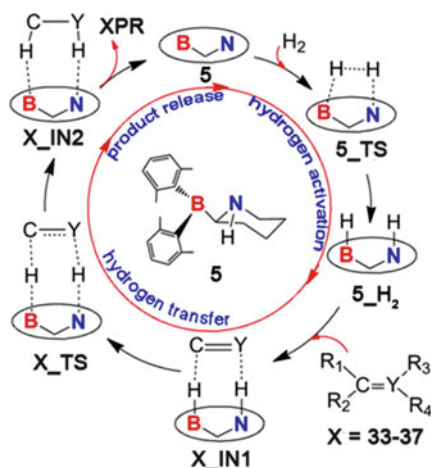
same side of the catalysts, which can facilitate the hydrogen transfer step in the catalytic cycles. (3) The relatively rigid frameworks of our designed catalysts may help realize asymmetric hydrogenation because, like MLBHCs (**10**), one can design proper substituents to favor the reaction channel to give the desired enantiomer over the other. Efforts have been made to realize asymmetric hydrogenation of imines based on FLP chemistry [68, 154].

#### 4.4 Catalytic Hydrogenations of Various Unsaturated Compounds

In our previous study we have shown that the molecule **5** is able to activate H<sub>2</sub> reversibly [107] but it was unknown whether **5** can be used as a hydrogenation catalyst. Although our designed molecules have not been synthesized, the active sites in our designed molecules have features present in the compounds synthesized later [156–161]. The compounds **29** [155] prepared by Tamm and coworkers, **30** by Lammertsma–Uhl’s group [156], and **31** by Slootweg–Lammertsma group [157], drawn in Scheme 13, have features akin to those in **8**, **6**, and **7** (Scheme 5), respectively. In addition, **5** bears a resemblance to the intermediate (**32**) reported by Baceiredo et al. when they synthesized boryl(phosphino) carbene [158]. Encouraged by the experimental successes [155–157, 159–161] and the resemblance of **5** to the experimentally accessed **32** [158], we speculated that **5** may be synthesized and thus carried out a computational experiment in an attempt to encourage experimental preparations. Using ethylene (**33**), silyl enol ether (CH<sub>2</sub>=C(Me)OSiMe<sub>3</sub> (**34**)), imines (Me<sub>2</sub>C=NMe (**35**) and Ph(Me)C=NMe (**36**)),



**Scheme 13** Comparing the active sites in the computationally designed molecules (5–8, Scheme 5) and experimentally synthesized FLPs (29–32). 32 is an experimentally accessed intermediate akin to 5



**Scheme 14** General features of the catalytic hydrogenation cycle

and ketone ( $\text{Ph}(\text{Me})\text{C}=\text{O}$  (37)) as representatives, we computed the energetics of these 5-mediated hydrogenations.

To be a hydrogenation catalyst, molecule 5 must be able to overcome the deactivation issues due to side reactions. In addition to the side reactions described in Scheme 10 (I–III and V), another possible reaction that 5 may undergo – the borohydride elimination to give  $(2,6\text{-Me-Ph})_2\text{B-H}$  and 1,2,3,4-tetrahydro pyridine – was considered. The exclusions of these side reactions were detailed in [107]. We give below the energetic results of the main cycles. Scheme 14 shows the common features (three steps) of the catalytic cycles of the hydrogenations, including hydrogen activation ( $5 \rightarrow 5_{\text{TS}} \rightarrow 5_{\text{H}_2}$ ), hydride transfer ( $\text{X\_IN1} \rightarrow \text{X\_TS} \rightarrow \text{X\_IN2}$ ), and product release ( $\text{X\_IN2} \rightarrow 5 + \text{XPR}$ ) ( $\text{X} = 33\text{--}37$ ). Since the hydrogen activation step is reversible ( $\Delta G^\ddagger = 23.0$  kcal/mole and  $\Delta G = 1.5$  kcal/mole) and the hydrogenation reactions share this step, we only give the energetic results for the hydrogen transfer and product release steps in Table 5.

The energetic results in Table 5 indicate that 5 may serve as a catalyst for alkenes (e.g.,  $\text{CH}_2\text{CH}_2$  (33) and  $\text{CH}_2=\text{C}(\text{Me})\text{OSiMe}_3$  (34)) hydrogenations, but slightly forcing experimental conditions (i.e., at evaluated temperature and pressure) could benefit the reactions, because of the relatively high free energy barriers (ca. 33 kcal/

**Table 5** M05-2X(IEFPCM, solvent=THF)/6-311++G(d,p)//M05-2X/6-311++G(d,p) Energetics results (in kcal/mole) for the hydrogenations of **33–37**

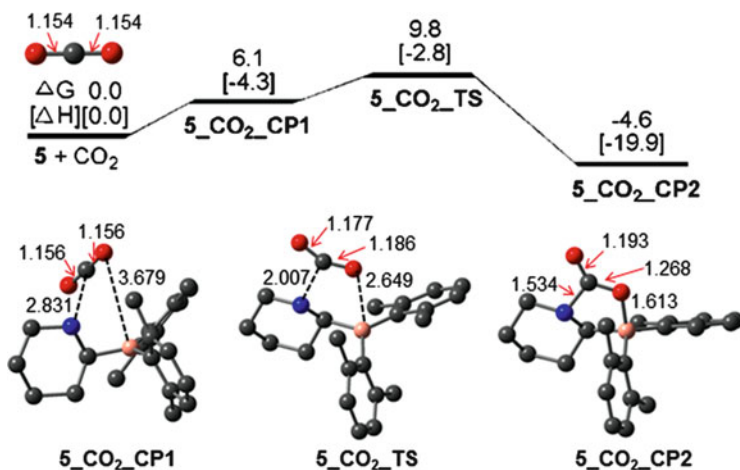
	<u>5</u> H <sub>2</sub> +X	X <u>IN1</u>	X <u>TS</u>	X <u>IN2</u>	<u>5</u> +XPR
	$\Delta G[\Delta H]$	$\Delta G[\Delta H]$	$\Delta G^\ddagger[\Delta H^\ddagger]$	$\Delta G[\Delta H]$	$\Delta G[\Delta H]$
CH <sub>2</sub> CH <sub>2</sub> ( <b>33</b> )	0.0[0.0]	8.9[−0.5]	33.6[19.6]	−18.5[−26.6]	−28.8[−26.4]
CH <sub>2</sub> =C(Me)OSiMe <sub>3</sub> ( <b>34</b> )	0.0[0.0]	9.5[−3.4]	32.6[17.5]	−9.0[−19.9]	−21.0[−19.5]
Me <sub>2</sub> C=NMe ( <b>35</b> )	0.0[0.0]	0.5[−12.1]	21.1[5.3]	−4.3[−14.3]	−14.1[−12.6]
Ph(Me)C=NMe ( <b>36R</b> ) <sup>a</sup>	0.0[0.0]	8.2[−5.3]	25.8[7.6]	−5.0[−17.7]	−13.5[−12.8]
Ph(Me)C=NMe ( <b>36S</b> )	0.0[0.0]	5.1[−6.2]	26.3[8.8]	−2.9[−14.9]	−13.5[−12.8]
Ph(Me)C=O ( <b>37R</b> ) <sup>a</sup>	0.0[0.0]	3.9[−9.4]	16.8[0.9]	−4.2[−13.5]	−7.7[−5.7]
Ph(Me)C=O ( <b>37S</b> )	0.0[0.0]	7.1[−6.0]	16.8[−0.3]	−5.7[−17.4]	−7.7[−5.7]

<sup>a</sup>For imine Ph(Me)C=NMe (**36**) and ketone (Ph(Me)C=O (**37**), two hydrogenation pathways leading to R- and S-enantiomers, respectively, have been considered

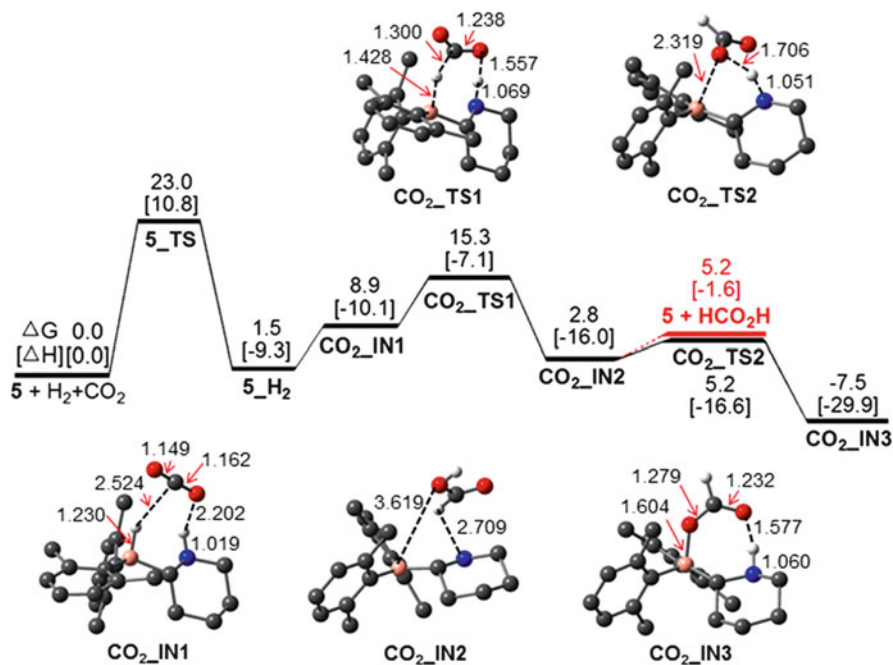
mole). The hydride transfer free energy barriers for the hydrogenation of the other compounds (e.g., imines (**35** and **36**) and bulky ketone (**37**)) are less than 27.0 kcal/mole, which are within the range for experimental realization. Because the imine **36** and ketone **37** have a prochiral carbon center, two hydride transfer pathways leading to R- and S-enantiomer products, respectively, were considered [114]. The small free energy barrier differences for the two different pathways of **36** and **37** indicate that molecule **5** cannot serve as an effective asymmetric hydrogenation catalyst. This is understandable because the B–C single bond in **5** can rotate easily and the two substituents on the boron atom are the same. To perform asymmetric hydrogenation, the molecule needs to be tailored to create asymmetric environments, e.g., incorporating the active site in relatively rigorous molecular frameworks or using different substituents on the B-center.

FLPs were initially developed for metal-free hydrogen activation and hydrogenation. Recently, FLPs have also found applications in CO<sub>2</sub> fixation, including CO<sub>2</sub> adsorption [86, 156] and chemical conversions [162]. Stimulated by these studies, the binding of CO<sub>2</sub> to **5** and the hydrogenation of CO<sub>2</sub> mediated by **5** were investigated. The energetic and geometric results in Fig. 9 indicate that the binding of CO<sub>2</sub> to **5** is reversible and energetically feasible for experimental realization. To verify this conclusion, the energetics for the reversible CO<sub>2</sub> binding to the (Me<sub>3</sub>C<sub>6</sub>H<sub>2</sub>)<sub>2</sub>PCH<sub>2</sub>CH<sub>2</sub>B(C<sub>6</sub>F<sub>5</sub>)<sub>2</sub> [86] was calculated at the same level of calculations. The addition barrier and the free energy of binding of the system were predicted to be 13.3 and −3.3 kcal/mole, respectively, comparable to the values, 9.8 and −4.6 kcal/mole, for the binding of CO<sub>2</sub> to **5**.

The binding of CO<sub>2</sub> to **5** is reversible and the H<sub>2</sub> activation can take place favorably. It is interesting to investigate the reaction of H<sub>2</sub> with CO<sub>2</sub> mediated by **5** [114]. The energetic and geometric results in Fig. 10 indicate that the reaction of H<sub>2</sub> and CO<sub>2</sub> under the catalytic influence of **5** is kinetically feasible and thermodynamically possible. However, similar to the some TM-mediated carbonyl reduction reactions [152, 153, 163, 164], the OH bond of HCOOH can easily be broken by **5** to form a stable formate complex CO<sub>2</sub>\_IN3. If no additional reaction conditions were afforded, the final product of **5**-mediated CO<sub>2</sub> hydrogenation would be



**Fig. 9** M05-2X(IEFPCM, solvent=THF)/6-311++G(d,p)//M05-2X/6-311++G(d,p) energetic (kcal/mole) and geometric results for the binding of **5** to CO<sub>2</sub>. The bond lengths are given in Å. Trivial hydrogen atoms are omitted for clarity (color code, C: black, B: pink, N: blue, O: red, H: gray)



**Fig. 10** M05-2X(IEFPCM, solvent=THF)/6-311++G(d,p)//M05-2X/6-311++G(d,p) energetic (in kcal/mole) and geometric results of **5**-mediated CO<sub>2</sub> hydrogenation; the optimized bond parameters are given in Å. Trivial hydrogen atoms are omitted for clarity (color code, C: black, B: pink, N: blue, O: red, H: gray)

the formate complex **CO<sub>2</sub>\_IN3** rather than HCOOH. However, one may promote the product release and the catalyst liberation by using a proper base to extract the product.

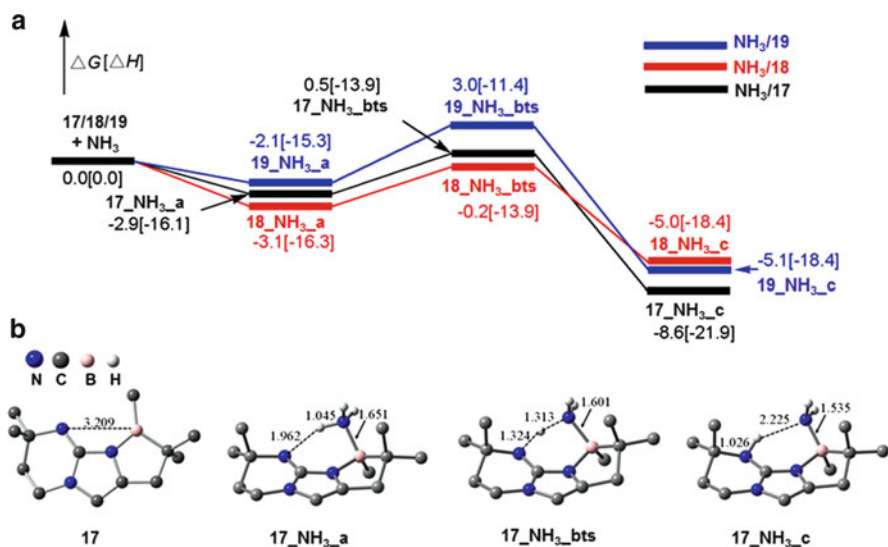
The computational results predicted that the designed molecule **5** could go further to serve as a catalyst for the hydrogenations of unsaturated compounds such as olefins, imines, and bulky ketones. In addition, the binding reaction of CO<sub>2</sub> to **5** is reversible. The promising results call for experimentalists to try to synthesize **5** or molecules with similar active sites.

#### 4.5 *Catalytic Intramolecular Hydroaminations of Non-activated Aminoalkenes*

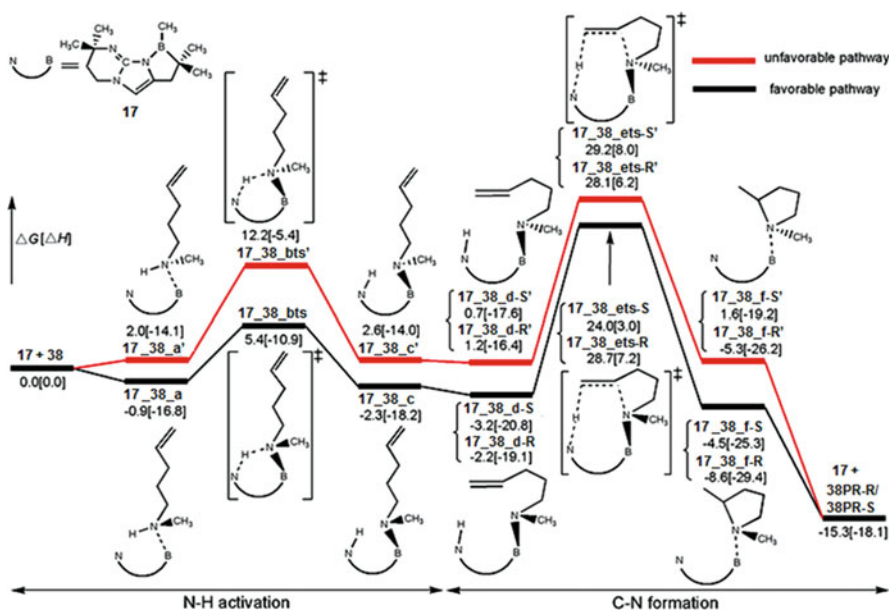
FLPs have been employed to carry out metal-free hydrogenation [47–49] but not yet to catalyze hydroamination, although NH<sub>3</sub> activation by main group compounds have been reported [11–13, 78]. For NH<sub>3</sub> activation, because NH<sub>3</sub> is a small Lewis base and tends to form stable complexes with Lewis acids including TM complexes (i.e., Werner-type complexes) and main group compounds (i.e., Lewis acid/base adducts), NH<sub>3</sub> activation is challenging and successful examples have been reported [13, 78, 149, 165–169]. Because the boron centers in **17–19** are weakly Lewis acidic, due to the electron donation of nitrogen, to circumvent the problem of forming stable Lewis acid/base adduct we envisioned that these molecules could activate NH<sub>3</sub> and subsequently perform hydroamination [109].

Figure 11 shows the energetic results for the NH<sub>3</sub> activations by **17–19**, along with the optimized geometries of stationary points involved in the **17**-mediated NH<sub>3</sub> activation. In agreement with our speculation, NH<sub>3</sub> cannot form stable complexes with **17–19**; the binding free energies of the complexes **X\_NH<sub>3</sub>\_a** (**X** = **17–19**) are 2.1–2.9 kcal/mole. The barriers for N–H bond cleavage range from 2.9–5.1 kcal/mole and the reactions are exergonic by 5.0–8.6 kcal/mole. The energetic results signify the possibility of using these molecules as hydroamination catalysts. To verify this we examined the intramolecular hydroamination (Eq. 1) catalyzed by **17–19** using  $\gamma$ -aminoalkene (**38**) as the substrate. Aminoalkene hydroamination via intramolecular cyclization is an efficient and atom-economical approach to synthesizing nitrogen heterocycles. Because the direct addition of the N–H bond to the C=C bond is symmetry-forbidden, catalysts are required. Much effort has been devoted to developing hydroamination catalysts including TM (e.g., Rh, Ir, and lanthanide) complexes [170–172] and main group compounds (e.g., TfOH) [173–175].

As an example, Fig. 12 shows the free energy results for the **17**-catalyzed Eq. (1) reaction. Possible side reactions which may cause catalyst deactivation were confirmed to be energetically unfavorable [111]. When amine **38** interacts with the catalyst **17**, it can bind to the B-site of **17** from either side of the plane of **17**.

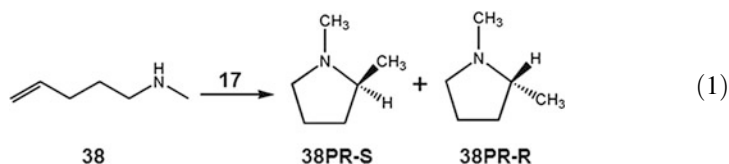


**Fig. 11** (a) M05-2X(IEFPCM, solvent=THF)/6-311++G(2d,p)//M05-2X/6-31G(d,p) free energy (in kcal/mole) profiles for  $\text{NH}_3$  activations by **17**–**19**. (b) M05-2X/6-31G(d,p) optimized geometries of stationary points involved in the activation by **17**, together with key bond lengths in Å. Trivial hydrogen atoms are omitted for clarity (similarly henceforth). Geometries for the other two reactions are included in [109]



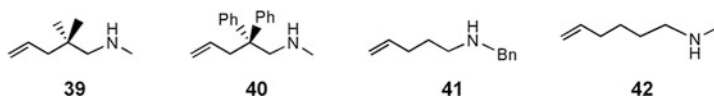
**Fig. 12** M05-2X(IEFPCM, solvent=THF)/6-311++G(2d,p)//M05-2X/6-31G(d,p) free energy (in kcal/mole) profiles of the **17**-catalyzed **38** hydroamination

Because **17** is nearly planar symmetric, we only considered the scenario in which **38** lies above the molecular plane. On the basis of the arrangement of the N-methyl group of **38** and the B-methyl group of **17**, there are two possible pathways, both of which can lead to products (S-enantiomer, **38PR-S**, and R-enantiomer, **38PR-R**). On the black pathway the N-methyl and B-methyl groups *trans* to each other, while the two are *cis* to each other on the red pathway. Because the *cis* arrangement causes larger steric effect than the *trans* arrangement, as compared in Fig. 12, the black pathway is more favorable than the red pathway. The reaction proceeds via two steps; **17** first mediates aminoalkene (**38**) N–H bond cleavage and the C–N bond then forms by transferring the hydrogen and amino group to the C=C double bond, respectively. The N–H bond activation is reversible. The C–N bond formation undergoing a concerted mechanism follows the Markovnikov addition rule. Along the most favorable pathway, the highest transition state is **17\_38\_ets-S** which is 24.0 kcal/mole higher than **17** + **38** and the reaction is exergonic by 15.3 kcal/mol. Therefore, the catalytic reaction is feasible both kinetically and thermodynamically.



Because the transition state **17\_38\_ets-S** is 4.7 kcal/mole lower than **17\_38\_ets-R**, **17** seems to be able to catalyze the hydroamination to produce **38PR-S** selectively. However, it should be emphasized that Fig. 12 only considers the scenario in which **38** binds to the B-site of **17** from above the molecular plane. Alternatively, **38** can also bind to the B-site from below the molecular plane of **17**. In this scenario, the favorable pathway should be that leading to **38PR-R** according to the stereochemistry. Because of the nearly symmetric character of the catalyst, the two scenarios of substrate binding to the catalyst could not result in much energetic difference. Therefore, the intramolecular hydroamination of **38** catalyzed by **17** could give racemic mixture of **38PR-S** and **38PR-R**. On the other hand, the catalyst **17** may change its chirality via interconversion, which also limits the catalytic reaction selectively to give one enantiomer (**38PR-S** or **38PR-R**).

We further extended the substrate in Eq. (1) to other aminoalkenes, including the methyl and phenyl  $\beta$ -substituted aminoalkenes (i.e., **39** and **40**, respectively), the benzyl-protected primary aminoalkene (**41**), and the  $\delta$ -aminoalkene (**42**) [176]. It has been found that these intramolecular hydroaminations also have feasible energetics; the free energies of the highest stationary points relative to the respective reactants, corresponding to the **17\_38\_ets-R** in Fig. 12, are 31.0 (**39**), 29.7 (**40**), 25.2 (**41**), and 23.8 kcal/mole (**42**), respectively and the reactions are exergonic by ca. 14–17 kcal/mole [111] (Scheme 15).



**Scheme 15** Schematic drawing of other aminoalkenes (39–42)

## 5 Concluding Remarks

Traditionally, hydrogen activation/hydrogenation is considered to be achievable only by transition metal complexes. The recent advances in metal-free hydrogen activation/hydrogenation (in particular, the discovery of FLP chemistry) demonstrate that this view needs to be changed. TM complexes and metal-free molecules share the same basic principle to achieve high reactivity toward  $H_2$ . If properly designed to utilize the Lewis acid/base bifunctional reactivity optimally, the metal-free systems can reach the reactivity comparable with that of TM complexes. This is shown by the methane activation by our designed molecules. Although FLPs can catalyze the hydrogenation of a variety of unsaturated substrates, the asymmetric metal-free hydrogenations with high *ee* values have been rarely reported. Realization of metal-free asymmetric hydrogenation with high *ee* value would be the next goal of the field. In addition, metal-free hydrogenations of ketones and small imines and FLP-based hydroaminations are awaiting experimental development, although these have been demonstrated computationally.

Computational chemistry contributed to the understanding of the FLP reactivity and the catalytic mechanisms of reactions involving FLPs. On the basis of the FLP principle, we demonstrated that computational chemistry can be utilized to design new molecules/catalysts. However, there is a gap between computational design and experimental realizations. To bridge the gap, on the one hand, computational chemists should keep it in mind to construct molecules closer to experimental reality. The side reactions which may deactivate designed molecules should be carefully checked and avoided. On the other hand, experimentalists should not be limited to the proposed molecules. While the reported molecules designed by computational chemists may be good targets, these are often used to demonstrate the applicability of principles. The principles behind the molecules could be more important than the molecules themselves. Experimentalists can use the principles to synthesize similar molecules. Indeed, our proposed  $\pi$ -FLP strategy has been borrowed by experimentalists to synthesize new metal-free molecules with similar active sites, capable of activating hydrogen and binding  $CO_2$ . Finally, we call for experimental effort to synthesize the molecules we have reported or molecules with active sites similar to those in our designed molecules.

**Acknowledgments** The authors acknowledge NSFC (20773160 and 20973197) for financial support.



## References

1. Tolman WB (2006) Activation of small molecules. Wiley-VCH, Weinheim
2. Kubas GJ (2001) Metal dihydrogen and  $\sigma$ -bond complexes. Kluwer Academic/Plenum Publishers, New York
3. Kubas GJ (1988) Molecular-hydrogen complexes-coordination of a sigma-bond to transition-metals. *Acc Chem Res* 21:120–128
4. Crabtree RH (1990) Dihydrogen complexes-some structural and chemical studies. *Acc Chem Res* 23:95–101
5. Jessop PG, Morris RH (1992) Reactions of transition-metal dihydrogen complexes. *Coord Chem Rev* 121:155–284
6. Kubas GJ (2004) Heterolytic splitting of H-H, Si-H, and other sigma bonds on electrophilic metal centers. *Adv Inorg Chem* 56:127–177
7. Kubas GJ (2006) Chemistry – breaking the H<sub>2</sub> marriage and reuniting the couple. *Science* 314:1096–1097
8. Kubas GJ (2007) Fundamentals of H<sub>2</sub> binding and reactivity on transition metals underlying hydrogenase function and H<sub>2</sub> production and storage. *Chem Rev* 107:4152–4205
9. Spikes GH, Fettinger JC, Power PP (2005) Facile activation of dihydrogen by an unsaturated heavier main group compound. *J Am Chem Soc* 127:12232–12233
10. Peng Y, Brynda M, Ellis BD et al (2008) Addition of H<sub>2</sub> to distannynes under ambient conditions. *Chem Commun* 6042–6044
11. Peng Y, Ellis BD, Wang X et al (2008) Diarylstannylenes activation of hydrogen or ammonia with arene elimination. *J Am Chem Soc* 130:12268–12269
12. Peng Y, Guo JD, Ellis BD et al (2009) Reaction of hydrogen or ammonia with unsaturated germanium or tin molecules under ambient conditions: oxidative addition versus arene elimination. *J Am Chem Soc* 131:16272–16282
13. Frey GD, Lavallo V, Donnadiu B et al (2007) Facile splitting of hydrogen and ammonia by nucleophilic activation at a single carbon center. *Science* 316:439–441
14. Xiao ZL, Hauge RH, Margrave JL (1993) Cryogenic reactions of gallium with molecular hydrogen and methane. *Inorg Chem* 32:642–646
15. Himmel HJ, Vollet J (2002) Probing the reactivity of aluminum(I) compounds: the reaction of pentamethylcyclopentadienyl-aluminum, Al[C<sub>5</sub>(CH<sub>3</sub>)<sub>5</sub>], monomers with dihydrogen in a solid Ar matrix to give the new aluminum hydride molecule H<sub>2</sub>Al[C<sub>5</sub>(CH<sub>3</sub>)<sub>5</sub>]. *Organometallics* 21:5972–5977
16. Himmel HJ (2003) Structural motifs and reactivity of small molecules containing subvalent Group 13 elements: matrix isolation and quantum chemical studies. *Dalton Trans* 3639–3649
17. Walling C, Bollyky L (1961) Base catalyzed homogeneous hydrogenation. *J Am Chem Soc* 83:2968–2969
18. Berkessel A, Schubert TJS, Muller TN (2002) Hydrogenation without a transition-metal catalyst: on the mechanism of the base-catalyzed hydrogenation of ketones. *J Am Chem Soc* 124:8693–8698
19. Senger S, Radom L (2000) Zeolites as transition-metal-free hydrogenation catalysts: a theoretical mechanistic study. *J Am Chem Soc* 122:2613–2620
20. Senger S, Radom L (2000) Toward a low-barrier transition-metal-free catalysis of hydrogenation reactions: a theoretical mechanistic study of HAlX<sub>4</sub>-catalyzed hydrogenations of ethene (X = F, Cl, and Br). *J Phys Chem A* 104:7375–7385
21. Chan B, Radom L (2004) Understanding metal-free catalytic hydrogenation: a systematic theoretical study of the hydrogenation of ethene. *Aust J Chem* 57:659–663
22. Chan B, Radom L (2005) Base-catalyzed hydrogenation: rationalizing the effects of catalyst and substrate structures and solvation. *J Am Chem Soc* 127:2443–2454
23. Chan B, Radom L (2006) Design of effective zeolite catalysts for the complete hydrogenation of CO<sub>2</sub>. *J Am Chem Soc* 128:5322–5323

24. Chan B, Radom L (2008) Zeolite-catalyzed hydrogenation of carbon dioxide and ethene. *J Am Chem Soc* 130:9790–9799
25. de Vries JG, Elsevier CJ (2007) *The hand book of homogeneous hydrogenation*. Wiley-VCH, Weinheim
26. Gallezot P, Cerino PJ, Blanc B et al (1994) Glucose hydrogenation on promoted Raney-nickel catalyst. *J Catal* 146:93–102
27. Masson J, Cividino P, Court J (1997) Selective hydrogenation of acetophenone on chromium promoted Raney nickel catalysts. 3. The influence of the nature of the solvent. *Appl Catal A Gen* 161:191–197
28. Thomas-Pryor SN, Manz TA, Liu Z et al (1998) Selective hydrogenation of butyronitrile over promoted Raney (R) nickel catalysts. *Catal Org React* 75:195–206
29. Osawa T, Yoshino K, Takimoto K et al (2006) Enantio-differentiating hydrogenation of methyl acetoacetate over modified Raney nickel catalysts prepared by two-step modifications. *Catal Lett* 112:167–171
30. Yamakawa M, Ito H, Noyori R (2000) The metal-ligand bifunctional catalysis: a theoretical study on the ruthenium(II)-catalyzed hydrogen transfer between alcohols and carbonyl compounds. *J Am Chem Soc* 122:1466–1478
31. Dalko PI, Moisan L (2004) In the golden age of organocatalysis. *Angew Chem Int Ed* 43:5138–5175
32. Yang JW, Fonseca MTH, List B (2004) A metal-free transfer hydrogenation: organocatalytic conjugate reduction of alpha, beta-unsaturated aldehydes. *Angew Chem Int Ed* 43:6660–6662
33. Adolfsson H (2005) Organocatalytic hydride transfers: a new concept in asymmetric hydrogenations. *Angew Chem Int Ed* 44:3340–3342
34. Gladiali S, Alberico E (2006) Asymmetric transfer hydrogenation: chiral ligands and applications. *Chem Soc Rev* 35:226–236
35. Tuttle JB, Ouellet SG, MacMillan DWC (2006) Organocatalytic transfer hydrogenation of cyclic enones. *J Am Chem Soc* 128:12662–12663
36. Ouellet SG, Walji AM, Macmillan DWC (2007) Enantioselective organocatalytic transfer hydrogenation reactions using Hantzsch esters. *Acc Chem Res* 40:1327–1339
37. Bolm C, Legros J, Le Paih J et al (2004) Iron-catalyzed reactions in organic synthesis. *Chem Rev* 104:6217–6254
38. Casey CP, Guan H (2007) An efficient and chemoselective iron catalyst for the hydrogenation of ketones. *J Am Chem Soc* 129:5816–5817
39. Enthaler S, Junge K, Beller M (2008) Sustainable metal catalysis with iron: from rust to a rising star? *Angew Chem Int Ed* 47:3317–3321
40. Furstner A, Majima K, Martin R et al (2008) A cheap metal for a "noble" task: preparative and mechanistic aspects of cycloisomerization and cycloaddition reactions catalyzed by low-valent iron complexes. *J Am Chem Soc* 130:1992–2004
41. Sui-Seng C, Freutel F, Lough AJ et al (2008) Highly efficient catalyst systems using iron complexes with a tetradentate PNNP ligand for the asymmetric hydrogenation of polar bonds. *Angew Chem Int Ed* 47:940–943
42. Li PH, Zhang YC, Wang L (2009) Iron-catalyzed ligand-free three-component coupling reactions of aldehydes, terminal alkynes, and amines. *Chem Eur J* 15:2045–2049
43. Wang M, Ren K, Wang L (2009) Iron-catalyzed ligand-free carbon-selenium (or tellurium) coupling of arylboronic acids with diselenides and ditellurides. *Adv Synth Catal* 351:1586–1594
44. Ren YL, Cheng L, Tian XZ et al (2010) Iron-catalyzed conversion of unactivated aryl halides to phenols in water. *Tetrahedron Lett* 51:43–45
45. Wang D, Zhang M, Bühlmann P et al (2010) Redox potential and C-H bond cleaving properties of a nonheme Fe<sup>IV</sup>=O complex in aqueous solution. *J Am Chem Soc* 132:7638–7644

46. Welch GC, Juan RRS, Masuda JD et al (2006) Reversible, metal-free hydrogen activation. *Science* 314:1124–1126
47. Stephan DW (2008) Frustrated Lewis pairs: a concept for new reactivity and catalysis. *Org Biomol Chem* 6:1535–1539
48. Stephan DW (2009) Frustrated Lewis pairs: a new strategy to small molecule activation and hydrogenation catalysis. *Dalton Trans* 3129–3136
49. Stephan DW, Erker G (2010) Frustrated Lewis pairs: metal-free hydrogen activation and more. *Angew Chem Int Ed* 49:46–76
50. Welch GC, Stephan DW (2007) Facile heterolytic cleavage of dihydrogen by phosphines and boranes. *J Am Chem Soc* 129:1880–1881
51. Spies P, Erker G, Kehr G et al (2007) Rapid intramolecular heterolytic dihydrogen activation by a four-membered heterocyclic phosphane-borane adduct. *Chem Commun* 5072–5074
52. Welch GC, Cabrera L, Chase PA et al (2007) Tuning Lewis acidity using the reactivity of “frustrated Lewis pairs”: facile formation of phosphine-boranes and cationic phosphonium-boranes. *Dalton Trans* 3407–3414
53. Geier SJ, Gilbert TM, Stephan DW (2008) Activation of H<sub>2</sub> by phosphinoboranes R<sub>2</sub>PB(C<sub>6</sub>F<sub>5</sub>)<sub>2</sub>. *J Am Chem Soc* 130:12632–12633
54. Jiang CF, Blacque O, Berke H (2009) Metal-free hydrogen activation by the frustrated Lewis pairs of ClB(C<sub>6</sub>F<sub>5</sub>)<sub>2</sub> and HB(C<sub>6</sub>F<sub>5</sub>)<sub>2</sub> and bulky Lewis bases. *Organometallics* 28:5233–5239
55. Ramos A, Lough AJ, Stephan DW (2009) Activation of H<sub>2</sub> by frustrated Lewis pairs derived from mono- and bis-phosphinoferrrocenes and B(C<sub>6</sub>F<sub>5</sub>)<sub>3</sub>. *Chem Commun* 1118–1120
56. Spies P, Kehr G, Bergander K et al (2009) Metal-free dihydrogen activation chemistry: structural and dynamic features of intramolecular P/B pairs. *Dalton Trans* 1534–1541
57. Ullrich M, Lough AJ, Stephan DW (2009) Reversible, metal-free, heterolytic activation of H<sub>2</sub> at room temperature. *J Am Chem Soc* 131:52–53
58. Mömning CM, Kehr G, Wibbeling B et al (2010) Formation of cyclic allenes and cumulenes by cooperative addition of frustrated Lewis pairs to conjugated enynes and diynes. *Angew Chem Int Ed* 49:2414–2417
59. Chase PA, Welch GC, Jurca T et al (2007) Metal-free catalytic hydrogenation. *Angew Chem Int Ed* 46:8050–8053
60. Spies P, Schwendemann S, Lange S et al (2008) Metal-free catalytic hydrogenation of enamines, imines, and conjugated phosphinoalkenylboranes. *Angew Chem Int Ed* 47:7543–7546
61. Mömning CM, Frömel S, Kehr G et al (2009) Reactions of an intramolecular frustrated Lewis pair with unsaturated substrates: evidence for a concerted olefin addition reaction. *J Am Chem Soc* 131:12280–12289
62. Wang HD, Fröhlich R, Kehr G et al (2008) Heterolytic dihydrogen activation with the 1,8-bis(diphenylphosphino)-naphthalene/B(C<sub>6</sub>F<sub>5</sub>)<sub>3</sub> pair and its application for metal-free catalytic hydrogenation of silyl enol ethers. *Chem Commun* 5966–5968
63. Dureen MA, Stephan DW (2009) Terminal alkyne activation by frustrated and classical Lewis acid/phosphine pairs. *J Am Chem Soc* 131:8396–8397
64. Welch GC, Prieto R, Dureen MA et al (2009) Reactions of phosphines with electron deficient boranes. *Dalton Trans* 1559–1570
65. Schulz F, Sumerin V, Leskela M et al (2010) Frustrated Lewis pairs: reactivities of TMS protected amines and phosphines in the presence of B(C<sub>6</sub>F<sub>5</sub>)<sub>3</sub>. *Dalton Trans* 39:1920–1922
66. Sumerin V, Schulz F, Nieger M et al (2009) Experimental and theoretical treatment of hydrogen splitting and storage in boron-nitrogen systems. *J Organomet Chem* 694:2654–2660
67. Chase PA, Jurca T, Stephan DW (2008) Lewis acid-catalyzed hydrogenation: B(C<sub>6</sub>F<sub>5</sub>)<sub>3</sub>-mediated reduction of imines and nitriles with H<sub>2</sub>. *Chem Commun* 1701–1703
68. Chen DJ, Klankermayer J (2008) Metal-free catalytic hydrogenation of imines with tris(perfluorophenyl) borane. *Chem Commun* 2130–2131

69. Sumerin V, Schulz F, Atsumi M et al (2008) Molecular tweezers for hydrogen: synthesis, characterization, and reactivity. *J Am Chem Soc* 130:14117–14118
70. Axenov KV, Kehr G, Fröhlich R et al (2009) Functional group chemistry at the group 4 bent metallocene frameworks: formation and “metal-free” catalytic hydrogenation of bis(imino-Cp)zirconium complexes. *Organometallics* 28:5148–5158
71. Jiang CF, Blacque O, Berke H (2009) Metal-free hydrogen activation and hydrogenation of imines by 1,8-bis(dipentafluorophenylboryl)naphthalene. *Chem Commun* 5518–5520
72. Sumerin V, Schulz F, Nieger M et al (2008) Facile heterolytic H<sub>2</sub> activation by amines and B(C<sub>6</sub>F<sub>5</sub>)<sub>3</sub>. *Angew Chem Int Ed* 47:6001–6003
73. Geier SJ, Gille AL, Gilbert TM et al (2009) From classical adducts to frustrated Lewis pairs: steric effects in the interactions of pyridines and B(C<sub>6</sub>F<sub>5</sub>)<sub>3</sub>. *Inorg Chem* 48:10466–10474
74. Geier SJ, Stephan DW (2009) Lutidine/B(C<sub>6</sub>F<sub>5</sub>)<sub>3</sub>: at the boundary of classical and frustrated Lewis pair reactivity. *J Am Chem Soc* 131:3476–3477
75. Jiang CF, Blacque O, Berke H (2010) Activation of terminal alkynes by frustrated Lewis pairs. *Organometallics* 29:125–133
76. Voss T, Chen C, Kehr G et al (2010) Cyclizations via frustrated Lewis pairs: Lewis acid induced intramolecular additions of amines to olefins and alkynes. *Chem Eur J* 16:3005–3008
77. Axenov KV, Kehr G, Fröhlich R et al (2009) Catalytic hydrogenation of sensitive organometallic compounds by antagonistic N/B Lewis pair catalyst systems. *J Am Chem Soc* 131:3454–3455
78. Chase PA, Stephan DW (2008) Hydrogen and amine activation by a frustrated Lewis pair of a bulky N-heterocyclic carbene and B(C<sub>6</sub>F<sub>5</sub>)<sub>3</sub>. *Angew Chem Int Ed* 47:7433–7437
79. Holschumacher D, Bannenberg T, Hrib CG et al (2008) Heterolytic dihydrogen activation by a frustrated carbene-borane Lewis pair. *Angew Chem Int Ed* 47:7428–7432
80. Chase PA, Gille AL, Gilbert TM et al (2009) Frustrated Lewis pairs derived from N-heterocyclic carbenes and Lewis acids. *Dalton Trans* 7179–7188
81. Holschumacher D, Taouss C, Bannenberg T et al (2009) Dehydrogenation reactivity of a frustrated carbene-borane Lewis pair. *Dalton Trans* 6927–6929
82. Menard G, Stephan DW (2010) Room temperature reduction of CO<sub>2</sub> to methanol by Al-based frustrated Lewis pairs and ammonia borane. *J Am Chem Soc* 132:1796–1797
83. Otten E, Neu RC, Stephan DW (2009) Complexation of nitrous oxide by frustrated Lewis pairs. *J Am Chem Soc* 131:9918–9919
84. Welch GC, Masuda JD, Stephan DW (2006) Phosphonium-borate zwitterions, anionic phosphines, and dianionic phosphonium-dialkoxides via tetrahydrofuran ring-opening reactions. *Inorg Chem* 45:478–480
85. McCahill JSJ, Welch GC, Stephan DW (2007) Reactivity of “frustrated Lewis pairs”: three-component reactions of phosphines, a borane, and olefins. *Angew Chem Int Ed* 46:4968–4971
86. Mömning CM, Otten E, Kehr G et al (2009) Reversible metal-free carbon dioxide binding by frustrated Lewis pairs. *Angew Chem Int Ed* 48:6643–6646
87. Ullrich M, Seto KSH, Lough AJ et al (2009) 1,4-Addition reactions of frustrated Lewis pairs to 1,3-dienes. *Chem Commun* 2335–2337
88. Li HX, Jiang JL, Lu G et al (2011) On the “reverse gear” mechanism of the reversible dehydrogenation/hydrogenation of a nitrogen heterocycle catalyzed by a Cp\*Ir complex: a computational study. *Organometallics* 30:3131–3141
89. Kenward AL, Piers WE (2008) H<sub>2</sub> activation – heterolytic H<sub>2</sub> activation by nonmetals. *Angew Chem Int Ed* 47:38–41
90. Rokob TA, Hamza A, Stirling A et al (2008) Turning frustration into bond activation: a theoretical mechanistic study on heterolytic hydrogen splitting by frustrated Lewis pairs. *Angew Chem Int Ed* 47:2435–2438
91. Guo Y, Li SH (2008) Unusual concerted Lewis acid-Lewis base mechanism for hydrogen activation by a phosphine-borane compound. *Inorg Chem* 47:6212–6219

92. Guo Y, Li SH (2008) A novel addition mechanism for the reaction of “frustrated Lewis pairs” with olefins. *Eur J Inorg Chem* 2501–2505
93. Hamza A, Stirling A, Rokob TA et al (2009) Mechanism of hydrogen activation by frustrated Lewis pairs: a molecular orbital approach. *Int J Quantum Chem* 109:2416–2425
94. Nyhlén J, Privalov T (2009) “Frustration” of orbital interactions in Lewis base/Lewis acid adducts: a computational study of H<sub>2</sub> uptake by phosphanylboranes R<sub>2</sub>P=BR’<sub>2</sub>. *Eur J Inorg Chem* 2759–2764
95. Rokob TA, Hamza A, Pápai I (2009) Rationalizing the reactivity of frustrated Lewis pairs: thermodynamics of H<sub>2</sub> activation and the role of acid–base properties. *J Am Chem Soc* 131:10701–10710
96. Kim HW, Rhee YM (2009) Dispersion-oriented soft interaction in a frustrated Lewis pair and the entropic encouragement effect in its formation. *Chem Eur J* 15:13348–13355
97. Rajeev R, Sunoj RB (2009) On the origin of reversible hydrogen activation by phosphine-boranes. *Chem Eur J* 15:12846–12855
98. Gao SL, Wu W, Mo YR (2009) The B–H–H–P dihydrogen bonding in ion pair complexes [(CF<sub>3</sub>)<sub>3</sub>BH-][HPH<sub>3</sub>-n(Me)<sub>n+</sub>] (n = 0–3) and its implication in H<sub>2</sub> elimination and activation reactions. *J Phys Chem A* 113:8108–8117
99. Grimme S, Kruse H, Goerigk L et al (2010) The mechanism of dihydrogen activation by frustrated Lewis pairs revisited. *Angew Chem Int Ed* 49:1402–1405
100. Li HX, Zhao LL, Lu G et al (2010) Insight into the relative reactivity of frustrated Lewis pairs and stable carbenes in activating H<sub>2</sub> and CH<sub>4</sub>: a comparative computational study. *Phys Chem Chem Phys* 12:5268–5275
101. Guo Y, He X, Li ZS et al (2010) Theoretical study on the possibility of using frustrated Lewis pairs as bifunctional metal-free dehydrogenation catalysts of ammonia borane. *Inorg Chem* 49:3419–3423
102. Stirling A, Hamza A, Rokob TA et al (2008) Concerted attack of frustrated Lewis acid–base pairs on olefinic double bonds: a theoretical study. *Chem Commun* 3148–3150
103. Privalov T (2009) Hydrogenation of imines by phosphonium borate zwitterions: a theoretical study. *Dalton Trans* 1321–1327
104. Rokob TA, Hamza A, Stirling A et al (2009) On the mechanism of B(C<sub>6</sub>F<sub>5</sub>)<sub>3</sub>-catalyzed direct hydrogenation of imines: inherent and thermally induced frustration. *J Am Chem Soc* 131:2029–2036
105. Privalov T (2009) On the possibility of conversion of alcohols to ketones and aldehydes by phosphinoboranes R<sub>2</sub>PBR’R’’: a computational study. *Chem Eur J* 15:1825–1829
106. Privalov T (2009) The role of amine-B(C<sub>6</sub>F<sub>5</sub>)<sub>3</sub> adducts in the catalytic reduction of imines with H<sub>2</sub>: a computational study. *Eur J Inorg Chem* 15:2229–2237
107. Wang ZX, Lu G, Li HX et al (2009) Encumbering the intramolecular pi donation by using a bridge: a strategy for designing metal-free compounds to hydrogen activation. *Chin Sci Bull* 55:239–245
108. Lu G, Li HX, Zhao LL et al (2009) Computationally designed metal-free hydrogen activation site: reaching the reactivity of metal-ligand bifunctional hydrogenation catalysts. *Inorg Chem* 49:295–301
109. Lu G, Li HX, Zhao LL et al (2011) Designing metal-free catalysts by mimicking transition-metal pincer templates. *Chem Eur J* 17:2038–2043
110. Lu G, Zhao LL, Li HX et al (2010) Reversible heterolytic methane activation of metal-free closed-shell molecules: a computational proof-of-principle study. *Eur J Inorg Chem* 2010:2254–2260
111. Li HX, Wen MW, Lu G et al (2012) Catalytic metal-free intramolecular hydroaminations of non-activated aminoalkenes: a computational exploration. *Dalton Trans* 41:9091–9100
112. Zhao LL, Li HX, Lu G et al (2010) Computational design of metal-free catalysts for catalytic hydrogenation of imines. *Dalton Trans* 39:4038–4047
113. Zhao LL, Li HX, Lu G et al (2011) Metal-free catalysts for hydrogenation of both small and large imines: a computational experiment. *Dalton Trans* 40:1929–1937

114. Zhao LL, Lu G, Huang F et al (2010) A computational experiment to study hydrogenations of various unsaturated compounds catalyzed by a rationally designed metal-free catalyst. *Dalton Trans* 41:4674–4684
115. Li HX, Zhao LL, Lu G et al (2010) Catalytic metal-free ketone hydrogenation: a computational experiment. *Dalton Trans* 39:5519–5526
116. Momming CM, Kehr G, Wibbeling B et al (2010) Addition reactions to the intramolecular mesityl<sub>2</sub>P-CH<sub>2</sub>-CH<sub>2</sub>-B(C<sub>6</sub>F<sub>5</sub>)<sub>2</sub> frustrated Lewis pair. *Dalton Trans* 39:7556–7564
117. Power PP (2010) Main-group elements as transition metals. *Nature* 463:171–177
118. Power PP (2011) Interaction of multiple bonded and unsaturated heavier main group compounds with hydrogen, ammonia, olefins, and related molecules. *Acc Chem Res* 44:627–637
119. Jung Y, Brynda M, Power PP et al (2006) Ab initio quantum chemistry calculations on the electronic structure of heavier alkyne congeners: diradical character and reactivity. *J Am Chem Soc* 128:7185–7192
120. Zhao LL, Huang F, Lu G et al (2012) Why the mechanisms of digermynes and distannyne reactions with H<sub>2</sub> differ so greatly? *J Am Chem Soc* 134:8856–8868
121. Strajbl M, Sham YY, Villà J et al (2000) Calculations of activation entropies of chemical reactions in solution. *J Phys Chem B* 104:4578–4584
122. Yu ZX, Houk KN (2003) Intramolecular 1,3-dipolar ene reactions of nitrile oxides occur by stepwise 1,1-cycloaddition/retro-ene mechanisms. *J Am Chem Soc* 125:13825–13830
123. Chen Y, Ye S, Jiao L et al (2007) Mechanistic twist of the [8+2] cycloadditions of dienylobenzofurans and dimethyl acetylenedicarboxylate: stepwise [8+2] versus [4+2]/[1,5]-vinyl shift mechanisms revealed through a theoretical and experimental study. *J Am Chem Soc* 129:10773–10784
124. Liang Y, Liu S, Xia YZ et al (2008) Mechanism, regioselectivity, and the kinetics of phosphine-catalyzed [3+2] cycloaddition reactions of allenates and electron-deficient alkenes. *Chem Eur J* 14:4361–4373
125. Liang Y, Liu S, Yu ZX (2009) Thieme chemistry journal awardees – where are they now? Phosphine- and water-cocatalyzed [3+2] cycloaddition reactions of 2-methyl-2,3-butadienoate with fumarates: a computational and experimental study. *Synlett* 905–909
126. Zhang CG, Zhang RW, Wang ZX et al (2009) Computational analysis of amine-borane adducts as potential hydrogen storage materials with reversible hydrogen uptake. *Chem Eur J* 15:5910–5918
127. Abdur-Rashid K, Faatz M, Lough AJ et al (2001) Catalytic cycle for the asymmetric hydrogenation of prochiral ketones to chiral alcohols: direct hydride and proton transfer from chiral catalysts trans-Ru(H)<sub>2</sub>(diphosphine)(diamine) to ketones and direct addition of dihydrogen to the resulting hydridoamido complexes. *J Am Chem Soc* 123:7473–7474
128. Noyori R, Ohkuma T (2001) Asymmetric catalysis by architectural and functional molecular engineering: practical chemo- and stereoselective hydrogenation of ketones. *Angew Chem Int Ed* 40:40–73
129. Abdur-Rashid K, Clapham SE, Hadzovic A et al (2002) Mechanism of the hydrogenation of ketones catalyzed by trans-dihydrido(diamine)ruthenium(II) complexes. *J Am Chem Soc* 124:15104–15118
130. Noyori R (2002) Asymmetric catalysis: science and opportunities (Nobel lecture). *Angew Chem Int Ed* 41:2008–2022
131. Sandoval CA, Ohkuma T, Muniz K et al (2003) Mechanism of asymmetric hydrogenation of ketones catalyzed by BINAP/1,2-diamine-ruthenium(II) complexes. *J Am Chem Soc* 125:13490–13503
132. Clapham SE, Hadzovic A, Morris RH (2004) Mechanisms of the H<sub>2</sub>-hydrogenation and transfer hydrogenation of polar bonds catalyzed by ruthenium hydride complexes. *Coord Chem Rev* 248:2201–2237
133. Ohkuma T, Hattori T, Ooka H et al (2004) BINAP/1,4-diamine-ruthenium(II) complexes for efficient asymmetric hydrogenation of 1-tetralones and analogues. *Org Lett* 6:2681–2683

134. Noyori R, Sandoval CA, Muniz K et al (2005) Metal-ligand bifunctional catalysis for asymmetric hydrogenation. *Philos Trans R Soc Lond A* 363:901–912
135. Ikariya T, Murata K, Noyori R (2006) Bifunctional transition metal-based molecular catalysts for asymmetric syntheses. *Org Biomol Chem* 4:393–406
136. Grützmacher H (2008) Cooperating ligands in catalysis. *Angew Chem Int Ed* 47:1814–1818
137. Sandoval CA, Li YH, Ding KL et al (2008) The hydrogenation/transfer hydrogenation network in asymmetric reduction of ketones catalyzed by [RuCl<sub>2</sub>(binap)(pica)] complexes. *Chem Asian J* 3:1801–1810
138. Sandoval CA, Shi QX, Liu SS et al (2009) NH/π attraction: a role in asymmetric hydrogenation of aromatic ketones with binap/1,2-diamine-ruthenium(II) complexes. *Chem Asian J* 4:1221–1224
139. Zimmer-De Iulii M, Morris RH (2009) Kinetic hydrogen/deuterium effects in the direct hydrogenation of ketones catalyzed by a well-defined ruthenium diphosphine diamine complex. *J Am Chem Soc* 131:11263–11269
140. Goldberg KI, Goldman AS (2004) Activation and functionalization of C-H bonds. Oxford University Press, Washington
141. Cummins CC, Baxter SM, Wolczanski PT (1988) Methane and benzene activation via transient (tert-Bu<sub>3</sub>SiNH)<sub>2</sub>Zr:NSi-tert-Bu<sub>3</sub>. *J Am Chem Soc* 110:8731–8733
142. Ochi N, Nakao Y, Sato H et al (2007) Theoretical study of C–H and N–H σ-bond activation reactions by titanium(IV)-imido complex. Good understanding based on orbital interaction and theoretical proposal for N–H σ-bond activation of ammonia. *J Am Chem Soc* 129:8615–8624
143. Zhang J, Leitus G, Ben-David Y et al (2005) Facile conversion of alcohols into esters and dihydrogen catalyzed by new ruthenium complexes. *J Am Chem Soc* 127:10840–10841
144. Ben-Ari E, Leitus G, Shimon LJW et al (2006) Metal-ligand cooperation in C–H and H<sub>2</sub> activation by an electron-rich PNPIr(I) system: facile ligand dearomatization-aromatization as key steps. *J Am Chem Soc* 128:15390–15391
145. Gunanathan C, Ben-David Y, Milstein D (2007) Direct synthesis of amides from alcohols and amines with liberation of H<sub>2</sub>. *Science* 317:790–792
146. Kohl SW, Weiner L, Schwartsburd L et al (2009) Consecutive thermal H<sub>2</sub> and light-induced O<sub>2</sub> evolution from water promoted by a metal complex. *Science* 324:74–77
147. Gnanaprakasam B, Zhang J, Milstein D (2010) Direct synthesis of imines from alcohols and amines with liberation of H<sub>2</sub>. *Angew Chem Int Ed* 49:1468–1471
148. Milstein D (2010) Discovery of environmentally benign catalytic reactions of alcohols catalyzed by pyridine-based pincer Ru complexes, based on metal-ligand cooperation. *Top Catal* 53:915–923
149. Khaskin E, Iron MA, Shimon LJW et al (2010) N-H activation of amines and ammonia by Ru via metal-ligand cooperation. *J Am Chem Soc* 132:8542–8543
150. Ozerov OV (2009) Oxidative addition of water to transition metal complexes. *Chem Soc Rev* 38:83–88
151. Nyhlén J, Privalov T (2009) On the possibility of catalytic reduction of carbonyl moieties with tris(pentafluorophenyl)borane and H<sub>2</sub>: a computational study. *Dalton Trans* 5780–5786
152. Daley CJA, Bergens SH (2002) The first complete identification of a diastereomeric catalyst-substrate (alkoxide) species in an enantioselective ketone hydrogenation. Mechanistic investigations. *J Am Chem Soc* 124:3680–3691
153. Hamilton RJ, Bergens SH (2006) An unexpected possible role of base in asymmetric catalytic hydrogenations of ketones. Synthesis and characterization of several key catalytic intermediates. *J Am Chem Soc* 128:13700–13701
154. Chen DJ, Wang YT, Klankermayer J (2010) Enantioselective hydrogenation with chiral frustrated Lewis pairs. *Angew Chem Int Ed* 49:9475–9478
155. Theuergarten E, Schluns D, Grunenberg J et al (2010) Intramolecular heterolytic dihydrogen cleavage by a bifunctional frustrated pyrazolylborane Lewis pair. *Chem Commun* 8561–8563

156. Appelt C, Westenberg H, Bertini F, Ehlers AW, Slootweg JC, Lammertsma K, Uhl W (2011) Geminal phosphorus/aluminum-based frustrated Lewis pairs: C-H versus C equivalent to C activation and CO<sub>2</sub> fixation. *Angew Chem Int Ed* 50:3925–3928
157. Bertini F, Lyaskovskyy V, Timmer BJJ et al (2011) Preorganized frustrated Lewis pairs. *J Am Chem Soc* 134:201–204
158. Lavigne F, Maerten E, Alcaraz G et al (2010) Borylated methylenephosphonium salts: precursors of elusive boryl(phosphino)carbenes. *J Am Chem Soc* 132:8864–8865
159. Stute A, Kehr G, Fröhlich R et al (2011) Chemistry of a geminal frustrated Lewis pair featuring electron withdrawing C<sub>6</sub>F<sub>5</sub> substituents at both phosphorus and boron. *Chem Commun* 47:4288–4290
160. Rosorius C, Kehr G, Fröhlich R et al (2011) Electronic control of frustrated Lewis pair behavior: chemistry of a geminal alkylidene-bridged per-pentafluorophenylated P/B Pair. *Organometallics* 30:4211–4219
161. Tanur CA, Stephan DW (2011) The thioether–methyleneborane (PhSCH<sub>2</sub>B(C<sub>6</sub>F<sub>5</sub>)<sub>2</sub>)<sub>2</sub>: synthesis and reactivity with donors and alkynes. *Organometallics* 30:3652–3657
162. Ashley AE, Thompson AL, O'Hare D (2009) Non-metal-mediated homogeneous hydrogenation of CO<sub>2</sub> to CH<sub>3</sub>OH. *Angew Chem Int Ed* 48:9839–9843
163. Hamilton RJ, Bergens SH (2008) Direct observations of the metal–ligand bifunctional addition step in an enantioselective ketone hydrogenation. *J Am Chem Soc* 130:11979–11987
164. Iuliis MZD, Morris RH (2009) Kinetic hydrogen/deuterium effects in the direct hydrogenation of ketones catalyzed by a well-defined ruthenium diphosphine diamine complex. *J Am Chem Soc* 131:11263–11269
165. Zhao J, Goldman AS, Hartwig JF (2005) Oxidative addition of ammonia to form a stable monomeric amido hydride complex. *Science* 307:1080–1082
166. Koyanagi GK, Kapishon V, Bohme DK et al (2010) Reactivity pattern in the room-temperature activation of NH<sub>3</sub> by the main-group atomic ions Ga<sup>+</sup>, Ge<sup>+</sup>, As<sup>+</sup> and Se<sup>+</sup>. *Eur J Inorg Chem* 10:1516–1521
167. Gunanathan C, Gnanaprakasam B, Iron MA et al (2010) “Long-range” metal–ligand cooperation in H<sub>2</sub> activation and ammonia-promoted hydride transfer with a ruthenium–acridine pincer complex. *J Am Chem Soc* 132:14763–14765
168. Kanzelberger M, Zhang XW, Emge TJ et al (2003) Distinct thermodynamics for the formation and cleavage of N–H bonds in aniline and ammonia. Directly-observed reductive elimination of ammonia from an isolated amido hydride complex. *J Am Chem Soc* 125:13644–13645
169. Morgan E, MacLean DF, McDonald R et al (2009) Rhodium and iridium amido complexes supported by silyl pincer ligation: ammonia N–H bond activation by a [PSiP]Ir complex. *J Am Chem Soc* 131:14234–14236
170. Molander GA, Romero JAC (2002) Lanthanocene catalysts in selective organic synthesis. *Chem Rev* 102:2161–2186
171. Mueller TE, Hultsch KC, Yus M et al (2008) Hydroamination: direct addition of amines to alkenes and alkynes. *Chem Rev* 108:3795–3892
172. Harder S (2010) From limestone to catalysis: application of calcium compounds as homogeneous catalysts. *Chem Rev* 110:3852–3876
173. Anderson LL, Arnold J, Bergman RG (2005) Proton-catalyzed hydroamination and hydroarylation reactions of anilines and alkenes: a dramatic effect of counteranions on reaction efficiency. *J Am Chem Soc* 127:14542–14543
174. Schlummer B, Hartwig JF (2002) Brønsted acid-catalyzed intramolecular hydroamination of protected alkenylamines. Synthesis of pyrrolidines and piperidines. *Org Lett* 4:1471–1474
175. Shapiro ND, Rauniyar V, Hamilton GL et al (2011) Asymmetric additions to dienes catalysed by a dithiophosphoric acid. *Nature* 470:245–250
176. Crimmin MR, Arrowsmith M, Barrett AGM et al (2009) Intramolecular hydroamination of aminoalkenes by calcium and magnesium complexes: a synthetic and mechanistic study. *J Am Chem Soc* 131:9670–9685



# Computational Studies of Lewis Acidity and Basicity in Frustrated Lewis Pairs

Thomas M. Gilbert

**Abstract** Computational studies that characterize the effects of Lewis acidity/basicity on FLP formation and reactivity are reviewed. Formation of the FLP encounter complex “cage” depends on Lewis acidities and basicities of substituent “external” atoms, and their abilities to interact intramolecularly. Computations indicate that these interactions are worth 9–18 kcal mol<sup>-1</sup> for partly fluorinated FLPs such as (F<sub>5</sub>C<sub>6</sub>)<sub>3</sub>B⋯P(*t*-Bu)<sub>3</sub>, and less for less fluorinated species such as (H<sub>5</sub>C<sub>6</sub>)<sub>3</sub>B⋯P(*t*-Bu)<sub>3</sub>. Reactivity within the cage depends on the “classical” Lewis acidities/basicities of the internal atoms. Energetics here fall into the range of 5–50 kcal mol<sup>-1</sup>; the larger the value, the greater the ability of the FLP to capture or split a substrate. In several cases the computationally predicted reaction barriers differ little with internal Lewis acidity/basicity, indicating that the rate-determining step involves the substrate entering the cage rather than attack by the Lewis acid/base atoms. In others, barriers vary sizably with Lewis acidity/basicity, indicating the opposite. In one case it was shown that these effects cancel, such that the three component barriers are identical for a range of substituted Lewis acid FLP components.

**Keywords** Barrier · Computational · Frustrated Lewis pair · Lewis acidity · Lewis basicity

## Contents

1	Introduction .....	268
2	Calculations Regarding Lewis Acidities/Basicities of the Components of FLPs .....	270
2.1	Calculations Regarding Lewis Acidities/Basicities Associated with Dispersive Interactions Between External Atoms .....	271
2.2	Calculations Regarding Lewis Acidities/Basicities Associated with Interactions Between Internal Atoms .....	273

---

T.M. Gilbert (✉)

Department of Chemistry and Biochemistry, Northern Illinois University, DeKalb, IL 60115, USA  
e-mail: [tgilbert@niu.edu](mailto:tgilbert@niu.edu)

3	Calculations Involving Lewis Acidity/Basicity and FLP Reactivity .....	278
3.1	Heterolytic Splitting of H <sub>2</sub> .....	278
3.2	Trapping and Activation of CO <sub>2</sub> and N <sub>2</sub> O .....	282
3.3	Miscellaneous Reactions .....	283
4	Closing Comments .....	286
	References .....	287

## Abbreviations

ABCO	Azabicyclo[2,2,2]octane
Ad	1-Adamantyl
Ar	Arene or aryl
DABCO	Diazabicyclo[2,2,2]octane
DFT	Density functional theory
Dipp	2,6-Di-( <i>i</i> -propyl)phenyl
FLP	Frustrated Lewis pair
LA	Lewis acid
LB	Lewis base
Mes	1,3,5-C <sub>6</sub> Me <sub>3</sub> H <sub>2</sub>
NHC	N-Heterocyclic carbene
OG2R3	3-Layer ONIOM-based G2R composite theory
ONI	ONIOM-based composite method
Py	Pyridine
SCRF	Self consistent reaction field; continuum solvent correction model
Tmp	2,2,6,6-Tetramethylpiperidine

## 1 Introduction

Lewis acid/base interactions govern most chemical processes, including the behavior of frustrated Lewis pairs (FLPs). While other chapters in this volume will focus on computational studies of the mechanisms by which FLPs activate molecules, this one will focus entirely on computational studies that compare FLPs in terms of the Lewis acid/base strengths of the components. Both energetics of FLP formation and of FLP reactivity will be discussed, including how the energetics change with acid/base strength, and what this tells us about FLP characteristics. While the number of such studies is limited, many provide considerable insight into the symbiotic processes by which FLPs cause other molecules to react, and suggest avenues of potential importance for study.

It is worth considering the working definitions of Lewis acidity and basicity [1, 2]. The original definition involved the energy evolved when an acid and base coordinated, and this definition is generally used computationally as well. Lewis acidity and basicity are system dependent in that the degree of acidity for an acid depends on the

choice of base, and vice versa. Thus, degrees of Lewis acidity/basicity defined this way are relative; no absolute scale of acidity exists in the same way that acidity in a solvent is determined by the solvent's autoionization equilibrium constant. Attempts have been made to remove this restriction as applied to Lewis acidity by defining it in terms of some inherent property, such as electron deficiency of the acid atom. However, so far this has led to predictions inconsistent with experiment and chemical intuition [3]. Studies over the years have shown that Lewis acidity incorporates several structural/electronic factors beyond the electron poverty of the acid atom [4], including the energy required to deform structures from trigonal planar to pseudo-tetrahedral upon complexation to a base ( $\Delta E_{\text{prep}}$ ) [5, 6], the relative energy of the acid LUMO [7], and the ability of the substituents to support the lowered positive charge on the acid atom in the complex [8]. In this review, the energetic definition will be employed, despite the necessity to couch degrees of acidity and basicity in terms of the conjoining molecule.

As the science of FLPs has evolved, many types of FLPs have been characterized, and it is likely that many more will be in the future [9]. To keep the discussion manageable, this chapter will focus on FLPs comprised of main-group components including boranes, alanes, carbenes, amines, and phosphines. As for notation, systems that are known to be FLPs, or that are predicted to have LA–LB distances well in excess of typical bonding distances, will be denoted LA $\cdots$ LB (sometimes LA atom $\cdots$ LB atom). Systems that are known to be classical Lewis pairs, or that are predicted to have typical LA–LB bonding distances, will be denoted LA–LB. Systems where equilibrium exists between the two, where the interaction is ambiguous or unknown or variable, or where a generic pairing is meant, will be denoted LA/LB.

The term “model chemistry” is used below to denote a combination of a computational model and a basis set. The shorthand used is the common one: model chemistry used for energies/basis set used for energies//model chemistry used for structural optimization/basis set used for structural optimization, e.g., SCS-MP2/6-311++G(d, p)//B3LYP/6-31+G(d, p). This is shortened further when the model chemistries used for energies and optimizations are identical. Readers unfamiliar with computational model chemistries should be aware that numerous mixtures of computational models and basis sets are used in the field, and most research groups have particular favorites. Only rarely can results from different model chemistries, different computational models, or different basis sets be properly compared. This particularly holds when attempting to compare results from perturbation theory calculations with those from density functional theory calculations, or those using double-zeta basis sets with those using triple-zeta basis sets. Unfortunately, abbreviations used for model chemistries are often uninformative as to the likely accuracy of the calculation. Readers interested in this level of detail are strongly encouraged to read an introductory textbook in the field, and to view critically the information below and in the original work. When references are cited more than once in the text below, model chemistries used will generally be noted only when first cited.

## 2 Calculations Regarding Lewis Acidities/Basicities of the Components of FLPs

A number of computational studies have probed the structural nature of FLPs. Generally speaking, models suggest that the pair form an encounter complex that is structurally a “cage” held together by long-range Lewis acid/base dispersive interactions between substituent atoms (hereafter the external atoms), such that the Lewis acid/base atoms (those that would be bonded in a classical complex; hereafter the internal atoms) are held a sizable distance apart [10–12]. The dispersive interactions are number dependent, meaning that the greater the number of interactions, the more strongly the cage holds together. Thus systems with arene rings (allowing for atom- $\pi$  cloud interactions), fluorine atoms (allowing for strong dipolar interactions such as C-H $\cdots$ F-C), and large substituents that can extend sufficiently far into space to allow these interactions are more likely to form FLP cages. Dispersive interactions are also “position ambivalent,” meaning that, for the most part, they should be independent of which internal atom holds the donor/acceptor external atoms/substituents. For example, one expects these interactions to be approximately isoenergetic for the well-known (F<sub>5</sub>C<sub>6</sub>)<sub>3</sub>B $\cdots$ P(*t*-Bu)<sub>3</sub> FLP and for its “reverse” isomer (*t*-Bu)<sub>3</sub>B $\cdots$ P(C<sub>6</sub>F<sub>5</sub>)<sub>3</sub>.

The internal atoms generate an environment within the cage that forces the added substrate to react. The nature of this environment has been characterized as one where base HOMO and acid LUMO interact [12], and as one where the acid and base atoms generate a polarized electric field between them that assists in activating the substrate [10]. While these views diverge at points, basically they are similar in describing the environment as one where the three-dimensional distribution of electron density in the cage dictates reactivity between the FLP and substrate. Hereafter, this environment will simply be called the field. The field distorts in the direction of the Lewis acid as it draws electron density toward itself. The degree of distortion is directly related to the inherent electron poverty/richness of the internal acid and base atoms, plus additional poverty/richness engendered by the electron-withdrawing/donating properties of their substituents. This is what is usually meant by the term “inherent Lewis acidity/basicity,” and is the “chemical intuition” view of Lewis acidity/basicity. In contrast to the dispersive interactions, the internal interactions are highly “position dependent.” To use the example above, (F<sub>5</sub>C<sub>6</sub>)<sub>3</sub>B $\cdots$ P(*t*-Bu)<sub>3</sub> is properly organized, because the acceptor internal atom has acceptor substituents and the donor internal atom has donor substituents. It should exhibit a highly polarized field, and considerable reactivity. In turn, (*t*-Bu)<sub>3</sub>B $\cdots$ P(C<sub>6</sub>F<sub>5</sub>)<sub>3</sub> is mismatched, and so would be expected to exhibit a less polarized field and lower reactivity. Calculations and solid-state NMR experiments have recently addressed this concept [13].

Both types of Lewis acid–base interactions and their degrees must be considered in relating the behavior of an FLP to Lewis acidity/basicity of the components. One must understand the Lewis acidities/basicities of the external atom/substituents in order to evaluate the dispersion energetics that determine the strength of the cage

**Table 1** Predicted B...P distances (Å) and interaction energies (kcal mol<sup>-1</sup>) of (R<sub>5</sub>C<sub>6</sub>)<sub>3</sub>B...P(*t*-Bu)<sub>3</sub> FLPs (R = F, H)

Lewis acid	Lewis base	<i>d</i> (B...P)	$\Delta E$ model chemistry	$\Delta E$	Ref
B(C <sub>6</sub> H <sub>5</sub> ) <sub>3</sub>	P( <i>t</i> -Bu) <sub>3</sub>	3.7	SCS-MP2/cc-PVTZ//HF/6-31G(d, p)	-12.0	[16]
B(C <sub>6</sub> F <sub>5</sub> ) <sub>3</sub>	P( <i>t</i> -Bu) <sub>3</sub>	4.0	SCS-MP2/cc-PVTZ//HF/6-31G(d, p)	-14.9	[16]
B(C <sub>6</sub> H <sub>5</sub> ) <sub>3</sub>	P( <i>t</i> -Bu) <sub>3</sub>	4.2	OG2R3//ONIOM MPW1K/6-31+G(d)	-5.0	[15]
B(C <sub>6</sub> F <sub>5</sub> ) <sub>3</sub>	P( <i>t</i> -Bu) <sub>3</sub>	3.8	OG2R3//ONIOM MPW1K/6-31+G(d)	-19.0	[15]
B(C <sub>6</sub> H <sub>5</sub> ) <sub>3</sub>	P( <i>t</i> -Bu) <sub>3</sub>	3.7	SCS-MP2/cc-PVTZ//B3LYP/6-31G(d)	-8.5	[12]
B(C <sub>6</sub> F <sub>5</sub> ) <sub>3</sub>	P( <i>t</i> -Bu) <sub>3</sub>	4.2	SCS-MP2/cc-PVTZ//B3LYP/6-31G(d)	-11.5	[12]

and its ability to place the Lewis acid/base atoms in proximity. One must also understand the Lewis acidities/basicities of the internal atoms, as these will determine the strength of the polarized field, and in turn the ability of the FLP to cause the small molecule to react. It is challenging to isolate each type, but approaches have done so, with reasonable degrees of success.

## 2.1 Calculations Regarding Lewis Acidities/Basicities Associated with Dispersive Interactions Between External Atoms

Pápai et al. [12, 14], Gille and Gilbert [15], and Kim and Rhee [16] have provided data assessing dispersive Lewis acid/base interactions in FLPs by computationally comparing the interaction energies of (F<sub>5</sub>C<sub>6</sub>)<sub>3</sub>B...P(*t*-Bu)<sub>3</sub> and its parent (H<sub>5</sub>C<sub>6</sub>)<sub>3</sub>B...P(*t*-Bu)<sub>3</sub>. As shown in Table 1, different model chemistries gave rather different predictions. Focusing on the B...P distance, the HF and B3LYP optimizations suggest that substituting fluorine for hydrogen on the arene rings increases the distance, while MPW1K optimizations suggest the distance should decrease. It is unclear what merit to ascribe to this observation, as all models indicated that the potential energy surface for increasing/decreasing the distance is rather flat. Moreover, arguments can justify either result. Replacing arene hydrogen with fluorines provides for more possible C-H...F interactions, likely decreasing the B...P distance, but the increased steric bulk of the perfluorinated arenes could repel the phosphine moiety, increasing it. The latter view was supported by the prediction that the B-P/B...P distances in the series of classical complexes (F<sub>5</sub>C<sub>6</sub>)<sub>3</sub>B-P(CH<sub>3-x</sub>Me<sub>x</sub>)<sub>3</sub> (*x* = 0–3) increased nonlinearly with *x* [15]. The B-P bond distances for *x* = 0–2 (between PMe<sub>3</sub> and P(*i*-Pr)<sub>3</sub>) changed only from 2.068 to 2.194 Å. The distance then jumped dramatically to 3.8 Å for *x* = 3, P(*t*-Bu)<sub>3</sub>, where the complex converted to an FLP. That said, it is unclear that arguments applying to classical complexes also apply to FLPs.

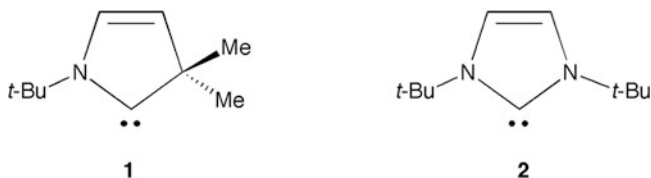
The predicted dispersive interaction energies differed with model chemistry as well. The SCS-MP2 models predicted that the dispersive interactions provided by C-H...F interactions and  $\pi$ -atom interactions enhanced by the increased Lewis acidity of the perfluorinated arene ring, if they exist at all, stabilize (F<sub>5</sub>C<sub>6</sub>)<sub>3</sub>B...P(*t*-Bu)<sub>3</sub> over (H<sub>5</sub>C<sub>6</sub>)<sub>3</sub>B...P(*t*-Bu)<sub>3</sub> by only ca. 3 kcal mol<sup>-1</sup>. This seems small

because each C–H···F–C interaction appears to be worth ca. 2 kcal mol<sup>-1</sup> of stabilization [17] (although it appears no case of C(alkyl)–H···F–C(aromatic) has been examined computationally), and optimized structures suggested the presence of at least a few of these in (F<sub>5</sub>C<sub>6</sub>)<sub>3</sub>B···P(*t*-Bu)<sub>3</sub>. In contrast, the OG2R3 composite model (which estimates the CCSD(T)/6-311++G(2df,2p) energy) suggested that the additional dispersive interactions stabilize the fluorinated FLP by 14 kcal mol<sup>-1</sup>. This seems rather too large.

Kim and Rhee [16] probed this further by examining interactions between P(*t*-Bu)<sub>3</sub> and the face of C<sub>6</sub>F<sub>6</sub>. Their data showed that the two interact with a maximum stabilization of ca. 12 kcal mol<sup>-1</sup>. The data were not partitioned to separate lone pair- $\pi$  cloud and C–H···F effects (although long range electrostatic effects were shown to be negligible), but nonetheless it appears that long range interactions such as occur in FLPs can be worth in excess of 10 kcal mol<sup>-1</sup>, as suggested by the OG2R3 results. It is worth noting that Kim and Rhee also estimated the energy associated with the internal B···P interaction in (F<sub>5</sub>C<sub>6</sub>)<sub>3</sub>B···P(*t*-Bu)<sub>3</sub> and (H<sub>5</sub>C<sub>6</sub>)<sub>3</sub>B···P(*t*-Bu)<sub>3</sub>. They found that this interaction in both FLPs is stabilizing by ca. 5 kcal mol<sup>-1</sup> at ca. 4 Å, a value that appears large, given that this distance is nearly twice the bonding distance. If this is correct (and see below) it implies that dispersive Lewis acid/base interactions here are worth 7 kcal mol<sup>-1</sup> in (H<sub>5</sub>C<sub>6</sub>)<sub>3</sub>B···P(*t*-Bu)<sub>3</sub> and 10 kcal mol<sup>-1</sup> in (F<sub>5</sub>C<sub>6</sub>)<sub>3</sub>B···P(*t*-Bu)<sub>3</sub>. The former represents a surprisingly large value for the  $\pi$ -atom interactions in (H<sub>5</sub>C<sub>6</sub>)<sub>3</sub>B···P(*t*-Bu)<sub>3</sub>, an FLP with no C–H···F–C interactions.

In related work, Grimme et al. predicted FLP formation energies between P(*t*-Bu)<sub>3</sub> and RB(C<sub>6</sub>F<sub>5</sub>)<sub>2</sub> (R = *n*-C<sub>6</sub>H<sub>13</sub>, *c*-C<sub>6</sub>H<sub>11</sub>, Cl, and H) as part of a study of CO<sub>2</sub> activation by FLPs (see below) [18]. In order, the values were –10.4, –7.3, –10.8, and –20.9 kcal mol<sup>-1</sup> (B2LYP-D3/def2-TZVP model). No B···P distance data were provided, but it seems likely that the first three have longer B···P distances than the last. It is notable that the values for the first three were near 10 kcal mol<sup>-1</sup>, similar to that predicted for (F<sub>5</sub>C<sub>6</sub>)<sub>3</sub>B···P(*t*-Bu)<sub>3</sub>, despite the fact these have at most two-thirds as many C–H···F–C interactions as this FLP. This argues that an interaction energy of  $\geq 14$  kcal mol<sup>-1</sup> for (F<sub>5</sub>C<sub>6</sub>)<sub>3</sub>B···P(*t*-Bu)<sub>3</sub> is more reasonable than a smaller value.

Wang et al. made direct computational comparisons between (F<sub>5</sub>C<sub>6</sub>)<sub>3</sub>B···N(*t*-Bu)<sub>3</sub> and (F<sub>5</sub>C<sub>6</sub>)<sub>3</sub>B···P(*t*-Bu)<sub>3</sub> [19]. They found the B···N distance in the amine FLP (4.779 Å) to be much longer than the B···P distance in the phosphine FLP (4.050 Å), consistent with the greater crowding and smaller size of the basic atom in the former (M05-2X/6-31G(d, p) model). Nonetheless, the FLP formation energies (M05-2X/6-311++G(d, p)/M05-2X/6-31G(d, p) model) were similar (–2.9 and –6.2 kcal mol<sup>-1</sup>), denoting that interaction energetics mostly involved the peripheral atoms. Given this, one might expect the formation energies to be more nearly equal. In this regard, the authors also examined the carbene-base FLPs (F<sub>5</sub>C<sub>6</sub>)<sub>3</sub>B···**1** and (F<sub>5</sub>C<sub>6</sub>)<sub>3</sub>B···**2** (Scheme 1). Optimizations of these again gave markedly different B···C distances (3.717 and 4.316 Å), but similar FLP formation energies (–5.7 and –4.4 kcal mol<sup>-1</sup>) that differed by less than did the amine/phosphine pairs. The data thus suggested that FLPs where the acids and bases have similar steric



**Scheme 1** NHCs used as Lewis bases in computational studies by Wang et al. [19]

environments and similar peripheral interactions will display similar formation energies, even if the acid atom/base atom distance differs substantially. This in turn supports the view that nearly all the interaction energy predicted for FLPs arises from external interactions rather than internal ones, so the 5 kcal mol<sup>-1</sup> contribution suggested for the latter by Kim and Rhee (see above) appears overestimated.

## 2.2 Calculations Regarding Lewis Acidities/Basicities Associated with Interactions Between Internal Atoms

Characterizing Lewis acidities/basicities of internal atoms in the context stated above requires examining coordination/dissociation energies for classical Lewis acid/base complexes. Many publications have focused on assessing the relative acidities/basicities of components of classical Lewis acid/base complexes. As noted above, discussion here will focus on main group systems relevant to FLPs.

### 2.2.1 Lewis Acids

As most FLPs involve B(C<sub>6</sub>F<sub>5</sub>)<sub>3</sub> or a variant, the Lewis acidity of this borane will be discussed first. Dissociation energies of classical (F<sub>5</sub>C<sub>6</sub>)<sub>3</sub>B–LB complexes have been predicted for an array of bases. Jacobsen et al. found a sizable range of bond energies for different LB, from 26.8 kcal mol<sup>-1</sup> for LB = CNMe to 12.4 kcal mol<sup>-1</sup> for LB = PH<sub>3</sub> to 9.1 kcal mol<sup>-1</sup> for LB = CO (BP86/ADF V model) [20]. Similarly, Gille and Gilbert examined (F<sub>5</sub>C<sub>6</sub>)<sub>3</sub>B–NMe<sub>3</sub> and (F<sub>5</sub>C<sub>6</sub>)<sub>3</sub>B–P(CH<sub>3-x</sub>Me<sub>x</sub>)<sub>3</sub> (x = 0–3), finding a value of 21 kcal mol<sup>-1</sup> for the amine base complex and values of 41, 36, and 32 kcal mol<sup>-1</sup> for the PMe<sub>3</sub>, PEt<sub>3</sub>, and P(*i*-Pr)<sub>3</sub> complexes, respectively (OG2R3/ONIOM MPW1K/6-31+G(d) model) [15]. Timoshkin and Frenking published computed bond energies between borane Lewis acids BCl<sub>3</sub>, B(C<sub>6</sub>H<sub>5</sub>)<sub>3</sub>, B(C<sub>6</sub>H<sub>4</sub>-4-F)<sub>3</sub>, and B(C<sub>6</sub>F<sub>5</sub>)<sub>3</sub>, and several Lewis bases [21]. The work compared the three triarylboranes with the well-studied BCl<sub>3</sub>, finding broadly that the relative Lewis acidities trended as B(C<sub>6</sub>H<sub>5</sub>)<sub>3</sub> ≈ B(C<sub>6</sub>H<sub>4</sub>-4-F)<sub>3</sub> ≪ B(C<sub>6</sub>F<sub>5</sub>)<sub>3</sub> ≈ BCl<sub>3</sub> (RI-BP86/def2-TZVPP model). The data in Table 2 expand on Timoshkin and Frenking's study by comparing X<sub>3</sub>B–YMe<sub>3</sub> complexes (X = F, Cl, C<sub>6</sub>F<sub>5</sub>; Y = N, P). One sees that the data are scattered, probably owing to the different model chemistries employed; nonetheless, qualitatively they confirm Timoshkin and Frenking's characterization of B(C<sub>6</sub>F<sub>5</sub>)<sub>3</sub> being about equal in Lewis acidity to BCl<sub>3</sub>.

**Table 2** Predicted interaction energies of amine-borane and phosphine-borane complexes  $X_3B-YMe_3$  ( $X = H, F, Cl, F_5C_6$ ;  $Y = N, P$ ; kcal mol $^{-1}$ )

Lewis acid	Lewis base	$\Delta E$ model chemistry	$\Delta E$	Ref
BF <sub>3</sub>	NMe <sub>3</sub>	MP2/6-311++G(d, p)	-51.9	[22]
BCl <sub>3</sub>	NMe <sub>3</sub>	BP86/TZ2P	-21.0	[4]
B(C <sub>6</sub> F <sub>5</sub> ) <sub>3</sub>	NMe <sub>3</sub>	OG2R3//ONIOM MPW1K/6-31+G(d)	-21.0	[15]
BF <sub>3</sub>	PMe <sub>3</sub>	MP2/6-311++G(d, p)	-41.7	[23]
BCl <sub>3</sub>	PMe <sub>3</sub>	MP2/6-311G(2d)//MP2/6-31G(d)	-33.1	[24]
B(C <sub>6</sub> F <sub>5</sub> ) <sub>3</sub>	PMe <sub>3</sub>	OG2R3//ONIOM MPW1K/6-31+G(d)	-41.0	[15]

**Table 3** Least-squares linear substituent effect energies and errors (OG2R3//M06-2X/6-311+G(d, p), kcal mol $^{-1}$ ) for amine-borane and phosphine-borane complexes (C<sub>6</sub>H<sub>x</sub>F<sub>5-x</sub>)<sub>3</sub>B-XMe<sub>3</sub> (modified from [25])

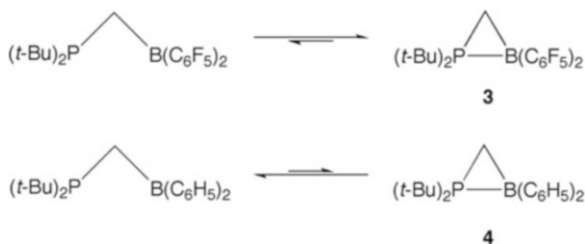
	(C <sub>6</sub> H <sub>x</sub> F <sub>5-x</sub> ) <sub>3</sub> B-NMe <sub>3</sub>	(C <sub>6</sub> H <sub>x</sub> F <sub>5-x</sub> ) <sub>3</sub> B-PMe <sub>3</sub>	Average
2-F	-12.6(2)	-14.7(8)	-13.7
3-F	-2.2(2)	-3.3(7)	-2.8
4-F	-0.1(1)	-0.5(7)	-0.3
5-F	-2.5(2)	-2.7(8)	-2.6
6-F	6.6(2)	3.2(9)	4.9

Caveats regarding these data should be noted. Showing the difficulties associated with different DFT model calculations, Timoshkin and Frenking found a bond dissociation energy for (F<sub>5</sub>C<sub>6</sub>)<sub>3</sub>B-PH<sub>3</sub> of 5.7 kcal mol $^{-1}$ , less than half the value of Jacobsen et al. Moreover, they found a dissociation energy of 23.2 kcal mol $^{-1}$  for (F<sub>5</sub>C<sub>6</sub>)<sub>3</sub>B-NH<sub>3</sub>, some four times the value for the phosphine homologue. This ratio is completely inconsistent with those for alkyl-substituted amines/phosphines (which are more relevant to FLPs; see Table 2), showing the difficulties associated with computing energetics when components contain small substituents. It is unclear why such oddities arise; amongst the possibilities are, first, competition between the increased donor ability of trialkyl bases vs the parents and the greater steric repulsions in the former and, second, basis set incompleteness for the more complex trialkyl bases.

To probe the effect of partial arene ring fluorination on the Lewis acidity of triarylboranes B(C<sub>6</sub>F<sub>x</sub>H<sub>5-x</sub>)<sub>3</sub>, Durfey and Gilbert determined association energies for all versions of (F<sub>x</sub>H<sub>5-x</sub>C<sub>6</sub>)<sub>3</sub>B-YMe<sub>3</sub> ( $x = 0-5$ ,  $Y = N, P$ ) [25]. Scaling the data by setting the association energies of (H<sub>5</sub>C<sub>6</sub>)<sub>3</sub>B-YMe<sub>3</sub> to zero, they found a remarkably linear correlation between the number and positions of F atoms on the arene rings and the Lewis acidity of the borane. Data appear in Table 3. As can be seen, substitution at the 2 position increased Lewis acidity by an average of 13.7 kcal mol $^{-1}$ , by far the largest effect. Substitution at the 3 and 5 positions increased acidity by ca. 3 kcal mol $^{-1}$ , substitution at the 4 position had essentially no effect, and substitution at the 6 position *decreased* the acidity by ca. 5 kcal mol $^{-1}$ . Taken together, the results indicate that B(C<sub>6</sub>F<sub>5</sub>)<sub>3</sub> should be only slightly more Lewis acidic than B(C<sub>6</sub>H<sub>4</sub>-2-F)<sub>3</sub>, and B(C<sub>6</sub>H<sub>2</sub>-2,3,5-F<sub>3</sub>)<sub>3</sub> and B(C<sub>6</sub>H-2,3,4,5-F<sub>4</sub>)<sub>3</sub> should be more Lewis acidic than both. B(C<sub>6</sub>H-2,3,5,6-F<sub>4</sub>)<sub>3</sub>, which is occasionally



**Scheme 2** Equilibria between open and closed forms of tethered FLPs, from Lammertsma et al. [27]



substituted for  $\text{B}(\text{C}_6\text{F}_5)_3$  in FLPs because the latter undergoes nucleophilic attack at the 4-F position [26], should show identical Lewis acidity, not less as is commonly assumed. Viewing acidity from the other direction,  $\text{B}(\text{C}_6\text{H}_4\text{-4-F})_3$  is only very slightly more Lewis acidic than  $\text{B}(\text{C}_6\text{H}_5)_3$ , meaning that it can be used as an electronic substitute for the parent with a  $^{19}\text{F}$  NMR “handle.” The decrease in acidity for 6-substituted arenes seems to arise because of steric repulsions which are, of course, integral to forming FLPs. Nonetheless, matching, for example,  $\text{B}(\text{C}_6\text{H}_2\text{-2,3,5-F}_3)_3$  with an amine or phosphine large enough to enforce FLP formation should give a very reactive environment within the cage.

An as yet untested possible benefit of this observation of a linear relationship is that one could estimate the Lewis acidity of a mixed or tethered system. For example, the mixed triarene borane  $\text{B}(\text{C}_6\text{H}_3\text{-2,5-F}_2)(\text{C}_6\text{F}_5)(\text{C}_6\text{H}_5)$  should be bulky enough to form an FLP with  $\text{P}(t\text{-Bu})_3$ . To predict its Lewis acidity, and in turn the FLP reactivity, relative to that of  $\text{B}(\text{C}_6\text{H}_5)_3$ , one compares the rings in the mixed borane with those in the parent. The fluorine at the 2 position in 2,5-F<sub>2</sub>-C<sub>6</sub>H<sub>3</sub> adds 13.7 kcal mol<sup>-1</sup> in acidity over the parent phenyl ring, while that at the 5 position adds 2.6 kcal mol<sup>-1</sup>, for a total of 16.3 kcal mol<sup>-1</sup>. Similarly, replacing all the hydrogens in the parent phenyl ring with fluorines adds 13.7 + 2.8 + 0.3 + 2.6 – 4.9 kcal mol<sup>-1</sup> = 14.5 kcal mol<sup>-1</sup>. Taking a weighted average of these to correspond to the arene substituents of  $\text{B}(\text{C}_6\text{H}_3\text{-2,5-F}_2)(\text{C}_6\text{F}_5)(\text{C}_6\text{H}_5)$  gives  $1/3[(16.3) + (14.5) + (0)] = 10.3$  kcal mol<sup>-1</sup>; that is, one estimates that  $\text{B}(\text{C}_6\text{H}_3\text{-2,5-F}_2)(\text{C}_6\text{F}_5)(\text{C}_6\text{H}_5)$  will be 10.3 kcal mol<sup>-1</sup> more exothermic/Lewis acidic than  $\text{B}(\text{C}_6\text{H}_5)_3$ . More usefully, one could predict the relative Lewis acidities of the acidic component of tethered FLPs. For example, the Lewis acid moiety in  $(\text{F}_5\text{C}_6)_2\text{B}(\text{arene tether})\text{P}(t\text{-Bu})_2$  would be expected to be 4.8 kcal mol<sup>-1</sup> less Lewis acidic than the boron in  $\text{B}(\text{C}_6\text{F}_5)_3$ .

Lammertsma et al. compared equilibrium positions between ring and open isomers of the tethered FLPs as shown in Scheme 2 [27]. In keeping with the greater internal Lewis acidity of the perfluorinated arene borane moiety, **3** prefers the cyclized form by 1.5 kcal mol<sup>-1</sup> (M06-2X/6-31+G(d, p) model), while parent **4** prefers the chain form. Both would likely act as FLPs under reasonable reaction conditions; unfortunately, experimentally **3** only exists transiently, rearranging to form a bicycle. Given Durfey and Gilbert’s results, an analogue of **3** using 3,4,5-F-substituted arene rings would clearly be of interest, displaying Lewis acidity somewhat less than that of the perfluorinated complex, but incapable of a similar rearrangement. In line with this, Gilbert’s calculations predict that  $\text{B}(\text{C}_6\text{H}_4\text{-2-F})_3$  should form an FLP with  $\text{P}(t\text{-Bu})_3$ , with a B⋯P distance of 3.547 Å, that is nearly as

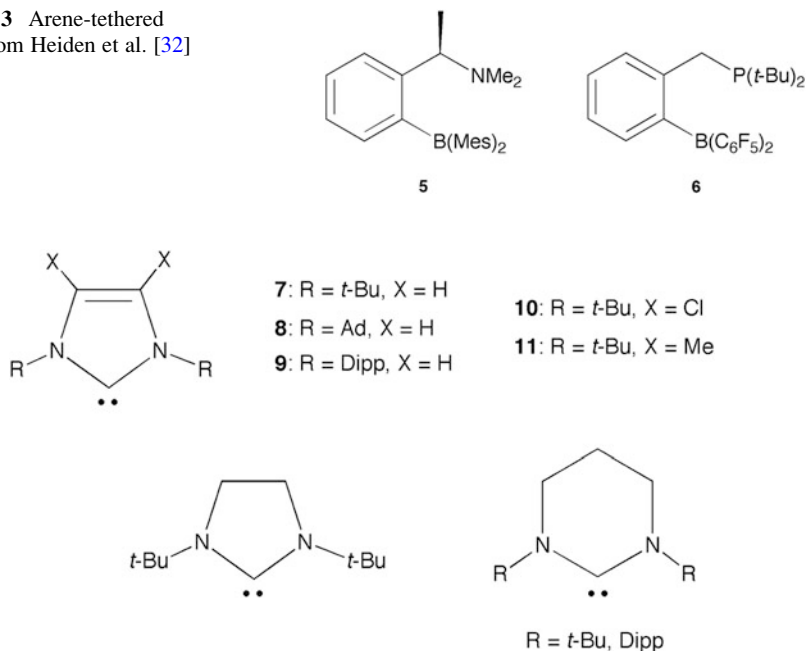
stable as the  $(F_5C_6)_3B \cdots P(t-Bu)_3$  FLP ( $-13.1$  vs  $-15.8$  kcal mol $^{-1}$ , OG2R3//ONIOM M06-2X/6-31 + G(d) model), and nearly as active at capturing  $N_2O$  (see Sect. 3.2) [28]. Interestingly, related calculations indicate that  $B(C_6H_4-4-F)_3$  should form a very weakly interacting FLP with  $P(t-Bu)_3$ , as seen experimentally, while  $B(C_6H_4-3-F)_3$  should form an equilibrium between classical and FLP complexes ( $B-P = 2.448$  Å, interaction energy  $-1.7$  kcal mol $^{-1}$ ). This illustrates the interplay between steric repulsions and intramolecular interactions associated with external Lewis acidity/basicity, and the interactions between Lewis acid/base atoms associated with internal acidity/basicity.

### 2.2.2 Lewis Bases

Basicities are generally computed as gas phase, 0 K, proton affinities, meaning that they do not relate directly to  $pK_a$  values of the relevant hydridophosphonium cations. Calculated hydrogen affinities for several free and tethered LBs used to form FLPs are given in [14]. Exothermicities range from 6 kcal mol $^{-1}$  for poorly basic  $P(C_6F_5)_3$  to 80 kcal mol $^{-1}$  for **2**, with most falling in the range of 40–60 kcal mol $^{-1}$ . Generally, LB proton affinities/basicities behave as expected from chemical intuition: trialkyl phosphines are more basic than triarylphosphines, phosphines with better donating substituents are more basic than those without.

Relatively few computational studies have addressed the effect of Lewis basicity on reactivity. Geier et al. illustrated the interplay between substituent-influenced donor strength and steric repulsion in FLPs through studies of  $(F_5C_6)_3B/2,6-(H_xMe_{2-x})py$  complexes [29]. When  $x = 0, 1$ , the pairs form strongly bonded classical complexes, with association energies of ca.  $-32$  kcal mol $^{-1}$  (M06-2X/6-311G(d, p)//ONIOM MPW1K/6-31 + G(d) model). When  $x = 2$ , the association energy is smaller,  $-25$  kcal mol $^{-1}$ . As this pair experimentally forms an equilibrium between a classical complex and an FLP that heterolytically splits  $H_2$ , it can be derived that the energy represents the “tipping point” bond energy above which a classical LA–LB complex forms, and below which an FLP forms. Wu et al. expanded this study through mapping the potential energy surfaces for interaction between  $B(C_6F_5)_3$  and  $py/2,6-Me_2py$  [30]. They showed that Fukui function descriptors (essentially, descriptors of the HOMO/LUMO energetics) track the classical complex/FLP equilibrium for  $(F_5C_6)_3B \cdots 2,6-Me_2py$ .

Erös et al. compared energetics of borane-amine FLPs  $(C_6F_5)_2(Mes)B/ABCO$  and  $(C_6F_5)_2(Mes)B \cdots tmp$  [31]. The former contains a “tied-back” base with a sterically uncongested nitrogen atom, while the latter contains a base with sterically encumbered nitrogen. Nonetheless, the proton affinities of the two bases were calculated to be essentially identical, meaning that energetic differences between the two FLPs should be attributed to steric effects. Potential energy surface scans showed that  $(C_6F_5)_2(Mes)B \cdots tmp$  has a single minimum with a  $B \cdots N$  distance of 4.52 Å (M05-2X/6-31G(d) model), and an energy relative to the components of  $-7.6$  kcal mol $^{-1}$  (M05-2X/6-311++G(d, p)//M05-2X/6-31G(d) model). In contrast,  $(C_6F_5)_2(Mes)B/ABCO$  exhibited two minima, one corresponding to a classical

**Scheme 3** Arene-tethered FLPs, from Heiden et al. [32]**Scheme 4** NHCs used as Lewis bases for FLPs in computations from Kronig et al. [33]

Lewis acid–base complex with  $B-N = 1.85 \text{ \AA}$  stabilized by  $8.8 \text{ kcal mol}^{-1}$  vs the components, and the other an FLP with  $B \cdots N = 3.77 \text{ \AA}$  stabilized by  $8.4 \text{ kcal mol}^{-1}$  vs the components. The barrier between the two was predicted to be ca.  $2 \text{ kcal mol}^{-1}$ . The similarity between formation energies of the two FLPs despite the dramatic differences in accessibility of the nitrogen atoms and in  $B \cdots N$  distances indicates that they reflect only the external atom energetics.

Heiden et al. investigated association energies of the tethered FLPs **5** and **6** shown in Scheme 3 [32]. Formation of a B–N bond stabilized amine-containing **5** by  $5.8 \text{ kcal mol}^{-1}$ , while formation of a B–P bond stabilized phosphine-containing **6** by  $3.0 \text{ kcal mol}^{-1}$  (B3LYP/6-31G(d) model). Both still heterolytically split  $H_2$  in the manner of FLPs (see below). That the former value is more exothermic than the latter appears due to decreased crowding in the former complex arising from its having smaller substituents on the nitrogen, given that B–P bonds are usually stronger than B–N bonds (see Table 2 and [25]), and that the  $C_6F_5$ -substituted boron in the latter should be more Lewis acidic than the Mes-substituted boron in the former. This is an interesting case of formation of an FLP involving an LB with rather small substituents.

Kronig et al. computed association energetics between  $B(C_6F_5)_3$  and several N-heterocyclic carbenes (Scheme 4), as well as acyclic carbene (*i*-Pr) $_2$ N–C–N (*i*-Pr) $_2$  [33]. While several of these pairs experimentally acted as FLPs and others did not, their predicted B–C (carbene) distances were all quite similar, averaging

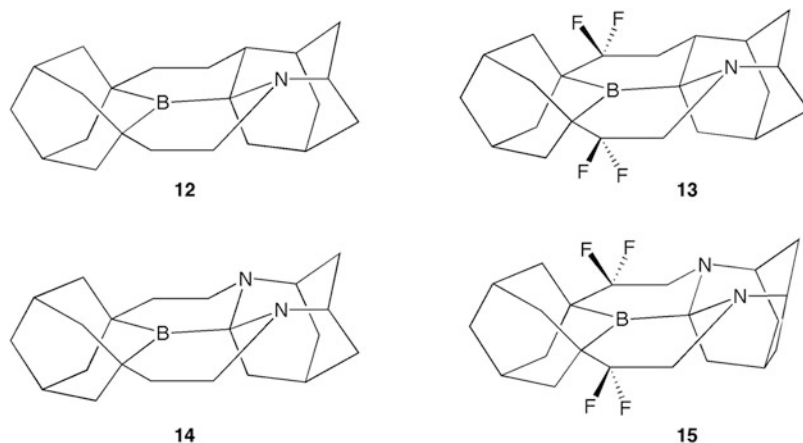
1.706(0.025) Å (M05-2X/6-311G(d, p) model). This suggests that the FLPs are in equilibrium with a classical pair, as in the  $(F_5C_6)_3B \cdots 2,6\text{-Me}_2\text{py}$  system above. Predicted energetics supported this, in that FLPs exhibited  $\Delta G_{298}$  of association values near zero, while classic pairs exhibited sizably exergonic  $\Delta G_{298}$  values. Interestingly, energetic data suggested that substitution at the 4 and 5 positions of the five-membered rings increased the steric bulk (and thus the propensity to form an FLP) of the carbenes, despite the distance of such substitution from the carbene carbon. Comparing  $(F_5C_6)_3B \cdots \mathbf{7}$  with  $(F_5C_6)_3B \cdots \mathbf{11}$  showed that replacing alkenyl hydrogens with methyl groups destabilized the FLP by  $6.0 \text{ kcal mol}^{-1}$ ; replacing them with chlorine atoms ( $(F_5C_6)_3B \cdots \mathbf{7}$  vs  $(F_5C_6)_3B \cdots \mathbf{10}$ ) destabilized the FLP by  $13.1 \text{ kcal mol}^{-1}$ . This implies that chlorine substitution decreases the basicity of the carbene carbon by at least  $7 \text{ kcal mol}^{-1}$ , a concept reflected in the lowered experimental FLP reactivity of  $(F_5C_6)_3B \cdots \mathbf{10}$  vs  $(F_5C_6)_3B \cdots \mathbf{11}$ .

### 3 Calculations Involving Lewis Acidity/Basicity and FLP Reactivity

#### 3.1 Heterolytic Splitting of $H_2$

By far the most computationally examined reaction of FLPs involves the heterolytic splitting of  $H_2$ . Other chapters from Grimme and Pápai in this volume will focus on mechanistic details regarding how FLPs split  $H_2$ , and the uses to which this reaction may be put. Generally speaking, workers in this area compute the energetics involving their particular FLP, so studies directly comparing FLP acidities/basicities are somewhat rare. This section will be restricted to such studies. Moreover, it will be restricted to computations within a single report, or those from one research group, to avoid “apples-to-oranges” comparisons involving related molecules but different model chemistries.

The most wide-ranging report in this area comes from Pápai et al. [14]. They calculated the energetics of  $H_2$ -splitting by all FLPs, free and tethered, known to be capable of doing so at the time of publication. They included for comparison some known FLPs that do not split  $H_2$ . The most active FLP was  $(F_5C_6)_3B \cdots 2,5\text{-}(t\text{-Bu})_2\text{NHC}$ , with  $\Delta G_{298} = -41 \text{ kcal mol}^{-1}$ , while the least active was  $\text{Mes}_3B \cdots P(t\text{-Bu})_3$ , with  $\Delta G_{298} = +28 \text{ kcal mol}^{-1}$  (M05-2X/6-311++G(d, p)/M05-2X/6-31G(d) model). Analysis of the data indicated clearly that distinctions between FLPs that do not split  $H_2$ , those that do so reversibly, and those that do so irreversibly were largely in keeping with the reaction free energy  $\Delta G_{298}$ . Moreover,  $\Delta G_{298}$  correlated reasonably with notions of increasing/decreasing Lewis acidity/basicity of the FLP components. A graph of  $\Delta G_{\text{reaction}}$  vs  $(\Delta G_{\text{pa}} + \Delta G_{\text{ha}})$ , where pa is the proton affinity of the base, and ha is the hydride affinity of the acid, showed few outliers from linearity, and a line of near-unitary slope. The work provides a solid



**Scheme 5** Rigidly tethered FLPs used for H<sub>2</sub> activation, computed by Wang et al. [34]

starting point for predictions regarding whether a hypothetical FLP will experimentally split H<sub>2</sub> simply by calculating the requisite affinities.

### 3.1.1 Comparisons of Lewis Acids

Lammertsma et al. compared energetics for the H<sub>2</sub>-splitting reaction for the tethered FLPs in Scheme 2 [27]. Splitting by perfluorinated FLP **3** exhibited a lower barrier (16.6 vs 22.6 kcal mol<sup>-1</sup>) and greater exothermicity (−14.8 vs −1.6 kcal mol<sup>-1</sup>) than it did by the parent **4**. It is clear that increased Lewis acidity of the FLP affected the reaction energy far more than the barrier. This suggests that most of the barrier energy involves positioning the H<sub>2</sub> molecule within the FLP cage, a need mostly independent of inherent borane Lewis acidity, more dependent on the steric effects that set the size of the channels into the cage.

As part of a study of the catalytic hydrogenation of imines, Wang et al. computed the H<sub>2</sub> splitting energies for the parent and fluorinated rigidly tethered FLPs shown in Scheme 5 [34]. Comparing **12** with **13**, and **14** with **15**, showed that fluorination lowered the barriers for splitting by only ca. 1 kcal mol<sup>-1</sup> and the reaction exothermicities by only ca. 3 kcal mol<sup>-1</sup> (M05-2X/6-311++G(2d, p)//M05-2X/6-31G(d, p) model). This suggests that little of the electron-withdrawing nature of the fluorines transmits through the alkyl bonds; i.e., that the internal Lewis acidities of the borons are nearly identical for each compound.

### 3.1.2 Comparisons of Lewis Bases

Wang and coworkers compared H<sub>2</sub> splitting energies for the seminal FLP (F<sub>5</sub>C<sub>6</sub>)<sub>3</sub>B⋯P(*t*-Bu)<sub>3</sub> and the congener (F<sub>5</sub>C<sub>6</sub>)<sub>3</sub>B⋯N(*t*-Bu)<sub>3</sub> [19]. As one expects, given the different channel sizes and volumes of the reaction field (see above), the latter exhibited a barrier

2.8 kcal mol<sup>-1</sup> greater than the former (M05-2X/6-311++G(d, p)//M05-2x/6-31G(d, p) model). Apparently the difference in inherent basicity between the phosphine and amine contributes little here, or the difference would likely be larger. The authors noted that calculated charges on the phosphorus and nitrogen atoms in the FLP differed in sign, and suggested this creates a preference for H<sub>2</sub> splitting by the amine FLP that compensates for the greater basicity of the phosphine FLP. The reaction exothermicities differed by nearly the same amount as the barriers, at -26.7 and -28.9 kcal mol<sup>-1</sup>. It is notable that the amine FLP splits H<sub>2</sub> more exothermically despite having lower basicity and providing what is presumably a very crowded HN(*t*-Bu)<sub>3</sub><sup>+</sup> cation. This might be a case where greater electrostatic effects in the products outweigh covalent interactions within the moieties.

In the same paper the authors examined H<sub>2</sub> splitting by the carbene-base FLPs (F<sub>5</sub>C<sub>6</sub>)<sub>3</sub>B⋯1 and (F<sub>5</sub>C<sub>6</sub>)<sub>3</sub>B⋯2 (Scheme 1). Barriers for the two differed by only 0.4 kcal mol<sup>-1</sup>, again a curious result given the differences in the B⋯C distances and resulting reaction field volumes. The reaction exothermicities were also nearly identical at -48.9 and -49.7 kcal mol<sup>-1</sup>. Evidently replacement of the CMe<sub>2</sub> group with an N-*t*-Bu group had little impact on the basicity of the carbene.

Geier et al. calculated H<sub>2</sub> splitting energies for B(C<sub>6</sub>F<sub>5</sub>)<sub>3</sub>/py and B(C<sub>6</sub>F<sub>5</sub>)<sub>3</sub>⋯2,6-Me<sub>2</sub>py [29]. The former, being a classical Lewis acid–base complex experimentally and computationally, split H<sub>2</sub> endothermically by 3–9 kcal mol<sup>-1</sup>, depending on model, while the latter, being an equilibrium mixture of classical complex and FLP, split H<sub>2</sub> exothermically by 13–15 kcal mol<sup>-1</sup>. Nearly all the difference between the two corresponded to the classical complex B–N bond energy, so the difference in inherent Lewis basicity between pyridine and lutidine was negligible. Wu et al. examined this system from another perspective, comparing mechanism pathway energies for H<sub>2</sub> splitting by B(C<sub>6</sub>F<sub>5</sub>)<sub>3</sub>⋯2,6-Me<sub>2</sub>py and BMe<sub>3</sub>/2,6-Me<sub>2</sub>py [30]. For the former FLP, they found a barrier of only 3.5 kcal mol<sup>-1</sup> and an exothermicity of -19.8 kcal mol<sup>-1</sup> (M05-2X/6-311G(d, p) model), the latter being in fair agreement with the data of Geier et al. Interestingly, for the latter pair, they found an FLP slightly lower in energy (2.7 kcal mol<sup>-1</sup>) than the classical complex. This exhibited a sizable barrier to H<sub>2</sub>-splitting (18.1 kcal mol<sup>-1</sup>), and an endothermic reaction (17.7 kcal mol<sup>-1</sup>). The difference between the two reactions arose mostly from the difference in hydride affinity of the two boranes; indeed, formation of FLP from the classical complex was *exergonic* for BMe<sub>3</sub>/2,6-Me<sub>2</sub>py and *endergonic* for B(C<sub>6</sub>F<sub>5</sub>)<sub>3</sub>/2,6-Me<sub>2</sub>py, despite the decreased steric issues in the former borane.

Rokob et al. examined the effect of Lewis basicity on FLPs in the context of investigating mechanisms for the FLP-stimulated hydrogenation of bulky imines [35]. Surprisingly, they found that the solvent phase free energy-based barrier for the borane/imine pair (F<sub>5</sub>C<sub>6</sub>)<sub>3</sub>B/*t*-BuN=CHPh splitting H<sub>2</sub> to form [*t*-BuNHCHPh<sup>+</sup>][(F<sub>5</sub>C<sub>6</sub>)<sub>3</sub>BH<sup>-</sup>] was identical to that for the borane/amine pair (F<sub>5</sub>C<sub>6</sub>)<sub>3</sub>B/*t*-BuNHCH<sub>2</sub>Ph and H<sub>2</sub> forming [*t*-BuNH<sub>2</sub>CH<sub>2</sub>Ph<sup>+</sup>][(F<sub>5</sub>C<sub>6</sub>)<sub>3</sub>BH<sup>-</sup>] (16.5 kcal mol<sup>-1</sup>, RI-SCS-MP2/cc-PVTZ//M05-2X/6-31G(d) model). As one would expect from basicities of imine vs amine, the latter reaction was 2.8 kcal mol<sup>-1</sup> more *exergonic*.

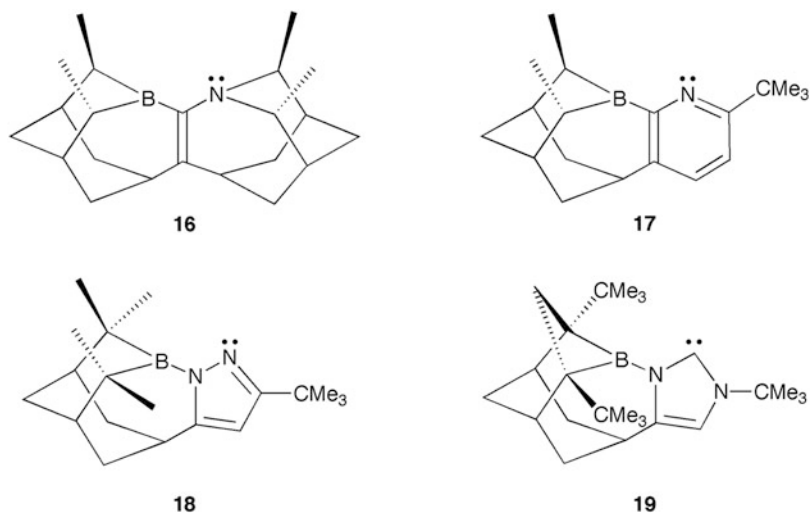
Lu et al. probed the effects of “tied-back” vs unfettered bases by calculating energetics of H<sub>2</sub> splitting by [2,4,6-(F<sub>3</sub>C)<sub>3</sub>C<sub>6</sub>H<sub>2</sub>]<sub>2</sub>BH and DABCO or NEt<sub>3</sub> [36].

They found different mechanisms for the two cases. When  $\text{NEt}_3$  was the base,  $\text{H}_2$  coordinated to the borane first in an  $\eta^2$  fashion, with the amine acting as a spectator. Subsequently, the amine attacked this complex, deprotonating bound  $\text{H}_2$  to form the product ion pair. The barrier for amine attack was very small ( $\Delta G_{298}^\ddagger = 0.1 \text{ kcal mol}^{-1}$ , M06-2X(SCRF)/6-311+G(2df,p)//M06-2X/mixed double zeta basis set model), and the process was predicted to be only  $1.5 \text{ kcal mol}^{-1}$  exergonic. Compared to the energy of the reactants, the barrier was  $26.6 \text{ kcal mol}^{-1}$ . The authors viewed the reaction as stepwise, despite the modest energetics of the amine attack step. In contrast, when DABCO was the base, the reaction was viewed as concerted. The base did not act as a spectator, but bound one end of the  $\text{H}_2$  molecule as the borane bound the other, in a more conventional FLP  $\text{H}_2$  splitting process. The barrier was computed to be  $22.9 \text{ kcal mol}^{-1}$ , presumably reflecting the greater basicity of DABCO resulting from its less congested nitrogen atom. Interestingly, the overall reaction was essentially as exergonic as the  $\text{NEt}_3$  reaction. This indicates that in this system Lewis basicity affected attainment of the transition state more than the energetics of the ion pair products.

In quite similar work, Erös et al. computed energetics of  $\text{H}_2$  splitting by FLPs ( $\text{C}_6\text{F}_5$ )<sub>2</sub>(Mes)B/ABCO and ( $\text{C}_6\text{F}_5$ )<sub>2</sub>(Mes)B...tmp [31]. As noted above, the FLPs were similarly stable with respect to their components. The two FLPs showed similar barriers to  $\text{H}_2$  activation as well,  $6.2$  and  $7.6 \text{ kcal mol}^{-1}$ , respectively. That the FLP containing the less congested base exhibited the smaller barrier was attributed to its shorter B...N distance, which allowed for better cooperation between acid and base. The reaction exothermicities favored the FLP with the smaller base as well, by a margin of  $-25.5$  to  $-23.0 \text{ kcal mol}^{-1}$ .

Heiden et al. compared energetics of the tethered amine and phosphine base FLPs shown in Scheme 3 in  $\text{H}_2$  splitting [32]. In stark contrast to most FLPs of these types, hydrogen splitting was predicted to be endergonic, by  $10.2 \text{ kcal mol}^{-1}$  for the phosphine and by  $24.3 \text{ kcal mol}^{-1}$  for the amine. These values are relatively consistent with the general concept that phosphines are more Lewis basic than amines. That the splitting reactions were endergonic explained why experimentally the processes continue with hydrogen addition to a borane aryl substituent and subsequent arene loss, along with cyclization to give cyclic borane-amines/borane-phosphines: arene loss provides the necessary driving energy for the reaction. Surprisingly, the barriers to  $\text{H}_2$  activation were predicted to be nearly identical at  $28.6 \text{ kcal mol}^{-1}$  for the phosphine and  $30.1 \text{ kcal mol}^{-1}$  for the amine. This stands in opposition to the results directly above. However, such a comparison might not be appropriate for a sterically congested phosphine vs a much less congested amine, as in Heiden's case.

Wang et al. investigated  $\text{H}_2$  splitting by the rigidly tethered systems shown in Scheme 6 [37]. These provided an informative series of nitrogen Lewis basicities ranging from amine to pyridine to imidazole, along with an NHC. Surprisingly, the barriers to splitting were remarkably similar; in particular, those for the nitrogen bases ranged from only  $3.8 \text{ kcal mol}^{-1}$  for **16** to  $5.8 \text{ kcal mol}^{-1}$  for **17** and  $5.9 \text{ kcal mol}^{-1}$  for **18** ( $\Delta H^\ddagger$ , M05-2X/6-311++G(d, p)//M05-2X/6-31G(d, p) model). The barrier for carbene **19** was  $5.4 \text{ kcal mol}^{-1}$ . These values suggested



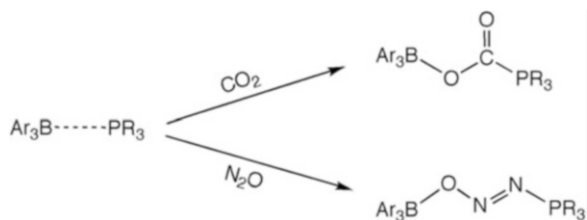
**Scheme 6** Rigidly tethered FLPs used for  $H_2$  activation, computed by Wang et al. [37]

that the greater inherent basicities in the amine and carbene systems were compensated for by lower steric congestion around nitrogen in the pyridine and imidazole systems. Some support for this view came from the reaction exothermicities, which were smallest for **16** ( $-11.8 \text{ kcal mol}^{-1}$ ), slightly larger for the less congested but less basic **17** and **18** ( $-16.7$  and  $-22.6 \text{ kcal mol}^{-1}$ ), and quite large for the less congested and very basic carbene **19** ( $-43.0 \text{ kcal mol}^{-1}$ ). The authors noted that **16**, with its low barrier and exothermicity, should act as a good hydrogenation catalyst. Plausibly it might also be a candidate for a hydrogen storage/release system.

### 3.2 Trapping and Activation of $CO_2$ and $N_2O$

The Stephan and Erker groups demonstrated that FLPs can capture  $CO_2$ , forming heteroesters (Scheme 7, top) [18]. The energetics of this process were examined computationally for the four boranes listed in Sect. 2.1. The energetics relative to the separate reactants differed little, ranging from  $-24.9 \text{ kcal mol}^{-1}$  for  $R = n\text{-C}_6\text{H}_{13}$  to  $-28.5 \text{ kcal mol}^{-1}$  for  $R = \text{Cl}$ . The differences were more distinct relative to the respective FLPs and  $CO_2$ , reflecting the differences in FLP formation energies (Sect. 2.1). The system that formed the most weakly bound FLP,  $(F_5C_6)_2(c\text{-C}_6\text{H}_{11})B \cdots P(t\text{-Bu})_3$ , released the greatest amount of energy ( $-19.8 \text{ kcal mol}^{-1}$ ) upon capturing  $CO_2$ , while an FLP containing a (presumably) more internally Lewis acidic borane,  $(F_5C_6)_2(\text{Cl})B \cdots P(t\text{-Bu})_3$ , released less energy upon capturing  $CO_2$  ( $-17.7 \text{ kcal mol}^{-1}$ ). The results provide an example of



**Scheme 7** Capture of three-atom molecules by FLPs

cancellation between internal and external FLP energetics, and thus cancellation of the effects of internal/external Lewis acidities.

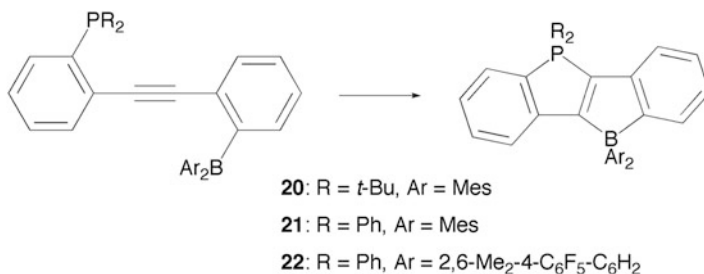
FLPs can also capture  $N_2O$ , although in this case “w”-shaped *trans–trans* chain complexes form (Scheme 7, bottom). Gilbert examined the effect of borane Lewis acidity on the energetics of  $N_2O$  capture by several  $Ar_3B \cdots P(t-Bu)_3$  FLPs [28]. Unsurprisingly, the more Lewis acidic the borane, the more exothermic was  $N_2O$  capture. The energetics were consistent with the linearity data observed by Durfey and Gilbert (Table 3), in that capture energies trended  $(F_5C_6)_3B \cdots P(t-Bu)_3 > (2-F-H_4C_6)_3B \cdots P(t-Bu)_3 > (3-F-H_4C_6)_3B \cdots P(t-Bu)_3 > (4-F-H_4C_6)_3B \cdots P(t-Bu)_3 \approx (H_5C_6)_3B \cdots P(t-Bu)_3$ .

The effect of borane Lewis acidity on the contributing resonance forms in these systems was also examined. The computed bond lengths changed predictably with the Lewis acidity of the borane: as acidity increased, the B–O and N–N distances decreased, while the O–N and N–P distances increased. The preferred resonance form shifted to place more electron density between boron and oxygen, and between the two nitrogens, giving the associated bonds multiple bond character.

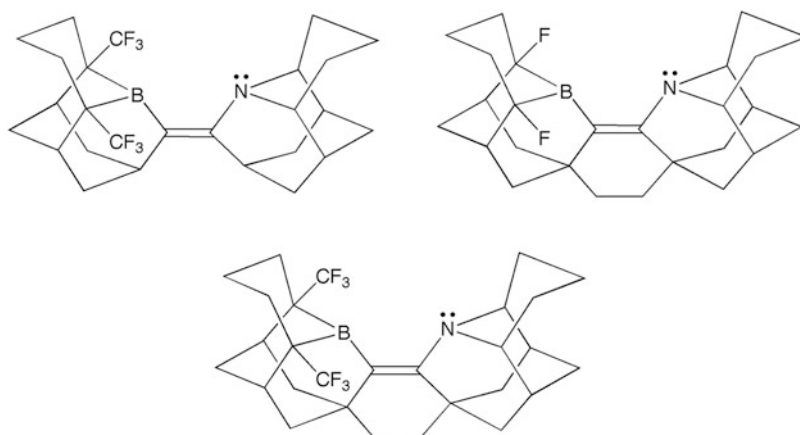
The relative stabilities of a number of constitutional isomers of  $Ar_3B/N_2O/P(t-Bu)_3$  ( $Ar = C_6F_5, C_6H_4-4-F$ ) were examined. In every case, those involving the more acidic borane  $B(C_6F_5)_3$  were significantly more stable than their  $B(C_6H_4-4-F)_3$  counterparts, indicating that increased B–X bond order is paramount in stabilizing all such complexes.

### 3.3 Miscellaneous Reactions

Fukazawa et al. described calculations exploring the thermal and photo-induced intramolecular FLP cyclization reactions shown in Scheme 8 [38]. Transition state searches in all cases indicated a stepwise process, with the phosphorus attacking the alkyne first (B3LYP/def2-SV(P) model). The barriers for **20** and **21** were similar despite the differences in Lewis basicity between the  $P(t-Bu)_2$  and  $PPh_2$  substituents (27.2 and 30.4 kcal mol<sup>-1</sup>, respectively), but consistent with greater basicity for the former. The cases showed somewhat different exothermicities, with cyclization of **20** being exothermic by –3.9 kcal mol<sup>-1</sup>, but that of **21** being endothermic at +3.0 kcal mol<sup>-1</sup>. The results were consistent with experiment in that cyclization occurs thermally with the more basic **20**, but not with **21** (for which cyclization can be induced photochemically). Interestingly, for **22**, containing the same phosphine moiety as **21** but a (conceptually) more Lewis acidic borane moiety, the barrier was



**Scheme 8** Intramolecular cyclization of an FLP, computed by Fukazawa et al. [38]



**Scheme 9** Rigidly tethered FLPs that might break the C–H bond of methane, computed by Wang et al. [39]

predicted to be 29.1 kcal mol<sup>-1</sup> and the exothermicity –2.5 kcal mol<sup>-1</sup>. These values lie between those for **20** and **21**, implying that the Lewis acidity of the borane has some impact on barrier energetics despite the fact that it is not directly involved in the primary mechanistic step. This implies in particular that the barrier reflects the basicity of the phosphine and the acidity of the borane, which in turn implies that the borane withdraws some electron density from the alkyne carbons. This is unexpected given Durfey and Gilbert's finding that electron-withdrawing substituents at the arene 4 position have negligible effect on the borane Lewis acidity [25].

Wang et al. extended their studies of H<sub>2</sub> splitting to splitting the C–H bonds in CH<sub>4</sub> using rigidly tethered FLPs based on those in Scheme 6 [39]. Systems that showed particular promise appear in Scheme 9. All three were predicted to exhibit barriers of ca. 10 kcal mol<sup>-1</sup> or less for methane C–H activation, and to give reactions exothermic by at least –13 kcal mol<sup>-1</sup> (M05-2X/6-311++G(2d, p)//M05-2X/6-31G(d, p) model). In contrast, systems identical to those in the scheme

but lacking electron-withdrawing substituents near boron typically displayed barriers above  $15 \text{ kcal mol}^{-1}$  and exothermicities close to zero.

The same authors explored methane activation by  $(\text{F}_5\text{C}_6)_3\text{B}\cdots\text{P}(t\text{-Bu})_3$  and  $(\text{F}_5\text{C}_6)_3\text{B}\cdots\text{N}(t\text{-Bu})_3$ . As in  $\text{H}_2$  splitting (see above), the two exhibited similar barriers in breaking the C–H bond, ones that were some  $22 \text{ kcal mol}^{-1}$  greater than required to break the H–H bond. Both the similarity and size of the barriers were ascribed to the orientation of the encapsulated  $\text{CH}_4$ ; optimizations indicated that the  $\text{CH}_3$  moiety covered the borane boron in an umbrella fashion, with the remaining hydrogen oriented toward the amine nitrogen/phosphine phosphorus. This orientation did not allow for straightforward donation of C–H bond density to the boron, or for donation of nitrogen/phosphorus lone pair density into a C–H  $\sigma^*$  orbital, resulting in a high barrier. This hypothesis also explained the similarity in barriers: methane orientation was determined by the Lewis acidity of the borane, so the two FLPs show similar barriers despite differences in base basicity. Interestingly, in the pairs  $(\text{F}_5\text{C}_6)_3\text{B}\cdots\mathbf{1}$  and  $(\text{F}_5\text{C}_6)_3\text{B}\cdots\mathbf{2}$  (Scheme 1), the barriers were again similar and larger than those for  $\text{H}_2$  activation ( $13.7$  and  $13.5 \text{ kcal mol}^{-1}$ ), but significantly lower than those for the FLPs above. This might signal the greater basicity of the carbenes vs amines/phosphines, or a different means by which the carbene carbon interacts with the methane C–H  $\sigma$  and  $\sigma^*$  orbitals.

FLPs add to alkenes to give zwitterionic 1,2-diheteroalkanes. Guo and Li examined addition of  $\text{B}(\text{C}_6\text{R}_5)_3/\text{P}(t\text{-Bu})_3$  ( $\text{R} = \text{H}, \text{F}$ ) to ethene as a three-component system (that is, not including stabilization afforded by formation of the FLP) [40]. The effects of greater Lewis acidity in the fluorinated case were stark. For the parent case, the barrier was predicted to be  $51.7 \text{ kcal mol}^{-1}$  and the reaction to be endergonic by  $36.6 \text{ kcal mol}^{-1}$  (B3LYP/mixed triple and double zeta basis set model). For the fluorinated system, the corresponding values were  $29.2$  and  $-3.4 \text{ kcal mol}^{-1}$ . Thus fluorinating the borane to increase its Lewis acidity approximately halved the barrier, and changed the reaction energetics from sizably endergonic to exergonic. The transition state structures for both systems suggested that the reaction occurred stepwise, with a stronger interaction between borane and ethene than between phosphine and ethene. Interestingly, the B $\cdots$ C distance in the transition state of the fluorinated system was  $0.32 \text{ \AA}$  longer than that in the parent, indicating that the increased Lewis acidity was countered to some degree by steric repulsions between the fluorines and alkene atoms. Nonetheless, the core bond distances in the two products were nearly identical, indicating that energy lowering in transition states and products was a function of electronic effects rather than steric effects.

In contrast to the energetic differences seen in the three-component ethene addition, Mmring et al. found little difference between the tethered FLPs  $\text{H}_2\text{BCH}_2\text{CH}_2\text{PH}_2$  and  $(\text{F}_5\text{C}_6)_2\text{BCH}_2\text{CH}_2\text{PMes}_2$  when added to the double bond in norbornene [41]. The barriers to addition to form the experimentally observed product were nearly identical at  $11.4$  and  $12.3 \text{ kcal mol}^{-1}$ , respectively (B2PLYP-D/def2-TZVP model), while the reaction energies were  $-13.5$  and  $-19.4 \text{ kcal mol}^{-1}$ . The data suggested that the gain in inherent Lewis acidity resulting from substituting fluoroarenes onto the boron was largely countered by the decrease in inherent Lewis

**Table 4** Energetics (kcal mol<sup>-1</sup>, OG2R3(SCRF)//ONIOM M06-2X(SCRF)/6-31+G(d) model) of reactions (4-F-H<sub>4</sub>C<sub>6</sub>)<sub>3</sub>B-ONN-P(*t*-Bu)<sub>3</sub> + LA → LA-ONN-P(*t*-Bu)<sub>3</sub> + B(C<sub>6</sub>H<sub>4</sub>-4-F)<sub>3</sub>

LA	ΔE
C(C <sub>6</sub> H <sub>5</sub> ) <sub>3</sub> <sup>+</sup>	-6.0
B(C <sub>6</sub> H <sub>5</sub> )(C <sub>6</sub> F <sub>5</sub> ) <sub>2</sub>	-12.4
B(C <sub>6</sub> F <sub>4</sub> -4-H) <sub>3</sub>	-20.3
B(C <sub>6</sub> F <sub>5</sub> ) <sub>3</sub>	-21.3

basicity resulting from substituting electron-withdrawing mesityl rings onto the phosphorus. It is notable that steric effects of the bulkier ligands were not manifested in the energetics. Presumably this arose because borane and phosphine moieties can freely rotate around the tethering C–C single bond, allowing them to find a low energy torsional relationship.

Stronger Lewis acids replace weaker acids in LA-ONN-P(*t*-Bu)<sub>3</sub> complexes of the type at the bottom of Scheme 7 [42]. For example, (4-F-H<sub>4</sub>C<sub>6</sub>)<sub>3</sub>B-ONN-P(*t*-Bu)<sub>3</sub> reacts with a number of boranes and transition metal Lewis acids to form [stronger LA]-ONN-P(*t*-Bu)<sub>3</sub>. It is intriguing that this occurs without disrupting the ONN-P(*t*-Bu)<sub>3</sub> moiety, despite the fact that this is computationally only weakly bound [28]. This reaction provides another means of comparing Lewis acidities. Relevant data appear in Table 4. It can be seen that B(C<sub>6</sub>F<sub>4</sub>-4-H)<sub>3</sub> was predicted to be essentially as strong a Lewis acid as B(C<sub>6</sub>F<sub>5</sub>)<sub>3</sub>, in agreement with the results of Durfey and Gilbert [25]. B(C<sub>6</sub>H<sub>5</sub>)(C<sub>6</sub>F<sub>5</sub>)<sub>2</sub> was found to be 58% as strong an acid as B(C<sub>6</sub>F<sub>5</sub>)<sub>3</sub>, arguing for an approximately linear decrease in Lewis acidity as each C<sub>6</sub>F<sub>5</sub> ring is replaced with a C<sub>6</sub>H<sub>5</sub> ring. Interestingly, scans of the potential surfaces for acid exchange gave “inclined plane” barriers rather than isolable transition states. It was found that degenerate exchange between (4-F-H<sub>4</sub>C<sub>6</sub>)<sub>3</sub>B-ONN-P(*t*-Bu)<sub>3</sub> and B(C<sub>6</sub>H<sub>4</sub>-4-F)<sub>3</sub> (which was observed experimentally) appeared to involve a classical A/I<sub>A</sub> pathway, as the lip of the inclined plane was associated with a structure containing short B–O distances for both the incoming and leaving boranes. In contrast, the reaction between (4-F-H<sub>4</sub>C<sub>6</sub>)<sub>3</sub>B-ONN-P(*t*-Bu)<sub>3</sub> and B(C<sub>6</sub>F<sub>5</sub>)<sub>3</sub> appeared to involve a classical D/I<sub>D</sub> pathway. Supporting this distinction, the “barrier” for the associative process was 3.5 kcal mol<sup>-1</sup> higher than that for the dissociative process, consistent with a conceptualization that the associative process involves considerable crowding (and so numerous repulsive interactions) between incoming and outgoing boranes, while the dissociative process involves less crowding and fewer repulsions.

## 4 Closing Comments

The efficacy of FLPs in activating substrates depends on both external and internal Lewis acidities/basicities of the components. While different substrates have different requirements, computational data suggest that, generally speaking, the peripheral atoms must create a cage that is stabilized by at least 6–8 kcal mol<sup>-1</sup> over the isolated components. This provides a structure sufficiently long-lived to

create a field and capture the substrate. That said, it remains unclear whether encounter complex energetics in excess of this are necessary, or even attained. Computational models have not yet iterated to trustworthy values for the external interactions even for the well-studied  $(F_5C_6)_3B \cdots P(t-Bu)_3$  system. At this point, experimental data are required to allow differentiation between accurate and inaccurate model chemistries. In this vein, it would be useful to determine the correctness and generality of Kim and Rhee's suggestion [16] that as much as 30% of the interaction energy between FLP acid and base is actually internal rather than external, even at large acid atom/base atom distances. This bears directly on the question of what energetics between peripheral substituents are necessary to form encounter complex cages.

In contrast, the data collated by Pápai et al. [14] show that internal Lewis acidity/basicity of components correlates well with substrate reactivity. This indicates that the field/electron density distribution generated by the acid/base atoms determines whether a substrate will be activated. It is notable that the likelihood that an FLP will split  $H_2$  is related to the hydride and proton affinities, which equate to the Lewis acidities/basicities of the acid and base, quantitatively. It will be of interest to see whether this holds for other FLP reactions, such as  $CO_2$  capture.

## References

1. Jensen WB (1980) The Lewis acid–base concepts: an overview. Wiley, New York
2. Klopman G (1974) The generalized perturbation theory of chemical reactivity and its applications. In: Klopman G (ed) Chemical reactivity and reaction paths. Wiley, New York
3. Plumley JA, Evanseck JD (2009) Periodic trends and index of boron Lewis acidity. *J Phys Chem A* 113:5985–5992
4. Bessac F, Frenking G (2006) Chemical bonding in phosphane and amine complexes of main group elements and transition metals. *Inorg Chem* 45:6956–6964
5. Rowsell BD, Gillespie RJ, Heard GL (1999) Ligand close-packing and the Lewis acidity of  $BF_3$  and  $BCl_3$ . *Inorg Chem* 38:4659–4662
6. Alkorta I, Elguero J, Del Bene JE, M6 O, Yáñez M (2010) New insights into factors influencing B–N bonding in  $X: BH_{3-n}F_n$  and  $X: BH_{3-n}Cl_n$  for  $X = N_2, HCN, LiCN, H_2CNH, NF_3, NH_3$  and  $n = 0–3$ : the importance of deformation. *Chem Eur J* 16:11897–11905
7. Bessac F, Frenking G (2003) Why is  $BCl_3$  a stronger Lewis acid with respect to strong bases than  $BF_3$ ? *Inorg Chem* 42:7990–7994
8. Brinck T, Murray JS, Politzer P (1993) A computational analysis of the bonding in boron trifluoride and boron trichloride and their complexes with ammonia. *Inorg Chem* 32:2622–2625
9. Chapman AM, Haddow MF, Wass DF (2012) Cationic group 4 metallocene–(*o*-phosphanylaryl)oxido complexes: synthetic routes to transition-metal frustrated Lewis pairs. *Eur J Inorg Chem* 2012(9):1546–1554
10. Grimme S, Kruse H, Goerigk L, Erker G (2010) The mechanism of dihydrogen activation by frustrated Lewis pairs revisited. *Angew Chem Int Ed* 49:1402–1405
11. Hamza A, Stirling A, Rokob TA, Pápai I (2009) Mechanism of hydrogen activation by frustrated Lewis pairs: a molecular orbital approach. *Int J Quantum Chem* 109:2416–2425
12. Rokob TA, Hamza A, Stirling A, Soós T, Pápai I (2008) Turning frustration into bond activation: a theoretical mechanistic study on heterolytic hydrogen splitting by frustrated Lewis pairs. *Angew Chem Int Ed* 47:2435–2438

13. Wiegand T, Eckert H, Ekkert O, Fröhlich R, Kehr G, Erker G, Grimme S (2012) New insights into frustrated Lewis pairs: structural investigations of intramolecular phosphane-borane adducts by using modern solid-state NMR techniques and DFT calculations. *J Am Chem Soc* 134:4236–4249
14. Rokob TA, Hamza A, Pápai I (2009) Rationalizing the reactivity of frustrated Lewis Pairs: thermodynamics of H<sub>2</sub> activation and the role of acid–base properties. *J Am Chem Soc* 131 (30):10701–10710
15. Gille AL, Gilbert TM (2008) Donor-acceptor dissociation energies of group 13–15 donor-acceptor complexes containing fluorinated substituents: approximate Lewis acidities of (F<sub>3</sub>C)<sub>3</sub>M vs (F<sub>5</sub>C<sub>6</sub>)<sub>3</sub>M and the effects of phosphine steric bulk. *J Chem Theory Comput* 3:1681–1689
16. Kim HW, Rhee YM (2009) Dispersion-oriented soft interaction in a frustrated Lewis pair and the entropic encouragement effect in its formation. *Chem Eur J* 15:13348–13355
17. Hyla-Kryspin I, Haufe G, Grimme S (2008) MP2 and QCISD(T) study on the convergence of interaction energies of weak O–H···F–C, C–H···O, and C–H···F–C hydrogen bridges. *Chem Phys* 346:224–236
18. Peuser I, Neu RC, Zhao X, Ulrich M, Schirmer B, Tannert JA, Kehr G, Fröhlich R, Grimme S, Erker G, Stephan D (2011) CO<sub>2</sub> and formate complexes of phosphine/borane frustrated Lewis pairs. *Chem Eur J* 17:9640–9650
19. Li H, Zhao L, Lu G, Mo Y, Wang Z-X (2010) Insight into the relative reactivity of “frustrated Lewis pairs” and stable carbenes in activating H<sub>2</sub> and CH<sub>4</sub>: a comparative computational study. *Phys Chem Chem Phys* 12:5268–5275
20. Jacobsen H, Berke H, Döring S, Kehr G, Erker G, Fröhlich R, Meyer O (1999) Lewis acid properties of tris(pentafluorophenyl)borane. Structure and bonding in L–B(C<sub>6</sub>F<sub>5</sub>)<sub>3</sub> complexes. *Organometallics* 18:1724–1735
21. Timoshkin AY, Frenking G (2008) Gas-phase Lewis acidity of perfluoroaryl derivatives of group 13 elements. *Organometallics* 27:371–380
22. Gaffoor F, Ford TA (2008) The vibrational spectra of the boron halides and their molecular complexes. *Spectrochim Acta* 71A:550–558
23. Ford TA (2008) Vibrational spectra of the boron halides and their molecular complexes. Part 11. Complexes of boron trifluoride with phosphine and its methyl derivatives. An *ab initio* study. *J Phys Chem A* 112:7296–7302
24. Loschen C, Voigt K, Frunzke J, Diefenbach A, Diedenhofen M, Frenking G (2002) Theoretical studies of inorganic compounds. 19. Quantum chemical investigations of the phosphane complexes X<sub>3</sub>B–PY<sub>3</sub> and X<sub>3</sub>Al–PY<sub>3</sub> (X = H, F, Cl; Y = F, Cl, Me, CN). *Z Anorg Allg Chem* 628:1294–1304
25. Durfey BL, Gilbert TM (2011) Computational studies of Lewis acidities of tris(fluorophenyl)-substituted boranes: an additive relationship between Lewis acidity and fluorine position. *Inorg Chem* 50:7871–7879
26. Welch GC, Cabrera L, Chase PA, Hollink E, Masuda JD, Wei P, Stephan DW (2007) Tuning Lewis acidity using the reactivity of “frustrated Lewis pairs”: facile formation of phosphine-boranes and cationic phosphonium-boranes. *Dalton Trans* 3407–3414
27. Bertini F, Lyaskovskyy V, Timmer BJJ, de Kanter FJJ, Lutz M, Ehlers AW, Slootweg JC, Lammertsma K (2012) Preorganized frustrated Lewis pairs. *J Am Chem Soc* 134:201–204
28. Gilbert TM (2012) Computational studies of complexation of nitrous oxide by borane-phosphine frustrated Lewis pairs. *Dalton Trans* 41:9046–9055
29. Geier SJ, Gille AL, Gilbert TM, Stephan DW (2009) From classical adducts to frustrated Lewis pairs: steric effects in the interactions of pyridines and B(C<sub>6</sub>F<sub>5</sub>)<sub>3</sub>. *Inorg Chem* 48:10466–10474
30. Wu D, Jia D, Liu L, Zhang L, Guo J (2010) Reactivity of 2,6-lutidine/BR<sub>3</sub> and pyridine/BR<sub>3</sub> Lewis pairs (R = F, Me, C<sub>6</sub>F<sub>5</sub>): a density functional study. *J Phys Chem A* 114:11738–11745

31. Erös G, Mehdi H, Pápai I, Rokob TA, Király P, Tárkányi G, Soós T (2010) Expanding the scope of metal-free catalytic hydrogenation through frustrated Lewis pair design. *Angew Chem Int Ed* 49:6559–6563
32. Heiden ZM, Schedler M, Stephan DW (2011) Synthesis and reactivity of *o*-benzylphosphido- and *o*- $\alpha$ -methylbenzyl(*N,N*-dimethyl)amine-boranes. *Inorg Chem* 50:1470–1479
33. Kronig S, Theuergarten E, Holschumacher D, Bannenberg T, Daniliuc CG, Jones PG, Tamm M (2011) Dihydrogen activation by frustrated carbene-borane Lewis pairs: an experimental and theoretical study of carbene variation. *Inorg Chem* 50:7344–7359
34. Zhao L, Li H, Lu G, Wang Z-X (2010) Computational design of metal-free catalysts for catalytic hydrogenation of imines. *Dalton Trans* 39:4038–4047
35. Rokob TA, Hamza A, Stirling A, Pápai I (2009) On the mechanism of  $B(C_6F_5)_3$ -catalyzed direct hydrogenation of imines: inherent and thermally induced frustration. *J Am Chem Soc* 131(5):2029–2036
36. Lu Z, Cheng Z, Chen Z, Weng L, Li ZH, Wang H (2011) Heterolytic cleavage of dihydrogen by “frustrated Lewis pairs” comprising bis(2,4,6-tris(trifluoromethyl)phenyl)borane and amines: stepwise versus concerted mechanism. *Angew Chem Int Ed* 50:12227–12231
37. Lu G, Li H, Zhai L, Huang F, Wang Z-X (2010) Computationally designed metal-free hydrogen activation site: reaching the reactivity of metal–ligand bifunctional hydrogenation catalysts. *Inorg Chem* 49:295–301
38. Fukazawa A, Yamaguchi E, Ito E, Yamada H, Wang J, Irle S, Yamaguchi S (2011) Zwitterionic ladder stilbenes with phosphonium and borate bridges: intramolecular cascade cyclization and structure-photophysical properties relationship. *Organometallics* 30:3870–3879
39. Lu G, Zhao L, Li H, Huang F, Wang Z-X (2010) Reversible heterolytic methane activation of metal-free closed-shell molecules: a computational proof-of-principle study. *Eur J Inorg Chem* 2010(15):2254–2260
40. Guo Y, Li S (2008) A novel addition mechanism for the reaction of “frustrated Lewis pairs” with olefins. *Eur J Inorg Chem* 2008(16):2501–2505
41. Mömmling CM, Frömel S, Kehr G, Fröhlich R, Grimme S, Erker G (2009) Reactions of an intramolecular frustrated Lewis pair with unsaturated substrates: evidence for a concerted olefin addition reaction. *J Am Chem Soc* 131:12280–12289
42. Neu RC, Otten E, Lough A, Stephan DW (2011) The synthesis and exchange chemistry of frustrated Lewis pair–nitrous oxide complexes. *Chem Sci* 2:170–176

# Solid-State NMR as a Spectroscopic Tool for Characterizing Phosphane–Borane Frustrated Lewis Pairs

Thomas Wiegand, Hellmut Eckert, and Stefan Grimme

**Abstract** Frustrated Lewis pair (FLP) chemistry has provided a new strategy for small molecule binding and/or catalytic activation. It is based on the cooperative reaction behavior of Lewis acid and Lewis base centers that are in close proximity to each other (e.g., within the same molecule) but cannot form a direct bond because of geometrical constraints. The most prominent FLPs are based on intramolecular phosphane–borane adducts, whose catalytic properties can be tailored over wide ranges of reactivity and selectivity. For the structural and chemical design of such systems, a fundamental understanding needs to be developed on how structure, dynamics and covalent interactions between the Lewis centers influence the reactivity profile. Advanced solid-state nuclear magnetic resonance (NMR) spectroscopic techniques afford new opportunities for addressing this challenge. Following a general introduction into the fundamentals of NMR spectroscopy, this review discusses the different types of internal interactions – magnetic shielding, nuclear electric quadrupolar coupling, indirect spin–spin interactions, and “through-space” dipole–dipole couplings – influencing NMR spectra in the solid state. As discussed in detail, each type of interaction bears specific informational content with regard to structural issues in FLP chemistry. One of the most attractive features of solid-state NMR is the possibility of tailoring the effective Hamiltonian by manipulations in either physical space or spin space. Using such “*decoupling*” or “*recoupling*” techniques certain types of interactions can be selectively turned off for spectral

---

T. Wiegand and H. Eckert (✉)

Institut für Physikalische Chemie and Graduate School of Chemistry, WWU Münster,  
Corrensstraße 30, 48149 Münster, Germany  
e-mail: [eckerth@uni-muenster.de](mailto:eckerth@uni-muenster.de)

S. Grimme

Mulliken Center for Theoretical Chemistry, Institut für Physikalische und Theoretische Chemie,  
Universität Bonn, Beringstrasse 4, 53115 Bonn, Germany  
e-mail: [grimme@thch.uni-bonn.de](mailto:grimme@thch.uni-bonn.de)



simplification or turned on for selective evaluation. The present review summarizes the most important *selective averaging* techniques that have found applications in the characterization of FLPs. In a second step the interaction parameters need to be connected with structure and bonding information. As illustrated in this chapter, ab initio calculations using density functional theory (DFT) methods have become indispensable for this task. Based on this comprehensive strategy including advanced NMR methodology, computer simulations, and ab initio calculations, the present review illustrates the utility of  $^{31}\text{P}$  and  $^{11}\text{B}$  NMR chemical shifts,  $^{11}\text{B}$  electric field gradient tensors, and  $^{31}\text{P}$ - $^{11}\text{B}$  indirect and direct dipole–dipole interactions for characterizing intramolecular borane–phosphane FLPs, illustrating the potential of this method to (1) quantify the extent of boron–phosphorus bonding interactions (and hence the “degree of frustration”) and (2) reveal specific structural details (i.e., boron–phosphorus distances and other local geometry aspects) relating to the catalytic activities of these exciting materials.

**Keywords** Ab initio calculation · B–P distance measurement · Degree of frustration · Frustrated Lewis pair · Magic angle spinning · Quadrupolar coupling constant · Solid-state  $^{11}\text{B}$  and  $^{31}\text{P}$  NMR · Spin–spin coupling

## Contents

1	Introduction .....	293
2	Fundamentals of Solid-State NMR Spectroscopy .....	296
2.1	General Aspects .....	296
2.2	Internal Interactions .....	297
2.3	Magnetic Shielding .....	298
2.4	Nuclear Electric Quadrupolar Coupling .....	299
2.5	Indirect Magnetic Dipolar Coupling .....	300
2.6	Direct Magnetic Dipole–Dipole Coupling .....	301
3	Experimental Techniques and Aspects of Their Application to FLPs .....	302
3.1	Signal Preparation and Lineshape .....	302
3.2	Measurement of Isotropic Chemical Shifts and Quadrupolar Coupling Parameters by Magic Angle Sample Spinning .....	304
3.3	Recovery of Indirect Spin–Spin Interactions .....	308
3.4	Dipolar Recoupling by Rotational Echo Double Resonance .....	311
4	$^{11}\text{B}$ NMR as a Probe for Structure and Bonding in FLPs .....	318
4.1	Spectral Features and Observables .....	318
4.2	DFT Calculations of $^{11}\text{B}$ Magnetic Shielding Parameters .....	323
4.3	DFT Calculations of Electric Field Gradients at Boron .....	326
5	$^{31}\text{P}$ NMR as a Probe of Structure and Bonding in FLPs .....	330
5.1	Spectroscopic Features and Observables .....	330
5.2	DFT-Calculations of $^{31}\text{P}$ Magnetic Shielding Parameters .....	334
5.3	DFT Calculations of $^{10}\text{B}/^{11}\text{B}$ – $^{31}\text{P}$ Indirect Spin–Spin Couplings .....	335
6	$^{31}\text{P}/^{11}\text{B}$ Direct Dipolar and Anisotropic Indirect $J$ -Couplings .....	338
7	Conclusions .....	341
	References .....	343

## Abbreviations

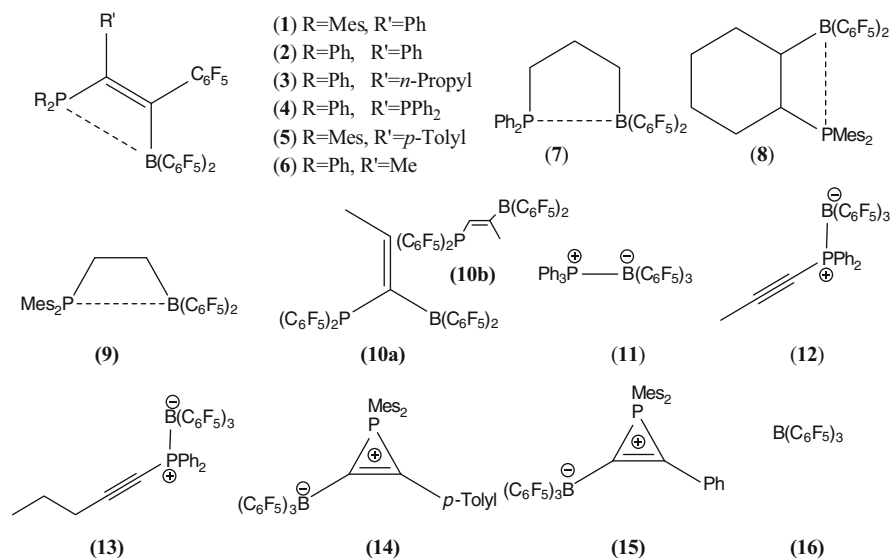
AO	Atomic orbital
B3-LYP	Becke-3-parameter Lee-Yang Parr (a hybrid density functional)
BP86	Becke-Perdew 86 (a GGA density functional)
CPMAS	Cross-polarization magic-angle spinning
CPREAPDOR	REAPDOR with cross-polarization as the preparation step
CT-REDOR	Constant-time REDOR
DFT	Density functional theory
EFG	Electric field gradient
FLP	Frustrated Lewis pair
GGA	Generalized gradient approximation
MAS	Magic-angle spinning
NAO	Natural atomic orbital
NBO	Natural bond orbital
NMR	Nuclear magnetic resonance
PAS	Principal axis system for the description of anisotropic NMR interactions
$R^2$	Linear regression factor
REAPDOR	Rotational echo adiabatic passage double resonance (REDOR for nuclei coupled to quadrupolar nuclei)
REDOR	Rotational echo double resonance
SATRAS	Satellite transition spectroscopy (quadrupolar nuclei)
SOQE	Second-order quadrupole effect
SWf-TPPM	Swept frequency TPPM (for decoupling in MAS-NMR)
TPPM	Two-pulse phase modulation, a proton decoupling scheme in NMR
TPSS	Meta-GGA density functional of Tao, Perdew, Staroverov, and Scuseria
TQMAS	Triple-quantum magic angle spinning, a technique for obtaining highly resolved spectra of quadrupolar nuclei
TZVP	Triple zeta valence plus polarization, a basis set
WBI	Wiberg bond order index

## 1 Introduction

Frustrated Lewis acid/base pairs (FLPs), which feature main group Lewis acid and Lewis base functionalities in close proximity, but within constrained geometries, are of great interest in the field of homogeneous catalysis. Their reactivity stems from the presence of bulky, sterically demanding ligands attached to the reactive centers, thereby inhibiting the anticipated Lewis acid/base adduct formation. The chemistry of these systems has witnessed high scientific interest within the last few years regarding the synthesis of new molecules [1], the experimental and theoretical

investigations of their reaction behaviors [2–4], and their detailed spectroscopic characterization [5]. The interest in these systems stems from the cooperative effects on the chemical reactivity behavior, which resembles in many cases that of organometallic systems. Important examples are the activation of dihydrogen [6–10], CO<sub>2</sub> [11], carbonyl compounds [12, 13], alkenes [14, 15], dienes [16], alkynes [17], and the capture of environmental pollutants such as NO [18]. The most prominent FLPs are based on a boron Lewis acid and a phosphorus Lewis base moiety (B/P pairs), even though other examples such as P/N, P/Al, C/B, and N/B pairs have also been reported [1]. In the reactivity design of these systems, the Lewis acidity of the boron site is usually enhanced by electron-withdrawing ligands such as C<sub>6</sub>F<sub>5</sub> while the Lewis basicity of the phosphorus site may be increased by electron-rich ligands such as phenyl, <sup>t</sup>Bu, or mesityl, or even moderated by electron-withdrawing ligands [19, 20].

A wide variety of phosphane–borane FLPs can be designed in an intermolecular or intramolecular manner. While in the former case a control of the B⋯P distances within the usual range of operation (200–250 pm) is difficult to achieve, the situation is fundamentally different in intramolecular FLPs where the constrained geometries are designed to bring the Lewis acid and Lewis base centers into close proximity, while, at the same time, attenuating the direct bonding interaction. The resulting structural arrangement, including the internuclear B⋯P distance, stems from the interplay of non-covalent dispersive interactions between the ligands (mainly of the  $\pi$ – $\pi$  type) as well as the covalent interactions between the Lewis centers. Through judicious choice of the electronegativity and steric properties of these ligands, the B⋯P distance can be tailored to values usually ranging between 200 and 400 pm, presenting a wide range of chemical reactivities towards suitable substrates. Important structural issues include (1) the detection and/or quantification of direct bonding interactions between those centers, relating to the “degree of the system’s frustration” encountered, (2) the measurement of internuclear B⋯P distances, particularly in systems not amenable to X-ray crystallography, (3) the correlation of those properties with chemical reactivity, and (4) the characterization of reaction intermediates or molecular adducts encountered during the catalytic activation process. As an element-selective, inherently quantitative technique with a focus on local structural environments, solid-state nuclear magnetic resonance (NMR) techniques are ideally suited for addressing the above questions. Even though the nuclei are influenced by multiple interactions, the NMR toolbox contains a plethora of powerful selective averaging experiments to simplify the complex spin Hamiltonian, resulting in very precise values of the different interaction parameters involved. The unique power of solid-state NMR in its application to FLP systems stems, however, from the ability to calculate these parameters with a high degree of accuracy using state-of-the-art methods of density functional theory (DFT) calculations from either crystallographic input or by geometry optimization methods. In this way the spectroscopic observables can be linked to very specific structure and bonding information at the reactive Lewis centers not available by other means. In this manner, the NMR observables can also serve as important



**Fig. 1** Molecular structures of those FLPs and model compounds characterized thus far by solid-state NMR

validation criteria for new theoretical tools and approaches predicting the structure and reactivity of FLPs.

The present manuscript focuses on intramolecular B/P adducts, to exemplify how the aforementioned questions can be addressed via <sup>11</sup>B, <sup>31</sup>P single resonance as well as <sup>11</sup>B/<sup>31</sup>P double resonance solid-state NMR spectroscopy. The systems characterized thus far by solid-state NMR are delineated in Fig. 1. The unsaturated C<sub>2</sub>-linked adducts **1–6** [21] which are synthesized by a 1,1-carboboration [22] possess an extraordinarily rigid backbone. While they do not activate hydrogen, they represent a new application of P–C bond activation chemistry. In contrast, the FLPs **7**, **8**, and **9** are linked via a trimethylene, cyclohexylene, and ethylene backbone, respectively, and have a more fluxional character. Consequently, they show a substantially higher reactivity; in particular the systems **8** and **9** are very reactive toward the activation of dihydrogen and undergo many other remarkable addition reactions [10]. The geminal alkylidene-bridged perfluorophenylated P/B pair **10** is structurally different since the Lewis basicity is significantly decreased by electron-withdrawing C<sub>6</sub>F<sub>5</sub> ligands. Nevertheless, experimental and theoretical work [19] has shown that the typical FLP behavior is maintained, leading to the conclusion that the generation of FLPs is also possible through electronic rather than steric control. In this case, the FLP behavior is, for example, expressed by the addition to unsaturated organic substrates to form the respective heterocyclic five-membered-ring adducts while the dihydrogen activation fails [19].

For comparison, we will also discuss the typical intermolecular B/P adducts **11**, **12**, and **13**, as well as the phosphirenium borate zwitterions [23] **14** and **15** which present significantly longer B...P distances. The latter four compounds are isolated as stable intermediates during the carboboration reaction. When the alkyne starting material contains phenyl ligands at the phosphorus site, the classical Lewis acid/base adducts **12** and **13** are obtained whereas in the case of the sterically more demanding mesityl ligands the phosphirenium borate zwitterions **14** and **15** are isolated as stable intermediates. For reference, we present a  $^{11}\text{B}$  solid-state NMR analysis for the trigonal coordinated boron system  $\text{B}(\text{C}_6\text{F}_5)_3$  (**16**) where the crystal structure has yet to be solved to date.

## 2 Fundamentals of Solid-State NMR Spectroscopy

### 2.1 General Aspects

The fundamental theory of solid-state NMR has been covered by number of excellent texts from different perspectives [24–26]. NMR is based on the *Zeeman interaction*, represented by the Hamiltonian

$$\mathcal{H}_z = -\mu_z B_0 \quad (1)$$

which lifts the energetic equivalence of the spin orientational states and causes a splitting into  $2I + 1$  individual levels with energies

$$E_m = -m\gamma\hbar B_0 \quad (2)$$

$\mathcal{H}_z$  is also responsible for a nuclear precessional motion, occurring with the angular frequency

$$\omega_p = \gamma B_{loc}, \text{ where } B_{loc} = B_0 + B_{int} \quad (3)$$

is the effective magnetic field felt by the nuclei. Because of the difference in interaction energies of the different spin orientational states, the energy levels in (2) are not equally populated, resulting in a macroscopic magnetization along the magnetic field direction. The NMR experiment generates a time dependent voltage signal oscillating at  $\omega_p$ . To this end, an electromagnetic wave oscillating with an angular frequency  $\omega_0$  close to  $\omega_p$  is applied perpendicular to the magnetic field direction. The interaction of the spins with the corresponding magnetic field component  $B_1$ , described by the Hamiltonian

$$\mathcal{H}_{rf} = -\gamma B_1 \mathbf{I}_x \quad (4)$$

stimulates transitions between the nuclear Zeeman levels and results in a rotation of the magnetization vector with a precession (“nutaton”) angular frequency  $\omega_1$ . Typically this field is applied in a pulsed mode, using short, intense pulses of radiowaves (typically 1–10  $\mu\text{s}$  in length), which tip the nuclear magnetization by  $90^\circ$  ( $90^\circ$  pulses). Following this *preparation* process the magnetization precesses in the plane perpendicular to  $B_0$  and induces an ac voltage in a detection coil. This *free induction decay* signal is then amplified, mixed with the radiowaves used for nuclear excitation (frequency  $\omega_0$ ), filtered, digitized, and stored. Following a waiting period needed to allow for restoration of the equilibrium magnetization along the magnetic field direction (*spin–lattice relaxation*), the process is repeated multiple times for continued signal accumulation. Subsequent Fourier-transformation of the stored accumulated time domain signal results in the frequency-domain signal, called the NMR lineshape.

## 2.2 Internal Interactions

As expressed by Eq. (3), the nuclear precession frequencies  $\omega_p$  reflect the effective magnetic field felt by the nuclei. While the effect of  $B_0$  is generally dominant, important modifications  $B_{\text{int}}$  arise from a number of different *internal interaction mechanisms*, whose parameters reflect the details of the local structural environment and whose effect on the energy levels can be calculated using standard perturbation theory. The corresponding interaction parameters are extracted from the NMR spectra using computer simulation techniques, and then related to details of structure and bonding with the help of ab initio calculations.

The total spin Hamiltonian determining the spectroscopic energy levels in solid-state NMR can be written as

$$\mathcal{H}_{\text{total}} = \mathcal{H}_z + \mathcal{H}_{\text{ms}} + \mathcal{H}_{\text{D}} + \mathcal{H}_{\text{J}} + \mathcal{H}_{\text{Q}} \quad (5)$$

where  $\mathcal{H}_{\text{ms}} + \mathcal{H}_{\text{D}} + \mathcal{H}_{\text{J}} + \mathcal{H}_{\text{Q}}$  define the relevant Hamiltonians of distinct types of internal interactions, namely (1) the magnetic interactions of the nuclei with the surrounding electrons (*magnetic shielding*),  $\mathcal{H}_{\text{ms}}$ , (2) the internuclear *direct and indirect magnetic dipole–dipole interactions*,  $\mathcal{H}_{\text{D}}$  and  $\mathcal{H}_{\text{J}}$ , respectively, and (3) interactions between the electric quadrupole moments of spin  $>1/2$  nuclei and the electrostatic field gradients sensed by these nuclei (*quadrupolar interaction*),  $\mathcal{H}_{\text{Q}}$ . In the solid state, all of these interactions are anisotropic, i.e., their influence on the precession frequency depends on molecular orientation in the magnetic field. As a result, extensive line-broadening is produced in powdered samples.

### 2.3 Magnetic Shielding

Magnetic polarization effects induced in the electronic environment of the nuclei under the influence of  $B_0$  modify the local magnetic fields experienced by the nuclei, hence influencing their precession frequencies. For a theoretical description of these effects, first-order perturbation theory suffices, and the secular Hamiltonian can be written as

$$\mathcal{H}_{\text{ms}} = \gamma \hat{\mathbf{I}} \overset{\leftrightarrow}{\sigma} B_0 \quad (6)$$

In Eq. (6),  $\overset{\leftrightarrow}{\sigma}$  is a second rank ( $3 \times 3$ ) tensor, which takes into account the anisotropy of the interaction and which adopts diagonal form in a specific coordinate system, denoted as the principal axis system (PAS). The PAS is determined by local symmetry. The diagonal parameters are usually characterized by the symbols  $\sigma_{11}$ ,  $\sigma_{22}$ , and  $\sigma_{33}$ , with the isotropic average being  $\sigma_{\text{iso}} = 1/3 (\sigma_{33} + \sigma_{22} + \sigma_{11})$ . Generally the convention

$$|\sigma_{33} - \sigma_{\text{iso}}| \geq |\sigma_{11} - \sigma_{\text{iso}}| \geq |\sigma_{22} - \sigma_{\text{iso}}| \quad (7)$$

is followed.

For the case of axial symmetry of the magnetic shielding tensor (existence of an  $n \geq 3$ -fold rotation axis) the orientational dependence of  $\omega_p$  is given by

$$w_p(\theta) = \gamma B_0 \left( 1 - \sigma_{\text{iso}} - \frac{1}{3} \Delta\sigma (3 \cos^2 \theta - 1) \right) \quad (8)$$

Here  $\Delta\sigma = \sigma_{33} - 1/2(\sigma_{11} + \sigma_{22})$  and the angle  $\theta$  specifies the orientation of the local symmetry axis relative to the magnetic field direction. Less symmetric environments are described by an asymmetry parameter  $\eta_\sigma = (\sigma_{22} - \sigma_{11}) / (\sigma_{33} - \sigma_{\text{iso}})$ .

In the liquid state, the effect of the magnetic shielding anisotropy is averaged out because the rapid molecular tumbling causes the angle  $\theta$  to change billions of times during the acquisition of the signal. In polycrystalline solid samples, however, Eq. (8) in connection with the statistical distribution of  $\theta$  leads to substantial line broadening, with spectral widths on the order of tens of kHz. Note, however, that for  $\theta = 54.7^\circ$ , the anisotropy vanishes, an effect that is exploited in the *magic-angle sample spinning* (MAS) technique used to measure highly resolved spectra in the solid state (see below). Magnetic shielding tensor values can nowadays be calculated with high precision using suitable ab initio methods, incorporating electron correlation effects by density functional theory, and even relativistic corrections for heavy atom nuclei [27, 28]. What are experimentally accessible, however, are not absolute shielding values (which would require comparisons with bare nuclei) but rather *chemical shifts* measured relative to the precession frequency of a reference compound:

$$\delta_{iso} = (\omega_{sample} - \omega_{ref})/\omega_{ref} \quad (9)$$

$^{11}\text{B}$  NMR chemical shifts offer an easy distinction between three- and four-coordinate environments. The boron coordination state in B/P FLPs can be considered “in-between” these two extremes, depending on the extent of the covalent interaction between the Lewis acid and Lewis base centers involved, resulting in intermediate chemical shifts. Likewise, the  $^{31}\text{P}$  chemical shifts are sensitive to this interaction. We will discuss in more detail below how  $^{11}\text{B}$  and  $^{31}\text{P}$  NMR chemical shifts can offer experimental access to the “degree of frustration” encountered.

## 2.4 Nuclear Electric Quadrupolar Coupling

For nuclei with spin  $I > 1/2$  the charge distribution is non-spherically symmetric. This asymmetry can be described by an electrical quadrupole moment superimposed upon a sphere containing the nuclear charge. Classical physics predict that such quadrupole moments can interact with inhomogeneous electric fields, i.e., electric field gradients (EFGs)  $V_{ij}$  present at the nuclear site. The latter are generated internally by the local electronic environment of the nuclei generated by electron density distributions, atomic coordination, and chemical bonding effects. The EFG is a symmetric second-rank tensor, which can be diagonalized in a molecular axis system. The sum of the diagonal elements  $V_{xx} + V_{yy} + V_{zz}$  vanishes (Laplace equation) so that the interaction can be described in terms of two parameters, the nuclear electric quadrupolar coupling constant  $C_Q = eV_{zz}Q$  and the asymmetry parameter

$$\eta_Q = (V_{xx} - V_{yy})/V_{zz} \quad (10)$$

with  $0 \leq \eta_Q \leq 1$ .

The quadrupolar interaction competes with the Zeeman interaction for spin alignment and the mathematical treatment is particularly straightforward if one interaction dominates. If  $\mathcal{H}_z > \mathcal{H}_Q$ , the influence of the nuclear electric quadrupolar interaction can be calculated within several levels of perturbation theory. Within the limit of first-order perturbation theory the relevant interaction Hamiltonian takes the form

$$\mathcal{H}_Q^{(1)} = \frac{C_Q}{2I(2I-1)} \cdot \frac{1}{2} (3\cos^2\theta - 1 - \eta_Q \sin^2\theta \cos 2\phi) \cdot \frac{1}{2} [3\hat{I}_z^2 - I(I+1)] \quad (11)$$

For each Zeeman state  $|m\rangle$  the corresponding energy corrections  $E_m^{(1)}$  are computed from the integrals  $\langle m | \mathcal{H}_Q | m \rangle$ . As the energy corrections are proportional to  $m^2$ , the energy level shifts of the  $|+1/2\rangle$  and  $|-1/2\rangle$  states are identical at each orientation, and the width of the central  $|+1/2\rangle \leftrightarrow |-1/2\rangle$  transition is thus



unaffected by the quadrupole interaction. In contrast, it follows from Eq. (11) that the frequencies of the  $|\pm 1/2\rangle \leftrightarrow |\pm 3/2\rangle$  transitions are orientationally dependent, giving rise to anisotropically broadened *satellite transitions* in powdered samples. If the condition  $\mathcal{H}_Q \ll \mathcal{H}_z$  is not fulfilled but still  $\mathcal{H}_Q < \mathcal{H}_z$ , the perturbation approach has to be extended to second-order. In this case, a more complicated orientational dependence causes anisotropic broadening even of the central transition. Highly characteristic lineshapes are observed, from which  $C_Q$  and  $\eta_Q$  can be extracted via lineshape simulation routines [29]. Theoretical ab initio values are available from optimized molecular geometries or crystal structure data using programs such as GAUSSIAN [30], TURBOMOLE [31, 32], or WIEN2k [33]. Thus the nuclear electric quadrupolar interaction parameters represent important structural validation criteria for unknown materials.

The trigonal planar local environments of three-coordinated boron atoms create a large electric field gradient at the  $^{11}\text{B}$  nuclei, with its maximum component perpendicular to the plane. In contrast, the electric field gradients encountered at the more symmetrically ligated four-coordinated boron species are relatively small. As discussed further below, the “in-between” state encountered with B/P FLPs affects sensitively both the  $^{11}\text{B}$  nuclear electric quadrupolar coupling constants and the electric field asymmetry parameters, offering experimental access to the “degree of frustration”.

## 2.5 Indirect Magnetic Dipolar Coupling

The Hamiltonian describing the indirect magnetic dipole–dipole coupling is given by the tensor product

$$\mathcal{H}_J = \hat{I} \vec{\vec{J}} \hat{S} \quad (12)$$

where  $\vec{\vec{J}}$  is the indirect spin–spin coupling tensor. Its magnitude and anisotropy depend to a great extent on the symmetry of the electron distribution in the chemical bond, but also on the sizes of the magnetic moments involved. For a two-spin interaction, the tensor is generally axially symmetric, and can be split into an isotropic component  $J_{\text{iso}}$  and an anisotropic component  $\Delta J$ . While the anisotropic part is averaged out by molecular tumbling in the liquid state, the isotropic part produces the peak splittings well-known in liquid state NMR. Heteronuclear spin–spin interactions of the observed nuclei to  $n$  nuclei having spin quantum number  $I$  yield a peak multiplicity of  $2nI + 1$ . In the solid state, the spectra are influenced both by isotropic and anisotropic  $J$ -couplings; however, the anisotropy can be eliminated by the magic angle spinning technique.

The magnitudes of the  $\vec{\vec{J}}$  tensor components depend not directly on distance but are greatly influenced by the electronic properties and bonding characteristics. Ab initio calculations of  $J_{\text{iso}}$  values with GAUSSIAN are possible in principle [27, 34],

even though the accuracy is lower than that of magnetic shielding calculations. Nevertheless, the experimental detection of  $^{11}\text{B}$ - $^{31}\text{P}$  isotropic spin–spin coupling in MAS-NMR spectra provides direct evidence of covalent interactions, and the magnitude of the isotropic spin–spin coupling constant can give insight into the “degree of frustration”, at least on a comparative basis.

## 2.6 Direct Magnetic Dipole–Dipole Coupling

Nuclear precession frequencies are further influenced by magnetic dipole–dipole interactions, as the spins feel the magnetic moments of their neighbors. The effect is anisotropic, depending on the orientation of the internuclear distance vector relative to  $B_0$ . This effect, too, results in strong line broadening effects for polycrystalline samples. There are two distinct mechanisms: (1) the *direct through-space* interaction, which merely reflects *spatial proximity*, and (2) the *indirect* interaction, where the coupling is transmitted via the polarization of bonding electrons. Both the direct and the indirect terms comprise a homonuclear and a heteronuclear contribution, respectively. The Hamiltonian of the direct through-space interaction is proportional to the inverse cube of the internuclear distance, providing a straightforward connection to geometric structure. In the limit of first-order perturbation theory it is given by the expressions [24]

$$\mathcal{H}_{\text{D,homo}} = -\left(\frac{\mu_0}{4\pi}\right) \frac{\gamma^2 \hbar^2}{d_{ij}^3} \left(\frac{3\cos^2\theta - 1}{2}\right) (3\hat{I}_z^2 - \hat{I}^2) \quad (13)$$

$$\mathcal{H}_{\text{D,hetero}} = -\left(\frac{\mu_0}{4\pi}\right) \frac{\gamma_I \gamma_S \hbar^2}{d_{IS}^3} \left(\frac{3\cos^2\theta - 1}{2}\right) (\hat{I}_z \hat{S}_z) \quad (14)$$

The orientational dependence is again described by the  $3\cos^2\theta - 1$  term where  $\theta$  is the angle between the internuclear distance vector and the magnetic field direction. In the liquid state the direct homo- and heteronuclear magnetic dipolar interactions are averaged to zero owing to the rapid molecular tumbling process. In the solid state, however, the effect results in broadened lineshapes. For isolated two-spin systems between nuclei  $I$  and  $S$ , we can specify the dipolar coupling constant

$$D_{IS} = (\mu_0/8\pi^2)h \gamma_I \gamma_S d_{IS}^{-3} \quad (15)$$

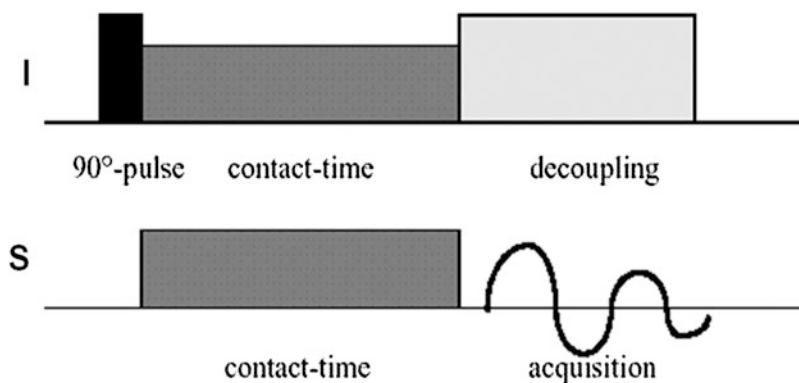
which provides a straightforward relation to internuclear distances  $d_{IS}$ . Thus, selective measurements of the magnetic dipole–dipole interactions in the solid state provide a powerful approach to structure elucidation. For FLPs, the principal application of the magnetic dipole–dipole interaction is the precise measurement of the B...P internuclear distance in those compounds not amenable to single-crystal X-ray crystallography.

### 3 Experimental Techniques and Aspects of Their Application to FLPs

#### 3.1 Signal Preparation and Lineshape

As described above, the standard preparation technique for recording NMR spectra in the solid state is the application of  $90^\circ$  pulses. For insensitive nuclei with small magnetic moments, low natural abundances, or long spin–lattice relaxation times, the preparation process often consists of *cross-polarization* from an abundant-spin reservoir [35]. This process uses the magnetic dipole–dipole couplings of the insensitive observed nuclei with nearby abundant spins. Figure 2 shows the pulse sequence involved. In general, transverse spin magnetization of the abundant nuclei (species *I*) is created by a  $90^\circ$  pulse, and spin-locked by applying a strong radiofrequency field along the direction of the magnetization in the rotating frame. During the application of this radiofrequency field, the spin states are now quantized in a direction orthogonal to  $B_0$  and the transverse magnetization is forced to precess around this direction with the *I*-spin nutation frequency  $\omega_{1I} = \gamma_I B_{1I}$ . As the spin-locked magnetization is much higher than the value corresponding to the value of  $B_{1I}$ , this situation reflects a non-equilibrium state, from which the system seeks to escape via relaxation. Cross-polarization facilitates a cross-relaxation channel involving magnetic dipole–dipole interactions with nearby *S* nuclei. This is accomplished by applying a second radio frequency field to those spins, whose amplitude is such that the nutation frequencies  $\omega_{1S}$  of both spin species are equal (*Hartmann–Hahn matching condition*) [36]:

$$\gamma_I B_{1I} = \gamma_S B_{1S} \quad (16)$$



**Fig. 2** Pulse sequence used for cross-polarization. The rf field applied to the *I* nuclei during the contact time is phase shifted by  $90^\circ$  relative to the corresponding preparation pulse

In this way, the excess  $I$ -spin polarization can be transferred to the  $S$ -spins, whose signal is then detected. In the spectroscopy of FLPs, this method is generally used to record  $^{13}\text{C}$  MAS-NMR spectra (1.1% natural abundance), the acquisition of which would not be possible by standard single-pulse excitation. As the requirements for the recycle delays to be used for signal accumulation depend on the spin–lattice relaxation times of the  $I$  nuclei in the abundant-spin reservoir rather than those of the detected  $S$  spins, cross-polarization is also often used with abundant  $S$ -spin nuclei if they relax more slowly compared to the  $I$  spins. For example, measuring  $^{31}\text{P}$  nuclei via cross-polarization from protons allows for much faster signal build-up compared to direct single-pulse  $^{31}\text{P}$  excitation. During the acquisition high-power multiple-pulse  $^1\text{H}$  decoupling is generally applied to eliminate broadening by dipolar spin–spin interactions most effectively.

Considering all of the interactions described in Sect. 2, the internal NMR Hamiltonian in the solid state is given by

$$\begin{aligned} \mathcal{H}_{\text{int}} = & \mathcal{H}_{\text{ms}}^{\text{aniso}} + \mathcal{H}_{\text{ms}}^{\text{iso}} + \mathcal{H}_{\text{D}}^{\text{homo}} + \mathcal{H}_{\text{D}}^{\text{hetero}} + \mathcal{H}_{\text{J}}^{\text{homo,iso}} + \mathcal{H}_{\text{J}}^{\text{homo,aniso}} + \mathcal{H}_{\text{J}}^{\text{hetero,iso}} \\ & + \mathcal{H}_{\text{J}}^{\text{hetero,aniso}} + \mathcal{H}_{\text{Q}}^{(1)} + \mathcal{H}_{\text{Q}}^{(2)} \end{aligned} \quad (17)$$

In the most general case, the NMR spectrum of a nuclear species in the solid state is influenced by all of these interactions simultaneously, restricting a meaningful analysis of the spectra to such cases, in which one particular interaction is completely dominant. Although there are numerous well-known examples of such special cases [24, 25], in general the various interaction strengths are often of comparable magnitude, resulting in featureless lineshapes that make a meaningful analysis impossible. For this general situation, advanced solid-state NMR methods, which serve to simplify the Hamiltonian of Eq. (17), are used to great advantage. The most important of these *selective averaging* techniques is the *magic angle sample spinning* (MAS) method [37]. Furthermore, it is possible to combine MAS with special *recoupling methods* that are designed to reintroduce selected interactions of the spin Hamiltonian. By combining several such methods, one can look selectively at individual parts of the spin Hamiltonian and extract the relevant interaction parameters. The design of new pulse sequences is greatly aided by the availability of program packages that calculate the behavior of the spins under the influence of the external and internal interaction Hamiltonians using standard time-dependent perturbation theory. Especially noteworthy is the program package *SIMPSON*, which enables the simulation of complex NMR experiments under the precise experimental conditions used at the spectrometer [38]. This freeware has proved to be invaluable in the analysis of complex experiments and has profoundly influenced NMR research in many laboratories. The following sections describe a number of useful individual experiments as well as some theoretical and practical aspects of their application to FLPs.

### 3.2 Measurement of Isotropic Chemical Shifts and Quadrupolar Coupling Parameters by Magic Angle Sample Spinning

Isotropic motion of the nuclei in solution affords the simplest form of selective averaging. If the correlation time describing this motion is short compared to the inverse frequency describing the spectral dispersion due to anisotropic interactions, all of the latter are being averaged out, and the NMR Hamiltonian simplifies to

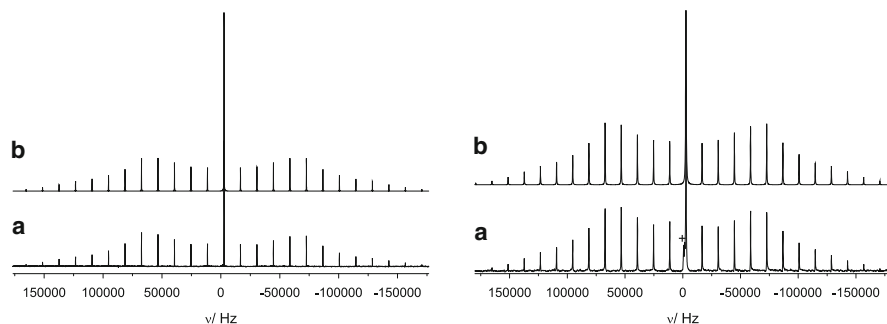
$$\mathcal{H}_{\text{tot}} = \mathcal{H}_{\text{ms}}^{\text{iso}} + \mathcal{H}_{\text{J}}^{\text{homo,iso}} + \mathcal{H}_{\text{J}}^{\text{hetero,iso}} \quad (18)$$

The success of high-resolution liquid state NMR spectroscopy as a structural tool in chemistry is based on this principle. A rather similar situation can be accomplished in polycrystalline solids by rotating the sample about an axis that is inclined by an angle of  $54^\circ 44'$  relative to the magnetic field direction (*magic angle sample spinning*) [37]. This manipulation replaces the actual orientation  $\theta$  by an orientational average over the rotor period, which simply corresponds to the orientational angle of the rotation axis. As for  $\theta = 54.7^\circ$  the term  $3\cos^2\theta - 1$  equals zero, all of the anisotropic interactions whose frequency dispersions scale with this term are canceled out, provided that the spinning frequency  $\omega_r$  is sufficiently large. In this case, the NMR Hamiltonian simplifies to the expression

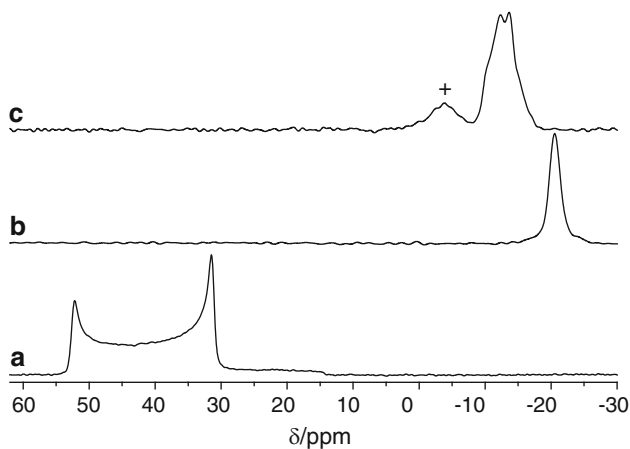
$$\mathcal{H}_{\text{tot}} = \mathcal{H}_{\text{ms}}^{\text{iso}} + \mathcal{H}_{\text{J}}^{\text{homo,iso}} + \mathcal{H}_{\text{J}}^{\text{hetero,iso}} + \mathcal{H}'_{\text{Q}}{}^{(1)} + \mathcal{H}'_{\text{Q}}{}^{(2)} \quad (19)$$

Here the terms  $\mathcal{H}'_{\text{Q}}{}^{(1)}$  and  $\mathcal{H}'_{\text{Q}}{}^{(2)}$  denote the relevant parts of the quadrupolar Hamiltonians in first- and second-order, which are modulated by MAS. Specifically,  $\mathcal{H}'_{\text{Q}}{}^{(1)}$  results in spinning sideband manifolds, whose envelope reflects the outer Zeeman (“satellite” transitions, SATRAS). A typical example is shown in Fig. 3 for compounds **14** and **15** where the boron atoms are four-coordinated and the nuclear electric quadrupolar coupling is rather weak. In this case the central transition lineshapes are sharp and values of  $C_{\text{Q}}$  and  $\eta_{\text{Q}}$  can be obtained by analyzing the spinning sideband envelope with the help of simulation programs. Figure 4a gives an example of a MAS-NMR lineshape influenced by second-order quadrupolar perturbations. In this case  $\mathcal{H}'_{\text{Q}}{}^{(2)}$  results in a structured lineshape for the central transition as mentioned above. The center of gravity of the signal is comprised both of the isotropic chemical shift contribution and a second-order quadrupolar shift, the magnitude of which decreases with increasing field strength [39]. Both these contributions can be separated by systematic studies of the field dependence or by the multiple-quantum NMR experiment (see below).

Thus Fig. 4 illustrates how  $^{11}\text{B}$  MAS-NMR is able to differentiate between three- and four-coordinated boron environments based on both the value of the isotropic chemical shifts and the nuclear electric quadrupolar coupling constant. In particular, this figure documents the typical “in-between” bonding state of the FLPs with intermediate values of chemical shift and nuclear quadrupolar coupling constants.

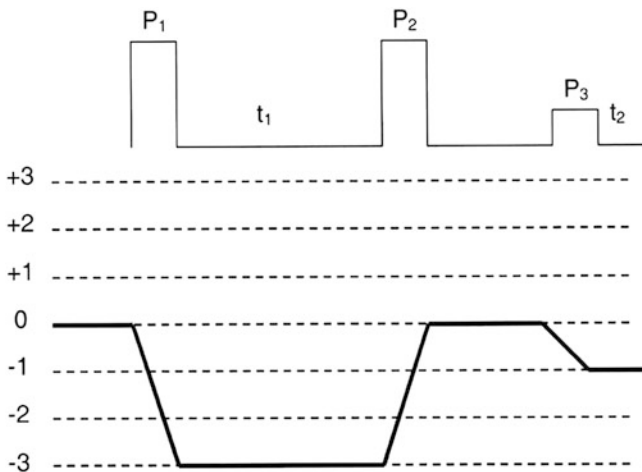


**Fig. 3** *Left:*  $^{11}\text{B}$  SATRAS spectrum (a) and the corresponding line shape simulation (b) of the phosphirenium borate zwitterion **14**. *Right:*  $^{11}\text{B}$  SATRAS spectrum (a) and the corresponding line shape simulation (b) of the phosphirenium borate zwitterion **15**. In both cases, comparable quadrupolar coupling parameters are obtained ( $C_Q \sim 0.3$  MHz and  $\eta_Q \sim 0.3$ ). The sharp intense line at the center corresponds to the  $|1/2\rangle \leftrightarrow |-1/2\rangle$  Zeeman transition. *plus* marks an impurity



**Fig. 4**  $^{11}\text{B}$  MAS-NMR spectra of (a) **16**, (b), **14** and (c) **7** highlighting the extremely high sensitivity of  $^{11}\text{B}$  solid-state NMR to the local environment of the boron site. *plus* marks an impurity. Chemical shifts are reported relative to  $\text{BF}_3 \cdot \text{Et}_2\text{O}$  solution

For quadrupolar nuclei affected by second-order quadrupolar perturbations the resolution can be improved by combining MAS-NMR with multiple quantum excitations. As shown by Frydman et al. [40], second-order quadrupolar broadening can be eliminated by correlating the evolution of a  $|m\rangle \leftrightarrow |-m\rangle$  multiple quantum transition with the central  $|1/2\rangle \leftrightarrow |-1/2\rangle$  transition during the course of a two-dimensional experiment, with corresponding coherence pathway selection by appropriate phase cycling. For sensitivity reasons, the triple-quantum coherence involving the  $|3/2\rangle \leftrightarrow |-3/2\rangle$  Zeeman states is usually selected, even for nuclei with  $I > 3/2$ .



**Fig. 5** Timing and coherence level diagram of a triple-quantum NMR experiment

Figure 5 shows a typical pulse sequence, along with a coherence level diagram. Triple-quantum coherence is excited (among other coherences) by the first short, intense radiofrequency pulse. The subsequent evolution during an incremented time period  $t_1$  is terminated by a second intense pulse, which generates zero-quantum coherence. Then a weak detection pulse produces transverse magnetization (single-quantum coherence) which is acquired during the detection period  $t_2$ . Double Fourier transformation with respect to both time domains  $t_1$  and  $t_2$ , followed by appropriate data manipulation, generates a 2D spectrum, from which the isotropic chemical shift  $\delta_{cs}^{iso}$  and the isotropic quadrupolar shift  $\delta_Q$  can be evaluated. The centers of gravity of the signals observed in the isotropic ( $F1$ -) and the anisotropic ( $F2$ -) dimensions of this experiment,  $\delta_{F1}$  and  $\delta_{F2}$  are given by [41]

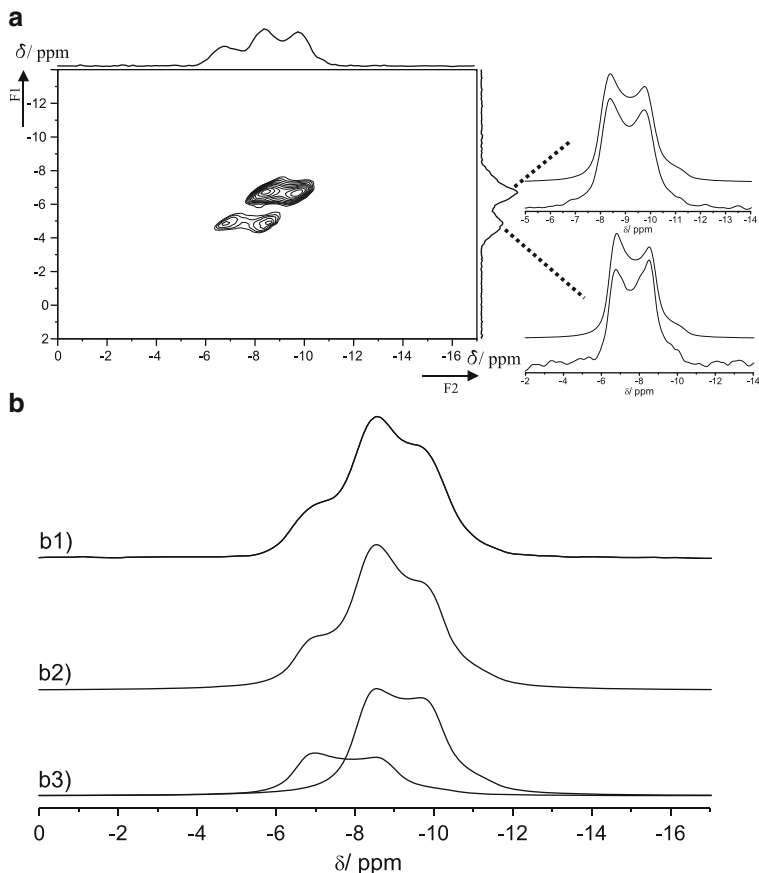
$$\delta_{F1} = (34\delta_{cs}^{iso} - 60\delta_Q)/9 \quad (20a)$$

$$\delta_{F2} = \delta_{cs}^{iso} + 3\delta_Q \quad (20b)$$

$$\text{where } \delta_Q = 3(SOQE)^2 / (10v_L^2[2I(2I - 1)]^2) \quad (20c)$$

In this expression  $v_L$  is the nuclear Larmor frequency, and the parameter  $SOQE$ , the so-called second-order quadrupolar effect is given by the relation

$$SOQE = C_Q \left(1 + \eta_Q^2/3\right)^{1/2} \quad (20d)$$



**Fig. 6** (a)  $^{11}\text{B}$  TQMAS-NMR spectrum (*left*) of the adduct **2** ( $\text{R} = \text{Ph}$ ,  $\text{R}' = \text{Ph}$ ) measured at 11.7 T with a spinning frequency of 14 kHz. The spectrum shows two slightly different resonances with isotropic chemical shifts of  $-7.6$  ppm and  $-5.9$  ppm, respectively and with a *SOQE* of 1.24 MHz and 1.31 MHz, respectively. The corresponding experimental *F1* slices and their simulations are shown on the right. (b)  $^{11}\text{B}$  MAS-NMR spectrum at 11.7 T (*b1*), simulated spectrum (*b2*) and individual contributions of the simulation (*b3*) showing two boron sites. For the simulations the quadrupolar parameters determined via the TQMAS experiment were chosen ( $C_Q = 1.25$  MHz,  $\eta_Q = 0.18$  and  $C_Q = 1.36$  MHz,  $\eta_Q = 0.15$ ). The intensity ratio is determined as 2.3:1

Thus, the analysis of the centers of gravity in both dimensions of such a triple quantum (TQ)-MAS NMR experiment results in the isotropic chemical shift  $\delta_{CS}^{iso}$  and the parameter *SOQE*.

A typical application to an FLP is given in Fig. 6 for the intramolecular adduct **2**. In this case the resolution in the regular MAS-NMR spectrum suffers from the partial overlap of two second-order quadrupolar broadened peak patterns.

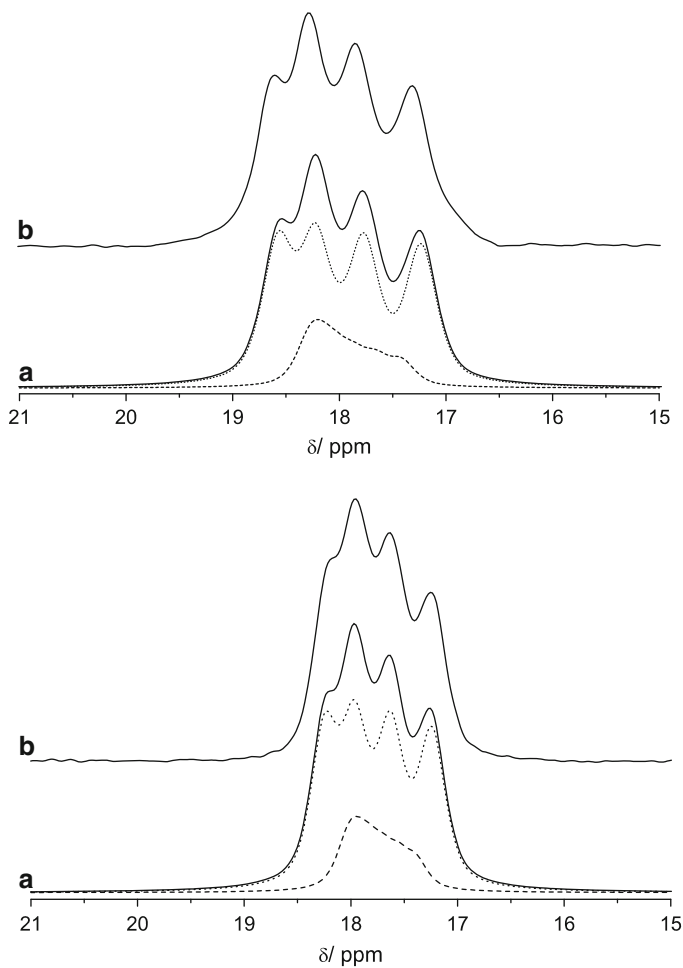


Using the TQMAS-NMR approach, the two lineshape contributions can be separated in the isotropic ( $F1$ ) dimension. By simulating the corresponding cross-sections along the anisotropic ( $F2$ ) dimension, the precise nuclear electric quadrupolar coupling and chemical shift parameters of the two individual components can be obtained. With these parameters the MAS-NMR lineshape can then be simulated in terms of both distinct sites, resulting in a 2.3:1 ratio in this case. Presumably these different sites arise from packing effects or disorder in the solid state (the crystal structure could not be solved to date).

### 3.3 Recovery of Indirect Spin–Spin Interactions

As indicated by the MAS-NMR Hamiltonian of Eq. (19) the high-resolution solid-state NMR lineshapes recorded under MAS conditions are in principle also influenced by isotropic indirect spin–spin interactions. In the case of  $^{11}\text{B}$  MAS-NMR these interactions are masked by anisotropic second-order quadrupolar broadening effects and thus in general are not directly observable. In contrast, the indirect  $^{10}\text{B}/^{11}\text{B}\cdots^{31}\text{P}$  spin–spin interactions produce multiplet structures in the  $^{31}\text{P}$  MAS-NMR spectra, with splittings (in Hertz) independent of the magnetic field strength. Figure 7 gives a typical example for compound **1**. The mere fact that these spin–spin couplings exist indicates the presence of covalent interactions between the two Lewis centers. To achieve optimum resolution of these multiplets it is essential to record the spectra with high-power  $^1\text{H}$  decoupling, using multiple-pulse schemes such as “Two Pulse Phase Modulated” (TPPM) pulses [43]. Since  $^{11}\text{B}$  (natural abundance 80.4%) and  $^{10}\text{B}$  (19.6%) have nuclear spin quantum numbers of 3/2 and 3, respectively, one might expect a  $^{31}\text{P}$  MAS-NMR line shape consisting of a quartet and septet, respectively, with isotropic  $J$  coupling constants being scaled according to the isotope-specific gyromagnetic ratios ( $\gamma(^{10}\text{B})/\gamma(^{11}\text{B}) = 0.33$ ). In reality, these patterns tend to be dominated by the four-line pattern expected due to coupling to the higher-abundant and larger-gamma  $^{11}\text{B}$  isotope. As it turns out, the patterns are not equally spaced and their shape possesses a small, but noticeable dependence on the magnetic field strength. This is the typical behavior expected theoretically and encountered experimentally when the dipolar interactions with a quadrupolar nucleus are not completely eliminated under MAS conditions because of strong quadrupolar perturbations of the  $^{10}\text{B}/^{11}\text{B}$  Zeeman energy levels. The effect can be described in the context of first-order perturbation theory, in which the  $^{31}\text{P}$  MAS-NMR transitions in the presence of this interaction are given as [44]

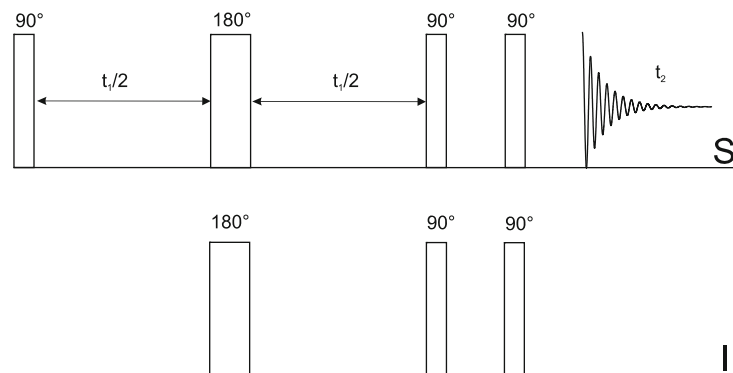
$$\nu_m = -m|J| - \frac{S(S+1) - 3m^2}{S(2S-1)}d \quad (21)$$



**Fig. 7**  $^{31}\text{P}\{^1\text{H}\}$  CPMAS spectra of compound **1** ( $\text{R} = \text{Mes}$ ,  $\text{R}' = \text{Ph}$ ) acquired at different field strengths (*top*: 7.1 T, swept-frequency TPPM (SWf-TPPM-15) [42]  $^1\text{H}$  decoupling, *bottom*: 9.4 T, TPPM-15  $^1\text{H}$  decoupling). In both cases (*a*) represents the line shape simulation (including the peak deconvolution due to  $^{31}\text{P}$ - $^{10}\text{B}$  (*dashed curve*) and  $^{31}\text{P}$ - $^{11}\text{B}$  (*dotted curve*) indirect dipolar couplings and (*b*) the measured spectrum

wherein  $J$  are the isotropic  $^{10/11}\text{B}$ - $^{31}\text{P}$  indirect spin–spin coupling constants,  $S$  are the nuclear spin quantum numbers for the quadrupolar nuclei ( $I = 3/2$  and 3 for  $^{11}\text{B}$  and  $^{10}\text{B}$ , respectively),  $m$  are the orientational quantum numbers, and  $d$  is the residual dipolar coupling [45, 46]. The latter value is given by

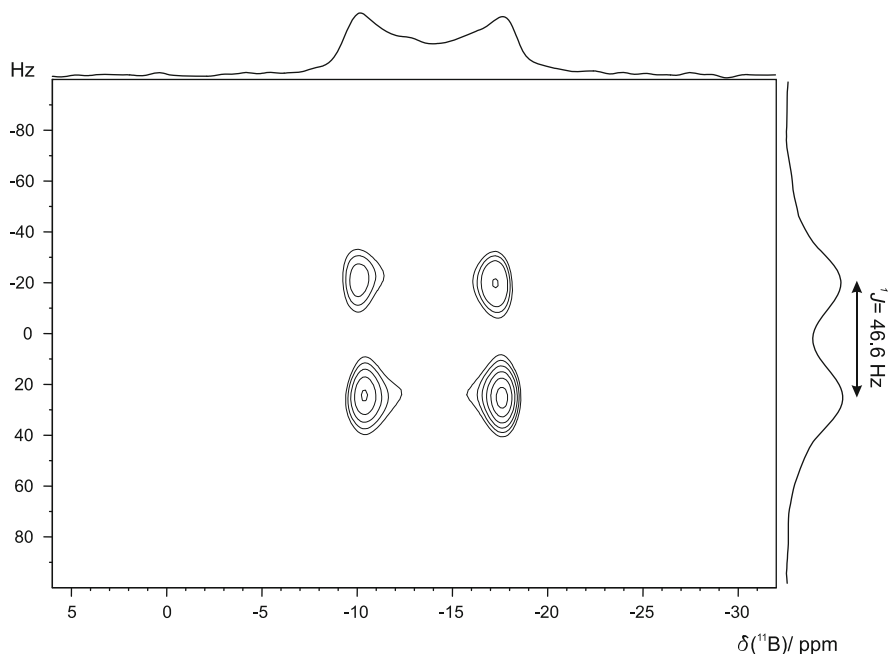
$$d = \frac{-3C_Q(D - \frac{\Delta I}{3})}{20\nu_S} [3\cos^2\beta^D - 1 + \eta\sin^2\beta^D \cos 2\alpha^D] \quad (22)$$



**Fig. 8** Timing diagram of the heteronuclear  $J$ -Resolved pulse sequence

with  $D$  describing the  $^{10/11}\text{B}$ - $^{31}\text{P}$  direct dipolar coupling constant,  $\Delta J$  the anisotropy of the indirect spin–spin coupling tensor,  $\nu_s$  the  $^{10}\text{B}$  or  $^{11}\text{B}$  Larmor frequency,  $C_Q$  the  $^{10}\text{B}$  or  $^{11}\text{B}$  quadrupolar coupling constant,  $\eta_Q$  the electric field gradient asymmetry parameter, and  $\alpha^D$  and  $\beta^D$  the Euler angles defining the orientation of the dipolar vector in the principal axis system of the EFG [44]. Figure 7 compares field dependent experimental spectra with simulated ones based on the following constraints: (1) the integrated peak areas of the two multiplets reflect the natural abundances of the two boron isotopes, (2) the  $J$  values are scaled according to the magnetogyric ratios, and (3) the  $d$  values are scaled according to the quadrupole moments ( $Q(^{10}\text{B})/Q(^{11}\text{B}) = 2.084$ ) [47]. Based on Fig. 7, a  $^1J(^{31}\text{P}\text{-}^{11}\text{B})$  coupling constant of about 55 Hz and a residual dipolar coupling value  $d(^{31}\text{P}\text{-}^{11}\text{B})$  of  $-5.5$  Hz were extracted from the spectra measured at 7.1 T. Appropriate linebroadening needs to be included for achieving the best fit of the superimposed peak patterns with the experimental data; as a result, the seven components originating from  $^{10}\text{B}$ - $^{31}\text{P}$   $J$ -coupling are not individually resolved. This lack of resolution might also reflect fluctuations of the  $^{10}\text{B}$  nuclei among their seven Zeeman states on the relevant NMR timescale.

In many cases, heteronuclear  $J$ -couplings of FLPs are too small to influence standard MAS-NMR lineshapes. In such cases, two-dimensional techniques such as the heteronuclear  $J$ -resolved spectroscopy method are used to great advantage [48]. Figure 8 illustrates the principal idea. Following the initial preparation process (either by  $90^\circ$  pulses or cross-polarization) the transverse  $S$ -magnetization initially evolves under the combined influence of magnetic shielding ( $\mathcal{H}_{\text{ms}}$ ) and heteronuclear  $J$ -coupling ( $\mathcal{H}_J$ ) during the first half of the evolution period  $t_1$ . The evolution under  $\mathcal{H}_{\text{ms}}$  is reversed, however, if the  $180^\circ$  pulse is placed in the center of the evolution period. In this case, no chemical shift evolution has taken place at the end of  $t_1$ . At the same time, the  $180^\circ$  pulse applied to the  $I$ -spins ensures that the indirect spin–spin interaction is *not* refocused but rather continues to influence the spin evolution during the entire  $t_1$ -period. For each value of  $t_1$  the signal is then detected during the regular signal acquisition time domain  $t_2$ . In this way, both

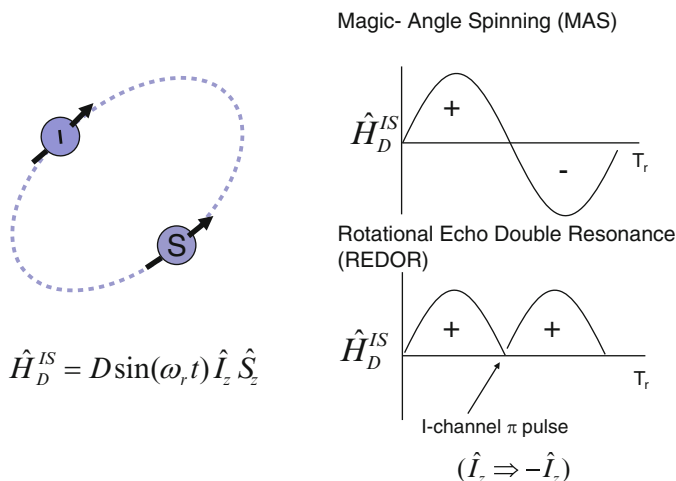


**Fig. 9**  $^{11}\text{B}\{^{31}\text{P}\}$  heteronuclear  $J$ -resolved spectrum of the B/P adduct **11** acquired at 7.1 T with a rotation frequency of 10 kHz. The  $F2$  projection shows the anisotropically broadened  $^{11}\text{B}$  MAS-NMR line shape while in the  $F1$  dimension the  $^1J$ -coupling between  $^{31}\text{P}$  and  $^{11}\text{B}$  is apparent

interactions have been effectively separated into two separate time domains  $t_1$  and  $t_2$  and can be read off a two-dimensional spectrum obtained upon a double Fourier transformation. In the case of FLPs the experiment can be conducted using either  $^{11}\text{B}$  or  $^{31}\text{P}$  observation. Figure 9 shows a  $^{11}\text{B}\{^{31}\text{P}\}$  –  $J$ -resolved NMR spectrum of compound **11**, whose  $^{31}\text{P}$  MAS-NMR spectrum is too broad for the detection of any  $J$ -coupling features. Likewise, this coupling is too weak to influence the  $^{11}\text{B}$  resonance, the shape of which is dominated by second-order quadrupolar perturbations. However, a clear  $J$ -doublet is seen in the  $F1$  dimension of the 2D  $J$ -resolved spectrum, from which a coupling constant of 46.6 Hz can be extracted.

### 3.4 Dipolar Recoupling by Rotational Echo Double Resonance

As illustrated by Eq. (19), the direct magnetic dipole–dipole interaction is eliminated by MAS. The interaction can, however, be reintroduced by a powerful double resonance experiment, termed *rotational echo double resonance (REDOR)*, which is able to provide site-selective dipolar coupling information under the high-resolution conditions afforded by magic angle spinning. As illustrated in Fig. 10,



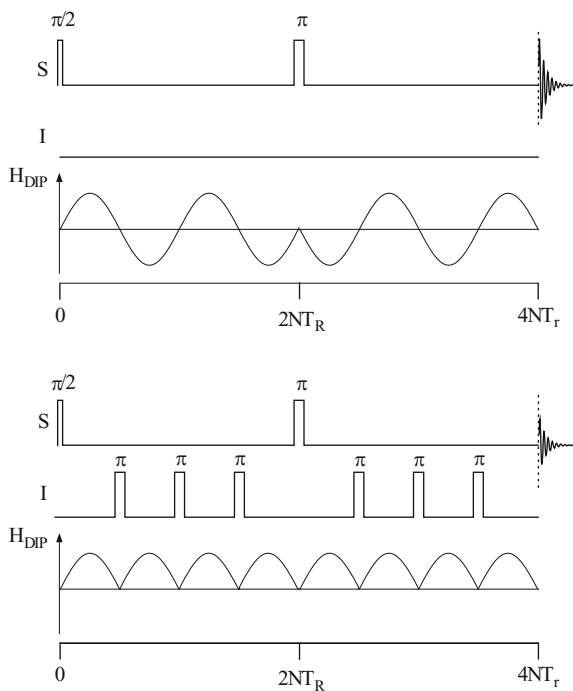
**Fig. 10** Principle of the REDOR experiment. Under MAS conditions the heteronuclear dipolar Hamiltonian oscillates sinusoidally with rotor orientation, leading to cancellation of  $H_D$  upon completion of the rotor cycle (*right, top*). Sign inversion created by a  $\pi$ -pulse applied to the non-observed  $I$  spins interferes with this cancellation (*right, bottom*) and the interaction is thus re-coupled

the dipolar coupling constant oscillates during the MAS rotor period according to the term  $\sin \omega_r t$  and is averaged out over the rotor cycle. However, if we invert the sign of the dipolar Hamiltonian by applying a  $\pi$ -pulse to the non-observed  $I$ -spins during the rotor period, this average is non-zero; the interaction is recoupled.

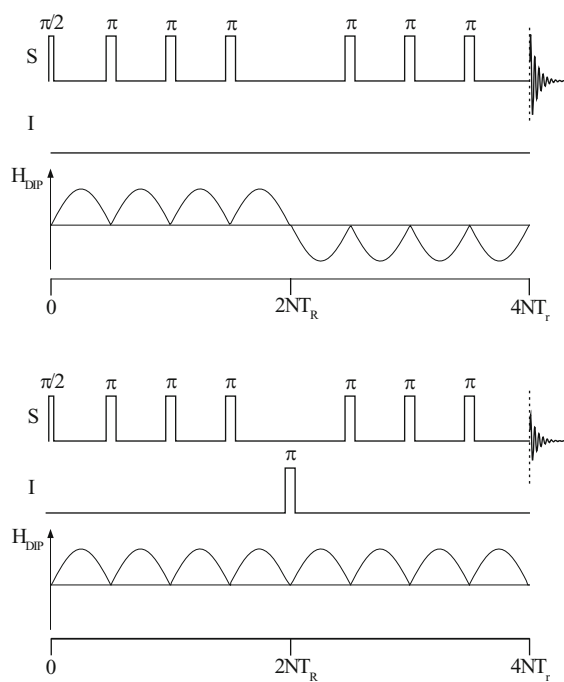
Figures 11 and 12 show two typical pulse sequences used for such purposes [49, 50]. In both sequences the recoupling is accomplished by  $180^\circ$  pulse trains and both yield identical results if  $I = 1/2$  and  $S = 1/2$ . Sequence (a), which applies the recoupling pulse trains to the non-observed  $I$ -spins, while the  $S$ -spin signal is detected by a rotor-synchronized Hahn spin echo sequence, is the preferred one if the observed nuclei are quadrupolar and coupled to  $I = 1/2$  spins ( $^{11}\text{B}\{^{31}\text{P}\}$  REDOR). In contrast, sequence (b) applies the pulse trains to the observed  $S$ -spins, while the non-observed  $I$ -spins are subjected only to one central  $\pi$ -pulse in the middle of the rotor period. This sequence is the preferred one if the observed spins have spin quantum number  $S = 1/2$  and are recoupled to quadrupolar nuclei (e.g., in  $^{31}\text{P}\{^{11}\text{B}\}$  REDOR). In both cases one measures the normalized difference signal  $\Delta S/S_0 = (S_0 - S)/S_0$  in the absence (intensity  $S_0$ ) and the presence (intensity  $S$ ) of the recoupling pulses. The degree of attenuation depends on the size of the heteronuclear magnetic dipole coupling constant  $D_{IS}$  and on the duration of the dipolar recoupling process, which is given by the product of the number  $N$  of rotor cycles during which the inversion pulse trains are applied and the rotor period  $T_r$ .

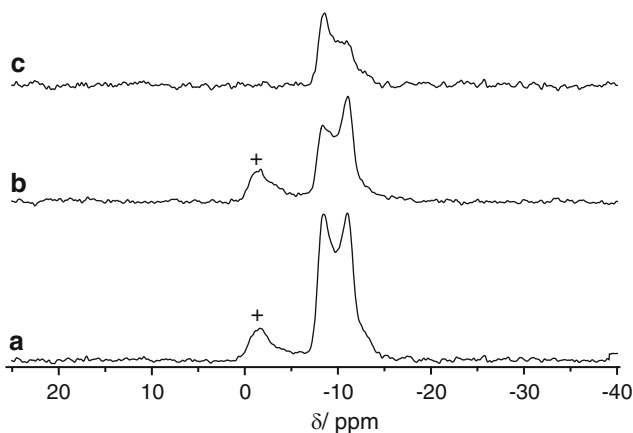
Figure 13 illustrates a simple application of a  $^{11}\text{B}\{^{31}\text{P}\}$  REDOR experiment to compound **3** in which at the chosen dipolar evolution time (0.43 ms) a significant loss in signal intensity is observed due to the recoupling of  $^{31}\text{P}$  dipolar interactions

**Fig. 11** Timing and coherence level diagrams of the REDOR pulse sequence of Schaefer and Gullion [49], preferred if the detected spin species  $S$  is quadrupolar



**Fig. 12** Timing and coherence level diagrams of the REDOR pulse sequence of Garbow and Gullion [50], preferred if the detected spins have quantum number  $S = 1/2$  and dephasing in the dipolar field of quadrupolar nuclei  $I > 1/2$  is studied





**Fig. 13** Single data point of a  $^{11}\text{B}\{^{31}\text{P}\}$  REDOR experiment acquired at 9.4 T with a rotor frequency of 14 kHz and an evolution time of 0.43 ms (*a*:  $S_0$ , *b*:  $S$ , *c*:  $S_0 - S$ ) for **3**. *plus* marks an impurity remote from  $^{11}\text{B}$  nuclei

(see Fig. 13b). A complete REDOR curve is then generated by measuring  $\Delta S/S_0$  under systematic incrementation of the dipolar evolution time  $NT_r$ . Under such conditions the normalized difference signal  $\Delta S = (S_0 - S)/S_0$  changes periodically (like  $\cos \Delta\Phi$ ) as a function of the dipolar evolution time  $NT_r$ , where

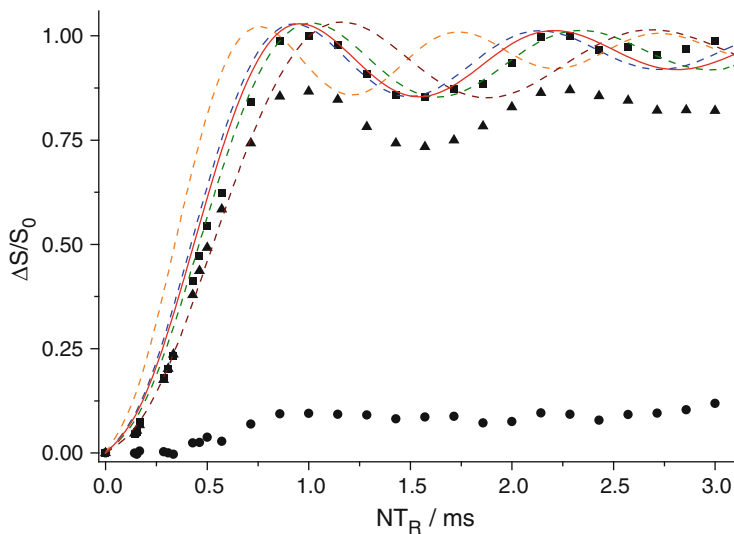
$$\Delta\Phi = 4\sqrt{2}NT_r D \sin\beta \cos\beta \sin\alpha \quad (23)$$

In this expression the angles  $\alpha$  and  $\beta$  are Euler angles describing the orientation of the dipolar vector in the MAS rotor axis system. For a polycrystalline sample, a powder average must be taken by appropriate integration over all the Euler angles:

$$\frac{\Delta S}{S_0} = 1 - \frac{1}{4\pi} \int_0^{2\pi} d\alpha \int_0^{\pi} \sin\beta \cos(\Delta\Phi) d\beta \quad (24)$$

For a two-spin system, simulation of this curve yields the dipolar coupling constant  $D_{IS}$  from which the internuclear distance  $d_{IS}$  can be extracted via Eq. (15). The intramolecular adducts of the present study can be considered as ideal  $^{31}\text{P}$ - $^{11}\text{B}$  two-spin systems, for which the distance should be easily measurable using either  $^{31}\text{P}\{^{11}\text{B}\}$  or  $^{11}\text{B}\{^{31}\text{P}\}$  REDOR experiments. In practice, the second experiment with observation of the quadrupolar  $^{11}\text{B}$  spin species has been preferred, because the  $^{11}\text{B}$  nuclei have shorter spin–lattice relaxation times.

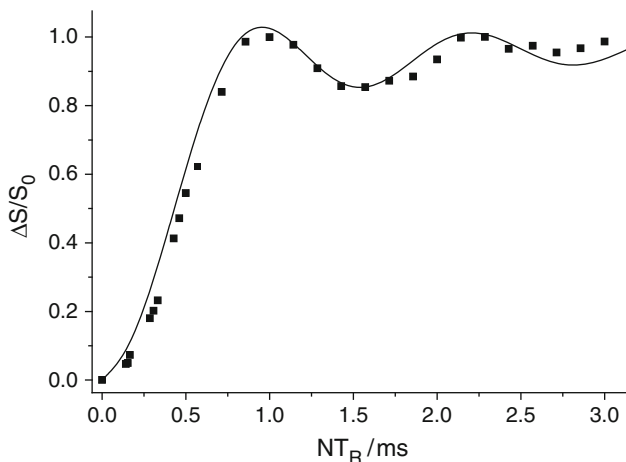
Figure 14 shows the complete  $^{11}\text{B}\{^{31}\text{P}\}$  REDOR curve for **3** as a representative example. The oscillatory behavior characteristic of an isolated two-spin system as predicted by Eqs. (23) and (24) is clearly evident, offering the prospect of internuclear distance measurements. To obtain high-fidelity results, however, a number



**Fig. 14**  $^{11}\text{B}\{^{31}\text{P}\}$  compensated REDOR curve (filled squares, calibration factor  $a = 1.4$ ), REDOR curve (filled triangles) and compensation (filled circles) for the intramolecular B/P adduct **3** (spinning frequency 14 kHz). SIMPSON simulations assuming a B...P distance of 1.9 Å (orange dashed curve), 2.038 Å (crystallographic value, blue dashed curve), 2.06 Å (red straight curve), 2.1 Å (green dashed curve) and 2.2 Å (brown dashed curve) are shown. Optimum agreement between the experimental and simulated REDOR curves is achieved by assuming a B...P distance of 2.06 Å. All simulations include the experimental  $^{31}\text{P}$  anisotropic shielding parameters ( $\Delta\sigma = 54$  ppm,  $\eta_\sigma = 0.56$ )

of corrections have to be applied. First of all, the REDOR curves are affected by the  $^{31}\text{P}$  chemical shift anisotropy. The corresponding  $\Delta\sigma$  values can be determined independently, usually by  $^{31}\text{P}$  MAS spinning sideband intensity profile analysis, for inclusion in the REDOR simulations. Second,  $\pi$ -pulse imperfections often lead to somewhat attenuated REDOR curves. Such effects can be accounted for in an experimental way by applying a compensation scheme developed in our laboratory [51]. In this compensation scheme a third series of signals as a function of evolution time is recorded, where an extra  $\pi$ -pulse is applied to the non-observed  $I$  nuclei during the middle of the evolution period. If the  $\pi(I)$  and  $\pi(S)$  pulses were all perfect, this would lead to an overall cancellation of the REDOR effect. However, if there are imperfections, a residual attenuation is observed, which is added (with some scaling factor) to the imperfect experimental REDOR curve. The effect of this correction is shown in Figs. 14, 15, and 16. While pulse imperfections mostly affect the size of the difference signal at long evolution times, their effect on the dipolar oscillatory parts are much less pronounced. Figures 14, 15, and 16 also compare the experimental REDOR curves with various simulated curves for different internuclear distances. The oscillating part of the experimental curve is best reproduced by a simulation based on an internuclear distance of 2.06 Å, which differs only slightly from the crystallographic value of 2.038 Å. The systematic deviation can be



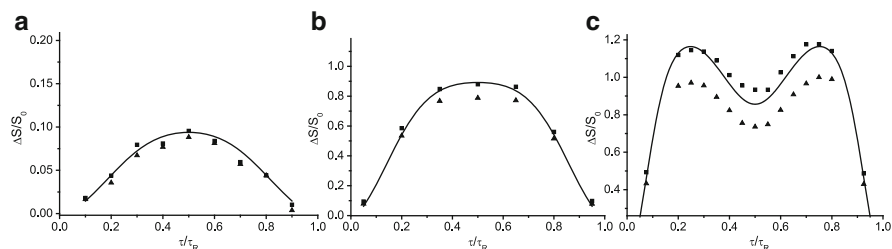


**Fig. 15**  $^{11}\text{B}\{^{31}\text{P}\}$  compensated REDOR curve for **3** (spinning frequency 14 kHz). The SIMPSON simulation assuming a B...P distance of 2.038 Å (crystallographic value, *solid curve*) is shown. Perfect agreement between the experimental and simulated REDOR curve based on the crystallographic B...P distance can only be achieved if a contribution arising from the  $J$ -coupling anisotropy ( $\Delta J$ ) is included in the simulations. The simulation includes the experimental  $^{31}\text{P}$  anisotropic magnetic shielding parameters ( $\Delta\sigma = 54$  ppm,  $\eta_\sigma = 0.56$ ) and an assumed  $J$ -coupling anisotropy of 60 Hz (coincident dipolar and  $J$ -coupling tensors are assumed)

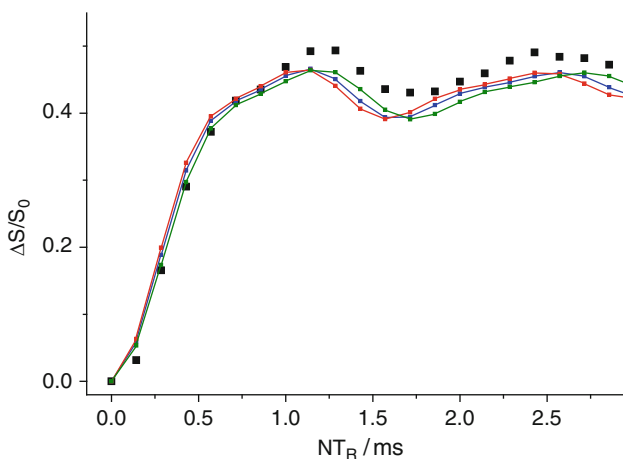
attributed to anisotropic indirect spin–spin ( $\Delta J$ ) interactions. Figure 15 shows that by using the  $J$ -anisotropy as an additional fitting parameter, optimum agreement with the experimental data can be reached.

In a promising alternative to this measurement, known as constant-time REDOR (CT-REDOR), the evolution time (i.e., the number of rotor periods) is held constant and the positions of the dephasing  $\pi$ -pulses are stepped through the rotation period [52]. This method can also be combined with a compensation scheme. Figure 16 shows compensated CT-REDOR curves for **3** with three different evolution times probing characteristic parts of the REDOR curve. The results are essentially the same as those obtained from the standard REDOR experiments. The boron-phosphorus distances extracted from the oscillatory part of the CT-REDOR curve tend to be over-estimated, and the experimental CT-REDOR curves can be correctly reproduced based on the crystallographic B...P distance if non-zero anisotropies of the  $J$ -coupling tensor (with  $\Delta J$  values ranging between 60 and 220 Hz) are included in the simulations. Especially in systems with long spin–lattice relaxation times, short spin–spin relaxation times and dilute nuclei, CT-REDOR experiments lead to significant savings in experimental time as compared to conventional REDOR measurements.

The reverse  $^{31}\text{P}\{^{11}\text{B}\}$  REDOR experiment frequently suffers from signal-to-noise ratio limitations since long  $^{31}\text{P}$ -spin lattice relaxation times often require slow signal accumulation rates. This drawback can be avoided by preparing the  $^{31}\text{P}$  spins via cross-polarization. In practice, a modification of the sequence shown in Fig. 12

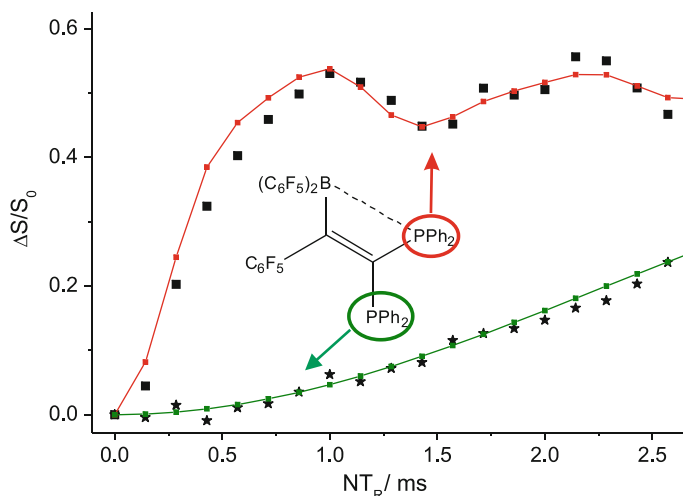


**Fig. 16**  $^{11}\text{B}\{^{31}\text{P}\}$  compensated CT-REDOR curve (filled squares) and CT-REDOR curve without compensation (filled triangles) for **3** with evolution times of 0.2 ms (a), 0.8 ms (b), and 1.6 ms (c), representing the initial region of a REDOR curve (a) and the oscillatory region (c). Perfect agreement between the experimental and simulated CT-REDOR curves based on the crystallographic B...P distance can only be achieved if a contribution arising from the  $J$ -coupling anisotropy ( $\Delta J$ ) is included in the simulations. The solid curves in (a) and (b) show SIMPSON simulations assuming a B...P distance of 2.038 Å and using the experimental  $^{31}\text{P}$  anisotropic magnetic shielding parameters ( $\Delta\sigma = 54$  ppm,  $\eta_\sigma = 0.56$ ) and  $\Delta J = 334$  Hz (coincidence of the dipolar and  $J$ -coupling tensors is assumed). In (c) the best agreement between simulation and experiment is obtained by assuming a B...P distance of 2.038 Å and  $\Delta J = 219$  Hz



**Fig. 17**  $^1\text{H} \rightarrow ^{31}\text{P}\{^{11}\text{B}\}$  CP-REAPDOR curve for the B/P adduct **1** acquired at 7.1 T with a spinning frequency of 14 kHz. SIMPSON simulations assuming different boron-phosphorus distances are shown additionally: red (2.115 Å), blue (2.115 Å and  $\Delta J = 60$  Hz), and green (2.18 Å)

is often used, where the duration of the mixing pulse applied to the  $I$ -spins (here the  $^{11}\text{B}$  nuclei) is extended to about 1/3 of the rotor period. Such extended mixing times during the MAS rotor period lead to significant interchange of the spin populations of the different  $^{11}\text{B}$  Zeeman states, enhancing the overall dipolar dephasing effect. This method, called REAPDOR (rotational echo adiabatic passage double resonance) [53] is now the preferred one for measuring dipolar interactions of spin-1/2 observer-nuclei  $S$  with quadrupolar  $I$ -nuclei. Figures 17 and 18 illustrate applications to **1** and **4**, respectively. Compared to the  $^{11}\text{B}\{^{31}\text{P}\}$  REDOR experiment, the  $\{^1\text{H}\}\text{-}^{31}\text{P}$



**Fig. 18**  $^1\text{H} \rightarrow ^{31}\text{P}\{^{11}\text{B}\}$  CP-REAPDOR curves for the  $^{31}\text{P}$  resonances at 24.5 ppm (filled black squares, P1) and  $-8.3$  ppm (filled black stars, P2), respectively, for the B/P adduct **4** acquired at 7.1 T with a spinning frequency of 14 kHz. The simulations assume B...P distances of 2.04 Å (red curve) and 4.25 Å (green curve), respectively. With the help of these results, the resonance at the higher frequency is unambiguously assigned to the crystallographic phosphorus species interacting with the Lewis acid site

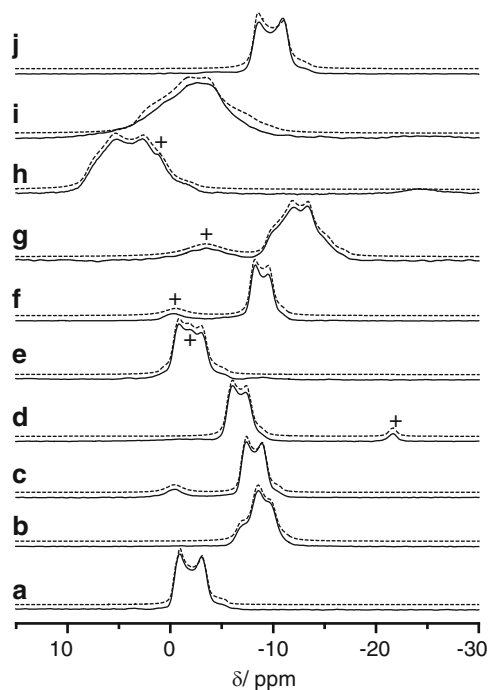
$\{^{11}\text{B}\}$  REAPDOR approach suffers from the disadvantage that the experimental (and simulated) curves are very sensitive to the  $^{11}\text{B}$  nutation frequency and nuclear electric quadrupolar coupling parameters. Hence, both of them must be accurately determined prior to the simulations.

Whichever experimental approach is used, the REDOR/REAPDOR curves have universal character and can be directly used to extract the internuclear distance. Thus this method offers the prospect of characterizing those FLPs for which no crystal structure data are available.

## 4 $^{11}\text{B}$ NMR as a Probe for Structure and Bonding in FLPs

### 4.1 Spectral Features and Observables

Figure 19 summarizes the spectra measured for the different intramolecular adducts investigated in this study. The substituted vinylene-bridged adducts **1–6** show chemical shift values (between  $-7.6$  and  $0.3$  ppm relative to  $\text{BF}_3 \cdot \text{Et}_2\text{O}$ ), and quadrupolar coupling constants (between 1.25 and 1.55 MHz), reflecting a bonding character that can be considered in-between three- and four-coordinate. These values clearly indicate the deviations from the ideal trigonal local geometry as present in **16**. The latter distortions are also readily apparent from the angle sums, obtained



**Fig. 19**  $^{11}\text{B}$  MAS-NMR spectra for P/B FLPs (solid curves) and their corresponding simulations (dashed curves): (a) **1** ( $\text{R} = \text{Mes}$ ,  $\text{R}' = \text{Ph}$ ), (b) **2** ( $\text{R} = \text{Ph}$ ,  $\text{R}' = \text{Ph}$ ), (c) **3** ( $\text{R} = \text{Ph}$ ,  $\text{R}' = n$ -Propyl), (d) **4** ( $\text{R} = \text{Ph}$ ,  $\text{R}' = \text{PPh}_2$ ), (e) **5** ( $\text{R} = \text{Mes}$ ,  $\text{R}' = p$ -Tolyl), (f) **6** ( $\text{R} = \text{Ph}$ ,  $\text{R}' = \text{Me}$ ), (g) **7**, (h) **8**, (i) **9**, and (j) **11**. All spectra were acquired at 11.7 T, except (g) and (i) which were measured at 9.4 T under TPPM-15 proton decoupling. *plus* marks impurities

from both the DFT calculations and the crystal structures (see Table 1). Notably, the local  $\text{C}_3$  axis is maintained, however, as reflected by the near-zero calculated and measured asymmetry parameters (see Table 2). For compound **2**, the two resonances differentiated in the TQMAS experiment (see Fig. 6) reveal that the two boron positions differ slightly ( $C_Q = 1.25$  and  $1.36$  MHz,  $\delta_{cs}^{iso} = -7.6$  and  $-5.9$  ppm). Our unconstrained DFT geometry optimizations yield a boron-phosphorus distance of  $2.05 \text{ \AA}$ , which is in good agreement with the experimentally determined distances within the series of these  $\text{C}_2$  unsaturated  $\text{P}\cdots\text{B}$  adducts.

The situation is somewhat different in compounds **7–9** in which large asymmetry parameters (between 0.4 and 0.6) reveal considerable distortions of the electric field gradient from axial symmetry. These distortions can be attributed to the less symmetric substitution patterns at the boron sites. With regard to the degree of Lewis center interaction, both the isotropic chemical shift and the  $C_Q$ -value for **7** suggest a similar situation as in **1–6**, whereas in the highly reactive FLPs **8** and **9** significantly larger quadrupolar coupling constants are measured (2.1 and 1.8 MHz, respectively). For compound **8** the significantly weaker Lewis center interaction is further confirmed by a comparatively large positive value of  $\delta_{iso}$ . Compound **9**

**Table 1** Comparison of crystallographic B...P distances and bond angle sums around B of the investigated intramolecular adducts with theoretical values from a full DFT geometry optimization on the TPSS level of theory (basis def2-TZVP) using the D3 dispersion correction

Compound	$d_{\text{cryst}} (\text{B} \cdots \text{P})/\text{\AA}$	$d_{\text{calc}} (\text{B} \cdots \text{P})/\text{\AA}$	Angle sum B(cryst.)/ $^{\circ}$	Angle sum B(calc.)/ $^{\circ}$
<b>1</b>	2.115(2)	2.130	344.1(2)	346
<b>2</b>	– <sup>a</sup>	2.046	– <sup>a</sup>	352
<b>3</b>	2.038(3)	2.046	349.2(2)	351
<b>4</b>	2.038(7)	2.047	348.1(5)	350
<b>5</b>	2.094(2)	2.131	342.1(1)	346
<b>6</b>	2.026(2)	2.046	349.0(2)	351
<b>7</b>	2.060(2)	2.079	342.4(2)	345
<b>8</b>	2.188(5) <sup>b</sup> /2.206(5)	2.174	344.2(4)/343.8(4)	344
<b>9</b>	– <sup>a</sup>	2.172 <sup>d</sup>	– <sup>a</sup>	349 <sup>d</sup>
<b>10</b>	– <sup>a</sup>	3.036 <sup>c</sup> ; 2.845 <sup>c</sup>	– <sup>a</sup>	360 <sup>c</sup> ; 360 <sup>c</sup>
<b>11</b>	2.180(6)	2.221	339.9(4)	343
<b>12</b>	2.157(8)	2.231	340.5(5)	345
<b>13</b>	– <sup>a</sup>	2.197 <sup>d</sup>	– <sup>a</sup>	345 <sup>d</sup>
<b>14</b>	3.257(6) <sup>b</sup> /3.232(5)	3.234	326.5(4)/329.0(4)	334
<b>15</b>	3.236(5)	3.222	332.3(3)	334

<sup>a</sup>No crystal structure available

<sup>b</sup>Used within the DFT calculations

<sup>c</sup>For details see [19]

<sup>d</sup>The D3 dispersion correction with Becke Johnson damping (D3-BJ) was used

presents an interesting anomaly. While its calculated  $^{11}\text{B}$  chemical shifts and quadrupolar coupling constants are even larger than those of **8**, in agreement with its experimentally observed high reactivity, the experimental  $^{11}\text{B}$  NMR parameters deviate significantly from the calculated ones. We attribute this effect to a more fluxional character of this compound in the solid state, which may lead to partial averaging of the nuclear electric quadrupolar interaction and may also affect the mean state of bonding reflected by the chemical shift value. Computationally, this fluxionality can be accounted for by including an averaging process over multiple conformations, which will be done in future studies.

Comparable quadrupolar coupling parameters ( $C_Q \sim 1.6$  MHz,  $\eta_Q$  close to zero) are also measured for the intermolecular Lewis acid/base adducts **11**–**13** (see Fig. 20). In the case of compound **13**, where no crystal structure is available, the adduct-like structure is thus inferred from solid-state NMR. Figure 20 also includes the spectra of the phosphirenium-borate zwitterions **14** and **15**, which are formed by an alternative reaction pathway of substituted alkyne-phosphanes with  $\text{B}(\text{C}_6\text{F}_5)_3$ . Here, the bulkier mesityl substituents at the phosphane site inhibit intermolecular adduct formation and addition to the triple bond is preferred. The corresponding spectra (Fig. 20c, d) reflect cases with nearly symmetrical (three identical  $\text{C}_6\text{F}_5$  groups and one unsaturated carbon) ligation patterns at the boron site. The sum of the three C–B–C bond angles involving these  $\text{C}_6\text{F}_5$  ligands is about  $330^{\circ}$  (as determined both crystallographically and computationally), which is close to that of a fully tetrahedral environment with an expected angle sum of  $328^{\circ}$  (see Table 1).

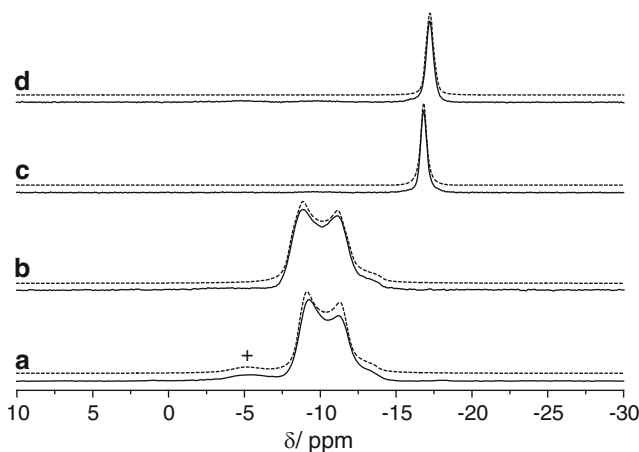
**Table 2** Experimentally and quantum-chemically determined  $^{11}\text{B}$   $\delta_{\text{CS}}^{\text{iso}}$ ,  $C_{\text{Q}}$ , and  $\eta_{\text{Q}}$  values. Chemical shifts are calculated on a DFT B3-LYP/def2-TZVP, electric field gradients on a DFT B97-D/def2-TZVP (modified) level of theory

	$\delta_{\text{CS}}^{\text{iso}}$ (exp.)/ ppm ( $\pm 0.5$ )	$C_{\text{Q}}$ (exp.)/ MHz. $\pm 3\%$	$\eta_{\text{Q}}$ (exp.) $\pm 0.1$	$\delta_{\text{CS}}^{\text{iso}}$ (calc.)/ ppm	$C_{\text{Q}}$ (calc.)/ MHz	$\eta_{\text{Q}}$ (calc.)	Angle ( $V_{zz}$ , B, P)] <sup>°e</sup>
<b>1</b>	0.3 <sup>a</sup>	1.54 <sup>b</sup> /1.55 <sup>a</sup>	0.19 <sup>a</sup>	-0.6	1.58	0.12	22.4
<b>2</b>	-7.6 <sup>a</sup> ; -5.9 <sup>a</sup>	1.25 <sup>a</sup> ; 1.36 <sup>a</sup>	0.18 <sup>a</sup> ; 0.15 <sup>a</sup>	-7.4 <sup>d</sup>	1.43 <sup>d</sup>	0.05 <sup>d</sup>	21.6 <sup>d</sup>
<b>3</b>	-6.6 <sup>a</sup>	1.34 <sup>b</sup> /1.35 <sup>a</sup>	0.15 <sup>a</sup>	-7.6	1.37	0.04	23.2
<b>4</b>	-4.7 <sup>a</sup>	1.31 <sup>b</sup> /1.31 <sup>a</sup>	0.15 <sup>a</sup>	-6.6	1.36	0.05	24.2
<b>5</b>	0.3 <sup>a</sup>	1.55 <sup>b</sup> /1.57 <sup>a</sup>	0.17 <sup>a</sup>	-1.9	1.51	0.13	23.7
<b>6</b>	-7.5 <sup>a</sup>	1.25 <sup>b</sup> /1.27 <sup>a</sup>	0.16 <sup>a</sup>	-9.2	1.33	0.07	22.8
<b>7</b>	-9.1 <sup>b</sup>	1.43 <sup>b</sup>	0.55 <sup>b</sup>	-10.2	1.49	0.53	8.5
<b>8</b>	8.6 <sup>b</sup>	2.10 <sup>b</sup>	0.43 <sup>b</sup>	7.3	2.14	0.39	20.0
<b>9</b>	3.3 <sup>b</sup>	1.8 <sup>b</sup>	0.6 <sup>b</sup>	7.7 <sup>d</sup>	2.23 <sup>d</sup>	0.26 <sup>d</sup>	21.1 <sup>d</sup>
<b>10</b>	60.1 <sup>b</sup> ; 59.0 <sup>b</sup>	4.15 <sup>b</sup> ; 4.25 <sup>b</sup>	0.15 <sup>b</sup> ; 0.2 <sup>b</sup>	56.6 <sup>f</sup> ; 55.4 <sup>g</sup>	4.28 <sup>f</sup> ; 4.16 <sup>g</sup>	0.12 <sup>f</sup> ; 0.14 <sup>g</sup>	66.8 <sup>f</sup> ; 74.7 <sup>g</sup>
<b>11</b>	-7.4 <sup>b</sup>	1.59 <sup>b</sup> /1.63 <sup>a</sup>	0.15 <sup>a</sup>	-8.8	1.60	0.02	0.5
<b>12</b>	-8.0 <sup>b</sup>	1.54 <sup>b</sup>	0.16 <sup>b</sup>	-8.8	1.64	0.02	2.7
<b>13</b>	-7.4 <sup>b</sup>	1.64 <sup>b</sup>	0.24 <sup>b</sup>	-6.0 <sup>d</sup>	1.88 <sup>d</sup>	0.02 <sup>d</sup>	0.5 <sup>d</sup>
<b>14</b>	-16.7 <sup>b</sup>	0.33 <sup>c</sup>	0.30 <sup>c</sup>	-19.5	0.47	0.40	-
<b>15</b>	-16.9 <sup>b</sup>	0.34 <sup>c</sup>	0.30 <sup>c</sup>	-19.9	0.41	0.27	-
<b>16</b>	58.7 <sup>b</sup>	4.26 <sup>b</sup>	0.02 <sup>b</sup>	54.5 <sup>d</sup>	4.04 <sup>d</sup>	0.00 <sup>d</sup>	-

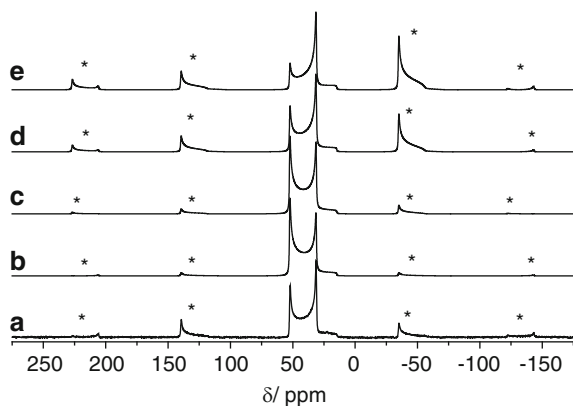
<sup>a</sup>Determined from lineshape analysis of slices from TQMAS experiments<sup>b</sup>Determined from lineshape analysis of  $^{11}\text{B}$  MAS-NMR spectra<sup>c</sup>Determined from  $^{11}\text{B}$  SATRAS spectrum<sup>d</sup>Fully geometry-optimized structures are used within the calculations<sup>e</sup>Orientation of the DFT calculated (B97-D, def2-TZVP (modified)) main principal component of the EFG tensor,  $V_{zz}$ , expressed by the angle between this parameter and the B...P distance vector<sup>f</sup>Fully optimized structure is used (energetically lowest, see ref. [19])<sup>g</sup>Fully optimized structure is used (energetically second lowest, see ref. [19])

Due to the relatively small quadrupolar coupling constants ( $\sim 0.3$  MHz), sharp central transition lineshapes are observed, appearing at the isotropic chemical shifts of  $-16.7$  and  $-16.9$  ppm, respectively. The quadrupolar coupling parameters are most easily extracted from the intensity distribution of the spinning sideband pattern observed for the satellite transitions (see Fig. 3).

Tris(pentafluorophenyl)borane ( $\text{B}(\text{C}_6\text{F}_5)_3$ , **16**) serves as a reference compound for purely three-coordinated environments. The  $^{11}\text{B}$  MAS-NMR spectrum appears at an isotropic chemical shift of 58.7 ppm and its line shape is dominated by second-order quadrupolar effects ( $C_{\text{Q}} = 4.3$  MHz and  $\eta_{\text{Q}} \sim 0$ , see Fig. 4). As previously noted by Bryce et al. for related compounds (e.g., trimesitylborane,  $\text{BMe}_3$ , and triphenyl borate,  $\text{B}(\text{OPh})_3$ ), the second-order quadrupolar perturbation line shape of the MAS center band is significantly affected by a large chemical shift anisotropy [54]. Line shape simulations show the best agreement between the simulated and experimental spectrum by assuming a chemical shift anisotropy parameter  $\Delta\sigma$  of 300 ppm and coincident  $^{11}\text{B}$  electric field gradient and magnetic shielding tensors (see Fig. 21). The zero asymmetry parameter is consistent with a local  $D_{3h}$  symmetry.

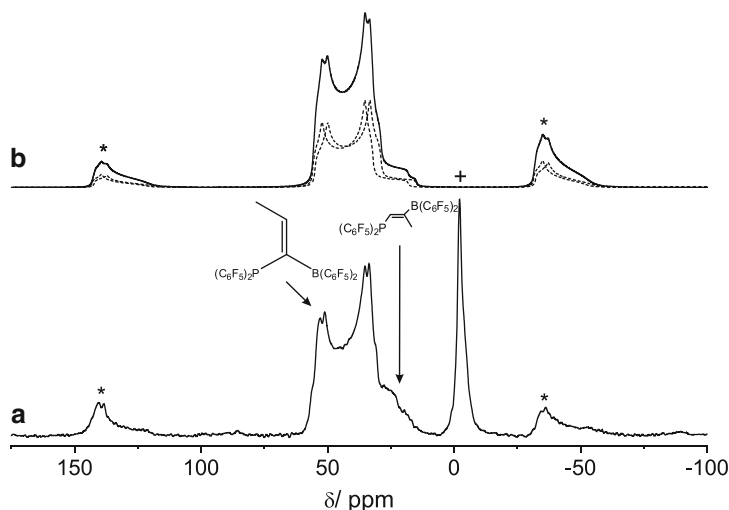


**Fig. 20**  $^{11}\text{B}$  MAS-NMR spectra for the investigated isolated intermediates of the 1,1-carboraboron (*solid curves*) and their corresponding simulations (*dashed curves*): (a) **12**, (b) **13**, (c) **14**, and (d) **15**. All spectra were acquired at 11.7 T. *plus* marks impurities



**Fig. 21**  $^{11}\text{B}$  MAS-NMR spectrum of  $\text{B}(\text{C}_6\text{F}_5)_3$  (**16**) acquired at 11.7 T with a rotation frequency of 14 kHz (a) and simulated spectra using the SIMPSON program package with a  $C_Q$  of 4.259 MHz, an  $\eta_Q$  value of 0.02 and different chemical shift anisotropies:  $\Delta\sigma = 0$  ppm (b),  $\Delta\sigma = 180$  ppm (c),  $\Delta\sigma = 300$  ppm (d), and  $\Delta\sigma = 360$  ppm (e). The intensity distribution of the central transition and the spinning sidebands (marked by *asterisks*) is strongly influenced by the chemical shielding anisotropy

Nearly perfect trigonal-planar local symmetry is also observed for the geminal alkylidene-bridged per-pentafluorophenylated P/B pair **10**. This molecule contains a  $\text{C}_1$ -bridge rather than a  $\text{C}_2$ -bridge, resulting in a larger separation between the Lewis centers. Theoretical calculations lead to P...B distances of 2.84 and 3.04 Å for the two energetically lowest conformers, which is about 0.5 Å larger than in common intramolecular FLPs [19]. The  $^{11}\text{B}$  MAS-NMR spectrum shows two resonances near 60 ppm which clearly reveal two fully trigonal coordinated boron sites in a 1:1 ratio;



**Fig. 22**  $^{11}\text{B}$  MAS-NMR spectrum (a) and simulation of the resonance of the main product (b) for compound **10**. For the main product **10a** two resonances with slightly different chemical shifts and quadrupolar coupling values are observed. The resonance for the second product **10b** is additionally marked. *asterisk* marks spinning sidebands, *plus* an impurity

see Fig. 22. The quadrupolar coupling constants of 4.15 and 4.25 MHz and a magnetic shielding anisotropy of 255 ppm are in agreement with this assessment. Nevertheless, a slight distortion from perfect trigonal geometry due to the different ligation pattern is expressed by asymmetry parameters of 0.15 and 0.20 for both species. We suspect that the observation of two resonances can be attributed to some disorder in the solid as it is also observed for the B/P adduct **2**. Possibly for this reason, no single crystals for an analysis of the crystal structure could be obtained. Yet the calculated structures for this geminal alkylidene-linked B/P pair [19] yields a bond angle sum of  $360^\circ$ , resulting in a quadrupolar coupling constant in excellent agreement with the experimentally observed values (see Table 2).

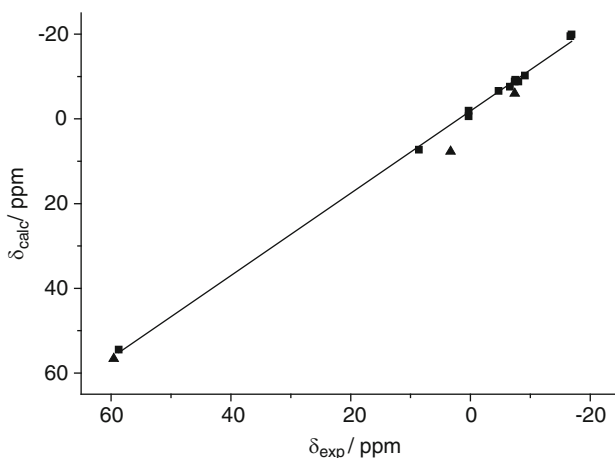
#### 4.2 DFT Calculations of $^{11}\text{B}$ Magnetic Shielding Parameters

The important question is whether the  $^{11}\text{B}$  chemical shifts and quadrupolar coupling parameters can be related to special structural characteristics that define the high reactivity of FLPs which may allow further insights into the reaction behavior of those molecules. Since previous theoretical studies suggest that the electric field generated by the Lewis acid and Lewis base functionality is responsible for the extremely efficient heterolytic splitting of dihydrogen, it is reasonable to assume that the B...P distance is an important structural parameter with which the reactivity can be correlated. This correlation can be explored in terms of B/P bonding details

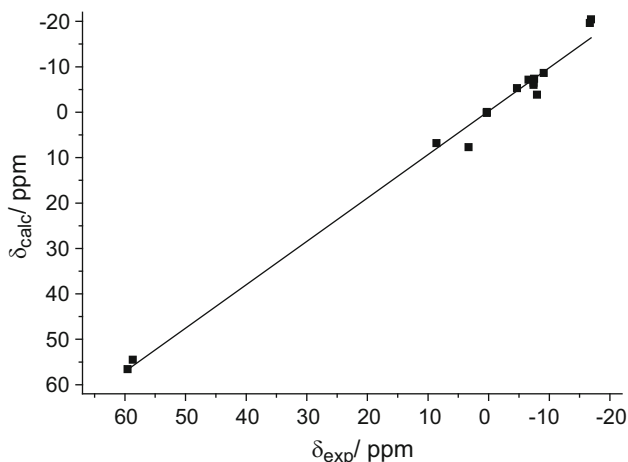


with the help of theoretical calculations of chemical shifts using DFT methods. As shown in Fig. 23, the experimentally determined  $^{11}\text{B}$  isotropic chemical shifts for the intramolecular adducts correlate well with the quantum-chemically determined values on a DFT B3-LYP/def2-TZVP level of theory ( $R^2 = 0.998$ ) based on their crystallographically determined molecular geometries. Likewise, a good correlation is observed between the experimental chemical shifts and the calculated ones based on the geometry-optimized molecules in the gas phase (Fig. 24). This agreement suggests that intermolecular interactions have little influence on the chemical shift values. The notable deviation from this correlation, observed for compound **9** in both plots, can be understood in terms of its fluxional character.

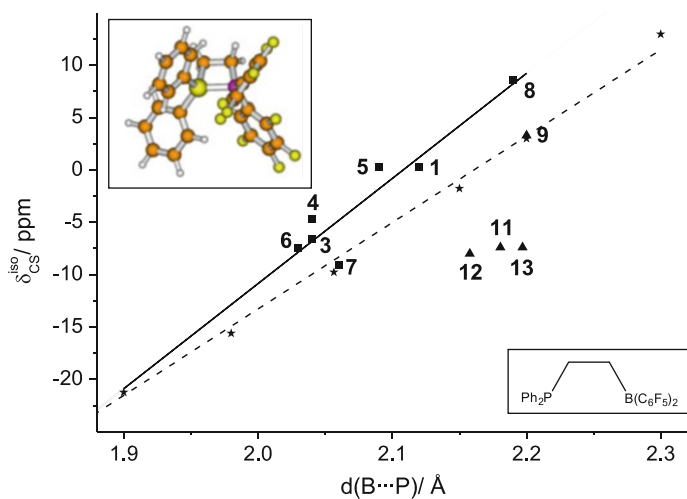
Figure 25 illustrates the high sensitivity of  $^{11}\text{B}$  isotropic chemical shifts to the B...P distances for the series of intramolecular adducts **1–9**: the larger the B...P distances the more high-frequency shifted are the  $^{11}\text{B}$  resonances. This is additionally confirmed by theoretical chemical shift calculations carried out for the model compound  $\text{Ph}_2\text{P-C}_2\text{H}_4\text{-B(C}_6\text{F}_5)_2$ , where the boron-phosphorus distance was changed systematically from 1.9 to 2.3 Å and full relaxation of all other degrees of freedom was allowed. Closely parallel chemical shift trends for the experimental and theoretical data with nearly identical slopes are observed. These studies show clearly that in the intramolecular adducts **1–9** the phosphorus Lewis base site significantly interacts with the boron Lewis acid site as expressed by the very sensitive  $^{11}\text{B}$  chemical shift parameter. Of course, this linear trend is only valid for structurally comparable FLPs with similar ligand types. Compounds **11–13** do not fit the correlation because of their different ligand substitution pattern: here B and P are bound to three aromatic ligands. In addition, compounds **9** and **10** have been omitted from the correlation since no experimental B...P distances are known and/or (in the case of **9**) due to the fluxional character of this compound.



**Fig. 23** Correlation between experimentally and quantum-chemically (B3-LYP, def2-TZVP) determined  $^{11}\text{B}$  chemical shifts (referenced to  $\text{BF}_3\cdot(\text{OEt}_2)$ ) based on the molecular geometries as realized in the crystal structures. Compounds where no crystal structures (*filled triangles*) are known are omitted from the correlation. The linear regression belongs to an  $R^2$  value of 0.998



**Fig. 24** Correlation between experimentally and quantum-chemically (B3-LYP, def2-TZVP) determined  $^{11}\text{B}$  chemical shifts (referenced to  $\text{BF}_3 \cdot (\text{OEt}_2)$ ), based on geometry optimized molecules in the gas phase. The linear regression belongs to an  $R^2$  value of 0.97 and exhibits a slope of 0.99

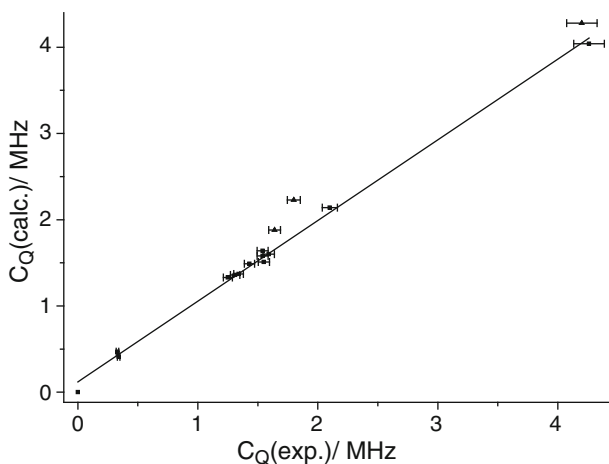


**Fig. 25** Correlation of experimental  $^{11}\text{B}$  chemical shifts with crystallographically determined (in the case of compounds **9** and **13**  $^{11}\text{B}\{^3\text{1P}\}$  REDOR data were used)  $\text{B}\cdots\text{P}$  distances. Stars denote calculated chemical shifts (BP-86/ def-TZVP level of theory) for a model compound (see inset) as a function of  $\text{B}\cdots\text{P}$  distance. The solid line represents a linear regression for the experimental values ( $R^2 = 0.85$ , filled squares). Compounds **9** and **11–13** are omitted from the correlation because of the fluxional character in the case of **9** and the different ligand substitution pattern of **11–13** (filled triangles). The dashed line shows the linear regression for the calculated model system ( $R^2 = 0.99$ )

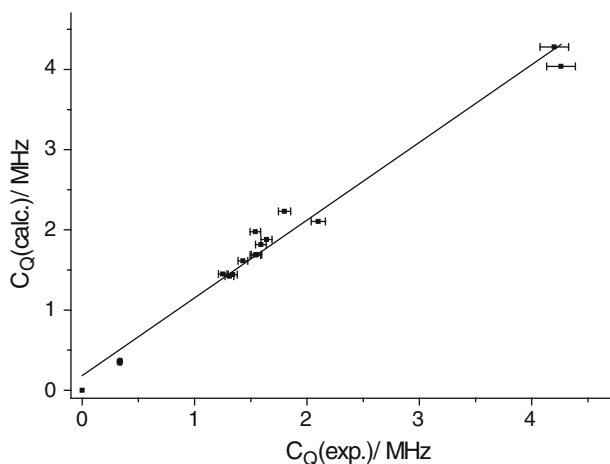
### 4.3 DFT Calculations of Electric Field Gradients at Boron

The nuclear electric quadrupolar coupling parameters were calculated on a GGA level of theory (functional B97-D) with the def2-TZVP basis set which is modified in such a way that tighter basis functions at the boron atom extracted out of Dunning's correlation consistent basis set are included (the full AO basis set is given in the Supplemental Materials section of [5]). This accurate description of both the valence and the core shell electrons is particularly useful since, in the case of main group elements such as boron, the EFG is dominated by the outer core and valence shell electronic distribution [55]. All of these theoretical studies are based on either crystallographic information (Fig. 26) or calculations in the gas phase (Fig. 27).

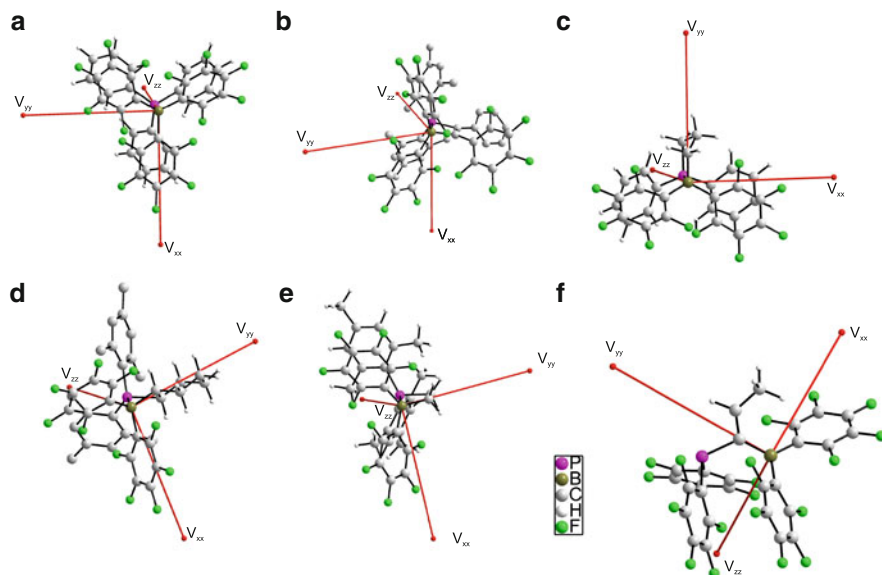
For the reference compound **16** the calculated  $C_Q$  value of 4.04 MHz and the asymmetry parameter  $\eta_Q = 0$  are in good agreement with the experimental data. Overall, Figs. 26 and 27 indicate excellent agreement between the experimental values and those calculated from either crystal data or optimized molecular structures in the gas phase, again with the notable exception of compound **9**. In the case of the substituted vinylene-linked intramolecular adducts the  $\eta_Q$  values range between 0.04 and 0.13. These values are consistent with a local boron geometry that is still close to trigonal as is also expected from the crystallographically determined bond angle sums of about 340–350°. Figure 28 visualizes the



**Fig. 26** Correlation between experimentally (from  $^{11}\text{B}$  MAS-NMR experiments) and theoretically (DFT, B97-D, def2-TZVP (modified)) determined  $C_Q$  values based on the molecular geometries as realized in the crystal structures. The linear regression for those compounds for which crystal structure data are available and **16** (filled squares) yields a slope of 0.94 and an  $R^2$  value of 0.996. The deviation from unity is partly attributed to uncertainties in the experimental values (estimated at  $\pm 3\%$ , see error bars). Data for compounds with unknown crystal structures are additionally included as filled triangles



**Fig. 27** Correlation between experimentally (from  $^{11}\text{B}$  MAS-NMR experiments) and theoretically (DFT, B97-D, def2-TZVP (modified)) determined  $C_Q$  values for the geometries obtained by a full geometry optimization for the compounds in the gas phase. The linear regression yields a slope of 0.97 and an  $R^2$  value of 0.98. The deviation from unity is partly attributed to uncertainties in the experimental values (estimated at  $\pm 3\%$ , see *error bars*)



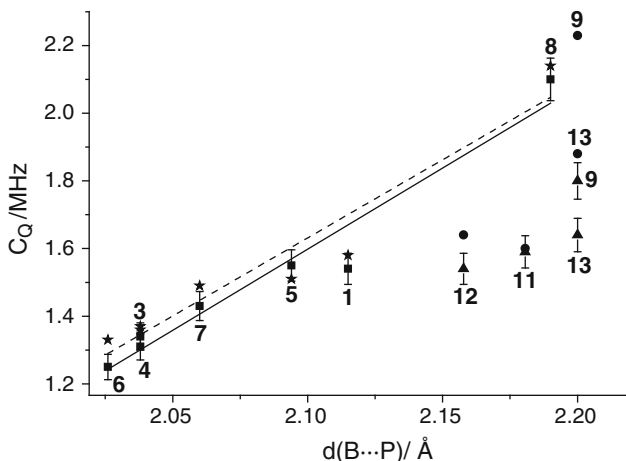
**Fig. 28** Representative tensor orientations of the  $^{11}\text{B}$  electric field gradients for **11** (a), **1** (b), **7** (c), **8** (d), **9** (e), and **10** (the energetically lowest conformer is used, see [19]) (f) obtained by DFT calculations on a GGA level (B97-D) with a slightly modified def2-TZVP basis set (for details see [5]). In nearly all cases a slight deviation from parallel alignment between the largest principal component  $V_{zz}$  and the B–P vector is observed (for detailed values see Table 2)

calculated EFG principal tensor components in the molecular axis frame. The presence of a  $C_3$ -axis results in identical components (per definition  $V_{xx}$  and  $V_{yy}$ ) within the coordination plane while the largest component ( $V_{zz}$ ) lies parallel to the  $C_3$  axis, i.e., perpendicular to the molecular plane. For the substituted vinylene adducts **1–6** the angle between the  $B\cdots V_{zz}$  and the B-P vectors is about  $20^\circ$ , which clearly illustrates the strong influence of the interaction between the Lewis centers on the  $^{11}\text{B}$  electric field gradients. In the case of the very reactive FLPs **7, 8, and 9**,  $V_{zz}$  is similarly oriented, albeit the angles tend to be slightly smaller. Possibly this may account for the higher FLP-characteristic reactivity of these intramolecular adducts. In contrast, for the unreactive classical Lewis acid/base adducts **11, 12, and 13**,  $V_{zz}$  is aligned fully parallel to the B-P director, which in this case is a direct covalent bond. The theoretical work performed by Grimme and co-workers emphasizes the importance of the electric field generated by the Lewis acid and Lewis base functionality which is responsible for the fast heterolytic cleavage of dihydrogen [2]. From the viewpoint of the boron site our analysis may describe the orientation of this electric field and therefore help us to understand why the intramolecular adducts are much more reactive than the typical intermolecular adducts despite comparable  $B\cdots P$  distances (in most cases even shorter distances are observed for the FLPs). For the intramolecular P/B pairs the constrained geometry leads to weaker  $B\cdots P$  interactions and the reactive pocket (determined by the electric field generated) is more easily accessible since the electric field gradient points away from the B-P axis. These considerations also allow the assumption that a completely linear geometry of the P–H–B unit is not necessarily an essential requirement for an efficient activation of  $\text{H}_2$  with the FLP [2].

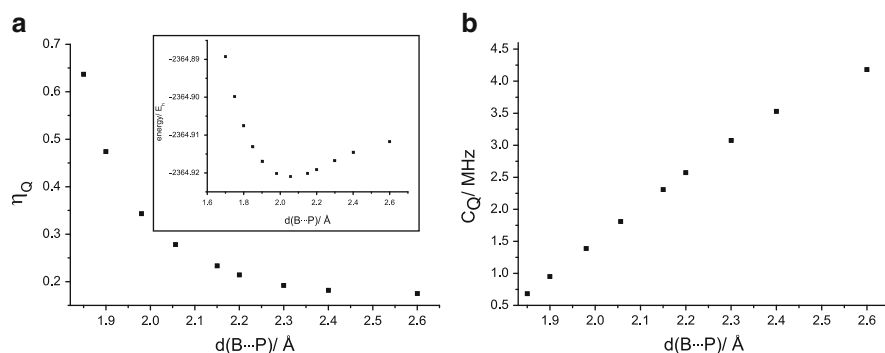
FLP **10** shows a completely different behavior. Here the electric field gradient points significantly away from the B-P director. For the two energetically lowest structures [19] angles of about  $70^\circ$  are calculated, in agreement with a geometry expected in the complete absence of  $B\cdots P$  interactions. The same conclusion was drawn from the  $^{11}\text{B}$  isotropic chemical shift values.

Figure 29 explores the correlation between the experimental  $C_Q$  values and the  $B\cdots P$  distances. For compounds **1–8** an excellent linear correlation ( $R^2 = 0.94$ ) is observed, indicating that the value of the  $^{11}\text{B}-C_Q$  is a rather sensitive parameter measuring the strength of interaction between the Lewis acid and base functionalities: larger  $B\cdots P$  distances are correlated with larger  $C_Q$  values. For compound **10** the measured  $C_Q$  value indicates that the interaction between Lewis acid and Lewis base is completely suppressed. These findings are again confirmed theoretically on the model system  $\text{Ph}_2\text{P}-\text{C}_2\text{H}_4-\text{B}(\text{C}_6\text{F}_5)_2$ . The  $C_Q$  values computed as a function of  $B\cdots P$  distance over the range 1.85–2.6 Å (followed by full optimization of all other degrees of freedom), are well-correlated with this parameter. Larger boron-phosphorus distances lead to larger  $C_Q$  values and smaller asymmetry parameters, indicating smaller deviations from the trigonal coordination geometry (see Fig. 30).

Overall, these results show that intramolecular interactions among the Lewis acid and base functionalities do influence the bonding geometry of the boron site, which is directly visualized by the solid-state NMR parameters  $\delta_{\text{iso}}$  and  $C_Q$ , as well as by the angle between the B-P director and the EFG principal axis at the boron site. The reactivity differences observed between the intramolecular FLPs **1–9** can

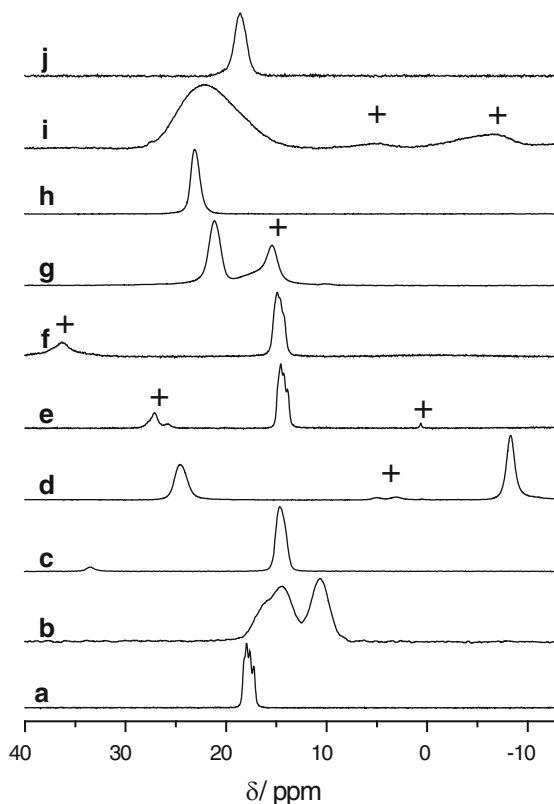


**Fig. 29** Correlation between experimentally determined (*filled squares*) and DFT-calculated (B97-D/ def2-TZVP (modified), *filled stars*)  $^{11}\text{B}$   $C_Q$  values and B...P distances: larger values result in larger  $C_Q$  values due to a lesser degree of distortion from trigonal boron bonding geometry. The *error bars* indicate an experimental uncertainty of about 3%. The *straight line* shows a linear regression for the experimental values ( $R^2 = 0.94$ ), the *dashed line* a linear regression for the DFT-calculated values ( $R^2 = 0.91$ ). Experimental (*filled triangles*) and DFT-calculated (*filled circles*) data points for compounds **9** and **11–13** are omitted from the correlation (see text). In the case of compounds **9** and **13** B...P distances from  $^{11}\text{B}\{^{31}\text{P}\}$  REDOR experiments were used



**Fig. 30** Calculated quadrupolar coupling parameters (B97-D, def2-TZVP) for the model compound  $\text{Ph}_2\text{P}-\text{C}_2\text{H}_4-\text{B}(\text{C}_6\text{F}_5)_2$  under variation of the B...P distance from 1.8 to 2.6 Å. (a) Asymmetry parameter,  $\eta_Q$ ; (b) quadrupolar coupling constant  $C_Q$ . The *inset* in (a) shows the potential energy curve with a minimum at 2.06 Å for the TPSS-D3/def2-TZVP level of theory

thus be understood on the basis of the differences in the bonding interactions between the Lewis centers. Owing to significantly weaker intramolecular Lewis pair formation in FLPs **7–10** these materials are much more reactive than compounds **1–6**.



**Fig. 31**  $^{31}\text{P}\{^1\text{H}\}$  CPMAS-NMR spectra acquired at 9.4 T with a spinning frequency of 10 kHz applying the TPPM-15 decoupling scheme for the following adducts: (a) **1** (R = Mes, R' = Ph), (b) **2** (R = Ph, R' = Ph), (c) **3** (R = Ph, R' = *n*-Propyl), (d) **4** (R = Ph, R' = PPh<sub>2</sub>), (e) **5** (R = Mes, R' = *p*-Tolyl), (f) **6** (R = Ph, R' = Me), (g) **7**, (h) **8**, (i) **9**, and (j) **11**. All the spectra were acquired at 9.4 T under TPPM-15 proton decoupling. *plus* marks impurities. Chemical shifts are relative to 85% H<sub>3</sub>PO<sub>4</sub>

## 5 $^{31}\text{P}$ NMR as a Probe of Structure and Bonding in FLPs

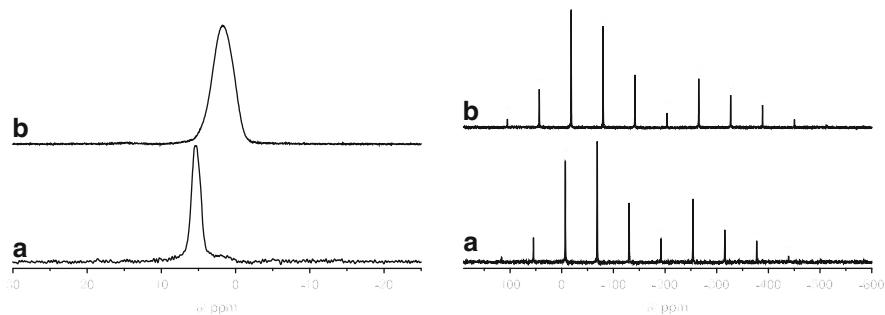
### 5.1 Spectroscopic Features and Observables

Figure 31 summarizes the  $^{31}\text{P}\{^1\text{H}\}$  CPMAS-NMR spectra of the intramolecular adducts **1–9** and of the intermolecular Lewis acid/base adduct **11**, and their spectroscopic parameters determined from them are given in Table 3. In general, the intramolecular adduct formation is evidenced by a narrow chemical shift window between approximately 25 and 5 ppm. In the case of the P/B pair **2**, two different

**Table 3** Isotropic chemical shifts (vs 85%  $H_3PO_4$ ), indirect  $^{10/11}B-^{31}P$  spin-spin coupling parameters, residual dipolar couplings<sup>d</sup> at 7.1 T,<sup>b</sup> at 9.4 T) and magnetic shielding anisotropy parameters (determined by lineshape analysis of slow-spinning MAS experiments) for compounds **1–15**. The calculated values of  $J$ ,  $\Delta\sigma$ , and  $\eta_\sigma$  result from DFT calculations (B3-LYP, TZVP). Calculated chemical shifts (DFT, B3-LYP, def2-TZVP) are referenced to phosphoric acid. <sup>c</sup>Determined from  $^{11}B\{^{31}P\}$  heteronuclear  $J$ -Resolved experiments (see text). <sup>d</sup>Fully optimized structure is used (second energetically lowest, see [19]). <sup>e</sup>Fully optimized structure is used (second energetically lowest, see [19])

$\delta_{iso}/ppm$	$J(^{31}P-^{11}B) \pm 5/Hz$	$J(^{31}P-^{10}B)/Hz$	$J(^{31}P-^{11}B)/Hz$	$J(^{31}P-^{11}B)/Hz$ (calc.)	$d$ $(^{31}P-^{11}B) \pm 3/Hz$	$d$ $(^{31}P-^{10}B) \pm 3/Hz$	$\delta_{iso}/ppm$ (calc.)	$ \Delta\sigma /ppm$	$\eta_\sigma$	$ \Delta\sigma /ppm$	$\eta_\sigma$
<b>1</b> 17.8	54.5	18.0	51.1	51.1	-5.5 <sup>a</sup> (-4.1 <sup>b</sup> )	-11.5 <sup>a</sup> (-8.6 <sup>b</sup> )	24.1	90.0	(0.40)	90.0	(0.40)
<b>2</b> ~15.3/10.7	-	-	47.1	47.1	-	-	17.0	60.6	(0.19)	60.6	(0.19)
<b>3</b> 14.5	52.0, 52.9 <sup>c</sup>	17.2	51.4	51.4	-6.0 <sup>a</sup> (-4.5 <sup>b</sup> )	-12.5 <sup>a</sup> (-9.4 <sup>b</sup> )	16.5	59.7	(0.32)	59.7	(0.32)
<b>4</b> 24.5/-8.3	51.0 <sup>c</sup>	-	52.4	52.4	-	-	23.6/-10.1	71.1/72.9	(0.66/0.89)	71.1/72.9	(0.66/0.89)
<b>5</b> 14.4	52.9	17.5	56.1	56.1	-6.0 <sup>a</sup> (-4.5 <sup>b</sup> )	-12.5 <sup>a</sup> (-9.4 <sup>b</sup> )	19.3	104.9	(0.48)	104.9	(0.48)
<b>6</b> 14.7	52.0	17.2	53.2	53.2	-6.0 <sup>a</sup> (-4.5 <sup>b</sup> )	-12.5 <sup>a</sup> (-9.4 <sup>b</sup> )	11.8	66.7	(0.51)	66.7	(0.51)
<b>7</b> 21.1	48.9 <sup>c</sup>	-	45.5	45.5	-	-	28.8	60.6	(1.00)	60.6	(1.00)
<b>8</b> 23.1	-	-	28.7	28.7	-	-	32.0	80.0	(0.37)	80.0	(0.37)
<b>9</b> 21.7	-	-	18.0	18.0	-	-	30.6	61.3	(0.81)	61.3	(0.81)
<b>10</b> -60.4;	-	-	-3.6 <sup>d</sup> , 28.9 <sup>e</sup>	-	-	-	-44.4 <sup>d</sup> ;	86.9 <sup>d</sup> ; 90.2 <sup>e</sup>	(0.91 <sup>d</sup> ;	86.9 <sup>d</sup> ; 90.2 <sup>e</sup>	(0.91 <sup>d</sup> ;
-64.3	-	-	-	-	-	-	-27.6 <sup>e</sup>	0.74 <sup>e</sup>		-27.6 <sup>e</sup>	
<b>11</b> 18.6	46.6 <sup>c</sup>	-	49.9	49.9	-	-	28.1	5.4	(0.28)	5.4	(0.28)
<b>12</b> 5.3	-	-	50.9	50.9	-	-	1.4	43.2	(0.48)	43.2	(0.48)
<b>13</b> 1.7	52.6 <sup>c</sup>	-	34.1	34.1	-	-	13.1	37.0	(0.98)	37.0	(0.98)
<b>14</b> -130.5	-	-	-	-	-	-	-161.1	478.2	(0.16)	478.2	(0.16)
<b>15</b> -141.8	-	-	-	-	-	-	-156.5	485.6	(0.15)	485.6	(0.15)

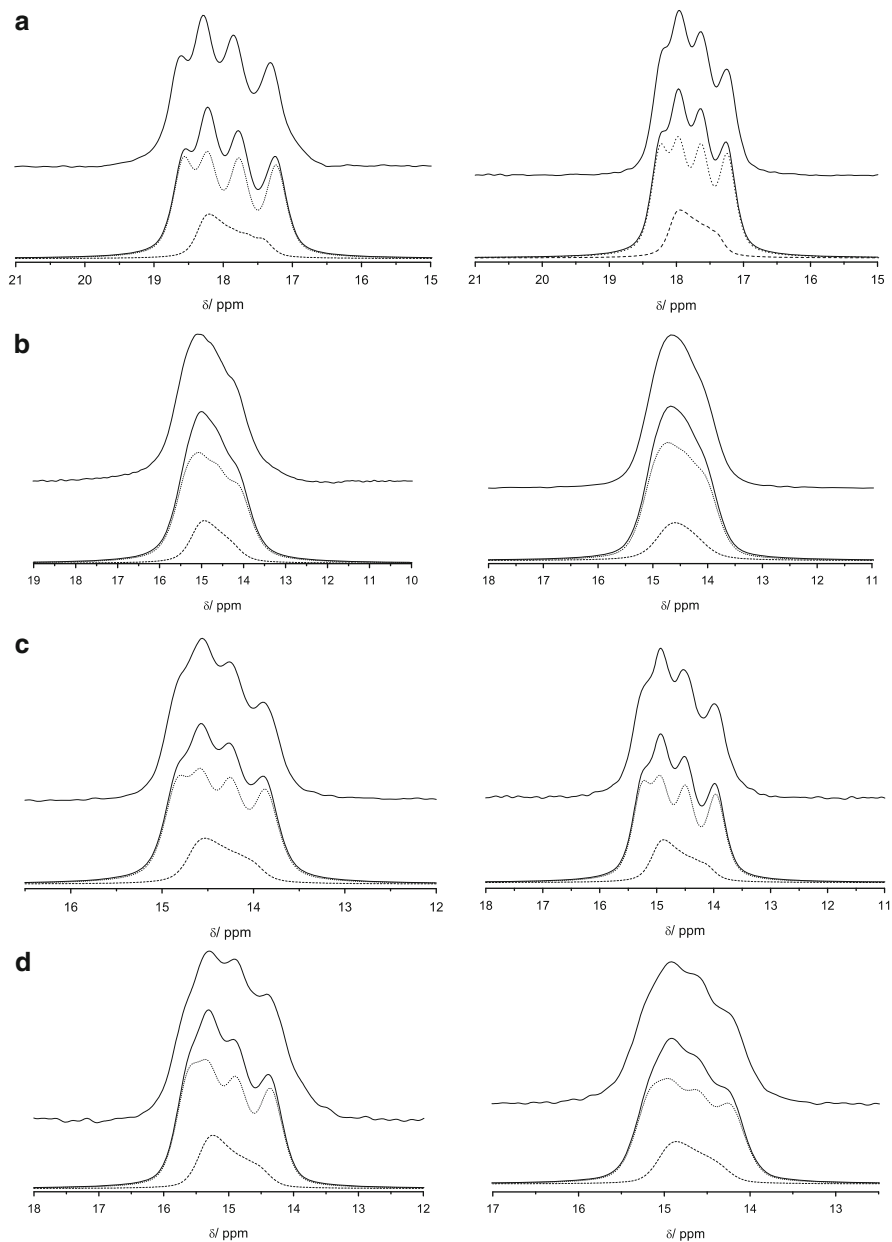




**Fig. 32** *Left:*  $^{31}\text{P}\{^1\text{H}\}$  CPMAS-NMR spectra of the intermolecular phosphane–borane adducts **12** (a) and **13** (b) acquired at 9.4 T under TPPM-15 decoupling and using a spinning frequency of 10 kHz. *Right:*  $^{31}\text{P}\{^1\text{H}\}$  CPMAS-NMR spectra of the phosphirenium-borate zwitterions **14** (a) and **15** (b) acquired under similar experimental conditions. Spinning sidebands are labelled by asterisks

resonances with slightly different chemical shifts are observed. For the crystallographically uncharacterized intermediate **13** the  $^{31}\text{P}$  spectra also clearly point to an adduct rather than a phosphirenium species, consistent with the results from  $^{11}\text{B}$  NMR. Compared to **12**, the  $^{31}\text{P}$  resonance of **13** is significantly broadened, suggesting solid-state disorder. Very different  $^{31}\text{P}$  NMR parameters are observed for the 1,1-carboration intermediate **14**. Here, the constrained geometry results in a strongly negative isotropic chemical shift ( $-130.5$  ppm) and a large chemical shift anisotropy (450 ppm). Surprisingly, a small asymmetry parameter  $\eta_\sigma$  of 0.05 is measured (and calculated) suggesting a near-axially symmetric magnetic shielding tensor. Based on the  $^{31}\text{P}$  NMR spectrum, compound **15** possesses an analogous structure (see Fig. 32). Overall, the NMR parameters of these phosphirenium zwitterions distinguish these phosphorus surroundings unequivocally from those of the P/B adducts.

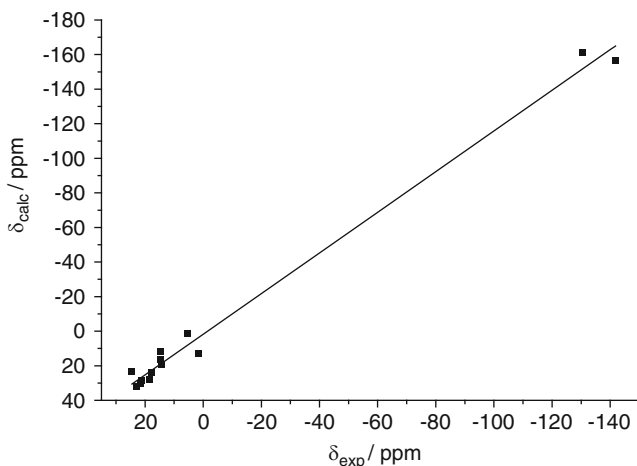
Finally, the  $^{31}\text{P}$  spectra of the intramolecular adducts **1**, **3**, **5**, and **6** show a characteristic multiplet structure which is attributed to indirect  $^{31}\text{P}$ - $^{10}\text{B}/^{11}\text{B}$  spin–spin couplings as discussed in Sect. 2.5. Figure 33 compares the experimental and simulated spectra obtained on the basis of this effect. While no such splittings are observable for the other FLPs, heteronuclear spin–spin couplings appear to dominate the experimental NMR line widths of these compounds as well, as the latter are found to be either independent of or tend to increase with decreasing magnetic field strength. A notable exception is compound **9** whose extremely broad  $^{31}\text{P}$  MAS-NMR spectrum increases with increasing field strength, suggesting that it is governed either by a chemical shift distribution or by dynamic effects. This is consistent with solid-state disorder of either static or dynamic origin as suspected from the fluxional character of this compound.



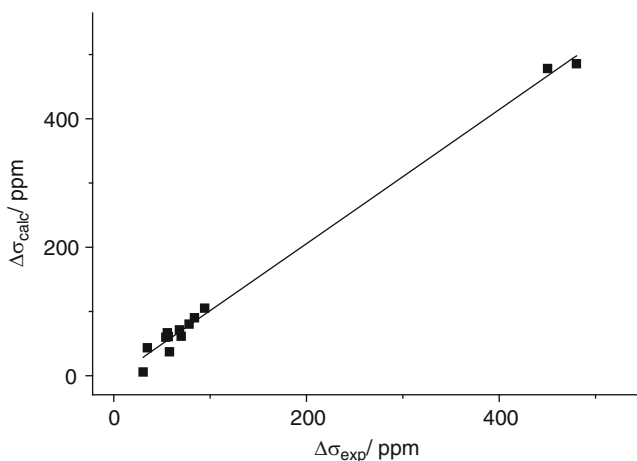
**Fig. 33** *Top:*  $^{31}\text{P}\{^1\text{H}\}$  CPMAS-NMR spectra acquired at 7.1 T with the SW-TPPM-15 decoupling scheme (*left*) and at 9.4 T with the TPPM-15 decoupling sequence (*right*) for compound **1** (**a**), **3** (**b**), **5** (**c**), and **6** (**d**). *Bottom:* Peak deconvolution (*solid curve*) consisting of  $^{31}\text{P}$ - $^{11}\text{B}$  coupling (*dotted curve*) and  $^{31}\text{P}$ - $^{10}\text{B}$  coupling (*dashed curve*)

## 5.2 DFT-Calculations of $^{31}\text{P}$ Magnetic Shielding Parameters

DFT calculations of  $^{31}\text{P}$  magnetic shielding tensors conducted at the B3-LYP/def2-TZVP level of theory show reasonably linear correlations between calculated and experimental isotropic chemical shifts (Fig. 34) and magnetic shielding anisotropies (Fig. 35), albeit with considerably more data scatter than in the case of the  $^{11}\text{B}$  NMR observables. Calculations on the model system  $\text{Ph}_2\text{P-C}_2\text{H}_4\text{-B}(\text{C}_6\text{F}_5)_2$  indicate a moderate, linear increase of the chemical shift by about 12 ppm as the B...P distance is increased over the range 190–230 pm and similar trends are observed for the magnetic shielding anisotropies (data not shown). For compound **4** the  $^{31}\text{P}$  chemical shifts calculated for P1 (*cis* to the B–C bond) and P2 (*trans*) are 23.6 ppm and –10.1 ppm, respectively, thus confirming the REAPDOR based peak assignment (Fig. 18). Thus, these  $^{31}\text{P}$  magnetic shielding parameters are potentially useful probes for assessing the degree of frustration as well. The observed and calculated spectroscopic parameters indicate, however, that isotropic  $^{31}\text{P}$  chemical shifts tend to be less suitable as a measure of the degree of electronic B...P interactions, as their detailed values prove to be rather sensitive to the chemical nature of the substituents at the phosphorus site. This is also true for the magnetic shielding anisotropy, which ranges between 50 and 85 ppm within the series of the closely related compounds **1–9**. Table 3 suggests that increased bonding overlap between the two Lewis centers tends to reduce the anisotropy. This correlation does not, however, include the intermolecular compounds **11–13**, whose symmetric bonding environment produces rather small  $\Delta\sigma$  values (near 30 ppm), despite weaker B...P interactions.



**Fig. 34** Correlation between experimentally and quantum-chemically (B3-LYP, def2-TZVP) determined  $^{31}\text{P}$  chemical shifts (referenced to  $\text{H}_3\text{PO}_4$ ). The linear regression belongs to an  $R^2$  value of 0.99. Compounds **2** and **10** are omitted from the correlation since the assignment of the two resonances observed experimentally is not clear



**Fig. 35** Correlation between experimentally and quantum-chemically (B3-LYP, TZVP) determined  $^{31}\text{P}$   $\Delta\sigma$  values. The linear regression belongs to an  $R^2$  value of 0.99. Compounds **2** and **10** are omitted from the correlation since the assignment of the two resonances observed experimentally is not clear

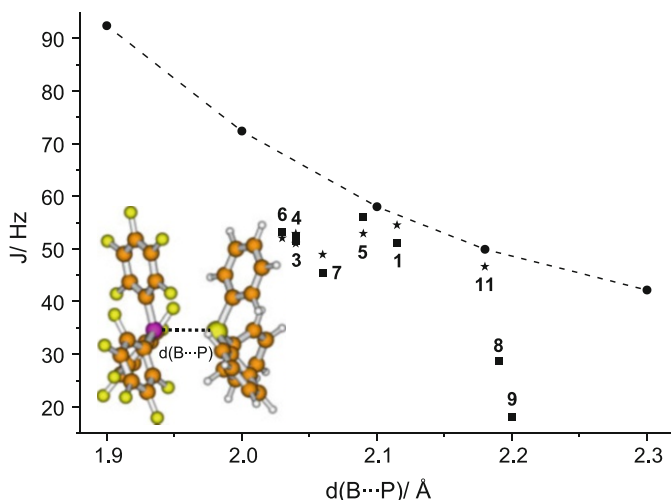
### 5.3 DFT Calculations of $^{10}\text{B}/^{11}\text{B} \cdots ^{31}\text{P}$ Indirect Spin–Spin Couplings

As already indicated, the relatively large indirect spin–spin couplings are attributed to  $^1J$ -couplings between the Lewis acidic borane and Lewis basic phosphane functionality. Since  $J$ -couplings between two nuclei are transmitted via electrons in a bond, two  $J$ -coupling pathways are in principle possible in the substituted vinylene-bridged B/P adducts:  $^1J$ -coupling via weak, but non-negligible covalent bonding between the Lewis functionalities or a  $^3J$ -coupling via the olefinic backbone. We can decide between these alternatives by analyzing the case of compound **4**, which has two carbon-phosphorus bonds oriented *cis* and *trans* with respect to the carbon boron bond. If the  $^1J$ -interaction pathway were absent and only a  $^3J$ -coupling were observed, the *trans* coupling to P(2) should be the stronger one. In contrast, our experimental result on **4** shows the opposite to be the case, despite the fact that the peak splittings are not resolved (most probably due to a lower sample crystallinity). The resonance of P(1), which is in *cis*-orientation to the Lewis acid site possesses a much larger linewidth than the resonance of P(2) oriented *trans* to the boron site (209 vs 119 Hz at 9.4 T). This difference can be attributed to a larger (unresolved)  $^1J$  coupling in the case of P(1). For answering this question satisfactorily from a theoretical point of view, DFT calculations of scalar coupling constants have been performed on a hybrid DFT level of theory using the functional B3-LYP and the sufficiently large triple zeta basis TZVP. For **1** these calculations lead to a  $^{11}\text{B}$ - $^{31}\text{P}$   $J$ -coupling constant of 51.1 Hz which is in excellent agreement

with the experimentally determined value (54.5 Hz). Such values are comparable in magnitude to  ${}^1J$  ( ${}^{11}\text{B}$ - ${}^{31}\text{P}$ ) values measured in solution for the adduct of  $\text{PPh}_3$  and  $\text{BH}_3$  (approximately 60 Hz) [56, 57]. Finally for the classical Lewis acid/base adduct **11** in which the remote possibility of a  ${}^3J$ -coupling is clearly excluded, the calculated  ${}^1J$ ( ${}^{31}\text{P}$ - ${}^{11}\text{B}$ ) is 52.4 Hz, in good agreement with the experimental value determined by heteronuclear  $J$ -resolved spectroscopy (46.6 Hz, see Fig. 9). Certainly the  ${}^3J$ -coupling pathway will contribute to the experimental value. For the *trans* isomer of **1** we calculate  ${}^3J$ ( ${}^{31}\text{P}$ - ${}^{11}\text{B}$ ) = 18.3 Hz, which corresponds to a maximum value based on the Karplus curve (dihedral angle  $\sim 180^\circ$ ) [58]. A significantly smaller value of  ${}^3J$  would be expected via the *cis*-pathway. Based on all these considerations it is safe to conclude that the observed peak splittings are dominated by  ${}^1J$ -rather than  ${}^3J$ -couplings between  ${}^{31}\text{P}$  and the boron nuclides.

Therefore a residual electron density between the Lewis acid and Lewis base site evidenced by solid-state NMR highlights the communication between both Lewis centers even in frustrated Lewis-pairs. It is reasonable to assume that the  ${}^1J$ -values should correlate with the boron-phosphorus distance as the most important structural parameter defining the reactivity of those molecules. We illustrate this distance-dependence with theoretical calculations of spin-spin coupling constants as a function of the boron-phosphorus distance for the intermolecular adduct **11**. In our DFT calculations (B3-LYP/TZVP) we systematically change the B...P distance within the geometry of the crystal structure and calculate  ${}^1J$ ( ${}^{11}\text{B}$ - ${}^{31}\text{P}$ ) for some characteristic points (see Fig. 36). As expected, a decrease is observed with increasing boron-phosphorus distance. In principle the coupling constant could be used as an NMR parameter probing the electronic interactions between the Lewis centers and describing “frustration” in an FLP. We have to note, however, that direct observation in the  ${}^{31}\text{P}$  NMR lineshape is often precluded by overlapping line broadening mechanisms and one would have to resort to heteronuclear  $J$ -resolved spectroscopy. Moreover, as illustrated by the calculated  $J$  values (see Table 3), while these values do show a general dependence on the boron-phosphorus distance, significant scattering is observed pointing to the high sensitivity of  $J$ -couplings towards electronic changes at the Lewis centers due to different kind of ligands or bridging units.

Our conclusion regarding a weak covalent B...P interaction is in accordance with the computed Wiberg bond order indices (WBIs) [59]. A bond order index of about one indicates the presence of a mostly covalent single bond while values close to zero point to ionic or van-der-Waals interactions. In the case of the vinylene-bridged intramolecular adducts the WBIs range from 0.73 to 0.91 in the Cartesian AO basis and from 0.72 to 0.82 in the natural atomic orbital (NAO) basis (see Table 4). While the WBIs in the AO basis do not correlate well with the B...P internuclear distances, a much more consistent trend for them is found in the NAO basis, even though individual differences are rather small (see Fig. 37). The covalent bonding interaction is further probed by a Natural Bond Orbitals (NBO) analysis [60, 61] which reveals a real bond between the phosphorus and boron moieties (see Table 4) in all of the intramolecular B/P FLPs investigated (except **10**). The percentage of the NBO on the natural atomic hybrid localized at B correlates



**Fig. 36** DFT calculated coupling constants  $^1J(^{31}\text{P}-^{11}\text{B})$  (B3-LYP, TZVP) for the Lewis acid/base adduct **11** as a function of B...P distances in the framework of the crystal structure (*filled circles*). The data show a strong distance-dependence of the coupling constants. *Filled stars* show experimentally determined coupling constants in the solid state, while *filled squares* represent DFT-calculated values (B3-LYP, TZVP) for the same compounds in the gas phase

**Table 4** Calculated Wiberg bond order indices (WBI) and results of a Natural Bond Orbital (NBO) analysis of the B...P bond for the bridged B/P adducts illustrating a significant covalent interaction

	WBI (AO basis) <sup>a</sup>	WBI (NAO basis) <sup>b</sup>	Occupancy (bond B...P) <sup>b</sup>	Percentage of the NBO on the natural atomic hybrid localized at P/% <sup>b</sup>	Percentage of the NBO on the natural atomic hybrid localized at B/% <sup>b</sup>
<b>1</b>	0.91	0.78	1.89	63.8	36.2
<b>2</b>	0.77 <sup>c</sup>	0.79 <sup>c</sup>	1.88 <sup>c</sup>	62.0 <sup>c</sup>	38.0 <sup>c</sup>
<b>3</b>	0.73	0.81	1.89	61.9	38.1
<b>4</b>	0.74	0.82	1.89	61.4	38.6
<b>5</b>	0.87	0.79	1.88	63.1	36.9
<b>6</b>	0.75	0.81	1.89	61.4	38.6
<b>7</b>	0.82	0.82	1.90	62.1	37.9
<b>8</b>	0.60	0.75	1.89	67.7	32.3
<b>9</b>	0.77 <sup>c</sup>	0.73 <sup>c</sup>	1.89 <sup>c</sup>	68.0 <sup>c</sup>	32.0 <sup>c</sup>
<b>10</b>	0.13 <sup>d</sup> /0.06 <sup>c</sup>	0.05 <sup>d</sup> /0.02 <sup>c</sup>	–	–	–
<b>11</b>	0.78	0.77	1.89	64.1	35.9
<b>12</b>	0.75	0.76	1.89	64.4	35.6
<b>13</b>	0.72 <sup>c</sup>	0.72 <sup>c</sup>	1.87 <sup>c</sup>	66.1 <sup>c</sup>	33.9 <sup>c</sup>

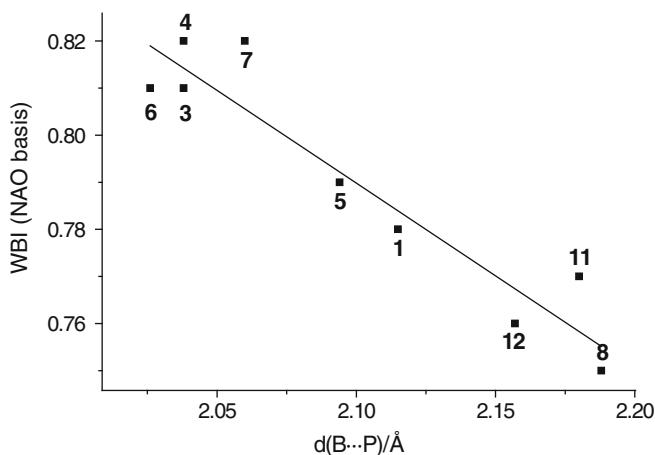
<sup>a</sup>DFT (TPSS-D3/def2-TZVP)

<sup>b</sup>Obtained from an NBO analysis (TPSS/def2-TZVP). The NBO analysis reveals in all cases a real covalent bond between the Lewis acid and base functionalities (except for **10**)

<sup>c</sup>Fully optimized structure is used

<sup>d</sup>Fully optimized structure is used (energetically lowest, see ref. [19])

<sup>e</sup>Fully optimized structure is used (second energetically lowest, see ref. [19])

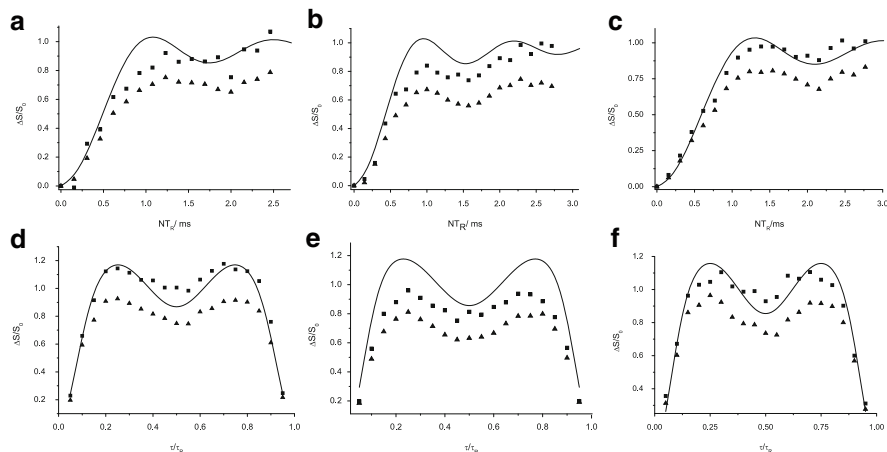


**Fig. 37** Correlation between Wiberg bond order indices (WBI) in the natural atomic orbital (NAO) basis (calculated from the TPSS Kohn-Sham determinants) and internuclear boron-phosphorus distances for compounds with known crystal structures. The *straight line* represents a linear regression with a  $R^2$  value of 0.88

well with the B $\cdots$ P internuclear distances, with the highest numbers being observed for compounds **3**, **4**, **6**, and **7** ( $d(\text{B}\cdots\text{P}) = 2.02\text{--}2.06$  Å), intermediate values for compounds **1** and **5** ( $d(\text{B}\cdots\text{P}) \sim 2.09\text{--}2.12$  Å) and much lower numbers being observed for compounds **8** and **9** (longest distances).

## 6 $^{31}\text{P}/^{11}\text{B}$ Direct Dipolar and Anisotropic Indirect $J$ -Couplings

Since the interaction among both Lewis centers is significantly correlated with the boron-phosphorus distances, the possibility of measuring this distance by REDOR or REAPDOR experiments is attractive. Our detailed results obtained on numerous FLPs indicate that the REDOR data always tend to underestimate the  $^{31}\text{P}\text{--}^{11}\text{B}$  dipolar coupling strengths slightly but systematically, leading to an overestimation of the internuclear distances in the absence of calibration. The experimental and simulated REDOR curves based on the crystallographic B $\cdots$ P distance can be made to agree with each other, however, by including a contribution arising from the  $J$ -coupling anisotropy ( $\Delta J$ ) in the simulations. As expressed by Eq. (22), the combination of the direct dipolar coupling and the  $J$ -anisotropy leads to a reduced effective dipole–dipole coupling constant, which ultimately determines the frequency of the dipolar oscillations. Typical experimental results are summarized in Fig. 38. The  $\Delta J$ -values determined for the intramolecular adducts range from 60 to 150 Hz. For the adduct **11** a slightly larger value of 200 Hz is observed; see Table 5. The non-zero contributions from the anisotropy of the  $J$ -tensor suggested by our REDOR



**Fig. 38**  $^{11}\text{B}\{^{31}\text{P}\}$  REDOR and CT-REDOR curves (REDOR data points: *filled triangles*, compensated REDOR data points: *filled squares*, calibration factor  $a = 1.8$  in the case of the REDOR experiment) for the intramolecular B/P adducts **1** (a, d) and **6** (b, e) and for the intermolecular adduct **11** (c, f). The simulation details are given in Table 5

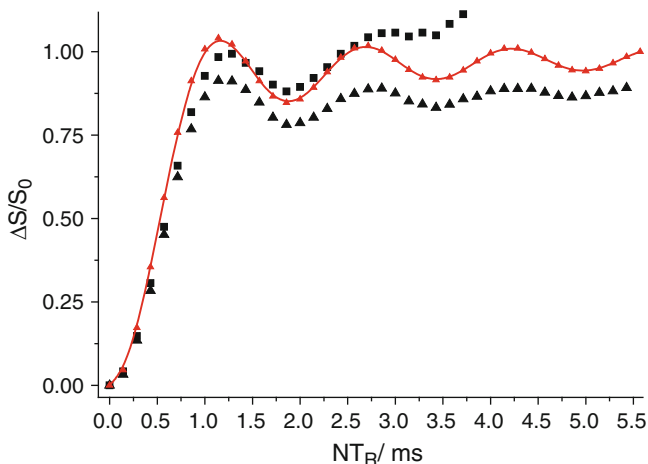
**Table 5** B...P distances from crystallography and “best-fit” values obtained from the oscillatory part of the  $^{11}\text{B}\{^{31}\text{P}\}$  REDOR curves, neglecting the influence of anisotropic  $J$ -coupling interactions ( $\Delta J = 0$ ). Numbers given in parentheses are such best-fit values from CT-REDOR data. Perfect agreement between the experimental and simulated REDOR and CT-REDOR curves based on the crystallographic B...P distance can only be achieved if a contribution arising from the  $J$ -coupling anisotropy ( $\Delta J$ ) is included in the simulations, and the corresponding “best-fit” values of  $\Delta J$  are listed

	$d_{\text{cryst.}}(\text{B}\cdots\text{P})/\text{\AA}$	$d_{\text{REDOR}}(\text{B}\cdots\text{P})$ ( $d_{\text{CT-REDOR}}(\text{B}\cdots\text{P})/\text{\AA}$ )	$\Delta J_{\text{REDOR}}$ ( $\Delta J_{\text{CT-REDOR}}/\text{Hz}$ )
<b>1</b>	2.115(2)	2.18 (2.14)	150 (60)
<b>3</b>	2.038(3)	2.06 (2.13)	60 (219)
<b>4</b>	2.038(7)	2.06 (—)	60 (—)
<b>6</b>	2.026(2)	2.06 (2.06)	80 (80)
<b>9</b>	—	2.20	—
<b>11</b>	2.180(6)	2.29 (2.29)	200 (200)
<b>13</b>	—	2.20	—

experiments lend further support to the presence of covalent interactions between the acid and base centers in the intramolecular adducts investigated.

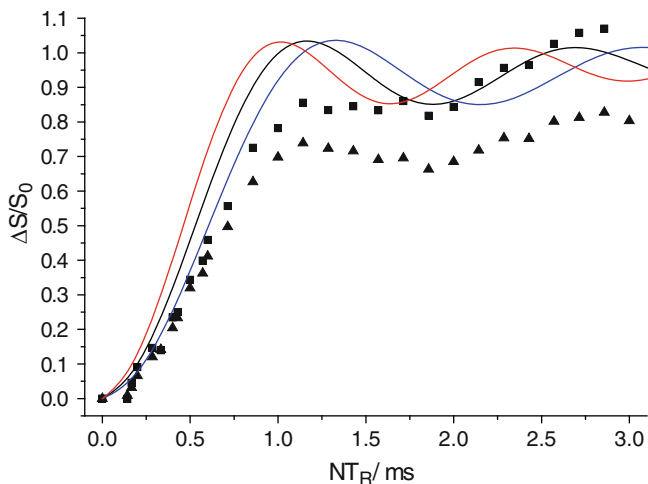
The most practical application of REDOR or REAPDOR experiments is the determination of internuclear B...P distances in FLPs not accessible to single crystal X-ray crystallography. Examples for such species include FLP materials that are disordered, amorphous or polymeric, adsorbed on surfaces, embedded in solid matrices, or distributed in other forms of nanocomposite matter. Figure 39 shows an application for compound **13**. Even though the compensation method does not perform well at long evolution times and the corrected data diverge from the simulated curve, the oscillatory part is hardly affected. Neglecting the anisotropic





**Fig. 39**  $^{11}\text{B}\{^{31}\text{P}\}$  compensated REDOR curve (*filled squares*) and REDOR curve (*filled triangles*) for the B/P adduct **13** (spinning frequency 14 kHz). The SIMPSON simulation (*solid red curve*) assumes a B...P distance of 2.20 Å and is based on experimental  $^{31}\text{P}$  anisotropic magnetic shielding parameters ( $\Delta\sigma = 58$  ppm,  $\eta_\sigma = 0.68$ ). Including a  $\Delta J \sim 60$  Hz leads to a B...P distance of 2.17 Å. In the case of long evolution times ( $>3$  ms) the compensation method does not perform well

$J$  coupling contribution to the REDOR curve leads to a distance of 2.20 Å, whereas assuming a  $\Delta J$ -value of 60 Hz would lead to 2.17 Å. Unconstrained DFT calculations (TPSS-D3(BJ)/def2-TZVP) for compound **13** lead to a boron-phosphorus distance of 2.197 Å in excellent agreement with these results. Figure 40 shows the  $^{11}\text{B}\{^{31}\text{P}\}$  REDOR curve for the extremely reactive FLP **9**. Although the oscillation of the curve is significantly damped in comparison to those of other FLPs (most probably due to the fluxional character leading to a distribution of structurally slightly different species), it can still be used for a distance determination leading to a B...P distance of 2.20 Å, which is also in good agreement with unconstrained DFT calculations [9]. Alternatively one could calibrate the technique by comparing the REDOR curve obtained on the compound of interest to one measured for an FLP with a crystallographically well-characterized B...P distance. Since the variations in the  $\Delta J$  values are moderately small, the calibration procedure then already accounts for potential systematic errors caused by the  $J$ -anisotropy. For systems with longer B...P distances, the oscillatory part of the REDOR curve may not be experimentally accessible (owing to transverse relaxation or damping by multi-spin interactions). In this case, the analysis must focus on the initial curvature of the REDOR dataset measured at short evolution times. With regard to this part, we have noticed a subtle distortion of the experimental REDOR curves in the sense that the extent of the initial dephasing in the limit of small dipolar evolution times falls slightly below the extent of dephasing predicted from the oscillatory part (see Figs. 39 and 40), i.e., both parts of the REDOR curve would actually result in slightly different values of effective dipolar coupling constants. We speculate that these distortions result mainly from heteronuclear interactions with the homonuclear coupled proton spin reservoir [62] and/or other systematic



**Fig. 40**  $^{11}\text{B}\{^{31}\text{P}\}$  compensated REDOR curve (filled squares) and REDOR curve (filled triangles) for FLP **9** (spinning frequency 14 kHz). Additionally, SIMPSON simulations assuming B...P distances of 2.10 Å (red curve), 2.20 Å (black curve), and 2.30 Å (blue curve) are shown. The best agreement in the oscillatory part is found for a B...P distance of 2.20 Å

errors as already described in the literature [63–65]. The origin of these deviations can be explored by conducting these REDOR experiments with  $^1\text{H}$  multipulse decoupling or on perdeuterated compounds, to be examined in future work. For the measurement of internuclear distances in unknown materials, the effect can again be eliminated by reference compound calibration.

## 7 Conclusions

We have described the utility of solid-state NMR techniques for the structural characterization of Frustrated Lewis Pairs (FLPs) allowing both the determination of structures and the analysis of their reaction behaviors using the information obtained on a local level. We have highlighted the high sensitivity of various NMR interaction parameters to the strength of electronic interactions (bonding) between the Lewis acid and base functionalities: the stronger this interaction, the lower are the isotropic  $^{11}\text{B}$  chemical shift values, the smaller are the quadrupolar coupling constants, and the larger are the values for the indirect  $^{31}\text{P}$ - $^{11}\text{B}$  spin–spin coupling constants. For illustrating these effects, we have explored a large variety of FLPs and related compounds ranging from the series of substituted vinylene-bridged P/B adducts, extremely reactive intramolecular P/B systems, inactive classical Lewis acid/base adducts to phosphirenium borate zwitterions isolated as stable intermediates during the 1,1-carbaboration reaction. Our results are supported and interpreted in a more profound way by performing DFT calculations of the NMR parameters mentioned above, which show in most cases excellent agreement with

the experimentally determined values. In particular, quadrupolar coupling parameters are calculated with high accuracy on a GGA level for single molecules in the gas phase, revealing only a small tilting of the largest principal electric field gradient,  $V_{zz}$ , away from the boron-phosphorus director. This behavior is responsible for the remarkable dependence of quadrupolar coupling constants on the boron-phosphorus distances, allowing one to interpret them as a physical parameter for quantifying “frustration”.

$^{31}\text{P}\{^1\text{H}\}$  CPMAS NMR experiments for the series of substituted vinylene-linked P/B adducts reveal in most cases the influence of indirect  $^{31}\text{P}$ - $^{11}\text{B}$  spin-spin couplings, manifesting themselves by asymmetric peak splittings in the MAS-NMR line shapes. Those  $J$ -coupling constants are on the order of 50 Hz (in close agreement with DFT calculations) and are attributed to  $^1J$ -spin-spin interactions directly pointing to a weak covalent bond between both Lewis centers. Field-dependent analysis of the  $^{31}\text{P}$  MAS-NMR lineshapes for nearly all the FLPs investigated illustrate that the observation of residual electron density is rather general. These results are complemented by  $^{11}\text{B}\{^{31}\text{P}\}$  REDOR and CT-REDOR experiments which suggest the influence of non-zero contributions of the  $J$ -coupling tensor anisotropy, again confirming the interaction between the Lewis centers. By taking  $\Delta J$ -values on the order of 100 Hz into consideration, such REDOR studies allow an accurate and precise determination of boron-phosphorus distances in FLPs, including those that are crystallographically inaccessible. Examples for such species include materials that are disordered, amorphous, or polymeric, adsorbed on surfaces, embedded in solid matrices, or distributed in other forms of nanocomposite matter.

From the results of this study it is clear that the term “frustration” does not mean the complete suppression of covalent bonding interactions. It remains to be investigated in detail, how “weak” or “strong” these electronic interactions should be for optimizing catalytic reactivity and selectivity. Clearly, the B...P internuclear distance is a reliable predictor only for those cases where it is controlled by the strength of this interaction within series of closely related compounds and where other aspects of the geometry are the same. Besides the fact that an optimum distance will clearly also depend on the kind of substrate chosen to be bound, activated, or dissociated, another important control parameter may be the orientation of the electric field gradient (and the electronic density distribution) relative to the B...P vector. While for the inactive intermolecular adducts **11–13** these directions coincide, all the active intramolecular FLPs have in common that there is a  $\sim 20^\circ$  tilt in relative orientation. Another factor enhancing the reactivity of an FLP may be the conformational flexibility (fluxionality) of the molecule. When such fluxionality is preserved in the solid state, as may be the case for compound **9** in the present study, the NMR parameters are affected as well, thereby influencing their correlations with the internuclear B...P distance. Such fluxionality in the solid state may in fact be desirable, particularly for molecular FLP catalysts adsorbed on surfaces or contained in nanocomposites. The continued refinement of existing and the development of new NMR strategies for characterizing structure, bonding and molecular dynamics of such systems will be an important subject of further investigations.

**Acknowledgments** We thank Prof. Dr. Gerhard Erker and his group (Olga Ekkert, Annika Klose, Christoph Rosorius, Dr. Muhammad Sajid, Dr. Gerald Kehr, and Dr. Roland Fröhlich) for providing us with all the samples discussed in this work and for outstanding and stimulating collaboration. We acknowledge support by the Deutsche Forschungsgemeinschaft, Sonderforschungsbereich SFB 858, *Synergetic Effects in Chemistry-From Additivity Towards Reactivity*. T.W. thanks the Fonds der Chemischen Industrie and the NRW Graduate School of Chemistry for personal fellowships.

## References

1. Stephan DW, Erker G (2010) Frustrated Lewis pairs: metal-free hydrogen activation and more. *Angew Chem Int Ed* 49(1):46–76
2. Grimme S, Kruse H, Goerigk L, Erker G (2010) The mechanism of dihydrogen activation by frustrated Lewis pairs revisited. *Angew Chem Int Ed* 49(8):1402–1405
3. Hamza A, Stirling A, András Rokob T, Pápai I (2009) Mechanism of hydrogen activation by frustrated Lewis pairs: a molecular orbital approach. *Int J Quantum Chem* 109(11):2416–2425
4. Rokob TA, Hamza A, Stirling A, Soós T, Pápai I (2008) Turning frustration into bond activation: a theoretical mechanistic study on heterolytic hydrogen splitting by frustrated Lewis pairs. *Angew Chem Int Ed* 47(13):2435–2438
5. Wiegand T, Eckert H, Ekkert O, Fröhlich R, Kehr G, Erker G, Grimme S (2012) New insights into frustrated Lewis pairs: structural investigations of intramolecular phosphane–borane adducts by using modern solid-state NMR techniques and DFT calculations. *J Am Chem Soc* 134(9):4236–4249
6. Stephan DW (2009) Frustrated Lewis pairs: a new strategy to small molecule activation and hydrogenation catalysis. *Dalton Trans* (17):3129–3136
7. Welch GC, Stephan DW (2007) Facile heterolytic cleavage of dihydrogen by phosphines and boranes. *J Am Chem Soc* 129(7):1880–1881
8. Welch GC, Juan RRS, Masuda JD, Stephan DW (2006) Reversible, metal-free hydrogen activation. *Science* 314(5802):1124–1126
9. Spies P, Erker G, Kehr G, Bergander K, Fröhlich R, Grimme S, Stephan DW (2007) Rapid intramolecular heterolytic dihydrogen activation by a four-membered heterocyclic phosphane–borane adduct. *Chem Commun* (47):5072–5074
10. Spies P, Kehr G, Bergander K, Wibbeling B, Fröhlich R, Erker G (2009) Metal-free dihydrogen activation chemistry: structural and dynamic features of intramolecular P/B pairs. *Dalton Trans* (9):1534–1541
11. Mömming CM, Otten E, Kehr G, Fröhlich R, Grimme S, Stephan DW, Erker G (2009) Reversible metal-free carbon dioxide binding by frustrated Lewis pairs. *Angew Chem Int Ed* 48(36):6643–6646
12. Moebs-Sanchez S, Bouhadir G, Saffon N, Maron L, Bourissou D (2008) Tracking reactive intermediates in phosphine-promoted reactions with ambiphilic phosphino–boranes. *Chem Commun* (29):3435–3437
13. Mömming CM, Kehr G, Wibbeling B, Fröhlich R, Erker G (2010) Addition reactions to the intramolecular (mesityl)<sub>2</sub>P–CH<sub>2</sub>–CH<sub>2</sub>–B(C<sub>6</sub>F<sub>5</sub>)<sub>2</sub> frustrated Lewis pair. *Dalton Trans* 39(32):7556–7564
14. McCahill JSJ, Welch GC, Stephan DW (2007) Reactivity of “frustrated Lewis pairs”: three-component reactions of phosphines, a borane, and olefins. *Angew Chem Int Ed* 46(26):4968–4971
15. Mömming CM, Fromel S, Kehr G, Fröhlich R, Grimme S, Erker G (2009) Reactions of an intramolecular frustrated Lewis pair with unsaturated substrates: evidence for a concerted olefin addition reaction. *J Am Chem Soc* 131(34):12280–12289
16. Ullrich M, Seto KSH, Lough AJ, Stephan DW (2009) 1,4-Addition reactions of frustrated Lewis pairs to 1,3-dienes. *Chem Commun* (17):2335–2337
17. Dureen MA, Stephan DW (2009) Terminal alkyne activation by frustrated and classical Lewis acid/phosphine pairs. *J Am Chem Soc* 131(24):8396–8397

18. Cardenas AJP, Culotta BJ, Warren TH, Grimme S, Stute A, Fröhlich R, Kehr G, Erker G (2011) Capture of NO by a frustrated Lewis pair: a new type of persistent N-oxy radical. *Angew Chem Int Ed* 50(33):7567–7571
19. Rosorius C, Kehr G, Fröhlich R, Grimme S, Erker G (2011) Electronic control of frustrated Lewis pair behavior: chemistry of a geminal alkylidene-bridged per-pentafluorophenylated P/B pair. *Organometallics* 30(15):4211–4219
20. Bertini F, Lyaskovskyy V, Timmer BJJ, de Kanter FJJ, Lutz M, Ehlers AW, Slootweg JC, Lammertsma K (2011) Preorganized frustrated Lewis pairs. *J Am Chem Soc* 134(1):201–204
21. Ekkert O, Kehr G, Fröhlich R, Erker G (2011) P–C bond activation chemistry: evidence for 1,1-carbaboration reactions proceeding with phosphorus–carbon bond cleavage. *J Am Chem Soc* 133(12):4610–4616
22. Kehr G, Erker G (2012) 1,1-Carbaboration. *Chem Commun* 48 (13)
23. Ekkert O, Kehr G, Fröhlich R, Erker G (2011) Phosphirenium-borate zwitterion: formation in the 1,1-carbaboration reaction of phosphinylalkynes. *Chem Commun* 47(37):10482–10484
24. Abragam A (1961) *The principles of nuclear magnetism*. Clarendon, Oxford
25. Slichter CP (1978) *Principles of magnetic resonance*. Springer, Heidelberg
26. Duer M (2004) *Introduction into solid state NMR spectroscopy*. Blackwell Publishing Ltd., Oxford
27. Kaupp M, Bühl M, Malkin VG (2004) *Calculation of NMR and EPR parameters*. Wiley-VCH, Weinheim
28. Gauss J, Stanton JF (2002) Electron-correlated approaches for the calculation of NMR chemical shifts. *Adv Chem Phys* 123:355–422
29. Massiot D, Fayon F, Capron M, King I, Le Calvé S, Alonso B, Durand J-O, Bujoli B, Gan Z, Hoatson G (2002) Modelling one- and two-dimensional solid-state NMR spectra. *Magn Reson Chem* 40(1):70–76
30. Frisch MJ et al (2009) *Gaussian 09*. Gaussian, Inc., Wallingford
31. Ahlrichs R, Furche F, Hättig C (2009) TURBOMOLE, version 6.0/ 6.3, Universität Karlsruhe
32. Ahlrichs R, Bär M, Häser M, Horn H, Kölmel C (1989) Electronic structure calculations on workstation computers: the program system turbomole. *Chem Phys Lett* 162(3):165–169
33. Blaha P, Schwarz K, Madsen G, Kvasnicka D, Luitz J (2001) WIEN2k, an augmented plane wave and local orbitals program for calculating crystal properties, Techn. Univ, Wien, ISBN 3-9501031-1
34. Cremer D, Grafenstein J (2007) Calculation and analysis of NMR spin-spin coupling constants. *Phys Chem Chem Phys* 9(22):2791–2816
35. Pines A, Gibby MG, Waugh JS (1973) Proton-enhanced NMR of dilute spins in solids. *J Chem Phys* 59(2):569–590
36. Hartmann SR, Hahn EL (1962) Nuclear double resonance in the rotating frame. *Phys Rev* 128 (5):2042–2053
37. Andrew ER, Bradbury A, Eades RG (1958) Nuclear magnetic resonance spectra from a crystal rotated at high speed. *Nature* 182(4650):1659
38. Bak M, Rasmussen JT, Nielsen NC (2000) SIMPSON: a general simulation program for solid-state NMR spectroscopy. *J Magn Reson* 147(2):296–330
39. Freude D, Haase J (1993) Quadrupole effects in solid state nuclear magnetic resonance. In: *NMR basic principles and progress*, vol 29. pp 1–90. Springer, Berlin
40. Frydman L, Harwood JS (1995) Isotropic spectra of half-integer quadrupolar spins from bidimensional magic-angle spinning NMR. *J Am Chem Soc* 117(19):5367–5368
41. Medek A, Frydman L (1999) Multiple-quantum magic-angle spinning NMR: a new technique for probing quadrupolar nuclei in solids. *J Braz Chem Soc* 10:63
42. Vinod Chandran C, Madhu PK, Kurur ND, Bräuniger T (2008) Swept-frequency two-pulse phase modulation (SWf-TPPM) sequences with linear sweep profile for heteronuclear decoupling in solid-state NMR. *Magn Reson Chem* 46(10):943–947
43. Bennett AE, Rienstra CM, Auger M, Lakshmi KV, Griffin RG (1995) Heteronuclear decoupling in rotating solids. *J Chem Phys* 103(16):6951–6958

44. Moran KL, Gier TE, Harrison WTA, Stucky GD, Eckert H, Eichele K, Wasylishen RE (1993) Synthesis and characterization of mixed ZnSe/GaP semiconductor species included in the sodalite structure. *J Am Chem Soc* 115(23):10553–10558
45. Olivieri A (1992) Study of quadrupole-perturbed quartets in the solid-state magic-angle spinning phosphorus-31 NMR spectra of phosphine-copper(I) complexes.  $^{63}\text{Cu}$  electric field gradients and anisotropy in the  $^{31}\text{P}$ ,  $^{63}\text{Cu}$  scalar coupling. *J Am Chem Soc* 114(14):5758–5763
46. Harris RK, Olivieri AC (1992) Quadrupolar effects transferred to spin- magic-angle spinning spectra of solids. *Prog Nucl Magn Reson Spectrosc* 24(5):435–456
47. Harris RK, Becker ED, Cabral de Menezes SM, Goodfellow R, Granger P (2001) NMR nomenclature. Nuclear spin properties and conventions for chemical shifts (IUPAC Recommendations 2001). *Pure Appl Chem* 73:1795
48. Massiot D, Fayon F, Alonso B, Trebosc J, Amoureux J-P (2003) Chemical bonding differences evidenced from  $J$ -coupling in solid state NMR experiments involving quadrupolar nuclei. *J Magn Reson* 164(1):160–164
49. Gullion T (1998) Introduction to rotational-echo, double-resonance NMR. *Conc Magn Reson* 10(5):277–289
50. Garbow JR, Gullion T (1991) Improvements in REDOR NMR spectroscopy. Minimizing resonance-offset effects. *J Magn Reson* 95(2):442–445
51. Chan JCC, Eckert H (2000) Dipolar coupling information in multi-spin systems: application of a compensated REDOR NMR approach to inorganic phosphates. *J Magn Reson* 147:170–178
52. Echelmeyer T, Wegner S, van Wüllen L (2008) A new application for an old concept: constant time (CT)-REDOR for an accurate determination of second moments in multiple spin systems with strong heteronuclear dipolar couplings. *Solid State Nucl Magn Reson* 34:14–19
53. Gullion T (1995) Measurement of dipolar interactions between spin-1/2 and quadrupolar nuclei by rotational-echo, adiabatic-passage, double-resonance NMR. *Chem Phys Lett* 246(3):325–330
54. Bryce DL, Wasylishen RE, Gee M (2001) Characterization of tricoordinate boron chemical shift tensors: definitive high-field solid-state NMR evidence for anisotropic boron shielding. *J Phys Chem A* 105(14):3633–3640
55. Autschbach J, Zheng S, Schurko RW (2010) Analysis of electric field gradient tensors at quadrupolar nuclei in common structural motifs. *Conc Magn Reson A* 36A(2):84–126
56. Power WP (1995) Phosphorus-31 solid-state NMR of a phosphine-borane adduct: phosphorus chemical shielding trends in the isoelectronic series  $\text{R}_3\text{PX}$ , where  $\text{X} = \text{BH}_3, \text{CH}_2, \text{NH}, \text{O}$ . *J Am Chem Soc* 117(6):1800–1806
57. Huffman JC, Skupinski WA, Caulton KG (1982) Structure of triphenylphosphine borane at  $-165^\circ$ . *C18H18BP*, *Cryst. Struct. Commun.* 11:1435
58. Karplus M (1959) Contact Electron-Spin Coupling of Nuclear Magnetic Moments. *J Chem Phys* 30(1):11–15
59. Wiberg KB (1968) Application of the Pople-Santry-Segal CNDO method to the cyclopropyl-carbinyl and cyclobutyl cation and to bicyclobutane. *Tetrahedron* 24(3):1083–1096
60. Foster JP, Weinhold F (1980) Natural hybrid orbitals. *J Am Chem Soc* 102(24):7211–7218
61. Reed AE, Weinhold F (1983) Natural bond orbital analysis of near-Hartree-Fock water dimer. *J Chem Phys* 78(6):4066–4073
62. Mitchell DJ, Evans JNS (1998) Improved heteronuclear decoupling in REDOR with the use of TPPM. *Chem Phys Lett* 292:656–661
63. Elbers S, Strojek W, Koudelka L, Eckert H (2005) Site connectivities in silver borophosphate glasses: new results from  $^{11}\text{B}\{^{31}\text{P}\}$  and  $^{31}\text{P}\{^{11}\text{B}\}$  rotational echo double resonance NMR spectroscopy. *Solid State Nucl Magn Reson* 27:65–76
64. Strojek W, Fehse CM, Eckert H, Ewald B, Kniep R (2007) Site discrimination in the crystalline borophosphate  $\text{Na}_5\text{B}_2\text{P}_3\text{O}_{13}$  using advanced solid-state NMR techniques. *Solid State Nucl Magn Reson* 32:89–98
65. Raskar DB, Eckert H, Ewald B, Kniep R (2008) Characterization of local environments in crystalline borophosphates using single and double resonance NMR. *Solid State Nucl Magn Reson* 34(1–2):20–31

# Index

## A

Ab initio calculations, 131, 291  
Aldimines, 88  
Alkenes  
    1,2-diheteroalkanes, 285  
    electron-poor, 101  
    unactivated, catalytic hydrogenation, 150  
Alkenylboranes, 102  
Alkylfluorides, 37  
Alkynes 1  
    activation, 18  
    Berke's reactions, 22  
    electron-poor, 101  
Amine/borane, 184  
Amines, 111  
Aminoalkenes, hydroamination, 255  
Aminoboranes, 111, 115  
Aminofulvene, 64  
Ammonia borane, 46  
Ammonium formatoborate, 124, 125  
Anilines, 49, 105, 116, 124  
    hydrogenations, 105  
*ansa*-Aminoboranes, 129  
Arenes, hydrogenation, 103  
Aromatic reductions, 85  
Azides, 45, 72  
Aziridines, 48, 85, 87

## B

Barriers, 267  
Basicity, 267  
Becke-Johnson damping, 219  
(C<sub>5</sub>H<sub>3</sub>Me<sub>2</sub>N)BF<sub>3</sub>, 2  
B-H bond activation, 1, 36

Bifunctional reactivity, 231  
Bis(pentafluorophenyl)chloroborane, 118  
Bis(dipentafluorophenylboryl)naphthalene,  
    118, 124  
Bis(diphenylphosphino)naphthalene, 10  
B3LYP, 220  
<sup>11</sup>B NMR, solid-state, 291, 323  
Boranes, 111  
    pendent olefins, 16  
Boron-amidinates, 61  
B-P distance measurement, 291  
B2PLYP, 220  
1-(2-Bromobenzyl)-2,2,6,6-  
    tetramethylpiperidine, 129  
Butadienes, 17

## C

Carbenes, 171, 184, 234, 277  
Carbon dioxide, 72  
    activation, 1, 29  
    catalytic deoxygenative hydrosilylation,  
        125  
    fixation, 124  
    to methane, 123  
    to methanol, 124  
    stoichiometric reduction, 30  
    trapping/activation, 282  
Carbon monoxide, 114  
Carbonyl/borane pairs, 184  
Carbonyl compounds, reduction, 124  
Catalysis, 157  
Catecholborane, activation, 35  
Chiral-7-isopropyl-3,3-dimethyl-2-  
    phenylindoline, 147

- CT-REDOR, 316  
 C–C bonds, triple, unactivated, 149  
 C–F activation, 1  
   heterolytic, 37  
 C–H activation, heterolytic, 37  
 Cumulenes, 69  
 Cyclohexenylphosphane, 49  
 Cyclohexylamines, 49  
 Cyclohexylammonium salts, 105  
 Cyclohexylbis(pentafluorophenyl)borane, 121  
 Cyclopropanes, ring-opening, 23, 28
- D**  
 D/A + H<sub>2</sub>, 183  
 DFT calculations, 213, 231, 291  
 1,4-Diazabicyclo[2.2.2]octane (DABCO), 187  
 Dienamines, 48  
   ferrocenophane-derived, 96  
 Dienes, activation, 17  
 Dihydrogen, 157  
   activation, linked FLPs, 190  
   heterolytic activation, 9  
   heterolytic cleavage, 1, 85, 162, 168, 278  
   vicinal phosphorus/boron FLPs, 47–55  
 Diimines, 88  
 Diisopropylamine, 117  
 Diisopropyltrimethylsilylamine, 120  
 Dimesitylalkenylphosphanes, 49  
 Dimesitylvinylphosphane, 47  
 6-Dimethylamino-6-methylpentafulvene, 65  
 2,3-Dimethylbutadiene, 99, 114  
*trans*-2,6-Dimethyl-2,6-diphenylpiperidine (DMDPP), 121, 184  
 Dimethylfumarate, 65  
 Dimethylpentafulvene, 64  
 Dioxane ring-opening, 27  
 1,1-Diphenylethene, 100  
 1,1-Diphenylethylene, 100  
 Dipolar recoupling, 311  
 Dipole–dipole coupling, 301  
 Disulfides, heterolytic activation, 1  
   heterolytic cleavage, 35  
 Di-*tert*-butylphosphinopropyne, hydroboration, 52  
 DMACATBH, 151  
 Double bonds, hydrogenation, 196
- E**  
 Electron donors/acceptors, 2  
 Enamines, 48, 56, 85  
   hydrogenation, 94, 140  
   transfer hydrogenation, 107
- Enones, 85  
   hydrogenation, 103  
 Enynes, 85  
 Ethers, ring-opening, 23  
 Ethylene, 8, 16  
   hydrogen addition, 235, 243  
   insertion, 37  
 Ethylvinylether, 63  
 Ethynylferrocene, 23
- F**  
 Ferrocenyl-phosphine derivatives, 10  
 Fluoroalkanes, 37  
 Free energies, 165  
   calculations, 213  
 Frustrated Lewis pairs, 1ff, 8  
   addition reactions, 45  
   arene-tethered, 277  
   carbene/borane, 12  
   geminal, 74  
   intermolecular/nonlinked, 163  
   intramolecular/linked, 163  
   nitrogen bases/boranes, 12, 55  
   olefinic carbon–carbon  $\pi$ -systems, 63  
   phosphine/borane, 10  
   vicinal/geminal, 45  
 Frustration, degree of, 291  
   notion/mechanism, 174  
   solvent-assisted, 187  
   thermally induced, 186
- G**  
 Gas phase, thermal corrections, 224  
 Geometry optimizations, 217  
 Gibbs activation energy, 50  
 Gibbs free energies, 165, 169, 188, 197, 201  
 Greenhouse gases, FLP activation, 29
- H**  
 Heterocumulenes, 45  
 Homogeneous catalysis, 111  
 Hydroaminations, 255  
 Hydrogen activation, 157, 213, 234  
   amines/boranes, 115  
   *ansa*-aminoborane, 133  
   heterolytic, 9  
   metal-free, 5, 231  
    $\pi$ -FLP, 235  
 Hydrogenation, 111  
   amines/boranes, 123  
   catalysis, 85



double bonds, 196  
enantioselective, 145  
metal-free, 231  
Hydrogen cleavage, thermodynamics, 162  
Hydrosilylation, 15

**I**

Imine/borane, 184  
Imines, 85, 88, 245  
    hydrogenations, 140  
        B(C<sub>6</sub>F<sub>5</sub>)<sub>3</sub>, 196  
    transfer hydrogenations, 105  
Iminium hydridoborate, 13  
Isonitriles, 61, 71

**J**

J-couplings, 300, 311, 335, 338

**K**

Ketones, hydrogenations, 249  
    hydrosilylation, 16

**L**

Lactides, ring-opening, 23, 28  
Lactone, 28  
LA-ONN-P(*t*-Bu)<sub>3</sub>, 286  
Lewis acceptors, 163  
Lewis acid(s), 2, 46, 273  
Lewis acidity, 2, 267  
Lewis acid–base reaction, 3, 157  
Lewis bases, 2, 46, 276  
Lewis basicity, 2, 267  
Lewis donors, 163  
London dispersion, 213  
Lutidine, 2, 14, 22, 114, 174, 280

**M**

Magic angle spinning, 291, 304  
Magnetic shielding, 298  
Mesitylazide, 74  
Metal-free catalysts, computational design, 245  
    design, 231  
Methane, activation, 240, 284  
Methoxy(bis(pentafluorophenyl)borane, 123  
N-(4-Methoxy)phenyl-1-  
    phenylethylideneamine, 145

2-Methylbutadiene, 99  
Mono-amino carbenes, 37  
Morpholinocyclohexene, 23

**N**

Na[Ph<sub>3</sub>CCH<sub>2</sub>(BPh<sub>3</sub>)CHCH<sub>2</sub>], 4  
Na[Ph<sub>3</sub>C(CH<sub>2</sub>)<sub>4</sub>OBPh<sub>3</sub>], 3  
N/B FLPs, intramolecular, 55  
N/C/O donors, 183  
2-Neosilylpropene, 99  
Nitriles, 71, 85–88  
Nitrogen-containing compounds, unsaturated,  
    139, 145  
NMR, solid-state, 296  
N<sub>2</sub>O, activation, 1, 282  
    FLP capture, 33  
    trapping, 282  
Norbornene, 63  
Nuclear electric quadrupolar coupling, 299  
N–H activation, heterolytic, 36

**O**

Olefins, 1  
    1,1-disubstituted, 85  
Organocatalysis, 111

**P**

<sup>31</sup>P/<sup>11</sup>B J-coupling, 338  
Perfluorophenylboranes, 125  
Perfluoro-1,4-phenylene, 190  
Phenylacetylene, 19  
Phenylazide, 71  
1-Phenyl-2-[bis(pentafluorophenyl)boryl]  
    ethane, 121  
Phenylisocyanate, 71  
2-Phenylpropene, 99  
Phosphinoborane, 114  
    *ansa*-Phosphinoborane, 134  
Phosphino-ferrocenes, 11  
Phosphirenium-borate betaine, 54  
Phosphonium fluoroborate salts, 37  
Phosphonium/hydridoborate, 47  
Phosphorus/boron, vicinal, 47  
Piers' aminoborane, 115  
Piers' ammonium borate, 115  
Piers' bis(pentafluorophenyl)borane, 118,  
    136, 138  
Piers' borane, 52

- 3-Pinanyl-bis(perfluorophenyl)borane, 145  
Piperidino-cyclohexene, 216  
 $^{31}\text{P}$  NMR, solid-state, 291, 330  
Potential energy surface (PES), 160  
PW6B95, 220  
Pyrazolium borates, 139  
Pyrazolylboranes, 139  
Pyridyliimines, 88  
Pyrroles, 24
- Q**  
Quadrupolar coupling constant, 291  
Quantum chemistry, 157, 213  
Quinolines, 188  
    catalytic hydrogenation, boranes, 126  
    hydrogenation, B(p-C<sub>6</sub>F<sub>4</sub>H)<sub>2</sub>Mes, 200  
Quinuclidine, 120, 128, 187
- R**  
Reaction mechanisms, 157  
REAPDOR, 317  
Ring-opening reactions, 1, 23, 27  
Rotational echo double resonance (REDOR), 311
- S**  
(SCS-)MP2, 213  
Sertraline, 88  
Silyl enol ethers, 48, 85  
    hydrogenation, 93  
Small molecules, 1, 9, 29, 38, 188, 213, 231  
    activation, 45, 235  
SO<sub>2</sub>, FLP capture, 33  
Solvation, 225  
Solvent effects, 144, 194, 213, 227  
Spin–spin coupling, 291  
    indirect, 308
- Stephan's phosphinoborane, 114  
Synergistic reactions, 45
- T**  
*t*-Bu<sub>3</sub>P/B(C<sub>6</sub>F<sub>5</sub>)<sub>3</sub> + H<sub>2</sub>, 175  
*tert*-Butylaniline, hydrogenation, 105  
Tetrahydrofuran, 5, 25, 114  
    FLP ring-opening, 25  
Tetramethylmorpholine, 135  
Tetramethylpiperidine, 117  
Thioxane ring-opening, 27  
2-Tolylpropene, 99  
TPSS-D3/def2-TZVP, 220  
Transfer hydrogenations, imines, 105  
Transition metals (TMs), 159  
    pincer catalysts, mimicking, 242  
Trimethylsilylcarbazole, 118  
Trimethylsilyldiphenylamine, 118  
Triphenylaziridine, 104  
Triphenylborane, 114  
Tris(pentafluorophenyl)borane, 117,  
    124, 164  
Tris(*tert*-butyl)phosphonium/chiral-alkyl-bis  
    (perfluorophenyl)hydroborate, 145  
Tritylsodium, 114
- X**  
X-ray diffraction, 219
- Y**  
Ynones, 49, 66–68, 101, 149  
    hydrogenation, 102
- Z**  
Zeeman interaction, 296  
Zero-damping, 219  
Zirconocene, 92